New Smart Materials via Metal Mediated Macromolecular Engineering

Edited by
Ezat Khosravi
Yusuf Yagci
Yuri Savelyev

 Springer

New Smart Materials via Metal Mediated Macromolecular Engineering

NATO Science for Peace and Security Series

This Series presents the results of scientific meetings supported under the NATO Programme: Science for Peace and Security (SPS).

The NATO SPS Programme supports meetings in the following Key Priority areas: (1) Defence Against Terrorism; (2) Countering other Threats to Security and (3) NATO, Partner and Mediterranean Dialogue Country Priorities. The types of meeting supported are generally "Advanced Study Institutes" and "Advanced Research Workshops". The NATO SPS Series collects together the results of these meetings. The meetings are co-organized by scientists from NATO countries and scientists from NATO's "Partner" or "Mediterranean Dialogue" countries. The observations and recommendations made at the meetings, as well as the contents of the volumes in the Series, reflect those of parti-cipants and contributors only; they should not necessarily be regarded as reflecting NATO views or policy.

Advanced Study Institutes (ASI) are high-level tutorial courses intended to convey the latest developments in a subject to an advanced-level audience

Advanced Research Workshops (ARW) are expert meetings where an intense but informal exchange of views at the frontiers of a subject aims at identifying directions for future action

Following a transformation of the programme in 2006 the Series has been re-named and re-organised. Recent volumes on topics not related to security, which result from meetings supported under the programme earlier, may be found in the NATO Science Series.

The Series is published by IOS Press, Amsterdam, and Springer, Dordrecht, in conjunction with the NATO Public Diplomacy Division.

Sub-Series

A.	Chemistry and Biology	Springer
B.	Physics and Biophysics	Springer
C.	Environmental Security	Springer
D.	Information and Communication Security	IOS Press
E.	Human and Societal Dynamics	IOS Press

http://www.nato.int/science
http://www.springer.com
http://www.iospress.nl

Series A: Chemistry and Biology

New Smart Materials via Metal Mediated Macromolecular Engineering

edited by

Ezat Khosravi

Polymer IRC, Chemistry Department
Durham University
Durham, United Kingdom

Yusuf Yagci

Department of Chemistry
Istanbul Technical University
Istanbul, Turkey

and

Yuri Savelyev

Institute of Macromolecular Chemistry
National Academy of Science
Kiev, Ukraine

CONTENTS

PREFACE

Control over macromolecular architecture and resulting material properties has been a central goal of polymer chemistry. There has been much interest in developing new synthetic routes to prepare smart materials with novel compositions and topologies for various applications. The considerable progress in the metal mediated macromolecular engineering over the past decade has had a major impact on the development of well-defined macromolecular architectures and the synthesis of smart materials. Particularly, remarkable strong developments have been observed for the synthesis of smart materials via four metal mediated macromolecular engineering techniques; Anionic, ROMP, ATRP and Click Chemistry. These materials have found uses in advanced microelectronics, technical and biomedical applications as well as in chemical sensors applications. Some of the materials produced via metal mediated macromolecular engineering, through self-assembly or other interactions resulted in the formation of nano or bio-nano smart materials and opened up a wide range of applications in nanotechnology.

The NATO ASI on "New Smart Materials via Metal Mediated Marcomolecular Engineering: From Complex to Nano Structures" was held at Dedeman Hotel and Resort, Antalya, Turkey from 1–12 September 2008. The ASI brought together 15 leading scientists as lecturers from NATO and Partner Countries who have greatly contributed in the area of Anionic, ROMP, ATRP and Click Chemistry. The aim of the ASI was to discuss the fundamental aspects and recent developments of these four powerful techniques and evaluate their potential in the syntheses of smart materials from complex structures (grafts, brushes, dendrimers, etc.) to nanostructures (self-assembly, nano-size, etc.) for a wide range of applications.

During the ASI, synthetic methodlogies of anionic, ATRP, ROMP and Click were presented for a wide range of well-defined complex polymeric systems. Thermoresponsive smart polymers, star copolymers, biocompatible polymers, amphipilic smart nano structured, conducting polymers, self assembled polymers, and hyperbranced polymers were part of the discussions. It became clear that the recent developments in the metal mediated polymerization methods facilitated preparation of materials with diverse properties. Particularly, the combination of different metal mediated methodologies extended the range of materials available that could not be prepared before with the conventional systems.

Both techniques of ATRP and Click chemistry are mediated by Copper catalysts and the complete removal of the copper residues from the products, crucial for biomedical and electronic applications, has always been problematic.

In order to alleviate this problem two methods were reported and discussed based on ARGET-ATRP, which uses very low concentartion of copper, and Click reaction using copper wire.

At the end of ASI, it was clear that the exploitation of new materials has become a new industry and that metal mediated polymerization reactions provided the possibilty to prepare smart materials. The future research is expected to focus on the development of more innovative and advanced materials for the industry and society.

The ASI was attended by 80 students from 13 NATO and 6 Partner and Dialogue Countries. The selection of Antalya for the location of ASI provided an exciting atmosphere for the exchange of scientific ideas. The ASI has provided a useful platform for scientific, social and cultural interactions amongst the participants.

ACKNOWLEDGEMENTS

CONTRIBUTORS

MICHAEL R. BUCHMEISER   Leibniz-Institute of Surface Modification, Permoserstrasse 15, 04318 Leipzig, Germany.

ALAIN DEFFIEUX   CNRS, Universite de Bordeaux, Laboratoire De Chimie des Polymeres Organiques, 16 Avenue Pey Berland 33607, Pessac Cedex, France.

FILIP DU PREZ   Department of Organic Chemistry, Ghent University, Krijgslaan 281 S4-bis, B9000 Gent, Belgium.

EUGENE SH. FINKELSTEIN   Topchiev Institute of Petrochemical Synthesis RAS, 29, Leninskii prospect, 119 991 Moscow, Russia.

KAROL GRELA   Institute of Organic Chemistry, Polish Academy of sciences, Kasprzaka 44/52, 01-224 Warsaw, Poland.

ROBERT H. GRUBBS   Division of Chemistry and Chemical Engineering, California Institute of Technology, 1200 E California Blvd MC 164-30 Pasadena, CA 91125, USA.

NIKOS HADJICHRISTIDIS   Department of chemistry, University of Athens, Panepistimiopolis Zografou, 15771 Athens, Greece.

ELNARA KALBALIYEVA   Institute of Petrochemical Processes, Azerbaijan Academy of Science, AZ 1025, Khodjaly Av. 30, Baku, Azerbaijan.

EZAT KHOSRAVI   Polymer IRC, Chemistry Department, Durham University, Durham DH1 3LE, UK.

PHILIPPE LECOMTE   Centre for Education and Research on
                                 Macromolecules (CERM), University
                                 of Liege, B6a Sart-Tilman, B-4000
                                 Liege, Belgium.

JEAN-FRANÇOIS LUTZ   Fraunhofer Institute for Applied
                                 Polymer Research, Geiselbergstrasse
                                 69, 14476 Potsdam, Germany.

KRZYSZTOF MATYJASZEWSKI   Chemistry Department, Carnegie
                                 Mellon University,
                                 4400 Fifth Avenue, Box 75,
                                 Pittsburg, 15213 PA, USA.

AXEL H. E. MÜLLER   Makromolekulare Chemie II,
                                 Universität Bayreuth, D-95440
                                 Bayreuth, Germany.

OSAMA M. MUSA   International Specialty Products (ISP),
                                 1361 Alps Road, Wayne, NJ 07470,
                                 USA.

YURI SAVELYEV   Institute of Macromolecular
                                 Chemistry, National Academy of
                                 Science, 48 Kharkivske Shausse,
                                 02660 Kiev, Ukraine.

YUSUF YAGCI   Department of Chemistry, Istanbul
                                 Technical University, Maslak, Istanbul
                                 80626, Turkey.

PART 1. ATOM TRANSFER RADICAL POLYMERIZATION (ATRP)

FROM MECHANISM AND KINETICS TO PRECISE ATRP SYNTHESIS

LAURA MUELLER, PATRICIA GOLAS,
AND KRZYSZTOF MATYJASZEWSKI[*]
*Department of Chemistry, Carnegie Mellon University,
4400 Fifth Avenue, Pittsburgh, PA 15213*

Abstract: Controlled/living radical polymerizations (CRP) give access to polymers with precisely controlled molecular weight, narrow molecular weight distribution, well-defined architecture and composition. CRP can be applied to a wide range of monomers and are tolerant to impurities and functional groups. Atom transfer radical polymerization (ATRP) is one of the most widely used CRP techniques. The mechanistic and kinetic studies of ATRP are of fundamental importance since they give access to polymers with various functionalities, compositions, and topologies.

1. Fundamentals of ATRP

The development of living polymerization[1, 2] enabled the production of polymers with precisely controlled molecular weight, narrow molecular weight distribution, and well-defined architecture and composition. There are a number of advantages of controlled/living radical polymerization (CRP),[3–8] such as applicability to a wide range of monomers and solvents, tolerance to impurities and functional groups, and ease of experimental set-up. Atom transfer radical polymerization (ATRP) is one of the most widely used CRP techniques.[9–12]

The mechanism for ATRP is shown in Scheme 1. Initiation occurs through a reversible reaction of $Mt^n L_m$ with an alkyl halide RX by a one-electron redox process to generate $X-Mt^{n+1}L_m$ and an organic radical $R^\bullet$, with a rate constant of activation k_{act}. The radical can then add to vinyl monomer with a rate constant of propagation k_p, be reversibly deactivated by $X-Mt^{n+1}L_m$ with a rate constant k_{deact}, or terminate by coupling or disproportionation with a rate constant k_t.

The dynamic equilibrium that is established between the low oxidation state transition metal complex (Mt^nL_m) and its higher oxidation state complex (X-$Mt^{n+1}L_m$) mediates control during ATRP. The ATRP equilibrium ($K_{ATRP} = k_{act}/k_{deact}$) is heavily shifted towards the dormant alkyl halide species, assuring even growth of polymer chains. During the initial stages of polymerization, a small amount of termination occurs (~5%) that leads to the accumulation of X-$Mt^{n+1}L_m$ species. This will then lessen further termination reactions via the persistent radical effect.[13, 14]

$$Mt^nL_m + P_n\text{-}X \underset{k_{deact}}{\overset{k_{act}}{\rightleftharpoons}} X\text{-}Mt^{n+1}L_m + P_n^\bullet$$

+M k_p

k_t

bimolecular
termination
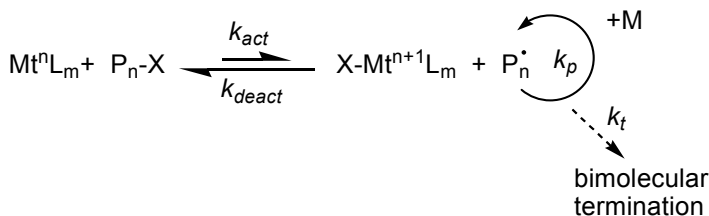
Scheme 1. Mechanism of ATRP.

1.1. COMPONENTS OF ATRP

The necessary components for a typical ATRP include an initiator, monomer, transition metal species, and complexing ligand. There are several commercially available alkyl halides which can be used as initiators for ATRP, typically containing a transferable halogen that is activated by α-carbonyl, phenyl, vinyl, or cyano substituents. It is important that initiation be fast and quantitative in order to obtain polymers of a predetermined molecular weight. An initiator that is characterized by sufficiently fast activation must be selected according to the following rules: activity depends on the degree of substitution (primary < secondary < tertiary), transferable group (Cl < Br < I), and radical stabilizing group (–Ph ~ –C(O)OR << –CN).[15]

Typically, a Cu-based transition metal complex is used to mediate ATRP, but several other metals have been used as well. In order to be an efficient catalyst, a transition metal center must possess at least two accessible oxidation states separated by one electron, it also must have an expandable coordination sphere and an affinity towards a halogen. In order to solubilize the transition metal and adjust the catalyst redox potential, a complexing ligand is required. An appropriate ligand will ensure a suitable equilibrium between dormant and propagating species. For copper, nitrogen-based ligands are typically used. Some examples include 2,2′-bipyridine (bpy),[9, 16] pyridine imine,[17, 18] diethylenetriamine (DETA),[19] tris[2-aminoethyl]amine (TREN),[20] and tetraazacyclotetradecane (CYCLAM),[21] among others.[22, 23]

Several monomers have been polymerized successfully by ATRP, including various (meth)acrylates, styrenes, (meth)acrylamides, and acrylonitrile. Each of these monomers contains substituents that are able to stabilize propagating radicals. It is necessary to choose optimal ATRP conditions to achieve a controlled polymerization for each monomer, including the correct initiator, catalyst, solvent, temperature, and concentration.

The rate of polymerization (R_p) in ATRP is determined by several factors, according to Equation (1). R_p is proportional to initiator concentration and the ratio of activator to deactivator concentrations. It is also influenced by the value of k_p, unique to each monomer, and K_{ATRP}, determined by the catalyst choice.

$$R_p = -d[M]/dt = k_p[M][P^\bullet] = k_p[M]K_{ATRP}[RX]([Mt^n/L]/[Mt^{n+1}X/L]) \quad (1)$$

1.2. MECHANISTIC CONSIDERATIONS OF ATRP

The K_{ATRP} value for any catalyst/initiator system is determined experimentally by mixing the alkyl halide initiator with transition metal activator and monitoring the increase in deactivator concentration over time. A plot is constructed of $F([Cu^{II}L_nX])$ versus time (Equation (2)) and K_{ATRP} is calculated from the slope.[14]

$$F\left(\left[Cu^{II}L_nX\right]\right) \equiv \frac{\left[Cu^IL_n\right]_0^2}{3\left(\left[Cu^IL_n\right]_0 - \left[Cu^{II}L_nX\right]\right)^3} - \frac{\left[Cu^IL_n\right]_0}{\left(\left[Cu^IL_n\right]_0 - \left[Cu^{II}L_nX\right]\right)^2} + \frac{1}{\left[Cu^IL_n\right]_0 - \left[Cu^{II}L_nX\right]} = (2)$$

$$= 2k_t K_{ATRP}^2 t + \frac{1}{3\left[Cu^IL_n\right]_0}$$

For most Cu-mediated ATRP, the K_{ATRP} value is typically between 10^{-10}–10^{-4}, where the larger values correspond to the more active catalysts.[14, 24–26] To better understand the factors that influence the ATRP equilibrium, it is possible to express it as a product of four reversible reactions: oxidation of the transition metal activator, or electron transfer (K_{ET}); formation of halide anion, or electron affinity (K_{EA}); bond homolysis of the alkyl halide initiator (K_{BH}); and association of halide anion with deactivator, or "halidophilicity" (K_X) (Scheme 2).[27] Of the four reactions, bond homolysis is the only that does not depend on the catalyst. If the same catalyst and conditions are considered for the other three reactions, the polymerization rate can be predicted from each of the calculated bond dissociation energies.

The typical method to determine the rate constant k_{act} is to spectroscopically (or chromatographically) monitor the consumption of alkyl halide upon activation by a Cu^I complex, which generated radicals that are trapped by an excess of scavenging agents (i.e. nitroxides).[29] The measurement of k_{deact} can be done by a type of clock reaction in which radicals are simultaneously trapped by a

transition metal deactivator and a nitroxide.[30] It can also be estimated from known values of K_{ATRP} and k_{act}.

$$Mt^n/L \xrightleftharpoons{K_{ET}} Mt^{n+1}X/L + e^{\ominus}$$

$$X^{\cdot} + e^{\ominus} \xrightleftharpoons{K_{EA}} X^{\ominus}$$

$$R-X \xrightleftharpoons{K_{BH}} R^{\cdot} + X^{\cdot}$$

$$X^{\ominus} + Mt^{n+1}/L \xrightleftharpoons{K_X} Mt^{n+1}X/L$$

$$K_{ATRP} = \frac{k_{act}}{k_{deact}} = K_{BH}K_{EA}K_X K_{ET}$$
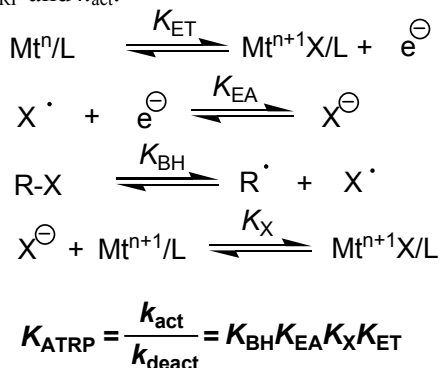
Scheme 2. Sub-equilibria in ATRP.[28]

In Cu-based ATRP, the k_{act} has been shown to depend on the complexing nitrogen-based ligand. The values generally obey several trends, with activity depending on: ligand topology (cyclic ~ linear < branched); linking unit between nitrogen atoms (C4 << C3 < C2) and/or coordination angle; nature of the ligand (aryl amine < aryl imine < alkyl imine < alkyl amine ~ pyridine); and steric bulk around the metal. For k_{deact}, ligands which are able to ease the structural reorganization of the Cu^{II} complex upon halogen abstraction give higher values than others.[31]

1.3. ATRP INITIATION SYSTEMS

1.3.1. *Normal/Reverse/Simultaneous Reverse and Normal ATRP*

In normal ATRP, an alkyl halide initiator is combined with a transition metal catalyst initially in its lower oxidation state. This technique requires relatively large amounts of the catalyst and deoxygenation of the system prior to poly-merization, making it difficult to bring to an industrial scale. Reverse ATRP was developed in order to avoid problems of oxidation. In this method, a conventional radical initiator (such as AIBN) is used to generate radicals that are deactivated by a higher oxidation state metal, in order to generate the ATRP activator *in situ*.[32–34] In this way, the more air-stable, higher oxidation state transition metal can be added to the initial polymerization mixture. Simultaneous reverse and normal initiation (SR&NI) is similar to reverse ATRP, except that it is carried out in the presence of an alkyl halide initiator along with AIBN. This way, handling problems can be avoided while the ability to make block copolymers is maintained. The SR&NI technique has been used in both bulk and miniemulsion systems.[35, 36]

1.3.2. Activators Generated by Electron Transfer (AGET)

SR&NI is limited in its ability to make pure block copolymers, because of the presence of a radical source that can initiate new chains. In activators generated by electron transfer (AGET) ATRP, this problem is avoided by the use of a reducing agent (which is not able to produce new polymer chains) to generate the lower oxidation state activator. Several reducing agents have been used for this process, including zero valent Cu,[37, 38] tin^{II} 2-ethylhexanoate,[39] ascorbic acid,[40, 41] and triethylamine.[42] This technique is very useful to aqueous and miniemulsion systems.[43–45]

1.3.3. Initiators for Continuous Activator Regeneration (ICAR) and Activators Regenerated by Electron Transfer (ARGET)

It is challenging to go to lower concentrations of copper in ATRP, because of the unavoidable radical termination reactions that occur which lead to the loss of activator and accumulation of deactivator. If the catalyst concentration is too low, polymerization will stop if the concentration of terminated chains is higher than that of catalyst. To avoid this problem, a new initiation process known as initiators for continuous activator regeneration (ICAR) was developed. In this technique, a conventional radical initiator (such as AIBN) is present in excess of the transition metal species to continuously regenerate the active, lower oxidation state transition metal species.[46] Similarly, a reducing agent can be used instead of a free radical source to generate activator. This method, known as activators regenerate by electron transfer (ARGET), has been used to prepare homopolymers and clean block copolymers in the presence of <50 ppm of copper catalyst.[47, 48] Similar to AGET, the reducing agents used in this process include hydrazine, phenol, glucose, ascorbic acid, Sn^{II} species, and Cu^0. The polymerization rate in ARGET and ICAR ATRP depends not on the nature of the catalyst, but on the concentration of the reducing agent and radical source, respectively. However, careful consideration must be made as to the choice of catalyst for ARGET and ICAR ATRP, as a number of side reactions are intensified at low catalyst concentration (such as halide dissociation and coordination of monomer to transition metal species). A number of the reducing agents in ARGET ATRP form acidic by-products which also have the potential to destroy the catalyst/ligand complex. It is of note that lower catalyst concentrations can lessen the occurrence of certain side reactions such as outer sphere electron transfer and β-H elimination. This has recently allowed the preparation of high molecular weight polystyrene and poly(styrene-*co*-acrylonitrile)[49] by ATRP.

2. Materials Prepared by ATRP

Polymers with various functionalities, compositions, and topologies have been prepared by ATRP (Figure 1).[50] Control over molecular weight distribution has also been recently demonstrated using ARGET ATRP. The formation of these polymers is discussed in the following sections.
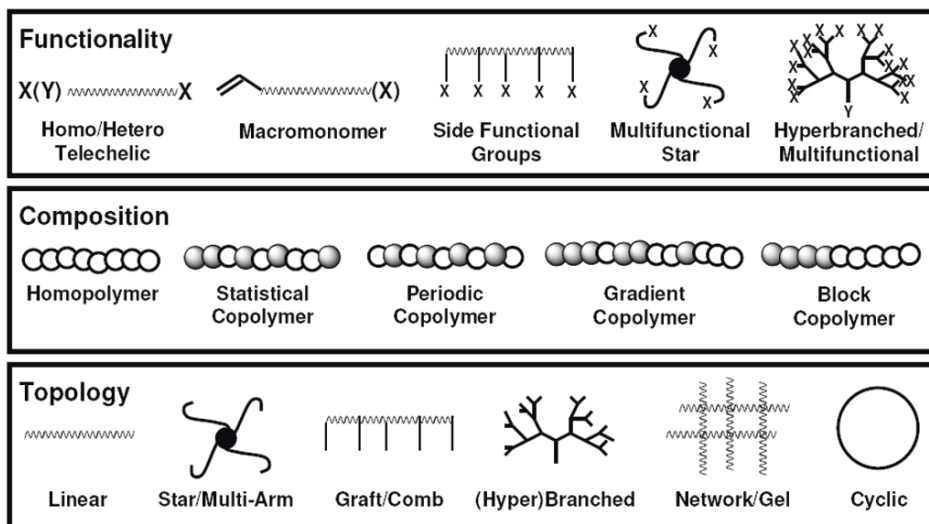
Figure 1. Illustration of polymers with controlled functionality, composition, and topology.

2.1. FUNCTIONALITY

Functionality within a polymer is important for fine-tuning many properties, such as elasticity, solubility, biocompatibility, tensile strength, melting/glass transition temperatures, crystallinity, electrical conductivity, etc. Functional groups can be incorporated into a polymer via modified monomer, initiators, or chain ends. Chain end functionality can lead to materials good for blend compatibilization, while functional monomers will have a greater effect over bulk properties. ATRP is tolerant to a wide variety of functional groups, although certain functionality (i.e. acidic groups) may interfere with the mechanism. However, these functional groups can easily be incorporated through post polymerization modification.

2.1.1. Functional Monomers

(Meth)acrylates represent the broadest range of monomers polymerizable by ATRP. Some examples include 2-hydroxyethyl (meth)acrylate, glycidyl

(meth)acrylate,[51] 2-trimethylsilyloxyethyl (meth)acrylate,[52–54] 2-(dimethyl-amino)ethyl methacrylate,[55] and allyl (meth)acrylate, among others. Several styrene derivatives have been polymerized via ATRP. Derivatives containing an electron withdrawing group (such as sulfonates, carbonyls, and halogens) lead to a faster polymerization, due to a decreased stability of the dormant species and thus faster propagation rates. The polymerization of 4-vinylpyridine by ATRP has also been demonstrated, although the catalytic complex should be carefully selected in order to prevent side reactions. (Meth)acrylamides are also polymerizable by ATRP.[56–59] Other types of functional monomers include bioconjugates (vinyl monomers with attached sugars,[60] or short nucleotide sequences,[61, 62]) macromonomers (a polymer chain with a polymerizable group at its terminus), monomers containing an ATRP initiator (leading to hyperbranched polymers), and monomers containing two or more polymerizable groups (leading to a cross-linked network).

2.1.2. Functional Initiators

The use of a functional initiator allows for direct incorporation of a functional group onto a chain end, yielding a telechelic polymer. There are several ways through which an initiator can be modified, as long as the functional group does not interfere with the ATRP mechanism. A polymer prepared using ATRP contains a halogen atom at its terminus and can subsequently be used to form a block copolymer. Initiators can also contain multiple initiating sites. Multifunctional ATRP initiators can be used to synthesize star copolymers and other hyperbranched materials as well. Difunctional ATRP initiators have been used to synthesize tri- and other multi-block copolymers.[63] Other types of difunctional initiators can combine one ATRP initiating site with an initiating group for another poly-merization mechanism to make block copolymers through mechanistic trans-formation.[64]

2.1.3. Chain-End Functionality

There are several examples of chain-end functionality which can be prepared from polymers prepared via ATRP. The halogen atom located at the end of the polymer chain can be easily displaced by numerous other functionalities. Some examples include a polymerizable double bond for the formation of a macromonomer, an initiating site for another polymerization mechanism, or a precursor for "click" chemistry. The most popular click reaction is the Cu^I-catalyzed azide–alkyne cycloaddition.[65, 66] This click reaction has been combined with ATRP to prepare pendant-functionalized polymers,[67] end-functional polymers,[68, 69] multisegmented block copolymers,[70] stars,[71] brushes,[51, 72] and other architectures.[73]

2.2. POLYMER COMPOSITION AND MICROSTRUCTURE

A polymer chain consisting of one type of monomer is known as a homopolymer. When more than one monomer is used, there are several combinations in which they can be arranged along the polymer chain, which is described by the instantaneous composition. A linear copolymer can have a random, periodic, block, or gradient structure, depending on the method of polymerization and the reactivities of each monomer. Polymers with similar molecular weights and monomer composition can have very different properties depending on the instantaneous chain composition. In ATRP, precise control of the composition along a single polymer chain is possible, because essentially all the polymer chains grow at the same rate throughout the polymerization. Tacticity control is not as simple, as will be discussed.

2.2.1. *Random/Gradient Copolymers*

The reactivity ratio between two monomers is defined as the ratio of the rate constants of homopropagation and crosspropagation. Comonomers with similar reactivity ratios will form a polymer with a random/statistical distribution of each monomer along the chain. If one monomer has a higher reactivity ratio than the other, a gradient copolymer is formed.[74] It is also possible to synthesize a forced-gradient copolymer of monomers with similar reactivity ratios by controlled addition of one comonomer to the reaction mixture throughout the reaction. Gradient copolymers tend to possess a broader glass transition temperature range, reduced order–disorder temperatures, can form new types of morphologies through self assembly as compared to statistical and block copolymers.

2.2.2. *Block Copolymers*

The extension of a macroinitiator with another monomer will lead to the formation of a block copolymer. In order to make well-defined block copolymers, it is important to extend a more reactive polymer chain end with a less reactive monomer. Otherwise, inefficient extension of the macroinitiator will lead to a product exhibiting a bimodal molecular weight distribution. If a less reactive macroinitiator needs to be extended with a more reactive monomer, a method known as halogen exchange (in which an alkyl bromide chain end is used in conjunction with a copper chloride catalyst) will prevent the problem of inefficient extension.[75, 76] Several types of block copolymers have been prepared by ATRP, including di-, tri-, and multi-block copolymers; block copolymers by mechanistic transformation; and organic/inorganic block copolymer hybrids.

2.2.3. *Control of Tacticity/Stereoblocks*

It is difficult to control tacticity in a radical polymerization, because the propagating radical center is a nearly planar sp^2 hybridized carbon, which results in

poor stereoselectivity. It has been shown though that the use of Lewis acids in ATRP has lead to the formation of highly isotactic acrylic polymers.[77–79] The carbonyl group of acrylic-based monomers coordinates to the Lewis acid, and will force the last two segments of a growing polymer chain into a meso configuration. This leads to an isotactic polymer containing a high percentage of meso dyads. Stereoblock copolymers have been prepared using this method by adding a Lewis acid to the polymerization of *N,N*-dimethylacrylamide after a certain conversion to yield an atactic-*b*-isotactic polymer.

2.3. POLYMER TOPOLOGY

There are various topologies which can be prepared by ATRP, including graft copolymers, star copolymers, cyclic copolymers, (hyper)branched materials, and cross-linked networks.

2.3.1. Graft/Brush Copolymers

A copolymer with many polymer chains originating from a linear polymer backbone is known as a graft or brush copolymer. There are three methods through which polymer brushes can be synthesized. In the first method, known as grafting onto, pre-formed polymeric side chains are grafted onto a backbone polymer. In the second method, known as grafting through, macromonomers are directly polymerized to form the brush copolymer. It is difficult to prepare brushes with a high grafting density using both of these methods, due to steric crowding of the reactive sites. The third and most often used method, known as grafting from, involves a linear polymer backbone functionalized with many ATRP initiating sites from which monomer is grown.

2.3.2. Star Copolymers

A non-linear structure with a central branch point is known as a star copolymer, where the polymer chains that are radiating out are known as arms.[80] A star copolymer can be synthesized using a couple different methods, and it is possible to have multiple arms with multiple functionalities. It is possible to polymerize the arms from an organic or inorganic multifunctional core, with 3, 4, 6, or 8 arms.[81–85] It was also demonstrated that a core with many different initiating sites (prepared by the polymerization of a monomer functionalized with an ATRP initiator) was used to prepare a star with ~80 arms.[50] Another method to create star copolymers is to start from pre-formed arms which can be attached to a functionalized core or cross-linked in the presence of a divinyl compound.[86–88]

2.3.3. Hyperbranched/Cross-Linked Networks

The synthesis of hyperbranched and cross-linked networks with well-defined structures has been realized through ATRP and other CRP processes. Branching is often unavoidable in radical polymerizations due to radical transfer to polymer. The amount of branching can be controlled in ATRP by polymerizing monomers containing initiator functionality,[89–91] or by polymerizing a dilute solution of divinyl monomer.[92] Branching is regulated in each case by controlling the degree of polymerization. Cross-linked topologies can be obtained directly by polymerization of divinyl monomers, or monomers containing cross-linkable pendant functionalities which are then connected in a post-polymerization step.[93] If the amount of cross-linker is high enough, a network is obtained.

2.3.4. Cyclic Polymers

The generation of cyclic polymers through a radical polymerization mechanism is difficult due to the unselective reactivity of the propagating radical, however cyclization of a telechelic polymer chain synthesized by ATRP has been reported.[94, 95] A polystyrene chain which contained an azide functionality on one end and an acetylene functionality on the other was cyclized using Cu^I-catalyzed click chemistry under high dilution.

2.4. CONTROL OVER MOLECULAR WEIGHT DISTRIBUTION

Molecular weight distribution, or polydispersity index (PDI), of a polymer prepared using ATRP can be predicted using the Equation (2).

$$PDI = \frac{M_w}{M_n} = 1 + \frac{1}{DP_n} + \left(\frac{[RX]_0 k_p}{k_{deact}[Mt^{n+1}X/L]} \right) \left(\frac{2}{Conv.} - 1 \right) \qquad (3)$$

As seen in Equation (3), PDI can be increased upon a decrease in the concentration of the deactivator species. In ICAR and ARGET ATRP, it is possible to use low concentrations of copper catalyst and still maintain control over molecular weight and chain-end functionality.[46, 47] With copper concentrations less than 10 ppm, polymers with high PDI (1.4–1.8) are obtained. As an example, two block copolymers polystyrene-b-poly(methyl acrylate) with similar compositions were synthesized using ARGET ATRP where the polydispersity of the PMA block was varied by adjusting the amount of copper catalyst. The block copolymer with low PDI in both blocks adopted a cylindrical morphology after thermal annealing, while the block copolymer with high PDI in the PMA block formed a hexagonally perforated lamellar morphology.[96] The observation of this morphology (which is considered to be metastable) demonstrates that PDI can have a dramatic effect over the morphology of block copolymers.

3. Conclusions

ATRP is a very powerful process that has been widely studied over the past decade in order to improve mechanistic understanding and to prepare a multitude of new and interesting materials. By choosing the proper starting materials and conditions, a wide variety of polymeric materials can be prepared in a timely and controlled manner. The recent development of new initiation systems, such as ICAR and ARGET ATRP, has allowed for successful polymerization with <50 ppm of catalyst. These methods are appropriate for industrial scale-up and the preparation of sensitive materials.

Acknowledgments

References

[1]   M. Szwarc, *Nature* **1956**, *178*, 1168.
[2]   M. Szwarc, M. Levy, R. Milkovich, *J. Am. Chem. Soc.* **1956**, *78*, 2656.
[3]   K. Matyjaszewski, in *Controlled Radical Polymerization (ACS Symp. Ser. 685)*, ACS, Washington, DC, **1998**.
[4]   K. Matyjaszewski, in *Controlled/Living Radical Polymerization. Progress in ATRP, NMP, and RAFT (ACS Symp. Ser. 768)*, ACS, Washington, DC, **2000**.
[5]   K. Matyjaszewski, T. P. Davis, Wiley, Hoboken, NJ, **2002**.
[6]   K. Matyjaszewski, in *Advances in Controlled/Living Radical Polymerization (ACS Symp. Ser. 854)*, ACS, Washington, DC, **2003**.
[7]   K. Matyjaszewski, in *Controlled/Living Radical Polymerization: From Synthesis to Materials (ACS Symp. Ser. 944)*, ACS, Washington, DC, **2006**.
[8]   W. A. Braunecker, K. Matyjaszewski, *Prog. Polym. Sci.* **2007**, *32*, 93.
[9]   J.-S. Wang, K. Matyjaszewski, *J. Am. Chem. Soc.* **1995**, *117*, 5614.
[10] M. Kato, M. Kamigaito, M. Sawamoto, T. Higashimura, *Macromolecules* **1995**, *28*, 1721.
[11] K. Matyjaszewski, J. Xia, *Chem. Rev.* **2001**, *101*, 2921.
[12] M. Kamigaito, T. Ando, M. Sawamoto, *Chem. Rev.* **2001**, *101*, 3689.
[13] H. Fischer, *Chem. Rev.* **2001**, *101*, 3581.
[14] W. Tang, N. V. Tsarevsky, K. Matyjaszewski, *J. Am. Chem. Soc.* **2006**, *128*, 1598.
[15] H. Kaneyoshi, Y. Inoue, K. Matyjaszewski, *Polym. Mater. Sci. Eng.* **2004**, *91*, 41.
[16] T. E. Patten, J. Xia, T. Abernathy, K. Matyjaszewski, *Science* **1996**, *272*, 866.
[17] D. M. Haddleton, C. B. Jasieczek, M. J. Hannon, A. J. Shooter, *Macromolecules* **1997**, *30*, 2190.
[18] W. Tang, A. K. Nanda, K. Matyjaszewski, *Macromol. Chem. Phys.* **2005**, *206*, 1171.

[19] J. Xia, K. Matyjaszewski, *Macromolecules* **1997**, *30*, 7697.

[20] J. Xia, S. G. Gaynor, K. Matyjaszewski, *Macromolecules* **1998**, *31*, 5958.

[21] C. Konak, B. Ganchev, M. Teodorescu, K. Matyjaszewski, P. Kopeckova, J. Kopecek, *Polymer* **2002**, *43*, 3735.

[22] J. Xia, K. Matyjaszewski, *Macromolecules* **1999**, *32*, 2434.

[23] J. Xia, X. Zhang, K. Matyjaszewski, *ACS Symp. Ser.* **2000**, *760*, 207.

[24] N. V. Tsarevsky, W. A. Braunecker, S. J. Brooks, K. Matyaszewski, *Macromolecules* **2006**, *39*, 6817.

[25] N. V. Tsarevsky, W. A. Braunecker, W. Tang, S. J. Brooks, K. Matyaszewski, G. R. Weisman, E. H. Wong, *J. Mol. Catal. A: Chem* **2006**, *257*, 132.

[26] H. Tang, N. Arulsamy, M. Radosz, Y. Shen, N. V. Tsarevsky, W. A. Braunecker, W. Tang, K. Matyjaszewski, *J. Am. Chem. Soc.* **2006**, *128*, 16277.

[27] T. Pintauer, B. McKenzie, K. Matyjaszewski, *ACS Symp. Ser.* **2003**, *854*, 130.

[28] M. K. Gray, H. Zhou, S. T. Nguyen, J. M. Torkelson, *Macromolecules* **2004**, *37*, 5586.

[29] K. Ohno, A. Goto, T. Fukuda, J. Xia, K. Matyjaszewski, *Macromolecules* **1998**, *31*, 2699.

[30] K. Matyjaszewski, H.-J. Paik, P. Zhou, S. J. Diamanti, *Macromolecules* **2001**, *34*, 5125.

[31] T. Pintauer, K. Matyjaszewski, *Coord. Chem. Rev.* **2005**, *249*, 1155.

[32] J. Xia, K. Matyjaszewski, *Macromolecules* **1997**, *30*, 7692.

[33] G. Moineau, P. Dubois, R. Jerome, T. Senninger, P. Teyssie, *Macromolecules* **1998**, *31*, 545.

[34] J. Xia, K. Matyjaszewski, *Macromolecules* **1999**, *32*, 5199.

[35] M. Li, N. M. Jahed, K. Min, K. Matyjaszewski, *Macromolecules* **2004**, *37*, 2434.

[36] K. Min, M. Li, K. Matyjaszewski, *J. Polym. Sci. Part A: Polym. Chem.* **2005**, *43*, 3616.

[37] J. Queffelec, S. G. Gaynor, K. Matyjaszewski, *Macromolecules* **2000**, *33*, 8629.

[38] K. Matyjaszewski, S. Coca, S. G. Gaynor, M. Wei, B. E. Woodworth, *Macromolecules* **1997**, *30*, 7348.

[39] W. Jakubowski, K. Matyjaszewski, *Macromolecules* **2005**, *38*, 4139.

[40] K. Min, H. Gao, K. Matyjaszewski, *J. Am. Chem. Soc.* **2005**, *127*, 3825.

[41] K. Min, H. Gao, K. Matyjaszewski, *Macromolecules* **2007**, *40*, 1789.

[42] H. Tang, M. Radosz, Y. Shen, *Macromol. Rapid Commun.* **2006**, *27*, 1127.

[43] K. Min, W. Jakubowski, K. Matyjaszewski, *Macromol. Rapid Commun.* **2006**, *27*, 594.

[44] J. K. Oh, K. Matyjaszewski, *J. Polym. Sci. Part A: Polym. Chem.* **2006**, *44*, 3787.

[45] J. K. Oh, C. Tang, H. Gao, N. V. Tsarevsky, K. Matyjaszewski, *J. Am. Chem. Soc.* **2006**, *128*, 5578.

[46] K. Matyjaszewski, K. Min, W. Tang, J. Huang, W. A. Braunecker, N. V. Tsarevsky, W. Jakubowski, *Proc. Natl. Acad. Sci. (U.S.A.)* **2006**, *103*, 15309.

[47] W. Jakubowski, K. Matyjaszewski, *Angew. Chem. Int. Ed.* **2006**, *45*, 4482.

[48] W. Jakubowski, K. Min, K. Matyjaszewski, *Macromolecules* **2006**, *39*, 39.

[49] J. Pietrasik, H. Dong, K. Matyjaszewski, *Macromolecules* **2006**, *39*, 6384.

[50] S. G. Gaynor, K. Matyjaszewski, *ACS Symp. Ser.* **1998**, *685*, 396.

[51] N. V. Tsarevsky, S. A. Bencherif, K. Matyjaszewski, *Macromolecules* **2007**, *40*, 4439.

[52] D. E. Betts, T. Johnson, D. Leroux, J. M. Desimone, *ACS Symp. Ser.* **1998**, *685*, 418.

[53] K. L. Beers, S. Boo, S. G. Gaynor, K. Matyjaszewski, *Macromolecules* **1999**, *32*, 5772.

[54] K. L. Beers, S. G. Gaynor, K. Matyjaszewski, S. S. Sheiko, M. Moeller, *Macromolecules* **1998**, *31*, 9413.

[55] X. Zhang, J. Xia, K. Matyjaszewski, *Macromolecules* **1998**, *31*, 5167.

[56] M. Teodorescu, K. Matyjaszewski, *Macromolecules* **1999**, *32*, 4826.

[57] M. Teodorescu, K. Matyjaszewski, *Macromol. Rapid Commun.* **2000**, *21*, 190.

[58] Y. Xia, X. Yin, N. A. D. Burke, H. D. H. Stoever, *Macromolecules* **2005**, *38*, 5937.

[59] D. Bontempo, R. C. Li, T. Ly, C. E. Brubaker, H. D. Maynard, *Chem. Commun.* **2005**, *37*, 4702.

[60] K. Ohno, Y. Tsujii, T. Fukuda, *J. Polym. Sci. Part A: Polym. Chem.* **1998**, *36*, 2473.

[61] A. Marsh, A. Khan, D. M. Haddleton, M. J. Hannon, *Polym. Prepr. (Am. Chem. Soc. Div. Polym. Chem.)* **2000**, *41*, 440.

[62] J.-F. Lutz, A. F. Thuenemann, R. Nehring, *J. Polym. Sci. Part A: Polym. Chem.* **2005**, *43*, 4805.

[63] D. A. Shipp, J.-L. Wang, K. Matyjaszewski, *Macromolecules* **1998**, *31*, 8005.

[64] D. Mecerreyes, G. Moineau, P. Dubois, R. Jerome, J. L. Hedrick, C. J. Hawker, E. E. Malmstrom, M. Trollsas, *Angew. Chem. Int. Ed.* **1998**, *37*, 1274.

[65] W. H. Binder, R. Sachsenhofer, *Macromol. Rapid Commun.* **2007**, *28*, 15.

[66] J.-F. Lutz, *Angew. Chem. Int. Ed.* **2007**, *46*, 1018.

[67] B. S. Sumerlin, N. V. Tsarevsky, G. Louche, R. Y. Lee, K. Matyjaszewski, *Macromolecules* **2005**, *38*, 7540.

[68] H. Gao, G. Louche, B. S. Sumerlin, N. Jahed, P. Golas, K. Matyjaszewski, *Macromolecules* **2005**, *38*, 8979.

[69] J.-F. Lutz, H. G. Boerner, K. Weichenhan, *Macromol. Rapid Commun.* **2005**, *26*, 514.

[70] P. L. Golas, N. V. Tsarevsky, B. S. Sumerlin, L. M. Walker, K. Matyjaszewski, *Aust. J. Chem.* **2007**, *60*, 1.

[71] H. Gao, K. Matyjaszewski, *Macromolecules* **2006**, *39*, 4960.

[72] H. Gao, K. Matyjaszewski, *J. Am. Chem. Soc.* **2007**, *129*, 6633.

[73] H. Durmaz, F. Karatas, U. Tunca, G. Hizal, *J. Polym. Sci. Part A: Polym. Chem.* **2006**, *44*, 3947.

[74] D. Greszta, K. Matyjaszewski, T. Pakula, *Polym. Prepr. (Am. Chem. Soc. Div. Polym. Chem.)* **1997**, *38*, 709.

[75] K. Matyjaszewski, D. A. Shipp, J.-L. Wang, T. Grimaud, T. E. Patten, *Macromolecules* **1998**, *31*, 6836.

[76] T. Kowalewski, N. V. Tsarevsky, K. Matyjaszewski, *J. Am. Chem. Soc.* **2002**, *124*, 10632.

[77] J.-F. Lutz, D. Neugebauer, K. Matyjaszewski, *J. Am. Chem. Soc.* **2003**, *125*, 6986.

[78] J.-F. Lutz, W. Jakubowski, K. Matyjaszewski, *Macromol. Rapid Commun.* **2004**, *25*, 486.

[79] Y. Okamoto, S. Habaue, Y. Isobe, *ACS Symp. Ser.* **2003**, *854*, 59.

[80] K. Matyjaszewski, *Polym. Int.* **2003**, *52*, 1559.

[81] K. Matyjaszewski, P. J. Miller, E. Fossum, Y. Nakagawa, *Appl. Organomet. Chem.* **1998**, *12*, 667.

[82] S. Angot, K. S. Murthy, D. Taton, Y. Gnanou, *Macromolecules* **1998**, *31*, 7218.

[83] A. Heise, C. Nguyen, R. Malek, J. L. Hedrick, C. W. Frank, R. D. Miller, *Macromolecules* **2000**, *33*, 2346.

[84] K. Matyjaszewski, P. J. Miller, J. Pyun, G. Kickelbick, S. Diamanti, *Macromolecules* **1999**, *32*, 6526.

[85] Y. Gnanou, D. Taton, *Macromol. Symp.* **2001**, *174*, 333.

[86] X. Zhang, J. Xia, K. Matyjaszewski, *Macromolecules* **2000**, *33*, 2340.

[87] J. Xia, X. Zhang, K. Matyjaszewski, *Macromolecules* **1999**, *32*, 4482.

[88] H. Gao, N. V. Tsarevsky, K. Matyjaszewski, *Macromolecules* **2005**, *38*, 5995.

[89] C. J. Hawker, J. M. J. Frechet, R. B. Grubbs, J. Dao, *J. Am. Chem. Soc.* **1995**, *117*, 10763.

[90] S. G. Gaynor, S. Edelman, K. Matyjaszewski, *Macromolecules* **1996**, *29*, 1079.

[91] K. Matyjaszewski, S. G. Gaynor, *Macromolecules* **1997**, *30*, 7042.

[92] R. Baudry, D. C. Sherrington, *Macromolecules* **2006**, *39*, 1455.

[93] N. V. Tsarevsky, K. Matyjaszewski, *Macromolecules* **2002**, *35*, 9009.

[94] N. V. Tsarevsky, B. S. Sumerlin, K. Matyjaszewski, *Macromolecules* **2005**, *38*, 3558.

[95] B. A. Laurent, S. M. Grayson, *J. Am. Chem. Soc.* **2006**, *128*, 4238.

[96] J. Listak, W. Jakubowski, L. Mueller, A. Plichta, K. Matyjaszewski, M. R. Bockstaller, *Macromolecules* **2008**, *41*, 5919.

POLYELECTROLYTE STARS AND CYLINDRICAL BRUSHES MADE BY ATRP: NEW BUILDING BLOCKS IN NANOTECHNOLOGY

FELIX PLAMPER, YOUYONG XU, JIAYIN YUAN, MATTHIAS BALLAUFF, AND AXEL H. E. MÜLLER*
Makromolekulare Chemie II, Universität Bayreuth, D-95440 Bayreuth, Germany

Abstract: Star polymers and cylindrical polymer brushes (CPBs), i.e. polymers possessing side groups densely grafted from a linear main chain, have attracted considerable experimental and theoretical interest over the past decade, owing to their peculiar solution and bulk properties. We have used the grafting-from approach via ATRP to synthesize well-defined star polymers and core–shell CPBs with homopolymer and block copolymer side chains. The diblock copolymer side chains may include combinations of soft-hard, hydrophilic-hydrophobic and crystalline-amorphous block segments. In particular, we have been interested in polyelectrolyte blocks; then the polymers resemble intramolecular spherical and cylindrical micelles, respectively. Star polymers of poly(acrylic acid) (PAA) and poly(N,N-dimethylaminoethyl methacrylate) (DMAEMA) were made using sugar- or silsesquioxane-based ATRP initiators. Their LCST and UCST phase behaviour depends on pH, counterion charge, temperature, and light. PDMAEMA CPBs react in a similar way, and on addition of trivalent counterions they even form helical structures. We have also synthesized hybrid nanowires of semiconducting CdS and CdSe or nanomagnets of γ-Fe$_2$O$_3$ inside the PAA core of CPBs. Here, we present novel water-soluble and biocompatible silica nanowires based on CPBs. They have a core consisting of a silsesquioxane network of crosslinked poly(3-acryloylpropyl trimethoxysilane) (PAPTS) and a shell of poly(oligoethyleneglycol methacrylate) (POEGMA). Sequential ATRP of APTS and OEGMA initiated by a polyinitiator backbone (DP = 3,200) was carried out in benzene. Due to the cylindrical shape of the brushes the functional TMS moieties were arranged into a 1D manner and then crosslinked via alkaline condensation, rendering the rigid core–shell hybrid CPBs. Finally, uniform silica nanowires were achieved by the simultaneous removal of the hybrid CPB template via pyrolysis. The length as well as the diameter of silica nanowires are well-defined.

1. Polyelectrolyte Stars

1.1. SYNTHESIS

#### *1.1.1. Poly(acrylic acid)*

Star-shaped poly(acrylic acid) (PAA) was prepared by a two-step strategy.[1] First *tert*-butyl acrylate (tBA) was polymerized by controlled radical polymerization using multifunctional initiators. Modified glucose, saccharose and β-cyclodextrin have been used aiming for stars with 5, 8 and 21 arms. Those initiators, bearing the α-bromoisobutyrate moiety, were prepared and carefully characterized by means of mass spectrometry and NMR. By choosing different molar ratios of monomer to initiation sites and varying the conversion different arm lengths could be obtained. The PtBA stars were analyzed in terms of their molecular weight distribution by gel permeation chromatography (GPC) with viscosity detection. The obtained number averaged molecular weights M_n do coincide with the expected M_n(theo) obtained by conversion and monomer to initiator ratio. The star-shaped PtBA was transformed to PAA by treatment with trifluoroacetic acid. The rather mild conditions provide almost quantitative elimination of iso-butylene, yielding $(PAA_n)_x$ (n equals number average degree of polymerization per arm, whereas x assigns the number average arm number). The ester groups used to attach the arms to the core stay almost completely intact (aqueous GPC). Those PAA stars could be methylated and again the molecular weights, obtained by mass spectrometry (matrix assisted laser desorption ionization – time of flight mass spectrometry; MALDI-ToF), do correlate with the theoretical molecular weights. After having obtained the star-shaped PAA, we could detach the arms by alkaline treatment for analysis of the arm length and arm length distribution. The experimentally determined arm lengths (DP_{arm}) obtained after alkaline cleavage do coincide with the expected arm lengths. This was verified by both endgroup determination (by NMR) and mass spectrometry (MALDI-ToF of the methylated PAA arms). This indicates that the initiation site efficiency is close to unity and our stars carry the maximum arm number, given by the initiator molecule.

1.1.2. Poly(dimethylaminoethyl methacrylate) and Its Quaternized Analog

The preparation of star-shaped Poly(*N,N*-dimethylaminoethyl methacrylate) $(PDMAEMA_n)_x$ followed the method for synthesis of PtBA, using the same initiators as mentioned above.[2] To increase the number of arms per star, a new initiator with a high number of initiation sites was required. Novel silsesquioxane nanoparticles bearing a high number of hydroxyl functions were prepared.[3]

Those particles, which are moderately polydisperse in terms of molecular weight ($PDI \sim 1.2$), were used to prepare initiators with an average 58 initiation sites per molecule (Scheme 1).[4]

$$14.5 \pm 4.5$$
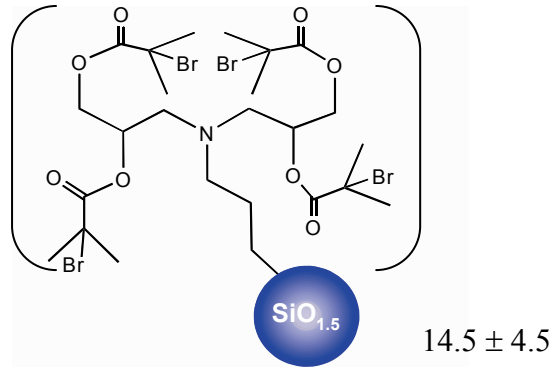
Scheme 1. Structure of ATRP initiator with 58 functions.

PDMAEMA stars could be easily quaternized to obtain strong polyelectrolytes (poly{[2-(methacryloyloxy)ethyl] trimethylammonium iodide}; PMETAI). The silsesquioxane core remains intact as seen by Asymmetric Field Flow Fractionation (AFFF).[2] The initiation site efficiency was considerably lowered (0.3–0.7) especially for the initiators with a high number of functionalities. The initiation site efficiency could be extracted by both conventional cleavage of the arms and by a statistical method: star-like fragments were detached from the core by HF and analyzed by GPC (Figure 1).
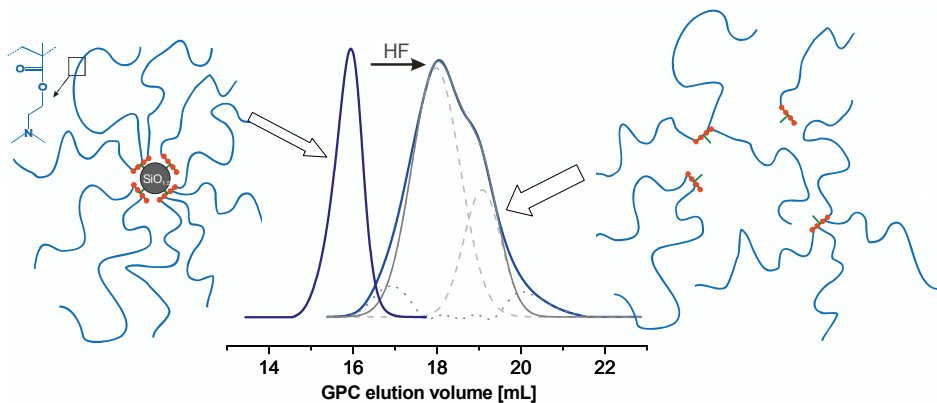
Figure 1. Comparison of eluograms of (PDMAEMA$_{170}$)$_{18}$ and the star-like PDMAEMA fragments obtained after treatment of (PDMAEMA$_{170}$)$_{18}$ with HF.

1.2. SOLUTION PROPERTIES

1.2.1. *Conformational Changes in Polycation Stars Induced by the Presence of Salt and the Use of Light-Sensitive Salt*

The high osmotic pressure inside the stars is responsible for the stretching of the arms in the absence of salt (hydrodynamic radius R_H is ca. 50% of their contour length).[2] NaCl leads to a shrinkage, as seen in the drop of the hydrodynamic radius R_h (measured by Dynamic Light Scattering, DLS) in dependence of the ionic strength. Electrostatic and osmotic screening (net osmotic pressure inside the star is lowered upon salt addition) leads to a retraction of the arms (Figure 2).
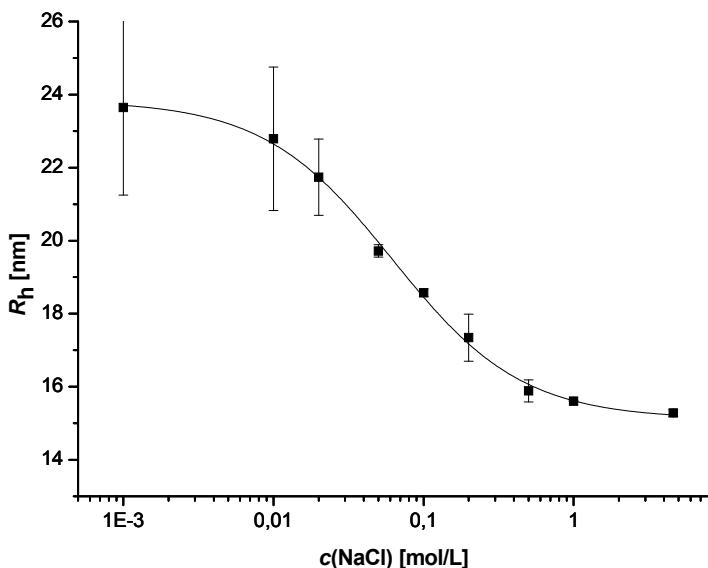
Figure 2. Dependence of the hydrodynamic radius of star-shaped quaternized PDMAEMA, $(PMETAI_{170})_{18}$, with ionic strength; the line is a guide for the eye. Reprinted by permission of ACS.

But not only ionic strength determines the hydrodynamic radius. Presence of multivalent counterions can also lead to a collapse and finally to a phase separation of the stars even at constant ionic strength.[5] This was shown by DLS of $(PMETAI_{170})_{18}$ solutions with hexacyanocobaltate(III) ($[Co(CN)_6]^{3-}$) and tetracy-anonickelate(II) ($[Ni(CN)_4]^{2-}$). The lower the valency of the counterions, the more counterions are needed to obtain the same collapse.

By use of $[Co(CN)_6]^{3-}$, we can reverse this contraction by UV irradiation.[5] Light exchanges one cyano ligand with water and the charge of the counterion is reduced (photoaquation).[6] One counterion is decomposed into two counterions. This leads again to an increase in osmotic pressure inside the star and the star's

arms stretch. We called those stars "nanoblossoms" due to the resemblance to real flowers (Figures 3 and 4).
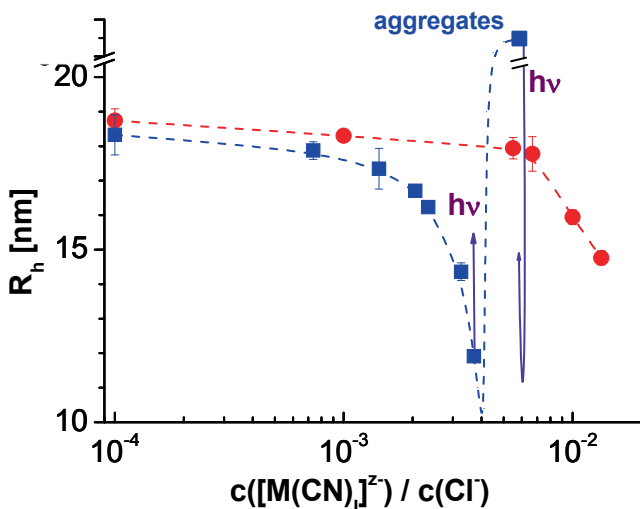
Figure 3. Change of the hydrodynamic radius of the cationic star polyelectrolyte (0.5 g/L of $(PMETAI_{180})_{17}$) in dilute aqueous solutions with same ionic strength (0.1 M NaCl) but different ratios of mono- to multivalent salt; circles: titrated with 0.033 n divalent $K_2[Ni(CN)_4]$; squares: titrated with 0.0167 n trivalent $K_3[Co(CN)_6]$; the arrows indicate the principle of photostretching or photodissolution; the dashed lines are a guide to the eye. Reprinted by permission of ACS.
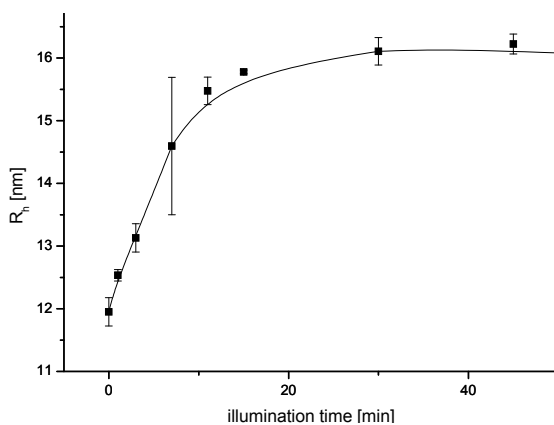
Figure 4. Photoinduced stretching measured by DLS of 0.5 g/L $(PMETAI_{170})_{18}$ in 0.1 N NaCl in presence of 3.7×10^{-4} mol/L $K_3[Co(CN)_6]$ in dependence of illumination time. Reprinted by permission of ACS.

We could further show a way of redissolving a precipitated polymer-counterion complex by UV-irradiation (photoinduced dissolution).[5] By improving this method, the same principle may be used for the easy modification of a huge variety of branched polyelectrolytes into light-sensitive materials.
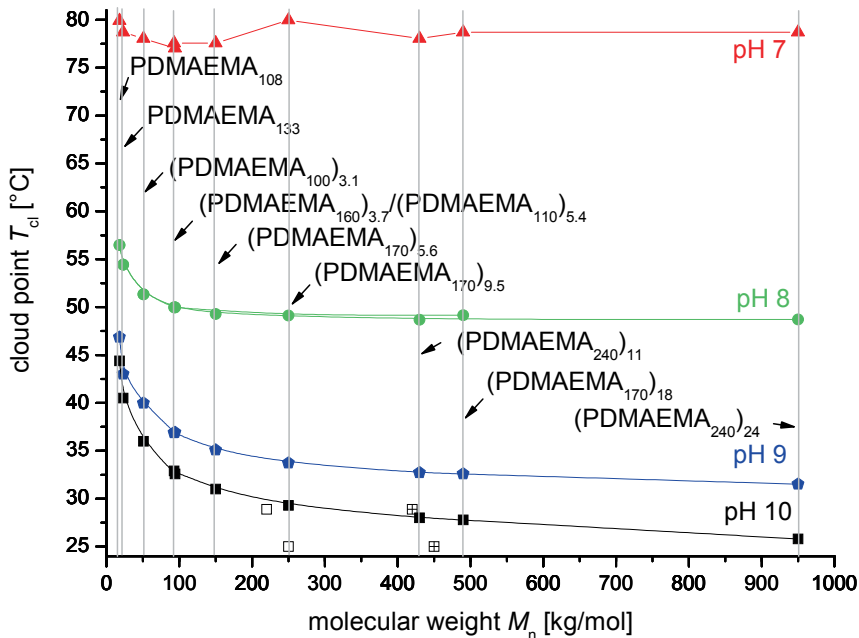
Figure 5. Cloud points T_{cl} at 0.1 g/L of star-shaped PDMAEMA in dependence of number averaged molecular weight and pH (black: pH = 10; blue: pH = 9, green: pH = 8; red: pH = 7); the solid lines are a guide to the eye. Reprinted by permission of ACS.

1.2.2. Temperature-Induced Phase Separation in Solutions of Star-Shaped and Linear PDMAEMA

We investigated the thermoresponsive behavior of the weak star-shaped polyelectrolyte PDMAEMA.[7] PDMAEMA belongs to the class of polymers that exhibit a lower critical solution temperature (LCST), i.e. the polymer becomes insoluble in water at elevated temperatures. The question, how far the observed cloud points depend on the architecture, should be answered. To assure constant pH for all samples, the polymers were investigated in buffer (Figure 5).

At high pH the observed cloud points show only dependence on the molecular weight (Flory–Huggins behavior). Architecture does not play a role. But for lower pH a slight modulation is observed: in addition to the shift of the whole cloud point curve to elevated temperatures, the cloud points of stars with higher segment densities are shifted to slightly higher temperatures compared to stars

with lower segment density. That means that charge density gains importance for lower pH.

Addition of multivalent counterions leads in buffered solutions of PDMAEMA even to the appearance of an upper critical solution temperature (UCST: insoluble at low temperatures).[8] The UCST-type miscibility gap shifts to higher temperatures when adding trivalent counterions, whereas the LCST-type cloud points hardly change. Therefore a new facile system has been invented: The LCST-type transition can be adjusted by pH, whereas the UCST-type cloud points can be adjusted by the concentration of trivalent counterions. The light-sensitivity of hexacyanocobaltate(III) can be employed to an UV-light induced switching of the UCST-behavior. The UCST-behavior disappears upon illumination. This photoinduced dissolution is related to the one described in previous chapter (Figure 6).
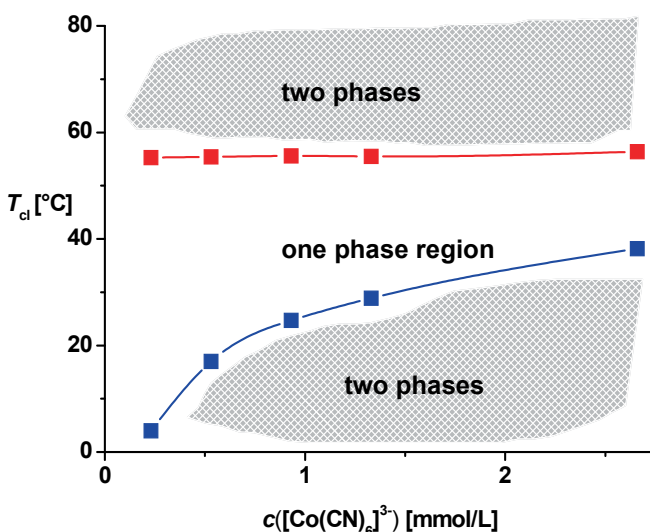
Figure 6. Dependence of the cloud points T_{cl} of aqueous $(PDMAEMA_{170})_{18}$ solutions (0.1 g/L in buffer of pH 8 + 0.1 n NaCl) on the $[Co(CN)_6]^{3-}$ concentration (red symbols assign LCST-type cloud points, blue ones refer to cloud points of the UCST-behavior). Reprinted by permission of ACS.

2. Cationic Cylindrical Polymer Brushes

Cylindrical polymer brushes (CPBs) are formed if the grafting density of polymer chains to a much longer linear chain is high enough. They have drawn more and more attentions because of the anisotropic nature and worm-like structures. Their special solution and bulk properties have given rise to their applications as single molecular responsive nano-objects.[9]

Three different strategies have been applied for the preparation of CPBs: grafting-onto,[10] grafting-from[11] and grafting-through.[12] Every strategy has its own advantages and disadvantages. Generally, grafting-from strategy can employ well-defined linear polymers as the macro-initiators and utilize the recently well-established controlled/living polymerization techniques such as atom transfer radical polymerization (ATRP),[13] nitroxide mediated radical polymerization (NMP),[14] ring-opening polymerization (ROP)[15] and ring-opening metathesis polymerization (ROMP)[16] for the grafting of the side chains. So far, this provides the most efficient and convenient ways of preparing well-defined CPBs, although it has its own inevitable disadvantages, for instance, relatively low grafting density of the side-chains.

Based on grafting-from strategy, CPBs with various architectures and functionalities have been prepared. Among them, Polyelectrolyte CPBs are a special type of macromolecules, carrying covalently large number of anions or cationic groups with counterions providing electro-neutrality. So far, most of the research was concentrated on the synthesis of polyelectrolyte CPBs.[17, 18] Few were conducted on the responsiveness and the transition of the polyelectrolyte CPBs.

Recently, we reported the synthesis of poly(N,N-dimethylaminoethyl methacrylate) (PDMAEMA) cylindrical brushes and their quaternized salts, poly{[2-(methacryloyloxy)ethyl] trimethylammonium iodide} (PMETAI) brushes.[19] Although Matyjaszewski et al. has showed the temperature responsiveness of the PDMAEMA brushes at various concentrations in solution,[20] we demonstrate here the response of this type of brushes on pH and the response of the quaternized brushes to mono- , di- , and tri-valent counterions.

2.1. SYNTHESIS OF PDMAEMA AND PMETAI BRUSHES

The PDMAEMA cylindrical brushes were prepared by the combination of anionic polymerization and ATRP using the grafting-from strategy. A macroinitiator with DP = 1,500 and a very low polydispersity[13] served as the backbone and linear PDMAEMA chains were grafted from it. It is known that the grafting-from can not give full initiating efficiency because of the inevitable steric hindrance. A lot of measures were taken to improve the grafting density, such as halogen exchange, lower monomer concentrations and slower growth by adding copper (II). When it comes to the determination of the initiating efficiency, PDMAEMA brushes were quaternized to their ammonium salt first, and cleavage of the side-chains and the ester groups in the monomer unit by strong base. This leaded to linear poly(methacrylic acid) (PMAA), which were subjected to water GPC measurements. The molecular weights of the linear PMAA were compared with calculated values, which provided the initiating efficiencies of the ATRP processes. We found that even with the above-mentioned measures having been

taken, the initiating efficiencies were all only around 50%. Scheme 2 displays the synthesis of PDMAEMA, PMETAI brushes and the process for the cleavage of side-chains.
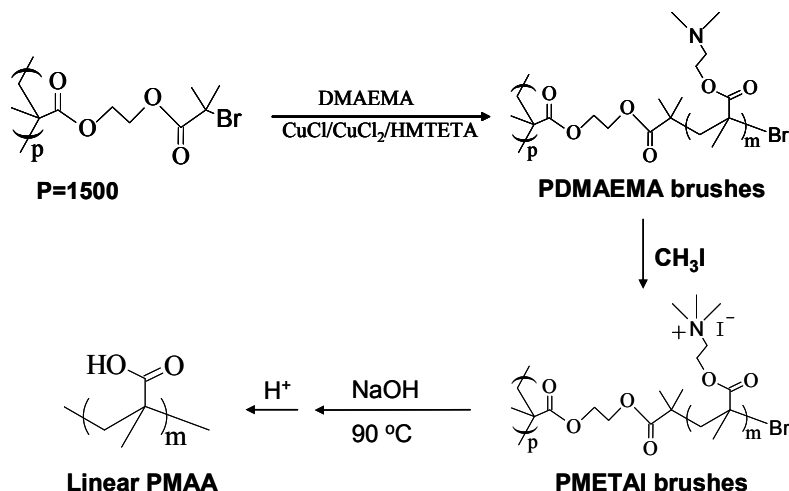
Scheme 2. Procedures for the synthesis of PDMAEMA, PMETAI brushes and side-chain cleavages.

AFM and cryo-TEM measurements were carried out to show the morphology of PDMAEMA and PMETAI brushes. Typical worm-like structures were observed for these brushes. Figure 7 shows the AFM and cryo-TEM images of the PMETAI brushes. The length of the brushes is around 180 nm both on the mica surface and in the vitrified solutions.
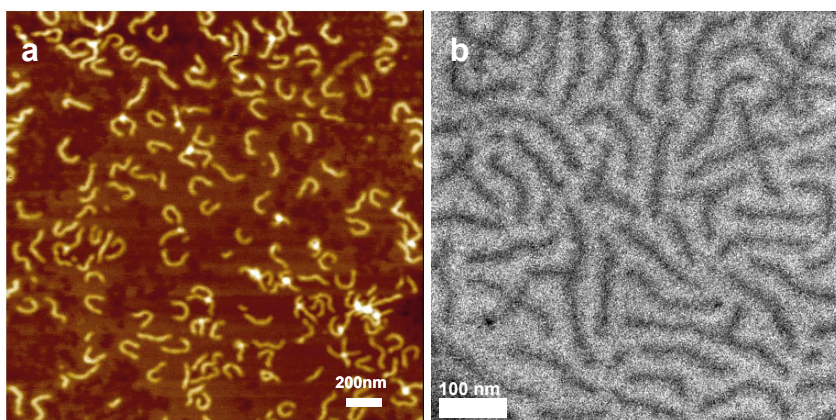
Figure 7. (**a**) AFM height image (Z range 7 nm) and (**b**) cryo-TEM image of PMETAI brushes. Reprinted by permission of ACS.

2.2. pH RESPONSIVENESS OF PDMAEMA BRUSHES

PDMAEMA is a weak cationic polyelectrolyte, and its degree of ionization depends on pH. The apparent pK_b value for PDMAEMA stars[1] with a large number of arms is around eight and the same behaviour are expected here. Hydrodynamic radii of the PDMAEMA brush at different pH values at very low concentration (0.2 g/L) were measured by DLS. The apparent hydrodynamic radii steadily decreased with the increasing pH values. Structural changes were directly observed by the cryo-TEM measurements at different pH values (see Figure 8). More extended structures appeared at low pH, while at high pH, the brushes were extraordinarily shortened.
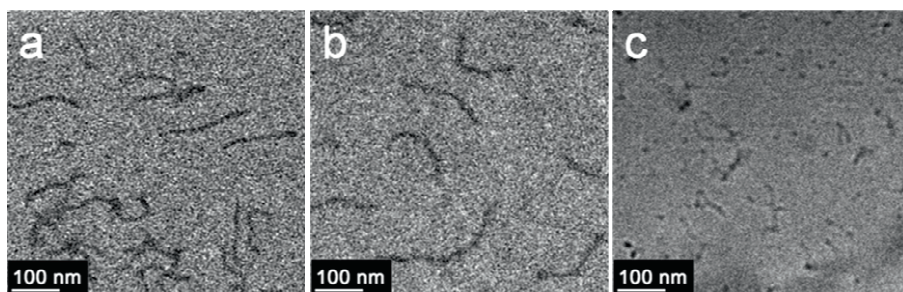
Figure 8. Cryo-TEM images of PDMAEMA brushes in vitrified 0.01 g/L aqueous solution at (**a**) pH 2, (**b**) pH 7 and (**c**) pH 10. Reprinted by permission of ACS.

2.3. SALT RESPONSIVENESS OF PMETAI BRUSHES

Due to the strong electrical repulsion of the charged side-chains, the strong polyelectrolyte PMETAI brushes exhibit rather elongated conformations. Addition of mono-valent salt to the solution will screen the electrostatic interaction within the polyelectrolyte. Figure 9 shows the change of the hydrodynamic radii of the PMETAI brush with increasing NaBr concentration. An obvious decrease of the apparent R_h was observed when added NaBr concentration moved from 0 to 1 M, which was caused by the screening effect of the added salt to the charges in the brushes. When the salt concentration was higher than 1 M, the apparent R_h increased again, which was probably caused by the re-swelling of the brushes with further adsorbed bromine ions.[21] The finding was also supported by the AFM measurements. At a NaBr concentration of 0.5 M, the brushes showed quite collapsed state.

When couterions with higher valencies (for example, di- and tri-valent) were put into the system, we found that the situation was totally different. When the brush concentration was high, aggregates or even precipitations appeared with added di- or tri-valent counterions. AFM and cryo-TEM measurements at very

low concentration of brushes revealed that with the charge ratio of the cations carried by the brushes and the added anions was near 1, worm-to-sphere collapses were observed. Interestingly, helical structures, the intermediate states were detected. The formation of the helix was prompted by the contraction of the polymer molecules along the long axis by the presence of the multivalent ions. Using a suitable tri-valent counterions, $[Co(CN)_6]^{3-}$, which can undergo photo-aquation and become a mixture of mono- and divalent ions, we were able to switch the morphologies of the brushes from extended one to collapsed state, and finally back to stretched one. The detailed findings were publishes elsewhere.[22]
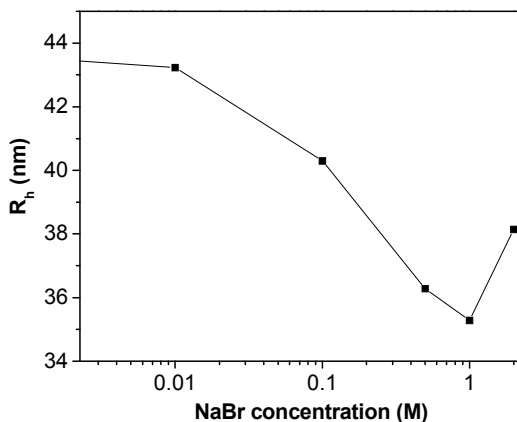
Figure 9. Apparent hydrodynamic radii of the PMETAI brushes as a function of NaBr concentration. Reprinted by permission of Elsevier.

3. Core–Shell Cylindrical Polymer Brushes as Templates for 1D Nanostructures

3.1. INTRODUCTION

The growing interest in one-dimensional (1D) nanostructures, such as nanowires, nanotubes, or nanorods, has intrigued many scientists, due to the size-dependent optical and electronic properties and their potential application as building blocks, interconnects and functional components for assembling nanodevices.[23, 24] Although great efforts have been made for exploring various techniques to develop unique 1D structures, the strict control of the distinctive geometry at extremely small size for 1D nanostructures remains a great challenge.[25, 26]

Owing to the possibility of forming extended chain conformations, cylindrical polymer brushes (CPBs), have been frequently employed as a unimolecular template for the preparation of 1D nanostructured materials.[27, 28] Among the different structures, core–shell superstructured CPBs which contain phase-separated diblock copolymer side chains, are of special interest. Generally,

these core–shell CPBs can be divided into two basic groups in terms of the core structure which can be either polyelectrolyte or trimethylsilyl (TMS)-based functions. In both cases, the brush core governs the nanowire dimension, and the shell protects the nanowires from agglomeration and precipitation in solution.

3.2.   POLYELCTROLYTE AS THE CORE

Polyelectrolytes, like poly(acrylic acid) (PAA) and poly(2-vinylpyridine), are well-known for the ability to complex with metal ions. This behavior is of great importance for the core–shell CPBs to realize the fabrication process of 1D hybrid nanostructures. As an example, the amphiphilic CPBs, $[PAA_x\text{-}b\text{-}PnBA_y]_z$ (x,y and z: the repeating units of the side chains and the backbone), with a hydrophilic PAA core and a hydrophobic poly(n-butyl acrylate) (PnBA) shell were synthesized via a combination of anionic polymerization (for the backbone) and ATRP (for the side chain), using the "grafting from" technique.[13]

Scheme 3. Schematic route to a CPB with amphiphilic diblock copolymer side chains (M1: TMS-HEMA; M2: tBA; M3: nBA; star: initiating site).

The synthetic strategy is detailed in Scheme 3, which includes the following steps: (1) the synthesis of a well-defined polyinitiator, poly(2-bromoisobutyryl-oxyethyl methacrylate) (PBIEM), by the esterfication of poly(2-hydroxyethyl methacrylate) (PHEMA), which was synthesized via anionic polymerization of 2-(Trimethylsilyloxy)ethyl methacrylate (TMS-HE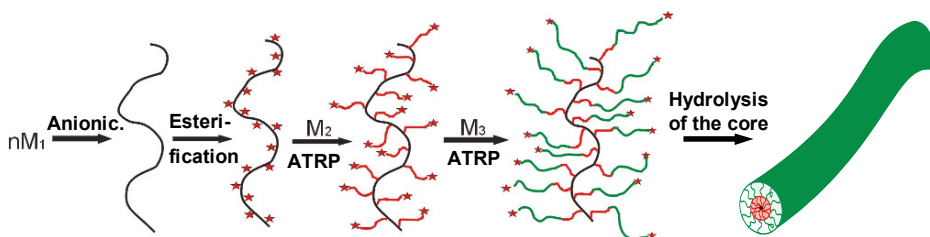MA); (2) ATRP of t-butyl acrylate (tBA) initiated by the pendant a-bromoester groups of PBIEM, yielding cylindrical brushes with PtBA homopolymer side chains; (3) sequential ATRP of nBA forming the cylindrical brushes with diblock copolymer PtBA-*b*-PnBA side chains; and (4) the hydrolysis of the PtBA block to produce the hydrophilic PAA block forming the core of an amphiphilic core–shell CPB. The characteristic wormlike morphology of the amphiphilic core–shell CPBs, for instance $[AA_{37}\text{-}b\text{-}nBA_{76}]_{1500}$, is visualized via scanning force microscopy (SFM) in Figure 10. The high uniformity as well as the regular cylindrical shape of the polymer brushes indicates that the CPBs are structurally well-defined. A statistical analysis give the number-average and weight-average lengths of 179 and 186 nm, respectively, with a polydispersity $l_w/l_n = 1.04$ which agrees well with the polydispersity of the backbone $M_w/M_n = 1.08$.
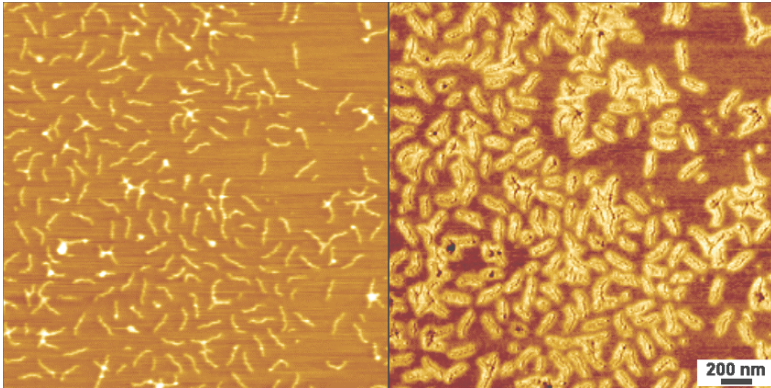
Figure 10. Tapping-mode SFM images of the CPB [AA37-b-nBA$_{76}$]$_{1500}$. Left, height image; right, phase image. the Z range are 6 nm, and 40°, respectively. Reprinted by permission of Elsevier.
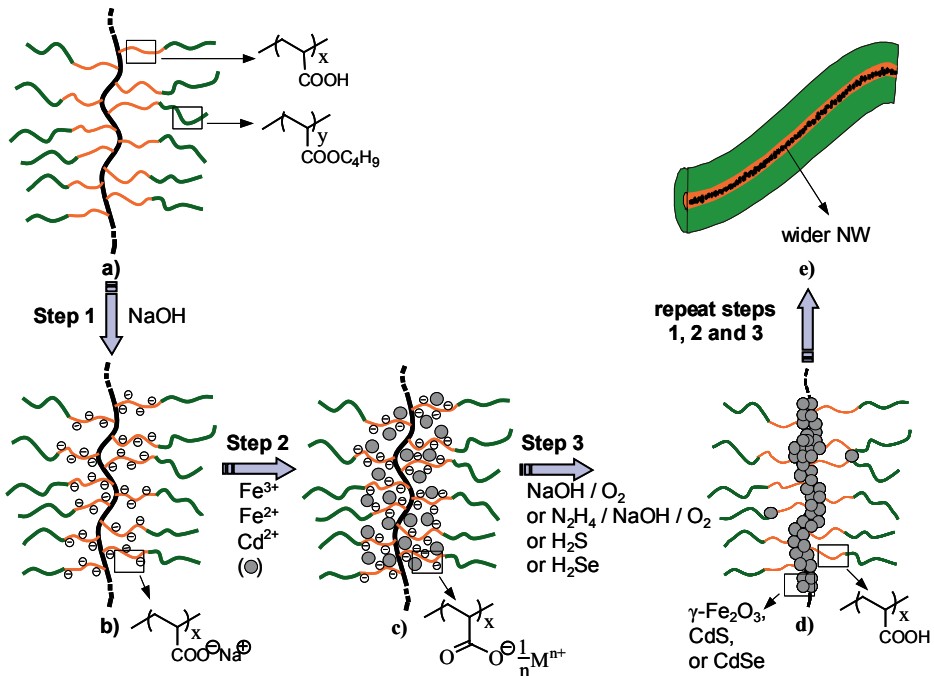
Scheme 4. Schematic illustration of the synthesis of a wirelike assembly of magnetic/ semi-conducting nanoparticles inside a core–shell CPB: (**a**) a CPB with 25 units of AA in the core and 63 units of nBA in the shell; (**b**) a neutralized polymer brush with a poly(sodium acrylate) core (Na$^+$ ions are not shown); (**c**) a polychelate of a polymer brush with Fe2$^+$, Fe3$^+$ or Cd2$^+$ ions; (**d**) a hybrid nanocylinder of a polymer brush and a wirelike assembly of magnetic/semiconducting nanoparticles, and (**e**) the double-loading process by repeating step 1 to 3 to increase the diameter of the nanowires.

The fabrication of 1D inorganic nanostructures by CPBs is closely relate to each unique aspect of the CPB structure: the PAA core, which possesses carboxylate groups capable of coordinating with metal ions (e.g., Fe^{2+}, Fe^{3+}, or Cd^{2+}), works as a nanoreactor for the nanoparticle formation and directs the nanoparticle distribution along the brush backbone; and the shell protects the fabricated nanoparticles from aggregation and provides the solubility of the hybrid cylinders in organic solvents. In Scheme 4, the preparation of one-dimensionally aligned superparamagnetic (Fe_2O_3) and semiconducting (CdS, CdSe) nanoparticles within these amphiphilic polymer brushes is displayed.[29–31] In the first step (a to b), the carboxylic groups in the PAA core were neutralized by NaOH. Via ion exchange, Fe^{2+}, Fe^{3+} or Cd^{2+} ions replace Na^+ ions (step 2: b to c), forming a polychelates (composites of CPB and metal ions,). Through corresponding chemical reactions, the purified polychelates were converted to Fe_2O_3, CdS or CdSe nanoparticles which were simultaneously aligned into 1D manner within the cylindrical core (step 3: c to d). Meanwhile, the PAA core resumes the initial chemical structure (i.e., acrylic acid functions) which enables the double-loading process by repeating steps 1 to 3.
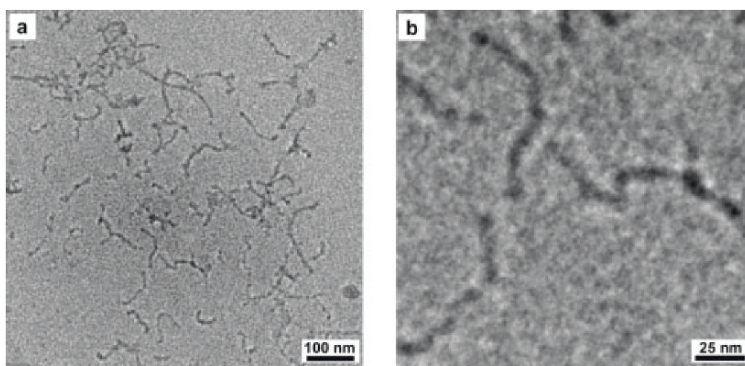
Figure 11. Nonstained TEM images of a hybrid magnetic nanocylinder of a polymer brush [AA25-*b*-nBA$_{61}$]$_{1500}$ and magnetic iron oxide nanoparticles. Reprinted by permission of Wiley-VCH.
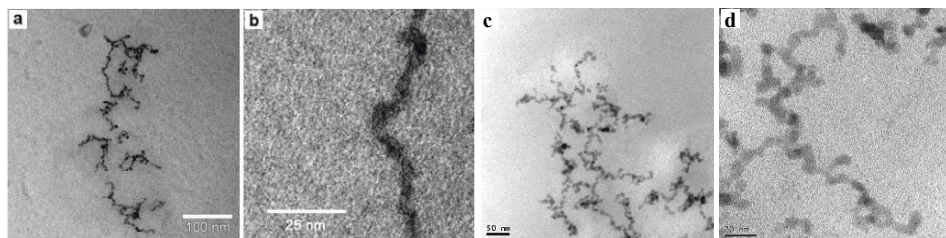
Figure 12. Nonstained TEM images of the wirelike assembly of CdS (**a** and **b**) and CdSe (**c** and **d**) nanoparticles formed inside a polymer brush [AA25-*b*-nBA$_{61}$]$_{1500}$. Reprinted by permission of Elsevier.

The typical TEM images of the hybrid of the polymer brush and generated Fe_2O_3, CdS and CdSe nanoparticles are shown in Figures 11 and 12. In all cases, wirelike assemblies of nanoparticles are clearly visible. These hybrid nanowires are 4–5, 6 and 7.6 nm wide respectively. It is worth noting that due to the protective PnBA polymer shell, the wormlike morphology remains and all hybrid nanowires are soluble and stable in solution.

It is known that bulk CdSe material shows an absorbance edge in the ultraviolet-visible (UV-vis) spectrum at a wavelength of 715 nm. With decreasing particle size, the absorption threshold shifts to shorter wavelengths as a result of quantum confinement effects. Figure 13 shows the UV-vis absorption spectrum of the polychelates, and the 1st loaded and double-loaded hybrid of the polymer brush and CdSe nanoparticles. Because the polychelate has nearly no absorption in the observed wavelength range, the absorption shown in Figure 4 can be attributed exclusively to the CdSe nanoparticles. Apparently, the double-loaded hybrid shows stronger absorption than the 1st loaded hybrid, which confirms the increase of the CdSe amount during the double-loading process. The 1st loaded hybrid shows an absorption onset at 679 nm and the double-loaded one at 705 nm. Both display a blue-shift relative to that of bulk CdSe, indicating the existence of the quantized transition. According to Murray's empirical curve, the threshold corresponds to CdSe nanoparticles with a rough size of 7 and 10 nm, respectively, which proves the growth of CdSe nanowires by width during the double-loading process.
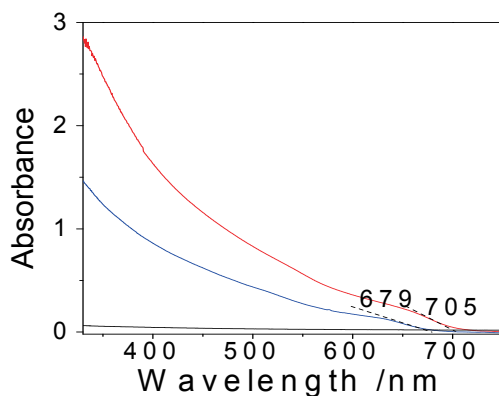
Figure 13. UV-vis spectra of the $Cd2^+$ polychelate (black line), 1st loaded hybrid (blue line) and double-loaded hybrid (red line) of the polymer brush and CdSe nanowires, the concentration for all is 0.4 g/L (polymer content). Reprinted by permission of Elsevier.

3.3. TRIMETHYLSILYL (TMS)-BASED FUNCTIONS AS THE CORE[32]

Differently, CPB's with a TMS-containing core represents a new synthetic strategy for the fabrication of 1D inorganic/hybrid nanostructures. Here, CPBs with a

silsesquioxane (R-$SiO_{1.5}$) core, and a corona made up of oligo(ethylene glycol) methacrylate (OEGMA) serve as the in-situ template for the pyrolytic formation of purely inorganic silica nanowires. The silica precursor is directly incorporated within the monomer, 3-acryloylpropyl trimethoxysilane (APTS), rather than being added.

The synthetic strategy is illustrated in Figure 14. The CPBs, [APTS$_{20}$-b-OEGMA$_{57}$]$_{3200}$ were similarly prepared by sequential ATRP of APTS and OEGMA from polyinitiator, PBIEM, with 3,200 initiating sites. Hydrolysis of the trimethoxysilyl (TMS) moieties and subsequent condensation led to a crosslinked silsesquioxane core, solubilized by the poly(OEGMA) shell. Pyrolysis at 700°C can be used to generate inorganic silica nanowires.

Molecular visualization of the products at each step was undertaken by SFM to verify the success of the synthetic strategy. In all cases, SFM revealed individual wormlike/wirelike structures lying flat on the substrate. Comparing the objects in Figures 15a and b, obviously the [APTS$_{20}$-b-OEGMA$_{57}$]$_{3200}$ CPBs are much more stretched than [APTS$_{20}$]$_{3200}$, due to the introduction of the bulky POEGMA blocks. Moreover, the cross-section analysis shows that the typical [APTS$_{20}$]$_{3200}$ brush (green) is 1.4 nm high in its center and 35 nm in width, while the [APTS$_{20}$-b-OEGMA$_{57}$]$_{3200}$ CPBs increases the center height to 4.4 nm and width to 76 nm. From the regular cylindrical shape of the [APTS$_{20}$-b-OEGMA$_{57}$]$_{3200}$ CPBs in Figure 15b, a statistical analysis points out that the number- and weight-average lengths are $L_n = 322$ nm and $L_w = 355$ nm, respectively, giving a polydispersity $L_w/L_n = 1.10$, which agrees well with that of the PBIEM backbone ($M_w/M_n = 1.14$).

The condensation of the APTS units, catalyzed by ammonia in a methanol/water mixture via the Stöber method, introduced a continuous silsesquioxane network in the core. After condensation, the SFM image shows that the formed hybrids [(SiO$_{1.5}$)$_{20}$-b-OEGMA$_{57}$]$_{3200}$ (Figure 15c) are averagely 283 nm long, 39 nm (12%) shorter than before. The width decreases by 24% from 76 to 58 nm. Such kind of shrinkage results from the successful hydrolysis and condensation process of the TMS groups in the core. In contrast, the height increases by 45% from 4.4 to 6.4 nm (Figure 6e), since the crosslinked poly(APTS) (PAPTS) block can no longer spread to be flatly adsorbed on mica surface. Additionally, the silsesquioxane network hardens the core and reduces the penetration of the AFM tip into the CPB. In the final step, the hybrid nanowires were converted to inorganic silica nanowires by a pyrolysis process at 700°C. Figure 15d shows the AFM image of the obtained uniform silica nanowires on mica. Apparently the nanowires are thinner than the hybrid nanowires, stemming from the loss of the POEGMA shell during the pyrolysis. The width and height are only 31 and 1.3 nm, respectively. The dimensions are very close to those of the [APTS$_{20}$]$_{3200}$ CPB (35 and 1.4 nm). Only the number-average length is 276 nm, 14% smaller.
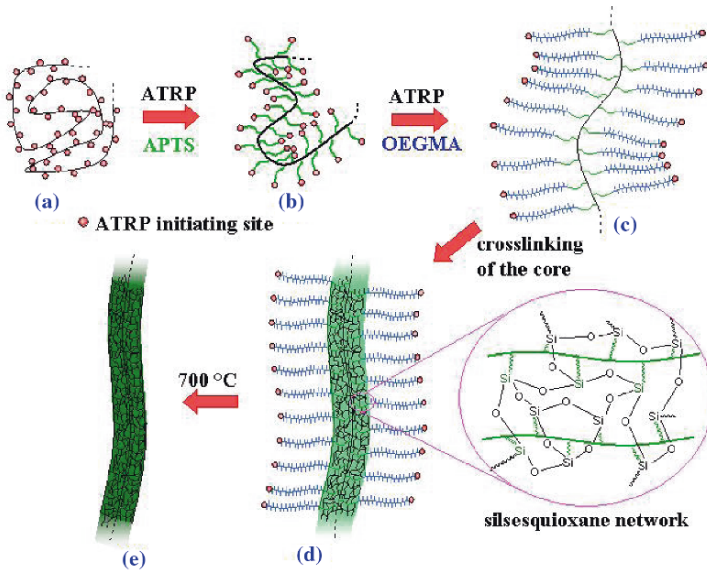
Figure 14. Synthesis of soluble organo-silica and inorganic silica nanowires. (**a**) ATRP polyinitiator PBIEM with DP = 3,200; (**b**) CPB with side chains of 20 APTS units; (**c**) core–shell CPB with additional 57 OEGMA units; (**d**) soluble organo-silica hybrid nanowires with crosslinked silsesquioxane network in the core; (**e**) inorganic silica nanowires after pyrolysis. Reprinted by permission of Nature.
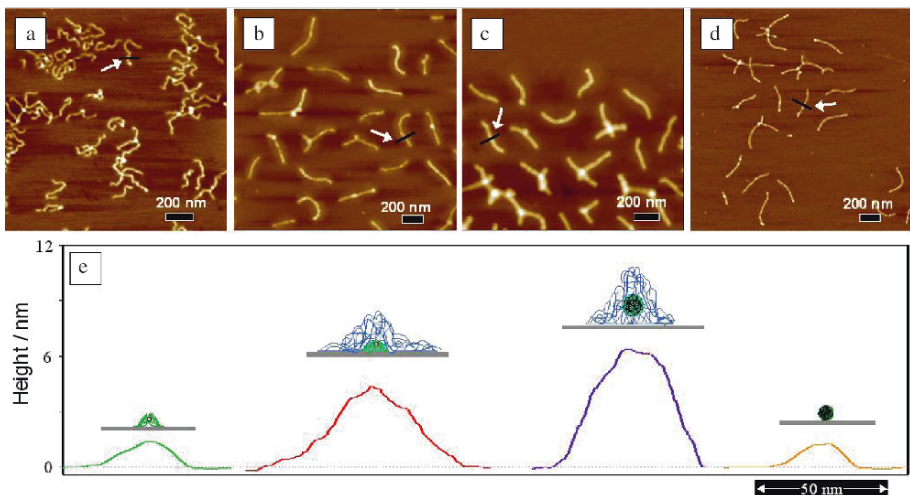
Figure 15. SFM height images on mica: (**a**) [APTS$_{20}$]$_{3200}$ CPBs (z range, 4 nm), (**b**) [APTS$_{20}$-*b*-OEGMA$_{57}$]$_{3200}$ core–shell CPBs (z range, 15 nm), (**c**) soluble organo-silica hybrid nanowires [(SiO1.5)$_{20}$-*b*-OEGMA$_{57}$]$_{3200}$ (z range, 20 nm), (**d**) inorganic silica nanowires (z range, 4 nm). (**e**) cross-sectional analysis of objects marked with an arrow. Reprinted by permission of Nature.

It is worth noting that although the POEGMA shell is removed during pyrolysis, it is essential in the condensation process, as it screens the intermolecular crosslinking, stretches the backbone, and most importantly, solubilizes the hybrid nanowires in methanol, in which the condensation reaction takes place. Additionally, the biocompatibility of the POEGMA shell may bring the soluble hybrid nanowires into bio-related potential applications, such as biosensors.

The absolute dimensions of the organo-silica hybrid nanowires were determined by scanning electron microscopy (SEM), transmission electron microscopy (TEM) and cryogenic TEM (cryo-TEM), respectively. Figure 16a shows a non-stained TEM image of the hybrid nanowires. The characteristic, wire-like dark domains represent the silsesquioxane core, whereas the organic corona is not visible due to low contrast. The number-average length of these dark objects is $L_n = 276 \pm 29$ nm (close to the AFM value) and the diameter is 9 nm, giving an aspect ratio of 30. In the SEM image (Figure 16b), the collapsed POEGMA shell is visible. Here, $L_n = 280 \pm 30$ nm and $d = 21 \pm 3$ nm are observed, leading to an aspect ratio of 13. Thus, the thickness of POEGMA shell is 6~7 nm. The structure of the hybrid nanowires in water was identified by cryo-TEM measurements (in Figure 16c). The dark line represents the nanowire core, and the gray corona stands for the POEGMA shell. The inset illustrates the compact superstructure of a single hybrid nanowire in solution. The size of the nanowire core ($L_n = 285 \pm 40$ nm, $d = 9.5 \pm 1$ nm) remains the same as that in Figure 16a, while the diameter, including the solvent-swollen corona, has dramatically expanded to 45 ± 5 nm, leading to a thickness of the swollen corona of ~18 nm.
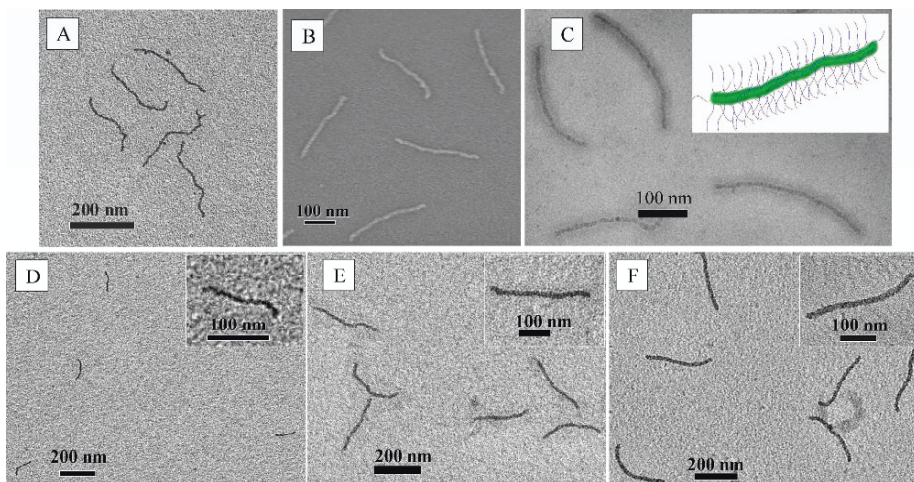
Figure 16. Electron microscopy characterization of soluble organo-silica hybrid nanowires. (**a**) Non-stained TEM image of $[(SiO1.5)_{20}\text{-}b\text{-}OEGMA_{57}]_{3200}$; (**b**) its SEM image and (**c**) its non-stained cryo-TEM image in water; (**d**), (**e**) and (**f**) are non-stained TEM images of $[(SiO1.5)_{21}\text{-}b\text{-}OEGMA_{58}]_{1500}$, $[(SiO1.5)_{41}\text{-}b\text{-}OEGMA_{68}]_{3200}$, and $[(SiO1.5)_{72}\text{-}b\text{-}OEGMA_{95}]_{3200}$, respectively. Reprinted by permission of Nature.

As the living polymerization techniques like anionic polymerization and ATRP can precisely define the degree of polymerization (DP), the dimension of the hybrid nanowires is tunable. To demonstrate the structural control, different-sized nanowires were prepared and compared with the $[APTS_{20}$-b-$OEGMA_{57}]_{3200}$ in Figure 16d–f. As expected, a decrease of the backbone DP from 3,200 to 1,500 with constant DPs of the side-chain blocks decreases the nanowire length from 276 to 138 nm, while the diameter kept constant (Figure 7d). At constant DP of the backbone we increased the PATPS block DP from 20 to 41 and 72, respectively, and the diameter increased from 9 to 15 and 21 nm, respectively (Figure 16e, f). Here the length increased very slightly (3% and 7%, respectively), due to the stronger repulsion of the enlarged side chains.

In conclusion, core–shell superstructured CPBs can be used as robust tools to design various 1D hybrid nanowires, such as magnetic(iron oxide), semi-conducting(CdS or CdSe), and silica or hybrid silica nanowires. The dimension of the nanowires can be tuned by the size of the core, e.g., the repeating units of the core monomer. The shell renders the nanowires solubility in organic solvent or aqueous solution. In the TMS-based CPBs, the hybrid silica nanowires are stretched enough to construct lyotropic phases.

Acknowledgment

References

[1]   F. A. Plamper; H. Becker; M. Lanzendörfer; M. Patel; A. Wittemann; M. Ballauff; A. H. E. Müller *Macromol. Chem. Phys.* **2005**, *206*, 1813.
[2]   F. A. Plamper; A. Schmalz; E. Penott-Chang; M. Drechsler; A. Jusufi; M. Ballauff; A. H. E. Müller *Macromolecules* **2007**, *40*, 5689.
[3]   H. Mori; A. H. E. Müller; J. E. Klee *J. Am. Chem. Soc.* **2003**, *125*, 3712.
[4]   S. Muthukrishnan; F. Plamper; H. Mori; A. H. E. Müller *Macromolecules* **2005**, *38*, 10631.
[5]   F. A. Plamper; A. Walther; A. H. E. Müller; M. Ballauff *Nano Lett.* **2007**, *7*, 167.
[6]   M. Wrighton; G. S. Hammond; H. B. Gray *J. Am. Chem. Soc.* **1971**, *93*, 5254.
[7]   F. A. Plamper; M. Ruppel; A. Schmalz; O. Borisov; M. Ballauff; A. H. E. Müller *Macromolecules* **2007**, *40*, 8361.
[8]   F. A. Plamper; A. Schmalz; M. Ballauff; A. H. E. Müller *J. Am. Chem. Soc.* **2007**, *129*, 14538.
[9]   M. Zhang; A. H. E. Müller *J. Polym. Sci. Part A: Polym. Chem.* **2005**, *43*, 3461.
[10] H. Gao; K. Matyjaszewski *J. Am. Chem. Soc.* **2007**, *129*, 6633.
[11] G. Cheng; A. Böker; M. Zhang; G. Krausch; A. H. E. Müller *Macromolecules* **2001**, *34*, 6883.

[12]   P. Dziezok; S. S. Sheiko; K. Fischer; M. Schmidt; M. Möller *Angew. Chem. Int. Ed.* **1997**, *36*, 2812.

[13]   M. Zhang; T. Breiner; H. Mori; A. H. E. Müller *Polymer* **2003**, *44*, 1449.

[14]   C. Cheng; K. Qi; E. Khoshdel; K. L. Wooley *J. Am. Chem. Soc.* **2006**, *128*, 6808.

[15]   H. Lee; W. Jakubowski; K. Matyjaszewski; S. Yu; S. S. Sheiko *Macromolecules* **2006**, *39*, 4983.

[16]   C. Cheng; E. Khoshdel; K. L. Wooley *Nano Lett.* **2006**, *6*, 1741.

[17]   J. Rühe; M. Ballauff; M. Biesalski; P. Dziezok; F. Gröhn; D. Johannsmann; N. Houbenov; N. Hugenberg; R. Konradi; S. Minko; M. Motornov; R. R. Netz; M. Schmidt; C. Seidel; M. Stamm; T. Stephan; D. Usov; H. Zhang *Adv. Polym. Sci.* **2004**, *165*, 79.

[18]   K. Lienkamp; L. Noe; M.-H. Breniaux; I. Lieberwirth; F. Gröhn; G. Wegner *Macromolecules* **2007**, *40*, 2486.

[19]   Y. Xu; S. Bolisetty; M. Drechsler; B. Fang; J. Yuan; M. Ballauff; A. H. E. Müller *Polymer* **2008**, *49*, 3957.

[20]   J. Pietrasik; B. S. Sumerlin; R. Y. Lee; K. Matyjaszewski *Macromol. Chem. Phys.* **2007**, *208*, 30.

[21]   Y. Mei; M. Ballauff *Eur Phys J E* **2005**, *16*, 341.

[22]   Y. Xu; S. Bolisetty; M. Drechsler; B. Fang; J. Yuan; L. Harnau; M. Ballauff; A. H. E. Müller *Soft Matter* **2009**, *5*, 379.

[23]   J. C. Johnson; H.-J. Choi; K. P. Knutsen; R. D. Schaller; P. Yang; R. J. Saykally *Nat. Mater.* **2002**, *1*, 106.

[24]   Z. L. Wang; J. Song *Science* **2006**, *312*, 242.

[25]   R. Adelung; O. C. Aktas; J. Franc; A. Biswas; R. Kunz; M. Elbahri; J. Kanzow; U. Schuermann; F. Faupel *Nat. Mater.* **2004**, *3*, 375.

[26]   X. Duan; C. M. Lieber *Adv. Mater.* **2000**, *12*, 298.

[27]   R. Djalali; S.-Y. Li; M. Schmidt *Macromolecules* **2002**, *35*, 4282.

[28]   M. Zhang; M. Drechsler; A. H. E. Mueller *Polym. Prepr. (Am. Chem. Soc., Div. Polym. Chem.)* **2004**, *45*, 454.

[29]   M. Zhang; C. Estournes; W. Bietsch; A. H. E. Mueller *Adv. Funct. Mater.* **2004**, *14*, 871.

[30]   M. Zhang; M. Drechsler; A. H. E. Mueller *Chem. Mater.* **2004**, *16*, 537.

[31]   J. Yuan; M. Drechsler; Y. Xu; M. Zhang; A. H. E. Müller *Polymer* **2008**, *49*, 1547.

[32]   J. Yuan, Y. Xu, A. Walther, S. Bolisetty, M. Schumacher, H. Schmalz, M. Ballauff, A. H. E. Müller *Nat. Mater.* **2008**, *7,* 718

SYNTHESIS OF SMART MATERIALS BY ATRP
OF OLIGO(ETHYLENE GLYCOL) METHACRYLATES

JEAN-FRANÇOIS LUTZ
*Research Group Nanotechnology for Life Science, Fraunhofer
Institute for Applied Polymer Research, Geiselbergstrasse 69,
14476 Potsdam-Golm, Germany*

Abstract: Well-defined thermoresponsive copolymers can be easily synthesized
via atom transfer radical polymerization (ATRP) of commercially available
oligo(ethylene glycol) methacrylates. This new class of smart biocompatible
polymers constitutes an interesting alternative to conventional thermoresponsive
macromolecules such as poly(N-isopropylacrylamide). In the present chapter,
our recent efforts for preparing PEG-based stimuli-responsive materials are
discussed in details.

Keywords: Polymer synthesis; Controlled radical polymerization; Atom transfer radical
polymerization (ATRP); Biocompatible polymers; Stimuli-responsive polymers

1. Introduction

Synthetic macromolecules undergoing rapid conformational change in response
to an external stimulus such as pH, temperature, ionic strength or irradiation
became lately very important in applied materials science.[1] For example,
thermoresponsive polymers exhibiting a lower critical solution temperature
(LCST) in aqueous medium are very promising materials for bio-applications
such as enzyme recycling, protein chromatography, controlled bio-adhesion,
hyperthermia-induced drug delivery or tissue engineering.[2] Such polymers are
soluble in water below the LCST but precipitate at temperatures above it. Hence,
temperature can be used as a simple external trigger for controlling the hydro-
philicity and therefore the structural shape of these macromolecules. Classic
examples of synthetic polymers exhibiting an aqueous LCST include poly(N,N′-
diethyl acrylamide), poly(dimethylaminoethyl methacrylate), poly(N-acryloyl-
pyrrolidine), poly(2-isopropyl-2-oxazoline), elastin-like artificial polypeptides,
poly(vinyl methyl ether) and poly(N-isopropylacrylamide) (PNIPAM, Scheme 1).

The latter has been by far the most studied and applied thermoresponsive polymer and therefore can be considered as the "gold standard" in this field of research.[3] During the last decades, several thousands of research articles and patents described the synthesis, the properties and the applications of this fascinating macromolecule.
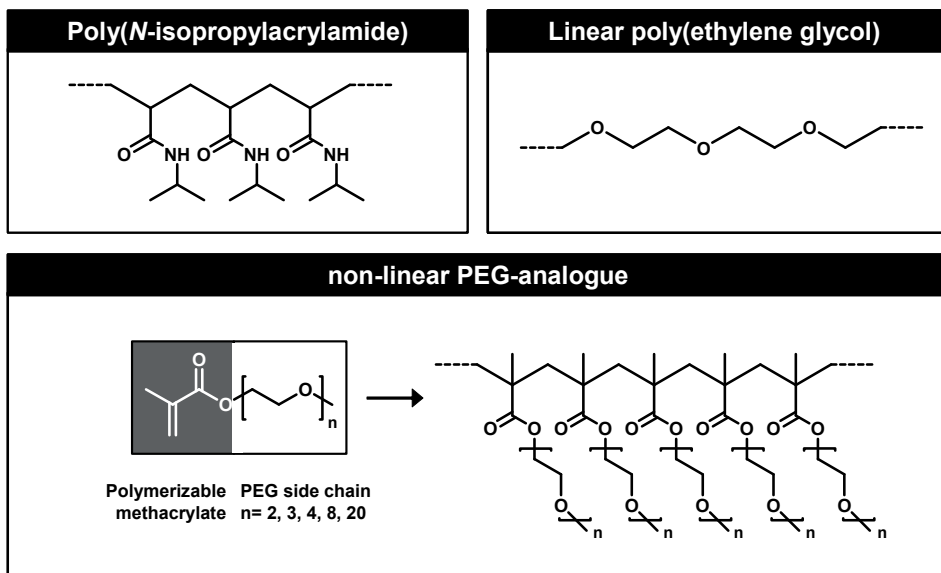
Scheme 1. Molecular structure of various biorelevant polymers.

However, despite its widespread popularity in material science, PNIPAM has inherent disadvantages such as an irreversible phase transition and, for short polymers, a significant   influence of end-groups on the thermal behavior.[3] Moreover, strictly speaking, PNIPAM is not a bio-inert polymer. Indeed, the presence of multiple secondary amide functions in the molecular structure of PNIPAM may lead to the formation of cooperative H-bonding interactions with other amide polymers, in particular with proteins.[4, 5] Thus, the design of new types of thermoresponsive polymers is a crucial topic in contemporary polymer chemistry.

In this context, this chapter describes the synthesis and the characterization of a novel family of thermoresponsive copolymers prepared from oligo(ethylene glycol) (macro)monomers. Such polymers are not standard linear poly(ethylene oxides) but graft structures composed of a carbon–carbon backbone and multiple oligo(ethylene glycol) side-chains (Scheme 1). Prior to our work, a few research groups reported that some of these polymers exhibit a LCST in aqueous medium. For example, Aoshima and Sugihara studied the living cationic polymerization of

vinyl ethers with oligo(ethylene glycol) side chains.[6] The resulting homopolymers and copolymers displayed interesting thermoresponsive behaviors in water.

Shortly after, in 2003, Ishizone and coworkers investigated the solution behaviors of homopolymers of either di(ethylene glycol) methyl ether methacrylate (MEO$_2$MA) or tri(ethylene glycol) methyl ether methacrylate (MEO$_3$MA) and reported that these macromolecules exhibit sharp phase transitions in aqueous medium.[7] This last publication clearly served as inspiration for the present work. Indeed, the family of oligo(ethylene glycol) methacrylates presents some obvious advantages. Firstly, these monomers are frequently commercially available and can be polymerized via a variety of techniques such a conventional free-radical-, controlled radical- or anionic-polymerization. Moreover, the resulting polymers are certainly promising for bio-applications as they are principally composed of biocompatible oligo(ethylene glycol) segments. Indeed, PEG (Scheme 1) is an uncharged, water soluble, non-toxic, non-immunogenic, FDA-approved polymer, and thus is probably the most widely applied synthetic polymer in biotechnology and medicine in recent years. Thus, it was very tempting to investigate further this class of monomers for preparing novel generations of biorelevant polymers. Different scientific aspects were investigated in our research group during the last 4 years. The most relevant findings are summarized within the next pages.

2. ATRP of Oligo(Ethylene Glycol) Methacrylates

PEG macromonomers (i.e. molecule composed of a polymerizable moiety connected to a short oligo(ethylene) glycol chain) first appeared in scientific literature during the 1980s.[8] The initial motivation behind the use of such compounds was clearly the design of novel macromolecular architectures (e.g. comb/graft polymers or networks). However, another significant advantage of PEG macromonomers is the possibility to access high-molecular weight PEG-based polymers using relatively mild synthetic conditions. Indeed, PEG macro-monomers may be polymerized via a variety of mechanisms such as anionic, cationic, ring opening metathesis or free-radical polymerization. Nevertheless, the latter approach is probably the most straightforward and versatile method for preparing non-linear PEG analogues. Free-radical polymerizations can be applied in a wide range of experimental conditions (i.e. apolar medium, pure water, physiological medium). Furthermore, the recent discovery of controlled radical polymerization techniques such as atom transfer radical polymerization (ATRP) has considerably broadened the possibilities of macromolecular design with PEG macromonomers.

Various types of radically polymerizable PEG macromonomers can be found in the literature. Yet, the most frequently used structures are styrene, acrylate or methacrylate derivatives. Besides the α-polymerizable moiety, the

ω-end group of the PEG chain is, in most cases, a methoxy function but ethoxy- or hydroxy-terminal groups are also frequent. Among these possible structures, the oligo(ethylene glycol) methyl ether methacrylates series is particularly appealing as most of its members are commercially available. Moreover, this class of monomers may lead to new types of PEG-based polymers with interesting stimuli-responsive properties (see following paragraphs). The research group of Armes first described the ATRP of an oligo(ethylene glycol) methyl ether methacrylate (OEGMA) with 7/8 ethylene oxide (EO) units.[9] The controlled radical polymerization of this monomer was performed in aqueous environment at room temperature and lead to the formation of POEGMA with a narrow molecular weight distribution. However, although important for large-scale synthesis and biological applications (e.g. protein PEGylation), ATRP in aqueous medium remains a complicated and rather challenging process. On a lab scale, ATRP in organic solvents is probably preferable to access well-defined POEGMA. Thus, in the present work, the ATRP of either MEO_2MA or oligo(ethylene glycol) methacrylate with 8/9 EO units (OEGMA$_{475}$, M_n = 475 g/mol) was performed in pure ethanol.[10] Indeed, alcohols exhibit some advantages of organic solvents but are also polar enough to generate fast polymerization kinetics.

Table 1 shows the molecular structure and the properties of a series of P(MEO_2MA-*co*-OEGMA$_{475}$) copolymers prepared by atom transfer radical copolymerization of MEO_2MA and OEGMA$_{475}$ in ethanol solution. In this series, the initial molar fractions of MEO_2MA and OEGMA$_{475}$ monomers were

TABLE 1. Properties of copolymers of OEGMA$_{475}$ and MEO_2MA prepared using ATRP.[a]

	[OEGMA]$_0$/[MEO$_2$-MA]$_0$	Conv.[b]	F_{OEGMA}[c] (%)	M_n[d]	$M_{n\,th}$[e]	M_w/M_n[c]
1	100:0	0.91	100	10,000	43,200	1.18
2	30:70	0.93	33	35,000	25,500	1.22
3	20:80	0.91	20	29,700	22,300	1.33
4	15:85	0.88	16	19,900	20,300	1.57
5	10:90	0.92	10	24,300	19,900	1.57
6	08:92	0.90	8	24,800	19,000	1.45
7	05:95	0.86	6	18,300	17,400	1.66
8	0:100	0.90	0	16,700	16,900	1.72

[a] Experimental conditions: 3 h, 60°C ; in ethanol solution (monomer/ethanol = 1:1.25 (v/v)) ; ([OEGMA$_{475}$]$_0$ + [MEO2-MA]$_0$)/[MBP]$_0$/[CuBr]$_0$/[Bipy]$_0$ = 100/1/1/2.

[b] Overall monomer conversion measured by ^{1}H NMR.

[c] Molar fraction of OEGMA$_{475}$ in the formed copolymer as calculated by ^{1}H NMR.

[d] measured by SEC in THF.

[e] $M_{n\,th}$ = conversion (475 [OEGMA$_{475}$]$_0$ + 188 [MEO$_2$-MA]$_0$)/[MBP]$_0$.

variable, but an overall average degree of polymerization of 100 was targeted in all cases. The copolymers were prepared at 60°C in the presence of the homogeneous ATRP catalytic system copper(I) bromide/2-2′ bipyridyl (Bipy). These synthetic conditions were first selected as a fast screening system since bromide-based catalysts and polar protic solvents are both known to generate very fast ATRP kinetics.

As expected, in such conditions, homopolymers or copolymers of MEO$_2$MA and OEGMA$_{475}$ could be obtained in high yields in a rather short time. However, the results of Table 1 underlines major differences between POEGMA$_{475}$ homopolymers and P(MEO$_2$MA-co-OEGMA$_{475}$) copolymers. Indeed, in the case of POEGMA$_{475}$, experimental molecular weights measured by size exclusion chromatography were found to be much lower than theoretical values. The latter is probably a consequence of the unusual solution behavior of graft polymers with long side-chains (i.e. stiff macromolecular brushes). Experimental molecular weights measured for P(MEO$_2$MA-co-OEGMA$_{475}$) copolymers were much closer to theoretical values, which indicates that these copolymers are more flexible and therefore adopt a random coil conformation in THF solution. Furthermore, P(MEO$_2$MA-co-OEGMA$_{475}$) copolymers exhibited a controlled composition. NMR analysis indicated that the comonomer composition of the purified copolymers correspond to the initial comonomer feed in all cases (Table 1). Still, this aspect is not extremely surprising considering that (i) both comonomers most probably exhibit relatively similar reactivities and (ii) the copolymers were isolated at high monomer conversions.

Generally speaking, ATRP in ethanol was found to be a very straightforward method for preparing P(MEO$_2$MA-co-OEGMA$_{475}$) copolymers. However, in the presence of the ATRP catalyst CuBr/Bipy, broad molecular weight distributions were obtained for the copolymers. For POEGMA$_{475}$ homopolymers, very narrow molecular weight distributions were obtained with CuBr/Bipy (these low polydispersies are maybe just apparent due to the globular shape of the stiff macromolecular brushes or can be due to the fact that termination reactions are usually disfavored with macromonomers). On the other hand, for P(MEO$_2$MA-co-OEGMA$_{475}$), it appears from Table 1 that polydispersity index increases with the molar fraction of MEO$_2$MA in the copolymer. Chloride-based ATRP catalysts usually lead to a much better control of the radical polymerization of methacrylates than bromide-based catalysts. Thus, the catalytic system CuCl/Bipy was tested for preparing POEGMA$_{475}$, P(MEO$_2$MA-co-OEGMA$_{475}$) and PMEO$_2$MA samples. As expected, this catalyst allowed a much better control of the molecular structure of the polymers. Experimental molecular weights of P(MEO$_2$MA-co-OEGMA$_{475}$) and PMEO$_2$MA were found to be close to theoretical values in all cases (for POEGMA$_{475}$, molecular weights measured by GPC were always found to be underestimated, independently of the catalyst structure). Nevertheless, a narrow molecular weight distribution was obtained for all samples (Mw/Mn < 1.3).[10]

3.   Properties in Aqueous Solutions

Polymers constructed from PEG (macro)monomers exhibit fascinating solution properties in aqueous medium. Depending on the molecular structure of their monomer units (i.e. nature of the polymerizable moiety, length of the PEG side chain, ω-end-group of the PEG chain), non linear PEG analogues can be either insoluble in water, readily soluble up to 100°C or thermoresponsive. In fact, the balance between hydrophilic and hydrophobic moieties in the molecular structure of the polymers is the key-parameter that determines their solution properties. For instance, in the case of (oligo ethylene glycol) methyl ether methacrylates, the ether oxygens of PEG form stabilizing H-bonds with water, whereas the apolar carbon–carbon backbone leads to a competitive hydrophobic effect (Scheme 2).[11, 12] Thus, polymers with very short PEG side-chains are not water soluble or only weakly hydrophilic. For example, polymers of 2-methoxyethyl methacrylate (MEMA, 1 EO unit, Scheme 2) are not water-soluble at room temperature.[13] On the other hand, polymers with long PEG side chains (i.e. 10 EO units and more) are soluble in water, even at high temperatures. In between these two extremes, non-linear PEG analogues with side-chains of intermediate length (i.e. 2 ≤ EO units < 10) generally exhibit a lower critical solution temperature (LCST) in aqueous solution. In other words, these polymers are soluble in water below the LCST but precipitate at temperatures above it. For example, monomers such as MEO2MA (2 EO units) or MEO3MA (3 EO units) lead to water-soluble thermoresponsive polymers with a LCST of 26°C or 52°C respectively.[7] Commercially available oligo(ethylene glycol) methyl ether methacrylates with slightly longer side-chains (i.e. 4/5 or 8/9 EO units in average, Scheme 2) lead to very hydrophilic polymers with rather high LCST values (i.e. in the range 60–90°C).[14]
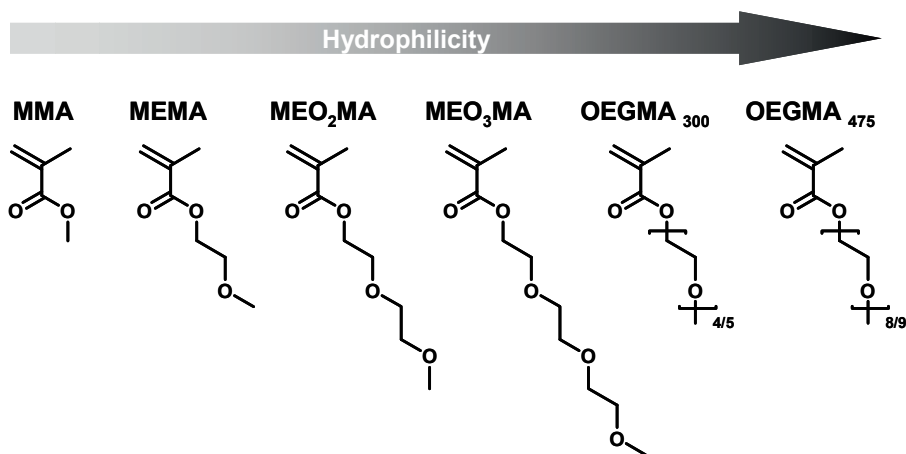
Scheme 2. Molecular structures of various oligo(ethylene glycol) methacrylates.

This interesting thermoresponsive behavior is almost certainly a consequence of the amphiphilicity of the polymer chains.[11, 12] At room temperature, the balance between favorable polymer–water interactions and unfavorable hydrophobic interactions is sufficient to allow solubilization. Above LCST, this balance is disrupted and polymer–polymer interactions are thermodynamically favored as compared to polymer–water interactions. In that regard, the thermoresponsive mechanism of poly(oligo ethylene glycol) methyl ether methacrylates is very comparable to the one of poly(*N*-alkyl acrylamides) such as PNIPAM.[3] However, the phase transitions of non-linear PEG analogues are generally reversible (i.e. heating and cooling behaviors are almost similar), whereas PNIPAM usually shows a significant hysteresis. The latter phenomenon has been cautiously explained by Wu and coworkers.[15] Above LCST, PNIPAM chains become partially dehydrated globules. In this collapsed state, the amide groups of PNIPAM lead to the formation of intramolecular and intermolecular NH···O=C hydrogen bonding interactions. Hence, during the cooling process, the rehydration of PNIPAM is hindered by these additional interactions, leading to a marked hysteresis. In comparison, poly(oligo ethylene glycol) methyl ether methacrylates exhibit a reversible dehydration as there is no strong H-bond donor in the molecular structure of these polymers and therefore no possibility of forming stabilizing H-bonds in the collapsed state.[16] Moreover, the phase transitions observed for non-linear PEG analogues are relatively insensitive to external physical conditions. In fact, for a given type of polymer, the cloud points depend to some degree on molecular weight, main-chain end-groups, tacticity, concentration and ionic strength. However, the observed variations in LCST are generally rather small.
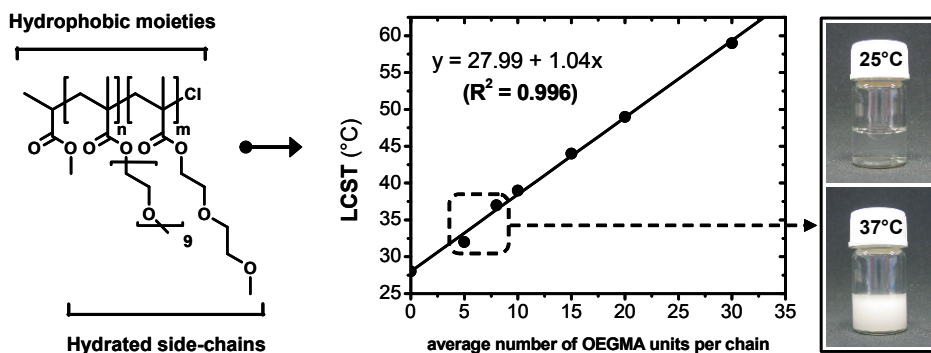

Figure 1. Plots of the measured lower critical solution temperature (LCST) as a function of the theoretical average number of OEGMA$_{475}$ units per chain for a series of P(MEO$_2$MA-*co*-OEGMA$_{475}$) copolymers of various composition.

Furthermore, we recently reported that the thermoresponsive behavior of non-linear PEG analogues can be precisely adjusted using a simple random

copolymerization strategy (Figure 1).[10] In this approach, PEG macromonomers of different chain-lengths (i.e. of different hydrophilicity but similar chemical nature) were copolymerized by ATRP (see previous paragraph). For example, random copolymers of MEO$_2$MA and OEGMA$_{475}$ exhibit LCST values in between 26°C and 90°C, which can be precisely adjusted by varying the comonomer composition (Figure 1). For example, cloud points of either 32°C (comparable to the standard LCST of PNIPAM), 37°C (body temperature, see inset in Figure 1) or 39–40°C (fever temperatures) were observed in pure water for copolymers possessing in average respectively 5%, 8% or 10% of OEGMA$_{475}$ units per chain.[10] Although copolymerization strategies for tuning LCST have been reported in the past, the present approach is rather unique in the sense that both comonomers are of the same kind (i.e. both only contain a PEG segment and a methacrylate moiety). Thus, chemically speaking, random copolymers P(MEO$_2$MA-co-OEGMA$_{475}$) can be considered as homopolymers. Furthermore, the comonomer pair MEO$_2$MA/OEGMA$_{475}$ is not the only one, which can be exploited for preparing defined thermoresponsive polymers.[17] In fact, virtually all the structures shown in Scheme 2 can be used in such copolymerization strategy, thus making oligo(ethylene glycol) methyl ether methacrylates a very appealing and versatile class of monomers for preparing stimuli-responsive materials.

4.   Stimuli-Responsive Materials

The thermoresponsive properties of non-linear PEG analogues are potentially interesting for a wide range of applications. For instance, Huck and Jonas first reported the preparation of thermoresponsive P(MEO$_2$MA-co-OEGMA$_{475}$) polymer brushes on planar surfaces.[18] These polymers were grown on a model silicon wafer coated with a silane ATRP initiator (i.e. "grafting from" strategy). The resulting surface brushes exhibited a clear thermoresponsive behavior and displayed LCST values roughly similar to those observed for P(MEO$_2$MA-co-OEGMA$_{475}$) copolymers in solution. We recently studied this interesting surface behavior to design smart bioactive substrates. For instance, it was demonstrated that thermoresponsive oligo(ethylene glycol)-based gold surfaces allow efficient control over fibroblast-adhesion within a convenient and applicable temperature range (25–37°C).[19]

Our research group also reported the synthesis of thermoresponsive P(MEO$_2$MA-co-OEGMA$_{475}$) hydrogels.[11] These macroscopic hydrogels were prepared using ethylene glycol dimethacrylate (EGDM) as a crosslinker. Although such hydrogels could be easily synthesized by conventional radical polymerization, the ATRP method was selected to insure a homogeneous comonomer composition in each region of the macromolecular network. Such precaution would not be necessary if one is only interested in the swelling

of the hydrogel at room temperature. However, if a thermoresponsive gel is targeted, a defined composition of the network is probably essential. Hydrogels samples exhibited a satisfying swelling capacity in pure water and appeared as homogeneous transparent materials in the swollen state. However, the swelling rates and the maximum swelling ratios were found to be proportional to the fraction of OEGMA grafts in the network, which is a logical behavior previously observed for PEG grafted hydrogels. Moreover, both hydrogels were found to be thermoresponsive and exhibited LCST values comparable to those measured for their single-chains analogues.[11]

Very recently, Hu and coworkers fabricated thermoresponsive microgels based on P(MEO$_2$MA-co-OEGMA$_{475}$) networks.[20] These monodisperse particles were prepared via conventional radical polymerization and therefore exhibited relatively broad phase transitions. Nevertheless, in semidilute aqueous solutions (4–10 wt%), these microgels self-assembled into interesting crystalline phases with iridescent properties. Other types of PEG-based stimuli-responsive colloids were lately described in the literature, for example thermoresponsive dendrimers, carbon nanotubes, silica particles, gold particles and block-copolymer micelles.[21–26]

Acknowledgements

References

[1] E. S. Gil; S. M. Hudson, Stimuli responsive polymers and their bioconjugates, *Prog. Polym. Sci.* 29, 1173–1222 (2004).

[2] C. de las Heras Alarcón; S. Pennadam; C. Alexander, Stimuli responsive polymers for biomedical applications, *Chem. Soc. Rev.* 34(3), 276–285 (2005).

[3] H. G. Schild, Poly(N-isopropylacrylamide): experiment, theory and application, *Prog. Polym. Sci.* 17(2), 163–249 (1992).

[4] J.-Y. Wu; S.-Q. Liu; P. W.-S. Heng; Y.-Y. Yang, Evaluating proteins release from, and their interactions with, thermosensitive poly (N-isopropylacrylamide) hydrogels, *J. Contr. Rel.* 102(2), 361–372 (2005).

[5] M. Keerl; V. Smirnovas; R. Winter; W. Richtering, Interplay between hydrogen bonding and macromolecular architecture leading to unusual phase behavior in thermosensitive microgels, *Angew. Chem. Int. Ed.* 47(2), 338–341 (2008).

[6]   S. Aoshima; S. Sugihara, Syntheses of stimuli-responsive block copolymers of vinyl ethers with side oxyethylene groups by living cationic polymerization and their thermosensitive physical gelation, *J. Polym. Sci. A: Polym. Chem.* 38(21), 3962–3965 (2000).

[7]   S. Han; M. Hagiwara; T. Ishizone, Synthesis of thermally sensitive water-soluble polymethacrylates by living anionic polymerizations of oligo(ethylene glycol) methyl ether methacrylates, *Macromolecules* 26(22), 8312–8319 (2003).

[8]   D. Neugebauer, Graft copolymers with poly(ethylene oxide) segments, *Polym. Int.* 56(12), 1469–1498 (2007).

[9]   X.-S. Wang; S. F. Lascelles; R. A. Jackson; S. P. Armes, Facile synthesis of well-defined water-soluble polymers via atom transfer radical polymerization in aqueous media at ambient temperature, *Chem. Commun.* (18), 1817–1818 (1999).

[10] J.-F. Lutz; A. Hoth, Preparation of ideal PEG analogues with a tunable thermo-sensitivity by controlled radical copolymerization of 2-(2-methoxyethoxy)ethyl methacrylate and oligo(ethylene glycol) methacrylate, *Macromolecules* 39(2), 893–896 (2006).

[11] J.-F. Lutz; K. Weichenhan; Ö. Akdemir; A. Hoth, About the phase transitions in aqueous solutions of thermoresponsive copolymers and hydrogels based on 2-(2-methoxyethoxy)ethyl methacrylate and oligo(ethylene glycol) methacrylate, *Macro-molecules* 40(7), 2503–2508 (2007).

[12] Y. Maeda; T. Kubota; H. Yamauchi; T. Nakaji; H. Kitano, Hydration changes of poly(2-(2-methoxyethoxy)ethyl methacrylate) during thermosensitive phase separation in water, *Langmuir* 23(22), 11259–11265 (2007).

[13] M. Tanaka; A. Mochizuki, Effect of water structure on blood compatibility – thermal analysis of water in poly(meth)acrylate, *J. Biomed. Mat. Res. Part A* 68A(4), 684–695 (2004).

[14] M. Mertoglu; S. Garnier; A. Laschewsky; K. Skrabania; J. Storsberg, Stimuli responsive amphiphilic block copolymers for aqueous media synthesised via reversible addition fragmentation chain transfer polymerisation (RAFT), *Polymer* 46, 7726–7740 (2005).

[15] X. Wang; X. Qiu; C. Wu, Comparison of the coil-to-globule and the globule-to-coil transitions of a single poly(N-isopropylacrylamide) homopolymer chain in water, *Macromolecules* 31(9), 2972–2976 (1998).

[16] J.-F. Lutz; O. Akdemir; A. Hoth, Point by point comparison of two thermo-sensitive polymers exhibiting a similar LCST: is the age of poly(NIPAM) over? *J. Am. Chem. Soc.* 128(40), 13046–13047 (2006).

[17] S. I. Yamamoto; J. Pietrasik; K. Matyjaszewski, The effect of structure on the thermoresponsive nature of well-defined poly(oligo(ethylene oxide) methacrylates) synthesized by ATRP, *J. Polym. Sci. Part A: Polym. Chem.* 46(1), 194–202 (2008).

[18] A. M. Jonas; K. Glinel; R. Oren; B. Nysten; W. T. S. Huck, Thermo-responsive polymer brushes with tunable collapse temperatures in the physiological range, *Macromolecules* 40(13), 4403–4405 (2007).

[19] E. Wischerhoff; K. Uhlig; A. Lankenau; Hans G. Börner; A. Laschewsky; C. Duschl; J.-F. Lutz, Controlled cell adhesion on PEG-based switchable surfaces, *Angew. Chem. Int. Ed.* 47(30), 5666–5668 (2008).

[20] T. Cai; M. Marquez; Z. Hu, Monodisperse thermoresponsive microgels of poly(ethylene glycol) analogue-based biopolymers, *Langmuir* 23(17), 8663–8666 (2007).

[21] F. Hua; X. Jiang; B. Zhao, Temperature-induced self-association of doubly thermosensitive diblock copolymers with pendant methoxytris(oxyethylene) groups in dilute aqueous solutions, *Macromolecules* 39(10), 3476–3479 (2006).

[22] D. Li; G. L. Jones; J. R. Dunlap; F. Hua; B. Zhao, Thermosensitive hairy hybrid nanoparticles synthesized by surface-initiated atom transfer radical polymerization, *Langmuir* 22(7), 3344–3351 (2006).

[23] J.-F. Lutz; S. Pfeifer; Z. Zarafshani, In situ functionalization of thermoresponsive polymeric micelles using the "click" cycloaddition of azides and alkynes, *QSAR Comb. Sci.* 26(11–12), 1151–1158 (2007).

[24] G. Chen; P. M. Wright; J. Geng; G. Mantovani; D. M. Haddleton, Tunable thermoresponsive water-dispersed multiwalled carbon nanotubes, *Chem. Commun.* 1097–1099 (2008).

[25] E. W. Edwards; M. Chanana; D. Wang; H. Möhwald, Stimuli-responsive reversible transport of nanoparticles across water/oil interfaces, *Angew. Chem. Int. Ed.* 47(2), 320–323 (2008).

[26] H.-I. Lee; J. A. Lee; Z. Poon; P. T. Hammond, Temperature-triggered reversible micellar self-assembly of linear-dendritic block copolymers, *Chem. Commun.* 3726–3728 (2008).

NEW POLYMERS WITH OPTOELECTRONIC PROPERTIES BY COMBINATION OF ATRP, ROP AND COUPLING PROCESSES

DEMET G. COLAK, IOAN CIANGA, SEDA YURTERI,
AND YUSUF YAGCI[*]
*Department of Chemistry, Istanbul Technical University,
34469 Maslak, Istanbul, Turkey*

Abstract: The present chapter describes the synthetic strategies used for the preparation of electroluminescent conjugated polymers via metal catalyzed coupling reactions. Synthesis of these polymeric materials having complex macromolecular architectures, composition or functionalities involves the use of several controlled polymerization methods, namely Atom Transfer Radical Polymerization (ATRP) and Ring Opening Polymerization (ROP). Essentially, new functional compounds as initiators in the above-mentioned methods, were designed, synthesized and used to obtain different types of telechelics or macro-monomers. New poly(p-phenylene) (PP) and poly(*p*-phenylene vinylene) (PPV) derivatives bearing macromolecular side chains were readily synthesized by cross-coupling processes (Suzuki or Yamamoto coupling) or/and Wittig reaction of appropriate combination of these well-defined macromolecules. The final soluble and processable conjugated polymers could find applications as high technology materials due to their properties such as conductivity and luminescence.

Keywords: Controlled polymerization methods (ATRP, ROP); Suzuki coupling; Yamamoto coupling; Conjugated polymers; Poly(*p*-phenylene); Poly(*p*-phenylene vinylene)

1. Introduction

The synthesis and design of new polymeric materials to accomplish particular and specialized applications involving advanced complex structures is a continuously developing domain in polymer chemistry. When designing a synthesis, there is a variety of synthetic processes each having advantages and disadvantages. If one considers the interdisciplinary connection between synthesis and material science to generate a defined architecture, it is necessary to achieve an impetus

for research.[1–3] The necessary requirements for the design of new advanced materials include both precise control of molecular structure through synthesis and processing. Elaborate correlation between molecular structure and properties is one of the final targets of polymer science. For designing new high-performance materials, exact information on functionality, composition, topology and chain uniformity are required. "Living/controlled polymerization" is the only technique available to control molecular architecture in macromolecular engineering and is the most suitable way to synthesize a polymer with a definite structure from one end to another. By combining different techniques such as living/controlled polymerization, macromonomer technique and coupling processes, one can synthesize new materials with novel properties.

The current chapter focuses on the synthetic key steps in tailoring new polymers with designed architectures and particular properties for high-tech applications. Structures of these polymers are mostly based on common polymers such as polystyrene (PSt), poly-ε-caprolactone (PCL), polytetrahydrofuran (PTHF) and poly(2-methyl-2-oxazoline) (POx).

2.   Brief Overview on the Processes Involved in the Synthesis

Before discussing the synthesis and properties of the final conjugated polymers, it is essential to first overview briefly the polymerization processes and techniques involved.

2.1.   TELECHELICS; MACROMONOMER TECHNIQUE

Telechelic polymers are defined as macromolecules that contain two reactive end groups and are important building blocks for the construction of polymeric materials.[4–6] They can be used as cross-linkers, chain extenders, and precursors for block and graft copolymers. Furthermore, various macromolecular architectures are possible by their reactions.[4] Telechelic polymers are called macromolecular monomers, macromonomers or macromers as they can also participate in polymerization reactions depending on their functionality. The macromonomer technique has proved to be a useful tool for preparing well-defined copolymers.[7, 8]

Telechelic polymers with various functionalities are synthesized by a wide range of polymerization methods such as anionic,[9] cationic,[10] ring opening,[11] group transfer,[12, 13] free radical,[14] metathesis,[15, 16] step growth[5] polymerization and chain scission[5] processes.
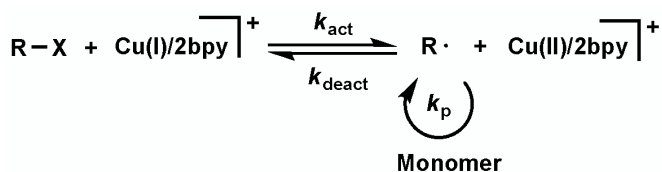
Exact control of polymerization is an important point for the preparation of well-defined telechelics and functional macromolecules. Recent developments in living/controlled radical polymerization provided the possibility to synthesize

well-defined telechelic polymers with controlled functionalities, via radical routes, as well.[17, 18]

2.2.   CONTROLLED POLYMERIZATION METHODS

2.2.1. *Atom Transfer Radical Polymerization (ATRP)*

Among the various controlled radical polymerization routes, ATRP seemed to be the most versatile system that can polymerize a wide variety of currently available monomers yielding polymers with different architectures and compositions by relatively simple means. The combination of synthetic versatility and simplicity makes ATRP a powerful technique for designing and preparing new materials. ATRP[19–21] involves reversible homolytic cleavage of a carbon–halogen bond by a redox reaction between an organic halide (R–X) and a transition metal, such as copper (I) complexed with 2,2′-bipyridine (bpy), as illustrated in Scheme 1.

$$R-X \; + \; Cu(I)/2bpy \Big]^{+} \quad \underset{k_{deact}}{\overset{k_{act}}{\rightleftharpoons}} \quad R\cdot \; + \; Cu(II)/2bpy \Big]^{+}$$

$$\curvearrowleft k_{p}$$

Monomer

Scheme 1. General reaction mechanism of ATRP.

Polymer functionalization by ATRP can be attained by using functional initiators and monomers or by the chemical transformation of the halogen end groups. By varying the initiator, RX, that contains both a functional group and an activated halide, it is quite easy to incorporate a functional group in to a polymer chain. A large number of functional initiators were successfully used in ATRP to synthesize functional styrene and acrylate type polymers.[21]

2.2.2. *Ring Opening Polymerization (ROP)*

Aliphatic polyesters are an attractive class of polymers that can be used in biomedical and pharmaceutical applications. The growing interest in this kind of degradable polymers is their physical and chemical properties which can be varied over a wide range by copolymerization and macromolecular architecture techniques. High molecular weight polylactones and polylactides are entirely produced by the ROP of corresponding cyclic monomers. If a cyclic ester is reacted with a catalyst/initiator under mild conditions, an aliphatic polyester of low polydispersity and high molecular weight is obtained in a short period of time. Scheme 2 presents the reaction pathway for the ROP of a cyclic ester.
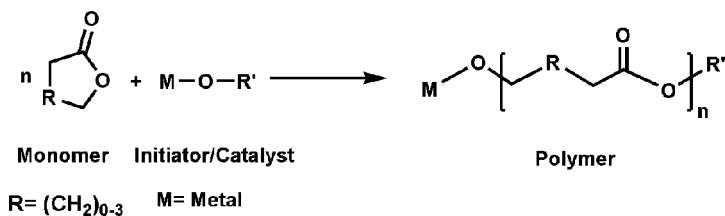
Scheme 2. ROP of a cyclic ester.

Each macromolecule formed generally contains one chain-end terminated with a functional group originating from the termination reaction and the other end capped with a functional group from the initiator. By varying the catalyst/ initiator and the termination reaction, the functional groups can be varied for the desired application.[22] Functional groups suitable to post-polymerization reactions can also be introduced into the polymer structure or they can be further modified for different purposes.

Depending on the initiator, the polymerization proceeds according to three different major reaction mechanisms,[23] via cationic, anionic, or "coordination-insertion" mechanisms.[24–26] In coordination insertion ROP, propagation is thought to proceed by coordination of the monomer to the active species, followed by insertion of the monomer into the metal–oxygen bond by rearrangement of the electrons.[24, 25] Scheme 3 shows a schematic presentation of the proposed reaction pathway for the ROP of a cyclic ester by coordination-insertion mechanism. The reaction is terminated by hydrolysis forming a hydroxy end group.
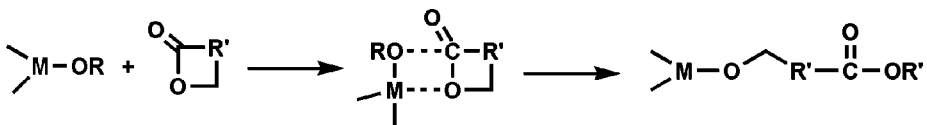
Scheme 3. ROP of a cyclic ester by coordination-insertion mechanism.

The coordination-insertion type of polymerization has been thoroughly investigated since it may yield well-defined polyesters through living polymerization.[25] PCL is a typical aliphatic semi crystalline biodegradable polyester accessible via such polymerization method.

## 2.3. METAL-CATALYZED CARBON–CARBON BOND FORMATION; COUPLING PROCESSES (YAMAMOTO AND SUZUKI COUPLING)

Most of the carbon–carbon bond-forming reactions are rooted in the reaction of stoichiometric quantities of the carbon nucleophile and the carbon electrophile. These classical methods work well and have been used successfully to design various organic structures. Recently developed methods make use of transition

metal-complexes as catalysts and have many advantages over the classical ones.[27] These include molecular design flexibility, tolerance to wide range of functional groups, high yields and efficiencies without by-products. Moreover, the use of very small amount of catalyst and simple workup and purifications make these methods economical and industrially attractive. A large number of transition metals have been used to form carbon–carbon bonds in different reactions. However, in particular, two metals have receieved the greatest attention. The use of palladium (Pd) and nickel (Ni) has led new strategies for the synthetic planning of different structures and architectures.

Ni-catalyzed coupling reaction of organic halides in the presence of neutral ligands (e.g. PPh$_3$, bpy) and zinc is known as "Yamamoto Coupling" and has been a typical method for the synthesis of conjugated polymers such as poly(phenylene)s (PP), with nearly quantitative yields.[28]
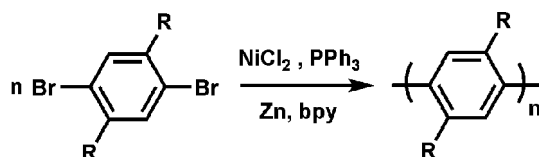
Scheme 4. Yamamoto coupling/polycondensation.

The Pd-catalyzed coupling reaction between organoboron compounds and organic halides (or triflates) is known as "Suzuki Coupling" and is a powerful methodology for the formation of carbon–carbon bonds.[29]
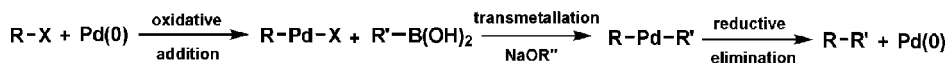
Scheme 5. Suzuki coupling.

The availability of the reagents and the mild reaction conditions contribute to the versatility of this reaction. It also offers several additional advantages, such as being insensitive to moisture, tolerating a broad range of functional groups, and proceeding generally regio- and stereoselectively.[30, 31] The reaction is carried out in the presence of a negatively charged base, such as sodium or potassium carbonate and the bases can be used as aqueous solutions.
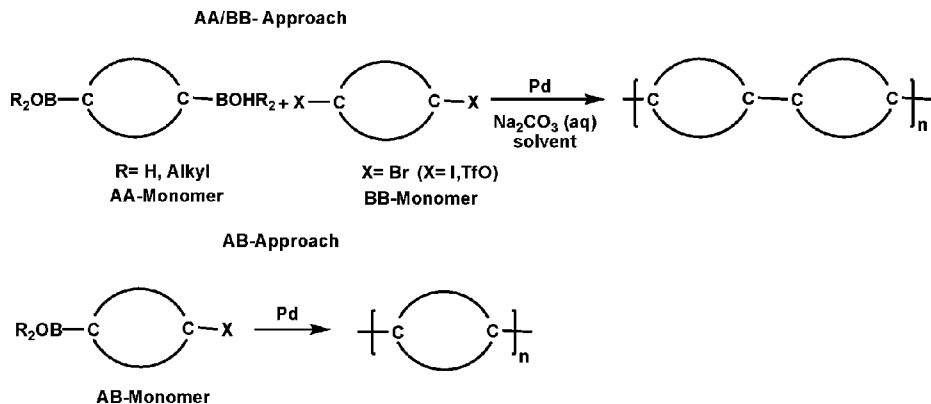
Suzuki coupling is successfully transferred to Suzuki Polycondensation (SPC) reaction, which is a step-growth polymerization of bifunctional aromatic monomers yielding PPs and its derivatives.[31–33] The required functional groups, boronic acid or esters and halides, may be present in different monomers (AA/BB approach) or can exist in the same monomer (AB approach) as depicted in Scheme 6.

3. Architectural Polymer Design and Synthesis of PPs and Poly(Phenylene Vinylene)s (PPVs) with Well-Defined Polymeric Side Chains

Since the discovery that PP conducts electricity when doped with oxidizing or reducing agents,[34] a great deal of research has gone into the study of this material and its derivatives.[31, 35, 36] PP is a typical conjugated polymer with excellent mechanical properties and thermal and thermooxidative stability. PP is used as a coating material in the packaging industry to protect integrated circuits from breakage, humidity, and corrosion. Other interesting and important properties of PPs include liquid crystallinity[37] and photoluminescence and electroluminescence.[38] PPs exhibit a rod-like architecture that differentiates them from flexible polymers.[39] Unfortunately, PPs are insoluble in many organic solvents, and this limits their processability. Therefore, the attachment of conformationally mobile alkyl side chains to the backbone has been important as it has allowed the controlled synthesis of soluble and processable PPs with high molecular weights. Due to the length of the main chain and the flexibility of the side chains, such molecules have been named as "hairy-rod" polymers.[40] Current methodologies for the direct synthesis of derivatized PPs are mainly based on Ni- and Pd-mediated cross-coupling reactions, due to their preservation of regiochemistry and nearly quantitative yields.[28, 31, 38]

Among the variety of conjugated polymers the other most thoroughly investigated series are PPVs.[41, 42] PPV was the first conjugated polymer to show electroluminescence. Since the first report of polymeric light-emitting diodes (PLEDs) based on PPVs,[43] PPV and its derivatives are still the leading candidates and are important π-conjugated polymers that exhibit interesting properties such as electroluminescence, liquid crystallinity, high third-order non-linearity, good thermal and chemical stability and excellent mechanical properties. However, PPVs are also almost insoluble in many organic solvents as their main chain is a rigid structure. To enhance the solubility and subsequent processability for various applications, it is beneficial to introduce side chains to the main chain structures. The grafted side-chains play an important role not only in solubility, but also in the order of molecular self-assembly, optical and electronical properties of optoelectronic materials. Well-defined macromolecular architectures have been regarded as a promising way for the formation of interesting materials and by combining stiff, insoluble, rod-like polymers such as PPP or PPV with a soft coil (e.g. PSt or PCL), it is possible to form new polymers with novel and interesting properties.

The synthetic strategies for the preparation of soluble and processable PPs and PPVs with complex structures and good optoelectronic properties by combination of controlled polymerization methods with metal-catalyzed cross-coupling reactions will be described in the following section.

AA/BB- Approach

R₂OB—C⟨⟩C—BOHR₂ + X—C⟨⟩C—X →(Pd / Na₂CO₃ (aq) / solvent)→ [C⟨⟩C—C⟨⟩C]ₙ

R= H, Alkyl
AA-Monomer

X= Br (X= I,TfO)
BB-Monomer

AB-Approach

R₂OB—C⟨⟩C—X →(Pd)→ [C⟨⟩C]ₙ

AB-Monomer

Scheme 6. Suzuki polycondensation (SPC).

3.1.   INITIATORS

Following the already anounced aim, the first step in our synthetic strategy for the preparation of PPs and PPVs was the design of initiators for different controlled polymerization techniques. Initiators should have two different functionalities that are active in different processes without disturbing each other. Scheme 7 shows the synthetic design on this purpose.
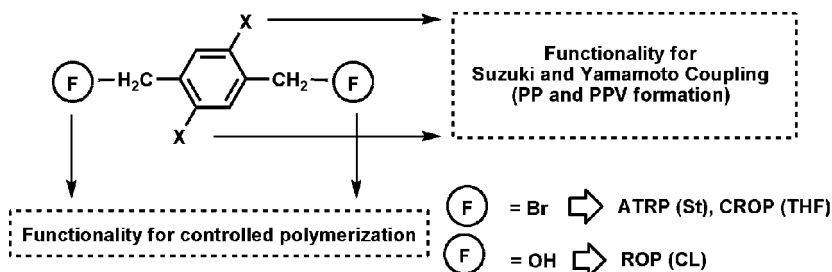
Scheme 7. Synthetic design of initiators.

They are mono- or bi-functional initiators with low molecular weights. Aliphatic –CH₂Br groups were active in the polymerization of St by ATRP technique or polymerization of THF by cationic ring opening polymerization (CROP), whereas –CH₂OH groups were the active sites for ROP of ε-caprolactone (CL) in conjunction with Sn(Oct)₂ as catalyst.[44] Additional to these active sites, initiators also contain aromatic bromine or boronate functionalities which are both inactive sites for controlled polymerizations, but useful in Yamamoto or Suzuki type couplings/polycondensations for the formation of PPs and PPVs.

The synthetic path is presented in Scheme 8 and our synthesized initiators are summarized in Chart 1.
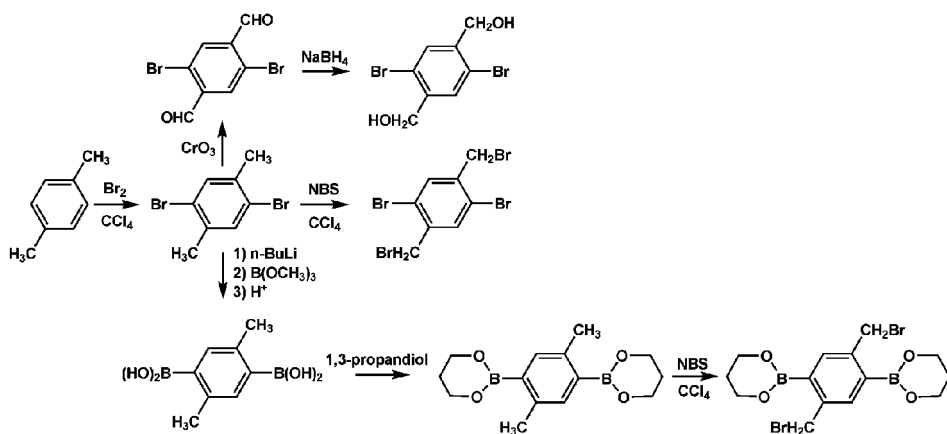
Scheme 8. Synthesis of bifunctional initiators for ATRP, CROP and ROP.
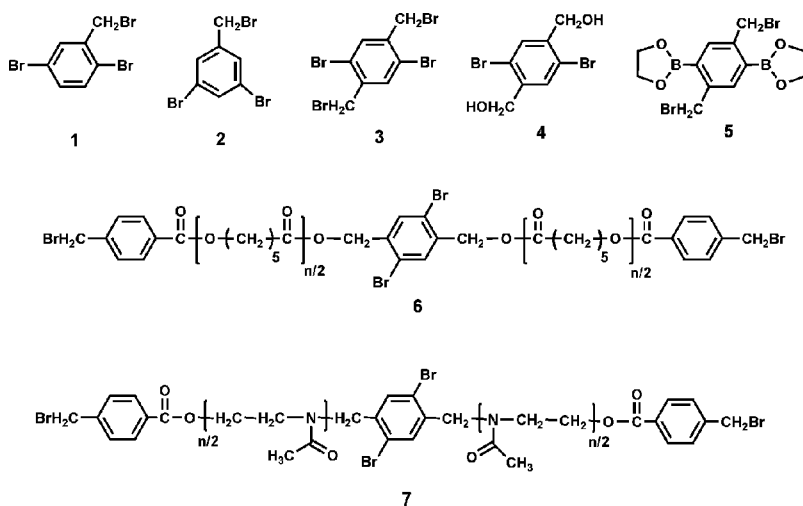
Chart 1. Synthesized initiators.

If a "polymer chain" holds a functional group that is active for a polymerization technique, then it can be used as a "macroinitiator". The transformation approach is a helpful method in polymer synthesis allowing several combinations of monomers.[45] Transformation reactions involve sequentially combined polymerization mechanisms. First, monomer 1 is polymerized by a mechanism 'A' by using a functional initiator or terminator yielding a polymer with a functional group F, which can initiate another polymerization by a different mechanism

'B'. The macroinitiators **6** and **7** in Chart 1 were synthesized in two steps. In the case of **6**, bifunctional initiator **4** was first used in the polymerization of CL,[44] then the macromolecule having hydroxyl end groups at both sides was esterified with proper low molecular weight compound[46] to introduce –CH$_2$Br end groups as the active sites for ATRP.

3.2. SYNTHESIS OF MACROMONOMERS

As stated earlier, macromonomers have been widely used as building blocks for the synthesis of various polymers and macromolecular architectures. They can be synthesized by termination method, initiation method or by transformation of any functional end-group.

In our strategy, we synthesized different types of new well-defined macro-monomers, which are summarized in Chart 2, using the initiators presented in Section 3.1. Scheme 9 shows the synthetic path for the macromonomers. Compounds containing benzylbromide groups initiated the polymerization of styrene under ATRP conditions[47, 48] or were used in CROP of cyclic monomers such as tetrahydrofuran (THF),[49] and 2-methyl-2-oxazoline (MeOx).[44] Compound **4**, 2,5-dibromo-1,4-di(hydroxymethyl)benzene was used in ROP of ε-CL.[44]
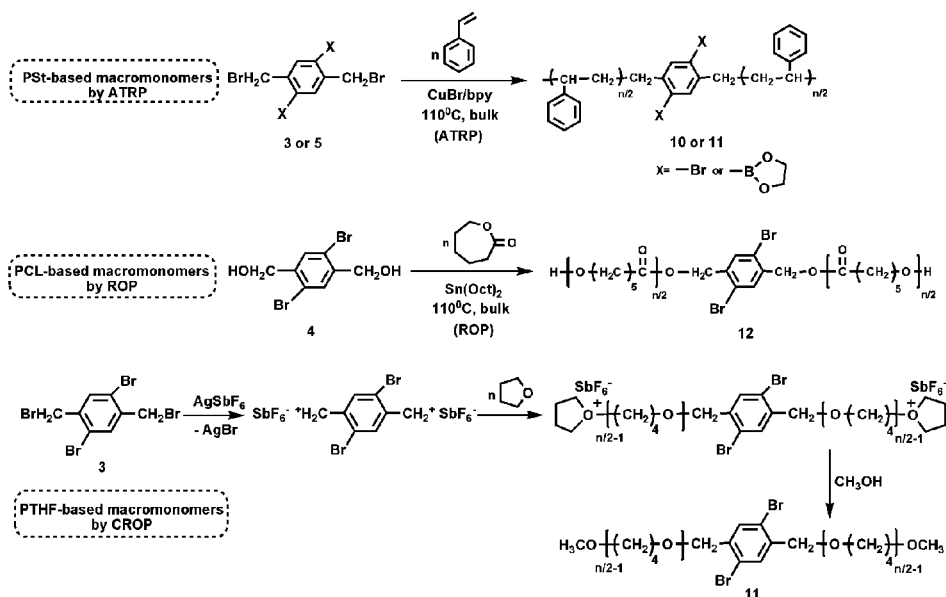
Scheme 9. Synthetic pathway for the synthesis of macromonomers.

In the case of ε-CL, the end groups of the macromonomers were –CH$_2$OH groups due to the nature of ROP process. The subsequent reaction of these hydroxyl groups with proper compounds yielded macroinitiators for ATRP and as a result block-copolymer macromonomers with more complex structures, but still with controlled molecular weights and polydispersities (such as Mn = 5,200 and PD = 1.07) were obtained.[46, 50] Macromonomers **14** and **15** (Chart 2) were synthesized in this sense by combining different polymerization modes in the frame of transformation approach.

As these polymers were intended to be used in further reactions, our efforts were driven to obtain low molecular weights and polydispersities with convenient yields. The molecular weights of the macromonomers were between 1,500–5,500 g/mol and the polydispersities were in the range of 1.07–1.3. The GPC traces were unimodal and narrow revealing that no side reactions took place. The calculated theoretical molecular weights fit very well with the GPC values. Furthermore, due to the low molecular weights, an evaluation from ^{1}H-NMR analysis was also possible.[51] (Mn = 3,800 for **10** and Mn = 4,700 for **13**, with PD = 1.2–1.3). It should be noted that all the macromonomers still preserve the necessary functionalities for Yamamoto and Suzuki type couplings, hence PP and PPV formation.
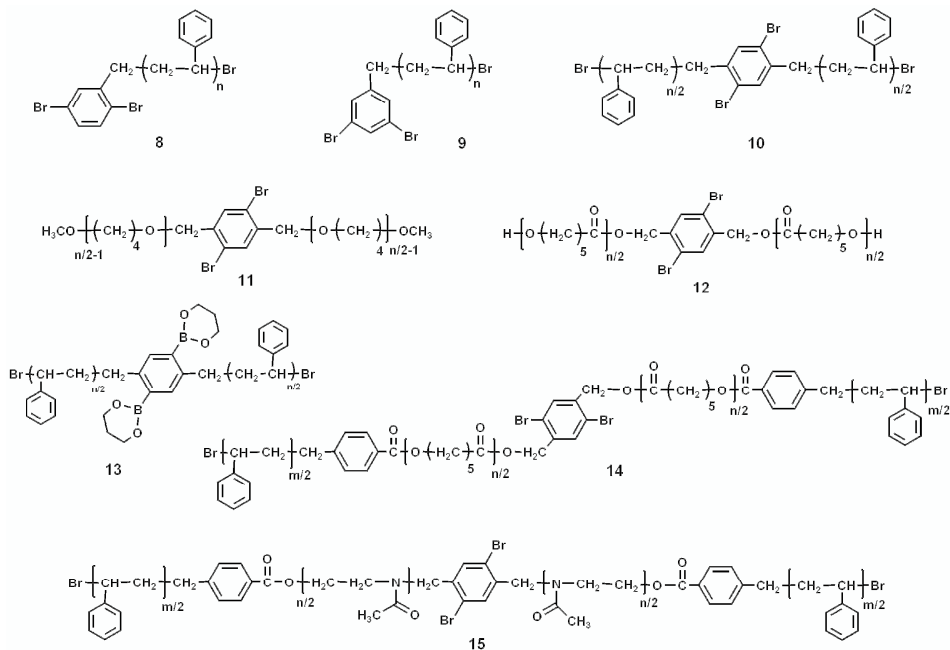
Chart 2. Synthesized macromonomers.

PPs with macromolecular side chains (PSt, PCL or PTHF)

Where ∿∿∿ is PTHF or PCL
ᗯᗯᗯ is PSt

16   17   18 (PTHF)
19 (PCL)
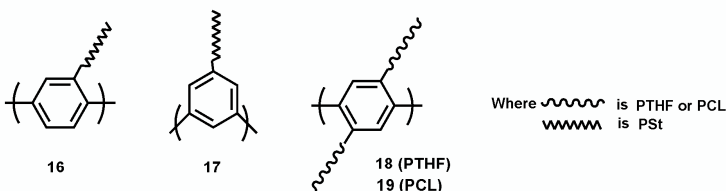
PPs with alternating macromolecular side chains

20   21

Where ᗯᗯᗯ is PSt

Where ∿∿∿ is PSt (22), PTHF (23)
PCL (24)
PCL-b-PSt (25)

26

Where ∿∿∿ is PTHF
ᗯᗯᗯ is PSt
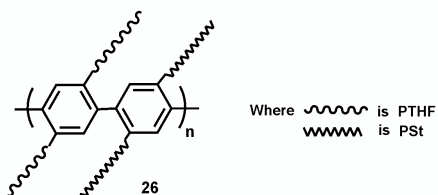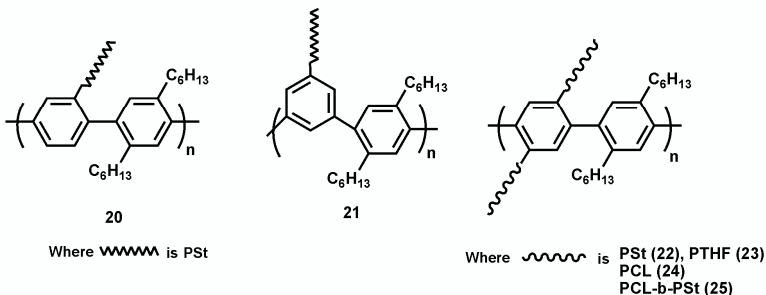
Segmented PPs with PSt and PCL side chains

27   28

Where ∿∿∿ is PCL
ᗯᗯᗯ is PSt
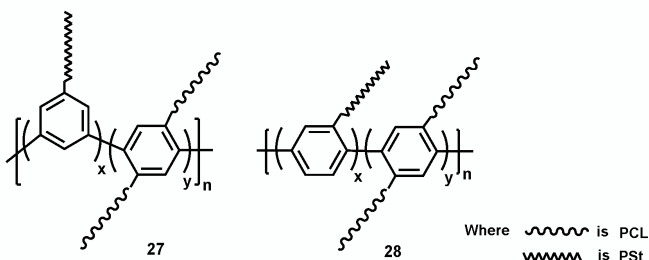
Chart 3. Synthesized PPs with complex structures.

3.3. SYNTHESIS OF PPS WITH WELL-DEFINED MACROMOLECULAR SIDE CHAINS

Aforementioned synthesized macromonomers were used in preparation of PPs bearing well-defined polymeric side-chains with complex structures and

architectures. Macromonomers were either homopolymerized or copolymerized by Yamamoto or Suzuki polycondensation reactions. The homopolymerization of macromonomers by Yamamoto method yielded comb-like polymers having regularly adjusted densed side-chains along the backbone. When macromonomers were copolymerized with another macromonomer, PPs having a random structure were formed. In the case of Suzuki polycondensation, copolymerization of macromonomers with a low molecular weight comonomer afforded alternating graft copolymers with loosely distributed side-chains, whereas copolymerization with different macromonomers resulted PPs with completely perfect alternating architectures. These polymers are referred as "*hairy rod molecules*" which is an important concept to overcome the limitations of a rigid, rod-like polymer.[40] Some examples of synthesized PP derivatives are shown in Chart 3 and are summarized in Table 1.

3.3.1. PPs by Homopolymerization of the Macromonomers

The synthetic pathway for the preparation of comb-like polymers (**16** and **17**) is presented in Scheme 10. PPs (**18** and **19**, in Chart 3) that have two side chains connected at the same benzene ring were also obtained in the same way from the corresponding macromonomers (**11** and **12** in Chart 2). Some details about the structure, molecular weight, polydispersity and some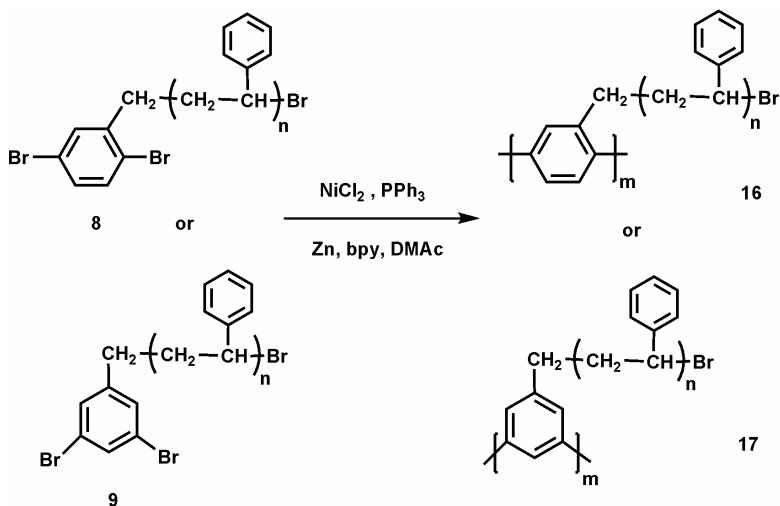 thermal characteristics are included in Table 1. The polydispersities are not so high taking into account that polycondensation is not a controlled method. The low molecular weights for **16** and **17** can be due to steric hindrances or to the self-termination of Ni-catalyzed polycondensation, most likely debromination.

Scheme 10. Synthesis of comb-like polymers by Yamamoto polycondensation.

Figure 1 shows the UV absorption spectra of macromonomers and corresponding PPs registered in dichloromethane solutions of the same concentrations. The spectrum reveals that absorptions of PPs differ from those of the starting macromonomers. The amplified absorption peaks are in the ranges of 225–230 and 252–257 nm, the latter being attributed to the presence of the phenylene rings in the main chain, indicating the formation of PPs.
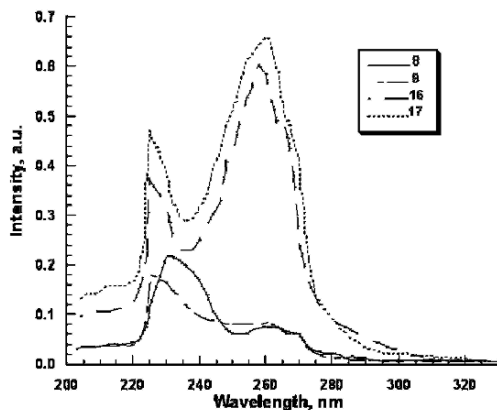
Figure 1. UV spectra of PPs 16 and 17 and the starting macromonomers.

Thermal behaviours of all polymers were investigated by differential scanning calorimetry (DSC) and thermogravimetric analysis (TGA). As can be noticed from Table 1, no glass transition temperatures (Tg) were determined for the rigid-rod main chains of PPs (**16–19**), which is a well known phenomenon for such kind of polymers. Only the thermal characteristics of the side chains such as melting points (T_m) of PTHF and PCL or Tg of PSt were observed in DSC measurements. The values depend on the lengths of the main chains and also those of the side chains. All the PPs showed a good thermal stability if the initial degradation temperatures (IDT) or the temperatures for which the weight loss is 10% (T_{w10}) are taken into consideration. Morphologies of the polymers were also examined by atomic force microscopy (AFM) in order to understand the architecture–property relations. Figure 2 shows the AFM pictures of macromonomer **12** (a) and the corresponding PP **19** (b) obtained by Yamamoto polycondensation. PP **19** with PCL side chains showed a layered morphology in thin films on hydroxylated SiO_2 substrates.[50] The layered structure was more regular compared to macromonomer **12**, and different microstructures were observed in different layers.

                    (a)   **(b)**   **(c)**

Figure 2. AFM pictures of macromonomer **12** and the corresponding PP **19** **(a)** AFM height picture of thin film of macromonomer **12** on UV-ozone-treated SiO$_2$ substrates. **(b)** AFM height picture of 5 × 5 μm area of a 34 nm thick PP **19** polymer film after melting (at 75°C, 1 h) and recrystallization (at 30°C). **(c)** Variation of height along a 5 μm horizontal distance (for (b)).

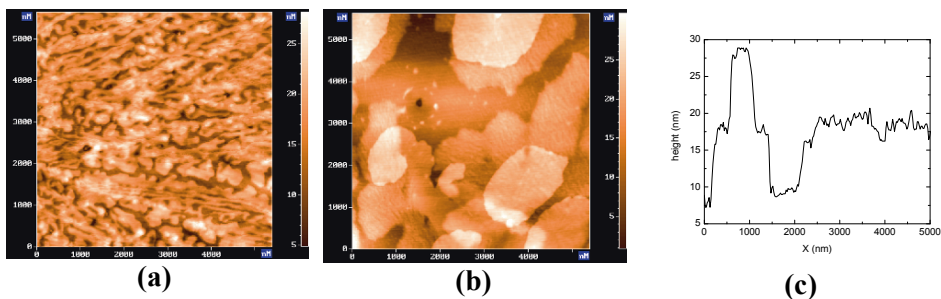The strong interactions of –OH end-groups of PCL side blocks with the hydroxylated SiO$_2$ substrate and the recrystallization of the PCL side groups induces the planarity of the phenyl rings in the backbone and a stable layered morphology is formed in thin films. From Figure 2b it can be seen that there are three different layers; layer 1 (bottom), layer 2 (middle) and layer 3 (top). Layers 1 and 3 showed relatively smooth microstructures while rough features within layer 2 were observed. This alternation of smooth and rough microstructures wihin the layers depend on whether the layer is finished with PCL side-chains (rough microstructure) or with the rigid backbone of PP (smooth microstructure) and it is expected to continue as the film gets thicker.

3.3.2.   *PPs by Copolymerization of the Macromonomers*

We also synthesized different PPs of perfectly or randomly alternating constitutions by using Suzuki or Yamamoto polycondensation methods (Chart 3, Table 1). Generally, we combined macromonomers containing different side chains in order to synthesize materials of different architectures, nature and properties. PP **26** containing as side chains well-defined PTHF and PSt in a perfectly alternating manner was synthesized by Suzuki polycondensation.[49] (Scheme 11). When thermal characteristics of this polymer were investigated, both, T$_m$ of PTHF and T_g of PSt side chains were not detected in DSC traces. The absence of the T$_m$ of PTHF side chains can be explained by the loss of their crystallinity as a result of alternation with PSt side chains. The absence of the T_g of PSt side chains can be a consequence of their inclusion into the PTHF ones, leading to a decrease in the mobility.
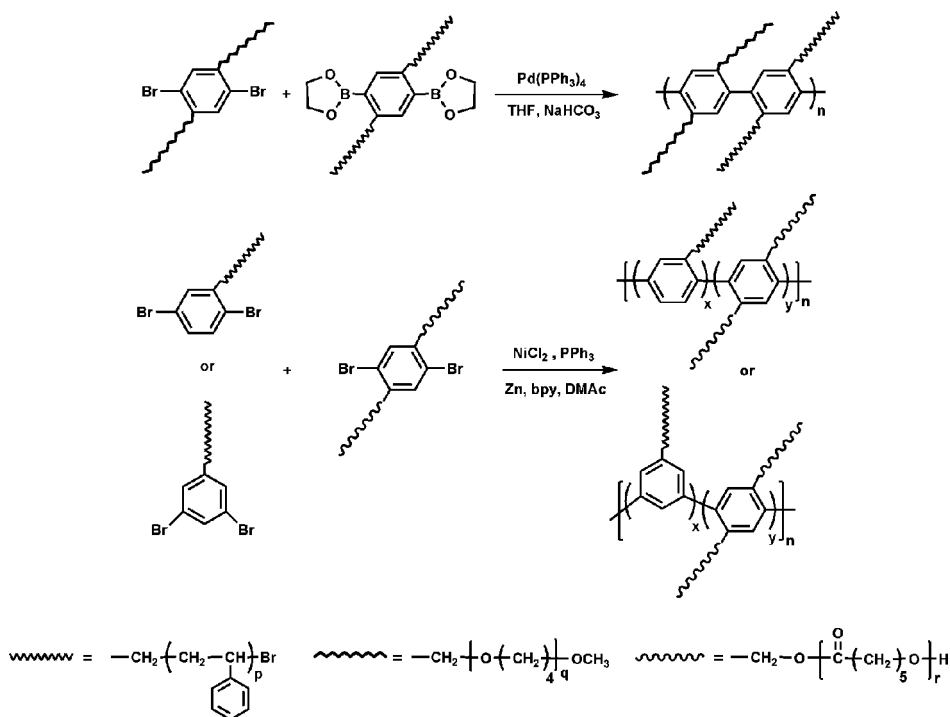
Scheme 11. Alternating PPs by Suzuki or Yamamoto polycondensation.

Other alternating graft copolymers (a polymeric side-chain alternating with a low molar mass substituent, hexyl) presented in Chart 3 were obtained also by Suzuki polycondensation of the macromonomers **8**–**10** and **14** (Chart 2) with 2,5-dihexylbenzene-1,4-diboronic acid.[52] Mn values for **21**–**25** ranged between 20,000 and 628,000 g/mol and the polydispersities were in the range of 2.76–4.7 in the case of samples **20**–**22** that bear PSt as polymeric side chains. This attitude could be assigned to the differences in the polar nature of hydrophobic side chains and the high polarity of the Suzuki reaction medium. In the case of copolymers **23** and **24** PD was 1.71. PP **25** containing alternating PCL-*b*-PSt side-chains was also prepared.[46]

Yamamoto polycondensation of macromonomers containing hydrophobic PSt side-chains (**8** or **9**) with macromonomer **12** having hydrophilic PCL side-chains afforded amphiphilic random PPs (**27** and **28**).[52] feed ratio of the two macromonomers was 1:1. The percentage of the PSt side chains, calculated from ^{1}H-NMR spectra in the final PPs **27** and **28**, was 49.2% and 42.1%, respectively. PP **27** has a more regular structure because of the structure of macromonomer **9** as the two aromatic bromine functions have equal reactivity because of their substitution position in phenyl ring. For macromonomer **8**, the reactivity of these functions is different. The substitution positions of PSt

side-chains in both PPs **27** and **28** also leads to different steric hindrance which affect their characteristics. The GPC traces of these polymers were symmetrical but broader and were shifted to higher molecular weights compared to starting materials as shown in Figure 3.
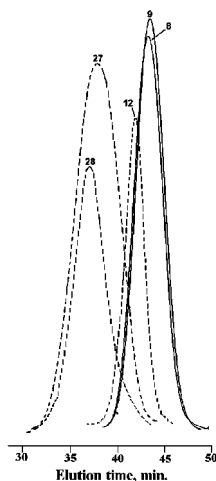
Figure 3. GPC traces of macromonomers **8**, **9**, **12** and PPs **27** and **28**.

Thermal behaviors of the polymers were followed by DSC and TGA measurements. When the data for PPs **27** and **28** from these measurements were taken into account and compared, it was obvious that the thermal characteristics of the polymers were strongly influenced by the steric effects due to the substitutions of the phenyl ring. For PP **27**, it is possible to detect both mp and T_g by DSC as PCL and PSt side chains have different positions. In the case of PP **28** the mp of the PCL side chains was apparent ($T_m = 55°C$) while the T_g of PSt side-chains was missing. The absence of the T_g of PSt chains was attributed to restriction of their molecular motions by the crystalline regions. For a better understanding of this thermal behavior model molecule for polymer fragments of PP **28** was obtained by molecular mechanics (mm+) after energy minimization and three dimensional ball-and-stick model is given in Figure 4.

The polymers **27** and **28** have good solubility in common organic solvents similar to the starting materials, thus spin-coated thin-films were prepared to observe their morphologies by AFM measurements (Figure 5). PPs containing both PSt and PCL side chains, **27** and **28**, showed microphase separated morphology after annealing. A 40 nm thick film of polymer **28** showed some layering after spin coating on hydroxylated surface and after annealing this film at 75°C (above T_m of PCL and the expected T_g of PSt) for 45 min a microphase separated morphology was observed as shown Figure 5b. The AFM picture

points out four alternating layers of PCL and PSt, having PCL on the substrate as the –OH end-groups prefer hydroxylated surface; and PSt on top due to its lower surface energy. Layered morphology was very stable in thin films so that even after annealing a 20 nm thick film at 160°C for 1 h, layers still could be observed. This also indicates the strong interaction between –OH end groups of PCL and the substrate. Polymer **27** also showed similar layered morphology in thin films (PSt layer on top). Figure 5a shows the phase image of a 20 nm (two periods) thick film on hydroxylated substrate after annealing at 160°C for 1 h. A variance could be observed between top (PSt) and underlying (PCL) layers showing a significant difference in their viscoelasticity.
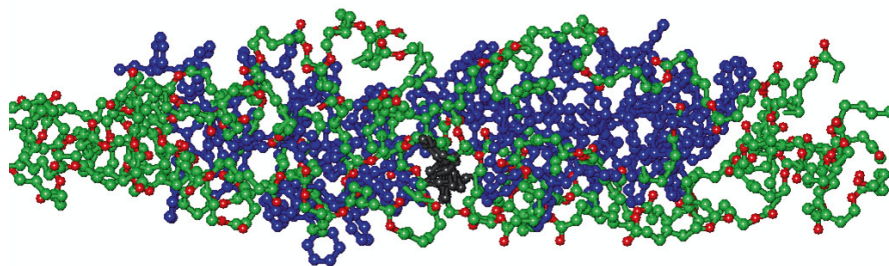
Figure 4. Three-dimensional ball-and-stick model of PP **28** (frontal image) (black: PPP main chain, blue: PSt segments, green: PCL segments).

(a)   (b)
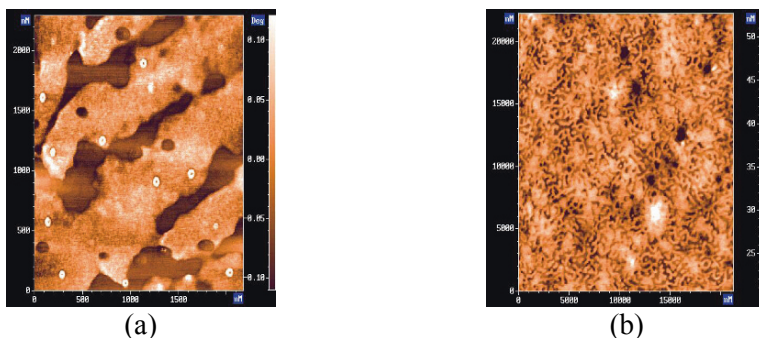
Figure 5. AFM images of PPs **27** and **28** **(a)** Phase image of a 20-nm thick film of PP **27** on a hydroxylated SiO_2 surface after annealing at 160°C for 1 h. **(b)** Height image of a 40-nm-thick film of PP **28** on a hydroxylated SiO_2 surface after annealing at 75°C for 45 min.

Various chemical structures of POx and PCL substituted PPs have also been synthesized.[53] The Yamamoto polycondensation of POx-based macromonomers with a PCL one facilitated pps with POx and PCL side chains in a random manner. Morphologies of the polymers were investigated by AFM. Spin-coated thin films of PPs showed morphological transitions after annealing at temperatures

above T_m and T_g of the components. The effect of the side-chain structures and the architecture on the resulting morphology was also examined. PPs showed layered morphologies in thin films and the structure of the side-chains was important in determining the orientations of the layers. PPs with statistically distributed POx and PCL side chains showed layers perpendicular to the underlying substrate due to the interactions of the blocks with each other and the tendency of the both blocks to interact with the hydrophilic substrate. Introduction of PSt blocks to PCL chain caused microphase separation between PCL-*b*-PSt and POx chains. The tendency of the hydrophilic POx for the substrate and hydrophobic PSt for the opposite direction resulted in a layered morphology where layers were parallel to the substrate. As a result, it is clear that the substitution of functional side groups or polymeric chains of different nature to PPs not only improves the solubility, but also gives them ability to self-organize into nanoscale structures. The self-organization and the resulting morphology are also important for their optoelectronic properties.

3.4. SYNTHESIS OF PPVS WITH PST OR PCL-BASED MACROMOLECULAR SIDE CHAINS

For the preparation of PPV derivatives[54] with polymeric side-chains, a strategy which is very similar to the synthesis of PPs with complex structures[55] was applied. First, ATRP of St and ROP of ε-CL, in the presence of proper initiators (Chart 2, **1** and **2**), provided well-defined low molecular weight polymers with dibromobenzene moieties at the end or in the middle of the chain. One of the current methodologies for the synthesis of PPVs is the Wittig polycondensation. In Wittig reaction, aldehyde functional compounds are reacted with triphenyl phosphonium salts in the presence of potassium *tert*-butoxide. Hence, well-defined polymers with aromatic bromine functions were further modified to introduce aldehyde groups. The Suzuki coupling of these bromobenzene moieties with 4-formylphenyl boronic acid, macromonomers having 4,4′-dicarbaldehyde terphenyl moieties were obtained. In the last step, PPVs with PSt or PCL chains as lateral substituents were synthesized by following a Wittig polycondensation in combination with bis-(triphenylphosphonium) salts. Scheme 12 presents the synthetic pathway for the final PPV derivatives. Colored PPV derivatives with good solubility in common organic solvents and also good film forming properties were obtained. The solutions of the polymers also show blue or green fluorescence under daylight or UV light. This behaviour is interesting as the composition of these polymers is 85–90% PCL or PSt. It should be noted that when PPs with macromolecular side chains were obtained starting from such macromonomers, they usually resulted in white polymers, similar to the starting materials. Some characteristics of the PPVs are shown in Table 2.

TABLE 1. Characteristics of synthesized PPs.

Macromon. /PP	Side chains	Polycond. type	$M_{n,GPC}$	PDI	Characteristics	Ref.
11 **/PP 18**	PTHF	Yamamoto	21,150	1.82	M_p PTHF = 31°C; IDT = 311°C T_{w10} = 400°C	[49, 51]
12 **/PP 19**	PCL	Yamamoto	27,150	1.41	M_p PCL = 60°C; IDT = 286°C T_{w10} = 335°C	[44, 50]
8 **/PP 16**	PSt	Yamamoto	17,300	1.5	T_g, PSt = 92°C	[52]
9 **/PP 17**	PSt	Yamamoto	16,400	1.7	T_g, PSt = 76°C	[52]
11+13 **/PP 26**	PTHF/ PSt	Suzuki	40,850	1.67	M_p,PCL: nd, T_g,PSt: nd IDT = 230°C; T_{w10} = 357°C	[49, 51]
8+12 **/PP 28**	PSt/ PCL	Yamamoto	23,400	1.35	M_p, PCL = 55°C; T_g,PSt: nd Layered morphology in thin films	[52]
9+12 **/PP 27**	PSt/ PCL	Yamamoto	19,700	1.5	M_p,PCL = 58°C; T_g, PSt = 68°C; Microphase separation; Layered morphology in thin films	[52]

M_p – melting point; T_g – glass transition temperature; IDT– initial degradation temperature; T_{w10} – temperature for which the weight loss is 10%; nd – not detected.

Thermal behaviors of the polymers were followed by DSC and TGA measurements. In DSC traces, a decrease in Mp of PCL was observed with the increasing complexity of polymers. The PCL chains are linked to a rigid conjugated chain at certain distances so the lengths of ordering and consequently the melting points are decreased. The Br substituents that alternate with PCL chains have also influence on this characteristic.
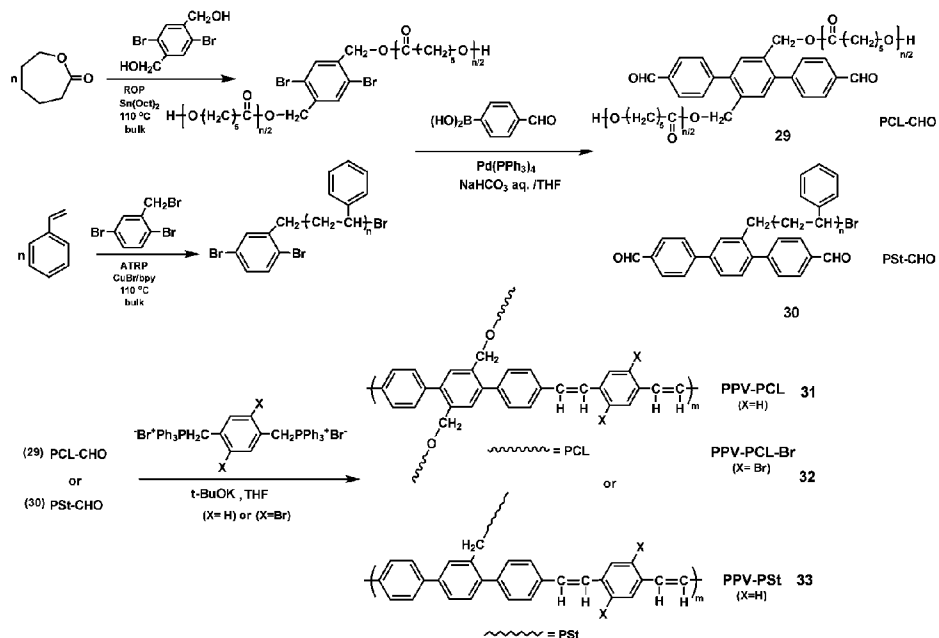
Scheme 12. Synthesis of PPVs with macromolecular side chains.

TABLE 2. Some characteristics of starting macromonomers and the final PPVs.

Polymer	Color	$M_{n,GPC}$	PDI	Mp[a] (°C)	Tg[a] (°C)	IDT[b] (°C)	T_{w10}[c] (°C)
29	White	3,720	1.36	47	–	318	378
31	Bright yellow	28,320	2.59	41	–	302	390
32	Dark yellow	320,00	2.31	38.5	–	231	262
30	White	2,480	1.34	–	99	250	377
33	Bright green	18,600	3.05	–	120	300	405

[a] From DSC analysis.

[b] Initial degradation temperature(IDT).

[c] The temperature at which the weight loss is 10%.

In the case of PSt-based PPVs **30** and **33**, T_g of PSt chains are slightly shifted to higher values as the complexity of the molecule increases, which can be a consequence of the decrease in mobility of PSt segments. From TGA measurements, for both series, it can be observed that the IDT and T_{w10} increases as

the complexity of the molecule increase. The highest values were registered for PPV **33** with PSt side chains whereas the lowest values were obtained for PPV **32** with PCL side chains that alternate with Br substituents; the loss of which can be expected at lower temperatures. Besides confirming the proposed structures, ^{1}H-NMR analysis of the PPVs also give information about *cis* and *trans* conformations of the vinylene bonds. In the case of **31**, 50% of the double bonds are in a *cis* conformation, whereas in the case of **32** the percentage of double bonds in *cis* conformation is 75. This increase could be attributed to the bulky bromine atoms as side groups near to PCL ones. For a better understanding of *cis* and *trans* conformations of PPV main chain as well as the distrubition of the PCL side chains, model molecules of polymer fragments were obtained by molecular mechanics (MM+).

The three-dimensional ball and stick models obtained after energy minimization are shownn in Figure 6. In both cases, *cis* and *trans* conformations, the molecule structure is of hairy-rod type with a pronounced cylindrical symmetry. In the case of *cis* conformation there is a slight deviation from this symmetry. Such cylindrical rods could potentially be used for construction in nanometer scale due to their high bending moduli. The absorption and emission spectra of all polymers were investigated in THF and CHCl$_3$ solutions and as films. In the UV spectra of polymers, a new maxima assigned to the conjugated chain is observed and also the absorption range is larger and red-shifted when compared with the starting materials, as shown in Figure 7. A clear bathochromic shift of the λ max is observed for all polymers with respect to macromonomers due to the extension of the conjugated chain. The PL spectra of all polymer films showed a red shift and some broadening of the emission bands in comparison to their solution spectra which can be due to the intermolecular interactions in the films. The PL spectra of PPVs are shown in Figure 8 and absorption and emission wavelengths are listed in Table 3. Absolute quantum yields (as bulk, thin films and solutions)[56] are given in Table 4.
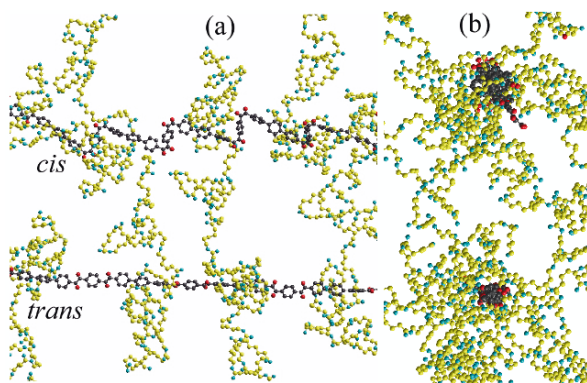
Figure 6. Three-dimensional ball and stick models of **31** in *cis* and *trans* conformations (**a**) top (**b**) frontal.
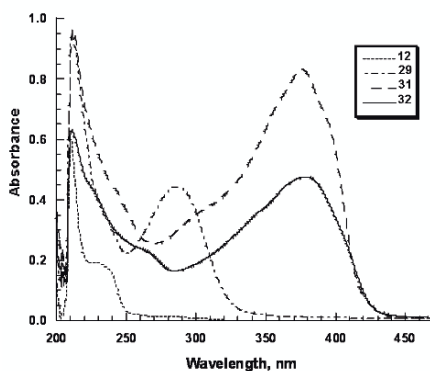
Figure 7. UV spectra of PCL polymers (in THF solutions, 0.04 g/L) [**1**(PCL-Br); **3**(PCL-CHO); **7**(PPV-PCL); **8**(PPV-PCL-Br)].
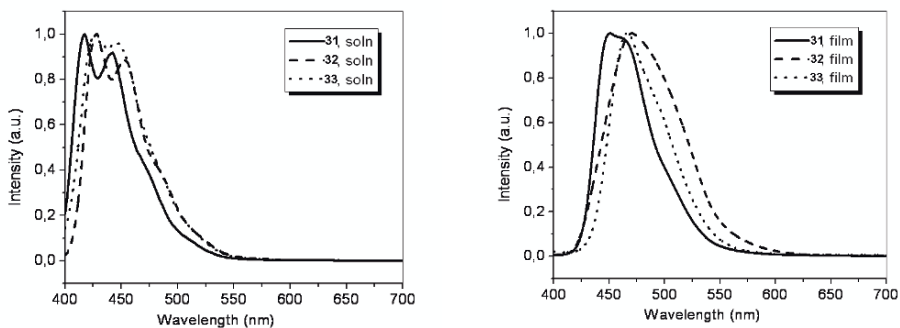
Figure 8. Photoluminescence spectra for **31–33** in chloroform (**a**) and as solid films cast on quartz plates (**b**) [7(PPV-PCL)(**31**); 8(PPV-PCL-Br)(**32**); 9(PPV-PSt)(**33**)].

TABLE 3. Photophysical properties of **31–33** in CHCl₃ solutions and in film.

Polymer	λ_{max}^{Abs} (nm)[a]	λ_{max}^{Abs} (nm)[b]	λ_{max}^{PL} (nm)[a]	λ_{max}^{PL} (nm)[b]
31	373	380	418	451
32	373	376	428	470
33	382	390	428	467

[a] Chloroform solution.

[b] Neat film on quartz.

TABLE 4. Absolute quantum yields in solution, thin films and bulk polymer materials.

Compound	Bulk	Inkjet printed film	Spin coated film	Solution
PPV-PCL (31)	0.12	0.20	0.25	0.56
PPV-PCL-Br (32)	0.08	0.10	0.09	0.34
PPV-PSt (33)	0.43	0.48	0.52	0.89

4. Conclusions

Soluble and processable PPs possessing randomly or completely and perfectly alternating side chain polymers with controlled chain length and complex macromolecular architectures were prepared. Also PPVs bearing macromolecular side chains with desired photophysical properties as well as good film forming properties were also synthesized. The synthetic strategy introduced by us opens new pathways for the design of materials with different and interesting properties by varying the composition and the architecture of the polymers. By mechanistic transformation approach, macromonomer technique and the appropriate combination of different polymerization routes, it is possible to combine conjugated polymers with conventional polymers as illustrated by the examples presented in this chapter.

References

[1]   Berlin, A., Zotti, G. (2000) Macromol. Rapid Commun., 21, 301.
[2]   Li, X.-G., Zhou, H.-J., Huang, M.-R., Zhu, M.-F., Chen, Y.-M. (2004) J. Polym. Sci. Part A: Polym. Chem., 42, 3380.
[3]   Guijun, Y., Boqiu, W., Yuping, D., Maofeng, Z., Zhaohui, Y., Qiaoling, Y., Yip, L. J. W., Benzhong, T. J. (2004) J. Polym. Sci. Part A: Polym. Chem., 42, 3229.
[4]   Yagci, Y., Nuyken, O., Graubner, V. (2005) "Telechelic Polymers", in: Encyclopedia of Polymer Science and Technology, 3rd edn.; Kroschwitz, J. I. (Ed.); Wiley, New York, Vol. 12, pp. 57–130.
[5]   Percec, V., Pugh, C., Nuyken, O., Pask, S. D. (1989) Comprehensive Polymer Science; Allen, G., Bevington, J. C. (Eds.); Pergamon, Oxford, VI, Ch. 6.
[6]   Goethals, E. J. (Ed.) (1989) Telechelic Polymers: Synthesis and Applications; CRC Press, Boca Raton, FL.
[7]   Hadjichristidis, N., Pitsikalis, M., Iatrou, H., Pispas, S. (2003) Macromol. Rapid Commun., 24, 979.
[8]   Cristova, D., Velichkova, R., Goethals, A. J. (1997) Macromol. Rapid Commun., 18, 1067.
[9]   Fontanille, M. (1989) Comprehensive Polymer Science; Allen, G., Bevington, J. C. (Eds.); Pergamon, Oxford, Vol. III, Ch. 27.

[10] Kennedy, J. P., Ivan, B. (1992) Designed Polymers by Carbocationic Macro-
      molecular Engineering: Theory and Practice; Hanser Verlag, Munchen, p. 167.
[11] Goethals, E. J. (1986) Makromol. Chem. Macromol. Symp., 6, 53.
[12] Webster, O. W. (1993) Makromol. Chem. Macromol. Symp., 70, 75.
[13] Webster, O. W. (2000) J. Polym. Sci. Polym. Chem. Ed., 38, 2855.
[14] Brosse, J. C., Depouet, D., Epaillard, F., Soatif, J. C., Legeay, G., Dusek, K.
      (1987) Adv. Polym. Sci., 81, 167.
[15] Hillmyer, M. A.; Nguyen, S. T.; Grubbs, R. H. (1997) Macromolecules, 30, 718.
[16] Morita, T., Maughan, B. R., Bielawski, C. W., Grubbs, R. H. (2000) Macro-
      molecules, 33, 6621.
[17] Matyjaszewski, K. (Ed.) (1998) Controlled Radical Polymerization, ACS
      Symposium Series; American Chemical Society, Washington, DC, p. 685.
[18] Mishra, M. K.; Yagci, Y. (1998) Handbook of Radical Vinyl Polymerization;
      Marcel Dekker, New York, p. 233.
[19] Wang, J. S., Matyjaszewski, K. (1995) Macromolecules, 28, 7901.
[20] Kato, M., Kamigaito, M., Sawamoto, M., Higashimura, T. (1995) Macromolecules,
      28, 1721.
[21] Matyjaszewski, K., Xia, J. (2001) Chem. Rev., 101, 2921.
[22] Degee, P., Dubois, P., Jerome, R. (1997) Macromol. Chem. Phys., 198(6), 1985–
      1995.
[23] Johns, Db., Lenz, R. W., Luecke, A. (1984) "Lactones", in: Ring-Opening
      Polymerization; Ivin K. J., Saegusa, T. (Eds.); Elsevier, London, Vol. 1, p. 464.
[24] Löfgren, A., Albertsson, A. C., Dubois, P., Jerome, R. (1995) J. Macromol. Sci.
      Rev. Macromol. Chem. Phys., C35(3), 379–418.
[25] Mecerreyes, D., Jerome, R., Dubois, P. (1999) Adv. Polym. Sci., 147, 1–59.
[26] Kricheldorf, H. R., Kreiser, S. I. (1996) Macromol. Symp., 103, 85–102.
[27] Hoffman, R. V. (2004) Organic Chemistry: An Intermediate Text, 2nd edn.;
      Wiley, Hoboken, NJ, pp. 246–272.
[28] Yamamoto, T. (1992) Prog. Polym. Sci., 17, 1153.
[29] Myaura, N., Suzuki, A. (1995) Chem. Rev., 95, 2457.
[30] Suzuki, A. (1999) J. Organomet. Chem., 576, 147.
[31] Schluter, A. D., Wegner, G. (1993) Acta Polym., 44, 59.
[32] Tour, J. M. (1994) Adv. Mater. 6(3), 190–198.
[33] Schluter, A. D. (1998) "Progress", in: Handbook of Conducting Polymers;
      Skotheim, T. A., Elsenbaumer, R. L., Reynolds, J. R. (Eds.); Marcel Dekker,
      New York, p. 209.
[34] Ivory, D. M., Miller, G. G., Sowa, J. M., Shacklette, L. W., Chance, R. R.,
      Baughman, R. H. (1979) J. Chem. Phys., 71, 1506.
[35] Schluter, A. D. (2001) J. Polym. Sci. Part A: Polym Chem., 39, 1533.
[36] Gin, D. L., Conticello, V. P. (1996) Trends. Polym. Sci.,4, 217.
[37] Witteler, H., Lieser, G., Wegner, G., Schulze, M. (1993) Makromol. Chem.
      Rapid Commun., 14, 471.
[38] Grem, G., Leising, G. (1993) Synth. Met., 55, 4105.
[39] Berresheim, A. J., Muller, M., Mullen, K. (1999) Chem. Rev., 99, 1747.
[40] Lauter, U., Meyer, W. H., Wegner, G. (1997) Macromolecules, 30, 2092.
[41] Kraft, A., Grimsdale, A. C., Holmes, A. B. (1998) Angew. Chem., Int. Ed., 37, 402.

[42] Friend, R. H., Gymer, R. W., Holmes, A. B., Burroughes, J. H., Marks, R. N., Taliani, C., Bradley, D. D. C., Dos Santos, D. A., Bredas, J. L., Logdlun, M., Salaneck, W. R. (1999) Nature (Lond), 397, 121.

[43] Burroughes, J. H., Bradley, D. D. C., Brown, A. R., Marks, R. N., MacCay, K., Friend, R. H., Burn, P. L., Holmes, A. B. (1990) Nature (Lond), 347, 539.

[44] Yurteri, S., Cianga, I., Degirmenci, M., Yagci, Y. (2004) Polym. Int., 53, 1219.

[45] Yagci, Y., Tasdelen, M. (2006) Prog. Polym. Sci., 31, 1133–1170.

[46] Yurteri, S., Cianga, I., Yagci, Y. (2005) Des. Monom. Polym., 8, 61.

[47] Cianga, I., Yagci, Y. (2002) Eur. Polym. J., 38, 695–703.

[48] Cianga, I., Yagci, Y. (2001) Polym. Bull., 47, 17–24.

[49] Cianga, I., Hepuzer, Y., Yagci, Y. (2002) Polymer, 43, 2141–2149.

[50] Demirel, A. L, Yurteri, S., Cianga, I., Yagci, Y. (2005) Macromolecules, 38, 6402.

[51] Cianga, I., Hepuzer, Y., Yagci, Y. (2002) Macromol. Symp., 183(1), 145–158.

[52] Yurteri, S., Cianga, I., Demirel, A. L., Yagci, Y. (2005) J. Polym. Sci. Polym. Chem. Ed., 43, 879.

[53] Demirel, A. L., Yurteri, S., Cianga, I., Yagci, Y. (2007) J. Polym. Sci. Polym. Chem. Ed., 45, 2091.

[54] Colak, D. G., Cianga, I., Yagci, Y., Cırpan, A., Karasz, F. E. (2007) Macromolecules, 40, 5301.

[55] Cianga, I., Cianga, L., Yagci, Y. (2006) New Applications of Living/Controlled Polymerization Methods for Synthesis of Copolymers with Designed Architectures and Properties, in: New Trends in Nonionic (Co)Polymers and Hybrids; Dragan, E. S. (Ed.); Nova Science, New York, pp. 1–53.

[56] Colak, D. G., Egbe, D. A. M., Birckner, E., Yurteri, S., Cianga, I., Tekin, E., Schubert, U. S., Yagci, Y. (2009) Eur. Polym. J., 45, 940–945.

PART 2. CLICK CHEMISTRY

SYNTHESIS OF FUNCTIONALIZED ALIPHATIC POLYESTERS BY THE "CLICK" COPPER-CATALYZED ALKYNE–AZIDE CYCLOADDITION

PHILIPPE LECOMTE[*], RAPHAEL RIVA,
AND CHRISTINE JEROME
*Center for Education and Research on Macromolecules,
University of Liege, B6 Sart-Tilman, B-4000 Liege, Belgium*

Abstract: The functionalization of aliphatic polyesters by the copper-mediated azide–alkyne Huisgen's cycloaddition is very efficient under mild conditions, which prevents degradation from occurring. The implementation of this reaction requires the synthesis of aliphatic polyesters bearing pendant alkynes and azides, which can be carried out either by polycondensation or by ring-opening polymerization.

1. Introduction

Aliphatic polyesters combine the rarely met properties of biodegradability and biocompatibility, which accounts for their wide use as biomaterials and as environmentally friendly thermoplastics. Nevertheless, the lack of functional groups along the chains is a severe limitation to develop new applications. It is thus highly desirable to implement efficient processes to graft functional groups onto aliphatic polyesters in order to tailor properties such as hydrophilicity, crystallinity, biodegradation rate or bioadherence. Moreover, the presence of functional groups along the chains paves the way to their use for any coupling reaction enabling to graft drugs, targeting molecules or probes in view of biomedical applications.

Aliphatic polyesters can be synthesized either by step-growth polymerization or by chain-growth polymerization. At the one hand, step-growth polymerization relies mainly on the polycondensation of diols and diacids or on the direct polycondensation of hydroxyacids. Nevertheless, it is very difficult to synthesize

aliphatic polyesters with high molecular weights by this approach. At the other hand, chain-growth polymerization is based on the ring-opening polymerization of lactones and lactides. Many initiators/catalysts have been found to be selective enough to prevent transesterification reactions from occurring, which allows synthesizing aliphatic polyesters with predetermined and high molecular weights. The more widely used initiators are metal alkoxides (Al, Sn, Y, Ti, Ca,…) and tin octoate.

In order to graft functional groups onto aliphatic polyesters, two main routes were investigated. The first approach relies on the synthesis and the polymerization of a lactone or a dilactone substituted by a functional group. Nevertheless, this strategy suffers from several drawbacks. Firstly, several functions such as alcohol, carboxylic acid or epoxide are not tolerated by metal alkoxides. The use of protection/deprotection reactions is then unavoidable, which complicate the synthetic strategy. Secondly, the synthesis of each novel aliphatic polyesters requires the synthesis of new monomer. Thirdly, the presence of the functional substituent might modify the polymerizability of the monomer, which is a further complication.

A straightforward approach relies on the direct grafting of functional groups onto aliphatic polyesters. Vert et al.[1, 2] reported on the metallation of poly(oxepan-2-one) (PCL for poly(ε-caprolactone) by lithium diisopropylamide (LDA) into a poly(enolate), which was finally reacted with a series of electrophiles, such as carbon dioxide and benzaldehyde (Scheme 1). The use of protection/deprotection reactions is not necessary anymore because the functionalization takes place after the polymerization step. Interestingly enough, no toxic reagents are used, which is a prerequisite for the developments of applications in the biomedical field. Nevertheless, enolates are nucleophilic species prone to react with esters. Chain degradation is thus unavoidable and can only be minimized under optimized conditions. Furthermore, the functionalization efficiency is not very high because no more than 30% of the repeating units can be functionalized.
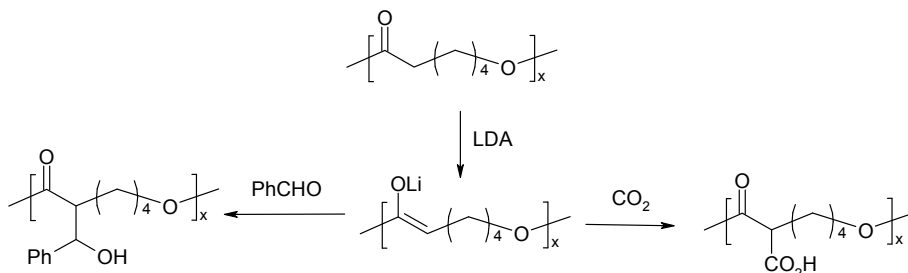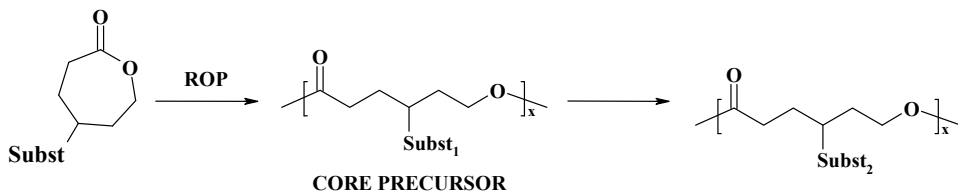

Scheme 1. Chemical functionalization of PCL by an anionic route.

In order to overcome these problems, it appears that a two-step process might be a valuable alternative (Scheme 2).[3] Thus, oxepan-2-one (εCL for ε-caprolactone) substituted by a properly selected functional group might be

polymerized. The derivatization of the first substituent into a variety of other functional groups might be carried out by any reaction known in the state of the art. A wide range of aliphatic polyesters could accordingly be made available from a single precursor.


Scheme 2. Direct chemical functionalization of PCL.

Several reactions such as Michael addition, ring-opening of epoxides, reaction of ketones and oxyamines, atom transfer radical addition, were used to implement the strategy shown in Scheme 2. Nevertheless, if some success was met, it remains highly desirable to find more efficient reactions, which tolerate many functional groups and can be carried out under mild conditions to prevent degradation from occurring.

Recently, Meldal et al.[4] and Sharpless et al.[5] reported the beneficial effect of copper(I) catalysts on the azide–alkyne Huisgen's cycloaddition. Interestingly, this reaction fulfill the requirements of a click reaction.[6] This reaction is highly efficient and regioselective, can be carried out under mild conditions and tolerates many functional groups, which avoids the use of protection/deprotection reactions. Nowadays, the copper azide–alkyne cycloaddition (CuAAC) is so popular that this reaction is many times considered as the only click reaction. The CuAAC reaction is often used in macromolecular engineering, as witnessed by several reviews recently published.[7–15] All these recent advances prompted us to investigate the efficiency of this reaction to functionalize aliphatic polyesters.

2. Functionalization of the Chain-End

The more simple and direct approach allowing functionalizing aliphatic polyesters by the CuAAC reaction is based on the derivatization of chain-ends. For instance, Li et al. reacted azide-containing sugars with α-alkynyl-PCL synthesized by ring-opening polymerization (Scheme 3).[16] Remarkably, no protection of the hydroxyl groups is required. Moreover, the CuAAC reaction is quantitative and no significant degradation of the aliphatic polyester was reported.
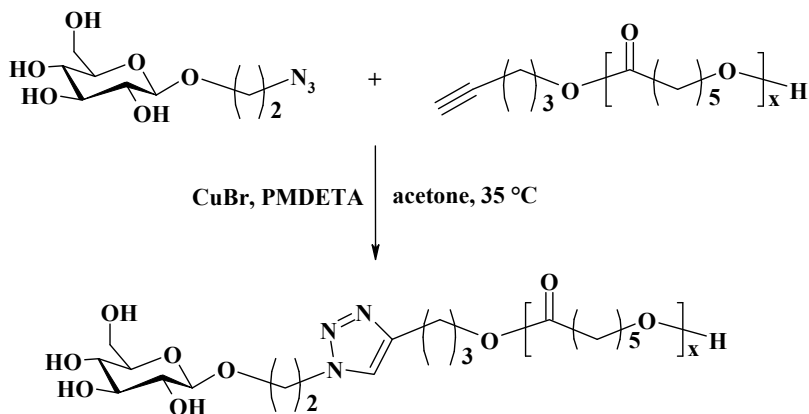
Scheme 3. Coupling of an azide-containing sugar with α-alkynyl-PCL.[16]

3. Random Functionalization

In order to increase the number of functional groups along the polyester chains, it was decided to extend the strategy shown in Scheme 2 to the CuAAC reaction, which requires the synthesis of aliphatic polyesters containing pendant alkynes or azides.

3.1. SYNTHESIS OF ALIPHATIC POLYESTERS BY RING-OPENING POLYMERIZATION

In order to prepare aliphatic polyesters by ring-opening polymerization, Emrick et al. synthesized 3-(prop-2-yn-1-yl)tetrahydro-*2H*-pyran-2-one (αAδVL for α-alkyne-δ-valerolactone) by a two step-procedure. Tetrahydro-*2H*-pyran-2-one (δVL for δ-valerolactone) was firstly reacted with LDA to obtain the corresponding enolate, which was finally reacted with 3-bromoprop-1-yne to obtain the targeted αAδVL with a yield of 74% (Scheme 4).[17] Nevertheless, the yields depend on the size of the ring. Indeed, when the reaction is carried out onto εCL rather than δVL, the yield is low (<50%), even under optimized conditions, due to the occurrence of the undesired lactone oligomerization initiated by the enolate.[18]
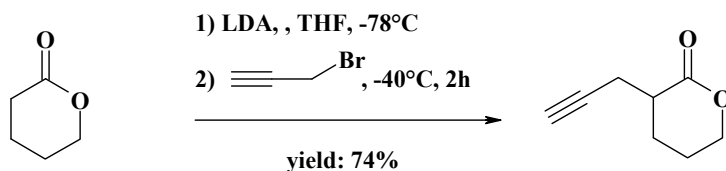
Scheme 4. Synthesis of α-alkynyl δ-valerolactone according to Emrick et al.[17]

The ring-opening hompolymerization of the αAδVL was successfully mediated by Sn(OTf)$_2$ in the presence of ethanol as reported by Emrick et al.[17] The molecular weight increased steadily with conversion and was predetermined by the monomer-to-alcohol molar ratio. The initiation was fast compared to propagation and a very low polydispersity index around 1.1 was obtained provided that the polymerization was stopped before reaching complete conversion. When the polymerization was allowed to proceed to full conversion, the polyesters displayed a higher polydispersity index (around 1.3–1.4) due to the occurrence of transesterification reactions, which competes with propagation at low monomer concentration. Last but not least, the number of pendant functional groups can be chosen at will by copolymerizing αAδVL and εCL.
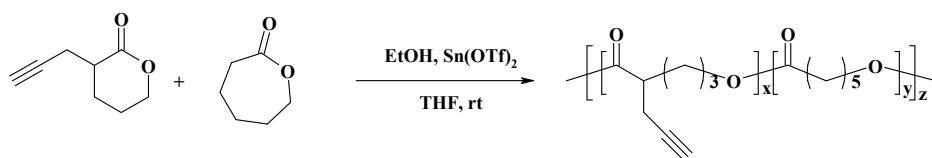
Scheme 5. Copolymerization of αAδVL and εCL according to Emrick et al.[17]

Very recently, Baker et al. reported on the synthesis of 3,6-di(prop-2-yn-1-yl)-1,4-dioxane-2,5-dione from ethyl oxoacetate by a three-step procedure shown in Scheme 6.[19] It is worth noting that the yield is quite low (15%), This monomer was homopolymerized in bulk at 130°C by using tin octoate as a catalyst and 4-tert-butylbenzylalcohol as an initiator (Scheme 7). The synthesis of statistical and block copolyesters with lactide was also reported (Scheme 7).
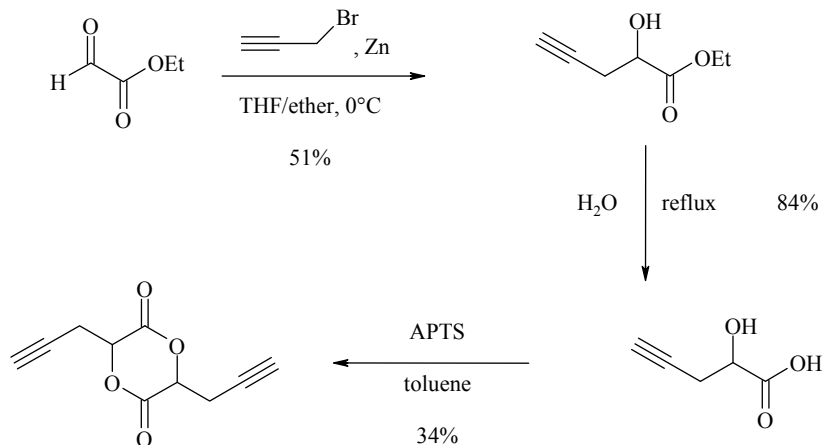
Scheme 6. Synthesis of 3,6-di(prop-2-yn-1-yl)-1,4-dioxane-2,5-dione according to Baker et al.[19]
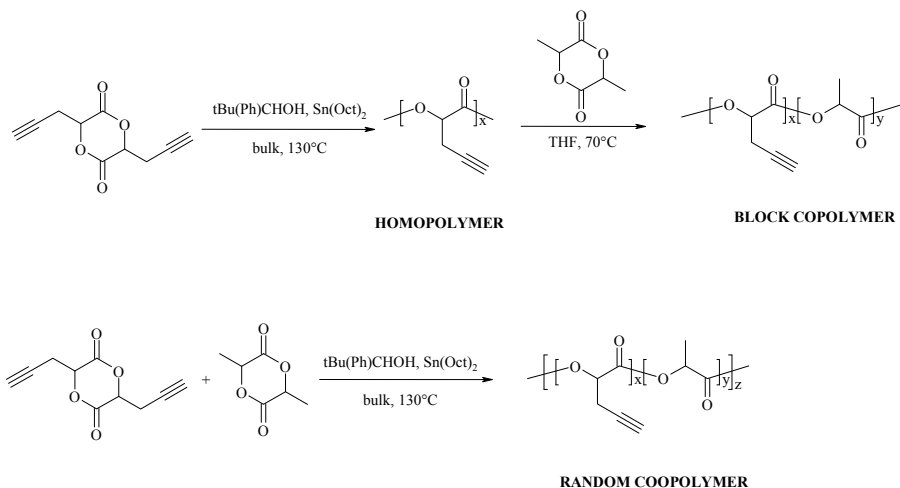
Scheme 7. Homopolymerization of 3,6-di(prop-2-yn-1-yl)-1,4-dioxane-2,5-dione according to Baker et al.[19]

Riva et al. reported on the synthesis of an azide-containing PCL by a strategy based on ring-opening polymerization.[20, 21] For this purpose, 3-chlorooxepan-2-one (αClεCL for α-chloro-ε-caprolactone) was synthesized by the Baeyer-Villiger oxidation of 2-chlorocyclohexanone and copolymerized with εCL (Scheme 8).[22] Unfortunately, aluminum isopropoxide was not efficient for the control of the polymerization for reasons which are still unclear. Nevertheless, tin(IV) alkoxides turned out to be more efficient to control the molecular weight, even though the polydispersity index was high (1.2–1.5) due to slow initiation. The statistical polymerization of a mixture of αClεCL and εCL was also reported.[22] Later on, Lee and Huang showed that the ring-opening polymerization of αClεCL can be initiated by alcohols in the presence of tin octoate.[23] The α-chloro substituents were then reacted with sodium azide with formation of the expected poly(εCL-co-αN$_3$εCL) copolymer (Scheme 8).
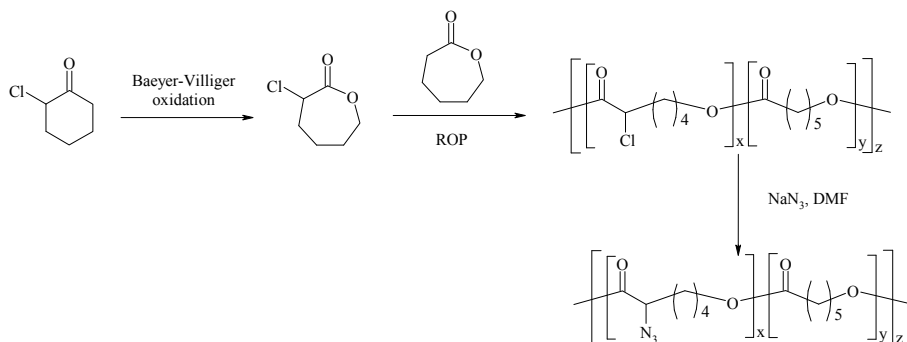
Scheme 8. Synthesis of aliphatic polyesters bearing pendant azides according to Jérôme et al.[20–22]

An alternative strategy relies on the ring-opening polymerization of 5-bromooxepan-2-one (γBrεCL for γ-bromo-ε-caprolactone) followed by the conversion of pendant bromides into azides by reaction with sodium azide. Unlike αClεCL, aluminum isopropoxide turned out to be a very efficient initiator of the ring-opening polymerization of γBrεCL and polyesters with predetermined molecular weight and low polydispersity indexes were synthesized.[24] The main drawback relies on the more difficult synthesis of γBrεCL, which requires three steps as shown in another chapter in this book dedicated to the functionalization of aliphatic polyesters.

3.2. SYNTHESIS OF ALIPHATIC POLYESTERS BY STEP-GROWTH POLYMERIZATION

Aliphatic polyesters containing pendant azides and alkynes were alternatively made available by step-growth polymerization. Du Prez et al. reported very recently the synthesis of aliphatic polyesters bearing pendant alkynes by step-growth polycondensation of 2-methyl-2-(prop-2-yn-1-yl)propane-1,3-diol (Scheme 9).[25] The step-growth polycondensation was carried out by a two-step process. Firstly, oligomers were obtained in the presence of tin tetrabutoxide. In order to prevent undesired radical reaction of the alkyne, hydroquinone was added in the medium. Finally, higher molecular weights were obtained by removing water at high temperature (200°C) and under reduced pressure.
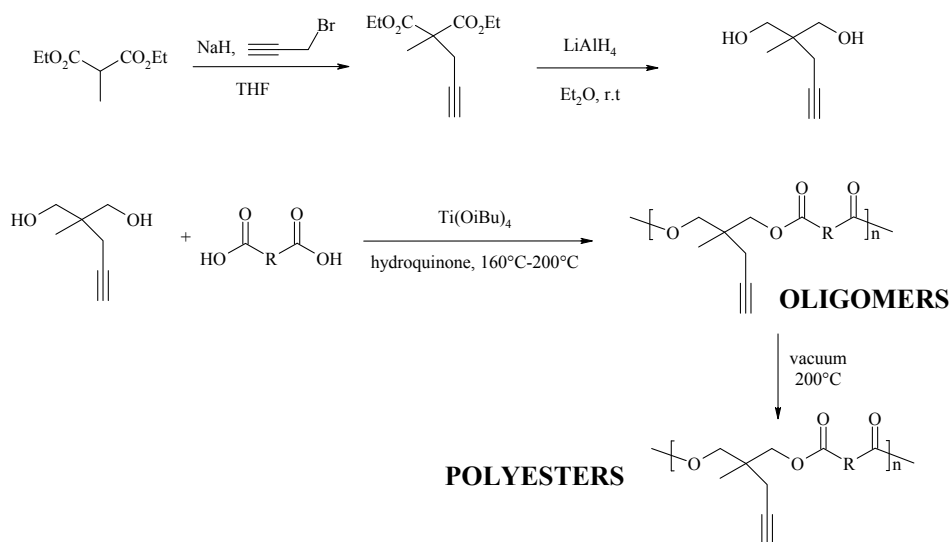
Scheme 9. Synthesis of aliphatic polyesters attached with pendant alkynes according to Du Prez et al.[25]

Sheares et al. reported the polycondensation of diols and diethyl 2,5-diazidoadipate, easily synthesized by reaction of diethyl 2,5-dibromohexanedioate with sodium azide (Scheme 10).[26] Due to the known trend of azides to explode, especially at high temperature, it is mandatory to avoid using the conditions used by Du Prez et al.,[25] because the temperature (200°C) is too high to handle azides safely. In the work of Brown and Sheares, [26] the polycondensation was catalyzed at 80°C by Novozyme 435 (Scheme 10).
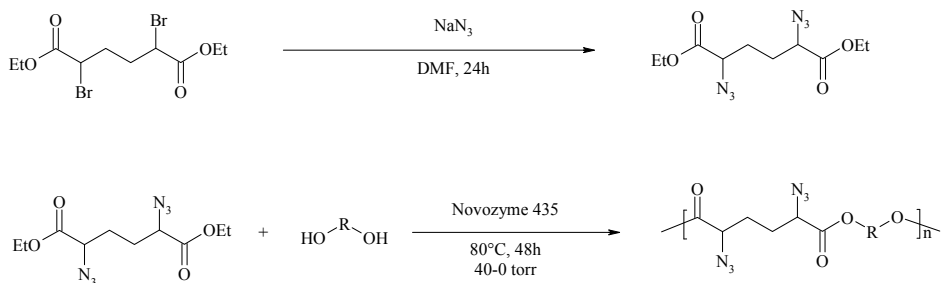
Scheme 10. Synthesis of aliphatic polyesters bearing pendant azides according to Brown and Sheares.[26]

The main advantage of the approach based on step-growth polymerization is the very easy synthesis of the monomers. Interestingly, a wide range of azide-functionalized aliphatic polyesters might be synthesized just by changing the structure of one of the partners of the polycondenation (diacid or diol). As far as the strategy based on ring-opening polymerization is concerned, only a very limited number of lactones substituted by alkynes and halogenides are reported, which limits severely the number of aliphatic polyesters, which can be made available. At the other hand, the control of the polymerization in terms of molecular weight and molecular weight distribution is by far better by ring-opening polymerization compared to step-growth polymerization. Ring-opening polymerization must also be preferred to prepare aliphatic polyesters of high molecular weight.

3.3. FUNCTIONALIZATION OF ALIPHATIC POLYESTERS BY CUAAC

Emrick et al. were the very first ones to report the functionalization of aliphatic polyesters by the CuAAC reaction.[17] Indeed, α,ω-PEG monomethyl ether azide was grafted onto a copolyester of αAδVL and εCL (Scheme 11), whose synthesis was shown in Scheme 5. The reaction was carried out in water at 80°C by in the presence of copper(II) sulfate and sodium ascorbate. The role of sodium ascorbate is to reduce copper(II) into Cu(I), which is the active catalyst

for the CuAAc reaction. Nevertheless, the polyester is not water-soluble, and was solubilized in a minimum amount of acetone before being added to the polymerization mixture. This solvent evaporates during the grafting. Interestingly, the coupling took place very quantitatively after one night of stirring. The use of water instead of organic solvents is very advantageous in view of future developments of biomedical applications. The strategy was successfully extended to the grafting of an azide-terminated GRGDS peptide onto the poly(αAδVL) homopolyester (Scheme 12).[17] Interestingly, the authors claim that no degradation by hydrolysis was detected. The copolyester based on PCL used by Emrick et al. is not very sensitive to hydrolysis. Nevertheless, Riva et al. observed that many other polyesters are more sensitive and degrade in water at 80°C in the presence of a copper salt.[20] It was thus necessary to implement milder conditions in order to functionalize a wider range of aliphatic polyesters without degradation. Riva et al. proposed to carry out the functionalization of aliphatic polyesters by CuAAC in an organic solvent (DMF or THF) rather than in water.[20] They showed that prop-2-yn-1-yl benzoate was grafted onto poly(εCL-co-αN₃εCL) in the presence of 10 mol% of copper iodide and 10 mol% of 1,8-diazabicyclo[5.4.0]undec-7-ene (DBU) or triethylamine, in THF and in DMF, at 35°C (Scheme 13). The reaction reached completion within 2 h and no degradation was observed by SEC.
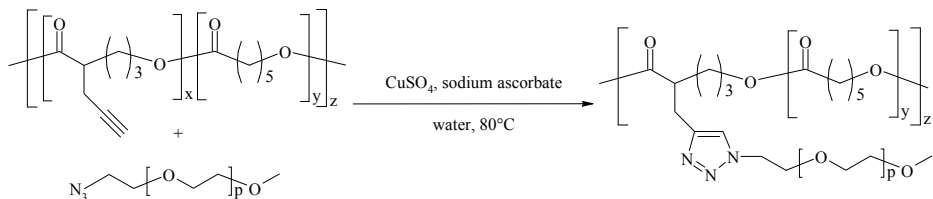
Scheme 11. Graftging of PEO onto alkyne-containing PCLs by the CuAAC reaction according to Emrick et al.[17]
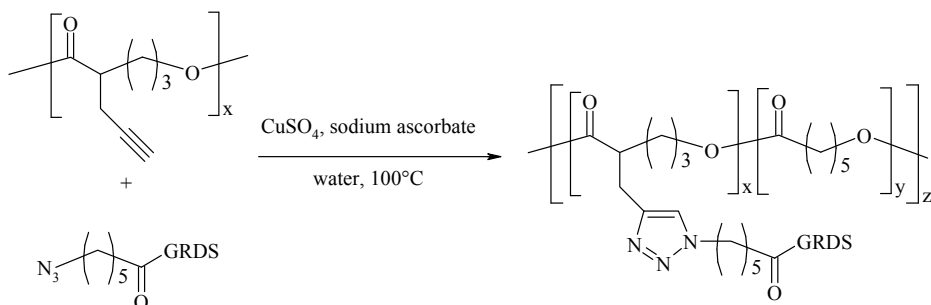
Scheme 12. Graftging of a peptide onto alkyne-containing PCLs by the CuAAC reaction according to Emrick et al.[17]
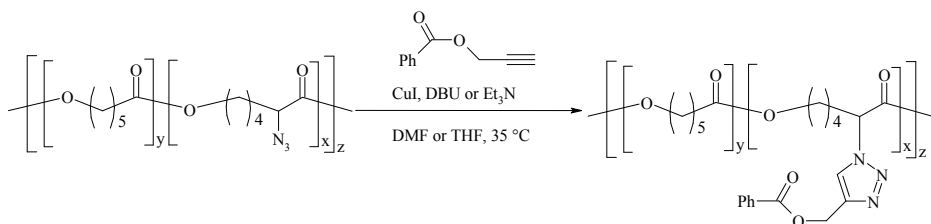
Scheme 13. Derivatization of azide-containing PCLs by the CuAAC reaction according to Riva et al.[20]

One main advantage of the CuAAC reaction remains its high tolerance to many functional groups without any need of cumbersome protection/deprotection reaction. Riva et al. grafted various functional groups onto PCL, e.g. hydroxyl, bromide, acrylic unsaturation, amine and ammonium salt (Scheme 14).[21, 27] A slight degradation by transesterification reactions was only observed when but-3-yn-1-ol was used to graft hydroxyl groups. In all the other instances, lack of degradation was the rule. The strategy was then extended to the grafting of alkyne-terminated PEO onto azide-containing copolyesters.[21, 27–29] It is worth noting that, although CuAAC is very efficient, the grafting efficiency was lower than the unity, most probably for steric reasons, especially when high grafting density was targeted. The same trend was reported for similar reactions.[30, 31] Finally, the coupling of α,ω-dialkynyl-PEG with azide-containing PCL was successfully implemented to synthesize amphiphilic conetworks.[32] Interestingly, CuAAC was used to obtain functional networks by a two-step procedure based on the functionalization of azide-containing polyesters followed the final cross-linking step.

The strategy based on the CuAAC reaction is thus an effective tool for tailoring extensively the properties and reactivity of PCL. For instance, the grafting of hydroxyl groups increases importantly the hydrophilicity of PCL. Ammonium-containing PCL is hydrosoluble, which is also the case of amine-containing PCL as far as the pH is low enough for the amino groups to be protonated. More recently, Brown and Sheares extended this approach to the grafting of pent-4-ynoic acid onto the azide-functionalized aliphatic polyester prepared by polycondensation as shown in Scheme 15.[26] Besides, the CuAAC reaction is also a very efficient tool to couple biologically active molecules in view of biomedical application. For example, Parish and Emrick grafted azide-substituted camptothecin, an anticancer drug, onto poly(αAδVL-*co*-εCL).[33] In another example, azide-functionalized sugars, such as glucose and mannose, were grafted onto an alkyne-containing polycarbonate, that was prepared by ring-opening copolymerization of lactide and 5-methyl-5-propargyloxycarbonyl-1,3-dioxan-2-one (Scheme 16).[34] The binding affinity of the grafted sugars for lectins makes the copolymer prone to target living cells, which is a key issue in controlled drug delivery.
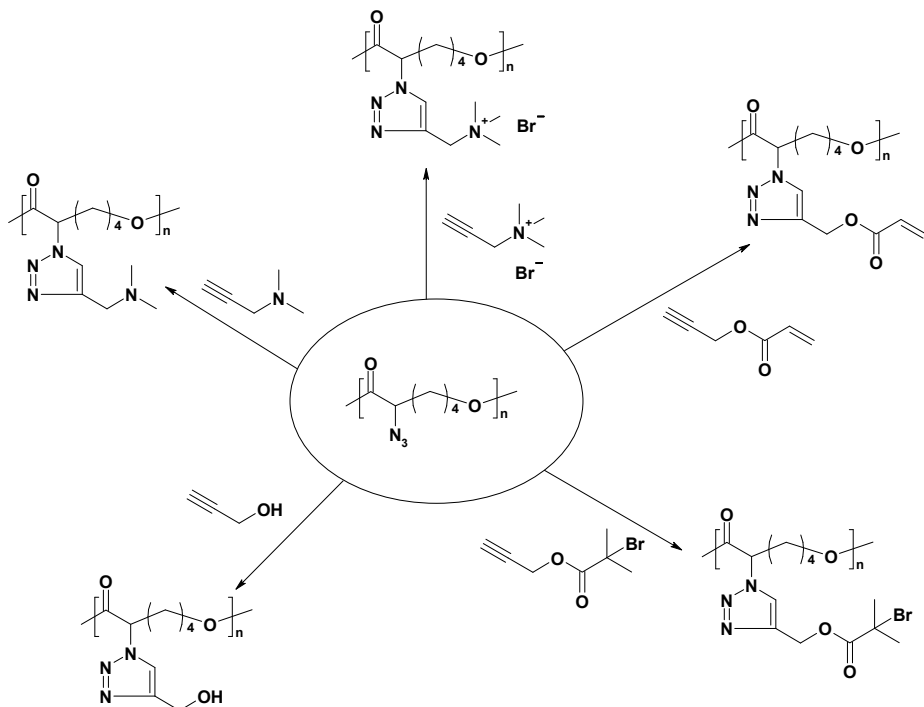
Scheme 14. Grafting of various functional groups onto azide-functionalized aliphatic polyesters according to Riva et al.[21]
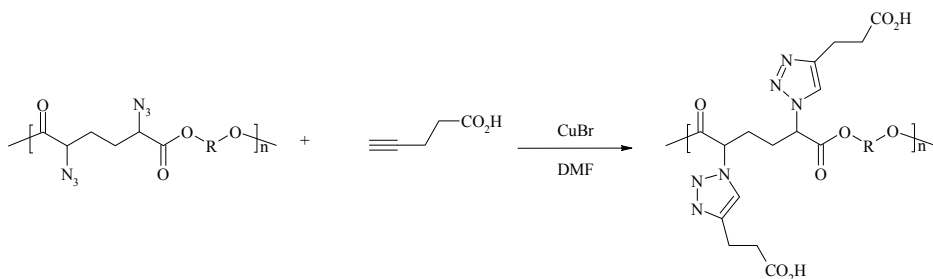
Scheme 15. Grafting of carboxylic acids onto azide-functionalized aliphatic polyesters according to Brown and Sheares.[26]

It must be pointed out that when a polymer with a high content of azides is handled, the risk of explosion may not be disregarded. The storage of this polymer at low temperature ($-20°C$) is a basic precaution. Whenever possible, a "one-pot" procedure should be worked out, such that the azide-containing polymer is not isolated but directly reacted with the derivatization agent. For instance, a poly(αClεCL-*co*-εCL) copolyester containing 50 mol% of pendant chlorides was reacted with 60 mol% of sodium azide in DMF overnight. A

solution of 65 mol% of *N,N*-dimethylprop-2-yn-1-amine and 6 mol% of copper iodide in THF was added to the reactor, and the click reaction went to completion within 2 h at 35°C (Scheme 17).[21] In this example, the amino substituent of the terminal alkyne acted as a base, which explains that DBU or triethylamine was not added to the reaction medium. As a rule, the "one-pot" procedure turned out to be as efficient as the common "two-pot" technique.
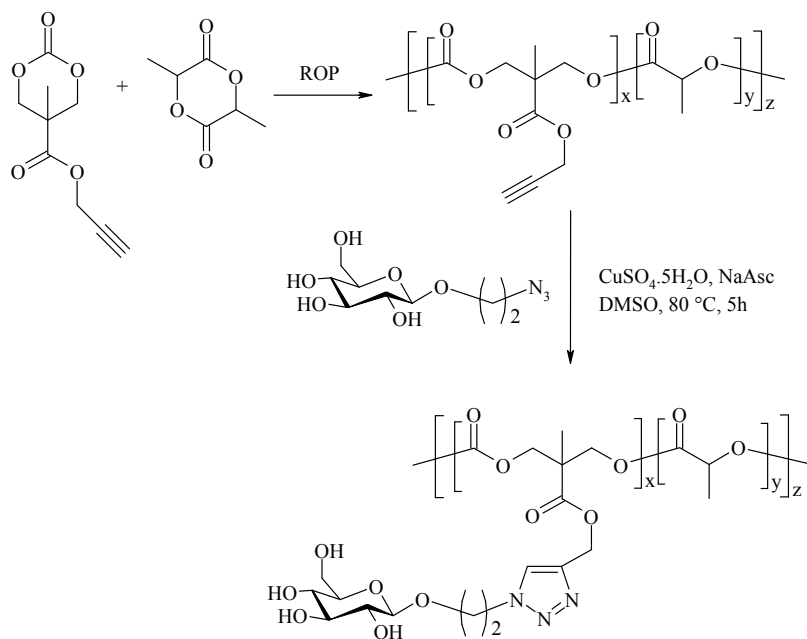
Scheme 16. Grafting of glucose onto a terminal alkyne containing PLA.[34]
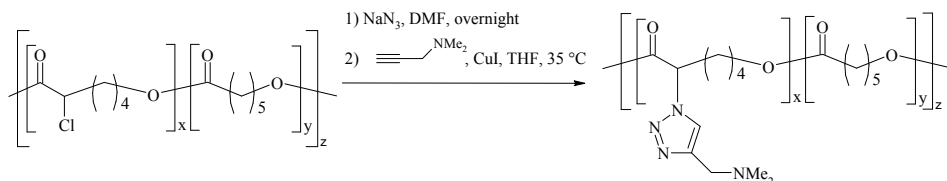
Scheme 17. "One-pot" process in which the intermediate azide derivative is not isolated.[21]

The successful implementation of the CuAAC reaction to functionalize azide- and alkyne-containing PCL paves the way to the extension of the process of aliphatic polyesters more sensitive to degradation than PCL. Riva et al. succeeded to graft PEO end-capped by an alkyne and prop-2-yn-1-yl benzoate onto an azide–copolyester obtained by ring-opening copolymerization of lactide and αClεCL followed by conversion of pendant chlorides into azides by reaction

with sodium azide. The grafting by the CuAAC reaction turned out to be more difficult due to highest sensibility of the copolyester. It was necessary to protect the hydroxyl end-groups by reaction with acetyl chloride. Besides, when the first trials of CuAAC were attempted, DBU turned out to be too basic and was replaced by triethylamine. Under these conditions, the grafting by CuAAC turned out to be very efficient and no degradation was observed. Later on, Baker et al. reported the functionalization by the CuAAC reaction of alkyne-containing poly(lactide) synthesized as shown in Schemes 6 and 7.[19]

4. Synthesis of Functional Lactones

Riva et al. implemented a reverse strategy by achieving the functionalization by the CuAAC reaction prior to polymerization. Indeed, a wide range of functionalized lactones were synthesized by coupling duly substituted terminal alkynes onto $\gamma N_3\varepsilon CL$ (Scheme 18).[35] One main advantage relies on the easy purification of these lactones by simple crystallization. Nevertheless, their use as monomer for ring-opening polymerization has not yet been reported. It must be noted that although the grafting of terminal alkynes onto $\alpha N_3\varepsilon CL$ was successful, the lactone was unstable and rearranged into a non cyclic compound. The position of the substituent on the lactone ring has thus a decisive impact on the ring stability.
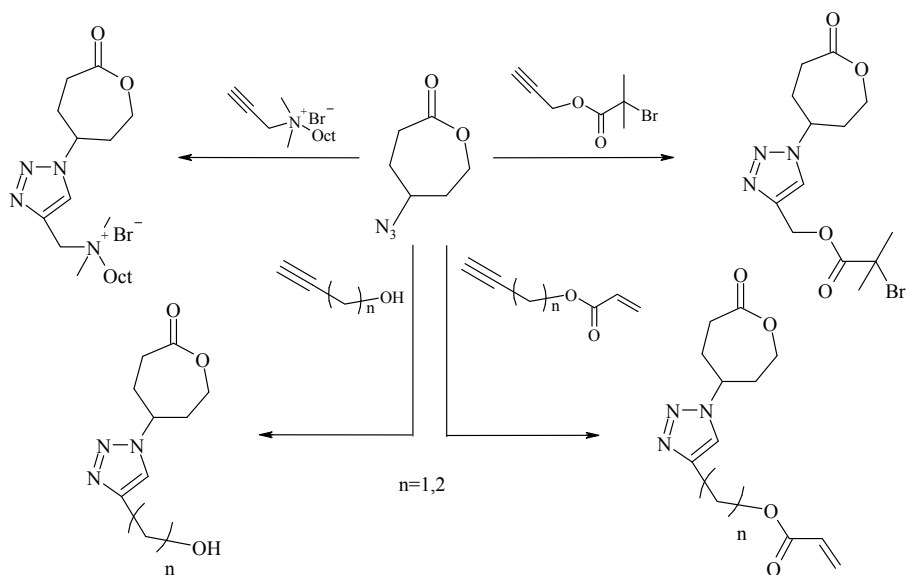
Scheme 18. New functional εCLs synthesized by Riva et al.[35]

5.   Conclusions

The CuAAC reaction turned out to be a very efficient reaction to functionalize aliphatic polyesters under mild conditions for which no degradation was observed. The best conditions rely on the use of an organic solvent such as DMF or THF at low temperature (20–40°C). The CuAAC reaction can even be carried out in water provided that the aliphatic polyester is not too sensitive to hydrolytic degradation.[17] The CuAAC reaction is very efficient to synthesize polyesters with various architectures, as recently reviewed.[36] This reaction has thus a great potential for the synthesis of novel degradable and biocompatible aliphatic polyesters with tailored properties. Nevertheless, the contamination of the polyester by catalytic residues is a severe limitation, especially if biomedical applications are targeted. In the future, it will be highly desirable to find efficient processes to eliminate the use of the metal or to find new metal-free reactions as efficient as the CuAAC reaction.

Acknowledgements

References

[1]   S. Ponsart, J. Coudane, M. Vert, Biomacromolecules 1, 275–281 (2000).
[2]   B. Saulnier, S. Ponsart, J. Coudane, H. Garreau, M. Vert, Macromol. Biosci. 4, 232–237 (2004).
[3]   P. Lecomte, R. Riva, S. Schmeits, J. Rieger, K. Van Butsele, C. Jérôme, R. Jérôme, Macromol. Symp. 240, 157–165 (2006).
[4]   C. W. Tornøe, C. Christensen, M. Meldal, J. Org. Chem. 67, 3057–3064 (2002).
[5]   V. V. Rostovstev, L. G. Green, V. V. Fokin, K. B. Sharpless, Ang. Chem. Int. Ed. 42, 2596–2599 (2002).
[6]   H. C. Kolb, M. G. Finn, K. B. Sharpless, Ang. Chem. Int. Ed. 41, 2004–2021 (2001).
[7]   J.-F. Lutz, Ang. Chem. Int. Ed. 46, 1018–1025 (2007).
[8]   R. A. Evans, Aust. J. Chem. 60, 384–395 (2007).
[9]   J. E. Moses, A. D. Moorhouse, Chem. Soc. Rev. 36, 1249–1262 (2007).
[10]   D. Fournier, R. Hoogenboom, U. S. Schubert, Chem. Soc. Rev. 36, 1369–1380 (2007).
[11]   H. Himabindu, X. Jiang, J. Lahann, Adv. Mat. 19, 2197–2208 (2007).
[12]   W. H. Binder, R. Sachsenhofer, Macromol. Rapid Commun. 28, 15–24 (2007).

[13] J. A. Johnson, M. G. Finn, J. T. Koberstein, N. J. Turro, Macromol. Rapid Commun. 29, 1052–1072 (2008).

[14] P. Lundberg, C. J. Hawker, A. Hult, M. Malkoch, Macromol. Rapid Commun. 29, 998–1015 (2008).

[15] M. Meldal, C. W. Tornøe, Chem. Rev. 108, 2952–3015 (2008).

[16] N. Xu, F.-Z. Lu, F.-S. Du, Z.-C. Li, Macromol. Chem. Phys. 208, 730–738 (2007).

[17] B. Parrish, T. Breitenkamp, T. Emrick, J. Am. Chem. Soc. 127, 7404–7410 (2005).

[18] B. Parrish, J. K. Quansah, T. Emrick, J. Polym. Sci.: Part A: Polym. Chem. 40, 1983–1990 (2002).

[19] X. Jiang, E. B. Vogel, M. R. Smith III, G. L. Baker, Macromolecules 41, 1937–1944 (2008).

[20] R. Riva, S. Schmeits, F. Stoffelbach, C. Jérôme, R. Jérôme, Ph. Lecomte, Chem. Commun. 5334–5336 (2005).

[21] R. Riva, S. Schmeits, Ch. Jérôme, R. Jérôme, Ph. Lecomte, Macromolecules 40, 796–803 (2007).

[22] S. Lenoir, R. Riva, X. Lou, C. Detrembleur, R. Jérôme, Ph. Lecomte, Macromolecules 37, 4055–4061 (2004).

[23]   R.-S. Lee, Y.-T. Huang, J. Polym. Sci.: Part A: Polym. Chem. 46, 4320–4331 (2008).

[24] C. Detrembleur, M. Mazza, O. Halleux, Ph. Lecomte, D. Mecerreyes, J. L. Hedrick, R. Jérôme, Macromolecules 33, 14–18 (2000).

[25] L. Billiet, D. Fournier, F. Du Prez, J. Polym. Sci.: Part A: Polym. Chem. 46, 6552–6564 (2008).

[26] A. H. Brown, V. V. Sheares, Am. Chem. Soc. 49(1), 181–182 (2008).

[27] R. Riva, P. Lussis, C. Jérôme, R. Jérôme, Ph. Lecomte, Polymer 49, 2023–2028 (2008).

[28] H. Li, R. Riva, H. R. Kricheldorf, R. Jerome, Ph. Lecomte, Chem. – Eur. J. 14, 358–368 (2008).

[29] H. Li, R. Riva, R. Jerome, Ph. Lecomte, Macromolecules 40, 824–831 (2007).

[30] K. Matyjaszewski, H. Gao, J. Am. Chem. Soc. 129, 6633–6639 (2007).

[31] N. V. Tsarevsky, S. A. Bencherif, K. Matyjaszewski, Macromolecules 40, 4439–4445 (2007).

[32] J. Zednik, R. Riva, C. Jérôme, R. Jérôme, Ph. Lecomte, Polymer 49, 697–702 (2008).

[33] B. Parish, T. Emrick, Bioconj. Chem. 18, 263–267 (2007).

[34] C. Lu, Q. Shi, X. Chen, T. Lu, Z. Xie, X. Hu, J. Ma, X. Jing, J. Polym. Sci.: Part A: Polym. Chem. 45, 3204–3217 (2007).

[35] R. Riva, L. Chafaqi, R. Jérôme, P. Lecomte, Arkivoc 10, 292–306 (2007).

[36] Ph. Lecomte, R. Riva, C. Jérôme, R. Jérôme, Macromol. Rapid Commun. 29, 982–997 (2008).

EXPLORATION OF 'CLICK' CHEMISTRY
FOR MICROELECTRONIC APPLICATIONS

OSAMA M. MUSA[*] AND LAXMISHA M. SRIDHAR
Bridgewater Applied Research Group, National Starch and Chemical Company/ICI, 10 Finderne Ave. Bridgewater, NJ 0880

Abstract: The 'Click' chemistry was explored for low temperature snap cure and for possible use as an adhesion promoter in electronic applications. Several azide and alkyne resins were synthesized and their curing potential was evaluated with a special emphasis on exploring Cu(I) catalyst effect. The preliminary curing study in the absence of catalysts showed a strong dependence of cure temperatures on the electronic nature of alkynes. The cure temperatures showed a tendency to increase with decreasing electronegativity of the substituent on alkynes. The capability of Cu(I) catalysts to accelerate the 'Click' chemistry was demonstrated for the first time in bulk phase. Using several Cu(I) catalysts, the cure temperatures could be lowered by as much as 40–100°C compared to the control, depending on the nature of catalyst and the catalyst loading. We discovered a novel synergistic effect between Cu(I) and silver filler in lowering the cure temperatures. Using this combination, lower cure temperatures could be obtained than using either alone. Among several resins screened, one resin system has shown promise for 80°C snap-cure in which the aforementioned synergistic effect is operative. Solution phase 'Click' chemistry was employed for the synthesis of a hybrid triazole-epoxy resin system. This system was found to cure without added amine curative. The triazole group here serves as a linker as well as an internal adhesion promoter. To address the incompatibility and volatility issues, which arose during evaluation, a controlled oligomerization method has been developed using controlled heating of azides and alkynes in solution phase.

1. Introduction

The Huisgen 1,3-dipolar cycloaddition between a terminal alkyne and an azide are exergonic fusion process that generates a triazole aromatic unit. Unlike other cycloaddition reactions, this process is irreversible and is thermodynamically favored by approximately 30–35 kcal/mol.[1] However, likely because of concerns about the safety of working with organic azides, chemists, in both pure and applied fields, have not given this transformation the due attention it deserves. Although the actual cycloaddition may be faster with other dipoles than azides, the latter gives by far the cleanest reaction, which is nearly devoid of any side products. The cycloaddition can be performed either in a solvent or in neat form (with liquid substrates), the yields are nearly quantitative, and as the process can be run neat, no purification is needed. What makes this process unique is the extraordinary stability of the reactants and products toward H_2O, O_2 and a majority of synthetic conditions.

The formation of triazoles via cycloaddition of azides and alkynes was first reported by Dimorth in the early 1900s but the generality, scope, and mechanism of these cycloadditions was not fully realized until the 1960s. This reaction generates a mixture of 1,4- and 1,5-disubstituted triazoles as depicted in Figure 1. Various attempts to control the regioselectivity have been reported without much success until the discovery of the Cu(I)-catalyzed reaction in 2002, which exclusively yields the 1,4-disubstituted 1,2,3-triazole.[2] The use of copper (I) salts accelerates this process by factors up to 10^7 while preserving the inertness of both azides and alkynes toward the vast majority of functional groups and conditions that are typical of terrestrial environment.

1,4-regioisomer   **1,5-regioisomer**
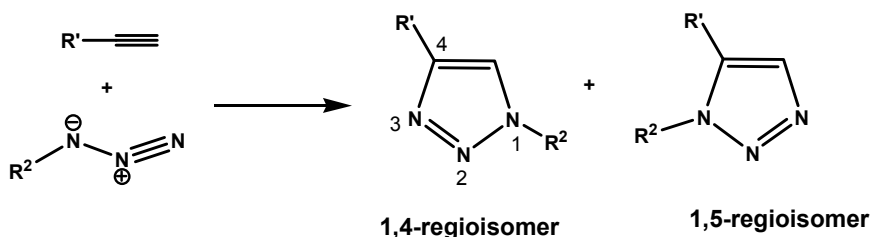
Figure 1. Huisgen cycloaddition of azides and alkynes.

Several copper(I) salts such as CuI, $CuOTf.C_6H_6$ can be employed but the reactions generally must be run with acetonitrile as cosolvent, require a nitrogen base. The *in situ* reduction of Cu(II) salts such as $CuSO_4.5H_2O$ with sodium ascorbate in aqueous alcoholic solvents allows the exclusive formation of 1,4-triazoles at r.t. in high yields with less than 2 mol% catalyst loading. Numerous terminal acetylenes and azide components participate in the transformation and the reaction is compatible with a wide range of functionalities such as esters,

acids, alkenes, alcohols and amines. Mechanistically, in contrast to the thermal cycloaddition, the Cu(I) catalyzed 'Click' chemistry is believed to proceed in a stepwise manner starting with the generation of copper(I)acetylide (step A, Figure 2). Density functional theory calculations show a preference for the stepwise addition (steps B-1→B-2→B-3) over the concerted cycloaddition (B-direct) by approximately 12–15 kcal/mol, leading to the intriguing metallacycle **1**. This undergoes ring contraction and protonation to complete the catalytic cycle generating triazole **2**.

Sharpless and coworkers from Scripps research institute, in patent WO 2003101972, described in detail the copper catalyzed 'Click' chemistry process in solution phase and its advantages such as dramatic acceleration of rate and exclusive 1,4-regioselectivity. The same authors have also described the use of 'Click' chemistry for the preparation of triazole polymers for use as metal adhesives, especially for copper, some of which outperformed the best available product in the market.[3] Since our focus is on developing low temperature snap cure resin system, it was reasoned that the demonstrated capability of Cu(I)catalysts to dramatically accelerate the 'Click' chemistry process might offer opportunities for low temperature snap cure. In addition, the reported good adhesion properties of triazole polymers provided an incentive to pursue this chemistry for electronic applications. Along with the aforementioned opportunities, the 'Click' chemistry also offers advantages such as mild and forgiving reaction condition, which is insensitive to air and moisture. This is in stark contrast to radical polymerization, which is often inhibited by oxygen leading to incomplete polymerization and reduced yield. Since the bulk phase 'Click' chemistry has not been reported so far, it gave an impetus to explore this chemistry for electronic applications.
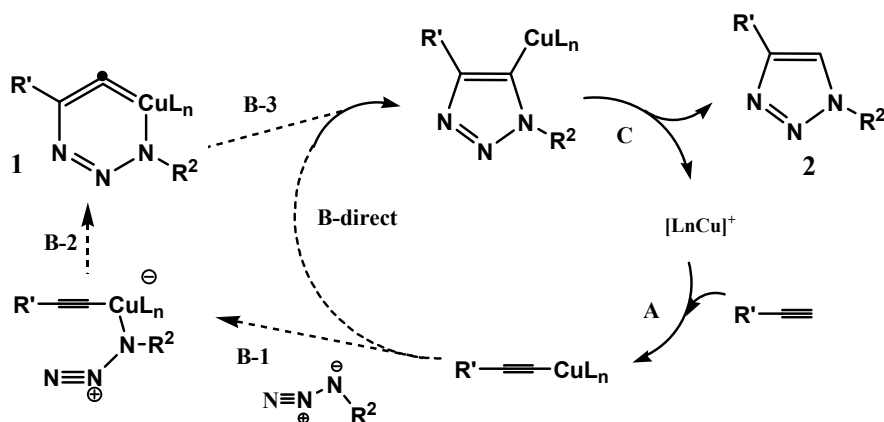

Figure 2. Proposed catalytic cycle for the Cu(1) catalyzed 'Click' chemistry.

2. Safety of Azides

Before Sharpless started working on 'Click' chemistry, the use of azides, either in organic or inorganic form, was not a popular choice in chemistry. This "azidophobia" seems to be largely based on the fact that a large number of metallic azides are shock sensitive. However, certain organic azides, especially small ones, are also explosive. The following points are noteworthy when handling azides. Sodium azide is relatively safe (it decomposes explosively when heated to 275°C-not normally the temperature used in synthetic laboratories),[4] especially in aqueous solutions, unless acidified to form HN_3, which is volatile and toxic. For organic azides to be safe, the "rule of six" is very useful: six carbons (or other atoms of comparable size) per energetic functionality provides sufficient dilution to render the compound safe. Decomposition of organic azides can also be catalyzed by certain transition metals (especially from the Co and Fe triads) and by strong acids. Azide groups attached directly to aromatic, vinylic or carbonyl moieties are much less stable and, other things being equal, more dangerous than aliphatic azides (the approximate activation energies for unimolecular loss of N_2 being 29 and 49 kcal/mol, respectively).[5] With these safety criteria on handling of azides in mind we began the exploration of 'Click' chemistry.

3. Approach

The evaluation of 'Click' chemistry involved three different approaches. The first approach, which is called the 'monomer approach', involved the synthesis of requisite monomers and evaluation of their curing performance in the presence and absence of catalysts using the hitherto unreported bulk phase 'Click' chemistry (Figure 3). In the second approach, termed the 'hybrid approach', the synthesis and evaluation of triazoles possessing polymerizable units such as epoxy, maleimide or acrylate was planned. Here the triazole unit serves as linker as well as an internal adhesion promoter. One advantage of using triazoles as linkers is the extremely forgiving conditions (insensitive to air and moisture and r.t reaction) used for their generation. This is in contrast to the synthesis of maleimides possessing ester linkage, which requires harsh conditions and often gives gellation problems. In the third approach, called the 'oligomer approach', the synthesis of triazole oligomers was planned using controlled oligomerization of bisazides and bisalkynes either in bulk or solution phase. These oligomers can then be used in a secondary chain growth polymerization. It was anticipated that these polymers would exhibit thermoplastic behavior.
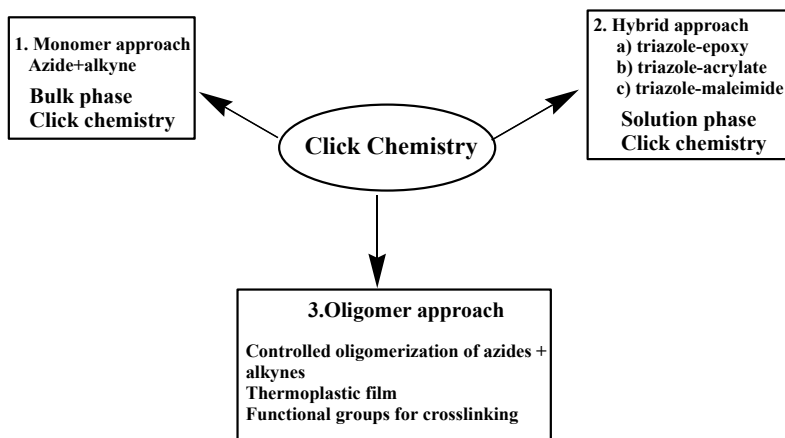
```
┌─────────────────────────┐                    ┌──────────────────────────┐
│ 1. Monomer approach     │                    │ 2. Hybrid approach       │
│    Azide+alkyne         │                    │    a) triazole-epoxy     │
│                         │                    │    b) triazole-acrylate  │
│ Bulk phase              │                    │    c) triazole-maleimide │
│ Click chemistry         │                    │                          │
│                         │                    │    Solution phase        │
└─────────────────────────┘                    │    Click chemistry       │
                          ↖            ↗        └──────────────────────────┘
                         ╭─────────────────╮
                         │  Click Chemistry │
                         ╰─────────────────╯
                                  │
                                  ↓
                  ┌──────────────────────────────────────┐
                  │        3.Oligomer approach           │
                  │                                      │
                  │ Controlled oligomerization of azides +│
                  │ alkynes                              │
                  │ Thermoplastic film                   │
                  │ Functional groups for crosslinking   │
                  └──────────────────────────────────────┘
```

Figure 3. Approaches to evaluate 'Click' chemistry.

4. Results and Discussion

The exploration of 'Click' chemistry began with the synthesis of required azide and alkyne monomers. Keeping the safety aspect in mind, two selective azide monomers possessing large molecular weights were synthesized starting from appropriate diols and triols. Azide **000021-14** was synthesized first from Uniqema dimerdiol in two steps as shown in Figure 4. Thus, reaction of dimerdiol with $MeSO_2Cl/Et_3N$ in CH_2Cl_2 afforded mesylate **13394-95**, which upon heating with NaN_3 in DMF at 85°C for 8 h, furnished azide **000021-14**. It is noteworthy that the reaction condition used here for the NaN_3 reaction is significantly milder than typical literature conditions, which require 120°C heating. Azide **000021-14** has a 16:1 ratio of carbon to azide functionality (well with in the safety limit of 6:1 ratio) and as it turned out, **000021-14** was found to be very safe to handle. While the thermal stability of azide **00002-14** was good under the normal resin cure temperature range (T_d = 270°C), the heat of decomposition (ΔH of 880 J/g) was higher than the acceptable limit (ΔH of 300 J/g). This indicated that the number of carbons (or other atoms of similar size) per energetic functionality is not sufficient enough to bring the heat of decom-position to ~300 J/g. To address this issue, azide **000021-37** was synthesized starting from commercially available low molecular weight polymer glycerolethoxylate-co-propoxylate triol. This triol has a M_n ~2,600, which was expected to be sufficient to bring the T_d to ~300 J/g. Following essentially the same sequence as used for the synthesis of **000021-14**, azide **000021-37** was synthesized in two steps (Figure 4). Azide **000021-37** exhibited a similar stability profile as **000021-14** but with significantly less T_d = 313 J/g.
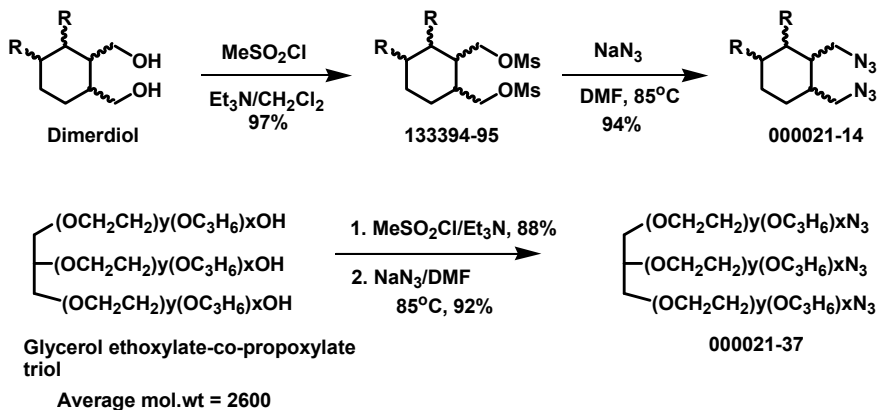
Figure 4. Synthesis of azide monomers **000021-14** and **000021-37**.

This demonstrated that the heat of decomposition (or in general heat of polymerization) can be lowered by increasing the molecular weight of the monomer. With the azide monomers in hand, we focused on the synthesis of alkyne monomers required for the curing study. Since aliphatic propargyl ethers have a viscosity advantage over aromatic propargyl ethers, the synthesis of aliphatic ethers was attempted first. Thus, following some literature procedures, the synthesis of several propargyl ethers possessing aliphatic backbones was investigated starting from corresponding triols and tetraols. However, several of these attempts using alcohols such as pentaerythritol and 1,1,1-*tris*hydroxy-methylethane led to incomplete alkylation to give a mixture of partially pro-pargylated products (Figure 5). In all of these attempts the desired peralkylated product was never obtained.
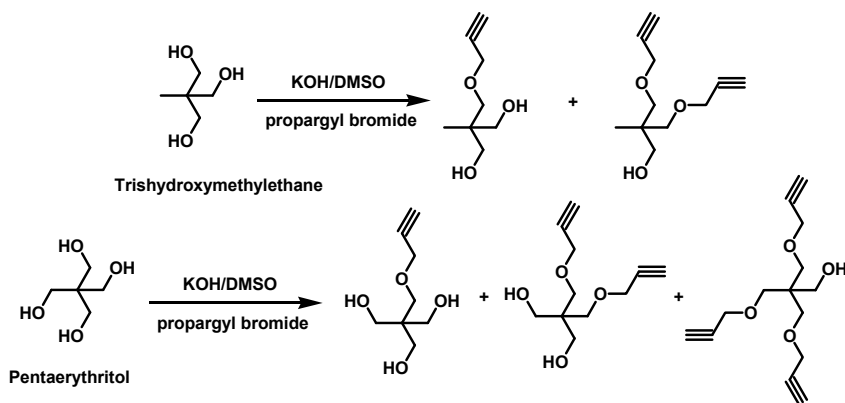

Figure 5. Attempted propargylation of pentaerythritol and trishydroxymethylethane.

Although propargylation of aliphatic alcohols led to incomplete conversion, the corresponding reaction with phenols was expected to be straightforward because of easy deprotonation of phenols. Toward this end, several phenols, such as resorcinol, bisphenol A, 1,1,1-tris(4-hydroxphenyl)ethane were propargylated using K_2CO_3/propargyl bromide in DMF under appropriate reaction conditions (Figure 6). While the propargylation of resorcinol and bisphenol A was straightforward at r.t to give **13394-113** and **000067-16**, respectively, the corresponding reaction with 1,1,1-tris(4-hydroxyphenyl)ethane required elevated temperatures to afford **000067-15**. Compound **13394-113** was obtained as a liquid where as both **000067-16** and **000067-15** turned out to be low melting solids (93°C and 65°C, respectively).
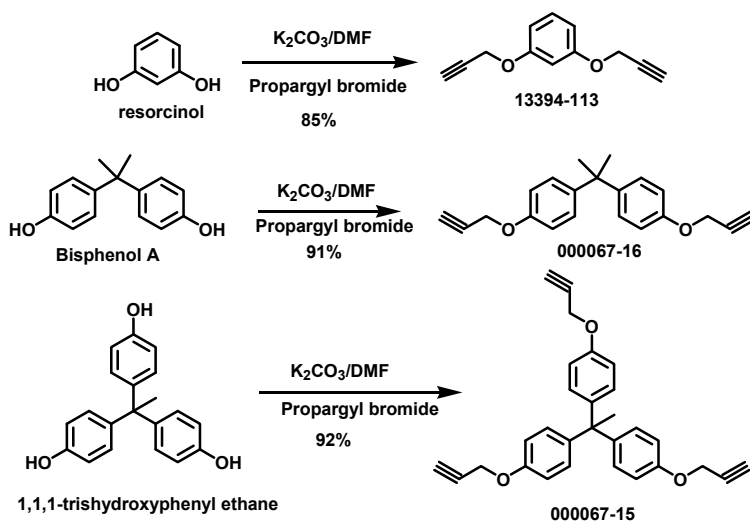
Figure 6. Synthesis of alkyne monomers **13394-113**, **000067-15** and **000067-16**.

To expand the 'Click chemistry' resin tool box and to study structure–property relationship, two aromatic propargyl amines were also prepared using similar reaction conditions. Thus, reaction of *p*-phenylenediamine and *m*-phenylenedioxydianiline with K_2CO_3/propargyl bromide in DMF at 0°C furnished the corresponding propargyl amines **000021-39** and **000021-38**, respectively (Figure 7). The reduced yields of these propargyl amines compared to those of propargyl ethers can be ascribed to the competing quaternization of these tertiary amines. This is supported by the observation that with aliphatic amines, none of the corresponding tertiary propargyl amine was obtained presumably due to product loss during work-up arising from quaternization.

Figure 7. Synthesis of propargyl amines **000021-39** and **000021-38**.

5. Electronic Effects on Cure Temperatures

With a number of structurally diverse azide and alkyne resin systems in hand, their curing behavior was investigated next in the absence of Cu(I) catalys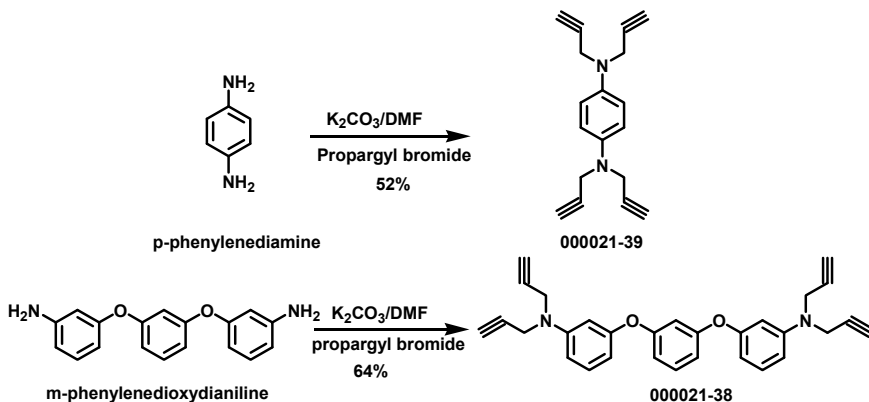ts. Toward this end, azide **000021-14** was mixed with some commercially available (tripropargylamine and nonadiyne) and in house alkynes (**000021-38**, **000021-39**, **13394-113**, **000067-15** and **000067-16**) and the results from the curing study are presented in Table 1. It was apparent from this study that the cure temperatures can be tuned by altering the substituent on the propargyl group (Figure 8). For example, all propargyl ethers (entries 1, 2, 3, Table 1) cured at ~150°C. No significant effect of degree of branching of alkynes on cure temperature was observed (**13394-113** vs. **000067-15**). This is in stark contrast to the polymerization of maleimides, in which increased degree of functionality in the monomer increases the cure temperature. For example, all other things being equal, monomaleimides cure at ~110°C while bismaleimides cure at ~125°C. In contrast to the propargyl ethers, the propargyl amines (tripropargylamine and **000021-38**) showed higher cure temperatures (entries 4 and 5). This gave a strong indication that the cure temperatures could be tuned by altering the electronegativity of the substituent attached to the propargyl group. Further credence to this theory was obtained when commercially available all-carbon alkyne, nonadiyne was used, which as anticipated, exhibited the highest cure temperature (entry 6). This study, thus established the reactivity order of alkynes in the uncatalyzed 'Click' chemistry as shown below. There is potential to further tune the cure temperature by attaching electron withdrawing substituents to the propargyl group. Results from this study will be reported in due course.

Decreasing reactivity
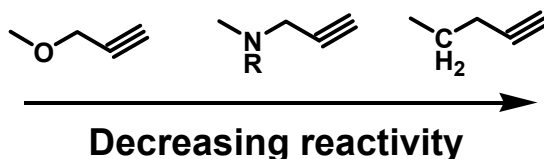
TABLE 1. Curing study of azide **000021-14** with different alkynes.

Entries	Resin systems	Cure temperatures
1	Azide **000021-14** and alkyne **13394-113**	148°C
2	Azide **000021-14** and alkyne **000067-15**	150°C
3	Azide **000021-14** and alkyne **000067-16**	150°C
4	Azide **000021-14** and tripropargylamine	165°C
5	Azide **000021-14** and **000021-38**	159°C
6	Azide **000021-14** and nonadiyne	186°C

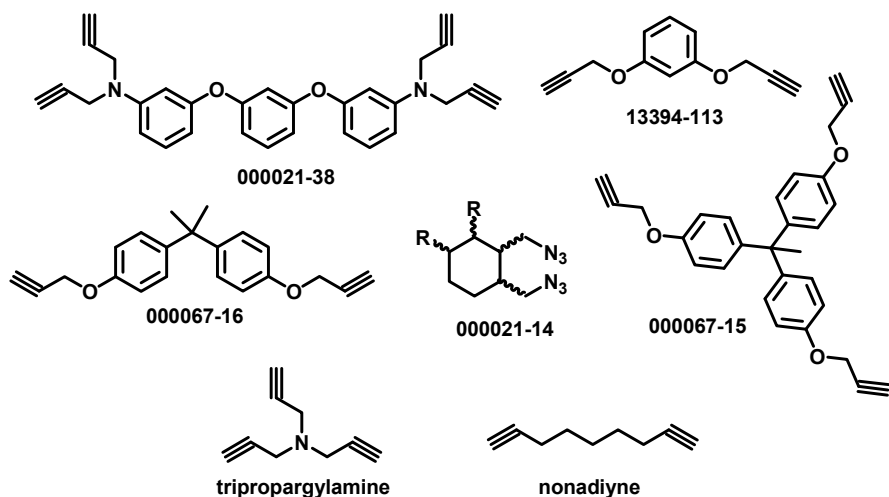*Figure 8.* Monomers used in the screening study.

6. Catalyst Screening Study

The copper(I) catalyst effect was explored next in bulk phase. Several commercially available copper catalysts were screened in an effort to bring the cure temperature to snap cure range (~100°C). With the use of copper catalysts, it was hoped that the cure temperatures could be lowered to the desired snap cure range. It turned

out that all of the catalysts used in the study decreased the cure temperature of formulations compared to the control (entries 2, 3, 4, 10 vs. entry 1; entries 6, 7 vs. entry 5; entry 9 vs. entry 8, Table 2; green vs. pink and blue curves in Cure profile A, blue vs. pink curve in Cure profile B, Figure 9). The magnitude of decrease depended on the catalyst loading and nature of the catalysts (hard or soft catalysts, entry 2 and 3 vs. entry 10). In addition to lowering the cure temperatures, the Cu(I) catalysts also narrowed the cure profiles considerably making them suitable for snap cure (see ΔT in entries 4, 6, 7, 9, compare with controls 1 and 5, Table 2; green curve in Cure profile A vs. green curve in Cure profile B, Figure 9). With hard Cu(I) catalysts, early onset was an issue with some azides and alkynes (see T_{onset} in entries 2,3, Table 1; pink and blue curves in Cure profile A, Figure 9). This early onset issue could be solved by the use of softer Cu(I) catalysts having sulfur ligands (entries 4, 7, green curve in Cure profile B).

TABLE 2. Catalyst effect on several azide/alkyne resin systems.

Entry	Resin system	Cure temp. (T_c)	T_{onset}	ΔT
1	**000021-14** + tripropargylamine (control)	165°C	118°C	47°C
2	**000021-14**+ tripropa.amine+CuI (1 wt%)	114°C	56°C	58°C
3	**000021-14**+triprop.amine+ CuPF$_6$ (1 wt%)	122°C	44°C	78°C
4	**000021-14**+triprop.amine+CuSBu (1 wt%)	124°C	99°C	25°C
5	**000021-37**+ triprop.amine (control)	186°C	140°C	46°C
6	**000021-37**+triprop.amine+CuI (1 wt%)	137°C	117°C	20°C
7	**000021-37**+triprop.amine+CuSBu (1 wt%)	124°C	106°C	18°C
8	**000021-37**+ **000021-39**(control)	180°C	128°C	52°C
9	**000021-37**+**000021-38** + CuI (1 wt%)	122°C	94°C	28°C
10	**000021-14**+triprop.amine+CuI (0.3%)	141°C	103°C	38°C

The hard Cu(I) catalysts, which showed poor results with **000021-14**, possessing hydrocarbon backbone, exhibited improved cure profile with azides possessing coordinating atoms such as **000021-37** (see higher T_{onset} in entry 6; pink curve in Cure profile B) and also under reduced catalyst loading (entry 10, compare with entry 2). These results proved that the early onset issue can depend on several factors such as resin, catalyst and stoichiometry.
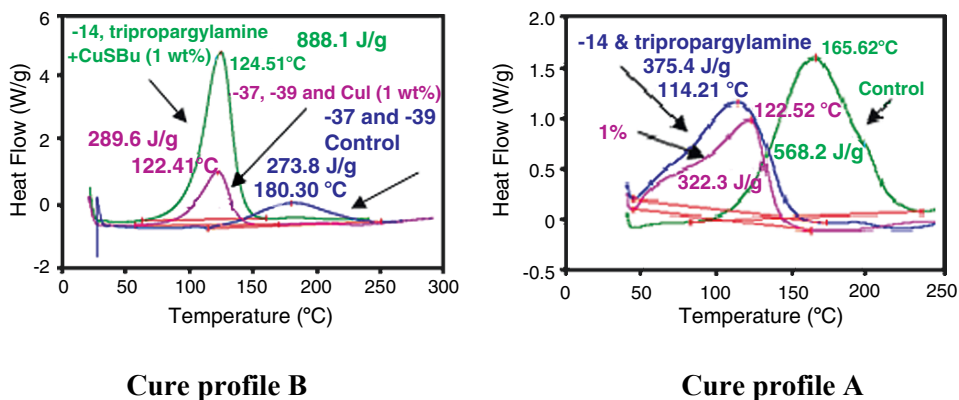
Figure 9. Curing profiles of azides **000021-14** and **000021-37** with different alkynes in the presence of several copper catalysts.

7. Compatibility of 'Click' Chemistry with Other Resin Systems

With the feasibility of 'bulk phase' 'Click' chemistry having been demonstrated for the first time, both in the presence and absence of catalysts, we next explored the compatibility of 'Click' chemistry with other resin systems such as epoxy or maleimides. It was reasoned that alkynes such as **000021-38** and **000021-39** can play a dual role both in 'Click' chemistry and in epoxy curing as a monomer or as amine initiators, respectively. The possibility of dual cure using a combination of 'Click' chemistry and epoxy cure without added amine curatives provided an impetus to explore this approach. The feasibility of monitoring each step in this projected dual cure system by monitoring the characteristic IR peaks of azide ($\sim$2,100 cm^{-1}), alkyne ($\sim$3,300 cm^{-1}) and epoxy ($\sim$890–930 cm^{-1}) (Figure 10) using hot-stage IR also provided a stimulus to investigate this. Toward this end, a mixture of azide **000021-37**, alkyne **000021-38**, BisF-epoxy (20 wt% of **000021-38** vs. BisF epoxy) and 1 wt% of Cu(I) was taken and a DSC scan was performed, which is shown Figure 10. With two peaks appearing in the DSC profile, the outcome of this experiment was along the expected lines. The first peak (T_c = 109°C) was presumed to be arising from 'Click' chemistry and the second curing peak from epoxy curing (T_c = 258°C).

To confirm this, a hot-stage experiment was performed using the above resin system in the temperature range 25–280°C. In the temperature range 70–120°C, the main changes were the decrease of the alkyne (C≡C–H) and azide band intensities at 3,350–3,150 and 2,200–2,000 cm^{-1} frequency region, respectively, confirming that the first curing peak was coming from 'Click' chemistry. At higher temperatures (>180°C), the absorption intensity of the oxirane group

(930–890 cm^{-1}) started to decrease. The analysis showed that the maximum reaction rate occurred at 220–260°C temperature range. This experiment, thus established the chemistry involved in both stages of the curing.
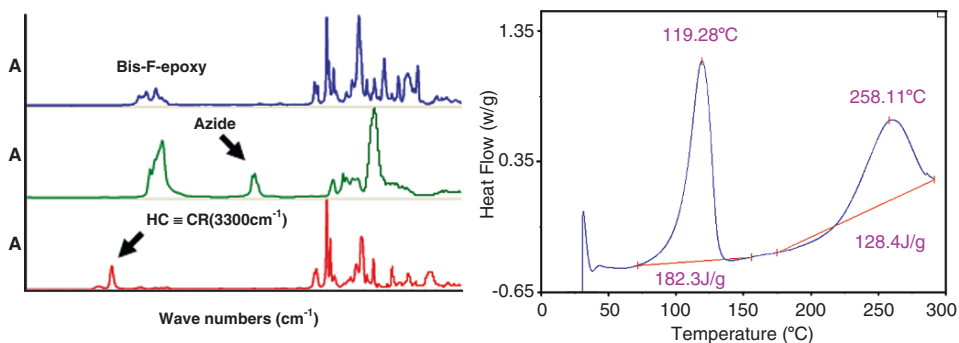
Figure 10. DSC profile of a mixture azide **000021-37**, alkyne **000021-38**, bisF-epoxy, 1 wt% CuI and the IR spectrum of individual resin components.

Figure 11 shows the normalized intensity profiles of azide, alkyne and the oxirane bands. The decrease in intensity of azide/alkynes and that of oxiranes with temperature is pretty much consistent with what was observed in the DSC of this system. The intensity profile showed that maximum reaction rate for the azide/alkyne occurred in the 70–110°C temperature range. The Alkyne signal disappeared completely at 120°C, suggesting that the alkyne/azide reaction reached completion at 120°C. The residual azide peak after 120°C is believed to be due to slightly excess azide in the mixture which began to decompose at approximately 220°C. The epoxy, in contrast, showed maximum reactivity between 220–260°C temperature range.

Figure 11. Normalized intensity profiles of azide, alkyne and epoxy bands.

8.   Mechanical Property Investigation and Synergistic Cu(I)-Silver Effect

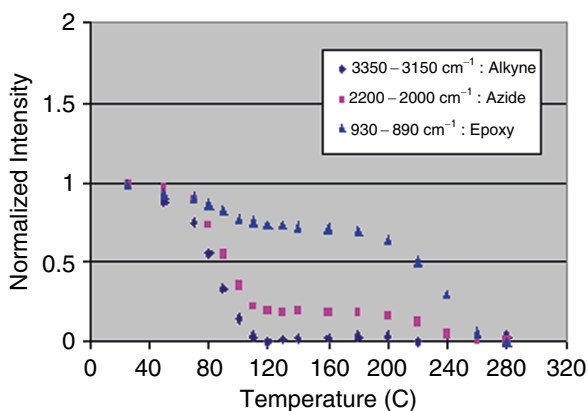In addition to the curing study, we also performed some curing evaluation of the 'Click chemistry' resin systems with a particular focus on testing the adhesion to metal leadframe both in the presence and absence of fillers. While the study of copper(I) catalyst effect was limited to propargylamines (tripropargylamine, **000021-38**, **000021-39**), we demonstrated that this effect was operative even when propargyl ethers were used. Thus, azide **000021-14** and alkyne **13394-113** cured at 88°C when 1 wt% CuI was used (compare with 150°C for the control). Under these conditions the resin gelled with in minutes after mixing CuI catalyst. As was observed before with propargylamines, the curing profiles however, could be improved using softer catalysts such as CuSBu under reduced loading (0.1 wt%). There was also an intriguing synergistic or cooperative cure temperature lowering effect when a combination of CuSBu and silver filler was used in the formulation. For example, while resins **000021-14** and **000067-16** cured at 133°C with 1 wt% CuSBu, addition of 75% silver filler to this resin mixture lowered the cure temperature to 69°C. In addition to this finding, we performed several die shear tests using the inhouse azides and alkynes. During this investigation, it turned out that azide **000021-1**4 was not compatible with all the alkynes except **000067-16** and the die shear tests gave very poor results (1 to 4 kg). In contrast, the compatible system, **000021-14** and **000067-16**, gave very good adhesion to the PPF lead frame (~25 kg at r.t) that was comparable to the control (30–35 kg). The good adhesion observed with this system was initially presumed to be due to good compatibility. However, this assumption turned out to be wrong since a perfectly compatible system, **000067-16** and **000021-37**, gave very poor adhesion to the PPF leadframe. A fundamental understanding of this issue is currently underway. Since **000067-16** and **000021-14** affords a linear polymeric system, it is believed that using a corsslinkable azide/alkyne system we might be able to improve the adhesion further.

Although **000067-16**, possessing the bisphenol A backbone exhibited good compatibility with **000021-14** and good adhesion properties, subsequent efforts to synthesize this resin afforded only solid material (m.p. 93°C), which turned out to be not miscible with **000021-14**. To resolve this issue, bisphenol E, possessing one carbon less and lower m.p. than bisphenol A, was used for the propargylation. Thus, reaction of bisphenol E with K_2CO_3/propargyl bromide furnished **000067-33** (Figure 12). As anticipated, **000067-33** turned out to be a liquid and the die shear showed similar results as observed for **000067-16** (~25 kg) on PPF leadframe. This result confirmed that backbone is critical to get good adhesion properties in 'Click' chemistry. A fundamental understanding of this adhesion phenomenon is currently underway.

While **000067-16** gave good adhesion properties, compatibility was still an issue with this system because of highly nonpolar nature of azide **000021-14**.

Efforts to address this issue involved the synthesis of diester **000067-40** (Figure 12), which has a similar dimerdiol backbone. Thus, reaction of dimer diacid with thionyl chloride followed by esterification with propargyl alcohol afforded ester **000067-40**. The structure of **000067-40** was established by ^{1}H NMR and GPC/MS.
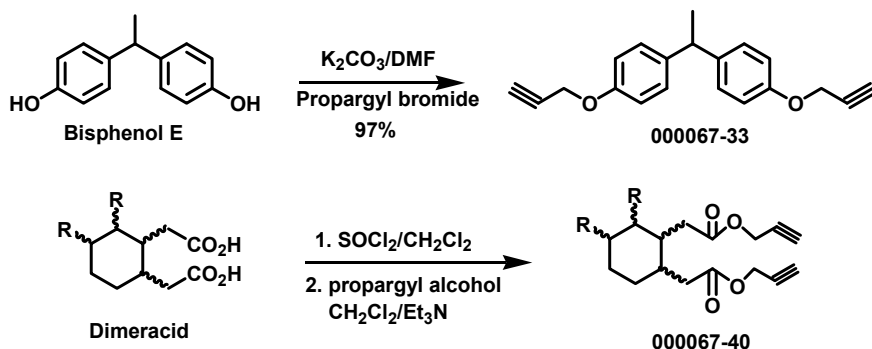

Figure 12. Synthesis of alkynes **000067-33** and **000067-40**.

9.   Hybrid Approach Using Solution Phase 'Click' Chemistry

As mentioned above, our second approach in 'Click' chemistry involved the synthesis of triazole hybrids using *in situ* generated Cu(I) catalyst in solution phase. Here the preformed triazole unit serves as a linker as well as an internal adhesion promoter. The advantages of using triazole as linkers include the extremely mild reaction conditions used for its formation and the compatibility of this chemistry with many functionalities. The *in situ* generation of catalytic Cu(I) species can be achieved using literature procedures employing Cu(II) salts along with a reducing agent such as sodium ascorbate. The polymerizable units can include epoxy, acrylate or maleimide groups containing alkyne functionality. To achieve these objectives, resin **000067-8**, containing both oxirane and triazole functionalities was synthesized from azide **000021-14** and commercially available glycidyl propargyl ether in the presence of $CuSO_4.5H_2O$ and sodium ascorbate in solution phase (Figure 13). Interestingly, resin **000067-8** was found to cure at ~160°C in the absence of any added amine catalysts. It is believed that the fairly nucleophilic triazole functionality initiates the polymerization of the epoxy group at elevated temperatures. Further exploration of the epoxy curing using triazoles as initiators is being planned under the initiator umbrella.
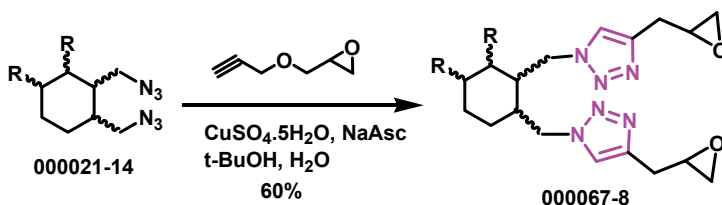
Figure 13. Synthesis of hybrid epoxy-triazole **000067-8**.

10. Controlled Oligomerization of Azide/Alkynes

The third approach in 'Click' chemistry involved controlled oligomerization of difunctional azides and alkynes in solution. These oligomers were expected to exhibit thermoplastic behavior. The incompatibility of azide **00002-14** with many propargyl ethers and volatility of propargyl ethers such as **13394-113**, provided a need to pursue this approach. It was reasoned that the above issues can be addressed by performing controlled oligomerization in a solvent to give oligomers, which can be used in a secondary chain growth polymerization. Initially we explored the controlled oligomerization in bulk phase using copper (I) catalysts, which however, gave access to polymers possessing molecular weights of >10,000 Da. To alleviate this uncontrolled oligomerization problem, the process was attempted in a solvent in the absence of catalysts. Thus, **000021-14** and **13394-113** in 1:1 ratio were heated in toluene at 100°C for 2 h to afford the oligomer **000067-25** (Figure 14). Two batches of this oligomer (**000067-21** and **000067-25**) were prepared and analyzed using GPC. The GPC profiles of these oligomer batches are shown in Figure 15, which were found to be not super imposable. One batch of oligomer (**000067-21**) showed a Mw = 2,217 Da (Table 3, entry 1), while the other batch (**000067-25**) had a Mw = 1,439 Da. The inconsistent molecular weight distributions obtained in this set of experiments was believed to be due to slow oligomerization of batch **000067-21** at r.t, which was prepared 3 weeks prior to the GPC experiment. To confirm this, another set of oligomerization was performed this time using azide **000021-14** and alkyne **000067-16** (incompatible solid in bulk phase). Two batches of the oligomers were prepared back to back (**000067-38** and **000067-41**) by heating the above resin mixture in toluene at 100°C for 3.5 h. Gratifyingly, the GPC showed reproducible results (GPC profile B, Figure 15) that showed identical molecular weight distribution of oligomers in both batches (entries 3 and 4, Table 3). This experiment proved that controlled oligomerization is indeed possible.
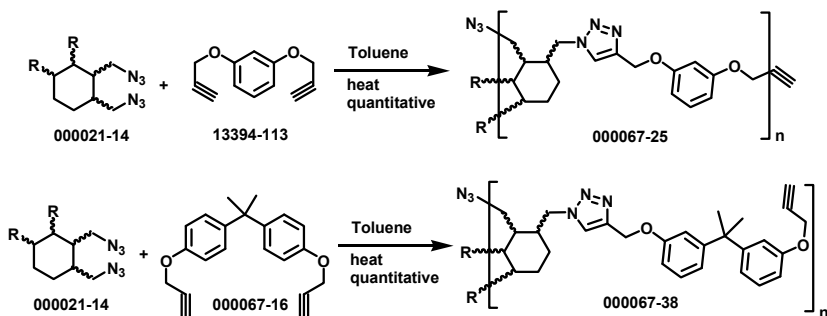
Figure 14. Oligomerization of **000021-14** with **13394-113** and **000067-16**.

GPC profile A   GPC profile B
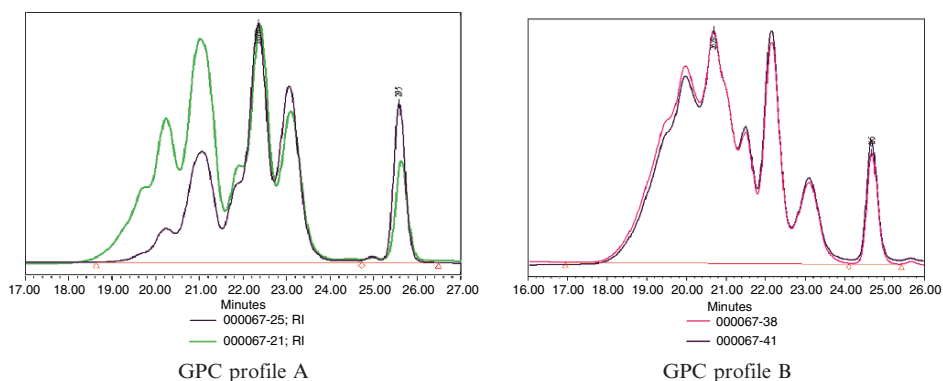
Figure 15. GPC profiles of oligomers.

TABLE 3. Molecular weight distribution averages (relative to polystyrene).

Entries	Sample	Mn	Mw	Mw/Mn
1	000067-21	1,478	2,217	1.5
2	000067-25	1,137	1,439	1.3
3	000067-38	2,036	3,343	1.6
4	000067-41	1,976	3,201	1.6

11. Conclusion

Several azide and alkyne resins were synthesized for "Click" chemistry and their curing potential was evaluated with a special emphasis on exploring Cu(I) catalyst effect. The preliminary curing study in the absence of catalysts showed a strong dependence of cure temperatures on the electronic nature of alkynes. The cure temperatures showed a tendency to increase with decreasing electronegativity of the substituent on alkynes. The capability of Cu(I) catalysts to accelerate the

'Click' chemistry was demonstrated for the first time in bulk phase. Using several Cu(I) catalysts, the cure temperatures could be lowered by as much as 40–100°C compared to the control, depending on the nature of catalyst and the catalyst loading. We discovered a novel synergistic effect between Cu(I) and silver filler in lowering the cure temperatures. Using this combination, lower cure temperatures could be obtained than using either alone. Solution phase 'Click' chemistry was employed for the synthesis of a hybrid triazole-epoxy resin system. This system was found to cure without added amine curative.

References

[1]   R. Huisgen, In *1,3-Dipolar Cycloaddition Chemistry*; A. Padwa (Ed.); Wiley, New York, 1984; Chapter 1, pp. 1–176.

[2]   V. Rostovtsev, L. G. Green, V. V. Fokin, K. B. Sharpless, *Angew. Chem. Int. Ed.* **2002**, *41*, 2596.

[3]   D. D. Diaz, S. Punna, P. Holzer, A. K. Mcpherson, K. B. Sharpless, V. V. Fokin, M. G. Finn, *J. Polym. Sci: PartA: Polym. Chem*. **2004**, *42*, 4392.

[4]   For a review of azide chemistry see, S. Brase, C. Gil, K. Knepper, V. Zimmermann, *Angew. Chem. Int. Ed.* **2005**, *44*, 5188.

[5]   H. C. Kolb, M. G. Finn, K. B. Sharpless, *Angew Chem. Int. Ed*. **2001**, *40*, 2004.

FROM NOVEL BLOCK-LIKE COPOLYMERS TO REACTIVE NANOPARTICLES: ATRP AND "CLICK" CHEMISTRY AS SYNTHETIC TOOLS

WIM VAN CAMP, BART DERVAUX, MIEKE LAMMENS, LIEVEN VAN RENTERGHEM, AND FILIP DU PREZ[*]
Department of Organic Chemistry, Ghent University, Polymer Chemistry Research Group, Krijgslaan 281 S4bis, B-9000 Gent, Belgium

Abstract: In this chapter, we report on the synthesis and characterization of well-defined amphiphilic block copolymers, 'block-like' copolymers and star copolymers composed of poly(isobornyl acrylate) (PiBA) and poly(acrylic acid) (PAA) by ATRP. As PiBA polymers exhibit interesting physical characteristics, we report first a detailed study of the homopolymerization of iBA. The precursor monomers 1-ethoxyethyl acrylate as well as tert-butyl acrylate have been used to synthesize the precursor polymers for the PiBA-co-PAA block copolymers. Furthermore, a combination of ATRP and 'click' chemistry was used to prepare block and graft copolymers using a modular approach. The PiBA-PAA block and 'block-like' copolymers were investigated as pigment stabilizers for aqueous pigment dispersions. In the second part of the research, well-defined PiBA star copolymers were prepared, and reactive nanoparticles were obtained by end group modification of the PiBA star polymers with reactive moieties. Finally, the control of the visco-elastic properties by the incorporation of these nanoparticles in an acrylate polymer matrix was investigated.

1. Design of Block- and 'Block-Like' Copolymers as Pigment Stabilizers

1.1. INTRODUCTION

In polymer research, on academic as well as industrial level, there is a huge interest for poly(acrylic acid) (PAA) containing polymers because of their pH-responsive

nature and hydrophilic characteristics, and for their interaction with metal ions.[1–4] This allows PAA to be used for applications such as super absorbents or as starting materials for the fabrication of a broad range of polyacrylic esters.

Stimuli-responsive amphiphilic block copolymers are a well-known class of intelligent polymers with a variety of promising potential applications such as entrapment of environmental pollutants,[5] catalysis,[6] stabilizers in emulsion polymerization,[7] drug carriers,[8] nanoreactors[9] and polymeric surfactants.[10, 11] PAA containing amphiphilic copolymers are used for example as emulsifiers, stabilizers,[7] surfactants, dispersants,[12–14] wetting agents, etc. Their application field includes cosmetics, paper industry,[12–14] coatings, bio-applications,[15] drug delivery systems and many others.

In order to further improve the properties of the current materials, the ability to synthesize these polymers with good control over the molar mass, chain architecture and polydispersity is of great importance. As radical polymerization has many advantages compared to other polymerization processes, several methods for controlling radical polymerization have been developed and extensively studied during the last 15 years. These include nitroxide mediated polymerization (NMP), reversible addition fragmentation chain transfer (RAFT) polymerization, and atom transfer radical polymerization (ATRP).

For this research project, well-defined amphiphilic block and "block-like" copolymer structures of acrylic acid (AA) and hydrophobic isobornyl acrylate (iBA) were synthesized by ATRP. These copolymers were evaluated as dye pigment stabilizers. Furthermore, the synthesis of PiBA-PAA block and graft copolymers by a combination of ATRP and Cu(I) catalyzed azide–alkyne 'click' reactions was investigated.

In the second part of this chapter, the preparation of a new type of nanoparticle starting from PiBA star-shaped polymers with reactive end groups is described.

1.2. HOMOPOLYMERIZATION OF IBA BY ATRP

PiBA was chosen as the hydrophobic segment for the amphiphilic copolymers because it has a number of interesting physical properties compared to other polyacrylates. For instance, due to the bulky side group of iBA (Figure 1), the corresponding polymer has a high glass transition temperature (T_g = 94°C), comparable to that for poly(methyl methacrylate) (PMMA) or polystyrene (PS).[16] PiBA is particularly interesting as an alternative to these polymers since the synthesis of PMMA or PS with ATRP with end group functionality (>90%) is not possible. However, only a limited amount of reports have been published about the synthesis of PiBA polymers. Therefore, a detailed study of the homopolymerization of iBA by ATRP was first performed in order to synthesize well-defined (block) copolymers in the next step.[17] Optimization of the reaction conditions resulted in well-defined PiBA homopolymers (Table 1).
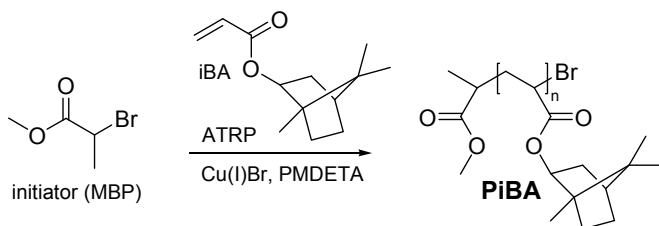
Figure 1. Polymerization of isobornyl acrylate to poly(isobornyl acrylate) (PiBA) by ATRP.

TABLE 1. Optimized reaction conditions and results of the homopolymerization of iBA by ATRP.

Entry[a]	$[M]_0/[In.]_0/$ $[Cu]_0/[ligand]$[b]	solvent	Time (min)	Conv.[c] (%)	$M_{n,exp}$[d] (g/mol)	M_w/M_n
1	100/1/0.5/0.75	EtOAc (25 v%)	60	27	3,300	1.26
2	200/1/0.5/0.5	EtOAc (25 v%)	390	28	8,300	1.25
3	100/1/1.5/1.5	EtOAc (33 v%)	250	93	145,00	1.16

[a.] All reactions were carried out using methyl-2-bromopropionate (MBP) as initiator, Cu(I)Br as catalyst and *N,N,N′,N″,N″*-pentamethyldiethylenetriamine (PMDETA) as ligand. Polymerization temperature = 77%.

[b.] $[M]_0$, $[In.]_0$, $[Cu]_0$ and [ligand] = initial concentration of monomer, initiator, copper catalyst and ligand respectively.

[c.] Calculated from ^{1}H NMR.

[d.] Relative to polystyrene standards.

For all reactions, high polymerization rates were obtained and PDIs were found to be as low as 1.16 for conversions up to 90%. The molecular weight of the polymers could be varied while maintaining control by increasing the monomer to initiator ratio ($[M]_0/[In]_0$) (entry 1 and 2) or increasing the copper concentration from 0.5 to 1.5 eq, resulting in a higher monomer conversion (entry 1 and 3). The first order kinetic plot shows a linear behaviour, indicating the controlled character of the polymerization reaction. Also, the number average molecular weight (M_n) increases as a function of conversion, while the PDI remains low throughout the polymerization reaction. Moreover, MALDI-TOF MS analysis of the different homopolymers revealed the controlled character of the poly-merization.[17]

1.3. SYNTHESIS OF PIBA-B-PTBUA AND PIBA-B-PEEA BLOCK COPOLYMERS

The above synthesized PiBA polymers were then used as a macroinitiator to synthesize amphiphilic PiBA-*b*-PAA block copolymers. As the ATRP mechanism is not able to polymerize AA in a direct way,[18] a precursor strategy has to be

used for the design of the PAA-containing polymer structures. Frequently used precursor monomers include *tert*-butyl acrylate (tBuA),[19, 20] benzyl acrylate,[21] as well as the 1-ethoxyethyl acrylate (EEA) precursor strategy which was recently developed in our research group.[22–24] Deprotection of the PtBuA segment is done by hydrolysis, including a subsequent purification step, while the PEEA segment is deprotected by thermolysis.[17, 22, 25, 26] In this study, both the tBuA and the EEA precursor strategy were evaluated for the synthesis of well-defined PiBA-PAA copolymers, and the synthetic strategy is depicted in Figure 2.
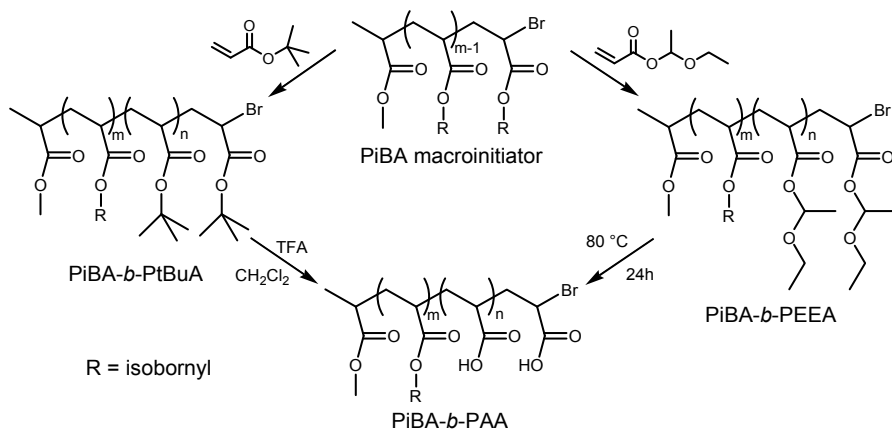
Figure 2. Synthesis of PiBA-*b*-PAA via ATRP by making use of a precursor strategy. (Reproduced with permission from J. Polym. Sci., Part A: Polym. Chem. **2008**, 46, 1649–1661. Copyright 2008 Wiley.)

An overview of the performed block copolymerizations is given in Table 2. In all cases, 3 eq of Cu catalyst compared to the macroinitiator concentration were used in order to have a sufficiently fast polymerization rate. Cu(I)Br was used in combination with PMDETA as the catalytic system. By varying the length of the macroinitiator and making use of various reaction conditions for the polymerization of the second block, a series of PiBA-*b*-PEEA block copolymers was prepared with different ratios of PiBA/PEEA and different lengths of both segments. The controlled character of the polymerization reactions was confirmed by a detailed kinetic analysis. Also, in GPC analysis, no unreacted macroinitiator was observed, indicating that pure block copolymer is obtained (Figure 3). Furthermore, these results demonstrate that the polymerization of iBA (synthesis of macroinitiator) occurs with negligible loss of the bromine end group.

TABLE 2. Summary of the reaction conditions and results for the synthesis of PiBA containing block copolymers by ATRP.

Entry[a]	$[M]_0/[In.]_0/$ $[Cu]_0/[ligand]$[b]	Solvent	Temp. (°C)	Time (min)	Conv.[c] (%)	$M_{n,exp}$[d] (g/mol)	M_w/M_n	Composition[e]
4	260/1/3/4.5	EtOAc (50 v%)	75	540	18	12,300	1.18	$PiBA_{73}\text{-}b\text{-}PtBuA_{38}$
5	200/1/3/4.5	EtOAc (25 v%)	50	270	36	13,800	1.15	$PiBA_{25}\text{-}b\text{-}PEEA_{70}$
6	200/1/3/4.5	–	50	250	19	13,700	1.21	$PiBA_{55}\text{-}b\text{-}PEEA_{38}$
7	200/1/3/4.5	–	60	240	37	17,700	1.26	$PiBA_{55}\text{-}b\text{-}PEEA_{75}$
8	150/1/3/4.5	–	70	245	45	14,100	1.22	$PiBA_{17}\text{-}b\text{-}PEEA_{72}$

[a.] All reactions were carried out using Cu(I)Br as catalyst and *N,N,N',N'',N''*- pentamethyldiethylenetriamine (PMDETA) as ligand.

[b.] $[M]_0$, $[In.]_0$, $[Cu]_0$ and $[ligand]$ = initial concentration of monomer, macroinitiator, copper catalyst and ligand respectively.

[c.] Calculated from ^{1}H NMR.

[d.] Relative to polystyrene standards.
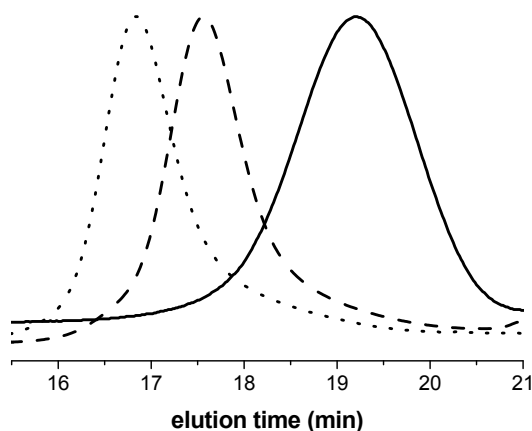
[e.] Determined from ^{1}H NMR.

Figure 3. GPC analysis of $PiBA_{17}$ macroinitiator (solid line) and the corresponding block copolymer $PiBA_{17}$-b-$PEEA_{72}$ (dotted line). The dashed line represents the GPC analysis of the deprotected block copolymer. (Reproduced with permission from J. Polym. Sci., Part A: Polym. Chem. **2008**, 46, 1649–1661. Copyright 2008 Wiley.)

1.4. SYNTHESIS OF PIBA-CO-PTBUA AND PIBA-CO-PEEA 'BLOCK-LIKE' COPOLYMERS

In addition to the synthesis of block copolymers via the macroinitiator strategy, copolymers of iBA and AA were also prepared via a sequential monomer addition[27] process, resulting in 'block-like' copolymers (Figure 4). The molecular

architecture of this type of copolymers is an intermediate between those of block and random copolymers and consists of a first block of pure iBA and a random second block of iBA and AA. Therefore, the repulsive inter-chain interactions are less strongly changing along the chain in comparison with a conventional block copolymer. Because of this, these polymers may be of particular interest for specific applications such as stabilization of dispersions.[28, 29] A copolymer with a structure close to that of a block copolymer can be obtained if a high conversion for the first block is reached prior to the addition of the second monomer. The major advantage of this synthetic approach is that time-consuming purification steps are avoided and replaced by a one-pot synthesis.
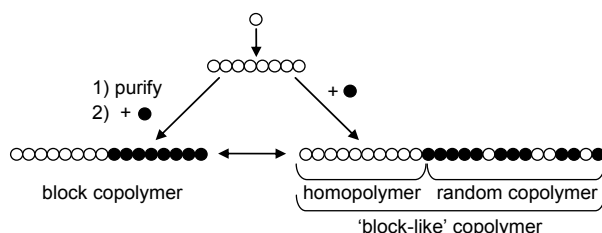
Figure 4. *Left*: Schematic depiction of the macroinitiator strategy yielding block copolymers. *Right*: Schematic depiction of sequential monomer addition, yielding 'block-like' copolymers. (Reproduced with permission from J. Polym. Sci., Part A: Polym. Chem. **2008**, 46, 1649–1661. Copyright 2008 Wiley.)

Table 3 gives an overview of the reaction conditions and results of the various 'block-like' copolymerizations. For all reactions, Cu(I)Br was used as catalyst, PMDETA as ligand and EtOAc as solvent. A second amount of Cu(I)Br/PMDETA was introduced with the addition of the second monomer in order to maintain a controlled and sufficiently fast polymerization.

The clear increase of the molecular weight after the addition of the second monomer shows that the PiBA segment efficiently initiates the formation of the second segment, even when the first segment has reached a high conversion (up to 81%) when the second monomer is added (Table 3, entry 9–10).

The molecular weight of the copolymer increases linearly as a function of time, even after the addition of the second monomer, while the PDI remains low during the polymerization reaction (Figure 5, left). The first order kinetic plot of the polymerization of both monomers also shows a linear behaviour (Figure 5, right). After the addition of the EEA monomer, the polymerization rate of iBA decreases as a result of dilution of the reaction mixture. It can be concluded that kinetic analysis of the 'block-like' copolymerization of iBA and EEA demonstrates the controlled behaviour of the copolymerization.

TABLE 3. Summary of the reaction conditions and results for the synthesis of PiBA containing "block-like" copolymers by ATRP.

Entry[a]	$[iBA]_0/[M_2]_0/[In.]_0/$ $[Cu]_0/[ligand]$[b]	Time[c] (min)	Conv. iBA[d, e] (%)	Conv. M_2[d] (%)	$M_{n,exp}$[f] (g/mol)	M_w/M_n	Composition[g, h]
9	67/200/1/1/1	126–310	81–95	63	26,600	1.25	$iBA_{54}//iBA_9/tBuA_{126}$
10	75/143/1/1.5/1.5	157–380	70–78	32	12,700	1.24	$iBA_{54}//iBA_6/PEEA_{46}$
11	75/200/1/1.5/1.5	95–380	53–56	6	8,000	1.17	$iBA_{46}//iBA_2/PEEA_{13}$
12	75/200/1/1.5/1.5	90–380	44–55	23	9,800	1.22	$iBA_{34}//iBA_9/PEEA_{46}$

[a.] All reactions were carried out at 70°C using methyl 2-bromopropionate (MBP) as initiator, Cu(I)Br as catalyst, N,N,N',N'',N''-pentamethyldiethylenetriamine (PMDETA) as ligand and ethyl acetate as solvent.

[b.] $[iBA]_0$, $[M_2]_0$, $[In.]_0$, $[Cu]_0$ and $[ligand]$ = initial concentration of isobornyl acrylate, second monomer, copper catalyst and ligand respectively.

[c.] Time before addition of the second monomer and at the end of the polymerization.

[d.] Determined by GC.

[e] Conversion before and after addition of the second monomer.

[f.] Relative to polystyrene standards.

[g.] Determined from ^{1}H NMR.

[h.] Notation 'block-like' copolymers: before double line PiBA segment with average DP; after double line, composition second segment after adding second monomer.
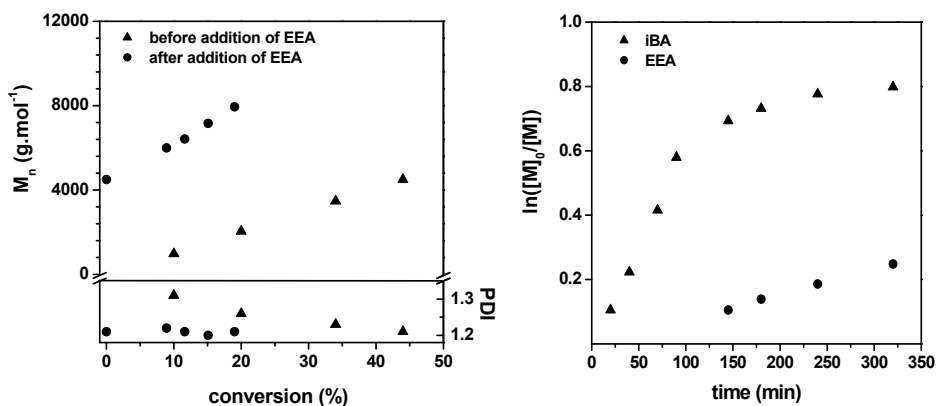
Figure 5. Synthesis of 'block-like' copolymers of iBA with EEA [entry 12, Table 3]. (*left*) increase of M_n (before and after addition of EEA) and evolution of PDI (before and after addition of EEA) as a function of conversion (after addition of EEA, the total conversion of iBA and EEA, since the addition, is used), (*right*) first order kinetic plot. (Reproduced with permission from J. Polym. Sci., Part A: Polym. Chem. **2008**, 46, 1649–1661. Copyright 2008 Wiley.)

1.5. DEPROTECTION OF THE PRECURSOR POLYMERS TO THE CORRESPONDING PAA-CONTAINING COPOLYMERS

In a next step, the PiBA-PtBuA block and 'block-like' copolymers were hydrolysed to PiBA-PAA using trifluoroacetic acid. FT-IR analysis revealed the hydrolysis of the *tert*-butyl ester group to carboxylic acid. However, it was found that the isobornyl ester is not stable under these reaction conditions. This shows that the *tert*-butyl protecting group strategy is not suitable to synthesize amphiphilic PiBA-PAA copolymers. In contrast, deprotection of the 1-ethoxyethyl protecting group of the PEEA segment by a heating step results in the desired amphiphilic PiBA-PAA copolymers.[17, 25] TGA analysis showed complete and selective deprotection of the PEEA segment without danger for degradation of the PiBA segment. This was also confirmed by ^{1}H-NMR analysis. GPC analysis before and after deprotection confirms the absence of side reactions (see Figure 3).

In another study, the morphological transition behavior during the *in situ* thermal deprotection of PiBA-*b*-PAA copolymers was visualized using atomic force microscopy.[26]

1.6. "CLICK" CHEMISTRY FOR THE DESIGN OF PAA CONTAINING BLOCK AND BRUSH COPOLYMERS

In addition, the combination of ATRP of EEA, our precursor monomer for acrylic acid, and the copper(I) catalyzed "click" 1,3-dipolar cycloaddition reaction of azides and terminal alkynes was evaluated as an alternative method to synthesize diverse PAA containing block and graft copolymer structures (Figure 6).[25]

A modular approach has been used. First, polymers with alkyne functionalities as well as azide functionalities have been synthesized. These polymers were subsequently "clicked" together to yield block copolymers. Furthermore, graft copolymers were synthesized by grafting alkyne-containing polymers onto a polymer backbone with multiple azide functions using the combination of ATRP and "click" reactions (see Figure 6).

Alkyne functionalities were introduced via polymerization of EEA with the alkyne containing initiator[30] propargyl 2-bromopropionate (Figure 7, right), while azide-containing polymers were obtained either via nucleophilic substitution of the bromide end group of hydrophobic poly(isobornyl acrylate) (PiBA) into an azide[31] (Figure 7, left), or by copolymerization with an azide containing monomer.[32] The azide containing monomer 3-azidopropyl methacrylate (AzMA) was copolymerized with MMA, yielding a random copolymer poly(MMA-*co*-AzMA).[25] The controlled behaviour of the polymerization reactions was demonstrated.
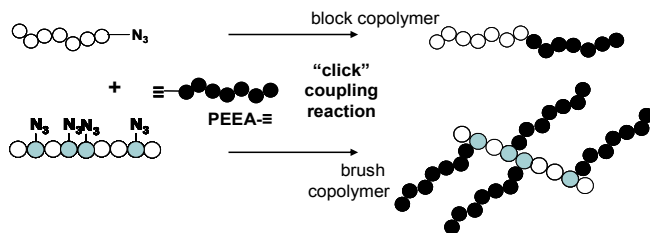
Figure 6. Schematic depiction of the synthesis of block and brush copolymers using "click" chemistry. (Reprinted from React. Funct. Polym. 2007, 67, 1168−1180, Copyright 2007, with permission from Elsevier.)
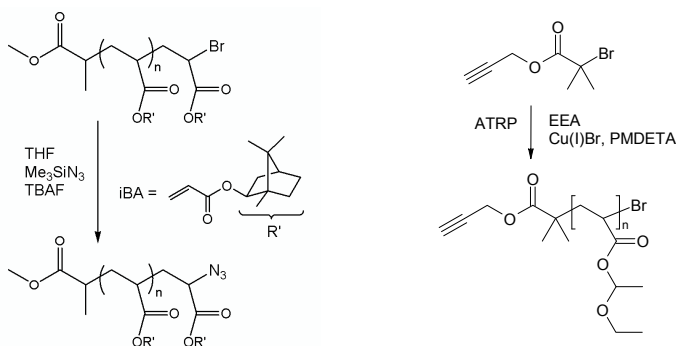

Figure 7. *Left*: Transformation of the bromide end group of PiBA to an azide by nucleophilic substitution. *Right*: ATRP of EEA using an alkyne-containing initiator. (Reprinted from React. Funct. Polym. **2007**, 67, 1168–1180, Copyright 2007, with permission from Elsevier.)

Block copolymers were obtained by "clicking" PEEA-≡ with PiBA-N₃. The reaction showed to be both quantitative and fast. After selective precipitation (PEEA-≡ was used in excess) and deprotection of the PEEA segment by a heating step,[22–25] the desired amphiphilic PAA-containing block copolymers were obtained (not shown).

Amphiphilic graft/brush copolymers were successfully prepared by "clicking" linear PEEA-≡ onto a polymer containing multiple azide functions, followed by deprotection of the PEEA side chains. Effective coupling of the PEEA-≡ chains onto the poly(MMA-*co*-AzMA) copolymer was observed, by the formation of a high molecular weight product in GPC analysis. Moreover, from a comparison of the M_n and peak molecular weight (M_p) values of the poly(MMA-*co*-AzMA) copolymer, the PEEA-≡ and the coupled product (Table 4), it was concluded that the "click" coupling reaction proceeded successfully.

TABLE 4. Summary of the results of the "click" coupling reaction between poly(MMA-*co*-AzMA) and PEEA-≡ , yielding a brush copolymer. (Reprinted from React. Funct. Polym. **2007**, 67, 1168–1180, Copyright 2007, with permission from Elsevier.)

Entry	$M_n/M_p/PDI$[a] copolymer poly(MMA$_{39}$-*co*-AzMA$_9$)[b]	$M_n/M_p/PDI$[a] PEEA-=	$M_n/M_p/PDI$[a] coupled product
13	7,000/9,900/1.25	4,600/5,400/1.21[c]	37,100/46,900/1.27
14	7,000/9,900/1.25	6,100/7,000/1.16[d]	42,200/56,800/1.23

[a.] Relative to polystyrene standards.

[b.] $[MMA]_0/[AzMA]_0/[In]_0/[Cu]_0/[ligand] =$. 60/15/1/0.5/0.5, 50°C, 60 min, conv. MMA= 48%, conv. AzMA= 47%.

[c.] $[M]_0/[In]_0/[Cu]_0/$ [ligand] = 100/1/1/1; 70°C, 307 min., conv. = 40%.

[d.] $[M]_0/[In]_0/[Cu]_0/$ [ligand] = 100/1/1/1; 70°C, 304 min., conv. = 37%.

1.7. PIBA-PAA BLOCK AND 'BLOCK-LIKE' COPOLYMERS AS PIGMENT STABILIZING POLYMER STRUCTURES

The amphiphilic block and 'block-like' copolymer structures as described above were compared as stabilizers for aqueous colloidal dispersions of hydrophobic copper phtalocyanine (CuPc) and hydrophilic titanium dioxide (TiO$_2$) pigments.[33] Pigments are colouring powders that are usually mixed with water or oil in order to produce paints and inks. In order to obtain a better storage and colour stability of the pigments, they have to be dispersed and stabilized as separate particles. Recently, aqueous colloidal dispersions of pigments have been of increasing interest from both scientific and practical points of view. Amphiphilic copolymers are known to be effective stabilizers of various colloidal dispersions, e.g. pigments in aqueous media.[34, 35]

The stabilization of aqueous dispersions by polymer surfactants is a result of the adsorption of amphiphilic macromolecules on the particle surface: often one segment of the amphipolar copolymer acts as an anchor. Depending on the characteristics of the pigment and the copolymer, mono- or multi-layers, which provide steric and/or electrostatic stabilization, are formed.

The sedimentation behaviour of the pigments was used to evaluate the pigment stabilizing properties of a series of polymers. The sedimentation measurements were performed with and without ultrasonic treatment since it is shown in literature that ultrasonic treatment has a positive effect on the stability of aqueous dispersions of pigments in the presence of polymeric stabilizers.[35]

All PiBA-PAA copolymers allow stabilizing pigment dispersions even without ultrasonic treatment (see Table 5). However, irrespective of the molecular composition of the copolymer, ultrasonic treatment significantly improves the dispersion stability as reflected by the sedimentation half times. It is also clear from the data that there is an optimal copolymer structure with regard to the

block length ratio. For dispersions of hydrophilic TiO$_2$, PiBA$_{17}$-b-PAA$_{72}$ with a long PAA block (block length ratio PiBA/PAA ~ 1/4) gives good stabilization, while for hydrophobic CuPc, PiBA$_{51}$-b-PAA$_{30}$ with a PiBA block exceeding the PAA block length (PiBA/PAA ~ 2) revealed the best stabilizing properties. Similar results were obtained for the PiBA-co-PAA 'block-like' copolymers: a higher content of AA unit results in a better stabilization of the hydrophilic TiO$_2$ pigment, while an increased PiBA block length relative to the iBA/AA copolymer blocks favours the dispersion stability of the hydrophobic CuPc pigment. However, 'block-like' copolymers are not as efficient for the stabilization of pigment dispersions as the pure block copolymers. This may be explained by the fact that the hydrophilicity of the pure PAA block is higher than the one of the PiBA/PAA block in 'block-like' copolymers as a result of the presence of hydrophobic iBA units.

TABLE 5. Suspension stability (half-time of sedimentation, in days) of TiO$_2$ and CuPc aqueous dispersions stabilized by PiBA-PAA block and 'block-like' copolymers.

Polymer	Suspension stability (days)[a]			
	No ultrasonic treatment		With ultrasonic treatment	
	TiO$_2$	CuPc	TiO$_2$	CuPc
PiBA$_{51}$-b-PAA$_{56}$	2	4	14	20
PiBA$_{51}$-b-PAA$_{30}$	0.1	5	1	45
PiBA$_{17}$-b-PAA$_{72}$	3	0.2	30	5
PiBA$_{54}$//PiBA$_6$/PAA$_{46}$	1	1	4	7
PiBA$_{41}$//PiBA$_2$/PAA$_{12}$	0.5	2	5	10
PiBA$_{21}$//PiBA$_{19}$/PAA$_{81}$	2	0.2	12	3
PiBA$_{34}$//PiBA$_{19}$/PAA$_{85}$	1.5	0.3	10	4
PiBA$_{34}$//PiBA$_9$/PAA$_{46}$	1	0.5	5	6

[a] Half time of sedimentation.

To explain these experimental results and the clear difference in pigment stabilization behaviour between block an 'block-like' copolymers, adsorption models have been proposed (see Figure 8).[33]

In the case of the PiBA-b-PAA *block copolymers* (Figure 8, top), the hydrophilic sites of the TiO$_2$ particle interact with the ionic groups of the PAA block in an extended flat conformation, while the PiBA block is in the collapsed state and creates a PiBA dominated shell. The orientation of the next layer of adsorbed molecules is inversed and originates from the hydrophobic interactions between PiBA blocks of block copolymers from the solution and the surface tethered PiBA blocks. This results in a PAA-dominated outer shell (Figure 8, B).

For CuPc pigments, the hydrophobic PiBA segments of the PiBA-*b*-PAA *block copolymers* are adsorbed on the hydrophobic CuPc surface while the hydrophilic PAA segments are pointing to the aqueous medium. The PAA segment can be completely extended or partially interacting with the anchor block (Figure 8, C).
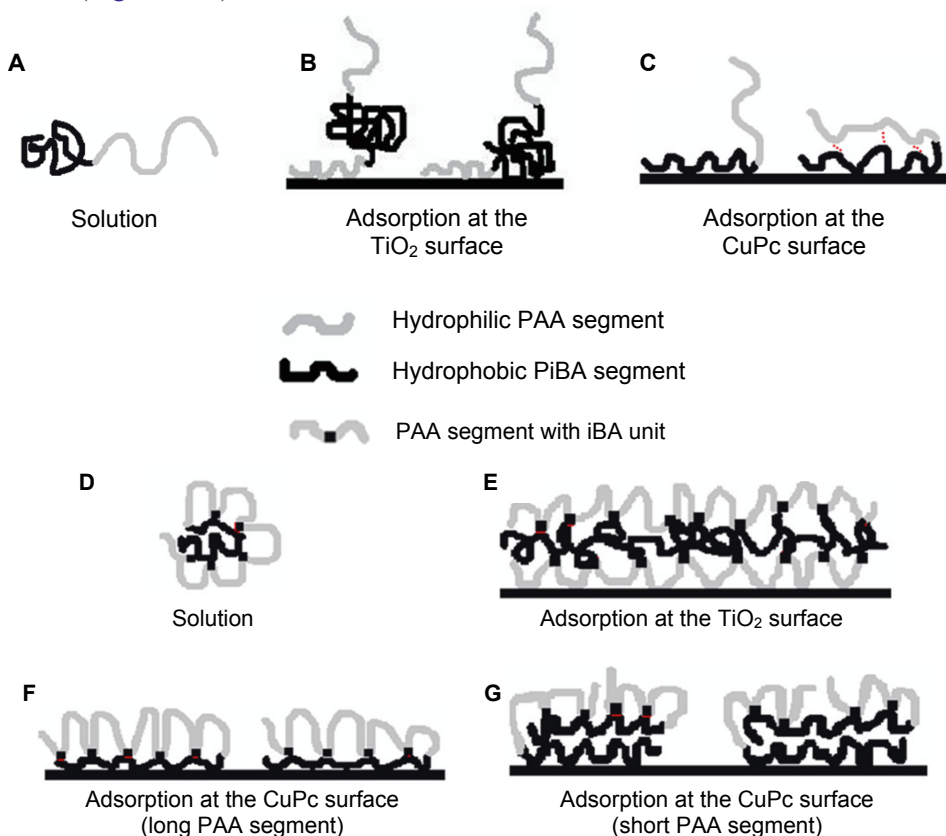

Figure 8. Schematic representation of the conformation of a PiBA-*b*-PAA *block copolymers* in aqueous media (A) and the assumed adsorption model in aqueous TiO_2 dispersions (B) and aqueous CuPc dispersions (C). Schematic representation of the conformation of PiBA-*co*-PAA *'block-like' copolymers* in aqueous media (D) and the assumed adsorption model in aqueous TiO_2 dispersions (E) and aqueous CuPc dispersions (long PAA segment: F; short PAA segment: G).

Adsorption models for the PiBA-*co*-PAA *'block-like' copolymers* are depicted in Figure 8, bottom part. The conformation of 'block-like' copolymers in an aqueous solution or at the particle surface is believed to differ substantially from that of block copolymers. The hydrophilic PAA block with incorporated iBA units (= second segment of the 'block-like' copolymers), is believed to be

partially coiled up due to the hydrophobic interaction of individual iBA units that also interact with the collapsed hydrophobic PiBA block. The conformation of a single 'block-like' copolymer in solution can thus be described as 'double-coil' or 'micelle-like' (Figure 8, D).

In the case of TiO$_2$ pigment, a colloid-formation mechanism[36] is assumed, which involves the formation of copolymer structures at the pigment surface with bilayers, where collapsed PiBA segments create a hydrophobic middle-layer that is located between two outer PAA layers (one adsorbed on the pigment surface and one exposed into the aqueous media) (Figure 8, E).

For aqueous dispersions of CuPc stabilized by *'block-like' copolymers*, the adsorption model includes two cases, mainly due to the different length of the hydrophilic block. For 'block-like' copolymers with a relatively long PiBA/PAA block, a similar adsorption mechanism is assumed as for pure block copolymers: the PiBA blocks adsorb on the pigment surface and are covered by the hydrophilic blocks, forming loops of PAA with anchoring iBA units (Figure 8, F). In the reverse case (short PiBA/PAA block), the PiBA adsorbed onto the pigment surface cannot be completely covered by the PAA segments. Different PiBA blocks aggregate on the surface and can be covered by the PAA segments (Figure 8, G).

2. Design of Reactive Nanoparticles from Star-Shaped Polymer Structures

2.1. INTRODUCTION

Because of their remarkable properties, star polymers continue to attract great attention in polymer research.[37, 38] In comparison to their linear analogues, star polymers have different rheological and mechanical properties and exhibit higher degrees of end group functionality. Controlled synthesis of star polymers also contributes to the elucidation of structure–property relationships in polymer science. Recent developments in atom transfer radical polymerization (ATRP) made it possible to use radical polymerization for the controlled synthesis of star polymers.[39–41] For these techniques, a variety of multifunctional initiators has been developed and successfully used.[42–45] Although end group reactive star polymers offer interesting perspectives to a number of applications as it is a novel way towards nanoparticles, nanocontainers or nanoporous layers,[46–49] limited amount of work has been done with regard to the synthesis of such reactive stars.[50–52]

In this part of our research, we aimed at the preparation of reactive star-shaped polymers by ATRP as precursor for a new type of nanoparticle.[53] Our approach consists of using an intramolecular cross-linking process to create unimolecular nanoparticles (see Figure 9). Therefore, multifunctional initiators developed by Heise et al.[42, 54] have been used to prepare star-shaped poly(isobornyl

acrylate) by ATRP in a controlled way. In a second step, the bromine end groups are transformed to a reactive end group by a nucleophilic substitution with methacrylic acid. The resulting reactive star polymers are then transformed to unimolecular nanoparticles by intramolecular polymerization. Finally, we investigated the use of such nanoparticles as noncovalent cross-linkers for linear polymers. In this way we aimed at the creation of similar properties as those of thermoplastic elastomers (TPEs) without having to prepare triblock copolymers.[55] As a model system, we investigated the viscoelastic properties of a material in which linear, rubbery poly(*n*-butyl acrylate) (PnBuA) chains are entangled with a variable amount of the organic nanoparticles.[53]
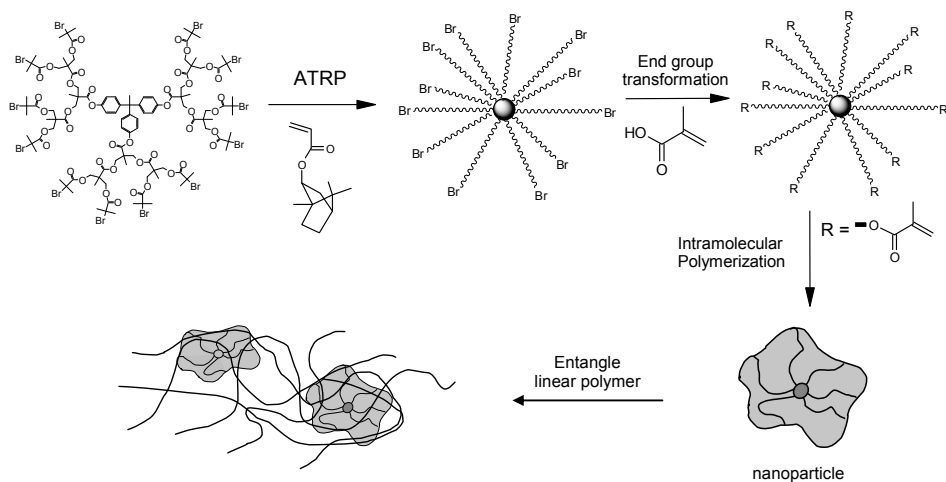

Figure 9. General scheme for the preparation of poly(isobornyl acrylate) nanoparticles and the subsequent incorporation of a linear polymer. (Reprinted with permission from Ref. [53]. Copyright 2008 American Chemical Society.)

2.2. STAR-SHAPED POLY(ISOBORNYL ACRYLATE) BY ATRP

The synthesis of star-shaped PiBA via the core first method using an initiator with 12 arms is depicted in Figure 9. ATRP was chosen as the controlled polymerization technique for two reasons. Firstly, by choosing the right reaction conditions, star-shaped polymers with a well-defined number of arms, controlled molecular weight and narrow polydispersity are obtained. Secondly, ATRP of acrylates, in our case iBA, results in secondary bromide end groups at the end of each arm of the stars, which are available for further modification into reactive end groups.

In the first step, multifunctional initiators were made *via* a route designed by Heise et al.[42, 54], based on a dendritic build-up of a few single blocks prepared by repeating esterification reactions. From this type of initiator, star-shaped

polymer structures with 4, 6 and 12 arms are synthesized. Then, ATRP reaction conditions were optimized to obtain star-shaped polymers with controlled molecular weight and low polydispersity index (PDI) using the synthesized multifunctional initiators. Well-defined structures were obtained using 4 eq of catalyst in comparison to the initiator system. Well-defined PiBA star-shaped polymers with varying molecular weight are shown in Table 6. The good control was also proven by kinetic studies (not shown). However, it has to be mentioned that above conversions of about 50%, star–star coupling occurs due to termination reactions. This is illustrated in Figure 10 in which the GPC curves are depicted as a function of reaction time for the synthesis of star-shaped PiBA with 12 arms. This phenomenon is inherent of the preparation of star-shaped polymers by ATRP,[44, 56, 57] but it can be controlled by terminating the polymerization at conversion below 50%, as also shown elsewhere by ^{1}H NMR analysis.[53]
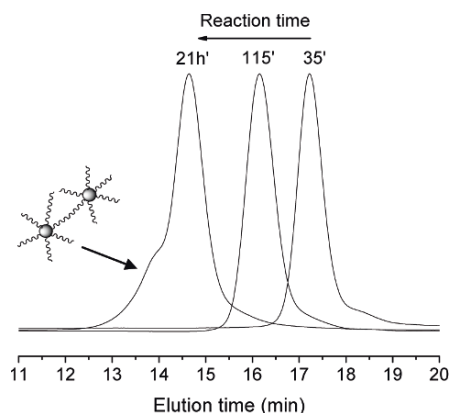

Figure 10. GPC curves as a function of reaction time for star-shaped PiBA with 12 arms (Table 6, Entry 1). (Reprinted with permission from Ref. [53]. Copyright 2008 American Chemical Society.)

In the second step, the star-shaped PiBA was converted into a reactive star polymer (Figure 11).[53] Methacrylate end groups have been introduced by a nucleophilic substitution of the end group using methacrylic acid according to a procedure described by Muehlebach and Rime.[58] The efficiency of this reaction is illustrated in the ^{1}H NMR spectrum in (*middle*) where the appearance of the typical methacrylate signals can be noticed (Figure 12). From the integration of these methacrylic protons (5.5 to 6 ppm), a conversion of more than 95% was calculated (Table 6). To examine the diversity of the reaction, end group modifications with acrylic acid were also performed (Table 6). Surprisingly, the reaction with acrylic acid did not have the same efficiency as the reaction with methacrylic acid. Only at elevated temperatures and longer reaction times, incomplete transformation (40%, entry 3-AA_3, Table 6) was observed. However, this resulted

also in side reactions that were detected by the appearance of shoulders in the GPC analysis.

TABLE 6. Reaction conditions and results for the synthesis of poly(isobornyl acrylate) nanoparticles.

Synthesis of star-shaped poly(isobornyl acrylate) with 12 arms[a]					
Entry	Time (min)	Conv. (%)	$M_{n,theo}$ (g/mol)	$M_{n,GPC}$[a] (g/mol)	M_w/M_n
1	1,260	95	182,000	84,000	1.35
2	125	21	42,000	21,000	1.10
3	135	30	59,000	24,600	1.09
4	116	7	17,000	6,600	1.05
5	100	22	44,000	22,000	1.07
6	90	16	34,000	25,500	1.06

End group modification with acrylic acid and methacrylic acid[b]						
Entry	M_n (g/mol)	Acid	Ratio acid/DBU[b]	Time (days)	T (°C)	Number of reactive groups[c]
3 – AA_1	59,000	Acrylic acid	2/2	3	45	–
3 – AA_2	59,000	Acrylic acid	4/4	3	50	–
3 – AA_3	59,000	Acrylic acid	4/4	6	55	5
3 – MA_1	59,000	Methacrylic acid	4/4	3	50	10
5 – MA_1	44,000	Methacrylic acid	4/4	4	50	11

Formation of nanoparticles[c]			
Entry	Conc. (mg/ml)	Mol% initiator (%)[d]	Conversion (%)[e]
5 – MA_UV_1	900	20	Network
5 – MA_UV_2	5	20	80
5 – MA_UV_3	4	20	75
5 – MA_UV_4	4	20	80

[a] Reactions performed at T = 50°C, 25V% of acetone and DP_{theo} = 75, $[In]_0/[Cu(I)]_0/[L]$ = ratio initiator/Cu(I)Br with [5% Cu]/ligand = 1/4/4; [a]determined via GPC in CHCl₃ using. PS-standards.

[b] Reactions done in ethyl acetate, AA: acrylic acid, MA: methacrylic acid, DBU = 1,8-diazobicyclo[5,4,0]undec-7-ene, [b] ratio compared to the number of bromine end groups; [c] number of bromine groups substituted to ester groups, determined by ^{1}H NMR.

[c] All reactions performed with UV initiation (using benzoin as initiator), reaction time: 4 h in toluene.

[d] Mol% initiator compared to methacrylate groups.

[e] determined by ^{1}H-NMR.
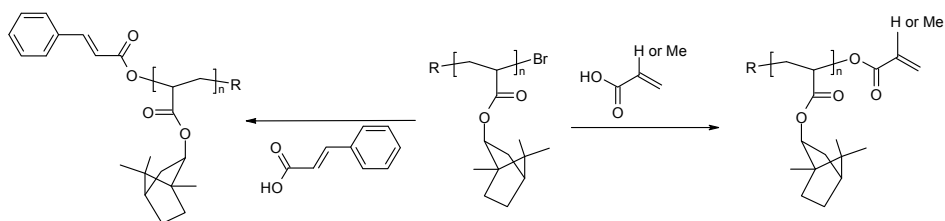
Figure 11. End group modification of poly(isobornyl acrylate) with different acids (*right*: (meth)acrylic acid, *left*: cinnamic acid).
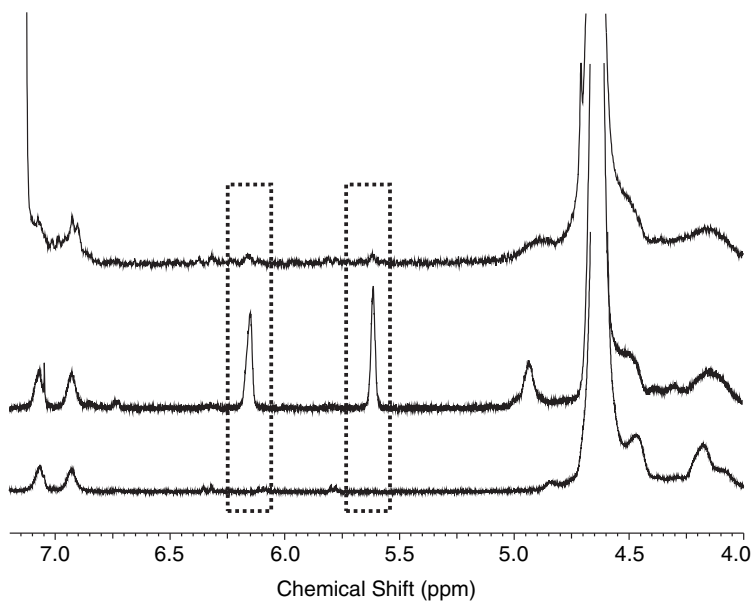

Figure 12. ^{1}H-NMR spectrum of PiBAstar with 12 arms (entry 5, *Table 6*) (*bottom*), the methacrylate functionalized polymer (5-MA_1) and the nanoparticle (entry 5, Table 6 – MA_UV_4) (*top*) (in CDCl$_3$, 500 MHz). (Reprinted with permission from Ref. [53]. Copyright 2008 American Chemical Society.)

2.3. REACTIVE STAR-SHAPED POLYMERS FOR THE PREPARATION OF NANOPARTICLES

For the preparation of the nanoparticles, an intramolecular reaction of the reactive methacrylate end groups of the described star-shaped polymers was performed. Due to the lower reactivity of methacrylate groups bound to a polymer, a UV initiation was chosen, resulting in shorter reaction times. An overview of a selection of reactions is given in Table 6. Since the ratio of *inter-* and *intra-*molecular reaction depends on the concentration of the polymer, a series of

reactions conditions (dilutions) was examined. The resulting products were then analysed by NMR spectroscopy to determine the conversion and by GPC to detect the possible presence of any coupled star polymers. As depicted in (*top*), the nearly complete disappearance of the methacrylate signals demonstrates nearly quantitative conversion. However, NMR analysis demonstrated that the remaining methacrylate groups survived the most stringent conditions, conforming that they would not interfere in the next reaction step.

In Figure 13, the GPC analyses for concentration of 50 and 5 mg/mL are shown. The shoulders at high molecular weight, caused by intermolecular reaction, gradually reduce with decreasing concentration. At 5 mg/mL, only a small fraction of coupled product can be detected. Finally, a concentration of 4 mg/mL was selected for scale-up of the reaction in view of the determination of material properties afterwards.
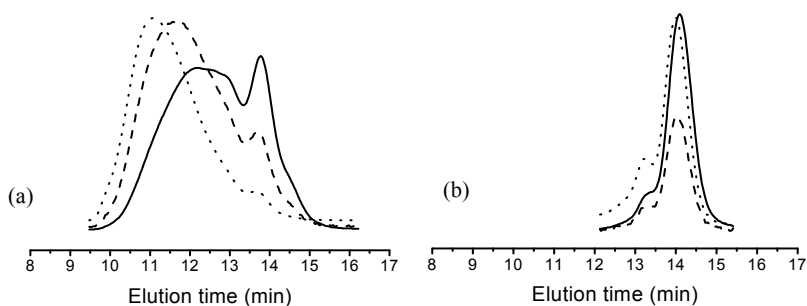

Figure 13. GPC-analyses of the UV-reaction of methacrylate functionalized star-shaped PiBA at different dilutions: (**a**) 50 mg/mL and (**b**) 5 mg/mL. Different detectors were used (refractive index (——), viscosity (- - -) and light scattering (· · ·)). (Reprinted with permission from Ref. [53]. Copyright 2008 American Chemical Society.)

In the last step of this new concept, the PiBA-nanoparticles were examined as a possible additive for a linear polymer, poly(n-butyl acrylate) (PnBuA) (see Figure 9). It was expected that the physical properties should change by entanglement of the nanoparticles with linear polymers. In this way, the addition of nanoparticles with a high glass transition temperature (T_g) to PnBuA with a low T_g ($-54°C$) should result in a viscosity increase and a reinforcement of the material. On the other hand, as no entanglement is expected with the corresponding star polymers, these should not have a significant effect.

In order to create the entanglements, the P*i*BA-nanoparticles were dissolved in the monomer (nBuA), after which it was polymerized by a free radical polymerization with AIBN. GPC measurements proved the successful incorporation of the nanoparticles into the PnBuA (not shown).[53]

The mechanical properties of the modified PnBuA have been examined by rheology measurements with a fixed stress and frequency as a function of

temperature (20°C to 130°C). From the values of the storage modulus (G′), the loss modulus (G″) and the dissipation factor (δ), an indication of the change in the visco-elastic behavior of the different polymer materials is obtained. In these studies, δ as a function of temperature is depicted for the two reference materials and for PnBuA modified with 5 wt% of nanoparticles (PnBuA_M3). For pure PnBuA, δ increases with temperature as a result of the increasing chain mobility (Figure 14). If a star-shaped polymer is added to the PnBuA (PnBuA_M1), no change in this behavior is noted. However, if the PnBuA is modified with PiBA-nanoparticles, the δ-value is clearly lower than for the blank sample and remains stable within the examined temperature range (20°C to 130°C). Thus, it can be concluded that the introduction of the nanoparticles drastically changes the visco-elastic behaviour.
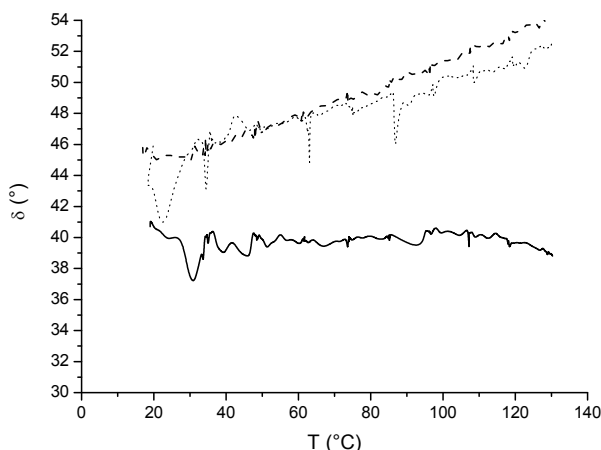

Figure 14. Dissipation factor δ as a function of temperature for PnBuA_blank (· · ·), PnBuA_M1 (- - -), PnBuA_M3 (——). (Reprinted with permission from Ref. [53]. Copyright 2008 American Chemical Society.)

3. Conclusion

In this research contribution, we have shown the synthesis of various amphiphilic copolymer structures composed of AA and iBA. Block and "block-like" co-polymers with a controlled molecular weight and composition were prepared by ATRP. In addition, block and graft copolymer structures were successfully prepared by combination of "click" chemistry and ATRP. The PAA segments were obtained by thermal deprotection of the PEEA segments. Pigment stabilization tests using the block and block-like structures as surfactants demonstrated several structure–property relations.

Furthermore, we have investigated a new concept for the preparation of polymeric nanoparticles. First, star-shaped PiBA polymers were prepared in a controlled way by ATRP. After end group conversion, the reactive star polymers were converted into a new type of nanoparticle by means of an intramolecular polymerization. It was clearly demonstrated that the incorporation of these nanoparticles in an acrylate polymer matrix can control the visco-elastic properties as a result of non-covalent chain entanglements.

Acknowledgements

References

[1]   Zhang, M. F.; Breiner, T.; Mori, H.; Muller, A. H. E. *Polymer* **2003**, 44, 1449–1458.
[2]   Porasso, R. D.; Benegas, J. C.; van den Hoop, M. *J. Phys. Chem. B* **1999**, 103, 2361–2365.
[3]   Rivas, B. L.; Pooley, S. A.; Soto, M.; Maturana, H. A.; Geckeler, K. E. *J. Appl. Polym. Sci.* **1998**, 67, 93–100.
[4]   Liu, Y. F.; Wang, S. Z.; Hua, J. D. *J. Appl. Polym. Sci.* **2000**, 76, 2093–2097.
[5]   Haulbrook, W. R.; Feerer, J. L.; Hatton, T. A.; Tester, J. W. *Environ. Sci. Technol.* **1993**, 27, 2783–2788.
[6]   Karymov, M. A.; Prochazka, K.; Mendenhall, J. M.; Martin, T. J.; Munk, P.; Webber, S. E. *Langmuir* **1996**, 12, 4748–4753.
[7]   Burguiere, C.; Pascual, S.; Bui, C.; Vairon, J. P.; Charleux, B.; Davis, K. A.; Matyjaszewski, K.; Betremieux, I. *Macromolecules* **2001**, 34, 4439–4450.
[8]   Rosler, A.; Vandermeulen, G. W. M.; Klok, H. A. *Adv. Drug Deliver. Rev.* **2001**, 53, 95–108.
[9]   Vamvakaki, M.; Papoutsakis, L.; Katsamanis, V.; Afchoudia, T.; Fragouli, P. G.; Iatrou, H.; Hadjichristidis, N.; Armes, S. P.; Sidorov, S.; Zhirov, D.; Zhirov, V.; Kostylev, M.; Bronstein, L. M.; Anastasiadis, S. H. *Faraday Discuss.* **2005**, 128, 129–147.
[10]   Verdonck, B.; Goethals, E. J.; Du Prez, F. E. *Macrom. Chem. Phys.* **2003**, 204, 2090–2098.

[11] Verbrugghe, S.; Bernaerts, K.; Du Prez, F. E. *Macrom. Chem. Phys.* **2003**, 204, 1217–1225.
[12] Ladaviere, C.; Dorr, N.; Claverie, J. P. *Macromolecules* **2001**, 34, 5370–5372.
[13] Loiseau, J.; Doerr, N.; Suau, J. M.; Egraz, J. B.; Llauro, M. F.; Ladaviere, C. *Macromolecules* **2003**, 36, 3066–3077.
[14] Loiseau, J.; Ladaviere, C.; Suau, J. M.; Claverie, J. *Polymer* **2005**, 46, 8565–8572.
[15] Chong, K. T.; Su, X. D.; Lee, E. J. D.; O'Shea, S. J. *Langmuir* **2002**, 18, 9932–9936.
[16] Brandrup, J.; Immergut, E. H.; Grulke, E. A. (Eds.), *Polymer Handbook*; 4th edition; Wiley, New York, **1999**.
[17] Dervaux, B.; Van Camp, W.; Van Renterghem, L.; Du Prez, F. E. *J. Polym. Sci., Part A: Polym. Chem.* **2008**, 46, 1649–1661.
[18] Patten, T. E.; Matyjaszewski, K. *Adv. Mater.* **1998**, 10, 901–915.
[19] Davis, K. A.; Matyjaszewski, K. *Macromolecules* **2000**, 33, 4039–4047.
[20] Haddleton, D. M.; Crossman, M. C.; Dana, B. H.; Duncalf, D. J.; Heming, A. M.; Kukulj, D.; Shooter, A. J. *Macromolecules* **1999**, 32, 2110–2119.
[21] Munirasu, S.; Ruhe, J.; Dhamodharan, R. *J. Polym. Sci.: Part A: Polym. Chem.* **2006**, 44, 2848–2861.
[22] Van Camp, W.; Du Prez, F. E.; Bon, S. A. F. *Macromolecules* **2004**, 37, 6673–6675.
[23] Hoogenboom, R.; Schubert, U. S.; Van Camp, W.; Du Prez, F. E. *Macromolecules* **2005**, 38, 7653–7659.
[24] Bernaerts, K. V.; Willet, N.; Van Camp, W.; Jerome, R.; Du Prez, F. E. *Macromolecules* **2006**, 39, 3760–3769.
[25] Van Camp, W.; Germonpre, V.; Mespouille, L.; Dubois, P.; Goethals, E. J.; Du Prez, F. E. *React. Funct. Polym.* **2007**, 67, 1168–1180.
[26] Wouters, D.; Van Camp, W.; Dervaux, B.; Du Prez, F. E.; Schubert, U. S. *Soft Matter* **2007**, 3, 1537–1541.
[27] Vidts, K. R. M.; Dervaux, B.; Du Prez, F. E. *Polymer* **2006**, 47, 6028–6037.
[28] Gray, M. K.; Zhou, H.; Nguyen, S. T.; Torkelson, J. M. *Macromolecules* **2004**, 37, 5586–5595.
[29] Kim, J.; Gray, M. K.; Zhou, H.; Nguyen, S. T.; Torkelson, J. M. *Macromolecules* **2005**, 38, 1037–1040.
[30] Tsarevsky, N. V.; Sumerlin, B. S.; Matyjaszewski, K. *Macromolecules* **2005**, 38, 3558–3561.
[31] Coessens, V.; Pintauer, T.; Matyjaszewski, K. *Progr. Polym. Sci.* **2001**, 26, 337–377.
[32] Sumerlin, B. S.; Tsarevsky, N. V.; Louche, G.; Lee, R. Y.; Matyjaszewski, K. *Macromolecules* **2005**, 38, 7540–7545.
[33] Dervaux, B.; Van Camp, W.; Bulychev, N. A.; Eisenbach, C. D.; Zubov, V. P.; Du Prez, F. E. *Macromol. Chem. Phys.* **2009**, 210, 287–298.
[34] Bulychev, N. A.; Arutunov, I. A.; Zubov, V. P.; Verdonck, B.; Zhang, T. Z.; Goethals, E. J.; Du Prez, F. E. *Macrom. Chem. Phys.* **2004**, 205, 2457–2463.
[35] Bulychev, N.; Dirnberger, K.; Arutunov, I.; Kopold, P.; Schauer, T.; Zubov, V.; Eisenbach, C. D. *Prog. Org. Coat.* **2008**, 62, 299–306.
[36] Somasundaran, P.; Krishnakumar, S. *Colloids Surf., A* **1997**, 123, 491–513.
[37] Mishra, M.; Kobayashi, S., *Star and hyperbranched polymers*; Marcel Dekker, New York, **1999**.
[38] Inoue, K. *Progr. Polym. Sci.* **2000**, 25, 453–571.

[39] Matyjaszewski, K., *Advances in controlled/living radical polymerization*; American Chemical Society, Washington, DC, **2003**.

[40] Matyjaszewski, K., *Controlled/living radical polymerization*; American Chemical Society, Washington, DC, **2000**.

[41] Matyjaszewski, K., *Controlled radical polymerization*; American Chemical Society, Washington, DC, **1998**.

[42] Heise, A.; Nguyen, C.; Malek, R.; Hedrick, J. L.; Frank, C. W.; Miller, R. D. *Macromolecules* **2000**, 33, 2346–2354.

[43] Huang, C. F.; Lee, H. F.; Kuo, S. W.; Xu, H. Y.; Chang, F. C. *Polymer* **2004**, 45, 2261–2269.

[44] Matyjaszewski, K.; Miller, P. J.; Pyun, J.; Kickelbick, G.; Diamanti, S. *Macromolecules* **1999**, 32, 6526–6535.

[45] Ohno, K.; Wong, B.; Haddleton, D. M. *J. Polym. Sci., Part A: Polym. Chem.* **2001**, 39, 2206–2214.

[46] Beil, J. B.; Zimmerman, S. C. *Macromolecules* **2004**, 37, 778–787.

[47] Zimmerman, S. C.; Wendland, M. S.; Rakow, N. A.; Zharov, I.; Suslick, K. S. *Nature* **2002**, 418, 399–403.

[48] Zimmerman, S. C.; Zharov, I.; Wendland, M. S.; Rakow, N. A.; Suslick, K. S. *J. Am. Chem. Soc.* **2003**, 125, 13504–13518.

[49] Harth, E.; Horn, B. V.; Lee, V. Y.; Germack, D. S.; Gonzales, C. P.; Miller, R. D.; Hawker, C. J. *J. Am. Chem. Soc.* **2002**, 124, 8653–8660.

[50] Hou, S.; Taton, D.; Saule, M.; Logan, J.; Chaikof, E. L.; Gnanou, Y. *Polymer* **2003**, 44, 5067–5074.

[51] Cloutet, E.; Fillaut, J. L.; Astruc, D.; Gnanou, Y. *Macromolecules* **1999**, 32, 1043–1054.

[52] Van Renterghem, L. M.; Goethals, E. J.; Du Prez, F. E. *Macromolecules* **2006**, 39, 528–534.

[53] Van Renterghem, L.; Lammens, M.; Dervaux, B.; Viville, P.; Lazzaroni, R.; Du Prez, F. E. *J. Am. Chem. Soc.* **2008**, 130, 10802–10811.

[54] Heise, A.; Hedrick, J. L.; Trollsas, M.; Miller, R. D.; Frank, C. W. *Macromolecules* **1999**, 32, 231–234.

[55] Holden, G.; Legge, N.; Quirk, R. P., *Thermoplastic elastomers*; Hanser & Hanser/Gardner, Munchen, **1996**.

[56] Ohno, K.; Wong, B.; Haddleton, D. M. *J. Polym. Sci. Part A: Polym. Chem.* **2001**, 39, 2206–2214.

[57] Angot, S.; Murthy, K. S.; Taton, D.; Gnanou, Y. *Macromolecules* **1998**, 31, 7218–7225.

[58] Muehlebach, A.; Rime, F. *J. Polym. Sci. Part A: Polym. Chem.* **2003**, 41, 3425–3439.

POLYMER- AND COLLOID-FUNCTIONALIZATION USING A COMBINATION OF ATRP AND CLICK CHEMISTRY

ZOYA ZARAFSHANI AND JEAN-FRANÇOIS LUTZ*
Research Group Nanotechnology for Life Science, Fraunhofer Institute for Applied Polymer Research, Geiselbergstrasse 69, 14476 Potsdam-Golm, Germany

Abstract: A straightforward click reaction (i.e. copper catalyzed 1,3 dipolar Huisgen cycloaddition of azides and terminal alkynes) was used as a complementary tool for functionalizing well-defined polymers prepared by atom transfer radical polymerization (ATRP). The bromine chain-ends of polystyrene or poly(acrylate) backbones were first transformed into azide end-groups via nucleophilic substitution and subsequently involved in "click" cycloaddition reactions with various functional alkynes. This efficient ATRP/"click" dual synthetic strategy was employed for preparing a wide variety of tailor-made functional materials such as telechelics, polymer-bioconjugates or shell-functionalized polymeric micelles.

Keywords: Polymer synthesis; Controlled radical polymerization; Atom transfer radical polymerization (ATRP); Micelles; Self-assembly

1. Introduction

Macromolecular chemistry requires, perhaps more than any other synthetic disciplines, simple, efficient and versatile chemical reactions.[1] Indeed, despite the enormous progress that has been made in this field of research over the last few decades, synthetic macromolecules remains generally rather undefined in comparison to biopolymers such as proteins or nucleic acids. Such limitations of polymer chemistry may surprise many non-specialists since modern organic synthesis offers practical solutions for the preparation of chemo-, regio- and stereo-controlled low molecular weight compounds. However, these chemical tools are not always readily transferable from the molecular scale to the macromolecular scale.[1] For instance, in standard organic synthesis, low-yield or unspecific chemical steps lead to the formation of distinct by-products,

which can be to some degree isolated and purified. Similar reactions at the macromolecular level lead to ill-defined polymer structures.

Hence, the set of chemical reactions commonly used for synthesizing or modifying polymers is, by necessity, limited to established straightforward tools. Yet, what appears at first as a significant limitation may in fact be an important advantage. For instance, Nature is only using a few chemical reactions and a very small library of monomers (20 amino acids and a few sugars and nucleobases) for synthesizing biopolymers and biological materials of remarkable structural and functional perfection. Through billions of years of optimization, Nature only selected robust chemical tools, which are perfectly adapted to earth's environmental conditions. Such selective approach may also be relevant in synthetic chemistry and could be an efficient strategy for building the materials of the future. Some recent trends in chemical sciences, such as the "click" chemistry concept introduced by Sharpless and coworkers, emphasize this aspect.[2]

The catchy term "click" refers to facile, efficient, selective and versatile chemical transformations, which lead to a single reaction product.[2] Although different chemical reactions (e.g. cycloadditions, nucleophilic substitutions, additions on carbon–carbon double bonds) can be considered to be of the click-type, the copper(I)-catalyzed azide–alkyne cycloaddition (CuAAC) is generally regarded as the quintessential example of click chemistry. Hence, the term "click" has been almost exclusively used to denote this reaction in recent literature.
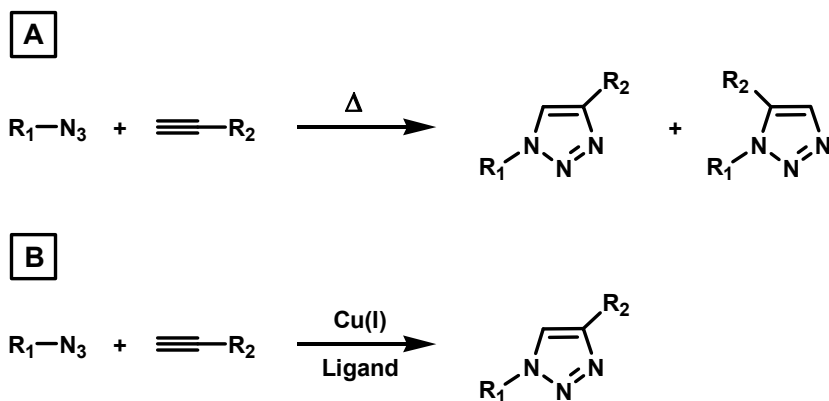
Scheme 1. Different types of azide–alkyne cycloaddition: (A) standard thermal cycloaddition, (B) copper(I)-catalyzed cycloaddition.

The synthesis of 1,2,3-triazoles via 1,3-dipolar cycloaddition of azides and terminal alkynes has been discovered by Arthur Michael at the end of the 19th century and significantly developed by Rolf Huisgen in the 1960s.[3–5] In the absence of transition-metal catalyst, these reactions are not regioselective, relatively slow, and require high temperature for reaching acceptable yields (Scheme 1A). However, in early 2002, Meldal and coworkers reported that the

use of catalytic amounts of copper(I), which can bind to terminal alkynes, leads to fast, highly efficient and regioselective azide–alkyne cycloadditions at room temperature in organic medium (Scheme 1B).[6] Moreover, shortly after, Sharpless and Fokin demonstrated that CuAAC can be successfully performed in polar media such as tert-butyl alcohol, ethanol or pure water.[7] These two important reports led to a remarkable renaissance of Huisgen cycloadditions in synthetic chemistry. Hence, CuAAC has been recently extensively investigated in various disciplines such as organic synthesis, inorganic chemistry, drug design, biochemistry and molecular biology.[8–10] Such rapid adoption of CuAAC in almost all areas of synthetic chemistry is rather unique and illustrates the versatility of this click reaction.

Although "click" chemistry was initially postulated as a general concept for organic synthesis, this strategy has also an enormous potential in polymer and materials science. The first communication, which illustrated this aspect was reported in 2004 by the research groups of Hawker, Fokin and Sharpless.[11] Afterward, the popularity of "click" chemistry within the materials science community grew exponentially and has been, in particular, significantly boosted by the influential works of Craig Hawker, Jean Fréchet and Finn.[11–13]

Our research on "click" chemistry started in mid-2004, shortly after the publication of these pioneer reports. At the time, no bridge had been built between the fields of controlled radical polymerization and "click" chemistry. Yet, the combination of these two robust synthetic tools was very tempting. Indeed, controlled radical polymerization techniques open up a wide range of possibilities for macromolecular engineering, whereas highly efficient and chemoselective click reactions such as CuAAC could provide interfaces with other disciplines (see above).[14, 15] In this context, our research group studied in details the combination of atom transfer radical polymerization (ATRP) and CuAAC. Our principal achievements are summarized in the present chapter. In particular two main aspects will be discussed in the next pages: (i) the possibility to functionalize "on demand" the terminal end-group of well-defined polymer chains via CuAAC and (ii) the modification of polymeric aggregates (i.e. spherical polymer micelles) in aqueous medium.
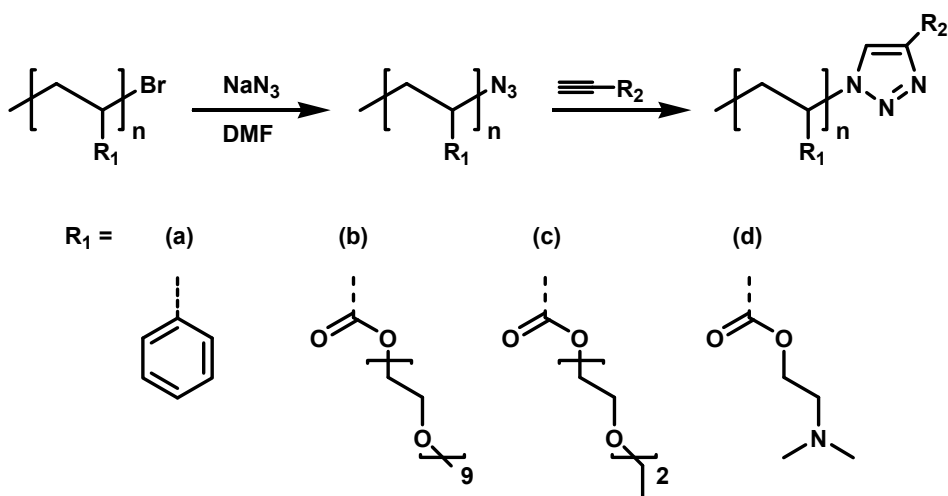
2. Preparation of Well-Defined Azido-functionalized Polymers

To be involved in CuAAC transformation reactions, well-defined polymers synthesized by ATRP should be pre-functionalized with either azide or alkyne reactive functions.[14] For instance, three main strategies were reported so far for preparing azido functional polymers using ATRP:

- Direct polymerization of an azido-functionalized monomer
- Use of an azido-functionalized initiator

- Transformation of the ω-halogen chain-ends into an azide by nucleophilic substitution (Scheme 2).[16]

Although this last approach requires one step more than the other two, it offers interesting advantages: (i) this strategy does not require the use of low molecular weight alkyl azides and is therefore relatively safe,[17] (ii) no azide functions are used during the free radical process (it was recently reported that side-reactions involving azides and polymerizable double bonds may occur)[18] and (iii) this approach is the only one that allows the terminal functionalization of surface brushes (i.e. polymers grown by ATRP on planar or spherical substrates).

Scheme 2. ATRP synthesis of well-defined ω-azido functional polymers and their subsequent functionalization via Huisgen cycloadditions.[16]

The transformation of ω-halogen chain-ends into azide functions is a rapid and experimentally simple step performed at room temperature in the presence of sodium azide. However, this substitution reaction is usually about 100 times faster for bromo-derivatives than for chloro-derivatives.[19] Such ω-end groups substitution can be employed for modifying well-defined polystyrene derivatives, poly(acrylates) or poly(methacrylates) synthesized by ATRP. Yet, poly(metha-crylates) usually require a large excess of sodium azide to be efficiently substituted.[19]

FT-IR and ¹H NMR studies indicated that the bromine chain-ends of either polystyrene (a) or poly(oligo(ethylene glycol) acrylate) (b) can be quantitatively converted into azide functions within a few hours using only a slight excess of sodium azide.[16, 20, 21] However, the fact that this step is quantitative does not necessarily imply that all the polymer chains are functionalized by an azide.

Indeed, atom transfer radical polymerizations are subject to side reactions (termination, transfer, elimination) leading to the formation of dead chains (i.e. polymer chains without halogen end groups).[22] These reactions cannot be completely suppressed. However, their occurrence can be consequently minimized if polymerizations are performed in appropriate conditions.[22, 23] For instance, polymers (**a**) and (**b**) with a high bromine content (and ultimately a high azide content) could be obtained by stopping the polymerizations at moderate monomer conversions.[16, 20] Nevertheless, some other polymers may be more problematic. For example, poly(2-(dimethylamino)ethyl acrylate) (**d**) usually exhibits a low content of bromine end-groups due to quaternization reactions occurring during the ATRP process.[24] Hence, this polymer can only be moderately functionalized using such ω-end group strategy.

3.   Functionalization via Azide–Alkyne Huisgen Cycloaddition

The ω-azido functional polymers, described in the above paragraph, may be efficiently functionalized via CuAAC. A very important advantage of azide–alkyne Huisgen cycloadditions is undoubtedly their high chemoselectivity. Thus, azido-functionalized polymers can be reacted with a variety of functional alkynes. For instance, we studied the cycloaddition of polymers (**a**) and (**b**) with several commercially available low molecular weight alkynes such as propargyl alcohol, 2-methyl-1-buten-3-yne, Nα-(9-fluorenylmethyloxycarbonyl)-L-propargylglycine, propiolic acid or propargyl amine.[16, 20] In all cases, the cycloaddition reactions were found to be quantitative, as evidenced by ^{1}H NMR, FT-IR or SEC-UV measurements. Hence, this versatile synthetic approach may be considered as a universal method for functionalizing polymers.

Furthermore, chemoselective CuAAC can be used for the "click" ligation of synthetic polymers with highly functional biopolymers such as sequence-defined oligopeptides. Polymer-peptide bioconjugates constitute a promising new class of macromolecules, which combine the advantages of standard synthetic polymers with advanced biological functions (e.g. molecular recognition, pro-grammed self-organization, biological targeting).[25] In this context, we studied the "click" cycloaddition of short alkyne-functionalized peptides such as RGD (cell adhesion sequence), TAT (protein transduction domain) or INF7 (membrane disruption peptide) with well-defined synthetic polymers synthesized by ATRP.[20, 26] Such CuAAC ligations can be performed in organic medium with protected peptides (i.e. the protecting side-groups of the amino-acids are not cleaved after solid-phase synthesis) or directly in aqueous medium with fully deprotected structures. In both cases, a high yield of bioconjugation can be obtained. However, the use of protected peptides greatly facilitates the char-acterization of the formed polymer bioconjugates (e.g. using SEC in organic medium).[20, 26]

R = CH₃, n~9 : OEGA (b)
R = CH₂-CH₃, n=2 : EEO₂A (c)

**Shell-functionalized
Aggregates**
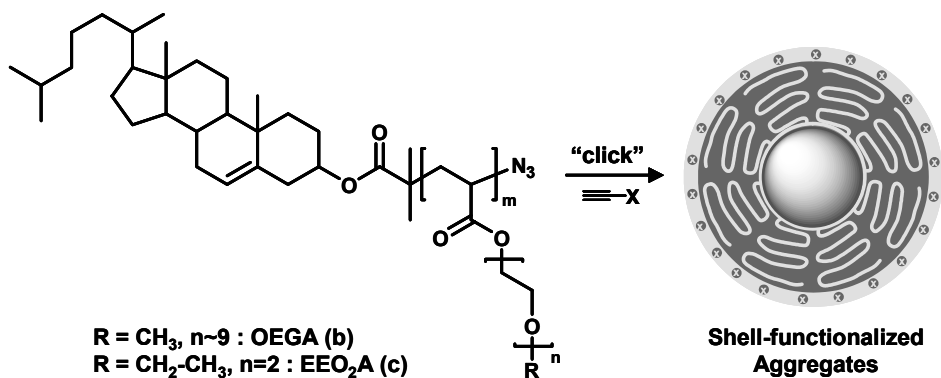
Scheme 3. General strategy for the *in situ* "click" functionalization of micellar aggregates in aqueous medium.[21]

Another important feature of copper catalyzed Huisgen cycloadditions is their high tolerance towards polar solvents (e.g. water/alcohol mixtures or pure water). Hence, these reactions are also potentially interesting for modifying fragile supramolecular assemblies (e.g. block copolymer aggregates) in aqueous solutions. Generally speaking, the micellization of macromolecular amphiphiles is a typical example of "bottom-up" approach. Polymeric surfactants are usually designed, synthesized and characterized at the molecular level and subsequently assembled into colloidal structures. Still, in some particular cases, the *in situ* modification of preformed micelles may be of interest. For example, post-functionalization is sometimes required in biomedical applications such as targeted drug- or gene-delivery when functional targeting moieties interact with encapsulated substances. However, the chemical modification of preformed micellar aggregates is indeed limited by the nature of the dispersion medium and therefore requires efficient chemical reactions, which can be performed in dilute aqueous solutions and at relatively moderate temperatures (i.e. room or physiological temperature).

Wooley and coworkers first pointed out the advantages of "click" CuAAC for functionalizing or crosslinking block copolymer micelles, composed of a polystyrene core and a poly(acrylic acid) shell.[27, 28] Additionally, we recently reported the *in situ* shell-functionalization of biocompatible micelles composed of a cholesterol-based hydrophobic core and a thermoresponsive PEG-based polymer shell (Scheme 3).[21] Well-defined surfactants were synthesized via the atom transfer radical (co)polymerization of oligo(ethylene glycol) acrylates (**b**) and (**c**) initiated by cholesteryl-2-bromoisobutyrate. After polymerization, the bromine ω-end-groups of the surfactants were transformed into azide functions as described above. Depending on their hydrophilic–hydrophobic balance, these novel surfactants lead to different types of micellar morphologies in pure deionized water.[21] Moreover, the outer-shell of these micellar assemblies could

be successfully functionalized *in situ* using CuAAC. For instance, the azide functions of the surfactants could be efficiently "clicked" to propargyl alcohol at room temperature and in dilute aqueous solutions. FT-IR and ^{1}H NMR measurements indicated that the yields of "click" cycloaddition were in most cases above 95%.
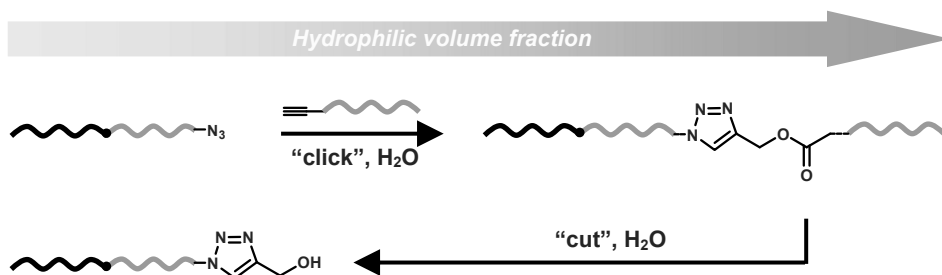
Scheme 4. Proposed strategy for tuning the hydrophilic–hydrophobic balance of polymeric macrosurfactants in aqueous medium. Black and dark-grey chains represent hydrophobic and hydrophilic segments, respectively.

Such efficient functionalization approach can be used for adding bigger molecules on the surface of the micelle. For instance, we recently reported an original method for tuning the hydrophilic–hydrophobic balance of polymeric macrosurfactants in aqueous medium.[29] This concept relies on the "click" ligation of an amphiphilic block copolymer (AB type) and a hydrophilic homopolymer (B type) (Scheme 4). The validity of this approach was examined with model polymers based on polystyrene (PS) and poly(oligo(ethylene glycol)acrylate) (POEGA, **b**) segments. In this coupling strategy, an ester group was introduced at the junction between AB and B segments. This labile moiety may be "cut" by hydrolysis (Scheme 4).

An ω-azido functional diblock copolymer PS-*b*-POEGA was synthesized in three steps. A well-defined PS macroinitiator was first prepared using ATRP in the presence of the catalyst system Cu(I)Br/PMDETA. The polymerization was stopped at moderate monomer conversion in order to isolate a PS with a high fraction of bromine end-groups (i.e. an efficient macroinitiator for block copolymer synthesis).[22, 23] After synthesis and purification, SEC analysis indicated the formation of a well-defined polymer with a controlled number average molecular weight (M_n = 2,300 g/mol, DP_n = 20) and a narrow molecular weight distribution (M_w/M_n = 1.17). This PS macroinitiator was subsequently used to initiate the ATRP of oligo(ethylene glycol) methyl ether acrylate (M_n = 454 g/mol) in toluene solution. This second polymerization step was also stopped at low OEGA conversion (i.e. 25%) to avoid significant loss of halogen end-groups. SEC measurements confirmed the successful stepwise synthesis of a tailor-made diblock copolymer (M_n = 6,300 g/mol; M_w/M_n =

1.22). The average degree of polymerization of the second block was estimated to be 13 by ^{1}H NMR (i.e. by comparing the integration of distinct PS and POEGA signals). In the last step, the bromine end-groups of the diblock copolymer PS-b-POEGA were transformed into azide moieties by nucleophilic substitution as described earlier. The chain-end substitution was confirmed by FT-IR analysis of the purified block copolymer. The resulting macrosurfactant self-assembled in dilute aqueous solution into compact spherical micelles with an average diameter of approximately 30 nm, as evidenced by dynamic light scattering and transmission electron microscopy.[29]

An α-alkyne functional homopolymer POEGA was synthesized via bulk ATRP of OEGA initiated by a trimethylsilyl (TMS)-protected alkyne initiator and subsequent deprotection.[30, 31] At the end of the polymerization step, the purified POEGA was characterized by SEC and ^{1}H NMR. The resulting homopolymer exhibited a number average molecular weight of 6,900 g/mol and a narrow molecular weight distribution (M_w/M_n = 1.15). Furthermore, the presence of the TMS-protected alkyne moiety at the α-chain end of the polymer was confirmed by two specific NMR signals at 4.73 and 0.12 ppm due to the methylene protons in alpha position of the alkyne moiety and the methyl groups of TMS, respectively. These signals allowed calculation of the average degree of polymerization of the homopolymer (DP_n = 18). The TMS-protecting groups were quantitatively removed via TBAF treatment in THF solution.[30]

The azide–alkyne "click" ligation of the ω-azido functional PS-b-POEGA and the α-alkyne functional POEGA (**b**) was investigated in aqueous solution in the presence of copper(II) sulfate and sodium L-ascorbate. It is important to emphasize that all POEGA chains possess an alkyne moiety, whereas only 85–90% of the PS-b-POEGA have a terminal azide moiety (see paragraph 2). Thus, a slight molar excess of diblock (i.e. 1.15 eq.) was used in the "click" reaction.

Various experimental conditions were screened in the present study. However, it was observed that the range of experimental conditions for performing this macromolecular ligation in aqueous solution is somewhat limited by the hydrolysis of POEGA side-chains. Polymers constructed from oligo(ethylene glycol) meth-acrylates were reported to be relatively insensitive to hydrolysis in acidic and basic conditions. However, their acrylate-counterparts seem at the first glance to be more easily hydrolyzable. For instance, high reaction temperatures (e.g. above 40–50°C) should be avoided for modifying POEGA-based polymers in water as it may result in side-chain hydrolysis. The ideal experimental conditions for performing the stoichiometric ligation of PS-b-POEGA and POEGA in water were found to be 48 h at 25°C. No side-chain hydrolysis occurred in these experimental conditions (i.e. NMR integration of side-chains signals correlate with backbone signals). Moreover, the successful "click" macromolecular ligation was confirmed by 500 MHz ^{1}H NMR measurements. Indeed, a broad signal due to the methylene protons located in between the formed triazole and the main-

chain ester was observed at 5.10–5.45 ppm, which is in good agreement with previous reports (high field NMR was necessary to visualize these junction protons as the formed polymers have a relatively high molecular weight).[31, 32] However, a weak signal due to methylene protons in alpha position of unreacted alkynes could also be observed at 4.73 ppm, indicating that the reaction was not quantitative. The integration of both signals at 5.10–5.45 ppm and 4.73 ppm indicated a yield of macromolecular coupling of approximately 80%.[29]

Acknowledgements

References

[1]   C. J. Hawker; K. L. Wooley, The convergence of synthetic organic and polymer chemistries, *Science* 309, 1200–1205 (2005).

[2]   H. C. Kolb; M. G. Finn; K. B. Sharpless, Click chemistry: Diverse chemical function from a few good reactions, *Angew. Chem. Int. Ed.* 40(11), 2004–2021 (2001).

[3]   A. Michael, Uebr die Einwirkung von Diazobenzolimid auf Acetylendicarbonsäuremethylester, *J. Prakt. Chem.* 48, 94 (1893).

[4]   R. Huisgen, Kinetics and mechanism of 1,3-dipolar cycloadditions, *Angew. Chem. Int. Ed. Engl.* 2(11), 633–645 (1963).

[5]   R. Huisgen, 1,3-dipolar cycloadditions. Past and future, *Angew. Chem. Int. Ed. Engl.* 2(11), 565–598 (1963).

[6]   C. W. Tornoe; C. Christensen; M. Meldal, Peptidotriazoles on solid phase: [1,2,3]-triazoles by regiospecific copper(I)-catalyzed 1,3-dipolar cycloadditions of terminal alkynes to azides, *J. Org. Chem.* 67(9), 3057–3064 (2002).

[7]   V. V. Rostovtsev; L. G. Green; V. V. Fokin; K. B. Sharpless, A stepwise huisgen cycloaddition process: Copper(I)-catalyzed regioselective "Ligation" of azides and terminal alkynes, *Angew. Chem. Int. Ed.* 41(14), 2596–2599 (2002).

[8]   V. D. Bock; H. Hiemstra; J. H. van Maarseveen, Cu(I)-catalyzed alkyne–azide "Click" cycloadditions from a mechanistic and synthetic perspective, *Eur. J. Org. Chem.* 2006, 1, 51–68 (2006).

[9]   Y. L. Angell; K. Burgess, Peptidomimetics via copper-catalyzed azide–alkyne cycloadditions, *Chem. Soc. Rev.* 36(10), 1674–1689 (2007).

[10] P. Wu; V. V. Fokin, Catalytic azide–alkyne cycloaddition: Reactivity and applications, *Aldrichimica Acta* 40(1), 7–17 (2007).

[11] P. Wu; A. K. Feldman; A. K. Nugent; C. J. Hawker; A. Scheel; B. Voit; J. Pyun; J. M. J. Frechet; K. B. Sharpless; V. V. Fokin, Efficiency and fidelity in a click-chemistry route to triazole dendrimers by the copper(I)-catalyzed ligation of azides and alkynes, *Angew. Chem. Int. Ed.* 43(30), 3928–3932 (2004).

[12] D. D. Díaz; S. Punna; P. Holzer; A. K. McPherson; K. B. Sharpless; V. V. Fokin; M. G. Finn, Click chemistry in materials synthesis. 1. Adhesive polymers from copper-catalyzed azide–alkyne cycloaddition, *J. Polym. Sci. Part A: Polym. Chem.* 42(17), 4392–4403 (2004).

[13] B. Helms; J. L. Mynar; C. J. Hawker; J. M. J. Frechet, Dendronized linear polymers via "click chemistry", *J. Am. Chem. Soc.* 126(46), 15020–15021 (2004).

[14] J.-F. Lutz, 1,3-dipolar cycloadditions of azides and alkynes: A universal ligation tool in polymer and materials science, *Angew. Chem. Int. Ed.* 46(7), 1018–1025 (2007).

[15] J.-F. Lutz; Z. Zarafshani, Efficient construction of therapeutics, bioconjugates, biomaterials and bioactive surfaces using azide-alkyne "click" chemistry, *Adv. Drug Del. Rev.* 60(9), 958–970 (2008).

[16] J.-F. Lutz; H. G. Börner; K. Weichenhan, Combining ATRP and click chemistry: A versatile method for preparing end-functional polymers, *Macromol. Rapid Commun.* 26, 514–518 (2005).

[17] S. Bräse; C. Gil; K. Knepper; V. Zimmermann, Organic azides: An exploding diversity of a unique class of compounds, *Angew. Chem. Int. Ed.* 44(33), 5188–5240 (2005).

[18] V. Ladmiral; T. M. Legge; Y. Zhao; S. Perrier, "Click" chemistry and radical polymerization: Potential loss of orthogonality, *Macromolecules*, 41, 6728–6732 (2008).

[19] V. Coessens; T. Pintauer; K. Matyjaszewski, Functional polymers by atom transfer radical polymerization, *Progr. Polym. Sci.* 26(3), 337–377 (2001).

[20] J.-F. Lutz; H. G. Börner; K. Weichenhan, Combining ATRP and "click" chemistry: A promising platform towards functional biocompatible polymers and polymer bioconjugates, *Macromolecules* 39(19), 6376–6383 (2006).

[21] J.-F. Lutz; S. Pfeifer; Z. Zarafshani, In situ functionalization of thermoresponsive polymeric micelles using the "click" cycloaddition of azides and alkynes, *QSAR Comb. Sci.* 26(11–12), 1151–1158 (2007).

[22] J.-F. Lutz; K. Matyjaszewski, Kinetic modeling of the chain-end functionality in atom transfer radical polymerization, *Macromol. Chem. Phys.* 203(10/11), 1385–1395 (2002).

[23] J.-F. Lutz; K. Matyjaszewski, Nuclear magnetic resonance monitoring of chain-end functionality in the atom transfer radical polymerization of styrene, *J. Polym. Sci. Part A: Polym. Chem.* 43(4), 897–910 (2005).

[24] F. Zeng; Y. Shen; S. Zhu, Atom-transfer radical polymerization of 2-(N,N-Dimethylamino)ethyl acrylate, *Macromol. Rapid Commun.* 23(18), 1113–1117 (2002).

[25] H. G. Börner; H. Schlaad, Bioinspired functional block copolymers, *Soft Matter*, 3, 394–408 (2007).

[26] J.-F. Lutz; H. G. Börner; K. Weichenhan, "Click" bioconjugation of a well-defined synthetic polymer and a protein transduction domain, *Aust. J. Chem.* 60(6), 410–413 (2007).

[27] R. K. O'Reilly; M. J. Joralemon; C. J. Hawker; K. L. Wooley, Facile syntheses of surface-functionalized micelles and shell cross-linked nanoparticles, *J. Polym Sci. Part A: Polym. Chem.* 44(17), 5203–5217 (2006).

[28] R. K. O'Reilly; M. J. Joralemon; C. J. Hawker; K. L. Wooley, Fluorogenic 1,3-dipolar cycloaddition within the hydrophobic core of a shell cross-linked nanoparticle, *Chem. Eur. J.* 12(26), 6776–6786 (2006).

[29] Z. Zarafshani; Ö. Akdemir; J.-F. Lutz, A "click" strategy for tuning in situ the hydrophilic–hydrophobic balance of AB macrosurfactants, *Macromol. Rapid Commun.* 29(12–13), 1161–1166 (2008).

[30] J. A. Opsteen; J. C. M. van Hest, Modular synthesis of block copolymers via cycloaddition of terminal azide and alkyne functionalized polymers, *Chem. Commun.*, 6, 57–59 (2005).

[31] J. A. Opsteen; J. C. M. van Hest, Modular synthesis of ABC type block copolymers by "click" chemistry, *J. Polym Sci. Part A: Polym. Chem.* 45(14), 2913–2924 (2007).

[32] A. P. Vogt; B. S. Sumerlin, An efficient route to macromonomers via ATRP and click chemistry, *Macromolecules* 39(16), 5286–5292 (2006).

CLICK CHEMISTRY AND STEP-GROWTH POLYMERIZATION:
THE IDEAL COMBINATION FOR THE REJUVENATION
OF INDUSTRIAL POLYMERS

DAVID FOURNIER, LEEN BILLIET, AND FILIP DU PREZ[*]
Department of Organic Chemistry, Ghent University, Polymer Chemistry Research Group, Krijgslaan 281 S4bis, B-9000 Gent, Belgium

Abstract: In this contribution, polyesters and polyurethanes were synthesized by step-growth polymerization in which alkyne pendant groups are located along the backbone. This was achieved via the use of different alkyne-based diols. For the polyesters, for which the synthesis occurs at high reaction temperatures, it has been proven that the alkyne functions are resistant upon heating. Thereafter, these universal alkyne-functionalized materials were used as a platform to further modify and broaden the properties of industrially relevant polymers. Click chemistry, which has recently been emerged as a powerful functionalization tool in polymer science, was used to modify the properties of these polyesters and polyurethanes. The desired functionality could be anchored by choosing the appropriate azide component. The post-functionalization via the Huisgen 1,3-dipolar cycloaddition was carried out in different reaction conditions leading to complete yields in all cases.

1. Introduction

Work in the field of step-growth polymerization has gained attention since the discovery of the Bakelite resins by the Belgian chemist Baekeland at the beginning of the 20th century[1] and also by Carothers' work 2 decades later.[2] Step-growth polymerization consists of a series of successive reactions, in which at least two complementary compounds can react at any time, leading to

increasing macromolecules. This process can be divided into two main classes: polycondensation and polyaddition reactions. The first class includes polyesters, polyamides and consists of the elimination of a small molecule (e.g. methanol, water) at each step of the condensation reaction. Secondly there is the class of polyaddition reactions such as polyurethanes, polyurea, in which no elimination of a small molecule occurs. As already extensively reviewed,[3–5] a few synthetic methodologies are suitable for the elaboration of materials *via* step-growth polymerization. The most widely used process is the nucleophilic attack to the complementary electrophilic carbonyl group, leading to the well-known commercial materials such as polyesters, polyurethanes, polycarbonates and polyamides. More recently, acyclic diene metathesis (ADMET) has received attention for the development of, for example, poly(arylenes) or poly(aryl alkenes).[6]

Step-growth polymerization is currently one of the most developed techniques allowing industries to synthesize a vast number of materials. These materials are suited for numerous applications in car industry, medicine, coatings, packaging, textiles and many others. The industrial applications mainly depend on the chemical nature of the starting components and on the properties of the synthesized materials. As an example, aromatic groups can be introduced directly in the polymer backbone by step-growth polymerization, leading to excellent properties for their use as fibers or electrical devices. Another promising topic, which is currently intensively investigated, is the step-growth polymerization of AB_x-monomers, leading to hyperbranched polymers.[7] Since this class of polymers has some unique properties such as low viscosity, good solubility and high functionalisation,[8–10] they can be applied in adhesives, micelles or as functional modifiers in crosslinking resins.[11]

In our research group, we are currently developing new functionalized materials made by step-growth polymerization. This chapter is focused on polyurethanes (PU) and polyesters due to their notable high impact on industry and extensive use in everyday life. Indeed, polyurethanes form a wide range of polymeric materials[12] due to the variety of the raw materials and processes. Furthermore, the generated properties allow their use in many applications[13] among which advanced fields like biomedical devices,[14] or dental and orthopedic applications.[15] Polyesters are also obtained by a wide range of reactions, the most widely used being the polyesterification between diacids and diols and their derivatives. This polymeric family forms a large class of commercially important polymers. Poly(ethylene terephthalate) (PET) is without doubt the most popular polyester and is commonly used as synthetic fibers, films or engineering thermoplastics. The synthesis, properties and applications of polyesters have been reviewed[16, 17] and driving forces are nowadays aimed at biodegradability studies.[18, 19] Nevertheless, for more specific applications, many of these polyesters and polyurethanes are limited in scope due to few drawbacks among which a lack of functionality

for further modification and tailoring.[20] It is expected that these functionalized materials may lead to applications that are outside of both polyurethane and polyester markets. In general, to introduce functionalities within materials made by step-growth polymerization, two main routes can be considered. Functionalities can be anchored either at the chain end or along the backbone of the polymers. The first route involves the use of monofunctional compounds, which leads to polymer chain terminations with the desired functional group at the chain end and to a reduced molecular weight. As an alternative, the chain end modification can also be performed after the synthesis of the materials.

The most promising strategy consists of the direct incorporation of the functional group along the polymer backbone during the step-growth polymerization in a one-pot process. This can be achieved by using a functionalized building block such as a functionalized diol, diisocyanate (PU chemistry) or diacid (polyester chemistry). Nevertheless, careful attention should be paid toward the inertness of the introduced functional groups during the step-growth polymerization, as this type of polymerization may require high temperatures in order to avoid secondary reactions, making the materials unusable for the desired final applications. In this way, the most reported strategies require additional protection/deprotection steps (path a, Scheme 1), which may be an important limitation.
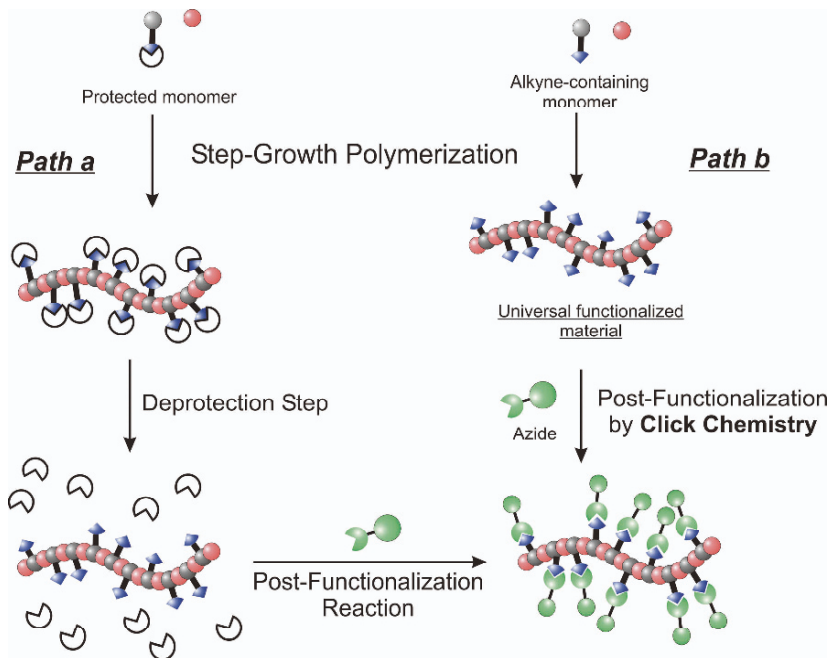
Scheme 1. Functionalization of materials *via* step-growth polymerization. *Path a*: using the common "protection/deprotection" way. *Path b*: using an universal approach involving click chemistry.

To overcome this drawback, we have recently developed in our group a promising method based on the combination of the step-growth polymerization and the Huisgen 1,3-dipolar cycloaddition (path b, Scheme 1) that fulfills the requirements of click chemistry, as defined by Sharpless in 2001.[21] To resume this concept, since it has already been largely reviewed,[22–37] this click reaction consists of the cycloaddition of an azide and an alkyne compound using a metallic catalyst leading to a tremendous acceleration of this reaction. In the case that copper is used (most common), the reaction is referred to as CuAAC (copper-catalyzed azide–alkyne cycloaddition). This simple reaction has won a great deal of attention due to its high selectivity, quantitative yield, mild reaction conditions, absence of by-product and inertness toward other functional groups. Nowadays, this reaction is becoming one of the most widely used methods for the post-functionalizations of polymers synthesized either by ionic polymerizations or radical processes.

In this chapter, the first part reviews the synthesis of alkyne-functionalized polyesters by step-growth polymerization and their further modifications by CuAAC.[38] The second part is focusing on the synthesis of alkyne-based polyurethanes and their modifications.[39] This promising concept of the in-situ incorporation of alkyne functions creates a unique advantage to obtain materials with easily adaptable physical properties.

2.   Synthesis of Functionalized Polyesters by Click Chemistry

The first part of the current research carried out by a Polymer Chemistry Research group[40] involves the synthesis of alkyne-functionalized aliphatic polyesters by the use of step-growth polymerization and their post-functionalization by the click chemistry concept. A few reports describing the combination of polyesters and click chemistry have witnessed some interesting issues for applications.[41, 42] However, these polyesters were synthesized by Ring-Opening Polymerization (ROP), including the laborious synthesis of azide- or alkyne-based cyclic monomers (i.e. lactones, lactides). The wide availability of monomers involved in step-growth polymerization attracted our attention since the structure of such polyesters can be tuned as desired.

Therefore, in our goal to synthesize highly interesting functionalized materials in a facile route, series of "clickable" poly(butylene adipate) (PBAd) and poly(ethylene succinate) (PESu) based polyesters were obtained by step-growth polymerization. These polyesters were synthesized starting from diols, including alkyne containing diols, and dicarboxylic acids, at high polymerization temperatures without any protection and deprotection steps (Scheme 2). To incorporate pendant acetylene groups into the polyester backbone, 2-methyl-2-propargyl-1,3-propanediol (MPPD, Scheme 2) has been prepared in large scale

by a straightforward synthesis in good yields from readily available compounds *via* a two-step reaction, following a modified literature procedure.[43, 44] All experimental data have already been given elsewhere.[38]

In the first stage (esterification, Scheme 2), the dicarboxylic acid (adipic acid (AdA) or succinic acid (SuA) reacted with the diols while water was eliminated as by-product. It is noteworthy to mention that on the one hand, a small excess of the diol mixture (1.1 eq) was used to limit the final molecular weights and facilitate the characterization and on the other hand, hydroquinone was added together with the monomers to prevent crosslinking in the polycondensation stage as reported elsewhere.[45, 46] At these reaction temperature (160–200°C), water can be easily removed from the reaction mixture and oligomers are formed. In order to increase the molecular weight, the oligomers were condensed at 200°C under vacuum in a second stage (polycondensation, Scheme 2).
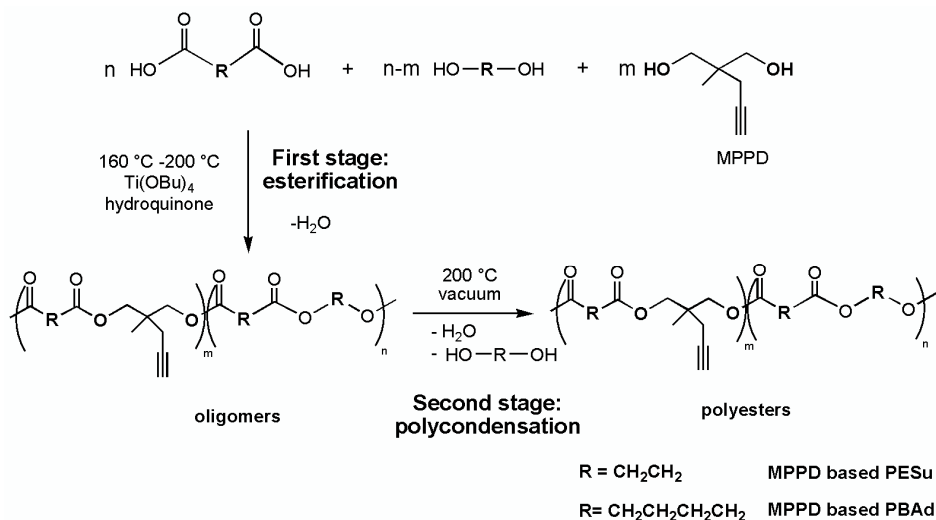
Scheme 2. Synthesis of MPPD based PESu and PBAd by a two-stage melt polycondensation method. (Reproduced from Ref. [38]. Copyright 2008 Wiley-VCH.)

In the present work, only results relating to the synthesized PBAd-based (co)polyesters with different amounts of adipic acid (AdA), butane-1,4-diol (BDO) and MPPD are presented. Experimental data are summarized in Table 1. As revealed by TGA measurements, all PBAd-based (co)polyesters are stable up to 340–350°C. These initial decomposition temperatures, defined as 5% weight loss (data in Table 1), do not depend on the MPPD content, showing that the incorporation of the alkyne group in the polyesters does not affect the thermal behavior at the early stage of the thermal decomposition process. In addition, the ^{1}H NMR spectra obtained from PBAd-25 (Figure 1, upper spectrum)

demonstrate the successful polymerization. The typical resonance of the alkyne proton at 2.87 ppm proves that the functionalized diol has been incorporated in the polymers without any side reaction as confirmed by the integrations. Moreover, the peaks at 0.96, 2.25 and 3.91 ppm are corresponding to the hydrogens of MPPD, clearly indicating that all expected signals are present in the aliphatic polyesters with pendant acetylene groups. These free alkyne groups withstand even the use of high polymerization temperatures without any additional protecting and deprotecting steps. Control over pendant acetylene concentration in the copolyesters was tailored by varying the BDO/MPPD molar ratio during the copolymerization. The amount of incorporated MPPD into the copolyester is calculated by integration of the ^{1}H NMR signal (Figure 1, upper spectrum) from the alkyne at 2.87 ppm (C≡C-$\underline{H}$ from MPPD) against the signal of BDO at 4.01 ppm (C$\underline{H_2}$CH$_2$CH$_2$C$\underline{H_2}$). As presented in Table 1, the calculated amounts of incorporated MPPD fit well with the predetermined feed ratios.

TABLE 1. Synthesis of PBAd-based (co)polyesters with pendant alkyne groups, based on MPPD, adipic acid and butane-1,4-diol.

Entry	Reference[a]	Theoretical composition	Experimental composition[b]	M_n[c] (g/mol)	T_m[d] (°C)	$T_{5\%}$[e] (°C)
1	PBAd-0	AdA/BDO/MPPD 1/1.1/0	AdA/BDO/MPPD 1/1.00/0	6,800	54	353
2	PBAd-5	AdA/BDO/MPPD 1/1.05/0.05	AdA/BDO/MPPD 1/0.98/0.07	7,900	53	354
3	PBAd-15	AdA/BDO/MPPD 1/0.95/0.15	AdA/BDO/MPPD 1/0.90/0.15	5,000	45	342
4	PBAd-25	AdA/BDO/MPPD 1/0.85/0.25	AdA/BDO/MPPD 1/0.82/0.28	10,900	41	352

[a] Indicated value in the reference names relates to the amount of incorporated MPPD (mol%) in the feed composition.

[b] Final composition determined by ^{1}H NMR in DMSO-d$_6$.

[c] Determined by THF-GPC calibrated with polystyrene standards.

[d] Melting temperature determined by DSC. Heating ramp: 20°C/min under nitrogen atmosphere from −40°C to 130°C.

[e] Temperature at 5% weight loss, as determined by TGA. Heating ramp: 10°C/min under air from 25°C to 800°C.

Subsequently, these aliphatic polyesters were successfully reacted with a number of azides *via* the Huisgen 1,3-dipolar cycloaddition reaction, yielding functionalized materials (Scheme 3).
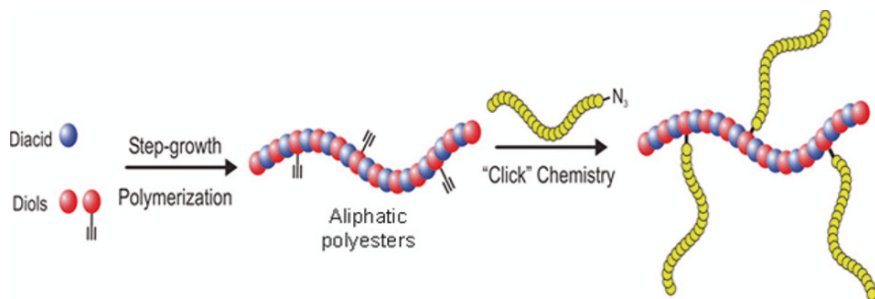
Scheme 3. Synthesis of polyesters via step-growth polymerization and their post-functionalization reactions using the click chemistry concept.

The Cu(I) catalyzed cycloaddition reactions of azides and alkynes can be performed in water or other polar solvents and are tolerant to a variety of functional groups, such as hydroxyl and carboxyl groups. Therefore, these click reactions appear to be a promising approach[39] to perform post-modification reactions on the polyester backbone containing pendant alkyne groups. The reactions were carried out in THF at 50°C in combination with the common copper catalyst system Cu(I)Br/PMDETA (1 eq each) which has been proved its efficiency towards the click reaction.[47] In this study, two azide compounds (2 eq), benzyl azide (BzN$_3$) and α-methoxy-ω-azido-PEG (PEG$_{550}$N$_3$), were used in a twofold excess. The results of the coupling reactions between the MPPD-based polyesters and the organic azide compounds are reported in Table 2.

TABLE 2. Results of the click reactions onto the MPPD-based poly(butylene adipate).

Entry	Sample	Azide compound	Mn[a] (g/mol)	Conversion[b] (%)
1	PBAd-5	BzN3	7,000	>99
2		PEG550N3	8,000	>99
3	PBAd-15	BzN3	7,100	>99
4		PEG550N3	13,800	>99
5	PBAd-25	BzN3	14,800	>99
6		PEG550N3	28,600	>99

Starting materials: PBAd-5: Mn = 7,900 g/mol. PBAd-15: Mn = 5,000 g/mol. PBAd-25: Mn = 10,900 g/mol.

[a] Determined by GPC using THF as solvent, calibrated with polystyrene standards.

[b] Determined by ^{1}H NMR in DMSO-d_6.
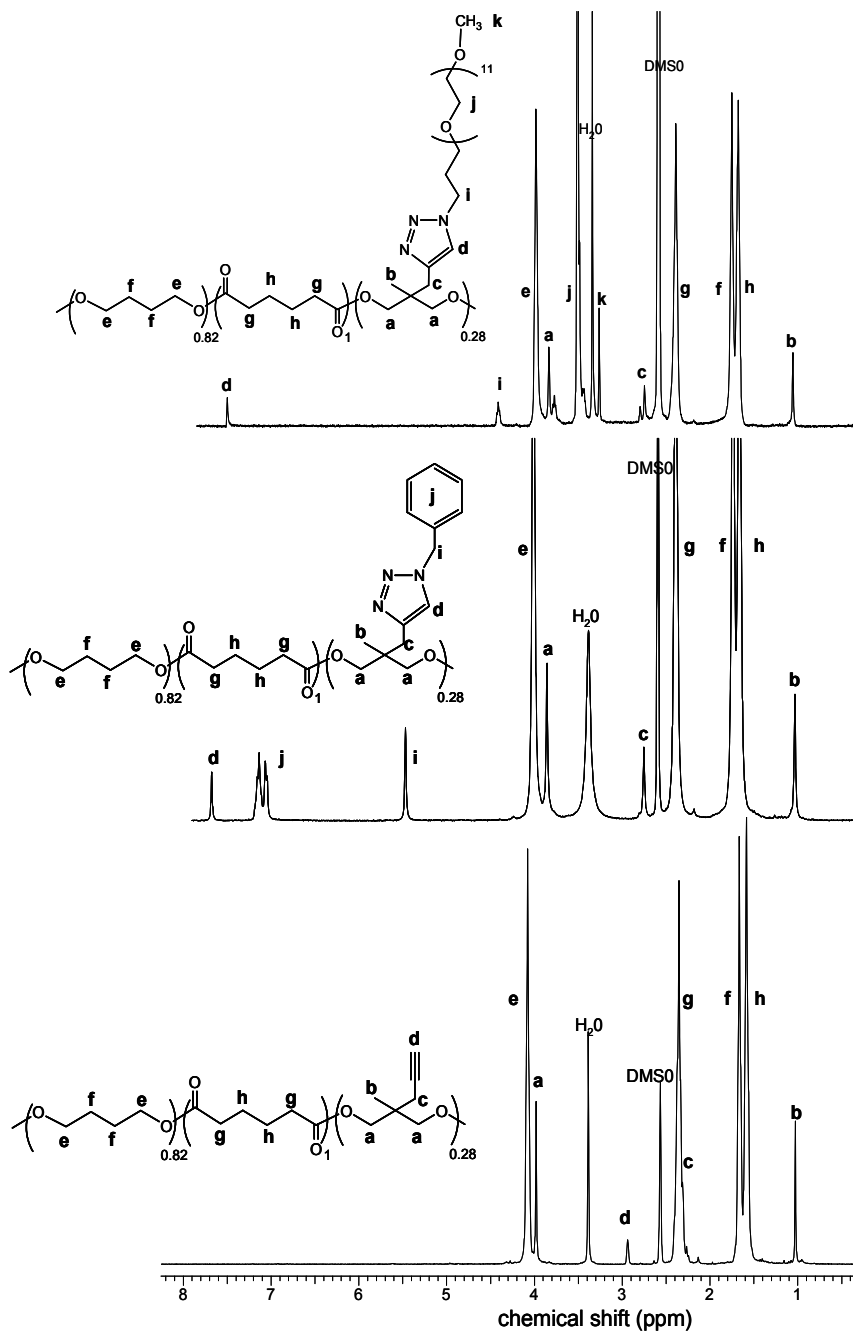
Figure 1. ¹H NMR spectra of the starting polyester PBAd-25 (lower spectrum) and the final polyesters after the click reaction with BzN₃ (middle spectrum) and PEG₅₅₀-N₃ (upper spectrum).

BzN$_3$, which could be considered as a model compound, was first screened with all the alkyne-functionalized polyesters (entries 1, 3 and 5 in Table 2). In all cases, quantitative reactions were observed. Samples taken during one of these reactions (entry 5, Table 3) after only 2 min showed that the functionalization is extremely fast under the conditions used (see further Table 3). Figure 3 shows the overlay of the ^{1}H NMR spectra of the starting material PBAd-25 (lower spectrum) and the final material obtained after the dipolar cycloaddition with BzN$_3$ (middle spectrum).

The success of the click reaction was confirmed by the complete disappearance of the alkyne signal at 2.87 ppm and the appearance of the proton linked to the formed triazole ring at 7.90 ppm (Figure 1). Furthermore, new peaks ascribed to BzN$_3$ appear at 5.55 ppm (**i**, C*H$_2$*) and at 7.3–7.4 ppm (**j**, aromatic protons). Our efforts to extend the Cu(I) catalyzed Huisgen cycloaddition reaction to polyesters prepared *via* step-growth polymerization have also focussed on PEG-grafting. Pegylation has been extensively used in drug delivery systems due to the physical properties of PEG such as non-toxicity, high water solubility, resistance to protein adsorption and amphiphilicity.[48, 49] In our case, graft copolymers are obtained by the click reaction of the previously synthesized alkyne containing polyesters and α-methoxy-ω-azido-PEG (Mn = 550 g/mol) and it has been observed that the PEG grafted PBAd-25 (Figure 1, entry 6) is now soluble in water. ^{1}H NMR analysis in DMSO-*d6* confirmed the efficient grafting of PEG by click chemistry (upper spectrum, Figure 1) due to the disappearance of the alkyne signal and the appearance of a typical resonance of the proton from the triazole ring and the one of the PEG-units at 3.50 ppm. It can also be noticed from Figure 1 that the functionalized polyesters have a higher number-average molecular weight than the starting materials, showing the success of the grafting reaction. Figure 2 shows the molecular weight and PDI of the polyester before and after the click reaction, as measured by GPC. The peak molecular weight is largely increasing, proving that α-methoxy-ω-azido-PEG has been grafted to the polyester backbone *via* the alkyne groups.

The good results obtained from the click reactions confirmed this interesting strategy for the functionalization of polyesters. Reaction conditions were changed in order to minimize the copper content and also to reduce the temperature. As a model system, PBAd-25 with the highest alkyne loading was considered. FT-IR analysis was reported very recently[50, 51] to follow the kinetics of click reactions but, to our knowledge, no investigations with an on-line FTIR technique in the mid-infrared region (4,000–400 cm^{-1}) have previously been reported. The continuous real-time generation of analytical data allows insights in reaction pathways and allows the determination of reaction rates.[52] Therefore, click reactions have been followed using an on-line ATR-FTIR monitoring system. In all on-line measurements, the polyester, solvent (THF) and catalyst were included in the background spectrum in order to eliminate their spectral

contributions. As the azide signal is a clearly distinguishable signal in the region of 2,150–2,000 cm^{-1}, the decrease in absorbance of this signal has been monitored as a function of time. At the end of each reaction, an ^{1}H NMR sample was taken to confirm the IR results. During click reactions performed at 50°C, kinetics have been followed by taking samples for ^{1}H NMR analysis.
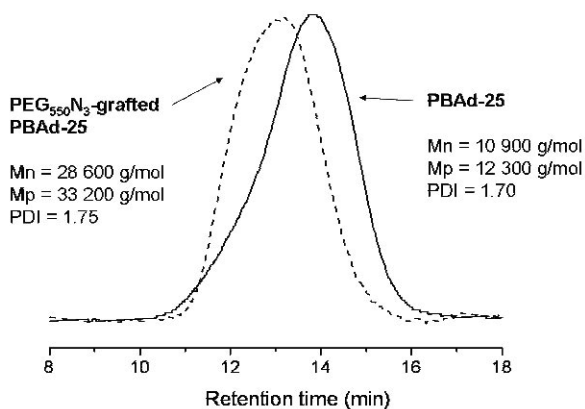

Figure 2. GPC traces of the starting polyester PBAd-25 (solid line) and the clicked $PEG_{550}N_3$-grafted PBAd-25 (dashed line). (Reproduced from Ref. [38]. Copyright 2008 Wiley-VCH.)

TABLE 3. Results of the click reaction on PBAd-25, monitored by on-line ATR-FTIR spectroscopy and ^{1}H NMR.

Entry	Azide compound	CuBr/PMDETA	T (°C)	Conversion[a] (%)	Time[b] (min)
1	BzN_3	1.0	50	>99	<2
2	BzN_3	0.5	r.t.	>99	50
3	BzN_3	0.3	r.t.	>99	120
4	$PEG_{550}N_3$	0.5	50	>99	600
5	$PEG_{550}N_3$	0.3	r.t.	$-^c$	120
6	$PEG_{550}N_3$	0.2	50	$-^c$	120

[a] Determined by ^{1}H NMR in DMSO-d6.

[b] For reactions at room temperature: determined by on-line FT-IR, for reactions at 50°C: determined by ^{1}H NMR in DMSO-d6.

[c] No conversion was observed by ^{1}H NMR after 120 min.

A typical example of an on-line ATR-FTIR experiment is presented in Figure 3, which represents the profile of the characteristic IR azide band during the click reaction of PBAd-25 with 2 eq of BzN_3 and 0.5 eq of the copper catalyst at room temperature (entry 2, Table 3). A decrease of the absorbance of the azide signal as a function of time is clearly visible. Within 50 min, all of the alkyne groups onto the poly(butylene adipate) backbone have reacted with BzN_3, which was also confirmed by ^1H NMR analysis. As shown in Figure 3, the azide signal is not disappearing completely because of the use of an excess BzN_3. When the amount of copper catalyst was lowered to 0.3 eq (entry 3, Table 3), the reaction time increased up to 2 h. The same reaction conditions were applied for the click reaction with $PEG_{550}N_3$ (entry 5, Table 3). However, even after 2 h no reaction was observed. In order to perform cycloaddition reactions between PBAd-25 and $PEG_{550}N_3$, higher temperatures and/or higher amounts of copper catalyst were expected to be required in comparison to a small molecule with an azide end group. After an increase of the reaction temperature to 50°C (entry 6, Table 3), the cycloaddition was also unsuccessful. Only when a higher amount of the copper catalyst was employed (0.5 eq, entry 4, Table 3) at 50°C, a quantitative click reaction was reached after 10 h.
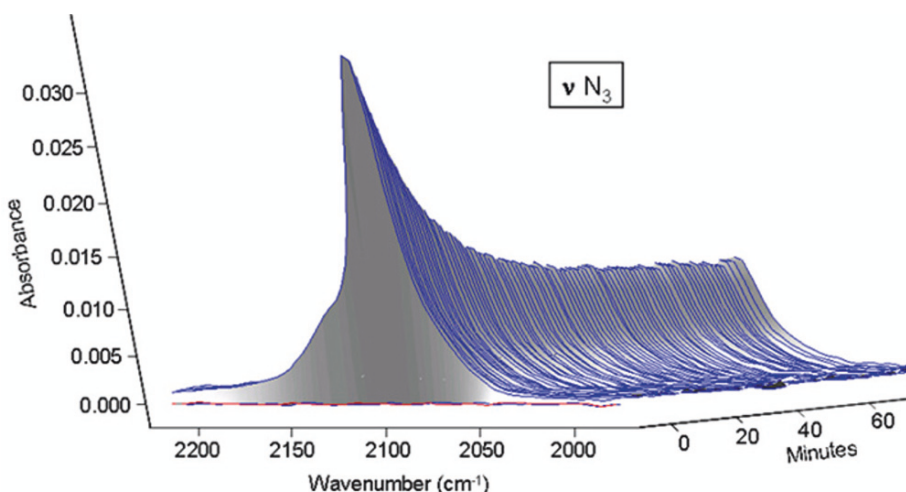
Figure 3. Waterfall plot and the absorbance of the azide signal as a function of time for the click reaction of PBAd-25 with BzN_3 (entry 2, Table 3).

These less mild reaction conditions can be ascribed to sterical constraints between the polymer and the oligomer in the case of graft copolymers, as described by Gao and Matyjaszewski.[53] Further investigations will be undertaken to check if the coupling is still quantitative when the content of pendant alkyne groups along the backbone is higher than 25%.

The first part of this chapter was related to the synthesis of functionalized polyesters by step-growth polymerization using an alkyne-based diol (MPPD). These polyesters were then successfully functionalized using the concept of click chemistry, which allowed us to obtain highly interesting functionalized polyesters. The efficiency of the post-modification of these materials has been proved either by ^{1}H NMR and on-line FTIR.

3. Synthesis of Functionalized Polyurethanes by Click Chemistry

As mentioned in the introduction part, the functionalization of PU materials has been a great challenge in order to develop new highly interesting materials in high added values domains. By incorporating an alkyne diol in the PU process, linear functionalized PUs were obtained with alkyne groups along the polymer backbone. For this purpose, 3,5-bis(hydroxymethyl)-1-propargyloxybenzene (PBM)[54] was synthesized as provider of alkyne functional groups. All experimental data can be found in Ref. [39].

This monoalkyne diol PBM was then reacted with hexamethylene diisocyanate (HDI) in ethyl acetate. According to the desired amount of PBM, butane-1,4-diol is added to the mixture. After the temperature was fixed at 50°C, a few microliters of dibutyltin dilaureate were added to the feed. As a result of the use of ethyl acetate as solvent, the PU polymer is precipitating during its formation, which facilitates the characterizations. Table 4 summarizes the results of the synthesized PUs with different amounts of incorporated PBM, from 0 mol% (PU-PBM-0, Table 4) to 50 mol% (PU-PBM-50, Table 4).

TABLE 4. Synthesis of linear PUs starting from HDI and the building block PBM.

Reference[a]	Composition[b] PBM/BDO/HDI	Mn[c] (g/mol)	PDI[c]	$T_{5\%}$[f] (°C)	Char yield[f] (%)
PU-PBM-50	50/0/50	8,100	1.33	302	23.9
PU-PBM-25	25/25/50	14,700	2.58	303	12.8
PU-PBM-8	8/42/50	6,000[d]	–[d]	304	5.1
PU-PBM-0	0/50/50	–[e]	–[e]	299	1.4

[a] Indicated values relate to the amount of incorporated PBM (mol%) in the final material.

[b] Final composition in mol% determined by ^{1}H NMR in DMSO-d$_6$.

[c] Determined by GPC calibrated with PMMA standards.

[d] The resulting trace is out of the calibration window and only the peak weight (Mp) could be determined.

[e] Not soluble in GPC solvent (DMA + LiCl).

[f] Temperature at 5% weight loss and final char yield, as determined by TGA. Heating ramp: 20°C/min under air from 25°C to 800°C.

The synthesized PUs were intensely washed to remove unreacted components and dried. Then, they were characterized by ^{1}H NMR spectroscopy and a typical spectrum (PU-PBM-25, Table 4) is shown in Figure 4. Among all attributed peaks, the alkyne proton clearly appears at 3.55 ppm proving the incorporation of the alkyne diol PBM in the PU material. Moreover, by taking into account the integration of the peaks at 4.75 ppm (2H, -C$\underline{H_2}$ from PBM), 3.9 ppm (4H, –O–C$\underline{H_2}$ from BDO) and 2.9 ppm (4H, -NH-C$\underline{H_2}$ from HDI), the molar ratio between HDI, BDO and PBM could be easily determined.
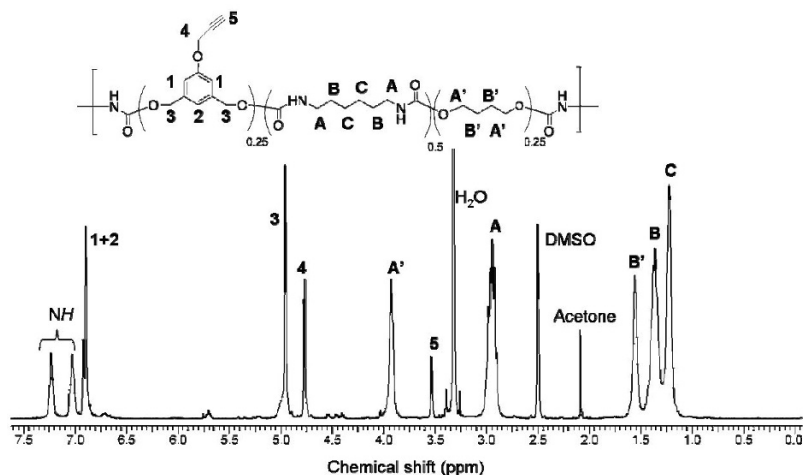
Figure 4. ^{1}H NMR spectrum (300 MHz, DMSO-*d6*) of PU-PBM-25. (Reproduced from Ref. [39]. Copyright 2008 American Chemical Society.)

FTIR spectroscopy was also used to characterize the obtained alkyne-based PUs. All spectra (data not shown) corresponding to the PU having PBM in their substructure showed several typical bands. The absorption at 1,740 cm^{-1} corresponding to the carbonyl function from the urethane groups and at 2,220 cm^{-1} (C≡C) relating to the terminal alkyne functions present in the material can clearly be seen. The thermal stability of the synthesized functionalized PU was studied by thermogravimetric analysis (TGA) measurements. The initial decomposition temperatures of synthesized PU-PBM, defined as 5% weight loss (data in Table 4), confirm that they are thermally stable up to 300°C and no effect due to the presence of PBM could be detected at the early stage of the thermal decomposition (Figure 5). However, when comparing their char yields, it can be observed that a larger amount of incorporated PBM leads to a higher final char yield, the maximum being 23.9%. Thus, PBM may act as a stabilizer agent as already reported elsewhere.[45, 55] Indeed, alkyne groups are known to act as a crosslinker upon heating by creation of reticulated alkenes and can participate in a reaction of cyclotrimerization making the materials flame-retardant. This is ascribed to the formation of char on the upper part of the

material, which prevents the formation of volatile compounds from the inner part. In addition, terminal alkynes have also been used to elaborate high-performance polymers and composites.[56] When final char yields were plotted against the amount of incorporated PBM (Figure 5, right), surprisingly a linear relationship was observed, meaning that a structure–property relationship may exist that can justify the above mentioned explanation about the thermal stability of alkyne-functionalized materials.
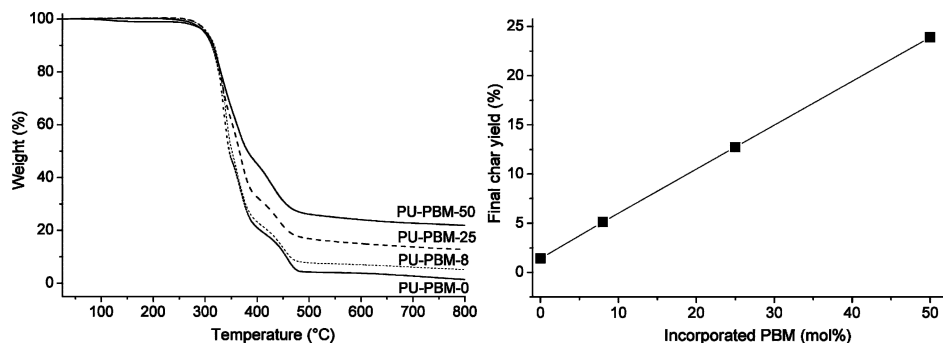
Figure 5. *Left*: TGA curves of the PU-PBM (heating ramp: 20°C/min under air from 25°C to 800°C). *Right*: Final char yield of the PU-PBM series versus the mol% of PBM incorporated in the material.

After showing the synthesis of alkyne-based PUs and their characterizations, the post-modification of PU side-chains has been undertaken *via* the copper(I) catalyzed azide–alkyne cycloadditions. This functionalization tool appears to be a promising approach to achieve modifications.[23, 28, 57] The availability of the alkyne functions present in the previously synthesized PUs has been studied by carrying out the click reaction with several azides (Scheme 4).
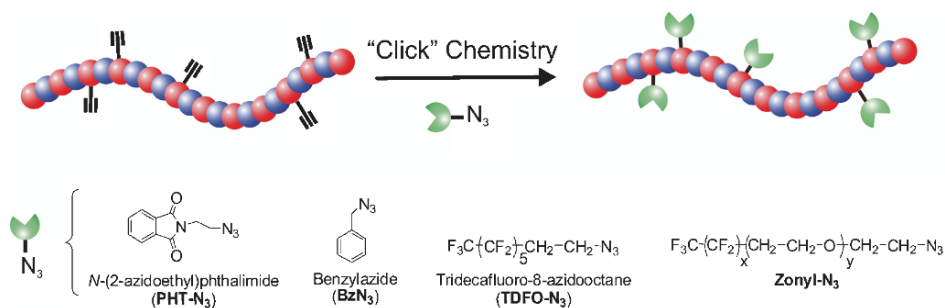
Scheme 4. Principle of the performed click reactions using alkyne-based PUs and various azide compounds.

The cycloaddition reactions were carried out either in dimethylsulfoxide (DMSO) at 50°C or in dimethylformamide (DMF) at 60°C in combination with Cu(I)Br/PMDETA or CuSO$_4$/Na$_{asc.}$. In this study, several azide compounds (Scheme 4) were used in a twofold excess such as benzyl azide (BzN$_3$), N-(azidoethyl)phthalimide (PHT-N$_3$), tridecafluoro-8-azidooctane (TDFO-N$_3$) or Zonyl-N$_3$. The results of the coupling reactions between PBM-based PUs and the organic azide compounds are reported in Table 5.

TABLE 5. Results of the click reactions onto PBM-based polyurethanes.

PU sample	Azide	Catalyst	Mn[c] (g/mol)	Yield[d] (%)	Char yield[f] (%)
PU-PBM-50	BzN$_3$	CuBr/PMDETA[a]	11,600	>99	14.1
	PHT-N$_3$	CuSO$_4$/Na$_{asc.}$[b]	11,400	>99	15.6
	TDFO-N$_3$	CuSO$_4$/Na$_{asc.}$[b]	7,800	>99	22.0
	Zonyl-N$_3$	CuSO$_4$/Na$_{asc.}$[b]	14,100	–[e]	2.16
PU-PBM-25	BzN$_3$	CuBr/PMDETA[a]	24,700	>99	18.5
	PHT-N$_3$	CuSO$_4$/Na$_{asc.}$[b]	18,300	>99	11.2
	TDFO-N$_3$	CuSO$_4$/Na$_{asc.}$[b]	16,000	>99	21.1

Starting materials: **PU-PBM-50**: Mn = 8,100 g/mol, PDI = 1.33. **PU-PBM-25**: Mn = 14,700 g/mol, PDI = 2.85. Reaction conditions: PU (1 eq), azide (2 eq), time = overnight.

[a] CuBr/PMDETA: 0.1 eq, DMSO, 50°C.

[b] CuSO$_4$/Na$_{asc.}$: 0.05 and 0.1 eq respectively, DMF, 60°C.

[c] Determined by GPC calibrated with PMMA standards.

[d] Determined by ^{1}H NMR in DMSO-d$_6$.

[e] Partially soluble in DMSO-d$_6$.

[f] Determined by TGA analysis. Heating ramp: 20°C/min under air from 25°C to 800°C.

When BzN$_3$, in this part also considered as a model compound, was reacted with both PU-PBM-50 and PU-PBM-25 (Table 5), reactions proceeded in good yields as demonstrated in Figure 6 where the ^{1}H NMR spectra of the compound PU-PBM-50 before (lower spectrum) and after (upper spectrum) cycloaddition of BzN$_3$ are shown. The arrow on Figure 6 clearly indicates the shift of the alkyne proton at 3.5 ppm (5, lower spectrum) to 8.2 ppm (5′, upper spectrum), corresponding to the proton linked to the formed triazole ring. Also, news peaks appear at 5.5 ppm (6′, CH_2 from BzN$_3$) and at 7.3–7.4 ppm (7′, aromatic protons from BzN$_3$), proving the success of the reaction. The complete disappearance of the alkyne proton at 3.5 ppm (Figure 6, lower spectrum) reveals that the reaction was quantitative. Also, N-(azidoethyl)phthalimide (PHT-N$_3$) was allowed to

react with PBM-based PUs using $CuSO_4/Na_{asc.}$ as copper catalyst in DMF at 60°C. As shown in Table 5, the click reactions with PU-PBM-50 and PU-PBM-25 occurred in a quantitative way since no peak from the starting alkyne proton could be detected in the final material by ^{1}H NMR. Phthalimide-based compounds were used as an amine-protecting group[58–60] and a simple deprotection step *via* hydrazine treatment was performed[61] leading to ethylamino-functionalized PU.
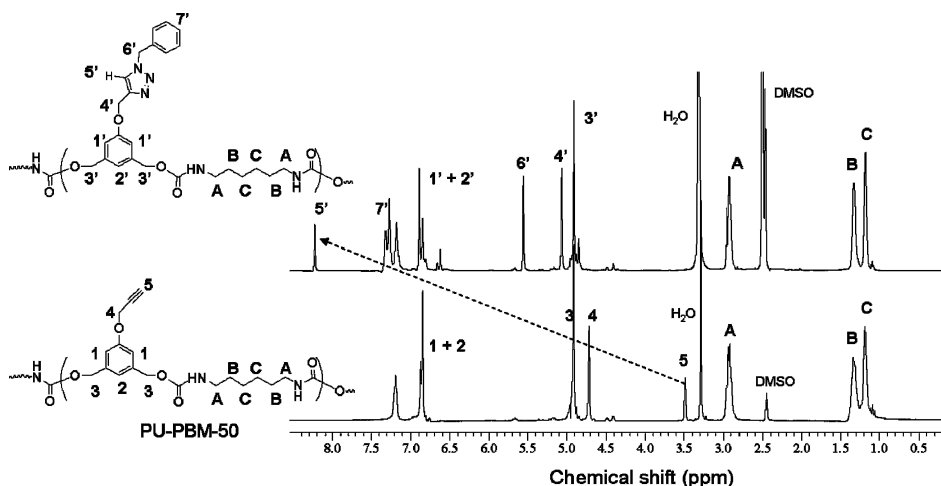

Figure 6. ^{1}H NMR spectra (300 MHz, DMSO-d6) of the starting polymer PU-PBM-50 (lower spectrum) and the final PU after the click reaction with BzN_3 (upper spectrum). (Reproduced from Ref. [39]. Copyright 2008 American Chemical Society.)

Last attempts on the series of PU-PBM were undertaken with fluorinated azide compounds in order to enlarge the concept of functionalized PUs by grafting hydrophobic pendant chains. Tridecafluoro-8-azidooctane (TDFO-N_3), which was synthesized from the iodide derivative,[39] was allowed to react with both PU-PBM-50 and PU-PBM-25 using copper sulfate and sodium ascorbate as catalyst system (Table 5). In both cases, the ^{1}H NMR revealed the appearance of the triazole proton. Integrations of this specific peak and the others from the PU backbone fit well, proving again the quantitative character of the click reactions. The high hydrophobicity of the fluorinated compound did not affect at all the dipolar cycloaddition. Finally, a last azide compound was used, namely Zonyl-N_3. This compound was synthesized from commercially available hydroxy-functionalized Zonyl FSO-100. This is a low molecular weight block copolymer having a first block based on a perfluoroalkyl chain followed by a second poly(ethylene glycol) block (Scheme 4). Zonyl FSO-100 is currently widely used in applications such as improved wetting agent, lubricant, antifogging and pigment compatibilizer in inks.[62] In the present work, Zonyl-N_3 was reacted with PU-PBM-50. As mentioned in Table 5, the resulting PU was only partially

soluble in the NMR solvent, making the measurement not suitable. Nevertheless, the change of solubility may be an indirect proof of the grafting process by click chemistry. On the other hand, Figure 7 represents the overlay of the GPC traces of PU-PBM-50 and the resulting PU with their macromolecular characteristics such as number average (M_n) and peak molecular weight (M_p) and polydispersity index (PDI). A shift of the macromolecular species toward lower retention time is clearly shown. Also, the peak molecular weight is largely increasing from 8,900 to 15,900 g/mol proving that the fluorinated compound has been grafted to the PU backbone *via* the alkyne functions.
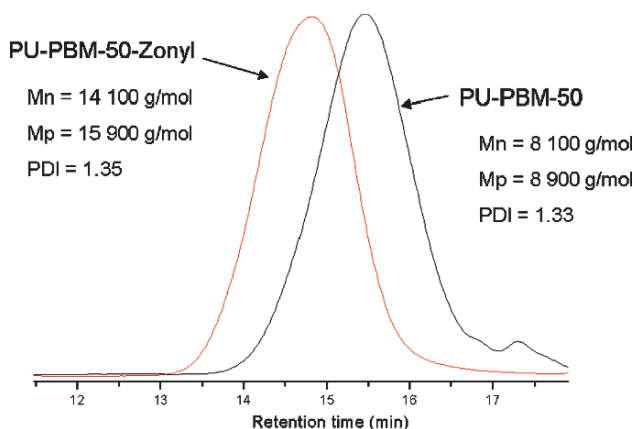
Figure 7. GPC traces of the starting material PU-PBM-50 and PU-PBM-50-Zonyl. (Reproduced from Ref. [39]. Copyright 2008 American Chemical Society.)

It can also be noticed from Table 5 that after the click reaction all the functionalized PUs have a higher number-average molecular mass than the starting PU-PBM-50 and PU-PBM-25, showing the success of the grafting reaction. As an exception, PU-PBM-50-TDFO (PU-PBM-50 after the click reaction with TDFO-N_3) has a slightly lower molecular mass (M_n = 7,800 g/mol, Table 5) than the starting material, which can be attributed to the change of hydrodynamic volume of the obtained macromolecules with quite hydrophobic side-chains.

4. Conclusion

Industrially important materials including polyesters and polyurethanes have been synthesized by step-growth polymerization bearing alkyne functions as pendant groups by incorporating an alkyne diol (MPPD and DPPD). These materials have been fully characterized using conventional techniques. It has been particularly demonstrated that the alkyne groups remained after the poly-merization although; in the case of polyester synthesis drastic polymerization

conditions (high temperature, vacuum) have been applied. By varying the initial ratio of each component, the alkyne loading can be easily tuned.

In the second part of the research, the Huisgen 1,3-dipolar cycloaddition was employed by reacting these alkyne functionalized materials with several azide compounds in the presence of a copper catalyst. After the success of the click reaction with BzN_3, other interesting hydrophilic or hydrophobic azide compounds have been grafted to the alkyne-functionalized materials. In all cases, a quantitative yield was obtained as observed by ^{1}H NMR, leading to polyesters and polyurethanes with new functionalities in the side-chains of the backbone. This concept of universal functionalized materials made by step-growth polymerization is believed to afford new classes of materials with easily adaptable physical properties by making use of readily accessible azide compounds.

Acknowledgements

References

[1]   *U.S. patent 0942699 Pat.*, 1907.
[2]   W. H. Carothers, *Chem. Rev.*, 1931, **8**, 353–426.
[3]   R. O. Ebewele, *Polymer Science and Technology*, CRC Press, Boca Raton, FL, 2000.
[4]   M. E. Rogers, T. E. Long and S. R. Turner, *Synthetic Methods in Step-Growth Polymers*, M. E. Rogers and T. E. Long (Eds.), Wiley, Hoboken, NJ, 2003, pp. 1–16.
[5]   T. Yokozawa, *Macromolecular Engineering: Precise Synthesis, Materials Properties, Applications*, K. Matyjaszewski, Y. Gnanou and L. Leibler (Eds.), Wiley-VCH, Weinheim, 2007, vol. 1, pp. 295–349.
[6]   K. B. Wagener, D. Valenti and S. F. Hahn, *Macromolecules*, 1997, **30**, 6688–6690.
[7]   P. J. Flory, *J. Am. Chem. Soc.*, 1952, **74**, 2718–2723.
[8]   M. Jikei and M.-A. Kakimoto, *Prog. Polym. Sci.*, 2001, **26**, 1233–1285.
[9]   J. M. J. Fréchet and D. A. Tomalia, *Dendrimers and Other Dendritic Polymers*, Wiley, New York, 2001.
[10]   C. Gao and D. Yan, *Prog. Polym. Sci.*, 2004, **29**, 183–275.

[11] R. Mezzenga, L. Boogh and J.-A. E. Månson, *Compos. Sci. Technol.*, 2001, **61**, 787–795.

[12] T. Thompson, *Design and Applications of Hydrophilic Polyurethanes: Medical, Agricultural and Other Applications*, Technomic, Lancaster, PA, 2000.

[13] T. Thomson, *Polyurethanes as Specialty Chemicals: Principles and Applications*, CRC Press, Boca Raton, FL, 2004.

[14] P. Vermette, H. J. Griesser, G. Laroche and R. Guidoin, *Biomedical Applications of Polyurethanes*, Landes Bioscience, Georgetown, TX, 2001.

[15] S. W. Shalaby and U. Salz, *Polymers for Dental and Orthopedic Applications*, CRC Press, Boca Raton, FL, 2006.

[16] J. Scheirs and T. E. Long, *Modern Polyesters: Chemistry and Technology of Polyesters and Copolyesters*, Wiley, New York, 2003.

[17] A.-C. Albertsson and I. K. Varma, *Adv. Polym. Sci.*, 2002, **157**, 1–40.

[18] R. Smith, *Biodegradable Polymers for Industrial Applications*, CRC Press, New York, 2005.

[19] J. E. Klee, C. Schneider, D. Hölter, A. Burgath, H. Frey and R. Mühlhaupt, *Polym. Adv. Technol.*, 2001, **12**, 1–9.

[20] C. K. Williams, *Chem. Soc. Rev.*, 2007, **36**, 1573–1580.

[21] H. C. Kolb, M. G. Finn and K. B. Sharpless, *Angew. Chem. Int. Ed.*, 2001, **40**, 2004–2021.

[22] H. C. Kolb and K. B. Sharpless, *Drug Discovery Today*, 2003, **8**, 1128–1137.

[23] C. J. Hawker and K. L. Wooley, *Science*, 2005, **309**, 1200–1205.

[24] Q. Wang, S. Chittaboina and H. N. Barnhill, *Lett. Org. Chem.*, 2005, **2**, 293–301.

[25] W. H. Binder and C. Kluger, *Curr. Org. Chem.*, 2006, **10**, 1791–1815.

[26] B. S. Sumerlin, N. V. Tsarevsky, H. Gao, P. Golas, G. Louche, R. Y. Lee and K. Matyjaszewski, *ACS Symp. Ser.*, 2006, **944**, 140.

[27] S. Diez-Gonzalez, A. Correa, L. Cavallo and S. P. Nolan, *Chem.-Eur. J.*, 2006, **12**, 7558–7564.

[28] D. Fournier, R. Hoogenboom and U. S. Schubert, *Chem. Soc. Rev.*, 2007, **36**, 1369–1380.

[29] H. Nandivada, X. W. Jiang and J. Lahann, *Adv. Mater.*, 2007, **19**, 2197–2208.

[30] J.-F. Lutz, *Angew. Chem. Int. Ed. Engl.*, 2007, **46**, 1018–1025.

[31] J. E. Moses and A. D. Moorhouse, *Chem. Soc. Rev.*, 2007, **36**, 1249–1262.

[32] M. V. Gil, M. J. Arevalo and O. Lopez, *Synthesis*, 2007, **11**, 1589–1620.

[33] C. J. Hawker, V. V. Fokin, M. G. Finn and K. B. Sharpless, *Aust. J. Chem.*, 2007, **60**, 381–383.

[34] W. H. Binder and R. Sachsenhofer, *Macromol. Rapid Commun.*, 2007, **28**, 15–54.

[35] W. H. Binder and R. Sachsenhofer, *Macromol. Rapid Commun.*, 2008, **29**, 952–981.

[36] J.-F. Lutz and Z. Zarafshani, *Adv. Drug Delivery Rev.*, 2008, **60**, 958–970.

[37] G. C. Tron, T. Pirali, R. A. Billington, P. L. Canonico, G. Sorba and A. A. Genazzani, *Med. Res. Rev.*, 2008, **28**, 278–308.

[38] L. Billiet, D. Fournier and F. E. Du Prez, *J. Polym. Sci., Part A: Polym. Chem.*, 2008, **46**, 6552–6564.

[39] D. Fournier and F. Du Prez, *Macromolecules*, 2008, **41**, 4622–4630.

[40] www.PCR.UGent.be

[41] B. Parrish, R. B. Breitenkamp and T. Emrick, *J. Am. Chem. Soc.*, 2005, **127**, 7404–7410.

[42] R. Riva, S. Schmeits, C. Jérôme, R. Jérôme and P. Lecomte, *Macromolecules*, 2007, **40**, 796–803.

[43] E. Buchta and H. Schlesinger, *Annalen Der Chemie-Justus Liebig*, 1956, **598**, 1–24.

[44] R. A. Findeis and L. H. J. Gade, *Dalton Trans.*, 2002, **21**, 3952–3960.

[45] A. B. Morgan and J. M. Tour, *Macromolecules*, 1998, **31**, 2857–2865.

[46] J. C. Saam, *J. Polym. Sci., Part A: Polym. Chem.*, 1998, **36**, 341–356.

[47] P. L. Golas, N. V. Tsarevsky, B. S. Sumerlin and K. Matyjaszewski, *Macromolecules*, 2006, **39**, 6451–6457.

[48] J. M. Harris and S. Zalipsky, *Poly(Ethylene Glycol): Chemistry and Biological Applications*, American Chemical Society, Washington, DC, 1997.

[49] G. Pasut, M. Sergi and F. M. Veronese, *Adv. Drug Delivery Rev.*, 2008, **60**, 69–78.

[50] C. J. Thode and M. E. Williams, *J. Colloid Interface Sci.*, 2008, **320**, 346–352.

[51] D. Quemener, M. Le Hellaye, C. Bissett, T. P. Davis, C. Barner-Kowollik and M. H. Stenzel, *J. Polym. Sci., Part A: Polym. Chem.*, 2008, **46**, 155–173.

[52] K. Sahre, U. Schulze, K.-J. Eichhorn and B. Voit, *Macromol. Chem. Phys.*, 2007, **208**, 1265–1273.

[53] H. Gao and K. Matyjaszewski, *J. Am. Chem. Soc.*, 2007, **129**, 6633–6639.

[54] M. J. Joralemon, R. K. O'Reilly, J. B. Matson, A. K. Nugent, C. J. Hawker and K. L. Wooley, *Macromolecules*, 2005, **38**, 5436–5443.

[55] F. Bertini, G. Audisio, J. Kiji and M. Fujita, *J. Anal. Appl. Pyrolysis*, 2003, **68–69**, 61–81.

[56] R. L. Knudsen and B. J. Jensen, *High Perform. Polym.*, 1996, **8**, 57–66.

[57] W. H. Binder and C. Kluger, *Curr. Org. Chem.*, 2006, **10**, 1791–1815.

[58] H. R. Ing and R. H. F. Manske, *J. Chem. Soc.*, 1926, 2348–2351.

[59] S. Gabriel, *Ber. Dtsch. Chem. Ges.*, 1887, **20**, 2224–2236.

[60] J. C. Sheehan and W. A. Bolhofer, *J. Am. Chem. Soc.*, 1950, **72**, 2786–2788.

[61] M. W. Weimer, J. M. J. Fréchet and I. Gitsov, *J. Polym. Sci., Part A: Polym. Chem.*, 1998, **36**, 955–970.

[62] www.dupont.com/zonyl.

PART 3. ANIONIC POLYMERIZATION

NEW AMPHIPHILIC NANOSTRUCTURES BASED ON BLOCK TERPOLYMERS MADE BY ANIONIC POLYMERIZATION

FELIX SCHACHER, STEFAN REINICKE,
ANDREAS WALTHER, HOLGER SCHMALZ,
AND AXEL H. E. MÜLLER[*]
*Makromolekulare Chemie II, Universität Bayreuth, D-95440
Bayreuth, Germany*

Abstract: Anionic polymerization is the method of choice to synthesize linear and miktoarm-star block copolymers with high molecular weights and very narrow molecular weight distributions. We report on the synthesis of some new block co- and terpolymers and on the self-organized nanostructures they form in the bulk and in solution. Bulk structures are used as novel stimuli-sensitive membranes, whereas solution structures are soft nanoparticles, which have either a compartmentalized core or corona: new multicompartment-core micelles, Janus nanoparticles and cylinders with multicompartment corona.

Anionic polymerization has been used to synthesize new block copolymers using monomers like glycidyl ethers, ethylene oxide, or N,N-dimethylaminoethyl methacrylate (DMAEMA), These polymers find applications in smart hydrogels and membranes. A triblock terpolymer of butadiene (B), 2-vinylpyridine (VP) and *tert*-butyl methacrylate (*t*BMA) forms multi-compartment core micelles in acetone solution via phase-separation of the insoluble PB and PVP blocks. The micelles are stabilized by crosslinking of the PB block. Hydrolysis of the *tert*-butyl ester of the *t*BMA and/or quaternization of the PVP block forms water-soluble particles with a poly(methacrylic acid) corona. In contrast, Janus particles form in the bulk by crosslinking of the PB middle block of PS-*b*-PB-*b*-P*t*BMA or poly(methyl methacrylate) (PMMA). After hydrolysis of the P*t*BMA or PMMA block they are promising interfacial agents. Janus particles have been applied as efficient surfactants for emulsion polymerization and as Pickering-style compatibilizers for polymer blends.
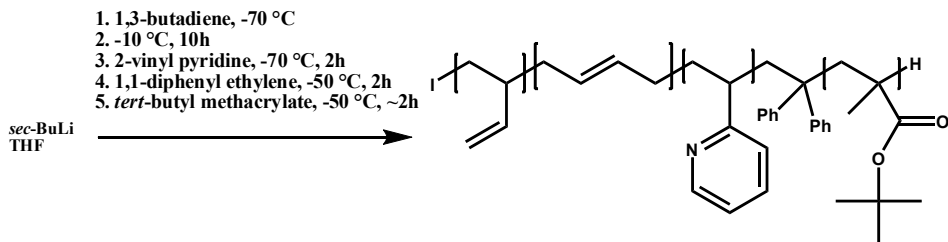
1. Block Terpolymer Micelles with a Compartmentalized Core

The term multicompartment micelles refers to self-assembled aggregates of block copolymers with cores that are further subdivided. The principal concept was introduced by Ringsdorf et al.[1] around 10 years ago and a recent review contributes to the progress within this field of research.[2] Those structures are of great interest when it comes to the simulation or understanding of biological systems, where different functionalities in close proximity are necessary to perform distinct biological functions.[3] It is known that complex structures in solution can be prepared from ABC triblock terpolymers.[4] Contrary to the large amount of reports on aggregates from diblock copolymers or the structures of ABC triblock terpolymers in the bulk, the number of contributions on triblock terpolymer micelles in block-selective solvents is still limited.[5–9] Most of the current approaches towards multicompartmental architectures are based on the mutual incompatibility of fluorocarbon and hydrocarbon segments of self-assembled systems in aqueous media.[10–13] One very recent example employs a ABCBA pentablock terpolymer, poly(ethylene oxide)-*b*-poly(γ-benzyl-L-glutamate)-*b*-poly(perfluoro ether)-*b*-poly(γ-benzyl-L-glutamate)-*b*-poly(ethylene oxide) (PEO-*b*-PBLG-*b*-PFPE-*b*-PBLG-*b*-PEO) in aqueous solution.[14] Besides, complex polymer architecture may also lead to the formation of multi-compartmental structures. Lodge et al. reported on ABC miktoarm star polymers, poly(ethyl ethylene)-*b*-poly(ethylene oxide)-*b*-poly(perfluoropropylene oxide).[3, 15] The star architecture is able to suppress the formation of concentric microphase domains. Additionally, charged polymer segments may induce a further compart-mentalization of either core or corona as well, as shown by Yan and coworkers[16] Theoretical aspects of the micelle formation from ABC terpolymers as model systems depending on block sequence, architecture and molecular weight have been addressed[17, 18] and broadened the scope and interest of multicompartment architectures.

1.1. SYNTHESIS AND CHARACTERIZATION OF THE BVT TERPOLYMERS

Linear polybutadiene-*b*-poly(2-vinylpyridine)-*b*-poly(*tert*-butyl methacrylate) BVT triblock terpolymers were synthesized through living sequential anionic polymerization. All synthesized polymers exhibit a very narrow molecular weight distribution. The synthetic procedure is shown in Scheme 1.

A series of BVT terpolymers with different weight fractions of the three blocks have been synthesized. A few representative SEC elution traces are shown in Figure 1.

1. 1,3-butadiene, -70 °C
2. -10 °C, 10h
3. 2-vinyl pyridine, -70 °C, 2h
4. 1,1-diphenyl ethylene, -50 °C, 2h
5. *tert*-butyl methacrylate, -50 °C, ~2h

sec-BuLi
THF

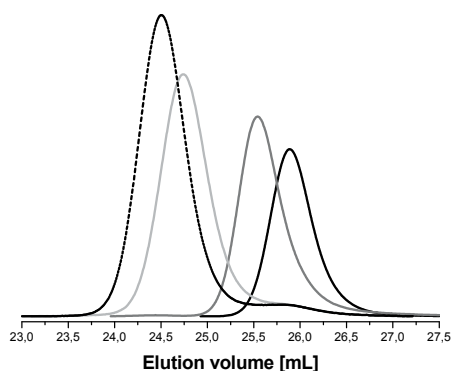*Scheme 1.* Synthesis of BVT terpolymers via sequential living anionic polymerization.

Elution volume [mL]

Figure 1. THF-SEC elution traces of B^{42} (solid black line), $B_{70}V_{30}^{63}$ (solid grey line), $B_{38}V_{18}T_{44}^{112}$ (solid light grey line) and $B_{32}V_{15}T_{53}^{132}$ (dashed black line); the subscripts denoting the weight fraction of the corresponding block in percent and the superscript the overall molecular weight in kg/mol. (Reprinted by permission from ACS.)

1.2. MULTICOMPARTMENT MICELLES IN ORGANIC SOLVENTS

To induce micellization, a block-selective solvent is required, acetone as a non-solvent for polybutadiene in this case. Due to the low glass transition temperature of PB ($-17°C$ for 90% 1,2-microstructure) the polymers can be directly dissolved in acetone, rendering turbid solutions. The so-formed micelles should consist of a polybutadiene core and be covered by a poly(2-vinylpyridine) shell. According to the block sequence, the poly(*tert*-butyl methacrylate) corona is emerging from the poly(2-vinylpyridine) compartment. Dynamic light scattering (DLS) and transmission electron microscopy (TEM) were used to investigate the formed aggregates. The results are shown in Figure 3 for $B_{38}V_{18}T_{44}^{112}$ in acetone at a concentration of 1 g/L.
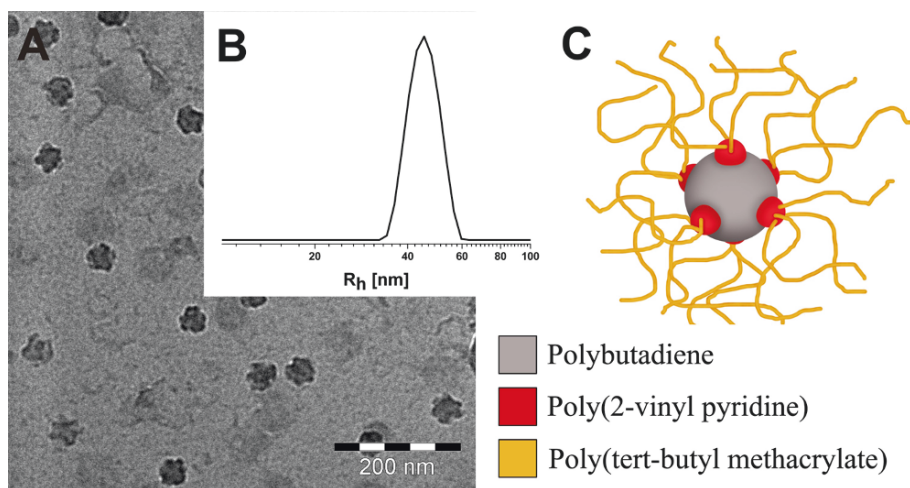
Figure 2. TEM micrograph of B38V18T44 micelles deposited from acetone solution (A); DLS plot for B38V18T44 micelles in acetone solution (c = 1 g/L, Θ = 90°) (B); schematic drawing of the proposed micellar structure in acetone solution (C). (Reprinted by permission from ACS.)

Figure 2A shows round-shaped aggregates with a diameter of around 40–50 nm, representing the micellar core. The central element (polybutadiene, grey) bears several (for the polymers investigated in this work numbers of 3–6 were found) black objects (poly(2 vinylpyridine), black), spherical in shape with an average diameter of 10–15 nm. The rather strong contrast originates from the difference in electron density between polybutadiene and poly(2 vinylpyridine). This type of micellar core is referred to as "spheres on sphere" or "raspberry-like".[11] This kind of morphology was first described by Stadler et al. for the bulk morphology of polystyrene-*b*-polybutadiene-*b*-poly(methyl methacrylate) (SBM) triblock terpolymers.[19] The inset, Figure 2B shows a DLS plot for the micelles in acetone solution, revealing $<R_h>_z$ = 44 nm and a $PDI_{app, DLS}$ = 1.01, rendering the micelles extremely monodisperse. Figure 2C depicts a scheme of the proposed structure in solution: a PB core with a non-continuous shell of P2VP, the P*t*BMA corona emerging from the latter.

There is a significant interest in the stabilization of polymer micelles. In that way, their dynamic structure can be altered in order to facilitate the transfer of such aggregates into different solvents or to provide their formation even below the critical micellar concentration.[20] Crosslinking of the core of the presented multicompartment micelles in acetone solution has been performed via applying a multifunctional acrylate (pentaerythrol tetraacrylate) compound as crosslinking agent and subsequent photopolymerization through UV-irradiation. The micelles were mixed with the desired amount of crosslinker (typically, 1 eq introduced functional groups calculated on the remaining 1,2-polybutadiene double bonds

in the polymer chain), left for 24 h to reach equilibrium state and afterwards subjected to UV-light for 2 h. The UV-lamp was equipped with a filter to cut off wavelengths below 300 nm to avoid photo-depolymerization of the PtBMA. The results (TEM and DLS) are shown in Figure 3.
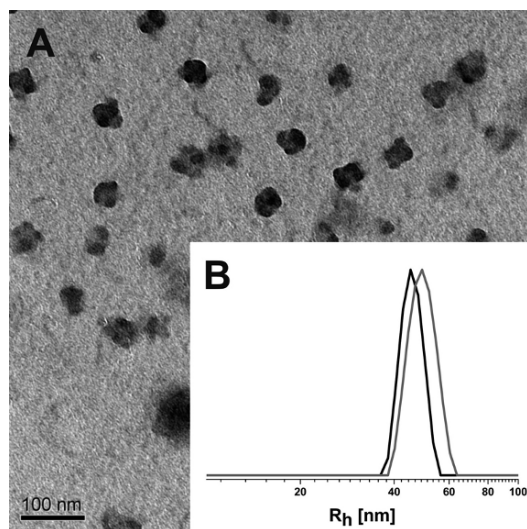

Figure 3. TEM micrograph of $B_{38}V_{18}T_{44}^{112}$ micelles after crosslinking with 1 eq multifunctional acrylate deposited from acetone solution (A); DLS plot in acetone solution (c = 1 g/L, $\Theta = 90°$) for the initial micelles (solid black line) and the micelles after crosslinking (solid grey line) (B). (Reprinted by permission from ACS.)

As can be seen in the TEM micrograph in Figure 3A, the multicompartmental character of the micelles is fully preserved. The size increased slightly, as shown in the DLS plots in Figure 3B. The initial size with $<R_h>_z = 44$ nm changed to $<R_h>_z = 48$ nm, probably due to the incorporation of the crosslinking agent inside the micellar core. The stabilized or crosslinked particles still exhibit a very narrow size distribution with $PDI_{app, DLS} = 1.02$. To further increase the versatility of the presented system, the PtBMA corona was converted into poly(methacrylic acid) (PMAA) through the hydrolysis of the ester moiety with hydrochloric acid.

1.3. MULTICOMPARTMENT MICELLES IN AQUEOUS SOLUTION

After hydrolysis of the PtBMA, the core-crosslinked micelles were transferred into aqueous solution through dialysis. However, sufficiently stable solutions could only be obtained at pH values higher than 6. This is due to the pH-dependant

solubility of PMAA. A cryo-TEM image of such a micellar solution is shown in Figure 4A.
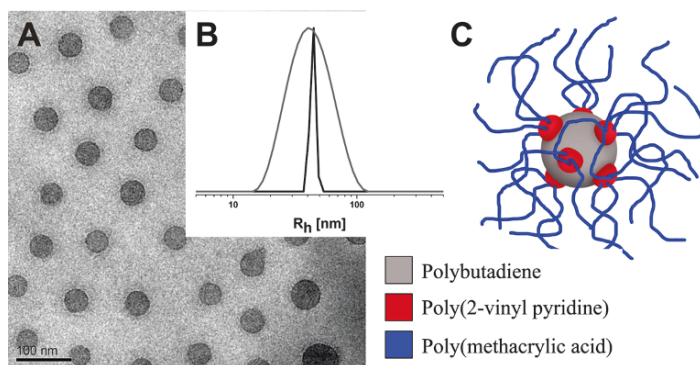
Figure 4. Cryo-TEM micrograph of $B_{46}V_{22}MAA_{32}^{92}$ micelles in aqueous solution at pH 10 (c = 1 g/L) (A); DLS plots for the micelles of $B_{38}V_{18}T_{44}^{112}$ in acetone (solid black line) and the $B_{46}V_{22}MAA_{32}^{92}$ micelles in aqueous solution (solid grey line) (c = 1 g/L in both cases, Θ = 90°) (B); proposed solution structure of $B_{46}V_{22}MAA_{32}^{92}$ micelles at high pH (C). (Reprinted by permission from ACS.)

In the cryo-TEM the multicompartmental character of the micellar core is not visible any more. This could be either due to a lack of contrast or simply due to swelling of the P2VP in water, causing the formation of a continuous shell around the PB core. The DLS plots in Figure 4B show a broadening of the peak for the hydrolyzed micelles ($<R_h>_z$ = 42 nm, $PDI_{app, DLS}$ = 1.18).

2. pH- and Temperature-Sensitive Hydrogels Based on Triblock Terpolymers

"Smart" hydrogels are networks of water soluble polymers, which form/disintegrate or swell/contract on external stimuli like a change in pH or temperature. Such stimuli responsive hydrogels find wide-spread use in biomedical applications and devices,[21] sensors,[22] damping elements, actuators, membranes[23] and nano-technology. They consist of chemically crosslinked stimuli sensitive polymers[24] or block copolymers forming networks with physical crosslinks above a certain temperature or pH.[25, 26] With a few exceptions,[27] these systems respond only to one stimulus, e.g. temperature or pH. Here, we report on double stimuli-responsive triblock terpolymers which respond to both, pH and temperature. These polymers contain a water-soluble poly(ethylene oxide) (PEO) middle block, a pH-sensitive poly(2-vinylpyridine) (P2VP), and a temperature-sensitive (LCST) outer block. Novel copolymers of methyl and ethyl glycidyl ether were

chosen as LSCT block. Depending on composition and concentration of the triblock terpolymers in water, a gel-sol-gel transition upon heating can be observed.[28]

Our concept of using trishydrophilic ABC triblock terpolymers with a neutral water-soluble PEO middle block (B block), a pH-sensitive A block, and a thermo-sensitive C block is illustrated in Scheme 2. Under conditions where only one of the endblocks is in a collapsed state the formation of soluble core-shell-corona (CSC) micelles is expected. These micelles themselves can form weak gels at sufficient high concentrations via hard-sphere crystallisation.[29, 30] Triggered by pH or temperature variations the second endblock will become insoluble. Depending on concentration, i.e. whether the CSC micelles already formed a soft gel or not, a hydrogel will be formed or the pre-formed hydrogel will transform into a stronger gel.
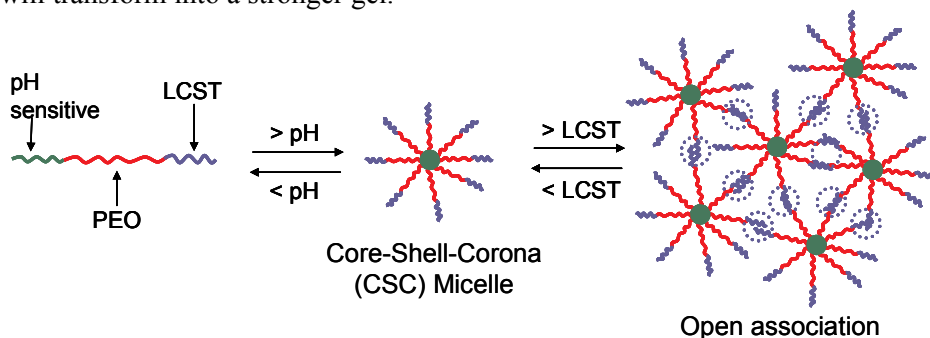
Scheme 2. Schematic depiction of hydrogel formation using trishydrophilic ABC triblock ter-polymers.

We have developed a new synthetic route[31] enabling the one-pot synthesis of block copolymers with well defined block lengths containing vinyl type monomers and epoxide monomers at the same time, using commercially available alkyllithium initiators in combination with the phosphazene base *t*-BuP$_4$. Applying this method, triblock terpolymers with poly(ethylene oxide) (PEO) as the water soluble middle block, poly(2-vinylpyridine) (P2VP) as the pH-sensitive moiety, and poly(glycidyl methyl ether-*co*-ethyl glycidyl ether) (P(GME-*co*-EGE)) as the thermo-sensitive block, were prepared (Scheme 3).

GME and EGE were the preferred monomers to form the thermo-sensitive block, since the corresponding homopolymers were shown to exhibit sharp coil-to-globule transitions at 58°C and 15°C, respectively.[32] Consequently, polymers with a sharp and tunable coil-to-globule transition might be obtained just by copolymerizing both monomers, which has indeed been shown by us recently (Figure 5A).[28] For anionic copolymerization with *t*-BuOK as initiator the reactivity ratios are 1.31 for GME and 0.55 for EGE, as determined by the

FINEMAN-ROSS method. A change of the initiating system from *t*-BuOK to
t-BuOLi/*t*-BuP$_4$ does not have a significant impact on the copolymerization
behavior, i.e. the reactivity ratios stay almost the same ($r_{GME} = 1.33$, $r_{EGE} = 0.72$).
Thus, copolymers with only a weak gradient in composition can be synthesized.
Furthermore, we could show that in contrast to poly(N-isopropyl acrylamide)
there is no hysteresis when performing a heating-cooling cycle. However, upon
cooling the transition is slightly broadened (Figure 5B).
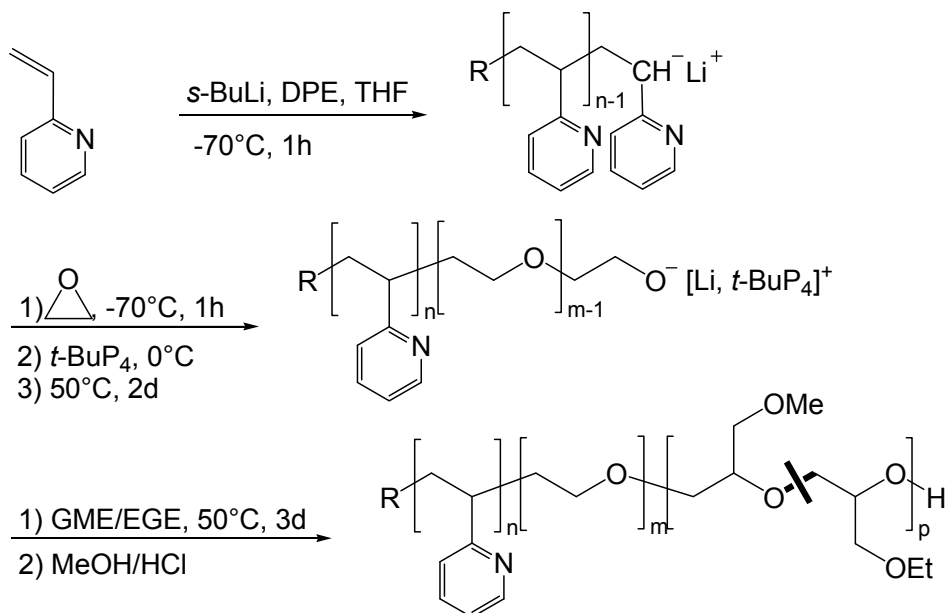
Scheme 3. One-pot synthesis of P2VP-b-PEO-b-P(GME-co-EGE) triblock terpolymers.

The temperature- and pH-dependent aggregation of the P2VP-*b*-PEO-*b*-
P(GME-*co*-EGE) triblock terpolymers in aqueous solution was investigated by
dynamic light scattering (DLS). Figure 6 shows, that a 2VP$_{57}$EO$_{477}$(GME$_{22}$-*co*-
EGE$_{22}$) triblock terpolymer (subscripts denote the degree of polymerization of
the corresponding block) forms reversibly micellar aggregates under conditions,
where only the pH-sensitive (pH > 4.5, room temperature) or the temperature-
sensitive (pH < 4.5, elevated temperature) block is insoluble. The coil-to-
globule transition of the thermo-sensitive P(GME-*co*-EGE) block within the
triblock terpolymers is shifted to higher temperatures (about 10°C) compared to
that of the corresponding pure copolymers, which is due to the attachment of
the hydrophilic PEO block.
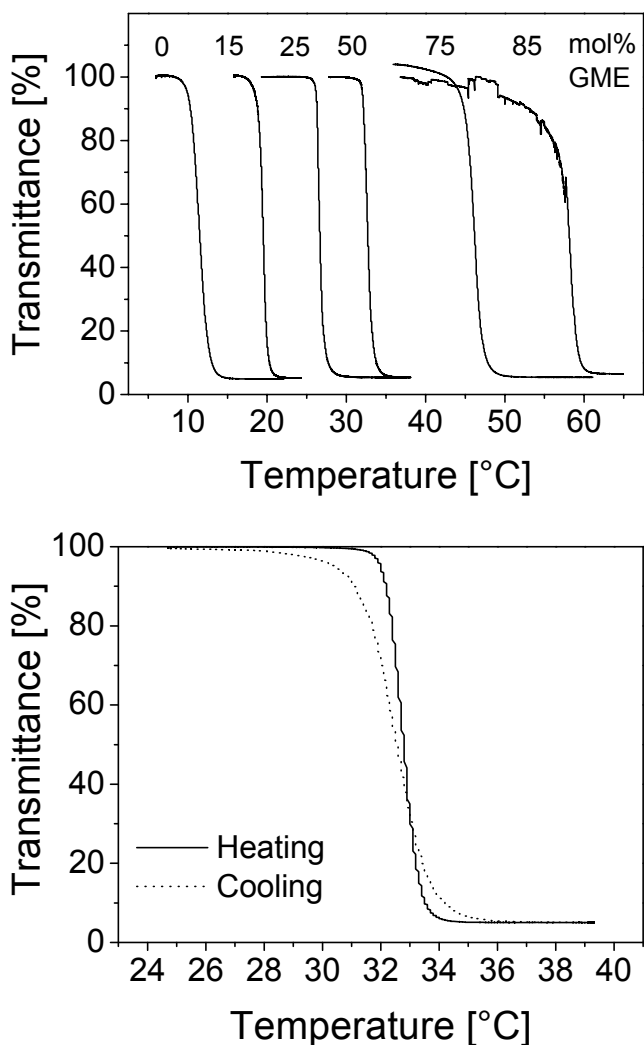
Figure 5. Transmittance as a function of temperature: (**a**) for aqueous solutions of P(GME-co-EGE) with varying GME content (2.5 g/L, Mn ca. 5,000 g/mol), (**b**) heating-cooling cycle for an aqueous solution of P(GME-co-EGE) with 50 mol% GME (c = 2.5 g/L).

The ability to form a hydrogel was demonstrated by rheological measurements, as well as by the so-called test tube inversion method. An 18 wt% solution of $2VP_{57}EO_{477}(GME_{22}\text{-}co\text{-}EGE_{22})$ at pH = 7 forms already a hydrogel at 20°C, becomes a liquid at intermediate temperatures, and finally forms a gel again above 50°C, i.e., shows a gel-sol-gel transition upon heating (Figure 7).
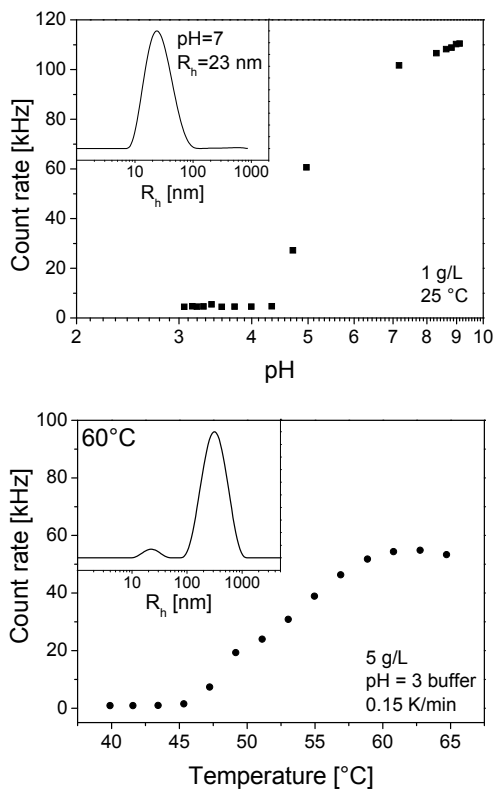
Figure 6. Scattering intensity of 2VP57EO477(GME22-co-EGE22) aqueous solutions at θ = 90°
in dependence of: (**a**) pH (1 g/L, room temperature), (**b**) temperature (5 g/L, pH = 3, citric acid
buffer). The insets show intensity weighted distribution functions of apparent hydrodynamic radii
(Rh,app) obtained via CONTIN analysis at the indicated conditions.

Interestingly, the storage modulus at 50°C is higher compared to that at
20°C, i.e., the gel is stiffer at higher temperatures. At concentrations below 14
wt% a gel is formed in the lower temperature region, only, whereas no gel
formation was observed for concentrations below 12 wt%. The critical con-
centration, at which a gel starts to reform at higher temperatures, i.e. a gel-sol-
gel transition is observed upon heating, is about 16 wt%. Small-angle neutron
scattering showed that the low temperature gel phase is built by a cubic packing
of spherical CSC micelles.[28]

Systematic variation of block lengths revealed, that a minimum overall molecular
weight is necessary in order to form a stable hydrogel. A 2VP$_{33}$EO$_{236}$(GME$_{11}$-*co*-
EGE$_{12}$) triblock terpolymer, i.e. comparable composition but lower molecular
weight compared to 2VP$_{57}$EO$_{477}$(GME$_{22}$-*co*-EGE$_{22}$), did not form a hydrogel at
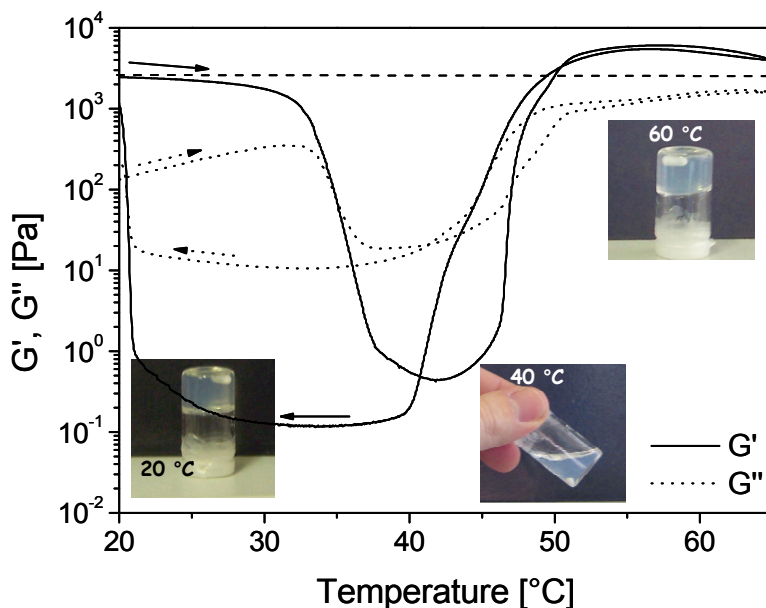
Figure 7. Temperature dependence of storage (G′) and loss (G″) modulus for an 18 wt% aqueous solution of 2VP57EO477(GME22-co-EGE22) at pH = 7 (1 Hz, 1% strain, 0.5 K/min). The photographs show free-standing gels at 20°C and 60°C (test tube inversion method). (Reprinted by permission from the Royal Society of Chemistry.)

concentrations up to 30 wt% regardless of pH and temperature. Increasing the block length of the thermo-sensitive block while keeping the other block lengths constant results in hydrogels, again showing a gel-sol-gel transition upon heating at sufficiently high concentration and neutral pH. However, these gels are significantly stiffer at high temperatures and show a more narrow sol region. Gelation can be induced at low pH, i.e. under conditions where the pH-sensitive P2VP block is still soluble, by increasing the temperature, too. Heating an 18 wt% solution of $2VP_{62}EO_{452}(GME_{36}\text{-}co\text{-}EGE_{36})$ at pH = 3.5 to temperatures above 45°C induces a sol-gel transition. This shows, that P2VP-*b*-PEO-*b*-P(GME-*co*-EGE) triblock terpolymers can form hydrogels in response to both, pH and temperature.

In conclusion, a new anionic polymerization route, using alkyllithium initiators in combination with the phosphazene base *t*-BuP$_4$, enables the synthesis of block copolymers containing vinyl monomers and epoxy monomers in a one-pot reaction. Additionally, we showed that a copolymerization of GME and EGE under these conditions leads to products with sharp and tunable LCST-type phase transitions. P2VP-*b*-PEO-*b*-P(GME-*co*-EGE) triblock terpolymers, containing a GME/EGE copolymer as thermo-sensitive block, form reversibly micellar aggregates in diluted aqueous solution, and gels in concentrated solution in response to changes in pH

and/or temperature. The block lengths and the composition play an important role in the micelle and hydrogel formation.

3. Janus Particles via Crosslinking Block Terpolymers in the Bulk

Anionic Polymerization provides one of the best means for the preparation of high-molecular weight block copolymers with tailored compositions and narrow molecular weight distributions. These factors give rise for the development of extremely well-defined microphase-segregated bulk structures. In recent years, increasing efforts have been devoted to utilize such solid state nanostructures for the preparation of soluble multicompartment colloids.[33, 34] The strategy to obtain this goal is based on crosslinking one of the non-continuous phases of the nanostructure. In our group, we have focused efforts on the preparation of Janus particles (see Scheme 4).[35]
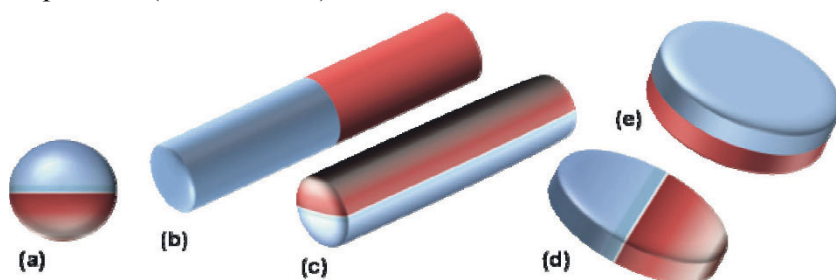
Scheme 4. Overview of possible Janus particle architectures. (**a**) Sphere, (**b**+**c**) cylinders, and (**d**+**e**) discs.

In general, Janus particles can be divided into several classes according to their architecture and dimensionality (see Scheme 4). Most commonly, spherical (3D) Janus particles can be imagined. In addition, two types of cylinders (1D) and two types of disc-like particles (2D) are conceivable. The lack of centro-symmetry is inherent to all of these particles and is the major challenging aspect in their preparation.

These synthetic difficulties can be overcome via selectively crosslinking the polybutadiene domains of polystyrene-block-polybutadiene-block-poly(methyl methacrylate) (SBM) and polystyrene-block-polybutadiene-block-poly(*tert*-butyl methacrylate) (SBT) block terpolymers.[33] The methodology is outlined in Scheme 5.

It requires block terpolymers with symmetric end blocks. This symmetry is necessary for the formation of overall lamella morphologies. Depending on the various interaction parameters of the constituting blocks and the weight fraction
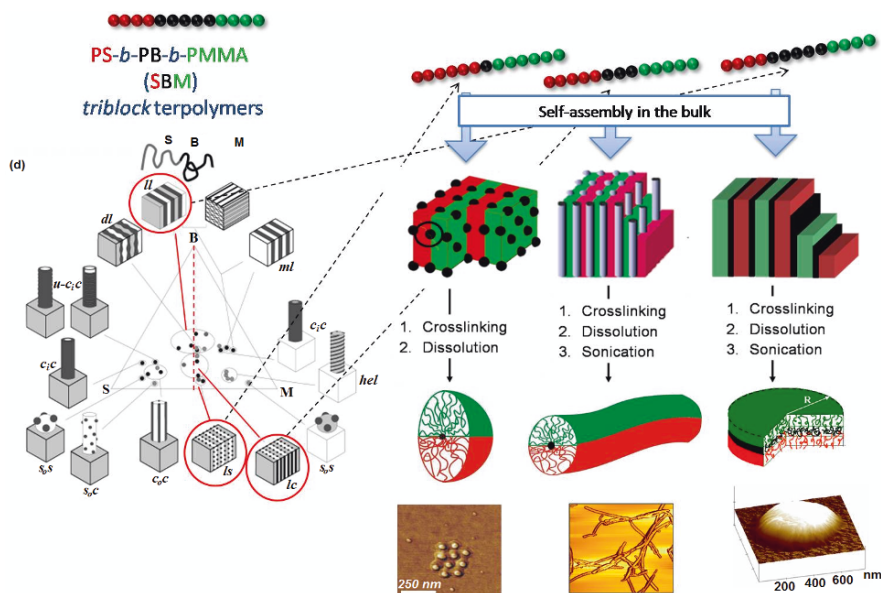
Scheme 5. Schematic preparation of Janus particles based on the selective crosslinking of polybutadiene containing SBM and SBT block terpolymers. The left-hand side shows the phase-diagram of SBM block terpolymers. The right-hand side displays the synthesis of Janus micelles, Janus cylinders and Janus discs. The bottom-right shows several atomic force microscopy and scanning electron microscopy images of the resulting materials.

of the inner block, three different morphologies, lamella-sphere (ls), lamella-cylinder (lc) and lamella-lamella (ll), can be obtained. The crosslinking of the inner polybutadiene domain (black) preserves the orientation of the two outer sides and unambiguously leads to the formation of Janus particles.[36–38] The particles can either be directly dissolved in the case of Janus micelles, whereas it needs to be assisted by sonication for the Janus cylinders and Janus discs. Janus particles are interesting for a variety of reasons.[35] Apart from showing unique self-assembly behavior, various application have been proposed or partially realized. In particular, the high interfacial activity of the Janus particles, combining amphiphilicity together with the Pickering effect, is appealing for large-scale applications.[39]

3.1. SELF-ASSEMBLY OF JANUS PARTICLES

The ability of a material to self-assemble into complex hierarchical structures is encoded into its architecture, proteins being the best example. Since Janus particles possess the unique and novel feature of being non-centrosymmetric,

many investigations have been concerned with the evaluation of the solution properties and self-assembly behavior of these particles.[36, 38, 40–43] As some techniques allow the preparation of non-spherical particles, it is also possible to study the effect of the geometry on the types of aggregates formed. Indeed, it turned out that Janus particles exhibit a variety of complex and partially unexpected aggregates.

In the case of spherical Janus micelles, having hemispheres of polystyrene (PS) and poly(methyl methacrylate) (PMMA), aggregation into clusters is observed in various organic solvents, e.g. THF.[38] Similarly, Janus discs composed of two sides of PS and poly(*tert*-butyl methacrylate) (P*t*BMA) undergo back-to-back stacking into superstructures in organic solvents.[36] The self-assembly behavior could be strikingly demonstrated with various imaging and scattering techniques. For instance, Figure 8a and c shows Transmission Electron Microscopy (TEM) images of back-to-back stacked Janus discs. The images were obtained from ultrathin sections after embedding the superstructures from THF or acetone into a crosslinkable silicone oil, microtome cutting and staining. A stacking of the PS sides of the Janus discs can clearly be seen and the multicompartment architecture can be visualized (see Figure 8c for a schematic representation of the layers).

Furthermore, Figure 8d exhibits a scanning force microscopy (SFM) image of individual Janus micelles (small isolated particles) and superstructured surface clusters composed out of supermicelles (clustered large "fried-egg"-like structures). Each supermicelle is constituted of several individual Janus micelles. The Scheme in Figure 8e serves as a cartoon of the proposed aggregation pattern of individual Janus micelles into the supermicelles. This aggregation of the Janus particles into superstructures is surprising to some extent as both sides of the particles alone, as well as the base terpolymer, are well soluble in the organic solvent used. It appears though that the very slight selectivity of the solvent is sufficient to induce a self-assembly of the particles into defined discrete clusters of Janus particles. Such kind of an aggregation can be expected neither for standard block copolymers nor for homogeneous particles and thus represents one of the unique features of Janus particles.

Turning to aqueous medium, the situation becomes even more complex and interesting. Extensive studies have been carried out with spherical Janus particles composed of one hemisphere of water-soluble poly(methacrylic acid) (PMAA) and another side of PS.[41] The detailed investigations revealed that the Janus particles aggregate on two hierarchical levels (see Figure 9). The first one is the assembly of single Janus particles into defined clusters, similar as in organic solution. The second is the aggregation into even larger aggregates, so-called giant micelles. The supermicelles and the giant micelles can be seen in the SFM and SEM (scanning electron microscopy) images below as small and very large structures, respectively. The structure of the very large supermicelles is unknown

so far, however, it was suggested that they may be similar to multilamellar vesicles. Interestingly, the critical aggregation concentration of the amphiphilic Janus micelles (PS-PMAA) in water is higher than for the Janus particles in organic solution. This again comes as a surprise as water is a much stronger selective solvent than the organic solvents used and thus a lower critical aggregation concentration is anticipated.
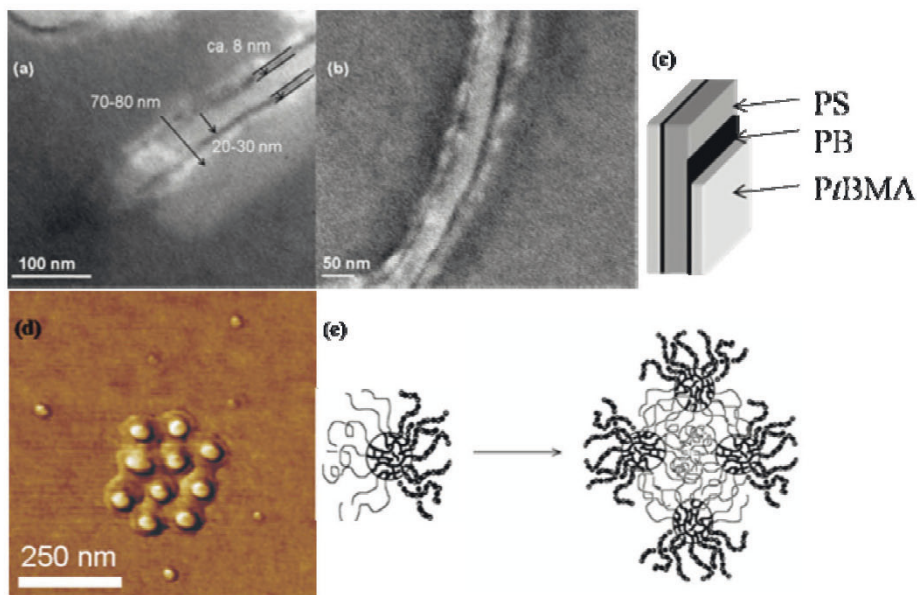
Figure 8. Superstructures formed by Janus discs, possessing one PS and one PtBMA side, in THF (**a**) and acetone (**b**). TEM images taken after embedding. (**d**) SFM height image (z-range = 30 nm) of single Janus micelles, composed of one PS and one PMMA side, and their supermicelles. The latter form ordered surface assemblies after deposition from THF onto mica. Scheme 1 -s (**c**) and (**e**) show the proposed aggregation patterns (polybutadiene = PB). (Reprinted by permission from ACS.)
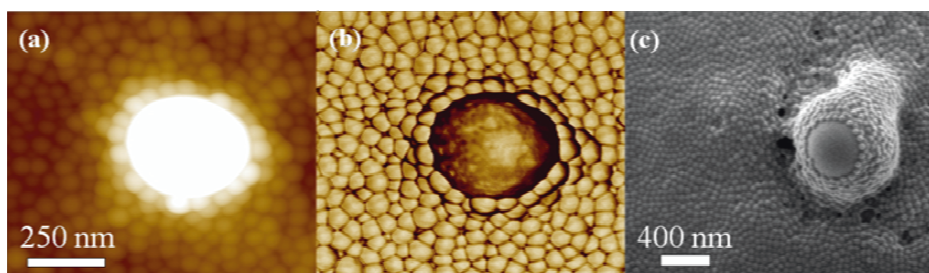
Figure 9. SFM height (a; z-range = 100 nm) and phase image (**b**), and SEM image (**c**) of amphiphilic Janus micelles, having one PS and one PMAA side, after deposition from aqueous solution. (Reprinted by permission from ACS.)

3.2. APPLICATIONS OF JANUS PARTICLES

After controlling the architecture of the Janus particles and gaining in-depth knowledge of their self-assembled structures, the attention is drawn to possible applications of Janus particles. From a scientific, as well as from an industrial point of view, the advanced surface-active properties of particles with a segregated corona over particles with a uniform wettability are very interesting. It was calculated that the surface activity of a Janus particle is up to three times higher at an oil/water interface than that of a uniform particle, leading to an enhanced adsorption at the interface. Janus particles uniquely combine the so-called Pickering effect, known from particles, with amphiphilicity – similar to block copolymers – induced by the Janus character.[39] This combination enables a firm attachment at interfaces and may lead to advanced stabilizing properties in dispersions. Unwanted coalescence of domains of the dispersed phase are thus expected to be diminished using this highly surface-active particles. Thus, the surface active properties are highly interesting for industrial application.

In a first approach, Pickering emulsion polymerization of standard monomers was explored using amphiphilic Janus particles as stabilizers.[44] The polymerizations could be performed with a simple conventional technique and no pre-homogenization to a miniemulsion was necessary as it is the case for Pickering emulsion polymerizations using homogeneous particles. The reactions led to extremely well-defined latex particles with very narrow size distributions, independently of the monomer used (Figure 10). A control of the latex particle size could easily be achieved by changing the concentration of the stabilizer. After the polymerization, the latex is stabilized by amphiphilic Janus particles, which can, due to their size, not be easily removed from the interface by thermal energy. Thus, a significant improvement of the long-term stability is found.
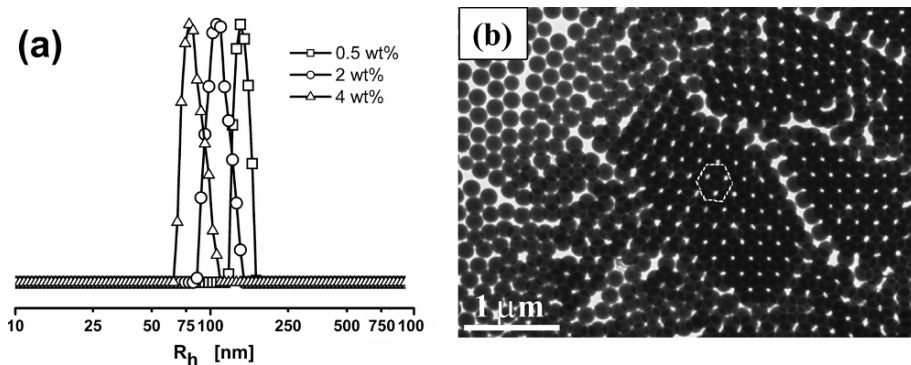

Figure 10. (**a**) CONTIN plots (dynamic light scattering) for PS latexes obtained at different contents of Janus particles. (**b**) TEM micrograph for a PS latex with a stabilizer content of 4 wt%. A double layer of particles can be seen in the micrograph. The hexagon guides the eye for a better recognition of the well ordered pattern. (Reprinted by permission from Wiley-VCH.)

A second application study deals with the utilization of Janus particles for the engineering of nanostructured polymer blends with controlled nanoparticle location.[45] The combination of polymer properties by blending and the introduction of inorganic particles are the most attractive ways for obtaining new products with superior material performances, such as for tailoring the electronic, mechanical or optical features. This does not only hold for large-scale industrial applications, but also for scientific problems as for instance in the case of polymer blend solar cells. In both fields, there is a constant search for better ways of compatibilization. In analogy to colloidal science, we conceived of a novel concept for blending polymers using surfactant-like particles.

Therefore, we applied Janus particles on a *multi-gram* scale for the blend compatibilization of two model polymers in a twin screw mini-mixer (Scheme 6).
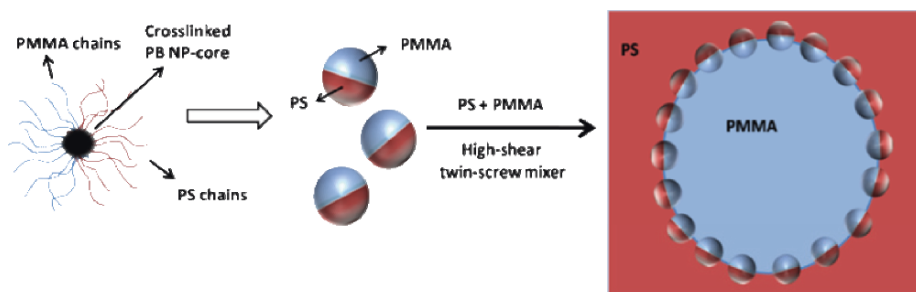
Scheme 6. Schematic representation of Janus particles and their adsorption at the blend interface of a PS/PMMA blend. (Reprinted by permission from ACS.)

It could be shown that the Janus particles can be located exclusively at the interface of the two polymer phases despite the high temperature and shear conditions. The domain sizes of the dispersed phase decrease with increasing content of Janus particles. The decrease is yet ongoing for high contents of Janus particles (Figure 11).

Furthermore, the biphasic particles exhibit an ordered arrangement at the interface, which may be a way of a lateral structuring of polymer interfaces. The strong adsorption at the interface is explained in terms of the increased desorption energy of Janus particles. A similarly high control of the nanoscopic structuring of polymer blends with homogenous nanoparticles has not yet been shown in the literature and is thus of tremendous interest. Furthermore, the compatibilization efficiency was critically compared to state-of-the-art comp-atibilizers such as block copolymers. It was found that the efficiency of the Janus particles is superior as compared to block copolymer based compatibilizers. This approach demonstrates convincingly that Janus particles are a very promising tool for nanostructuring blend and block copolymer interfaces. Moreover, Janus

particles provide a mean for the nanoscopic engineering of blend systems, while matching some macroscopic processing constraints. We are strongly convinced that the results will have an impact on materials science in general and will open up new ways of structuring nanocomposites and high-performance materials, thus bridging academic and industrial research. Developments based on modified Janus particles may take place in important fields like electro-optical polymeric devices (e.g. solar cells), nanocomposites with increased thermo-conductivity or improved crack characteristics and for self-healing materials.
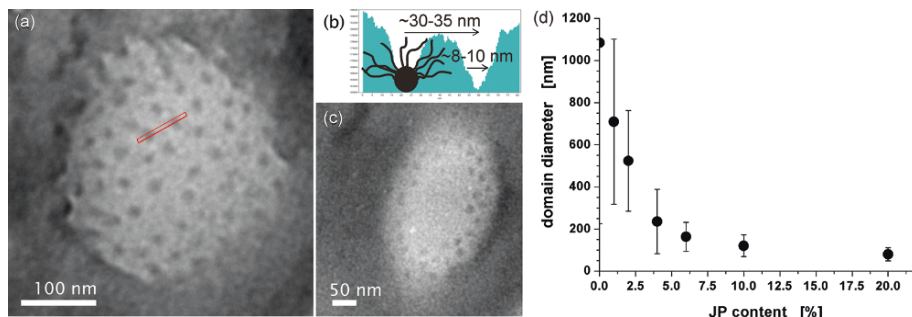
Figure 11. Endcaps of PMMA droplets in a PS matrix with Janus particles located at the interface (dark dots). (**b**) Section analysis of the red bar shown in image (**a**). One side of a Janus particle is schematically sketched to show its brush-like character and the location of the polybutadiene nanoparticle core. (**d**) Evolution of the PMMA domain size as a function of the Janus particle (JP). (Reprinted by permission from ACS.)

In conclusion, the transfer of well-defined block terpolymer bulk structures into solution via controlled crosslinking of selected micro domains allows the facile formation of multicompartment colloids. Biphasic Janus particles can be prepared in a variety of different architectures, i.e. spherical, cylindrical and disc-like colloids. The pathway enables to study the fascinating self-assembly behavior of these unique non-centrosymmetric materials. The amphiphilic character can be used for the Pickering emulsion polymerization and the polymer blend compatibilization. In both cases, an excellent performance of the particles in terms of stabilizing the interfaces and controlled location can be observed.

Acknowledgments

References

[1]   H. Ringsdorf; P. Lehman; R. Weberskirch *Book of Abstracts, 217th ACS National Meeting Anaheim*; American Chemical Society, Washington, DC, **1999**.

[2]   J.-F. Lutz; A. Laschewsky. *Macromol. Chem. Phys.* **2005**, *206*, 813.

[3]   Z. Li; M. A. Hillmyer; T. Lodge. *Langmuir* **2006**, *22*, 9409.

[4]   R. S. Underhill; G. Liu. *Chem. Mater.* **2000**, *12*, 2082.

[5]   C. S. Patrickios; C. Forder; S. P. Armes; N. C. Billingham. *J. Polym. Sci. A: Polym. Chem.* **1997**, *35*, 1181.

[6]   J. Kriz; B. Massar; J. Plestil; Z. Tuzar; H. Pospisil; D. Doskociloca. *Macromolecules* **1998**, *31*, 41.

[7]   W. Y. Chen; P. Alexandridis; C. K. Su; C. S. Patrickios; W. R. Hertler; T. A. Hatton. *Macromolecules* **1995**, *28*, 8604.

[8]   G. Yu; A. Eisenberg. *Macromolecules* **1998**, *31*, 5546.

[9]   S. Stewart; G. Liu. *Chem. Mater.* **1999**, *11*, 1048.

[10] K. Stähler; J. Selb; F. Candau. *Mat. Sci. Eng. C* **1999**, *10*, 171.

[11] S. Kubowicz; J.-F. Baussard; J.-F. Lutz; A. Thünemann; H. v. Berlepsch; A. Laschewsky. *Angew. Chem. Int. Ed.* **2005**, *44*, 5262.

[12] T. Lodge; A. Rasdal; Z. Li; M. A. Hillmyer. *J. Am. Chem. Soc.* **2005**, *127*, 17608.

[13] Z. Li; M. A. Hillmyer; T. P. Lodge. *Macromolecules* **2006**, *39*, 765.

[14] A. Thünemann; S. Kubowicz; H. v. Berlepsch; H. Möhwald. *Langmuir* **2006**, *22*, 2506.

[15] Z. Li; E. Kesselman; Y. Talmon; M. A. Hillmyer; T. P. Lodge. *Science* **2004**, *306*, 98.

[16] J. Mao; P. Ni; Y. Mai; D. Yan. *Langmuir* **2007**, *23*, 5127.

[17] S.-H. Chou; H.-K. Tsai; Y.-J. Sheng. *J. Chem. Phys.* **2006**, *125*, 194903.

[18] C. Zhong; D. Liu. *Macromol. Theory Simul.* **2007**, *16*, 141.

[19] U. Breiner; U. Krappe; T. Jakob; V. Abetz; R. Stadler. *Polym. Bull.* **1998**, *40*, 219.

[20] R. K. O'Reilly; C. Hawker; K. L. Wooley. *Chem. Soc. Rev.* **2006**, *35*, 1068.

[21] A. S. Hoffmann. *Adv. Drug Deliv. Rev.* **2002**, *54*, 3.

[22] G. Gerlach; M. Günther; J. Sorber; G. Suchaneck; K.-F. Arndt; A. Richter. *Sens. Actuators B* **2005**, *111–112*, 555.

[23] S. Abramchuk; E. Kramarenko; D. Grishin; G. Stepanov; L. V. Nikitin; G. Filipcsei; A. R. Khoklov; M. Zrinyi. *Polym. Adv. Technol.* **2007**, *18*, 513.

[24] F.-J. Xu; E.-T. Kang; K.-G. Neoh. *Biomaterials* **2006**, *27*, 2787.

[25] H. H. Lin; Y. L. Cheng. *Macromolecules* **2001**, *34*, 3710.

[26] A. Sotirios; C. T. Angelopoulos. *Macromol. Chem. Phys.* **2006**, *207*, 2188.

[27] K. Dayananda; B. S. Pi; B. S. Kim; T. G. Park; D. S. Lee. *Polymer* **2007**, *48*, 758.

[28] S. Reinicke; J. Schmelz; A. Lapp; M. Karg; T. Hellweg; H. Schmalz. *Soft Matter* **2009**, accepted.

[29] G. A. McConnell; A. P. Gast; J. S. Huang; S. D. Smith. *Phys. Rev. Lett.* **1993**, *71*, 2102.

[30] A. P. Gast. *Langmuir* **1996**, *12*, 4060.

[31] A. A. Toy; S. Reinicke; A. H. E. Müller; H. Schmalz. *Macromolecules* **2007**, *40*, 5241.

[32] S. Aoki; A. Koide; S. Imabayashi; M. Watanabe. *Chem. Lett.* **2002**, 1128.

[33] A. Walther; A. Göldel; A. H. E. Müller. *Polymer* **2008**, *49*, 3217.
[34] G. J. Liu; L. Z. Yan Xiaohu; J. Y. Zhou; S. Duncan. *J. Am. Chem. Soc.* **2003**, *125*, 14039.
[35] A. Walther; A. H. E. Müller. *Soft Matter* **2008**, *4*, 663.
[36] A. Walther; X. André; M. Drechsler; V. Abetz; A. H. E. Müller. *J. Am. Chem. Soc.* **2007**, *129*, 6187.
[37] Y. Liu; V. Abetz; A. H. E. Müller. *Macromolecules* **2003**, *36*, 7894.
[38] R. Erhardt; A. Böker; H. Zettl; H. Kaya; W. Pyckhout-Hintzen; G. Krausch; V. Abetz; A. H. E. Müller. *Macromolecules* **2001**, *34*, 1069.
[39] B. P. Binks; P. D. I. Fletcher *Langmuir* **2001**, *17*, 4708.
[40] Z. Nie; W. Li; M. Seo; S. Xu; E. Kumacheva. *J. Am. Chem. Soc.* **2006**, *128*, 9408.
[41] R. Erhardt; M. Zhang; A. Böker; H. Zettl; C. Abetz; P. Frederik; G. Krausch; V. Abetz; A. H. E. Müller. *J. Am. Chem. Soc.* **2003**, *125*, 3260.
[42] D. Dendukuri; T. A. Hatton; P. S. Doyle. *Langmuir* **2007**, *23*, 4669.
[43] L. Hong; A. Cacciuto; E. Luijten; S. Granick. *Nano Lett.* **2006**, *6*, 2510.
[44] A. Walther; M. Hoffmann; A. H. E. Müller. *Angew. Chem. Int. Ed.* **2007**, *120*, 723.
[45] A. Walther; K. Matussek; A. H. E. Müller. *ACS Nano* **2008**, *2*, 1167.

EPOXIDE ACTIVATED ANIONIC POLYMERIZATION: APPLICATION TO THE SYNTHESIS OF (CO)POLYETHERS WITH CONTROLLED STRUCTURE AND TUNED PROPERTIES

AMELIE LABBE, VIRGINIE REJSEK,
STEPHANE CARLOTTI, AND ALAIN DEFFIEUX[*]
*Laboratoire de Chimie des Polymères Organiques, UMR 5629
CNRS-ENSCPB-Université Bordeaux 1, 16 Avenue Pey Berland,
33607 Pessac cedex, France*

Abstract: A ring opening polymerization process allowing the fast and controlled anionic polymerization of epoxide monomers is described and applied to the synthesis of (co)polyethers with novel structure and composition. The approach is based on the simultaneous formation of complexes between an organometallic Lewis acid additive with both the anionic initiator and the monomer. In conjunction with the use of tetraalkylammonium or phosphonium salts as initiators, the addition of such additive allows the synthesis of polyethers and block copolyethers with controlled molar masses and narrow polydispersities, in hydrocarbon media, at low temperature, and in short reaction times. The low nucleophilic character of the propagating species involved in the polymerization avoids transfer to monomer, a side reaction which is often predominant in conventional anionic polymerizations. This also allows the controlled polymerization of functional epoxides such as glycidyl methacrylate and epichlorohydrin. Properties and potential applications of these new polyethers and copolyethers are also reported.

Keywords: Anionic polymerization; Activated monomer; Epoxide; Lewis acid; Onium salt

1. Introduction

Alkali metal derivatives are commonly used as initiator for the anionic poly-merization of three member ring cyclic ethers.[1] However, the high nucleophilicity of the corresponding propagating species generally results in important transfer reactions that lead to the formation of oligomers. In the case of propylene oxide (POx) for example only low molar mass polymers are obtained as a consequence

of proton abstraction on the POx-methyl group, which leads to the formation of hydroxy-ended chains and new allyl alkoxide initiators.

Another approach that allows a better control of the polymerization of substituted epoxides involves the use of aluminum porphyrin initiators in association with bulky aluminum derivatives as activator.[2] These systems yield PPOx with controlled molar masses in the range of 10,000 to 50,000 g/mol in short polymerization time. However, they result in the formation of coloured polymers and catalyst removal is necessary.[3] We report in this paper the use of new and quite simple initiating systems based on the combination of anionic initiators with a trialkylalkylaluminum additive.

2. Results and Discussion

2.1. PROPYLENE OXIDE ACTIVATED ANIONIC POLYMERIZATION

In recent works we have found that very simple initiators based on the association of alkali metal derivatives[4, 5] or tetralkylammonium or tetraalkylphosphonium salts[6] with triisobutylaluminum (*i*-Bu$_3$Al) yield a rapid and controlled polymerization of propylene oxide whereas transfer to monomer was strongly reduced or even suppressed. As it may be seen in Table 1, these systems are inactive at ratios [Al]/[Onium salt] lower or equal to one, even after a long polymerization time.

TABLE 1. Propylene oxide polymerization initiated by different initiating species in the presence of triisobutylaluminum, in toluene.

Initiator [I]	[Bu$_3$Al]/[I]	[POx]/[I]	T (°C)	Time (h)	Yield (%)	$\overline{M}_n$ th. (g/mol)	$\overline{M}_n$ exp. (g/mol)	$\dfrac{\overline{M}_w}{\overline{M}_n}$
i-PrONa	0	360	25	24	0	–	–	–
i-PrONa	1	360	25	24	0	–	–	–
i-PrONa	3.5	360	0	3.5	100	22 100	23 600	1.3
NBu$_4$Cl	0	360	20	24	0	–	–	–
NBu$_4$Cl	1	360	20	24	0	–	–	–
NBu$_4$Cl	1.3	350	0	2	100	20 000	21 100	1.07
NBu$_4$Cl	1.8	360	0	1	100	20 700	19 800	1.34
NOct$_4$Br	1.4	345	0	2	100	20 600	20 500	1.11
NOct$_4$Br	3.4	345	–30	2	100	200 000	185 000	1.21
PBu$_4$Cl	1.2	517	20	2	100	25 200	23 000	1.10

POx concentration: 2–4 mole/l

In contrast, in the presence of an excess of the aluminic compound, polymerization proceeds rapidly, up to complete monomer conversion. In the temperature

range 0°C to 20°C, experimental PPOx molar masses are closed to the expected values, considering the formation of one PPOx chain per onium salt, and poly-dispersities are narrow.

For the same ratio [Al]/[Onium salt] the highest rates of polymerization are obtained with the bulkiest ammonium NOct₄Br and the phosphonium PBu₄Cl salts , whereas for a given counterion the polymerization rate directly increases with the amount of trialkylaluminum which acts as an activator/catalyst for the polymerization. Since when initiators are used alone or at ratio initiator/*i*-Bu₃Al of 1:1, no polymerization proceeds, these results sustain the selective insertion of a *i*-Bu₃Al complexed monomer which is electrophilically activated. These results can be interpreted by a polymerization mechanism involving an acti-vation of the epoxide by *i*-Bu₃Al, through complexation, making the activated monomer more prone to nucleophilic attack by the 1:1 [*i*-Bu₃Al]/[X⁻Y⁺] "ate" complex (X = Br, Cl and Y = NR₄ or PR₄), see Scheme 1.

After monomer insertion, a new "ate" complex is formed between a *i*-Bu₃Al molecule and the growing chain end, whereas the second *i*-Bu₃Al molecule is released and can coordinate and activate a new POx molecule.
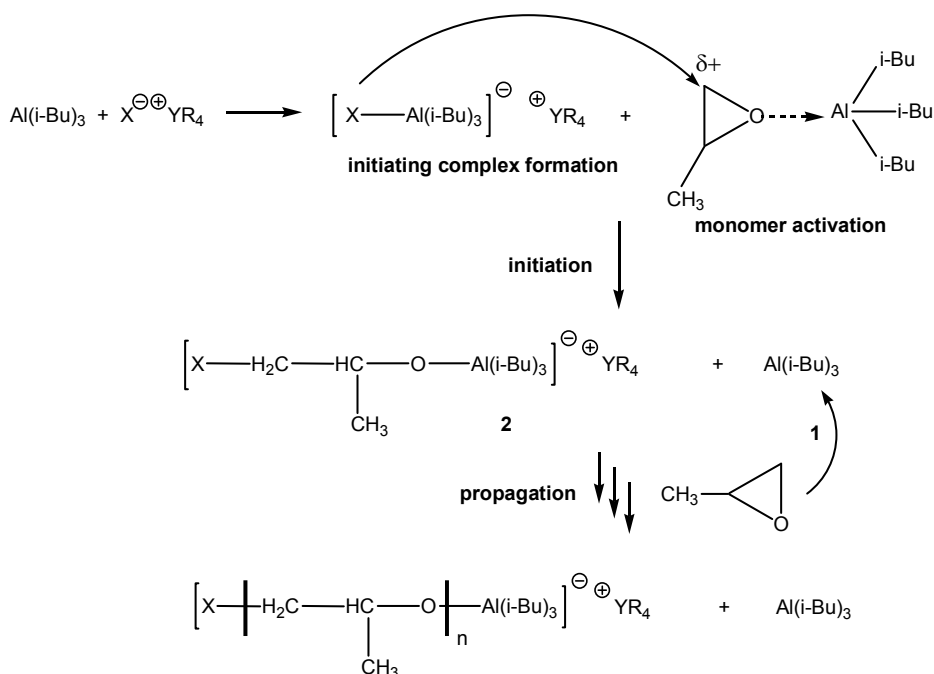
Scheme 1. Polymerization mechanism involving monomer activation followed by nucleophilic attack of the aluminate complex using onium salts as initiator.[6]

2.2. ACTIVATED ANIONIC POLYMERIZATION OF ETHYLENE OXIDE

As for propylene oxide, ethylene oxide (EO) polymerization readily takes place
in the presence of tetraalkylammonium salts in toluene and in dichloromethane,
a better solvent for poly(EO), when a slight excess of trialkylaluminum with
respect to the initiator ([Al]/[Initiator] > 1) is added to the system.[7] Some EO
polymerization data are collected in Table 2.

TABLE 2. Ethylene oxide (EO) polymerization initiated by NOct$_4$Br (I) in the presence of
triisobutylaluminum in dichloromethane, [EO] = 4 M.

[i-Bu$_3$Al]/[I]	T (°C)	Time (h)	Conversion (%)	$\overline{M}_n$ (th.) (g/mol)	$\overline{M}_n$ (exp.) (g/mol)	Ip
1.5	20	4	100	19,300	17,300	1.15
1.5	25	2	100	20,000	19,000	1.16
1.5	25	4	93	41,500	36,000	1.20

In most cases the PEO experimental molar masses are in good agreement
with calculated values assuming one chain formed per initiator molecule and
polydispersities are narrow. The linear variation of molar masses in direct
relation with the equation $\overline{M}_n$ = [EO]$_{consumed}$/[NOct$_4$Br] and the narrow poly-
dispersity of the final PEO are again consistent with a living-like polymerization
process.

To further confirm the livingness of the monomer activated anionic epoxide
polymerization, the synthesis by sequential monomer addition of diblock and
triblock EO and POx copolymers that found important applications as amphiphilic
copolymers[8–10] was investigated. Results are collected in Table 3. In toluene,
when EO is used as the first monomer, a short PEO block ($\overline{M}_n$ = 5,300 g/mol)
was prepared to avoid precipitation. Upon addition of POx, the formation of a
second block, with a molar mass in agreement with the calculated value, was
readily obtained in a short period of time, yielding PEO-*b*-POx diblock co-
polymers. Addition of a new EO feed yields a triblock copolymer, with narrow
molar mass distribution, constituted by two external water-soluble PEO blocks
and a central poorly hydrophilic and thermosensitive PPOx block. The reverse
addition order of the two monomers yields narrow polydisperse poly(POx-*b*-
EO-*b*-POx) triblocks, see Figure 1, with the more hydrophilic block in between
the two thermoresponsive ones.

In these two cases it is possible to prepare copolymers having molar masses
significantly higher than those obtained by conventional anionic polymerization,
especially regarding the PPOx block length. This allowed to broaden and to
tune the amphiphilic properties, the LCST behavior and the reversible gelation
characteristics of the EO/POx copolymers. In particular we observed that for

the same EO/POx composition and chain structure, gelation occurs at lower solution concentration with copolymers of higher molar masses.

TABLE 3. Block copolymerization of EO and POx initiated by NOct$_4$Br (I) in the presence of triisobutylaluminum in toluene, [EO+POx] = 7 M. Sequential addition order: POx-EO (runs 1 and 2); POx-EO-POx (run 3); EO-POx-EO (run 4).

Run	[i-Bu$_3$Al]/ [I]	Time (h)	Conv. (%)	$\overline{M}_n$ theor (g/mol) $\times 10^{-3}$			$\overline{M}_n$ (g/mol) $\times 10^{-3}$	Ip
				First block	Second block	Third block		
1	1.5	2 + 4	100	20	10	–	33.8	1.28
2	1.4	12 + 12	100	20	20	–	39.0	1.06
3	1.5	2 + 2 + 2	100	10	5	10	22.4	1.29
4	1.3	4 + 8 + 12	100	5.3	10	12	28.9	1.10
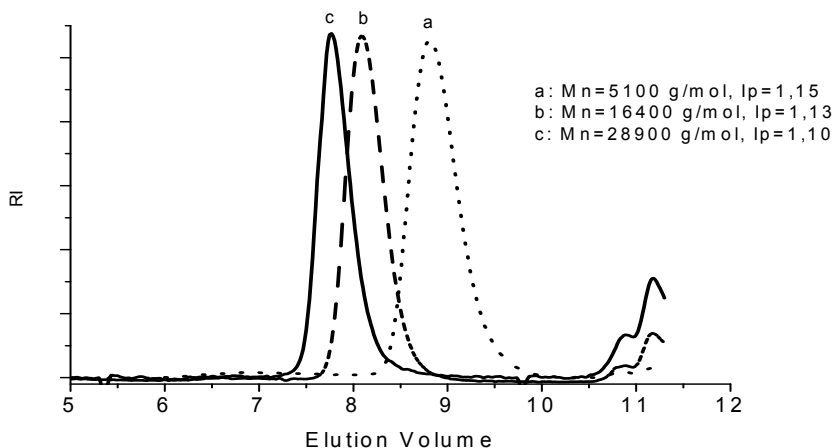
Figure 1. SEC traces corresponding to the different stages of the synthesis of a PEO-PPOx-PEO triblock copolymer (run 4, Table 3); (a) PEO first block; (b) PEO-PPOx diblock; (c) final triblock.

2.3. ACTIVATED ANIONIC POLYMERIZATION OF GLYCIDYL ETHERS (GE) AND EPICHLOROHYDRIN (ECH)

A similar strategy was then applied to the polymerization of glycidyl ethers, a broad family of epoxides that can be prepared from renewable resources such as glycerol available in large amount as a side product of the biofuel production. In this monomer family the properties of the corresponding polyethers can be tuned by the nature of the side group of the epoxide ring, thus allowing the

preparation of polyethers with hydrophilic or hydrophobic characteristics.[11] In similar conditions as described for POx a fast and controlled activated anionic polymerization takes place in non polar media at low temperature for all the glycidyl ether derivatives investigated. Some representative polymerization results are indicated in Table 4. The microstructure of the PPOx and PGEs polymers obtained from NR4X/i-Bu$_3$Al initiating systems, determined by ^{13}C NMR, corresponds to regio-regular head-to-tail monomer enchainments, without any detectable head-to-head and tail-to-tail linkages in agreement with a fully regiospecific monomer insertion process. The methylene signal, which is resolved in three distinct peaks corresponding to triad sequences, indicates the formation of atactic polyether chains, in agreement with a non stereoregulating polymerization process.

As it is noted in Table 4 even epoxide derivatives bearing a reactive side function, i.e. methacryloyl or chloromethyl, i.e. glycidyl methacrylate[12] and epichlorhydrin,[13] which would polymerize or be detrimental in conventional anionic polymerization, does not interfere in the conditions of the monomer activated anionic polymerization. This can be attributed to the weak basicity and nucleophilicity of aluminate complexes acting as propagating species, which, thanks to the strong monomer activation, can selectively ring open the activated epoxide rings.

TABLE 4. Glycidyl ethers and epichlorhohydrin anionic polymerizations initiated by NOct$_4$ Br (I) in the presence of triisobutylaluminum in toluene, [M] = 3–4 M.

Monomer	[i-Bu$_3$Al]/[I]	T (°C)	Time (h)	$\overline{M}_n$ (th.) (g/mol)	$\overline{M}_n$ (exp.) (g/mol)	Ip
Methyl glycidyl ether	1.3	0	5.3	3 000	3 100	1.16
	1.5	0	15	10 000	10 900	1.06
	2.6	0	4.8	30 000	28 700	1.07
	4.3		7	47 500	43 600	1.10
	7		7.5	93 000	87 100	1.16
Isopropyl glycidyl ether	1.5	0	3	5 000	5 600	1.07
	4	0	5.5	27 300	28 700	1.10
	6.5	0	24	50 000	50 200	1.15
Glycidyl methacrylate	1.5	−30	1.8	10 000	9 400	1.10
	1.5	−30	3.8	30 000	22 500	1.13
Epichlor-hydrin	1.5	− 40 ↑	2.3	10 000	9 400	1.14
	2.6	− 40 ↑	2.5	30 000	30 200	1.11
	2.7	− 35 ↑	7.3	50 000	44 300	1.12
	5.4	− 35 ↑	8	100 000	83 500	1.23

This allows in particular the direct preparation of reactive polyether systems. Poly(ECH) with molar mass up to 100,000 g/mol and narrow polydispersity, as well as random and block copolymers of ECH with other epoxide monomers can be readily prepared and used as precursor for the preparation of various functional polymers. In the same way photo- and thermo-curable poly(glycidyl methacrylate) and a series of co(polyether)s with glycidyl methacrylate units have been prepared. The pendant methacrylate groups were then crosslinked to prepare the corresponding polyether networks with a broad scope of properties.

In conclusion the monomer activated anionic polymerization of epoxides appears to be a very useful tool for the preparation of polyethers with tunable properties. This will allow valorizing this important monomer family which is readily available from epoxidation of olefins or from glycerol which both are available from a renewable feedstock.

References

[1]   Boileau, S. *Comprehensive Polymer Science, Chain Polymerization*, 1989, Pergamon, London, Vol. 3(1), p. 467.

[2]   (a) Sugimoto, H.; Aida, T.; Inoue, S.; Kuroki, M. *Macromolecules* 1994, 27, 2013. (b) Akatsuka, M.; Aida, T.; Inoue, S. *Macromolecules* 1994, 27, 2820.

[3]   Takeuchi, D.; Aida, T. *Macromolecules* 1996, 29, 8096.

[4]   Billouard, C.; Carlotti, S.; Desbois, P.; Deffieux, A. *Macromolecules* 2004, 37, 4038.

[5]   Deffieux, A.; Billouard, C.; Desbois, P.; Carlotti, S. *ACS Polym. Preprints* 2004, 45, 571.

[6]   Labbé, A.; Carlotti, S.; Billouard, C.; Desbois, P.; Deffieux, A. *Macromolecules* 2007, *40*, 7842.

[7]   Rejsek, V.; Sauvanier, D.; Billouard, C.; Desbois, P.; Deffieux, A.; Carlotti, S. *Macromolecules* 2007, *40*, 6510.

[8]   (a) Mortensen, K.; Brown, W.; Jorgensen, E. *Macromolecules* 1994, *27*, 5654. (b) Mortensen, K. *J. Phys.: Condens. Matter* 1996, *8*, A103.

[9]   Almgren, M.; Brown, B.; Hvidt, S. *Colloid Polym. Sci.* 1995, *273*, 2.

[10]   Alexandridis, P.; Nivaggioli, T.; Hatton, T. *Langmuir* 1995, *11*, 1468.

[11]   Labbé, A.; Carlotti, S. =; Deffieux, A.; Hirao, A. *Macromol. Symp.* 2007, *249–250*, 392.

[12]   Carlotti, S.; Labbe, A.; Deffieux, A., to be published.

[13]   Carlotti, S.; Labbe, A.; Rejsek, V.; Doutaz, S.; Gervais, M.; Deffieux, A. *Macromolecules*, 2008, *41*, 7058.

DESIGN OF SMART COMB MACROMOLECULES BY COMBINATION OF LIVING ANIONIC AND CATIONIC POLYMERIZATIONS

FUMI ARIURA, MICHEL SCHAPPACHER,
AND ALAIN DEFFIEUX[*]
*Laboratoire de Chimie des Polymères Organiques, UMR 5629
CNRS-ENSCPB-Université Bordeaux 1, 16 Avenue Pey Berland,
33607 Pessac cedex, France*

Abstract: The preparation and characteristics of a series of comb (co)polymers with different chain architectures and/or topologies are described. These structures are based on the preparation of poly(chloroethyl vinyl ether) (PCEVE) as a reactive backbone, which is used for grafting living anionic chains, typically polystyryllithium or polyisoprenyllithium. Since these different building blocks are synthesized by living ionic polymerizations, a precise control of the dimensions of both the branches and the backbone can be achieved, whereas the selectivity of the branch coupling reaction permits an almost quantitative substitution of the chloride groups of the PCEVE chain. This approach allows to precisely tune the dimensions and structure of the corresponding macromolecules and comb architectures displaying very different shapes. Linear, star-like, cylindrical, ring-like, have been prepared and characterized by different techniques including AFM imaging.

1. Introduction

In recent years, highly-branched (combs) and hyperbranched (dendritic) polymers have gained widespread attention due to their unique bulk and solution properties, which may strongly differ from their linear counterparts. This is illustrated for example by their large number of terminal functional groups, their intrinsic structure and shape (leading to specific rheological properties) as well as by the possibility to accommodate guest molecules within the macromolecule. Compared

to dendrimers and dendrigrafts of complex architecture, comb polymers characterized by a lower degree of branching still possess a highly compact architecture and a high number of chain-ends.[1–4] Since they can be prepared more rapidly and economically than hyperbranched polymers, they are good candidates to replace hyperbranched polymers in a number of applications.

In this paper, we describe the preparation and characteristics of a series of comb (co)polymers with different chain architectures and/or topologies. These structures are based on the preparation of poly(chloroethyl vinyl ether) (PCEVE) as a reactive backbone, which is used for grafting living anionic chains, typically polystyryllithium or polyisoprenyllithium.[5, 6] Since these different building blocks are synthesized by living ionic polymerization, a precise control of the dimensions of both the branches and the backbone can be achieved, whereas the selectivity of the branch coupling reaction permits an almost quantitative substitution of the chloride groups of the PCEVE chain. This approach allows to precisely tune the dimensions and structures of the corresponding macromolecules and comb architectures displaying very different shape, i.e. linear, star-like, cylindrical, ring-like, have been prepared.

As a step further, the possibility to prepare macromolecular objects with topologically organized elementary building blocks has been explored, paving the way to more sophisticated nano-structures. We show here that this strategy can be applied to the preparation of comb copolymers with amphipathic subdomains. Special emphasis is given to the correlation between the synthetic strategy, the molecular architecture and the supramolecular organization of those macromolecules.

2. Linear Combs

2.1. COMBS WITH HOMOPOLYMER BRANCHES[6–9]

The synthetic approach that is used to generate combs with polystyrene (PS) branches is summarized in Scheme 1. Poly(chloroethyl vinyl ether)(PCEVE) used as reactive backbone is first synthesized by living cationic polymerization of chloroethyl vinyl ether using hydrogen iodide as initiator and zinc chloride as catalyst (**a**). Living polystyryl lithium chains (**b**) are then prepared by anionic polymerization using *sec*-butyl lithium as initiator and grafted onto the PCEVE backbone (**a**) to form a comb polymer with polystyrene branches (**I-1**).

The grafting reaction is achieved by adding the living PS Li solution onto a known quantity of PCEVE in THF solution. The molecular architecture that is produced thus consists of a (PCEVE-*g*-PS) comb.
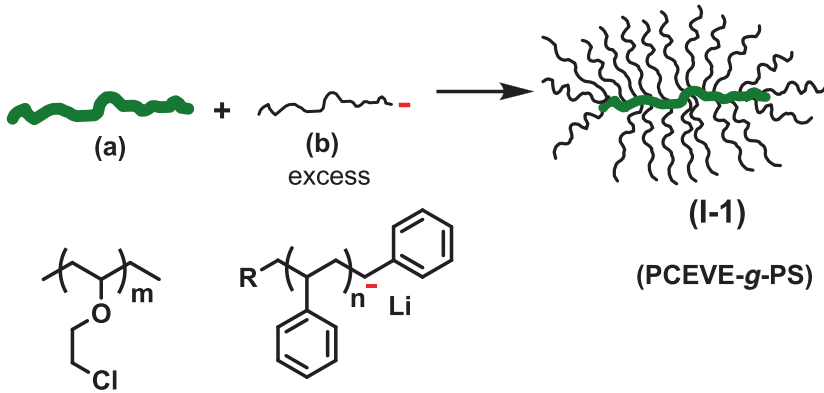
Scheme 1. Synthesis of (PCEVE-*g*-PS) copolymer.

The characteristics of some of the corresponding combs are collected in Table 1. They show a unimodal distribution, narrow polydispersity (I_p) and molar masses determined using elastic light scattering close to the theoretical values calculated assuming one PS graft per chloroethyl vinyl ether unit. This confirms very high grafting yields, which typically range between about 100% and 90% for the low and very long PCEVE backbone $\overline{DP}_n$s. The particular molecular architecture of the (PCEVE-*g*-PS) copolymer strongly affects their dimensions, i.e., size and shape, and their organization on surfaces.[10] For example the radius of gyration of a linear PS in THF is about four times higher that the corresponding comb of same molar mass, which means a density multiplied by 60 within an isolated comb molecules. The fact that (PCEVE-*g*-PS) combs exhibit very high molar masses and such high chain compacity

TABLE 1. Influence of PCEVE backbone and PS branch lengths on the molar mass of (PCEVE-*g*-PS) combs and on the grafting efficiency.

PCEVE $\overline{DP}_n D_{exp}$	PSLi $\overline{M}_{n\,exp}$	$\overline{M}_{n\,th}$ [a]	$\overline{M}_{w\,exp}$ [b]	I_p	f [c]
6	10,400	61,000	67,500	1.27	5.8
36	3,000	109,800	104,400	1.01	35
36	19,200	692,600	691,000	1.05	36
60	3,000	180,000	179,300	1.03	60
280	3,000	846,000	755,000	1.01	251
760	3,000	2,290,000	2,110,000	1.01	703
760	8,500	6,500,000	5,420,000	1.06	637
1,000	3,000	3,340,000	2,680,000	1.03	897

[a] Assuming one PS graft by CEVE unit.

[b] Measured by light scattering.

[c] Number of PS branches.

enables the observation of individual molecules by AFM. This technique appears to be a powerful tool to characterize the morphology of individual macromolecules and to determine their molecular characteristics, such as absolute molar mass, molar mass distribution and chain conformation.[11−16]

In practice, samples for AFM analysis are prepared by spin-casting on freshly-cleaved mica or Highly Oriented Pyrolytic Graphite (HOPG) substrate in ambient conditions starting from solutions. Samples are analyzed after complete evaporation of the solvent at room temperature. The probes are commercially available silicon tips with a typical radius of curvature of less than 10 nm and the magnitude of the tip-sample interactions are lowered as much as possible.

The AFM images presented below, Figure 1, were recorded in air in Tapping Mode (TM). They show images of isolated comb molecules one with a short PCEVE backbone and long PS branches and the other with a longer backbone and shorter branches.
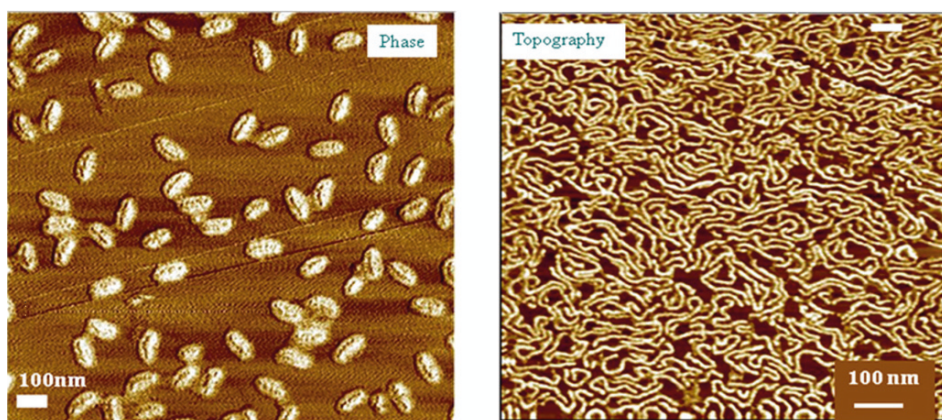
Figure 1. Phase and topographic AFM images of individual PCEVE-*g*-PS combs: PCEVE with $\overline{DP}_n$ = 300 and 760, PS with $\overline{DP}_n$ = 400 and 70 (*left* and *right* respectively).

The shorter molecules exhibit a rigid rice grain-like conformation whereas the more elongated and narrower ones show a wormlike conformation with the capacity of macromolecules to fold. Indeed, depending on the density of branches, the stiffness of the chain is modified. In a situation where the branch density is high, the steric repulsion between the side chains leads to stiffening of the backbone and the persistence length then becomes comparable to the contour length.

In most AFM images of homogeneous deposits (prepared from more con-centrated solutions), the molecules appear as continuous objects within which interruptions are discernable. Since these interruptions are chain ends, the contour length (L_{tot}) distribution of the molecules can be calculated. Considering that

the molecular mass is proportional to the contour length (L_{tot}) of the molecules, it is then possible to determine the molecular length distribution, similarly to the molecular mass distribution obtained from SEC measurements. The number average molecular length (L_n) and the length average molecular length (L_w), both determined from the distribution for sample in Figure 1 (right), are found to be 160 and 168 nm, respectively. It is worth noting here that the distribution is very narrow; the polydispersity index of the molecular length obtained from AFM images ($L_w/L_n = 1.05$) is in very good agreement with the value determined from SEC measurements ($\bar{M}_w/\bar{M}_n = 1.06$). Considering, as an extreme case, that a fully extended PCEVE backbone with 700 monomer units yields a theoretical value of ~175 nm for the main chain contour length, we can conclude that the objects appearing in the two images of Figure 1 correspond to single molecules with a fully extended backbone.

2.2. COMB COPOLYMERS WITH A AND B BRANCHES[17, 19]

In addition to the above general characteristics, the introduction by copolymerization of a second type of monomer in comb architectures adds a new topological parameter. According to the nature and distribution of the two elementary units, opportunities are thus open both for an internal self-organization within the macromolecule and for the self-assembly process of several macromolecules. Different block-like structures can be considered in comb macromolecules; (i) random distribution of A and B branches along the backbone, (ii) AB-type diblock copolymer branches and, (iii) Janus type combs constituted of A branches on one backbone side and B branches on the other side. These different structures are illustrated in Scheme 2.

random distribution of A:B branches

A-B diblock branches

Janus-like distribution of A and B branches
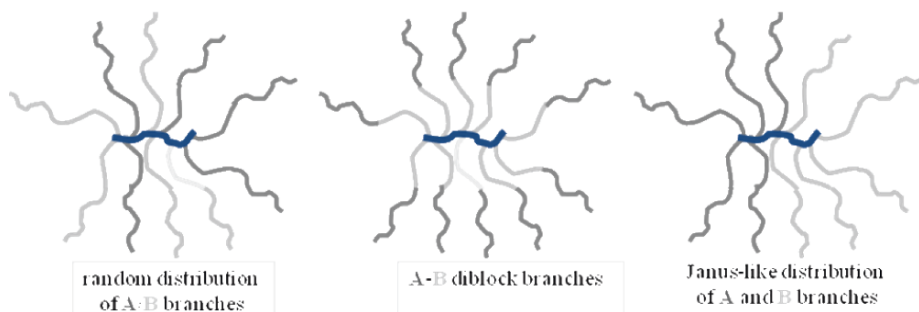
Scheme 2. Main topologies in comb-like block copolymers.

2.3. COMB COPOLYMERS WITH RANDOMLY DISTRIBUTED BRANCHES

Comb polymers having two types of chemically distinct branches, i.e., polystyrene and polybutadiene or polyisoprene, have been prepared using a slightly modified strategy: after partial substitution of the chloride groups of the PCEVE backbone by reaction with a controlled amount of PSLi chains, addition of anionic poly-butadienylLi (PButLi) or polyisoprenylLi (PILi) permits to substitute the remaining CEVE units, yielding a comb polymer with randomly distributed PS and PBut (or PI) branches,[17] Scheme 3. The conformation and organization of these comblike copolymers have been investigated in the bulk and in solution in a good solvent for the two branches as well as in a selective solvent of one type of branch. In hydrocarbon media, which are selective solvents of the PI branches, the combs form unimolecular micelles with a core formed of PS branches and a shell constituted by PI branches. In the bulk, their organization in a biphasic morphology is driven by the incompatibility between the polystyrene and polyisoprene branches. At a weight composition around to 50/50 between PS and PI branches, a lamellar morphology is observed in which the backbone of the comb copolymers are aligned forming the borderline between the PS moities located into one phase and the PI moities constituting the second phase, Figure 2.
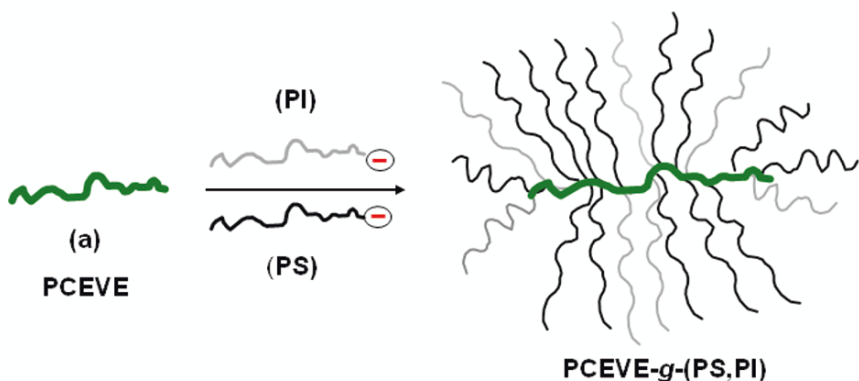
Scheme 3. Synthesis of a comb copolymer with randomly distributed PS and PI branches.

It was shown that combs constituted of diblock AB branches (PS-*b*-PI for example)[18] as well as Janus types AB[19] comb copolymers or more complex comb structures[20] can also self organize into different morphologies. In a selective solvent of one of the monomer aggregation into super micelles was reported whereas in the bulk biphasic organization generally takes place.
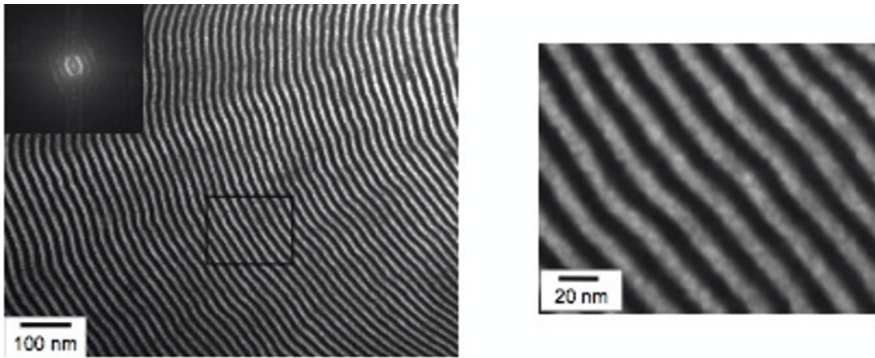
Figure 2. TEM image of a PCEVE-*g*-PS,PI (weight composition PS: 46, PI: 54) copolymer film showing lamellar morphology. The white and dark regions correspond to PS and PI domain, respectively.

3.   Stars with Comb Branches

Although similar structures were synthesized by controlled radical polymeri-zation,[21–23] star comb polystyrenes were prepared according to the present strategies either by a divergent or convergent approach.

3.1. DIVERGENT APPROACH[24, 25]

The synthesis of PS comb stars is achieved in two stages: (a) preparation of a multi-arm poly(styrene-*b*-chloroethyl vinyl ether) backbone[22] and (b) grafting polystyryl lithium chains onto the reactive chloroethyl ether functions of the poly(chloroethyl vinyl ether) blocks,[5, 6] as summarized in Scheme 4. For example, a four-arm star-like α-acetal-PS-*b*-PCEVE backbone is first prepared as the central connecting point. The four acetal-PS end-groups of the star precursor are then derived with TMSI and used to initiate the growth of PCEVE blocks, as already described. This yields a four-arms diblock copolymer in which the polystyryl chains act as a spacer between the central connecting point and the PCEVE branches (Figure 3). The grafting of a new series of polystyryl lithium chains onto the PCEVE blocks yields the corresponding four arms star poly-styrene comb.

The main features of such "4-arm" comb star polystyrene (I)-(PS-*b*-PCEVE-*g*-PS)[4] are collected in Table 2. The number of PS branches (F) per comb macromolecule corresponds to the substitution of 75–80% of the CEVE units of the PCEVE backbone. The $\overline{M}_{w\ RI(app)}/\overline{M}_{w\ LS}$ ratio, which is related to the volume contraction due to branching of 0.29 and 0.19 for the linear comb and the star comb respectively, in agreement both with their highly branched chain architecture and with a higher volume contraction for the comb star. The radius

of gyration (R_g) and hydrodynamic radius (R_h) of the star combs and the corresponding linear comb polymers can be compared in Table 2.
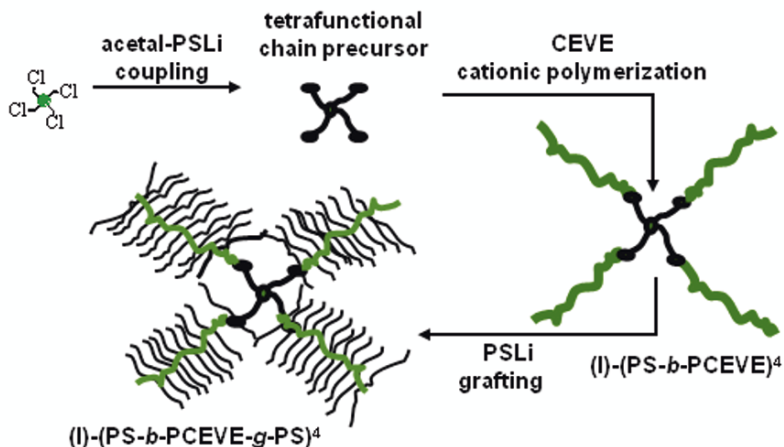
Scheme 4. Synthesis of multi arm poly (styrene-*b*-chloroethyl vinyl ether) backbone followed by grafting polystyrene chains.

TABLE 2. Main characteristics of the linear and corresponding four arm star PS combs.

Ref.	$\overline{M}_{w\,th.}$ (×10³)	$\overline{M}_w$ (×10³)	$\overline{M}_{W\,R}$ $I_{(app.)}$ (×10³)	I_p	$\overline{M}_w{}^b{}_{LS}$ (×10³)	F	Grafting (%)	$\dfrac{\overline{M}_{n\,app}}{\overline{M}_{n\,star}}$	$R_g{}^a$ (nm)	$R_h{}^a$ (nm)
*Lin*PCEVE-g-PS[e]	3,400	800		1.09	2,700		79	0.29	25	24
3.1.1.a. (I)-(PS-*b*-PCEVE-g-PS[e])⁴	11,800	1,700		1.07	900	3.34	76	0.19	45	45

[a] Determined in THF at 25°C.
[b] Determined from the ratio $\overline{M}_{w\,LS}$ (I)-(PS-*b*-PCEVE)⁴/($\overline{M}_{w\,SEC}$ linear PS₁-acetal + $\overline{M}_{w\,SEC}$ linear PCEVE).
[c] PS graft : $\overline{M}_{w\,SEC}$: 10,400 g/mol; $I_p = 1.03$.
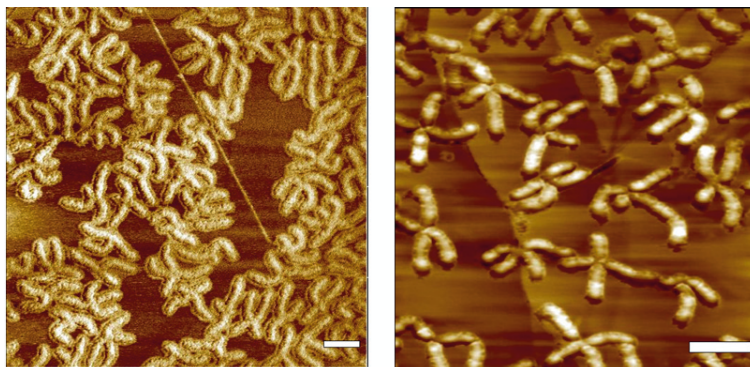
Figure 3. AFM images of the four-arm comb stars (I)-(PS-*b*-PCEVE-g-PS)⁴ obtained from deposition on HOPG from their CH_2Cl_2 solution. (**a**) phase and (**b**) topographical images: bar = 100 nm.

3.2. CONVERGENT APPROACH[26]

In this second approach star-like poly(CEVE) were prepared by sequential polymerization of CEVE and cyclohexyl divinyl ether (CDVE), the difunctional vinyl ether yielding both chain growth and crosslinking, see Scheme 5. The CEVE polymerization was initiated using HCl/ZnCl$_2$ in toluene at −20°C and CDVE was added after complete conversion of CEVE. In these conditions the cross linking reaction is slow and incomplete (entries 1 and 2, Table 3), thus SnCl$_4$ was added to trigger the final reaction (entries 3–6). To improve the crosslinking step the molar ratio of introduced CDVE to living polymer (r) was also increased up to 90. Since one main goal was to obtain very long PCEVE arms ($\overline{DP}_n$ > 500) with the aim to observe them by AFM, some chain termination/or transfer likely occurs during the polymerization, yielding some linear poly(CEVE) chains as side products. These were removed by fractionation precipitation. Then, in order to get the corresponding comb stars, the molecules were grafted with PSLi chains ($\overline{M}_n$ = 15,000 g/mol) as previously reported for other comb architectures. The stars were then separated from ungrafted PS by selective precipitation.
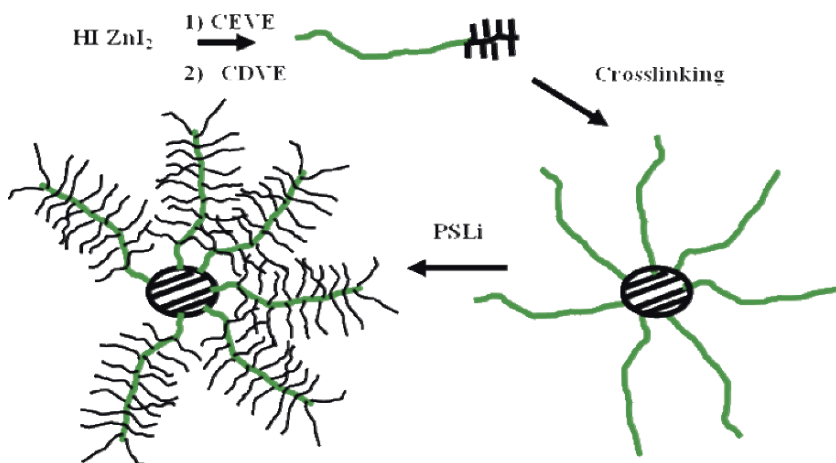
Scheme 5. Synthesis of star-like poly(CEVE) by sequential polymerization of CEVE and CDVE.

Table 4 resumes the main characteristics of comb star corresponding to entry 6 in Table 3. The star shape structure and characteristics of the combs were further confirmed by AFM. The AFM images of a series of PS comb stars are shown in Figure 4. The PS comb branches surrounding the central crosslinked core can be clearly visualized in the images.

TABLE 3. Characteristics of PS stars obtained by the convergent strategy.[26]

Entry	$\overline{M}_w \times 10^{-4}$ PCEVE arm[a]	I_p	r[b]	Temp. (°C)	$\overline{M}_w \times 10^{-5}$ star PCEVE[c]	I_p	N_a[d]
1	5.8	1.13	22	−10/−	–	Broad	
2	4.8	1.10	35	−20/−	–	Broad	
3	5.7	1.13	68	−20/−20[e]	–	Broad	
4	7.7	1.23	22	−15/−5[e]	–	Broad	
5	6.2	1.14	35	−15/−5[e]	7.5	1.25	12
6	13.0	1.08	90	−15/−5[e]	3.7	1.10	28

[a] SEC.

[b] [CDVE]/[P*].

[c] SEC-MALLS.

[d] $\overline{M}_w$ star/$\overline{M}_w$ arm.

[e] After addition of SnCl₄.
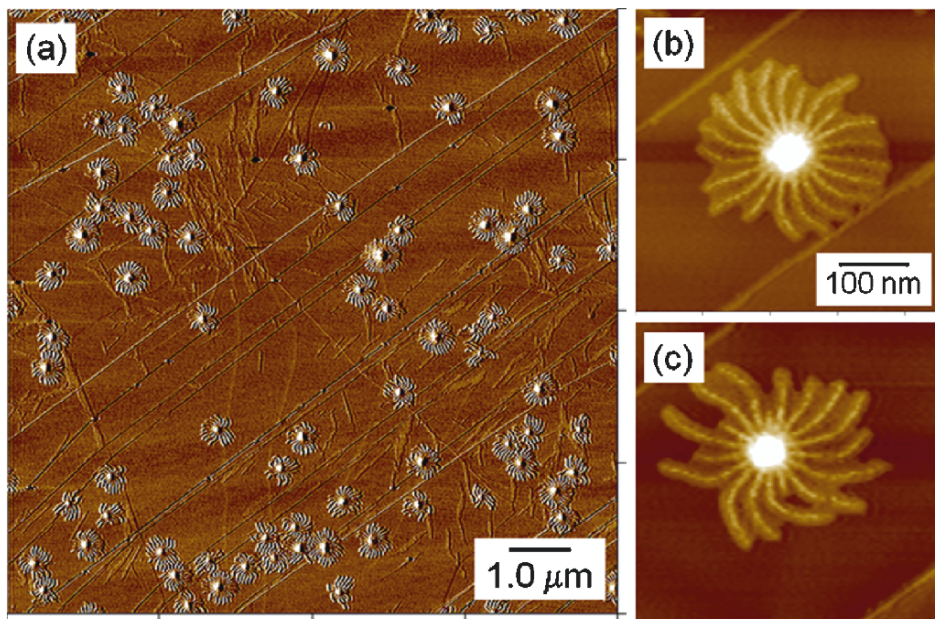
Figure 4. Topographic AFM images of comb stars (sample of **Table 4**) obtained by the divergent method. (**a**) general view; (**b**) and (**c**) images of isolated macromolecules showing the hard central crosslinked core (in white) and the relatively softer attached PS comb branches (light brown).

As it may be seen, the number of branches is much higher than in the previously reported divergent approach. The average number of branches estimated on a large number of star molecules was estimated to 18 with some noticeable heterogeneity between macromolecules. The discrepancy observed

in the number of branches between data of Table 4 and the AFM images can be attributed to a much lower PS grafting of the star as compared to the isolated branch, due to steric restrictions around the central core.

TABLE 4. Characteristics of PS comb star prepared by the convergent strategy after grafting of polystyrene with a $\overline{DP_n}$ of 160.

Comb architecture		$\overline{M}_w$	I_p	$R_g{}^a$ (nm)	$N_a{}^b$
Single arm	PCEVE$_{1220}$-g-PS$_{160}$	1.5×10^7	1.28	110	1
Star^c	star-(PCEVE$_{1220}$-g-PS$_{160)}$	2.8×10^8	1.12	190	14

[a] Measured in THF at 25°C.

[b] Number of arms measured by the molar mass ratio between comb star and single arm comb.

[c] Entry 6 of Table 3.

4. Ring Combs

The interest in cyclic macromolecules began more than 50 years ago with theoretical prediction of the effect of chain cyclization on the polymer properties[27, 28] and the discovery of naturally occurring macrocycles such as DNA.[29] However, large polymer macrocycles remain[30] a fascinating curiosity for theoreticians and physicists and a challenging area for synthetic chemists.

The most appropriate method for the synthesis of cyclic polymers with controlled size and narrow dispersity was first proposed by Cassassa[31] more than 40 years ago. It is based on the end-to-end chain coupling of linear α,ω difunctional chains in highly dilute conditions, however, cyclization yields in the case of large macrocycles are generally low. We have developed recently[32, 33] a more efficient method based on the synthesis of an A**B**C triblock copolymer, in which the two short A and C sequences bear reactive antagonist functions, that can be selectively activated under dilute conditions to allow intramolecular coupling and form the macrocyclic polymers. When the central B block is a poly(CEVE) the grafting of living polymer chain can then be achieved as previously described and ring combs can be prepared. The linear A**B**C copolymers were obtained by sequential living cationic polymerization of three different vinyl ethers, an hydroxyl functional vinyl ether for the A block, CEVE for central block **B** and cyclohexyl divinyl ether for block C (Scheme 6). Cyclization was achieved under high dilution via intramolecular reaction between hydroxyl and vinyl ether functions in the presence of an acid salt as a catalyst. The shift of the main SEC peak to higher elution volume was consistent with the reduction of the hydrodynamic volume of the macromolecule after chain cyclization although the slight peak broadening indicated both the presence of residual linear precursor and of dimers.
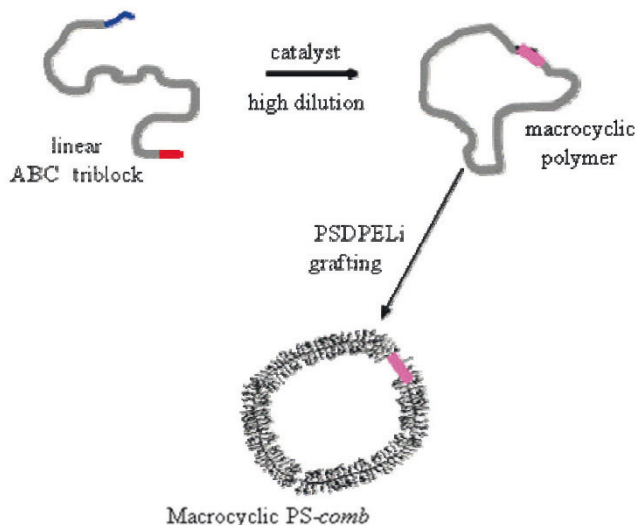
Scheme 6. Strategy for the synthesis of cyclic comb-like copolymers.

The characteristics of linear and cyclic **ABC** copolymers (L) are given in Table 5.

TABLE 5. Dimensional characteristics of linear (L) and cyclized (C) **ABC** copolymer and of the corresponding macrocyclic combs with different PS or PS/PI branch lengths.[32]

Chain architecture	PS graft[b] $\overline{DP}_n$	$\overline{M}_{n\ app}$[c] $(\times 10^{-3})$	I_p	$\overline{M}_{p\ app}$[c] $(\times 10^{-3})$	$\overline{M}_{pc}/\overline{M}_{pL}$	$\overline{M}_w$[d] $(\times 10^{-3})$
L	No	92	1.05	99		95
C	No	78	1.15	76	0.77	96
PS *comb*-Ca	90	740	1.14	800		5,900
PS *comb*-Cb	260	1,650	1.09	2,160		10,200

[a] $\overline{DP}_n$ of PCEVE: 870.

[b] $\overline{DP}_n$ of PS branches.

[c] Determined by SEC in THF using PS standards.

[d] Measured by static light scattering.

The synthesis of ring combs by grafting living PSLi onto macrocyclic PCEVE chains was then achieved as reported before for other PS combs. Direct imaging allowed us to get direct and quantitative information on the obtained cyclic polymer structures.

The AFM topographic image of *comb*-Ca, Figure 5a, shows single macro-molecules isolated on the HOPG. The majority of the structures observed are monodispered macrocyclic brushes, in agreement with a cyclization efficiency

of 50% to 60%. Among the other polymer architectures observed are linear brushes corresponding to uncyclized A**B**C copolymer, linear and macrocyclic dimers exhibiting about twice the size of the linear precursor or of the corresponding cyclics and tadpole structures.
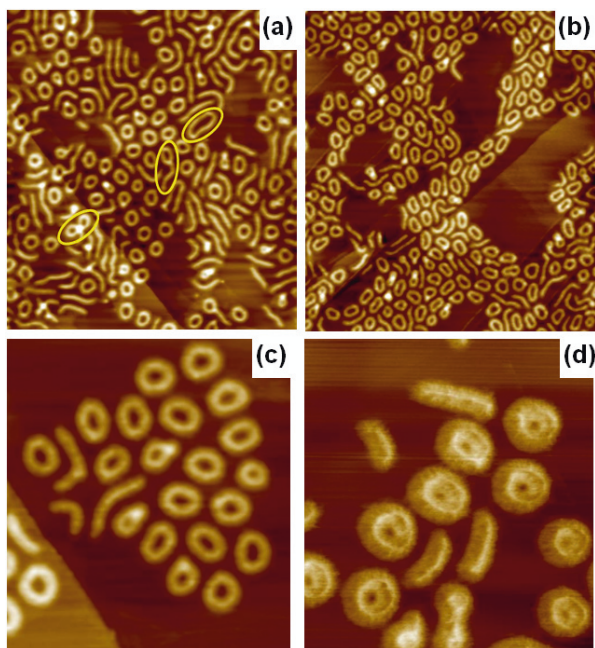
Figure 5. Topographic images of crude (**a**) and fractionated (**b**) cyclized PS combs showing the formation of cyclic PS combs and the presence of residual linear precursor, cyclic dimer and tadpole structures (yellow circles). (**c**) and (**d**) show topographic images of *comb*-Ca and *comb*-Cb with PS graft $\overline{DP_n}$ of 90 and 260, respectively.

Samples containing larger fractions of macrocyclic combs were readily obtained by selective precipitation from cyclohexane solution upon decreasing gradually the temperature, Figure 5b. Typically the fractionated samples contain about 80% to 85% of cyclic combs. The AFM image of the fractionated *comb*-Ca and *comb*-Cb are shown Figure 5c and d, emphasizing the influence of the PS graft dimensions on the characteristics of the comb macrocycles.

In conclusion we have developed a general approach based on the combination of living polymerization processes for the precise design of comb polymers with various chain architecture and composition. AFM provides the best technique for their characterization at the molecular level. These highly branched macromolecules behave as isolated nanoobjects with their own characteristics and are capable to develop both intra and supra molecular organizations which could be used for the design of new devices in nanotechnology.

Acknowledgements

References

[1]   Frechet, J. M. J.; Tomalia, D. A.; Dendrimers and Other Dendritic Polymers, New York: Wiley, 2002.
[2]   Bosman, A. W.; Janssen, H. M.; Meijer, E. W. *Chem. Rev.* (1999), *99*, 1665.
[3]   (a) Roovers, J. (Ed.); Branched Polymers I and II. In: Advances in Polymer Science, vols. 142 and 143; Berlin: Springer, 1999; (b) Frechet, J. M. J.; Tomalia, D. A. (Eds.); Dendrimers and Other Dendritic Polymers; Chichester: Wiley, 2001.
[4]   Teertstra, S. J.; Gauthier, M. *Prog. Polym. Sci.* (2004), *29*, 277.
[5]   Schappacher, M.; Deffieux, A. *Makromol. Chem. Phys.* (1997), *198*, 3953.
[6]   Deffieux, A.; Schappacher, M. *Macromolecules* (1999), *32*, 1797.
[7]   Schappacher, M.; Billaud, C.; Paulo, C.; Deffieux, A. *Macromol. Chem. Phys.* (1999), *200*, 2377.
[8]   Deffieux, A.; Schappacher, M. *Macromol. Symp.* (1998), *132*, 45.
[9]   Viville, P.; Leclère, P.; Deffieux, A.; Schappacher, M.; Bernard, J.; Borsali, R.; Brédas, J. L.; Lazzaroni, R. *Polymer* (2004), *45*, 1833.
[10] Dziezok, P.; Sheiko, S. S.; Fischer, K.; Schmidt, M.; Möller, M. *Angew. Chem. Int. Ed. Engl.* (1997), *36*, 2812.
[11] Prokhorova, S. A.; Sheiko, S. S.; Mourran, A.; Azumi, R.; Beginn, U.; Zipp, G.; Ahn, C-H.; Holerca, M. N.; Percec, V.; Möller, M. *Langmuir* (2000), *16*, 6862.
[12] Prokhorova, S. A.; Sheiko, S. S.; Ahn, C. H.; Percec, V.; Möller, M. *Macromolecules* (1999), *32*, 2653.
[13] Sheiko, S. S.; Gerle, M.; Fischer, K.; Schmidt, M.; Möller, M. *Langmuir* (1997), *13*, 5368.
[14] Gerle, M.; Fischer, K.; Roos, S.; Müller, A. H. E.; Schmidt, M.; Sheiko, S. S.; Prokhorova, S. A.; Möller, M. *Macromolecules* (1999), *32*, 2629.
[15] (a) Sheiko, S. S.; Möller, M. *Chem. Rev.* (2001), *101*, 4099. (b) Sheiko, S. S.; Prokhorova, S. A.; Beers, K. L.; Matyjaszewski, K.; Potemkin, I. I.; Khokhlov, A. R.; Möller, M. *Macromolecules* (2001), *34*, 8354.
[16] Sheiko, S. S. *Adv. Pol. Sci.* (2000), *151*, 61.
[17] Lanson, D.; Ariura, F.; Schappacher, M.; Borsali, R.; Deffieux, A. *Macromol. Res.* (2007), *15*(2), 173.
[18] Lanson, D.; Schappacher, M.; Deffieux, A.; Borsali, R. *Macromolecules* (2006), *39*, 7107.
[19] Lanson, D.; Schappacher, M.; Borsali, R.; Deffieux, A. *Macromolecules* (2007), *40*, 5559.
[20] Schappacher, M.; Deffieux, A. *Macromolecules* (2000), *33*, 7371.
[21] Matyjaszewski, K.; Qin, S.; Boyce, J. R.; Shirvayants, D.; Sheiko, S. S. *Macromolecules* (2003), *36*, 1843.

[22] Boyce, J. R.; Shirvayants, D.; Sheiko, S. S.; Ivanov, A. D.; Börner, H.; Qin, S.; Matyjaszewski, K. *Langmuir* (2004), *20*, 6005.
[23] Sheiko, S. S.; Da Silva, M.; Shirvayants, D.; LaRue, I.; Prokhorova, S.; Möller, M.; Beers, K.; Matyjaszewski, K. *J. Am. Chem. Soc.* (2003), *125*, 6725.
[24] Schappacher, M.; Deffieux A. *Macromolecules* (2005), *38*, 4942.
[25] Schappacher, M.; Deffieux A. *Macromolecules* (2005), *38*, 7209.
[26] Ariura, F.; Schelmtz, J.; Schappacher, M.; Deffieux, A. to be published.
[27] Zimm, B. H.; Stockmayer, W. H. *J. Chem. Phys*. (1949), *17*, 1301.
[28] Bloomfield, V.; Zimm, B. H. *J. Chem. Phys*. (1966), *315*, 44.
[29] Dubecco, R.; Vogt, M. *Proc. Natl. Acad. Sci. USA* (1963), *50*, 236.
[30] Deffieux, A.; Borsali, R.; Controlled Synthesis and Properties of Macrocyclic Polymers, in: *Macromolecular Engineering*, Matyjaszewski, K.; Gnanou, Y.; Leibler, L. (Eds.), Wiley-VCH, Weinheim, Germany, 2007, vol. 2, p. 875.
[31] Cassassa, E. F.; *J. Polym. Sci.: Part A* (1965), *3*, 605.
[32] Schappacher, M.; Deffieux, A. *Science* (2008), *319*, 1512.
[33] Schappacher, M.; Deffieux, A. *J. Am. Chem. Soc.* (2008), *130*, 44, 14684.

SMART MATERIALS FROM LIVING POLYPEPTIDES

HERMIS IATROU AND NIKOS HADJICHRISTIDIS[*]
*Department of Chemistry, University of Athens,
15771 Athens, Greece*

Abstract: Attempts to synthesize well-defined polypeptides by the ring-opening polymerization (ROP) of α-amino acid N-carboxyanhydrides (NCAs) with primary amines have been plagued, for more than 50 years, by unwanted side reactions. Recently, we have employed high vacuum techniques (HVT) to create living conditions for the amino-initiated ROP of NCAs (γ-benzyl L-glutamate, ε-Z L-lysine, proline, etc.). With this approach, a wide variety of novel block copolypeptides, having controlled molecular and architectural characteristics have been synthesized in ~100% yields. The same holds for hybrid-polypeptides (chimeras), only that the initiating amino group is attached to a conventional macromolecule rather than to a small molecule.

Along these synthetic lines, a series of novel amphiphilic triblock copolypeptides, poly(L-lysine)-b-poly(γ-benzyl-L-glutamate)-b-poly(L-lysine), were synthesized. Due to the macromolecular architecture of the tribock copolypeptides and the rigid nature of the poly(γ-benzyl-L-glutamate) middle block, the formation of bilayers was favored, and vesicles formed in water at neutral pH over the entire compositional range. Compared to other vesicular structures derived from conventional polymers, these polypeptidic vesicles possess the unique feature of being stimuli-responsive to pH and temperature (smart materials). In the presence of deoxyguanosine monophosphate, a multilevel self-assembly of the triblock copolypeptides in water was observed.

1. Introduction

Proteins are copolymers of α-amino acids linked together, through amide bonds, in a well-defined sequence, which characterizes their primary structure. Intra- and intermolecular interactions between the functional groups of the residual amino acids lead to organized higher order (secondary, tertiary, and quarternary) 3D structures,[1] which are responsible for the perfect performance of proteins in

Nature. Inspired by these remarkable materials, polymer chemists tried to develop, from the middle of the 20th century, synthetic routes leading to well-defined co-polypeptides for applications in biotechnology (tissue engineering, drug delivery, therapeutics).[2]

The most common way to prepare polypeptides involves the ring-opening polymerization (ROP) of α-amino acid *N*-carboxyanhydrides (NCAs) using primary amines (e.g., *n*-hexylamine) as initiators (Scheme 1).
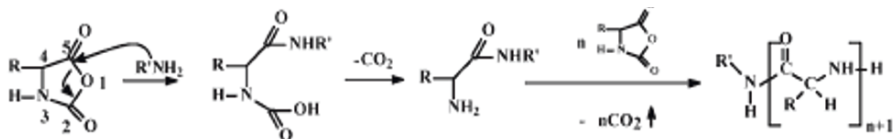
Scheme 1. Polymerization of NCAs by primary amines (normal amine mechanism).

The livingness of the ROP of NCAs is necessary for the preparation of well-defined polypeptide-based materials. Attempts to synthesize well-defined living polypeptides with amino initiators have been plagued, for more than 50 years, by unwanted polymerization mechanisms and termination reactions.[3] This problem has been overcome by the use of organonickel,[4] ammonium chloride initiators[5] and hexamethyldisilazane.[6]

We present here our method for the synthesis of living polypeptides. In addition, a few examples of how these living polypeptides can lead to new materials will be discussed, and a novel amphiphilic triblock copolypeptide with smart properties is presented.

2. Living Polypeptides: Synthesis of Polypeptide-Based Materials

Recently, we employed high vacuum techniques (HVT) to create living conditions for the amino-initiated ROP of NCAs. Apparently with this method, the unwanted side reactions are either avoided or are insignificant, thus leading to living polypeptides.[7]

The "living" nature of the ROP of NCAs was evaluated according to the following criteria:[8] (a) complete consumption of the monomer, (b) linearity of M_n with conversion, (c) stoichiometric control of the molecular weight, (d) narrow molecular weight distributions, and (e) synthesis of block copolypeptides by sequential monomer addition. All of these criteria are satisfied, and examples regarding criteria (a) (b) and (d) are given in Figures 1 and 2. The last criterion was verified with the synthesis of several diblock and triblock copolypeptides of various *a*-amino acid NCAs. Two examples are given in Figure 3.
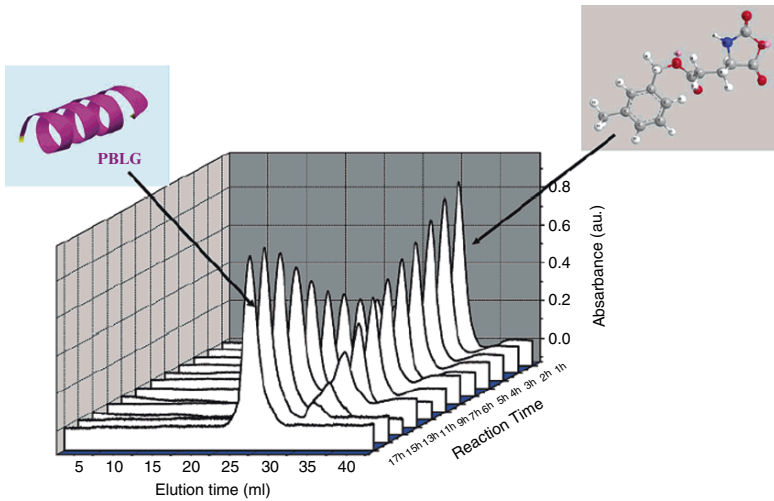
Figure 1. Monitoring the polymerization of the PBLG438 using size exclusion chromatograms with UV detector. After 17 h, more that 99.9% of the monomer has been consumed. It is well-known that PBLG and PZLL with DP > 80 exhibit 100% the a-helix conformation. (Reprinted from Ref. [7].)
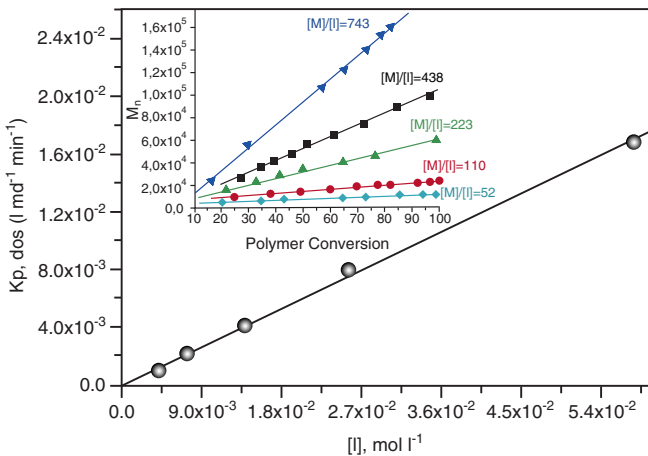
Figure 2. Linear dependence of Kp,obs of the PBLG samples with initiator concentration proves that the chains grow without termination. At the inset is the dependence of the Mn as a function of polymer conversion for several [M]/[I] ratios. (Reprinted from Ref. [7].)
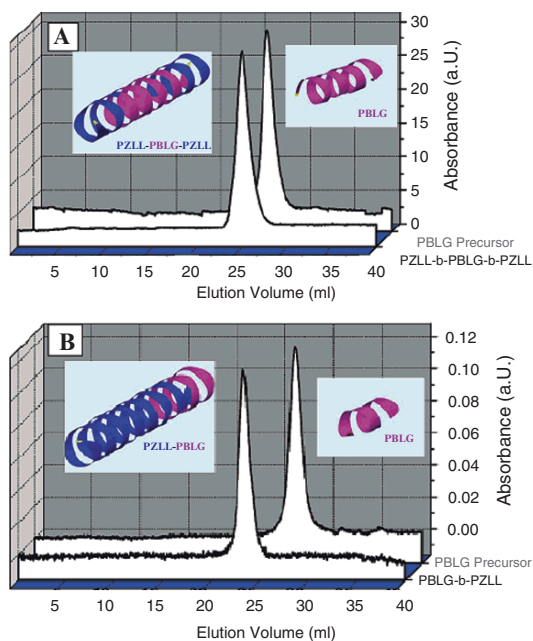
Figure 3. Monitoring the synthesis of PZLL90-PBLG150-PZLL90 (**a**) and PBLG130-PZLL320 (**b**) by SEC with a UV detector. (Reprinted from Ref. [7].)

Our methodology was applied, along with anionic polymerization and using HVT, for the synthesis of the following novel complex macromolecular *chimeras* shown in Scheme 2: PBLL-*b*-PBLG-*b*-PS-*b*-PBLG-*b*-PBLL (linear); (PS)$_2$(PBLG or PBLL), (PS)(PI)(PBLG or PBLL) (3μ-stars); (PS)$_2$[P(α-MeS)](PBLG or PBLL), (PS)$_2$(PBLG or PBLL)$_2$ (4μ-stars), where PS is polystyrene, PI is polyisoprene, P(α-MeS) is poly(α-methylstyrene), PBLG is poly(γ-benzyl-L-glutamate), and PBLL is poly(γ-*tert*-butyloxycarbonyl-L-Lysine).[9]

As an example, the synthesis of (PS)2(Polypeptide) is given in Scheme 3 and Figure 4

3. Smart Materials from Living Polypeptides

Well-defined block copolypeptides, which combine the self-assembly of block copolymers and the highly ordered 3D structures of proteins (α-helix, β-sheet), are potential candidates for novel supramolecular structures and biotech applications, such as biosensors, tissue engineering, and selective drug delivery.
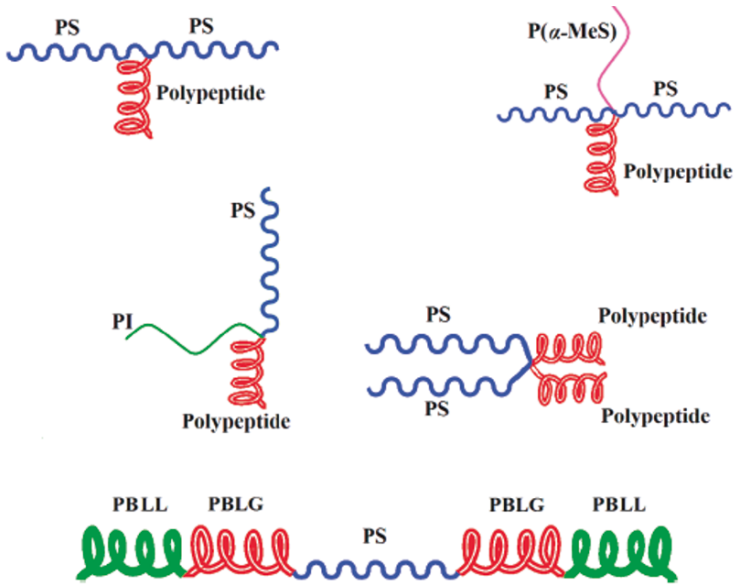
Scheme 2. Complex polymer/polypeptide hybrids (macromolecular *Chimeras*). (Reprinted from Ref. [9].)
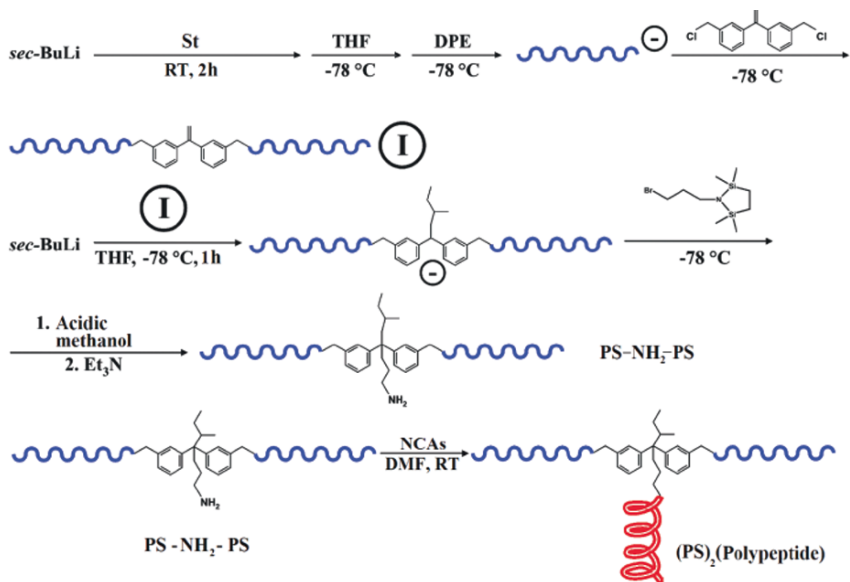
Scheme 3. Synthesis of the 3-Miktoarm Star *Chimeras* (PS)(PI)(Polypeptide). (Reprinted from Ref. [9].)
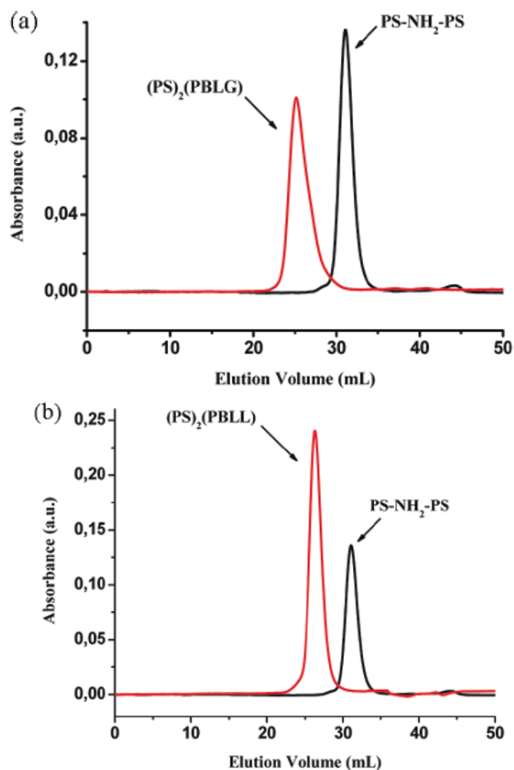
Figure 4. Monitoring the synthesis of the (PS2)(PBLG) (**a**) and (PS2)(PBLL) (**b**) 3-miktoarm star hybrid/polypeptide by SEC. (Reprinted from Ref. [9].)
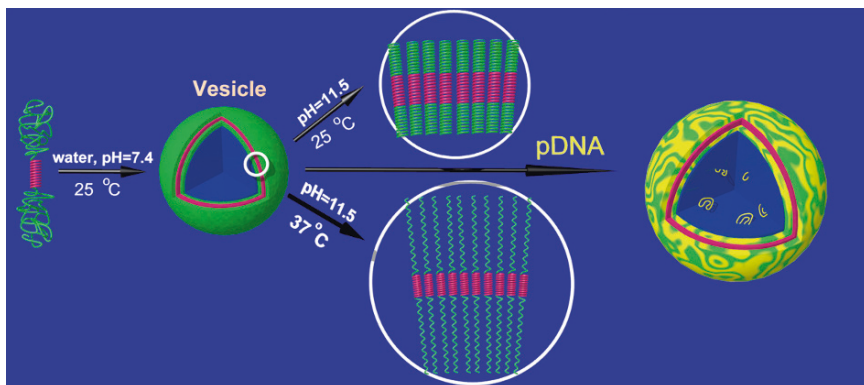
Scheme 4. Schematic representation of the micellar behavior of amphiphilic triblock copolypeptides, PLL-*b*-PBLG-d7-*b*-PLL, in water at pH 7.5 as confirmed by SANS, SLS, DLS, as well as AFM, cryoTEM and SEM. It was found that large vesicles are formed, with one or more walls, depending on the composition of the copolypeptides. The vesicles are pH/temperature responsive and are efficient carriers of DNA. (Reprinted from Ref. [10].)

Along these lines, a series of novel amphiphilic triblock copolypeptides, poly(L-lysine)-*b*-poly(γ-benzyl-L-glutamate)-*b*-poly(L-lysine), PLL-*b*-PBLG-d7-*b*-PLL, was synthesized by: (a) the sequential ROP of γ-benzyl-L-glutamate and ε-Boc-L-lysine N-carboxy anhydrides, with 1,6-diaminohexane as initiator, using HVT and (b) the subsequent selective deprotection of the Boc- groups. The synthesized copolypeptides had similar molecular weights, while the composition of the middle block ranged between 19% and 74%. Due to the macromolecular architecture of the copolypeptide and the rigid nature of the middle block, the formation of monolayers was favored, and surprisingly, vesicles were formed in water at neutral pH over the entire compositional range.[10] The vesicular structures were excessively characterized by static (SLS) and dynamic
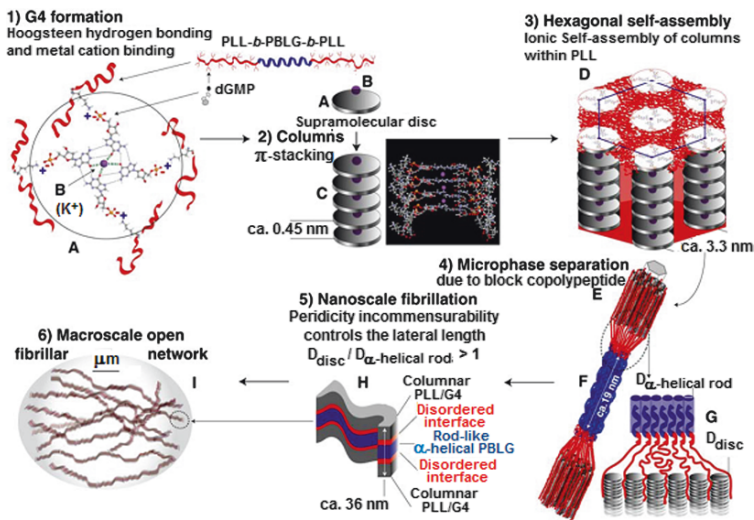
Scheme 5. Schematic representation of the multilevel hierarchical self-assembly of PLL-*b*-PBLG-d7-*b*-PLL in water in the presence of deoxyguanosine monophosphate (dGMP), as confirmed by SAXS, WAXS, FTIR and TEM. G4 supramolecular disk **(A)** formed by 4 Hoogsteen paired dGMP molecules (hydrogen bonds in dashed grey lines), stabilized by metallic cation K+ **(B)**, interacting with the carbonyl oxygen atoms. The disks are π-stacked to form discotic columns **(C)** with a periodicity of ca. 0.45 nm. The stacking may be tilted (not shown in the scheme). The acidic phosphate groups at the periphery of G4 disks are complexed with the basic PLL chains and lead to ionic self-assembly with hexagonal order **(D)** with a column separation of ca. 3.3 nm. The rod-like α-helical PBLG chains **(F)** of PLL(dGMP)-*b*-PBLG-*b*-PLL(dGMP) microphase separate from the PLL-containing domains **(E)** and lead to ribbon formation of width of ca. 36 nm **(H)** using the present molecular weight of PLL-*b*-PBLG-*b*-PLL. The block lengths of PLL-*b*-PBLG-*b*-PLL control the domain thicknesses within the fibrils to be ca. 8.5 nm, ca. 19 nm, and ca. 8.5 nm, including disordered interface layers **(G)** between them. As the periodicity of the G4-disks (diameter $_{Ddisc}$) is larger than the packing periodicity of the α-helical PBGL rod-like chains (diameter Dα-helical rod), a packing frustration results. The open fibrillar network extends to macroscopic length scale **(I).** The atoms in the chemical formulas are highlighted as follows: H in white, C in grey, N in blue, O in red, and P in orange. (Reprinted from Ref. [11].)

light scattering (DLS), small angle neutron scattering (SANS), atomic force microscopy (AFM), cryo-transmission electron microscopy (cryoTEM), scanning electron microscopy (SEM), UV and FT-IR spectroscopy and circular dichroism (Scheme 5). In contrast to other vesicular structures derived from conventional polymers, the formed polypeptidic vesicles possess the unique feature of being stimuli-responsive to pH and temperature. When the copolypeptides were mixed with plasmid DNA, large vesicular structures were also formed. The molecular characterization of the vectors was performed with most of the methods mentioned above and indicated that the pDNA is both partially condensed on the PLL phase and partially encapsulated inside the vesicle (Scheme 4).

When PLL-*b*-PBLG-d7-*b*-PLL was mixed with deoxyguanosine mono-phosphate (dGMP), in the presence of a metal cation, a multilevel hierarchical self-assembly was confirmed.

4.   Conclusions

The living polymerization of α-amino acids, a major synthetic challenge for more than 50 years, has been solved using high vacuum techniques, which ensure not only high purity of all reagents involved but also create and maintain all necessary conditions for the living polymerization of NCAs. The livingness of the polypeptides under high vacuum conditions can be preserved indefinitely, thus making possible the use of linking chemistry for the synthesis of a wide variety of macromolecular architectures.

Poly(L-lysine)-*b*-poly(γ-benzyl-L-glutamate)-*b*-poly(L-lysine), PLL-*b*-PBLG-d7-*b*-PLL, in water forms vesicular structures in all compositions. This is due to (a) the rigid middle block of the copolypeptide, which prevents the chains from bending, (b) the macromolecular architecture, which forms a monolayer more readily than the corresponding diblock copolypeptides that must adopt an antiparallel orientation to form a bilayer, and (c) similar curvature induced by the equal PLL blocks, which promotes the formation of planar monolayers rather than micelles. Compared to other vesicular structures formed by conventional amphiphilic copolymers, our "smart" vesicles possess the unique feature of being stimuli-responsive to pH and temperature.

When PLL-*b*-PBLG-d7-*b*-PLL was mixed in water with deoxyguanosine monophosphate (dGMP), in the presence of a metal cation, a multilevel hierarchical self-assembly was confirmed, leading to rigid fibrillar materials. We encode structures by ionic self-assembly of dGMPs within the PLL blocks of rod–coil block copolypeptide. The open rigid fibrillar material may be used as an en-capsulating template for cells and proteins, mimicking the extracellular matrix where the fiber density and pore sizes may be further customized and where the metal cations may be exchanged for functionalities. We expect that these

novel concepts and materials will be relevant as a toolbox for future bio-nanotechnology applications.

Acknowledgements

References

[1]   Alberts, B.; Bray, D.; Lewis, J.; Raff, M.; Roberts, K.; Watson, J. *Molecular Biology of The Cell*, 2nd edn.; Garland, New York, 1989; pp. 87–134, 820–830.

[2]   Deming, T. *Adv. Drug Deliv. Rev.* **2002**, 54, 1145. Kricheldorf, H. R. *Angew. Chem., Int. Ed.* **2006**, *45*, 5752.

[3]   Deming, T. *Nature* **1997**, *390,* 386.

[4]   Dimitrov, I.; Schlaad, H. *Chem. Commun.* **2003**, 23, 2944.

[5]   Lu, H.; Cheng, J. *J. Am. Chem. Soc.* **2007**, *129*, 14114.

[6]   Aliferis, T.; Iatrou, H.; Hadjichristidis, N. *Biomacromolecules* **2004**, *5*, 1653.

[7]   Fetters, L. *Encyclopedia of Polymer Science and Engineering*, 2nd edn.; Wiley-Interscience, New York, 1987; Vol. 10, pp. 19–25.

[8]   Karatzas, A.; Iatrou, H.; Hadjichristidis, N.; Inoue, K.; Sugiyama, K.; Hirao, A. *Biomacromolecules* **2008**, *9*, 2072.

[9]   Iatrou, H.; Frielinghaus, H.; Hanski, S.; Ferderigos, N.; Ruokolainen, J.; Ikkala, O.; Richter, D.; Mays, J.; Hadjichristidis, N. *Biomacromolecules* **2007**, *8*, 2173.

[10]   Houbenov, N.; Nykänen, A.; Iatrou, H.; Hadjichristidis, N.; Ruokolainen, J.; Faul, C. F. J.; Ikkala, O. *Adv. Funct. Mater.* **2008**, 18, 2041.

PART 4. RING OPENING METATHESIS POLYMERIZATION (ROMP)

ROMP: THE METHOD OF CHOICE FOR PRECISE MACROMOLECULAR ENGINEERING AND SYNTHESIS OF SMART MATERIALS

EZAT KHOSRAVI[*], THOMAS C. CASTLE, MARGARET KUJAWA, JAN LEEJARKPAI, LIAN R. HUTCHINGS, AND PETER J. HINE
Polymer IRC, Durham University, Durham DH1 3LE, UK

Abstract: The recent advances in olefin metathesis highlight the impact of Ring Opening Metathesis Polymerisation (ROMP) as a powerful technique for macromolecular engineering and synthesis of smart materials with well-defined structures. ROMP has attracted a considerable research attention recently particularly by industry largely due to the development of well-defined metal complexes as initiators and also because of the award of the Noble Prize for Chemistry in 2005 to three scientists (Chauvin, Grubbs, Schrock) for their contributions in this area. This chapter discusses several interesting examples in order to demonstrate that ROMP is a power tool in macromolecular engineering and that it allows the design and synthesis of polymers with novel topologies.

1. Synthesis of Copolymers

Control over macromolecular architecture and the resulting material properties has been a central goal of polymer chemistry. Copolymerisation is a very important process and allows, in many cases, the alteration of the physical, mechanical, and electronic properties of a material through adjustments to the ratio of the individual components in the copolymer. There have been a lot of interests in developing new synthetic route to prepare copolymers with novel compositions and topologies. Efforts have been directed toward developing new synthetic methodologies whereby precise placement of chemical functionality and monomer composition can be achieved. ROMP has attracted a considerable

research attention recently largely due to development of well-defined initiator systems. ROMP using well-defined initiators is a living process and therefore allows the synthesis of well-defined polymers with controlled architectures, molecular weights, polydispersities, and terminal functionalities.

This chapter aims at reviewing the synthetic routes developed recently for preparing novel copolymers based on ROMP and also based on its combination with other polymerisation techniques. It highlights the impact of the well-defined ROMP initiators and the utility of ROMP as a powerful technique for the synthesis of new materials with well-defined structures.

1.1. GRAFT (COMB) COPOLYMER

The potential of combining the capabilities of living anionic and ROMP methods has been explored to prepare polymers with well-defined structures and unusual topologies. This approach offers access to a range of graft copolymers that cannot be prepared by grafting onto or from homopolymer backbones Additionally and importantly, the method allows rational design and synthesis of graft copolymers with control over the main chain and graft chain molecular weights and the graft density.
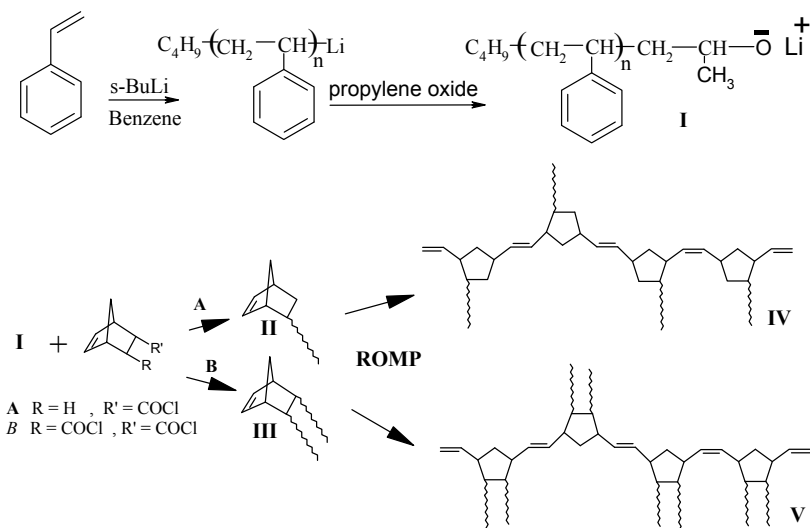
Scheme 1. Combination of anionic polymerization and ROMP for the preparartion of graft copolymers IV and V.

Well-characterised 5-norbornene-2,3-*trans*-bis(polystyrylcarboxylate) macro-monomers, **III**, were systhesised according to Scheme 1. The ROMP of the macromonomers using well-defined Schrock molybdenum initiators, Mo(N-2,6-i-Pr$_2$C$_6$H$_3$)(OCMe$_3$)$_2$(CHR) where R is CMe$_3$ or CMe$_2$Ph, produced well-defined graft copolymers, **V**.[1–4] The graft copolymers produced consisted of a

polynorbornene (PNB) backbone carrying two polystyrene (PS) grafts on each cyclopentane ring. Well-characterised macromonomers and comb graft copolymers with polystyryl grafts with average degrees of polymerisation ($\overline{DP}$s) of 4, 7, and 9 were successfully produced.[1] The graft copolymers exhibited single mode molecular weight distributions and narrow polydispersities, typically in the range 1.09 to 1.16. ROMP of macromonomers of different molecular weights, i.e. different PS graft lengths, revealed a limit to the length of the PNB backbone attainable in the graft copolymer, which was related to the length of PS graft in the macromonomer.[4] These results suggested that the graft copolymer backbone chain grows up to a certain length beyond which the ROMP reaction becomes sterically hindered and eventually stops. As the length of PS graft in the macro-monomer was increased the length of PNB backbone attainable in the graft copolymer decreased. The polymerisation reactions were demonstrated to be living by producing block and tapered copolymers with the sterically undemanding monomer 2,3-bis trifluoromethylnorbornadiene.[1–4]

Well-defined graft copolymers having a PNB backbone chain carrying only one PS graft on each cyclopentane ring has also been prepared. It was anticipated that this would provide a basis for comparison with our earlier results on the synthesis of graft copolymers with two PS grafts in each cyclopentane ring. With only one graft per norbornene (NB) repeat unit the steric hindrance effect was expected to be lower, allowing the formation of graft copolymers with longer grafts and backbone chains. The synthesis of *exo*-5-norbornene-2-(polystyrylcarboxylate) macromonomers, **II** was carried out in close analogy to the method described previously[1–4] and the reaction scheme is also outlined in Scheme 1. The well-characterised macromonomers, **II**, were subjected to ROMP using the same Schrock molybdenum initiators to give graft copolymer **IV**. The ^{1}H NMR spectrum of the living polymerisation reaction mixture showed two broad unresolved signals at 11.44 and 11.62 ppm characteristic of the hydrogens of the propagating alkylidenes. These signals could be due to *head or tail* insertion of the macromonomer to the active site leading to *head–tail, tail–tail or head–head* placements of repeat units in the polymer chain. The results suggest that, in contrast to two PS grafts on the same NB unit, with one PS graft on the NB unit graft copolymers with relatively long backbone and side chains can be prepared, probably as a consequence of lowered steric hindrance. As observed by ^{1}H NMR, the macromonomer can add *head or tail* fashion to the propagating chain end which reduces the steric hindrance at the growing chain end and allows the synthesis of high molecular weight graft copolymers.

The DSC and TGA results for graft copolymers revealed that in all cases, only one Tg was observed for these graft copolymers. This indicates that the PNB and PS segments do not undergo phase segregation. The Tg of these graft copolymers shows that there is an overall increase in Tg on going from graft

copolymers containing short PS chains to longer PS chains. The Tg of PNB is 35°C and that of PS is 100°C, thus the Tg process observed is primarily associated with PS grafts in these systems. A similar trend was observed in relation to thermal decomposition temperatures, using 2% weight loss as an arbitrary criterion for degradation. As the PS graft length increases, the thermal decomposition temperature also increases.

The well-characterised macromonomers **II** and **III** were also subjected to ROMP to synthesise well-defined comb copolymers containing one and two PS grafts per NB unit using ruthenium initiators **Ru1–Ru3**, Figure 1.[5]
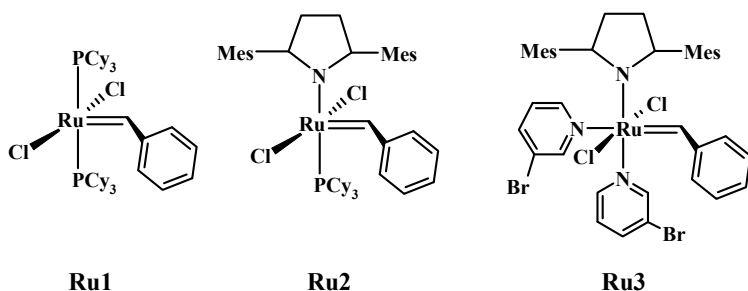
Figure 1. Structures of Grubbs ruthenium initiators used in this work.

In the case of macromonomers with one PS graft per NB unit (**II**), by increasing the reaction times to 2 or 3 days all the ROMP reactions with initiator **Ru1** went to completion and higher molecular weight comb (graft) copolymers than previously reported to Molybdenum initiators were obtained. In the case of macromonomers with two PS grafts per NB unit (**III**), the reaction for the graft length of 20 and 10 went to completion to much higher ratios of [M]/[I] than previously reported for the molybdenum initiators by increasing the reaction times to 2 or 3 days. However, for the longer PS graft length the ROMP reactions did not go completion, due to the presence of steric hindrance.

The study of the effect of the initiators of different activity revealed that for the ROMP of macromonomers with one PS graft per NB unit (**II**), initiator **Ru2** is more active than initiator **Ru1** and that they both are more active than initiator **Ru3**. The results showing the effect of solvent on the ROMP reaction of the macromonomer **II** showed that the graft copolymers prepared using initiator **Ru1** in benzene exhibit narrower PDI in comparison with the samples prepared in dichloromethane indicating a well-behaved reaction in benzene. The ROMP of the macromonomer with two PS grafts per NB unit using initiator **Ru3** did not go to completion, despite leaving the reaction for 3 days. The change of solvent from benzene to dichloromethane and also raising the reaction temperature from ambient to 40°C also resulted in the observation of

unreacted macromonomers. The reason for this behaviour is believed to be due to steric hindrance.

1.2. SYNTHESIS OF BLOCK COPOLYMERS

A series of novel well-defined block copolymers have been synthesised by the transformation of living anionic polymerisation into living ROMP (Scheme 2).[6] Ethylene oxide was polymerised anionically, initiated by diphenylmethyl-potassium and end-functionalised by a controlled termination reaction with a slight excess of 4-vinylbenzyl chloride (4-VBC) to produce a polyethylene oxide (PEO) macromonomer with a terminal vinyl group, (**VI** Scheme 2). ^{1}H NMR analysis of the macromonomers indicated the degree of vinyl functionalisation was at least 95%. The macromonomer (**VI**) was transformed into a ROMP macroinitiator (**VII**) by an alkylidene exchange reaction between bis(tricycle-hexylphospine)propylidene ruthenium dichloride catalyst (**Ru4**) and the PEO macromonomer **VI**. Such alkylidene exchange reactions, as with most metathesis reactions that involve olefin substrates, are reversible and to drive the reaction to completion it is necessary to remove the by-product of the reaction.[7–9]
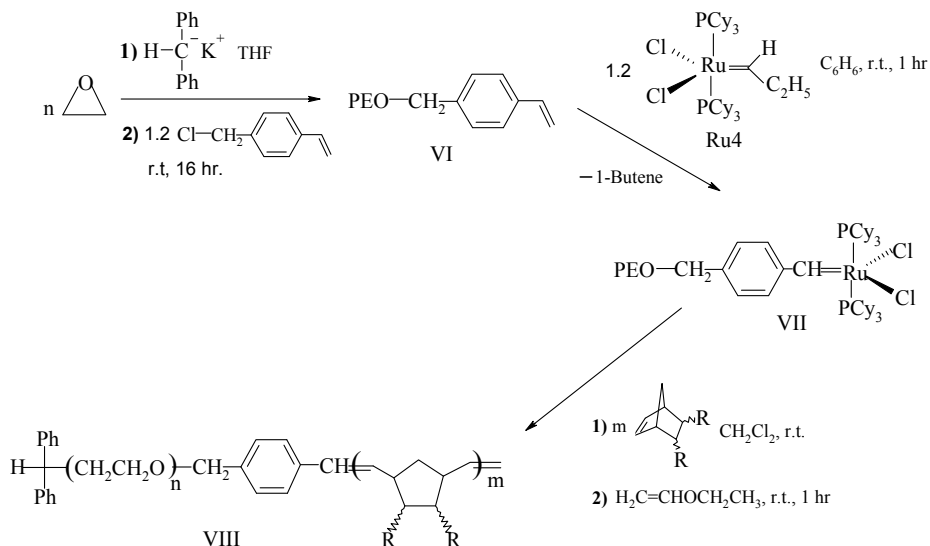
Scheme 2. Synthesis of a PEO-PNB block copolymer. PEO = polyethylene oxide, PNB = polynorbornene and Cy = cyclohexyl.

Using the ruthenium propylidene initiator **Ru4** for the synthesis of PS macroinitiator **VII** the by-product of the reaction is 1-butene, a gas at room temperature and atmospheric pressure. The by-product can be easily removed from the reaction mixture by bubbling a steady flow of an inert gas (e.g., argon)

through the reaction mixture thereby driving the exchange to completion. ^{1}H NMR (Figure 2) shows the complete loss of the signal for the alkylidene proton of the ruthenium propylidene **Ru4**, a triplet at 19.61 ppm in solution in C_6D_6 and the emergence of the new alkylidene proton signal for PEO-Ru macroinitiator (**VII**), a singlet at 20.56 ppm. Figure 2 also shows evidence of a small peak at 20.64 ppm, believe to be due to macroinitiator in which the PEO is in a *meta* position relative to the alkylidene proton. The 4-VBC used in this research contains a trace of 3-VBC. This will also react with the living PEO during the end functionalisation reaction and will eventually result in a trace of PEO ruthenium macroinitiator with the *meta* PEO substitution on the benzylidene moiety. A series of PEO macroinitiators were synthesized with the number average molecular weight (M_n) of PEO ranging from 2,400 to 38,800 g/mol, and narrow PDI (1.04–1.06), measured by SEC in DMF.
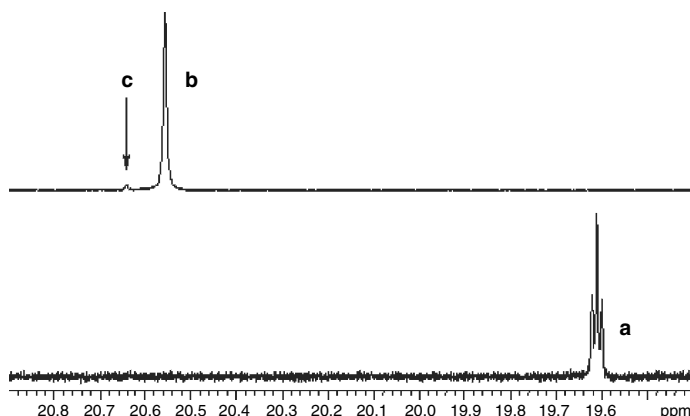
Figure 2. Comparison of the ^{1}H NMR analysis of the ruthenium propylidene initiator (**Ru4**) and the PEO macroinitiator (**VII**). Spectra recorded in C_6D_6, referenced against TMS: (a) Ruthenium propylidene initiator; (b) Ruthenium PEO macroinitiator from 4-VBC functionalized PEO macromonomer; (c) Ruthenium PEO macroinitiator from 3-VBC functionalised PEO macromonomer.

The PEO ruthenium macroinitiators (**VII**) were used to initiate the ROMP of three NB derivatives (**A–C**, Figure 3) to give a series of well-defined block copolymers of varying molecular weights and compositions. A range of molar ratios of PEO macroinitiator [M] to monomer [MI] were used, [M]/[MI] = 100, 200 and 500. In all cases the consumption of monomer was quantitative and the block copolymers exhibited narrow molecular weight distributions (1.1–1.2), consistent with a living polymerisation technique. This suggests that the PEO macroinitiators are efficient initiators for ROMP of the monomers used in this study.

The number average molecular weights (M_n) of the block copolymers were calculated both by SEC and ^{1}H NMR. The values calculated by SEC are much smaller than the predicted molecular weights, the reason for this being that the copolymers were analysed using a calibration curve generated from PEO/PEG standards. SEC columns separate the eluting polymers by molecular size (hydrodynamic volume) rather than molecular weight and since the block copolymers undoubtedly have different hydrodynamic properties to the standards we would not expect the data to be correct.[10] Despite this, the SEC data from the block copolymers is useful for qualitative analysis and determination of polydispersity. In order to obtain a quantative measure of the molecular weights of the block copolymers we also calculated the M_n by ^{1}H NMR, by comparing the intensity of the PEO (of known molecular weight) peak at 3.4 ppm to the olefinic protons of the PNB backbone, which fall between 5 and 6 ppm. The values obtained for M_n agree well with the predicted values.
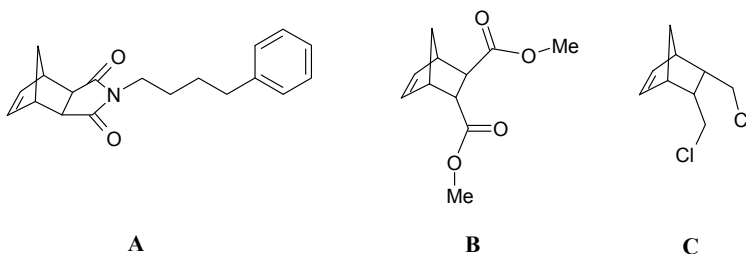
Figure 3. Norbornene derivatives used as monomers in block copolymer synthesis.

The synthesis of a range of block copolymers containing a PS and a PNB block has been achieved by the conversion of lithium initiated living anionic polymerisation into ruthenium catalysed ROMP.[11] For the synthesis of PS macromonomers was to use Quirk's method[12] was used to functionalise living PS (**IX**) with ethylene oxide (EO) to synthesise hydroxyethylated PS (**X**) (Scheme 3). The macromonomer (**XI**) was then synthesized by a coupling reaction, between **X** and 4-VBC, based on the Williamson ether synthesis.

The reaction of polymeric organolithium compounds with EO has been shown to be a useful method for the hydroxyl functionalisation of many polymers synthesized via an anionic polymerization mechanism.[12–15] In the case of PS (and polybutadiene) the reaction is well-characterised and leads to quantitative hydroxylation.[16, 17] Reaction of PS-Li (**IX**) with EO yields polymeric oxyanion chain ends, which aggregate strongly in solution.[16] This aggregation inhibits propagation of EO resulting in the introduction of a single EO monomer unit. However, oligomerisation of EO can occur with increased reaction times and concentrations of EO. The lithium alkoxide end group was
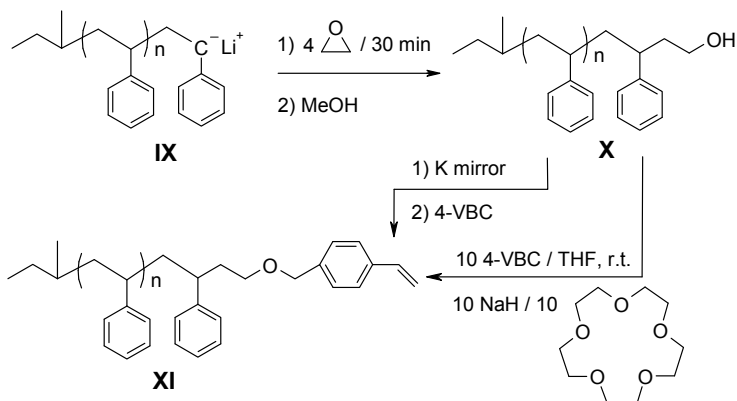
Scheme 3. Synthesis of poly(styrene–norbornene) block bopolymers.

protonated with N_2 sparged MeOH to yield hydroxyl terminated PS (**X**). Study of **X** via ^{1}H NMR spectroscopy indicated the presence of a single broad peak at 3.38–3.10 ppm corresponding to a single terminal methylene group adjacent to the hydroxyl group. Moreover, no evidence of the extra signals between 3 and 4 ppm that would result from the ether linkage formed via oligomerisation were observed.[16] Oligomerisation is not expected to present a problem for the synthesis of macromonomers as the oligomeric product would be functionalised with a hydroxyl group. However the ^{1}H NMR data suggests it did not occur to any detectable degree under our reaction conditions. Comparison of the integration values of the peak at 3.38–3.10 ppm corresponding to the CH_2OH methylene group with that from the aromatic phenyl protons of the PS polymer chain at 7.4–6.3 ppm confirmed that the reaction was approximately quantitative. In all cases a sample of PSLi (**IX**) was terminated with MeOH prior to the addition of EO, and used for the determination of M_n of the polymer using SEC.

The conversion of the hydroxyl functionalised PS (**X**) into PS macro-monomer (**XI**) was achieved using a Williamson coupling reaction with 4-VBC, and was attempted successfully by two different routes. Firstly, the hydroxyl group of **X** was deprotonated using a K mirror to yield a potassium alkoxide salt, which was then reacted with 4-VBC to form **XI**. In the second approach, the methodology of Aspinall et al.,[18] originally developed to allow the conversion of hindered alcohols into ethers at room temperature, was adapted for the synthesis of **XI**. In this case, the hydroxyl functionalised PS (**X**) was combined with 4-VBC, NaH, and 15-crown-5 and left stirring under dry N_2 until reaction was complete (48 h). Whilst the latter reaction was slower than the first method (K mirror), it needed less rigorous purification of 4-VBC and exclusion of moisture, and was catalysed by a milder base. This could prove particularly useful when adapting the described methodology, for polymers containing functionalities that are sensitive to nucleophilic attack. In each

case, the product of the functionalisation reaction was analysed by ^{1}H NMR spectroscopy. The spectra of the products from both routes were identical as expected, indicating the quantitative conversion of **X** into **XI** via both approaches.
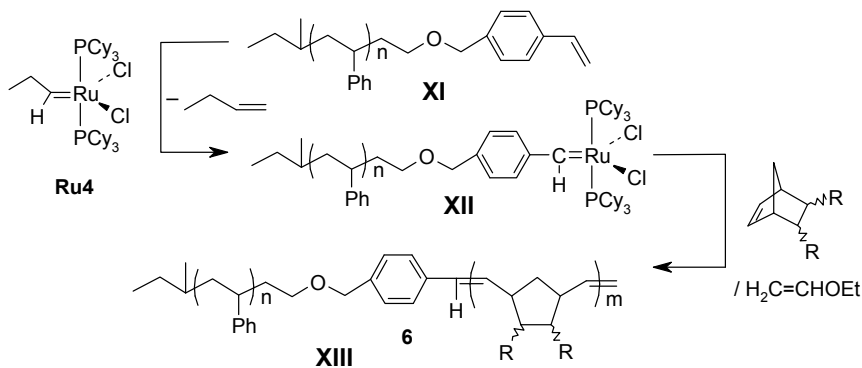
Cy = Cyclohexyl.

Scheme 4. Synthesis of poly(styrene–norbornene) block copolymers.

The synthesis of the ruthenium PS macroinitiators **XII** was achieved by an analogous alkylidene exchange reaction to that used to convert PEO macro-monomers into PEO ruthenium macrointiators.[6] The alkylidene exchange reaction of PS macromonomer **XI** with ruthenium propylidene initiator (**Ru4**), resulted in the synthesis of **XII**. Similarly, 1-butene side product was removed in order to effect complete conversion of macromonomer **XI** to macroinitiator **XII**.[6] The success of the reaction can also be monitored by the absence of the peaks from the vinyl functionality of the macromonomer **XI** in the ^{1}H NMR spectrum of the final product. ^{1}H NMR can also be used to monitor the conversion of the alkylidene proton of the propylidene initiator **Ru4** (**a**, Figure 4), into that of the macroinitiator **XII** (**b**, Figure 4).

A series of PS macroinitiators **XII** were synthesised with the number average molecular weight (M_n) of PS ranging from 2,850 to 10,500 g/mol, measured by SEC in THF Ruthenium PS macroinitiator **XII** was used for ROMP of NB derivatives (**A–C**), shown in Figure 3, to synthesise block copolymers (**XIII**). A series of block copolymers were synthesised in which the composition was controlled by altering the ratios of monomer [M] to macro-initiator [MI]; [M]/[MI] = 100, 200, and 500. Consumption of monomer was quantitative and the block copolymers possessed a narrow molecular weight distribution (PDI of 1.05–1.2). This suggests that as with the PEO macroinitiators, the ruthenium PS macroinitiators (**XII**) are efficient initiators for the ROMP of the NBE derivatives investigated.
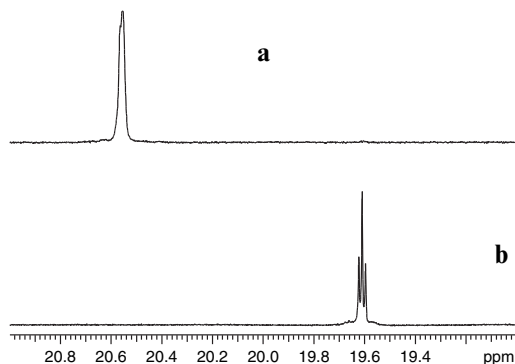
Figure 4. Comparison of the ^{1}H NMR analysis of the ruthenium propylidene initiator and the PS macroinitiator, in C$_6$D$_6$: (**a**) Ruthenium propylidene initiator; (**b**) PS Ruthenium PS macroinitiator.

The values of M_n for the block copolymers, calculated by SEC using triple detection were lower than those predicted by the stoichiometry of the reaction. The data obtained by triple detection SEC is based upon the parameters for PS measured in THF solution (e.g., refractive index [RI], specific refractive index increment [dn/dc], and intrinsic viscosity [η]), we would not therefore expect the values from SEC to be accurate.

The ^{1}H NMR spectra of the PS-PNB block copolymers can be used to calculate a quantitative value for the molecular weight (M_n) of the block copolymers, from the ratio of the integrals of a peak from each of the PNB and PS blocks in backbones. The values for M_n calculated by ^{1}H NMR are in good agreement with those predicted by the stoichiometry.

1.3. SYNTHESIS OF WELL-DEFINED CROSSLINKED SYSTEM

Dicyclopentadiene, DCPD, is cheap and can be polymerised by ROMP, which yields a crosslinked polymer. This polymerisation process is fast and can be tailored to either Reaction Injection Moulding (RIM) or Resin Transfer Moulding (RTM). The production of large moulded objects from DCPD-based feeds using RIM technology was developed mainly in the USA by BF Goodrich under the trade name of TELENE and by Hercules under the trade name METTON.[19–29] The advantages of DCPD include a rapid reaction and good product mechanical properties including low density, low water absorption and excellent toughness. The disadvantages include a nasty smell, an exothermic

reaction, which can be difficult to control, and the difficulty of regulating the crosslinking reaction, which reduces the processability and the range of mechanical properties available.

Recently, we developed a process which involves ROMP-Resin Transfer Moulding (RTM) copolymerisation of monofunctional and difunctional norbornene monomers to produce well-defined crosslinked polymers, Figure 5.[30–34] This in-mould processing gives a high conversion of monomers, which is essential. The incomplete reaction, and particularly residual monomer, will affect the physical and thermal properties of the product. More importantly, this system provides control over the degree of crosslinking through the addition of the amount of the difunctional monomer. A crucial factor in the development of the synthesis route was the availability of the ruthenium initiator, $RuCl_2(=CHPh)(PCy_3)_2$. The advantages of this initiator over others include its stability towards functional groups and water, the possibility of well-controlled living polymerisation and its solubility in the norbornene monomers.
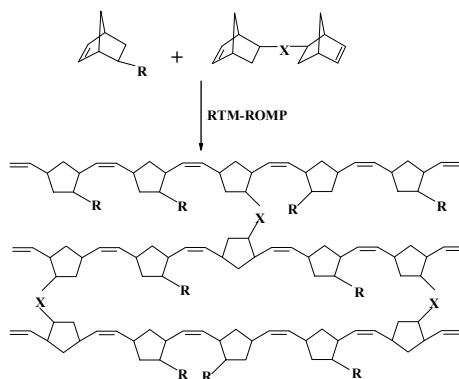
Figure 5. Schematic presentation of ROMP of the mixture of mono- and di-functional norbornene monomers to prepare well-defined crosslinked material.

Two types of monomers were used, both based on exo-N-alkyl dicarboximide norbornene. Monofunctional, exo-N-alkyl dicarboximide norbornenes, termed CnM, carrying pendant alkyl chains of different lengths, Figure 6a. The monofunctional monomers synthesised included n = 3, 4 and 5. The second type of monomers synthesised for this study were difunctional bis(exo-N-alkylenedicarboximide norbornenes) with an alkylene spacer, Figure 6b. These materials, termed CmD, were synthesised for values of m = 3, 5, 6, 9, and 12. Monofunctional exo-N-alkyl dicarboxyimide norbornenes were polymerised using RTM-ROMP processing to give linear polymers. The copolymerisation of monofunctional monomers with difunctional monomers produced crosslinked polymers.

a) Monofunctional monomer - CnM   b) Difunctional monomer - CmD

n= 2-9 and 12   m= 3,5,6,9 and 12
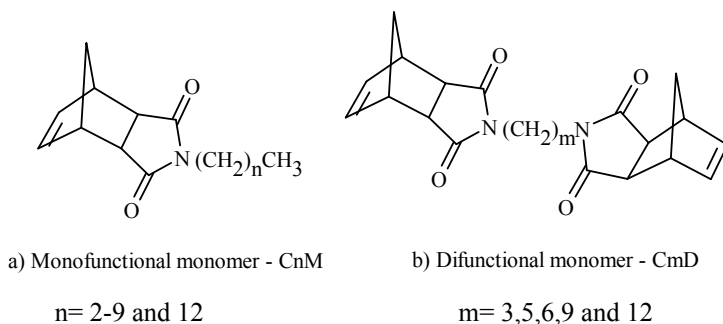
Figure 6. Structures of mono- and di-functional norbornene dicarboximides used for this work.

Dynamic mechanical analysis (DMTA) was employed to examine the variation in the relaxation behaviour, particularly the glass transition temperature T_g, with side chain length. DMTA also proved to be a useful way of establishing the optimum processing conditions and investigating the effects of molecular architecture such as the side chain length and the crosslink spacer length on mechanical properties. Particular attention was given to measurements of the shear modulus above the glass transition temperature. This was used to determine a value for the molecular weight between crosslinks, using simple rubber elasticity theory[35] and the results were compared to those expected from the stoichiometry of the monomer mixture. The results showed that the optimum M:I ratio for the C5M/CmD system was 8,000:1. Having established this fact, a range of samples was prepared using this ratio, to investigate the effect of varying the percentage of the difunctional component, and the length of the difunctional linkage.
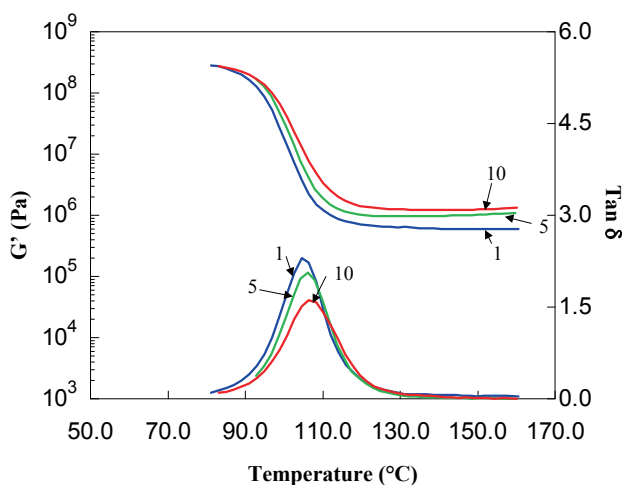
Figure 7. Dynamic shear modulus results for ROMP of the mixture of C5M with 1, 5 and 10 molar percentage of C12D.

Figure 7 shows the dynamic shear modulus results for the C5M/C12D combination, with 1, 5 and 10 molar percentage of the difunctional component. The results show that as the percentage of the difunctional, crosslinking unit, is increased the glass transition shifts to a higher temperature, the height of the tanδ peak decreases and the plateau shear modulus above T_g increases. These results are as expected for an increase in the crosslink density of a polymer. Nielsen[36] in his review of the crosslinking effect on the physical properties of polymers, describes these three effects. The system reported in this work turns out to be a textbook example of a well-defined and homogenously crosslinked system.

References

[1]   W.J. Feast, V.C. Gibson, A.F. Johnson, E. Khosravi, and M.A. Mohsin, Polymer, **1994**, 35, 3542.

[2]   W.J. Feast, V.C. Gibson, A.F. Johnson, E. Khosravi, and M.A. Mohsin, J. Mol. Catal. A: Chem., **1997**, 115, 37.

[3]   A.C.M. Rizmi, E. Khosravi, W.J. Feast, M.A. Mohsin, and A.F. Johnson, Polymer, **1998**, 39, 6605.

[4]   E. Khosravi, "Block Copolymers", A chapter in *Handbook of Metathesis*, R.H. Grubbs (Ed.), Wiley-VCH, Weinheim, **2003**, Vol. 3, pp. 72–117.

[5]   E. Khosravi, L.R. Hutchings, and M. Kujawa-Welten, Designed Monomers Polym., **2004**, 7, 619–632.

[6]   L.R. Hutchings, E. Khosravi, and T.C. Castle, Macromolecules, **2004**, 37, 2035–2040.

[7]   K.J. Ivin and J.C. Mol, *Olefin Metathesis and Metathesis Polymerization*, Academic Press, San Diego, CA, **1997**.

[8]   P.E. Schwab, R.H. Grubbs, and J.W. Ziller, J. Am. Chem. Soc., **1996**, 118, 100–110.

[9]   M. Ulman and R.H. Grubbs, Organometallics, **1998**, 17, 2484–2489.

[10] M. Netopilík and P. Kratochvíl, Polymer, **2003**, 44, 3431–3436.

[11] T.C. Castle, E. Khosravi, and L.R. Hutchings, Macromolecules **2006**, 39, 5639–5645.

[12] R.P. Quirk and J.J. Ma, J. Polym. Sci., Part A: Polym. Chem., **1988**, 26, 2031–2037.

[13] M.A. Hillmyer and F.S. Bates, Macromolecules, **1996**, 29, 6994–7002.

[14] Y. Deng, R.N. Young, A.J. Ryan, J.P.A. Fairclough, A.I. Norman, and R.D. Tack, Polymer, **2002**, 43, 7155–7160.

[15] R.P. Quirk, F. You, C. Wesdemiotis, and M.A. Arnould, Macromolecules, **2004**, 37, 1234–1242.

[16] R.P. Quirk, R.T. Mathers, C. Wesdemiotis, and M.A. Arnould, Macromolecules, **2002**, 35, 2912–2918.

[17] R.P. Quirk, Y. Guo, C. Wesdemiotis, and M.A. Arnould, Polymer, **2004**, 45, 3423–3428.

[18] H.C. Aspinall, N. Greeves, W.-M. Lee, E.G. McIver, and P.M. Smith, Tetrahedron Lett., **1997**, 38, 4679–4682.

[19] R.J. Minchak, US Patent 4,426,502, issued 17/01/**1984**.

[20] L. Matejka, C. Houtman, and C.W. Macosko, J. Appl. Polym. Sci., **1985**, 30, 2787.

[21] R.H. Grubbs, L.K. Johnson, and S.T. Nguyen, US Patent No. 5,312,940, issued 5/17/**1994**.

[22] R.H. Grubbs, L.K. Johnson, and S.T. Nguyen, US Patent No. 5,342,909, issued 8/30/**1994**.

[23] R.H. Grubbs, S.T. Nguyen, and L.K. Johnson, US Patent No. 5,710,298, issued 1/20/**1998**.

[24] R.H. Grubbs and C.S. Woodson, Jr., US Patent No. 5,728,785, issued 3/17/**1998**.

[25] C.S. Woodson, Jr. and R.H. Grubbs, US Patent No. 5,939,504, issued 8/17/**1999**.

[26] D.S. Breslow, Chemtech, **1990**, 20, 540.

[27] J.A. Johnson and M.F. Farona, Polym. Bull., **1991**, 25, 625–627.

[28] H. Ng, I. Manas-Zloczower, and M. Shmorhun, Polym. Eng. Sci., **1994**, 34, 921–928.

[29] A. Bell, Polym. Preprints, **1994**, 35, 694–695.

[30] E. Khosravi and A.A. Al-Hajaji, Eur. Polym. J., **1998**, 34, 153.

[31] E. Khosravi and A.A. Al-Hajaji, Polymer, **1998**, 39, 5619.

[32] E. Khosravi, W.J. Feast, A.A. Al-Hajaji, and T. Leejarkpai, Mol. Catal. A: Chem., **2000**,160, 1.

[33] T. Leejarkpai, Ph.D. thesis, University of Durham, UK, **2000**.

[34] P.J. Hine, T. Leejarkpai, E. Khosravi, R.A. Duckett, and W.J. Feast, Polymer, **2001**, 42, 9413.

[35] L.R.G. Treloar, *The Physics of Rubber Elasticity*, Oxford, London, UK, **1958**.

[36] L.E. Nielsen, Journal of macromolecular science – Revs. Macromol. Chem., **1969**, C3(1), 69.

SYNTHESIS OF FLUORINE-18 FUNCTIONALIZED NANOPARTICLES FOR USE AS IN VIVO MOLECULAR IMAGING AGENTS

JOHN B. MATSON AND ROBERT H. GRUBBS[*]
NanoSystems Biology Cancer Center, Division of Chemistry and Chemical Engineering, MC 127-72, California Institute of Technology, Pasadena, CA 91125

Abstract: Nanoparticles containing fluorine-18 were prepared from block copolymers made by ring-opening metathesis polymerization (ROMP). Using the fast initiating ruthenium metathesis catalyst $(H_2IMes)(pyr)_2(Cl)_2RuCHPh$, narrow polydispersity, amphiphilic block copolymers were prepared from a cinnamoyl-containing, hydrophobic norbornene monomer and a mesylate-terminated, PEG-containing hydrophilic norbornene monomer. Self-assembly into micelles and subsequent crosslinking of the micelle cores by light-activated dimerization of the cinnamoyl groups yielded stable nanoparticles. Incorporation of fluorine-18 was achieved by nucleophilic displacement of the mesylates with the radioactive fluoride ion with 31% incorporation of radioactivity. The resulting positron-emitting nanoparticles are to be used as *in vivo* molecular imaging agents in tumor imaging.

1. Introduction

The diagnosis, imaging and treatment of cancer stand to be revolutionized by the use of nanostructures as vehicles for imaging agents and chemotherapeutics.[1] High molecular weight species are known to localize more heavily in tumor tissue than in healthy tissue, prompting research in this area. This phenomenon, known as the enhanced permeability and retention effect (EPR effect), is due to the leaky vasculature exhibited in the tumor tissue.[2] Exploitation of the EPR effect is a common strategy for targeting tumor cells using nanostructures

including liposomes,[3] quantum dots,[4] dendrimers,[5] polymeric micelles,[6] and other molecular conjugates.[7]

The EPR effect was first observed in the 1980s when Maeda and coworkers reported that large molecules (>50 kDa) showed a tendency to enter and remain in cancer cells.[8] They attributed these results to four characteristics of tumor vascularization: (a) hypervascularization; (b) enhanced vascular permeability; (c) little recovery of macromolecules via the blood vessels; and (d) little recovery of macromolecules via the lymphatic system. Since then, the existence of the EPR effect across many types of tumors has been studied, and the phenomenon was later found to be consistent across all solid tumors.[9] Interestingly, the maximum size of a molecule that can cross into tumor tissue varies widely, from less than 100 nm up to 2 μm, depending on the tumor cell line.[10] Currently there are no reports that seek to optimize nanoparticle size to deliver the maximum amount of chemotherapeutic agents to tumors.

2. Tumor Imaging

Imaging of tumors using nanostructures designed to exploit the EPR effect has been accomplished using several *in vivo* imaging techniques, including magnetic resonance (MR),[11] near-IR fluorescence (NIR),[12] and positron emission tomography (PET).[13] PET is a specific, highly sensitive and versatile three-dimensional molecular imaging technique and the most sensitive and accurate method of measuring the temporal pattern in the biodistribution of labeled compounds. Fluorine-18 is the most widespread radionuclide used in PET imaging. Its relatively long half-life ($t_{1/2}$ = 109 min) makes fluorine-18-containing radiotracers more synthetically accessible than radiotracers containing other small positron emitting nuclides, such as carbon-11 ($t_{1/2}$ = 20 min), nitrogen-13 ($t_{1/2}$ = 10 min) and oxygen-15 ($t_{1/2}$ = 2 min). This has led to a dramatic increase in recent years in the production of fluorine-18, which is produced by the proton bombardment of $[^{18}O]H_2O$ in a cyclotron.

While nanoparticles incorporating positron-emitting metals such as copper-64 ($t_{1/2}$ = 12.7 h)[13a–c] have been synthesized, rapid and efficient incorporation of fluorine-18 into nanoparticles remained elusive until our report in 2008.[14] Incorporation of fluorine-18 into nanoparticles is expected to pave the way for precise and accurate *in vivo* PET imaging using nanostructured materials.

One of the most common imaging agents in PET scanning is 18-fluoro-deoxyglucose (FDG).[15] A hydrogen atom in a glucose molecule is replaced by a radioactive fluorine atom, and the positron-emitting compound is injected into the body where it is preferentially consumed by a growing tumor. A problem with using FDG, as well as other small molecule imaging agents, is that only a fraction of 1% of FDG molecules (depending on the activity of the batch) carries the radioactive label – the rest are unlabelled 19-fluorodeoxyglucose

molecules and cannot be visualized using a PET scan. Sites in the body that cannot quickly absorb over 1,000 glucose molecules can become saturated with unlabeled FDG, and the tumor cells are not imaged.[16] To solve this problem, either more ^{18}F-containing molecules relative to ^{19}F-containing molecules are needed (higher specific activity), or more sites for potential fluorination per molecule are needed. While significantly increasing the percent of radioactive fluorine is currently both difficult and unsafe, increasing the number of fluorination sites per molecule by incorporating multiple fluorine atoms into macromolecules is an attractive method for improving tumor imaging.

3. Nanoparticle Synthesis

Organic nanoparticles are typically made by the self assembly of amphiphilic block copolymers. By dissolving block copolymers with blocks of approximately equal lengths at the appropriate concentration in a solvent that is selective for only one of the blocks, the less soluble block will form a tight core, while the soluble block will form a loose shell or corona. Indeed, polymeric micelles have found use in medical diagnostic imaging[17] and drug delivery,[18] however, since there are no covalent bonds holding the micelles together, there is the possibility that they can dissociate into individual polymer chains upon dilution in the bloodstream. Crosslinking either the core or the corona avoids this problem by covalently linking all of the chains, turning the micelles into discrete nanoparticles. Since polymeric micelles are typically comprised of a few dozen to several hundred individual polymer chains, there can be thousands of sites available to incorporate functionality in each nanoparticle. In the case where each nanoparticle possesses thousands of potential radioactive sites, the chances of having a particle without a radioactive label are very low, and the oversaturation problem is avoided.

Due to the ability to control micelle size by modifying block lengths and ratios, the predictable self-assembly behavior in forming micelles, and the potentially high molar specific activity, we selected amphiphilic block copolymers as scaffolds from which to build nanoparticles. Ring opening metathesis polymerization (ROMP) provides a route to narrowly dispersed amphiphilic block copolymers without protecting group chemistry.[19] This is a distinct advantage over other living polymerization techniques, such as anionic polymerization, cationic polymerization and controlled free radical polymerization, including atom transfer radical polymerization (ATRP), nitroxide-mediated radical polymerization (NMRP) and reversible addition-fragmentation transfer polymerization (RAFT). Typical syntheses of nanoparticles using these techniques require multiple polymerization steps and one or more deprotection or post-polymerization functionalization steps. Additionally, many of the steps performed after polymerization requires lengthy purification procedures such as dialysis. ROMP can

be used to avoid these steps, which are neither efficient nor atom economical, by allowing for the direct polymerization of a variety of functional monomers.[20] Living ROMP using substituted norbornenes also produces polymers whose degrees of polymerization can be easily and precisely controlled by adjusting the monomer to catalyst ratio.[21] When substituted norbornenes are used as the monomers, ROMP is free of chain-transfer and termination events. Reactions are therefore typically run to complete conversion, allowing for extremely precise control over polymer molecular weight by modifying the monomer to catalyst ratio. Factors affecting nanoparticle size and shape, such as the length and relative ratio of the hydrophilic and hydrophobic blocks, can be easily modified to quickly produce a wide variety of nanoparticle architectures using ROMP.

3.1. MONOMER DESIGN AND SYNTHESIS

The synthesis of nanoparticles containing functional groups for crosslinking, biocompatibility and facile radiofluorination required the development of block copolymers that exhibited all of these elements. Substituted exo-norbornene imides were selected as the monomers due to their ability to undergo living ROMP, as well as their ability to be easily functionalized. Specifically, norbornene-imide monomers were used because the condensation of exo-anhydride **1** with function-alized amines is a versatile reaction capable of forming a variety of monomers (Scheme 1). Hydrophobic monomer **3** was synthesized by reaction of exo-norbornene anhydride **1** with aminoethanol to produce norbornene-imide **2**, followed by coupling with *trans*-cinnamic acid using EDC. The cinnamoyl group has recently become popular as a photo-crosslinking group in nanoparticle synthesis since its development by Liu in the mid-1990s.[22] Irradiation with ultraviolet light causes the *trans*-olefin to undergo a [2 + 2] dimerization, affording a tetrasubstituted cyclobutane ring.
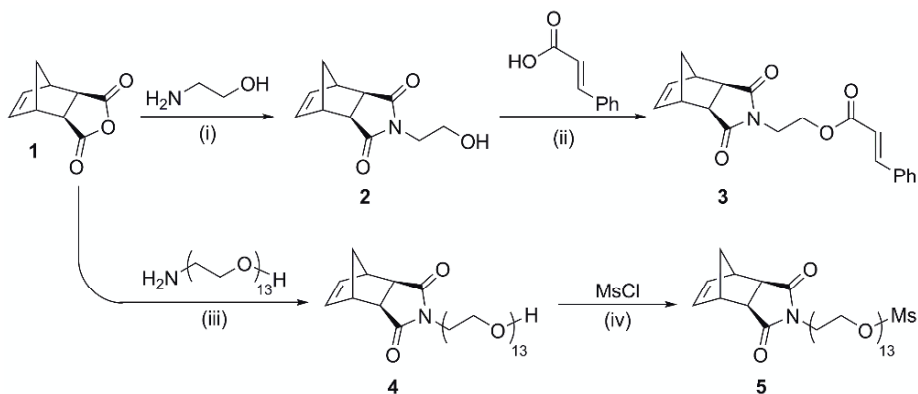
Scheme 1. Monomer syntheses. Reaction conditions: (i) NEt$_3$, toluene, reflux, DS-trap. (ii) EDC, DMAP, CH$_2$Cl$_2$, rt. (iii) C$_6$H$_6$, NEt$_3$, DS-trap, reflux. (iv) MsCl, NEt$_3$, −30°C.

The PEGylated norbornene imide **4** was synthesized by reaction of a previously reported[23] mono-aminated poly(ethylene glycol) (PEG) chain with exo-norbornene anhydride **1**, followed by installment of a mesylate using mesyl chloride to produce hydrophilic monomer **5**. PEG was chosen because it is well-known to be non-immunogenic and non-toxic, and both linear and grafted PEG chains have been shown to provide a stealth coating for nanoparticles in the bloodstream.[24] Many lengths of PEG chains were examined, but PEG600 provided the desired solubility while retaining high activity during ROMP.

We chose to incorporate fluorine-18 into the nanoparticles by mimicking well-known small molecule chemistry.[25] Many fluorine-18-containing molecular imaging agents rely on nucleophilic displacement of a sulfonate ester by the nucleophilic fluoride-18 anion. These types of reactions are typically run in acetonitrile, using kryptofix-222 to bind potassium. The mesylate group was chosen for displacement by fluorine after examination of a variety of leaving groups, including nosylates and triflates. While the latter two leaving groups are known to be more reactive, they were found to be unsuitable due to lack of solubility or stability, respectively.

3.2. POLYMER SYNTHESIS

To demonstrate the ability of this synthetic method in producing a broad range of narrowly dispersed nanoparticles, four block copolymers of varying molecular weights were synthesized. Known for producing extremely narrow polydispersity polymers, the ruthenium olefin metathesis catalyst $(H_2IMes)(pyr)_2(Cl)_2RuCHPh$ (**6**) was selected as the initiator (Scheme 2). Recently, pyridine-containing, fast-initiating ruthenium catalysts such as **6** have shown remarkable reactivity as initiators for living ROMP.[21, 26] The rate of dissociation of the two pyridine ligands from catalyst **6** has been shown to be over five orders of magnitude faster than the rate of phosphine dissociation of the parent complex $(H_2IMes)(PCy_3)$ $(Cl)_2RuCHPh$,[27] leading to polymer syntheses that can be completed in a few seconds.[28]
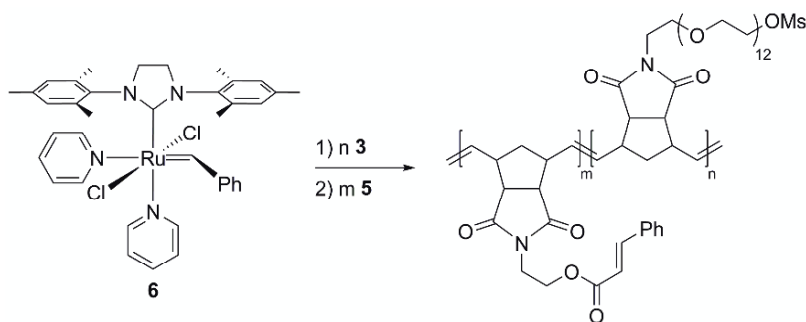
Scheme 2. Polymer synthesis.

TABLE 1. GPC characterization of block copolymers.

Entry	m	n	M_n (theo)	M_n (GPC)	PDI
1	50	150	140,400	133,200	1.01
2	100	300	280,500	280,000	1.03
3	200	600	560,100	544,000	1.18
4	400	1,200	1,124,000	1,222,000	1.73

Sequential copolymerization of the two monomers was carried out on the benchtop under argon in THF. After polymerization of the first monomer was complete (1–2 min), the second monomer was added to the reaction mixture. All reactions were complete in 30 min. Quenching with ethyl vinyl either, stirring for 10 min and precipitating into ether/hexanes (1:1) afforded the desired products in excellent yields. Characterization by gel permeation chromatography (GPC) showed monomodal, narrowly dispersed peaks for most of the polymers (Table 1, entries 1–3). The PDIs were typical for this catalyst, with the exception of the highest molecular weight polymer (Table 1, entry 4). This broadening is likely due to catalyst death. A block ratio of 3:1 hydrophilic/ hydrophobic was chosen after a thorough study of the solubility of nanoparticles with various block lengths. The nanoparticles were found to be soluble in acetonitrile, the solvent used for the radiofluorination reaction, while maintaining a large enough core to allow for crosslinking. Nanoparticles with a smaller hydrophilic/hydrophobic ratio were found to be insoluble in acetonitrile, while polymers with a larger hydrophilic/hydrophobic ratio were difficult to isolate and characterize.

3.3. MICELLE FORMATION AND CROSSLINKING

Micelle formation was accomplished by dissolving a given polymer in THF, a good solvent for both blocks, followed by slowly adding water to the solution (Scheme 3). Dialysis of the resulting micelle solution against water was used to remove the THF. The micelles were analyzed by dynamic light scattering (DLS) and atomic force microscopy (AFM) (Figure 1a). AFM measurements show that the micelles follow the expected trend of increasing micelle diameters with increasing polymer molecular weight. Additionally, the polydispersity of the micelles can be observed qualitatively by AFM. The largest micelles are clearly more polydisperse, while the smallest micelles are nearly monodisperse, in agreement with the PDIs of the constituent block copolymers.
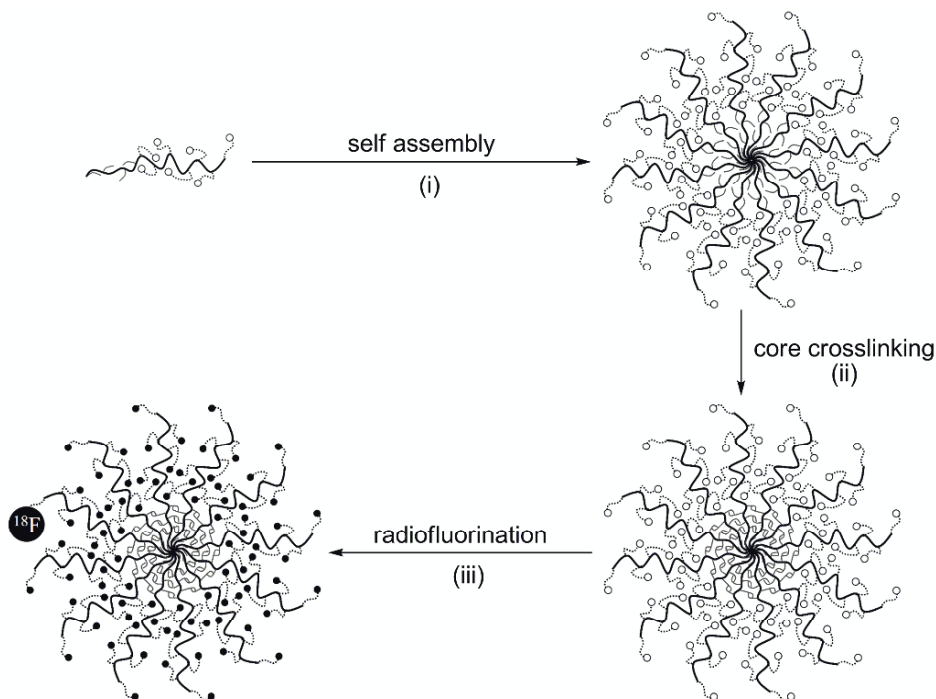
Scheme 3. Fluorinated nanoparticle synthesis. Solid, black lines represent the polymer backbone; dotted lines and gray lines represent pendent PEG and cinnamoyl groups, respectively. Empty balls represent mesylate groups and black balls represent fluorine atoms. Conditions: (i) dialysis against H_2O, 24 h (ii) hv, 3 min (iii) (1) $K^{18}F$, kryptofix 222, K_2CO_3, BHT, MeCN, 120°C, 60 min; (2) $K^{19}F$, kryptofix 222, MeCN, 80°C, 30 min.

To ensure that the nanoparticles stayed intact upon dilution in the bloodstream, crosslinking of the micelle cores was carried out. Crosslinking was achieved by using UV light from a mercury arc lamp in degassed water at room temperature. The percentage of crosslinking was determined by measurement of the peak absorbance at 278 nm before and after irradiation. Some amount of intra-chain crosslinking is likely, but this contribution is expected to be small due to the compact nature of the micelle core. After only 3 min of UV irradiation, samples were typically crosslinked to 15%. There is no evidence that significant cross-linking occurs while the micelle solution is standing in incident light. The extent of the reaction was kept between 15% and 25% as longer reaction times caused the nanoparticles to become insoluble.
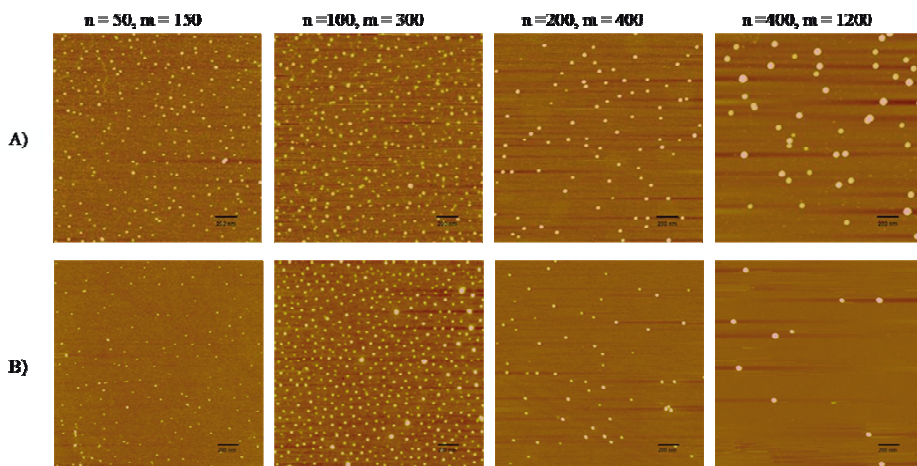
Figure 1. (**a**) AFM images of micelles. (**b**) AFM images of crosslinked nanoparticles. The nanoparticle diameters are observed to increase with increasing molecular weight of the constituent block copolymers.

Characterization of the nanoparticles (Table 2) was accomplished in the solid state by AFM, as shown in Figure 1b, and in solution by DLS. Similar to the micelles, the expected trend of increasing nanoparticle diameter with increasing polymer molecular weight is observed, with nanoparticle diameters ranging from 12.7 to 39.7 nm by AFM and 47.4 to 142.5 nm by DLS. These data are comparable to the values observed for the micelles. The apparent diameter of the nanoparticles is two to three times larger when measured using DLS than when measured using AFM. This effect is likely due to the swelling of the polymer chains in solution as well as the hydration sphere surrounding the particles in aqueous environments. Because AFM measures dehydrated particles on a substrate, hydrodynamic diameter as measured by DLS is a better indicator of the particle size *in vivo*. DLS measurements show that the particles fall into the desired range to effectively probe the limits of the EPR effect.[1e]

TABLE 2. Characterization of nanoparticles.

Entry	Polymer M_n	Diameter (AFM)	Diameter (DLS)
1	133,200	12.7 ± 2.6 nm	47.4 ± 7.5 nm
2	280,000	16.4 ± 4.5 nm	58.1 ± 1.8 nm
3	544,000	21.1 ± 3.9 nm	79.7 ± 9.7 nm
4	1,222,000	39.7 ± 4.0 nm	142.5 ± 6.8 nm

3.4. RADIOFLUORINATION

Lyophilized nanoparticle samples were used for the radiofluorination experiments. Fluorine-18 anion was transported in its hydrated form into the reaction vessel, and solutions of kryptofix 222, K_2CO_3 and BHT were added. Three consecutive additions and evaporations of acetonitrile were used to remove the water, which is typically detrimental to nucleophilic substitution reactions using fluoride ion.[25] The nanoparticles were added to the reaction vessel as a solution in acetonitrile, and the reaction mixture was heated in a sealed vessel for 1 h at 120°C. The mesylate groups remaining after radiofluorination were displaced with additional fluorine-19 to avoid undesired reactions *in vivo*. The radio-fluorinated particles were isolated by diluting the reaction mixture with water and passing this solution through neutral alumina and strongly acidic cation exchange resin. These conditions effectively removed all of the kryptofix and most of the unreacted fluoride. The extent of reaction was established by measurement of the radioactivity of the nanoparticles, as well as radio-TLC, which showed that 31% of the fluorine was incorporated into the nanoparticles. The product was recovered in 61% radiochemical purity.

4. Conclusions

Fluorine-18 functionalized nanoparticles have been synthesized for use as *in vivo* molecular imaging agents from amphiphilic block copolymers made by ROMP. A cinnamoyl-functionalized norbornene imide monomer was synthesized to be used in the photocrosslinkable, hydrophobic block, and a PEG-containing, mesylate-terminated norbornene imide monomer was synthesized to be used in the hydrophilic block. Sequential ROMP of the two monomers followed by dissolution in water yielded aqueous micelles. Crosslinking of the micelles using ultraviolet light yielded discrete nanoparticles that exhibited hydrodynamic diameters from 47 to 142 nm. Standard nucleophilic fluorination chemistry was employed to incorporate fluorine-18 into the nanoparticles in 61% radiochemical purity. Ongoing *in vivo* studies in mice will establish the optimal size range of nanoparticles for exploitation of the EPR effect.

References

[1]   (a) Brigger, I.; Dubernet, C.; Couvreur, P. *Adv. Drug Delivery. Rev.* **2002**, *54*, 631–651. (b) Sinha, R.; Kim, G. J.; Nie, S. M.; Shin, D. M. *Mol. Cancer Ther.* **2006**, *5*, 1909–1917. (c) Moghimi, S. M.; Hunter, A. C.; Murray, J. C. *FASEB J.* **2005**, *19*, 311–330. (d) Ferrari, M. *Nat. Rev. Cancer* **2005**, *5*, 161–171. (e) Heath, J. R.; Davis, M. E. *Annu. Rev. Med.* **2008**, *59*, 251–265.

[2]   Maeda, H.; Wu, J.; Sawa, T.; Matsumura, Y.; Hori, K. *J. Controlled Rel* **2000**, *65*, 271–284.

[3]   (a) Lee, S. M.; Chen, H.; Dettmer, C. M.; O'Halloran, T. V.; Nguyen, S. T. *J. Am. Chem. Soc.* **2007**, *129*, 15096–15097. (b) Torchilin, V. P. *Nat. Rev. Drug Discovery* **2005**, *4*, 145–160.

[4]   (a) Michalet, X.; Pinaud, F. F.; Bentolila, L. A.; Tsay, J. M.; Doose, S.; Li, J. J.; Sundaresan, G.; Wu, A. M.; Gambhir, S. S.; Weiss, S. *Science* **2005**, *307*, 538–544. (b) Smith, A. M.; Ruan, G.; Rhyner, M. N.; Nie, S. M. *Ann. Biomed. Eng.* **2006**, *34*, 3–14. (c) Bagalkot, V.; Zhang, L.; Levy-Nissenbaum, E.; Jon, S.; Kantoff, P. W.; Langer, R.; Farokhzad, O. C. *Nano Lett.* **2007**, *7*, 3065–3070.

[5]   (a) Ihre, H. R.; De Jesus, O. L. P.; Szoka, F. C.; Frechet, J. M. J. *Bioconjugate Chem.* **2002**, *13*, 443–452. (b) Lee, C. C.; MacKay, J. A.; Frechet, J. M. J.; Szoka, F. C. *Nat. Biotechnol.* **2005**, *23*, 1517–1526. (c) Malik, N.; Evagorou, E. G.; Duncan, R. *Anti-Cancer Drug.* **1999**, *10*, 767–776. (d) Jain, N. K.; Asthana, A. *Expert Opin. Drug Deliv.* **2007**, *4*, 495–512.

[6]   (a) Torchilin, V. P. *J. Controlled Rel* **2001**, *73*, 137–172. (b) Sun, X. K.; Rossin, R.; Turner, J. L.; Becker, M. L.; Joralemon, M. J.; Welch, M. J.; Wooley, K. L. *Biomacromolecules* **2005**, *6*, 2541–2554. (c) Licciardi, M.; Giammona, G.; Du, J. Z.; Armes, S. P.; Tang, Y. Q.; Lewis, A. L. *Polymer* **2006**, *47*, 2946–2955.

[7]   Heidel, J.; Mishra, S.; Davis, M. E. *Adv. Biochem. Eng. Biotechnol.* **2005**, *99*, 7–39.

[8]   Matsumura, Y.; Maeda, H. *Cancer Res.* **1986**, *46*, 6387–6392.

[9]   (a) Maeda, H.; Seymour, L. W.; Miyamoto, Y. *Bioconjugate Chem.* **1992**, *3*, 351–362. (b) Baban, D. F.; Seymour, L. W. *Adv. Drug Delivery Rev.* **1998**, *34*, 109–119. (c) Reddy, L. H. *J. Pharm. Pharmacol.* **2005**, *57*, 1231–1242.

[10] Hobbs, S. K.; Monsky, W. L.; Yuan, F.; Roberts, W. G.; Griffith, L.; Torchilin, V. P.; Jain, R. K. *Proc. Natl. Acad. Sci. U.S.A.* **1998**, *95*, 4607–4612.

[11] (a) Morawski, A. M.; Lanza, G. A.; Wickline, S. A. *Curr. Opin. Biotechnol.* **2005**, *16*, 89–92. (b) Seo, W. S.; Lee, J. H.; Sun, X. M.; Suzuki, Y.; Mann, D.; Liu, Z.; Terashima, M.; Yang, P. C.; McConnell, M. V.; Nishimura, D. G.; Dai, H. J. *Nat. Mater.* **2006**, *5*, 971–976. (c) Mulder, W. J. M.; Koole, R.; Brandwijk, R. J.; Storm, G.; Chin, P. T. K.; Strijkers, G. J.; Donega, C. D.; Nicolay, K.; Griffioen, A. W. *Nano Lett.* **2006**, *6*, 1–6. (d) Kobayashi, H.; Brechbiel, M. W. *Adv. Drug Delivery Rev.* **2005**, *57*, 2271–2286.

[12] Yang, Z.; Zheng, S. Y.; Harrison, W. J.; Harder, J.; Wen, X. X.; Gelovani, J. G.; Qiao, A.; Li, C. *Biomacromolecules* **2007**, *8*, 3422–3428.

[13] (a) Pressly, E. D.; Rossin, R.; Hagooly, A.; Fukukawa, K. I.; Messmore, B. W.; Welch, M. J.; Wooley, K. L.; Lamm, M. S.; Hule, R. A.; Pochan, D. J.; Hawker, C. J. *Biomacromolecules* **2007**, *8*, 3126–3134. (b) Bartlett, D. W.; Su, H.; Hildebrandt, I. J.; Weber, W. A.; Davis, M. E. *Proc. Nat. Acad. Sci. U.S.A.* **2007**, *104*, 15549–15554. (c) Fukukawa, K.; Rossin, R.; Hagooly, A.; Pressly, E. D.; Hunt, J. N.; Messmore, B. W.; Wooley, K. L.; Welch, M. J.; Hawker, C. J. *Biomacromolecules* **2008**, *9*, 1329–1339. (d) Schipper, M. L.; Cheng, Z.; Lee, S.-W.; Bentolila, L. A.; Iyer, G.; Rao, J.; Chen, X.; Wu, A. M.; Weiss, S.; Gambhir, S. S. *J. Nucl. Med.* **2007**, *48*, 1511–1518.

[14] Matson, J. B.; Grubbs, R. H. *J. Am. Chem. Soc.* **2008**, *130*, 6731–6733.

[15] (a) Nabi, H. A.; Zubeldia, J. M. *J. Nucl. Med. Technol.* **2002**, *30*, 3–9. (b) Rohren, E. M.; Turkington, T. G.; Coleman, R. E. *Radiology* **2004**, *231*, 305–332.

[16] Jagoda, E. M.; Vaquero, J. J.; Seidel, J.; Green, M. V.; Eckelman, W. C. *Nucl. Med. Biol.* **2004**, *31*, 771–779.

[17] (a) Torchilin, V. P. *J. Controlled Rel.* **2001**, *73*, 137–172. (b) Tochilin, V. P. *Colloids Surf. B* **1999**, *16*, 305–319.

[18] Adams, M. L.; Lavasanifar, A.; Kwon, G. S. *J. Pharm. Sci.* **2003**, *92*, 1343–1355.
[19] Bielawski, C. W.; Grubbs, R. H. *Prog. Polym. Sci.* **2007**, *32*, 1–29.
[20] (a) Maynard, H. D.; Okada, S. Y.; Grubbs, R. H. *Macromolecules* **2000**, *33*, 6239–6248. (b) Rawat, M.; Gama, C. I.; Matson, J. B.; Hsieh-Wilson, L. C. *J. Am. Chem. Soc.* **2008**, *130*, 2959–2961. (c) Ilker, M. F.; Nsslein, K.; Tew, G. N.; Coughlin, E. B. *J. Am. Chem. Soc.*, **2004**, *126*, 15870–15875.
[21] Choi, T. L.; Grubbs, R. H. *Angew. Chem. Int. Ed.* **2003**, *42*, 1743–1746.
[22] (a) Liu, G. J.; Hu, N. X.; Xu, X. Q.; Yao, H. *Macromolecules* **1994**, *27*, 3892–3895. (b) Guo, A.; Liu, G. J.; Tao, J. *Macromolecules* **1996**, *29*, 2487–2493. (c) Henselwood, F.; Liu, G. J. *Macromolecules* **1997**, *30*, 488–493.
[23] Menger, F. M.; Zhang, H. *J. Am. Chem. Soc.* **2006**, *128*, 1414–1415.
[24] Gref, R.; Minamitake, Y.; Peracchia, M. T.; Trubetskoy, V.; Torchilin, V. P.; Langer, R. *Science* **1994**, *263*, 1600–1603.
[25] Cai, L.; Lu, S.; Pike, V. W. *Eur. J. Org. Chem.* **2008**, *17*, 2853–2873.
[26] (a) Camm, K. D.; Castro, N. M.; Liu, Y. W.; Czechura, P.; Snelgrove, J. L.; Fogg, D. E. *J. Am. Chem. Soc.* **2007**, *129*, 4168–4169. (b) Slugovc, C.; Demel, S.; Stelzer, F. *Chem. Commun.* **2002**, *21*, 2572–2573.
[27] Love, J. A.; Morgan, J. P.; Trnka, T. M.; Grubbs, R. H. *Angew. Chem. Int. Ed. Engl.* **2002**, *41*, 4035–4037.
[28] Bielawski, C. W.; Benitez, D.; Morita, T.; Grubbs, R. H. *Macromolecules* **2001**, *34*, 8610–8618.

POLYMERIC MONOLITHS: NOVEL MATERIALS FOR SEPARATION SCIENCE, HETEROGENEOUS CATALYSIS AND REGENERATIVE MEDICINE

MICHAEL R. BUCHMEISER
Leibniz-Institut für Oberflächenmodifizierung e.V. (IOM), Permoserstraße 15, D-04318 Leipzig, Germany; Institut für Technische Chemie, Universität Leipzig, Linnéstraße 3, D-04103 Leipzig, Germany

Abstract: The chemistry of metathesis polymerization-derived monolithic supports is summarized. Since ring-opening metathesis polymerization (ROMP) triggered by well-defined transition metal alkylidenes is a living polymerization method, it allows for the controlled and highly reproducible synthesis of stationary phases in terms of both the nature and total content of the functional group(s) of interest. In addition, the high functionality tolerance of ROMP allows for creating monolithic supports with an unprecedented diversity in terms of functional groups that may be introduced. Applications in various areas of chemistry such as separation science heterogeneous catalysis and tissue engineering are summarized.

Keywords: Ring-opening metathesis polymerization; Monoliths

1. Introduction

Modern chemistry requires designed, high-performance materials with regard to particle size, particle shape, porosity, specific surface area, functionality and capacity, respectively. Enormous progress has been made in the areas of analytical chemistry and materials science that are relevant to this topic. This contribution intends to highlight both the motivation that has lead to the development of metathesis polymerization-based monolithic supports and the actual contributions of this polymerization technique to the areas of material science and separation science, respectively.

2.   Motivation and Starting Point

The "classic" approach to functional stationary phases entails the use of polymer analogous reactions on beaded, crosslinked and thus insoluble polymers. Consequently, the nature of the "working" functionality of the thus prepared stationary phases is sometimes still rather based on assumption than on real analysis. In many cases, the (fairly) reproducible generation of a mixture of functional groups located at the surface is responsible for the final chromatographic properties. In order to avoid any multi-step derivatization reactions, the polymerization of *functional monomers* therefore appeared favorable. In this context, polymerizations techniques that are both living[1, 2] and highly tolerant versus functional groups were of particular interest. Generally, such polymerizations techniques allow for the full control over both the molecular weight and architecture of the resulting polymers. In due consequence, this permits the stoichiometric and thus highly reproducible design of block-copolymers including cross-linked polymers. In due consequence, this facilitates correlating the polymers' and materials' structure with the resulting separation properties.

We commenced our research on ROMP-derived monolithic materials in 1998. At that time and long after, there were only very scattered activities in the synthesis of monoliths based on living or controlled polymerization techniques.[3] In view of the impressive achievements made in ring-opening-metathesis polymerization (ROMP) at that time,[4, 5] we decided to investigate the general applicability of this polymerization technique to the synthesis of monolithic supports. Using Grubbs-type initiators, a broad range of functional monomers based on substituted norborn-2-enes and norbornadienes bearing anhydrides, esters or amides may well be polymerized in a truly living manner.

3.   ROMP-Derived Monolithic Materials

3.1.   PROPERTIES OF MONOLITHIC MATERIALS

Within the context of stationary phases, the term "monolith" applies to any single-body structure containing interconnected repeating cells or channels, which is characterized by a defined porosity and which supports interactions/reactions between this solid and the surrounding liquid phase. Such supports are either prepared from inorganic mixtures, e.g. silanols, or from organic compounds, e.g. by a crosslinking polymerization. For a profound discussion of their history, their general properties and application refer to Refs. [6–11].

3.2. MONOLITHIC MATERIALS PREPARED FROM NBE-BASED MONOMERS

Our first experiments on the suitability of ROMP for the synthesis of monolithic supports entailed the copolymerization of NBE with DMNH6 in the presence of two porogenic solvents, 2-propanol and toluene, with $RuCl_2(PCy_3)_2(CHPh)$.[12] Such a setup in fact allowed for the realization of the first ROMP-derived monolithic supports (Scheme 1).
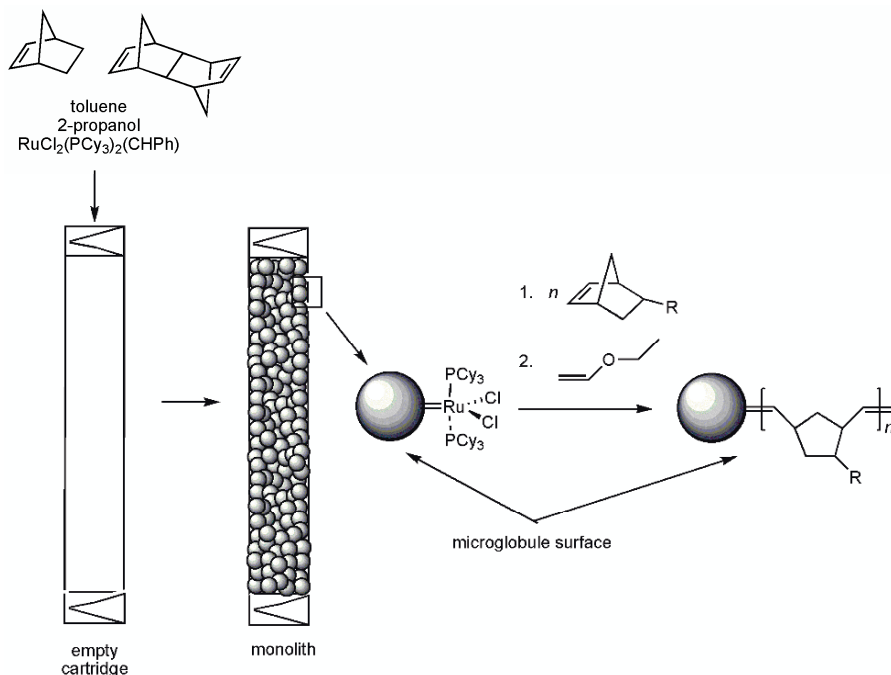
Scheme 1. Synthesis and functionalization of ROMP-derived monolithic supports.

By variation of the polymerization mixture in terms of monomer, crosslinker and porogen content, the volume fraction of the interglobular void volume (ε_z) as well as the total porosity ε_t were successfully varied within a range of 0–50% and 50–80%, respectively. The addition of small amounts of triphenylphosphine in the low ppm range allowed for tuning the polymerization kinetics. NBE-based monoliths prepared by ROMP displayed linear plots of pressure versus flow rate, which confirmed that the monoliths were not compressed even at high flow velocities exceeding 5 mm/s. ICP-OES measurements on totally dissolved samples of various monoliths revealed that the ruthenium introduced into the monolithic matrix in form of the initiator could in fact be totally removed by the use of appropriate capping agents, resulting in Ru-concentrations <10 µg/g, which corresponds to a metal removal >99.9%.

3.3. MONOLITHIC MATERIALS PREPARED FROM COE-BASED MONOMERS

In general, NBE-derived monomers result in polymer structures that comprise of *tertiary* allylic carbons. Despite the high mechanical and thermal stability of these structures,[13] which are by far sufficient for short and medium term analytical applications as well as applications in heterogeneous catalysis,[14–16] tertiary allylic carbons located at the surface of a monolithic structure tend to be oxidized, resulting in a slow change of surface polarity of such monolithic columns. In due consequence, the typical long-term stability of NBE-based, ROMP-derived columns is limited to less than 1,000 injections. We therefore tried to solve this problem by introducing a novel monomer/crosslinker system to the synthesis of monolithic structures. For these purposes, we developed a polymerization system based on *cis*-cyclooctene (COE) and tris(cyclooct-4-en-1-yloxy)methylsilane (TCOMS). Our efforts were guided by the idea that the polymer backbone of poly(COE)-derived materials consists of *secondary* allylic carbons and therefore presents an attractive alternative to NBE-based systems. However, compared to NBE-based monomers, COE-based ones are characterized by a significantly reduced ring strain, thus requiring more active initiators. This and the use of novel monomers made the comprehensive re-design of monolith synthesis inevitable. As a direct consequence of the reduced ring strain in COEs, the reactivity of the initiator had to be enhanced. Thus, the first-generation Grubbs initiator $RuCl_2(PCy_3)_2(CHPh)$ was replaced by a fast initiating derivative of the second-generation Grubbs initiator, i.e. by $RuCl_2(Py)_2(1,3-Mes_2$-imidazolin-2-ylidene)(CHC_6H_5) (Mes = mesityl, Py = pyridine).[17] In order to make reactivity feasible to the handling of the polymerization mixtures, i.e. to slow down kinetics, pyridine was added. Similar to the NBE-based system, the final polymerization system consisted of various amounts of the monomer (COE), the crosslinker (TCOMS), the macroporogen (2-propanol), the microporogen (toluene) and the modulator (pyridine). An initiator loading of 0.2 wt% was chosen throughout.

Some important differences between COE- and NBE-based, ROMP-derived monolithic supports need to be outlined. Figure 1 illustrates the different structure of an NBE- and COE-based ROMP-derived monolith applying the same recipe in terms of monomers, crosslinkers and porogens. Figure 1b illustrates the fast separation (<150 s) of a mix of proteins, i.e. ribonuclease A, lysozyme, insulin, cytochrome C, and myoglobin on a COE-based monolith applying gradient elution. Peak half widths ($\omega_{0.5}$) were <6 s, resolution (R_s) was >1.2 throughout. For purposes of comparison, an NBE-based monolith of the same recipe, i.e. using the same amounts of monomer, crosslinker and porogens was synthesized and used for separation (Figure 1a).
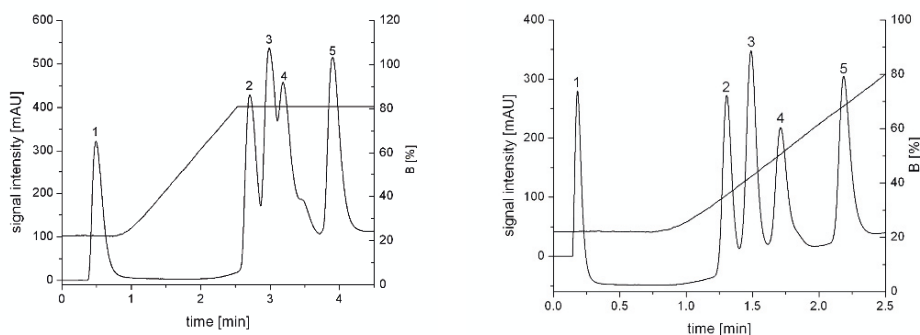
Figure 1. Separation of proteins (rinonuclease, insulin, cytochrome c, lysozyme, α-chymotrypsinogene A, catalase) on a monolith (0.2 × 220 mm). Mobile phase A: 0.05% aqueous TFA , B: ACN + 0.05 % TFA; linear gradient 10% to 100% B in 10 min; delay 2 min; RT, flow: 5.71 µL/min (400 mL/min+50/375/40 cm split); 180 bar; inj. vol. 500 nl; conc. 10 µg/ml. UV (218 nm).

Applying the identical gradient, peak half widths ($\omega_{0.5}$) were <7 s, resolution (R_s) was >1.1 throughout. Some important mechanistic aspects of the separation may be deduced from these experiments. Since lysozyme (M_w = 14,307 g/mol) and ribonuclease (M_w = 13,700 g/mol) were well separated (R_s = 10.6!), separation must be independent of the molecular weight, but dependant on the *tertiary structure* of these analytes. The most striking difference in separation behavior of both COE- and NBE-based columns is observed in the retention times of the analytes as well as in R_s and the values for the mean peak half width ($\omega_{0.5}$). These findings were related to the structural data obtained *via* ISEC[18] for both the COE- and the NBE-based monolith.[19]

3.4. APPLICATIONS IN THE SEPARATION OF BIOMOLECULES

Apolar, non-functionalized polymeric surfaces are widely used as stationary phases for both RP-HPLC and IP-RP-HPLC. While the former is the method of choice for high-resolution separations of peptides and proteins, the latter is eminently suited for the separation of single- and double-stranded nucleic acids. Using ROMP-derived, NBE-based monoliths, the separation of oligothymidylic acids $(dT)_{12-18}$ ranging in mass from 3,638 D (dT_{12}) to 5,456 D (dT_{18}) was accomplished on a semi-preparative scale within 2 min (Figure 2).[13]

As expected, the elution order of oligodeoxynucleotides strongly correlated with their molecular mass, suggesting that an increase in molecular mass directly translates into an increase in hydrophobic interaction of the corresponding analyte with the monolith. In addition, a mixture of eight proteins (ribonuclease A, insulin, cytochrome c, lysocyme, α-lactalbumin, α-chymotrypsinogen A, ß-lactoglobulin B, catalase) was separated in less than 90 s by RP-chromatography.[13]
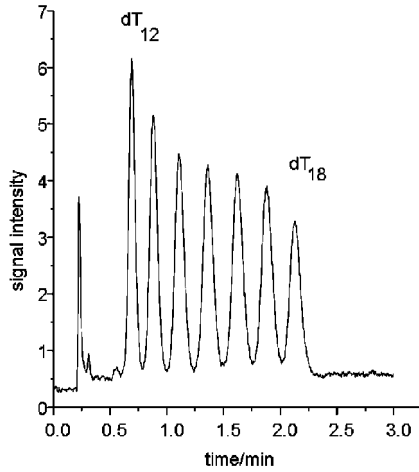
Figure 2. Separation of proteins on a capillary monolith (0.2 × mm). (1) ribonuclease A, (2) insulin (3) lysozyme, (4) albumin, (5) myoglobin, (6) β-lactoglobulin. Chromatographic conditions: mobile phase: (A) 95% water, 5% acetonitrile, 0.05% TFA, (B) 80% water, 20% acetonitrile, 0.04% TFA, 25°C; detector: UV 190 nm. Gradient (i): 0–60% (B) 0–30 min, 60–90% (B) within 5 min, flow 0.8 µL/min. Gradient (ii): 10–60% (B) within 7 min, 60–90% (B) within 2.5 min, flow 1.8 µL/min.
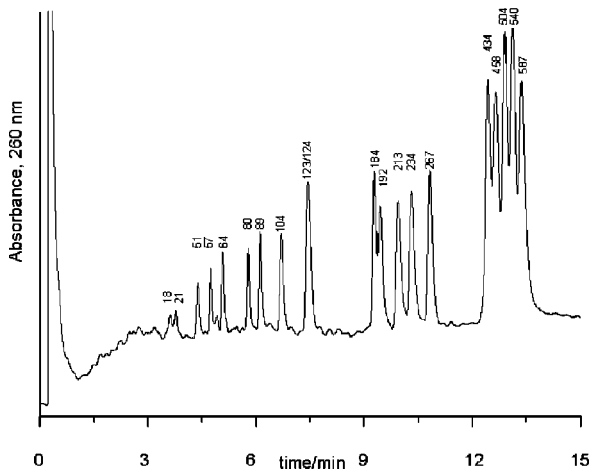
Figure 3. Analysis of human insulin in interstitial fluid samples using capillary monoliths of (a) 8 cm × 200 µm i.d. and (b) 8 cm × 50 µm i.d. Interstitial fluid samples diluted (a) 1:10 and (b) 1:160 and spiked with (1) human insulin (100 fmol/µL), injection volume 1 µL. Mobile phase: (A) 95% water, 5% acetonitrile, 0.05% TFA, (B) 20% water, 80% acetonitrile, 0.04% TFA; gradient: 0–30 min 0–60% B; 50–90% B within 5 min; flow (a) 1.5 µL/min, (b)0.5 µL/min; 25°C; UV 190 nm.

Encouraged by the high efficiency of these columns, we turned our attention to the separation of double-stranded (*ds*) DNA.[20] The separation of pBR322 DNA-HaeIII fragments could in fact be accomplished on monolithic systems using a two-step gradient (Figure 3). The amount of DNA material that could be loaded onto a 100×3 mm i.d. column without serious loss in separation efficiency was about 2.5 µg.

3.5. MINIATURIZED SYSTEMS: MONOLITHIC CAPILLARY COLUMNS[21]

In order to contribute to ongoing efforts towards the miniaturization of analytical devices and to develop systems applicable to the coupling to highly sensitive quantification methods such as mass spectroscopy, we investigated whether the concept of ROMP-derived monolithic supports could be extended to the synthesis of capillary columns. For that purpose, we simply used the synthetic concepts, recipes and procedures elaborated for semi-preparative scale separations to capillary columns. A separation of single-stranded oligodeoxynucleotides $(dT)_{12-18}$ by IP-RP-HPLC on a monolithic, ROMP-derived capillary column is illustrated in Figure 4.
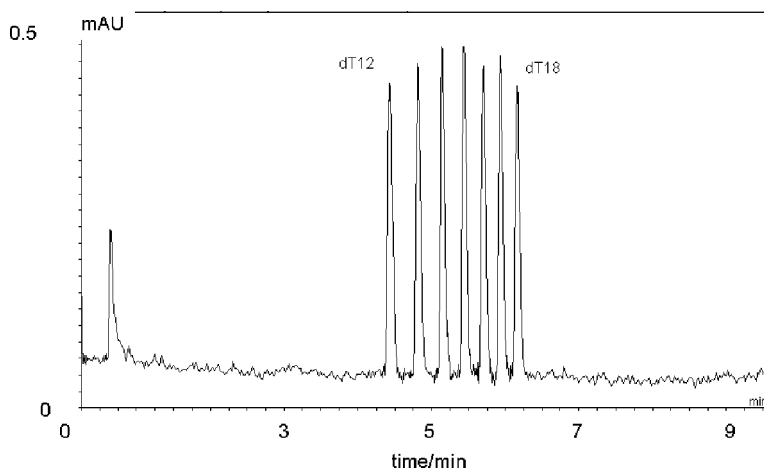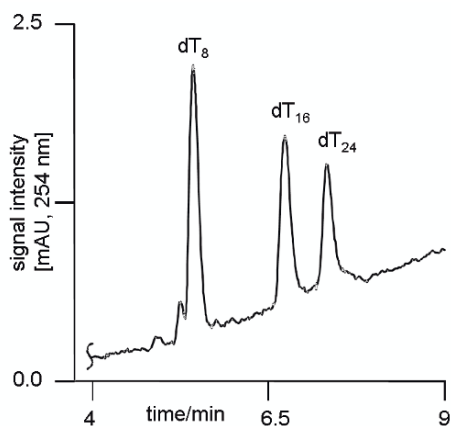

Figure 4. Separation of dT_8, dT_{16} and dT_{24} (2 ng each) on a functionalized, monolithic NBE-based capillary column (57×0.2 mm) *via* anion-exchange chromatography. Mobile phase: 20 mM ammonium acetate, pH = 5.0, 80% water, 20% acetonitrile, linear gradient 0–1.0 M NaCl within 10 min, flow = 3.1 µL/min, 25°C; UV (254 nm).

Using 0.2 mm i.d. capillaries, high resolution was achieved for all seven analytes ($2.27 < R_s < 3.47$). In addition, four homologous oligodeoxynucleotides, ranging in length from 24–27 nucleotides and differing from each other by the insertion of one, two and three thymidines after position 18 of the 24-mer were baseline separated within 7 min.[21] Using three different standard systems, we

also checked the run-to-run precision, the reproducibility of synthesis as well as the influence of changes in polymerization parameters on separation efficiency and counter pressure. Investigations on the run-to-run precision revealed that e.g. for proteins (lysozyme A, ribonuclease, insulin, cytochrome C, myoglobin), deviations in retention times were <1.4%.[22] The fragments ranging in size from 51 to 587 base pairs were separated by capillary IP-RP-HPLC. The excellent separation efficiency of ROMP-based monoliths for *ds*DNA was documented in peak widths at half height of 3.1–8.5 s for the fragments up to about 250 base pairs. Longer DNA fragments eluted with peak widths at half height around 10–12 s. These higher peak widths were a result of the shallower gradient required for total resolution. The use of a steep gradient ensured the rapid elution of the proteins as extremely sharp peaks with peak widths at half height between 1 and 2 s. The selectivity was high, allowing for the separation of all components to baseline within less than 5 min. Finally, it is worth mentioning that NBE-based monolithic supports were also found capable of separating diastereomeric phosphorothioates.[21]

Reproducibility of synthesis was checked by determining the relative standard deviation (RSD) in retention times (t_R), which was found to be in the range of 2.9% to 3.9% for all analytes. The long-term stability of the COE-based mono-lithic columns was checked after more than 1,000 runs at 50°C and revealed excellent stability of the columns, thus proofing the concept of replacing NBE- by COE-based monomers and crosslinkers (*vide supra*). No significant alteration in separation performance was observed, however retention times slightly decreased after 1,200 injections (approx. 1.6–7.2% for all analytes). ROMP-derived capillary monoliths were also found applicable to separation problems common in medical research.[23] Thus, insulin and various insulin analogues used in diabetic treatment were analyzed. A comparison of the separation efficiency of a monolithic capillary column with a particle-based capillary column was performed. The monolithic column showed equivalent separation efficiency compared to Vydac C4 and Zorbax C3-based stationary phases. Moreover, the high permeability of monoliths enabled chromatographic separations at higher flow rates, thus shortening analysis times to about one-third without any loss in separation efficiency. For the analysis of insulin in human biofluid samples, enhanced sensitivity was achieved by using a 50 μm i.d. ROMP-derived monolith. For purposes of completeness, it should be mentioned that ROMP-derived, NBE-based columns have also been successfully applied in voltage-assisted capillary LC.[24]

3.6. FUNCTIONALIZED ROMP-DERIVED POLYMERIC MONOLITHS

ROMP triggered with Schrock or Grubbs-type initiators is a living polymerization process. Using the active initiator covalently bound to the surface of the structure-forming microglobules after completed rod-formation, various functional

monomers have been grafted onto the monolith surface by simply passing solutions thereof through the mold. This way, linear polymer chains were attached to the inner surface of the monolith. This approach generally offers some advantages. First, the structure of the "parent" monolith is not affected by the functional monomer and can be optimized regardless of the functional monomer used later. Second, solvents other than the porogens, e.g. methanol, methylene chloride, dimethylformamide, can be used for this "*in situ*" derivatization.[25] The versatility of this concept was demonstrated by grafting various functional NBE- or 7-oxanorbornene-based monomers, e.g. ester-, amine-, phenol-, ß-cyclodextrin-, imidazolium salt-, carboxylic acid-containing ones onto the monoliths' surface. Using a ß-CD-derivatized monolith, the chiral separation of proglumide was accomplished.[12] In extension to this chemistry, a post-synthesis grafting method was developed that offers access to high capacity functionalized monolithic systems. By applying this method, the amounts of grafted monomers exceeded 1 mmol/g.[26] Recently, ROMP-derived, norborn-2-ene-based monoliths were subject to *in situ* surface functionalization using 2-(N,N-dimethylaminoethyl)norborn-5-ene-2-ylcarboxylic amide. The resulting functionalized monoliths were successfully used in anion-exchange chromatography of oligodeoxynucleotides.[27] Figure 5 illustrates the separation of oligo-deoxythymidylic acids dT_8, dT_{16} and dT_{24}. Though resolution was lower compared to octamethylferrocene-derivatized silica columns prepared *via* 1-alkyne graft polymerization[28] (*vide supra*), sufficient separation efficiency was achieved allowing for the base line separation of these analytes. Peak half widths were in the range of 8.4–11.4 s, peak resolution was 4.59 and 2.14, respectively.

Figure 5. Separation of dT_8, dT_{16} and dT_{24} (2 ng each) on a functionalized, monolithic NBE-based capillary column (57 × 0.2 mm) *via* anion-exchange chromatography. Mobile phase: 20 mM ammonium acetate, pH = 5.0, 80% water, 20% acetonitrile, linear gradient 0–1.0 M NaCl within 10 min, flow = 3.1 μL/min, 25°C; UV (254 nm).

Recently, ROMP has also been used for the post synthesis functionalization of electron-beam curing-derived,[29–32] (meth-)acrylate-based polymeric monolithic materials.[33] These were prepared *via* the copolymerization of norborn-2-ene-5-yl acrylate with TMPTA and EMA. In contrast to the acrylate and methacrylate moieties, the NBE groups did not undergo free radical polymerization in course of the electron-beam triggered process and could thus, after monolith formation, be reacted with either $RuCl_2(PCy_3)_2(CHPh)$ or $RuCl_2(PCy_3)(1,3$-dimesityl-dihydroimidazolin-2-ylidene)(CHPh). After the surface attachment of the initiators was completed, a variety of functional monomers was successfully grafted onto the surface of these supports (Scheme 2). Grafting densities up to 290 μmol monomer/g were realized. For purposes of completeness, a comparative study of the separation performance of ROMP-based NBE- and COE-derived monolithic columns with electron beam curing-derived ones shall be mentioned.[32] All columns investigated allowed for the rapid separation of proteins, however, the novel electron beam curing-derived polymeric columns allowed for the fastest separation of these analytes with sufficient peak resolution.
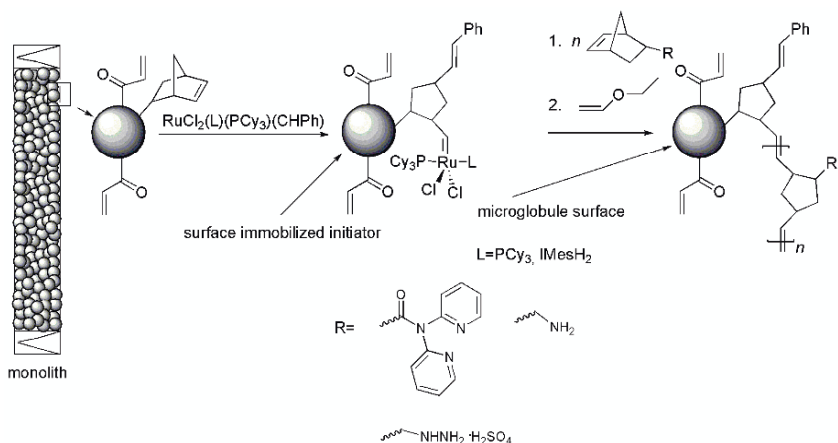
Scheme 2. Post synthesis functionalization of electron-beam curing-derived monolithic supports *via* ROMP ($IMesH_2$ = 1,3-dimesityldihydroimidazolin-2-ylidene).

4. Monolith-Immobilized Catalysts

In order to overcome the problems commonly related to catalysts immobilized to beaded catalysts, we aimed on the synthesis of non-porous supports suitable for continuous flow experiments, e.g. monolithic supports. Using a ROMP-based protocol, we were able to synthesize functionalized monoliths.[12, 34, 35] These were designed in a way that only interparticle porosity was generated, whereas the structure-forming microclobules were virtually non-porous. Taking advantage of the "living" character of ruthenium-catalyzed ROMP used for

their synthesis and the high tolerance of the catalytic system towards different functional monomers we were able to graft cationic NHC-precursors onto the surface. Tentacle-like polymer chains attached to the surface were formed. The free NHC necessary for catalyst formation were simply generated by passing a strong base such as 4-dimethylaminopyridine (DMAP) over the support. In a last step the catalyst was formed and simultaneously immobilized by passing a solution of $Cl_2Ru(CHPh)(PCy_3)_2$ over the rigid rod. Loadings of up to 1.4% of Grubbs-catalyst on NHC base were achieved. Monolith-immobilized metathesis catalysts prepared by this approach showed high activity in various metathesis-based reactions such as ROMP and RCM. The use of chain-transfer agents (CTAs, e.g. cis-1,4-diacetoxybut-2-ene, DEDAM, 2-hexene) allowed the regulation of molecular mass, in particular in the case of cyclooctene. The presence of CTAs additionally enhanced the lifetime of the catalytic centres by reducing the average concentration of ruthenium methylidenes, thus allowing the prolonged use of these systems. Additionally, both the tentacle-type structure and the designed microstructure of the support reduced diffusion to a minimum. In a benchmark reaction with DEDAM, these properties directly translated into high average TOFs of up to 0.5 s^{-1}.

In an alternative approach, we prepared a monolith-supported second-generation Grubbs catalysts containing the saturated IMesH2 ligand by a synthetic protocol summarized in Scheme 3.[36, 37] Surface-derivatization of the monolith was carried out with 7-oxanorborn-2-ene-5,6-dicarboxylic anhydride followed by conversion of the grafted poly(anhydride) into the corresponding poly-silver salt. This poly-silver salt was used for the halogen exchange with the second-generation Grubbs catalyst $RuCl_2(PCy_3)(IMesH_2)(=CHPh)$.

In the benchmark reaction with DEDAM, TONs close to 1,000 were achieved. It is worth mentioning that these systems benefit from the presence of free silver carboxylate groups, which act as a reversible scavenger for phosphine. Thus, the use of monocarboxylic acids such as 7-oxanorborn-2-ene-5-carboxylic acid instead of the anhydride results in a supported catalyst that shows significantly reduced TONs in the RCM of DEDAM. Again, the use of silica as support results in low TONs around 120. This comparably low activity of silica-based systems is attributed to both the non-reversible scavenging of the phosphine by residual silanol groups and to diffusion-controlled reactions and can in fact be overcome by the use of the above-mentioned monolithic systems.
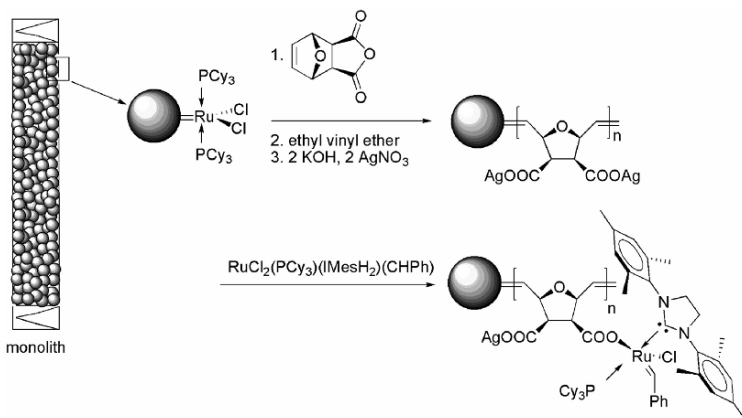
Scheme 3. Synthesis of a monolith-bound Grubbs-type catalyst based on *vic*-dicarboxylates.
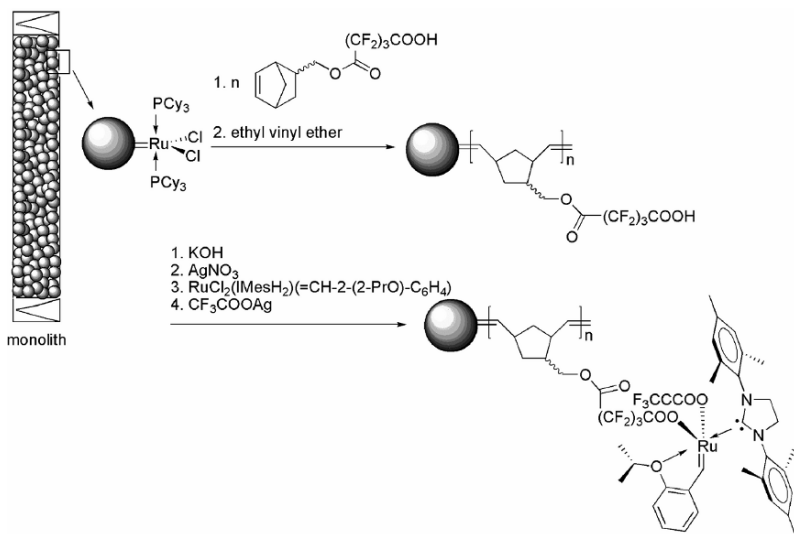
Scheme 4. Synthesis of a monolith-bound second-generation Grubbs-Hoveyda-type catalyst based on fluorocarboxylates.

In view of these results we tried to further enhance the reactivity of Ru-based metathesis catalysts and to avoid the use of phosphine ligands. In due consequence, numerous variations in Hoveyda-type catalysts of the general formula $RuCl_2(IMesH_2)(=CH-2-(2-PrO-C_6H_4))$ were carried out. Among the most important findings was that the exchange of chlorine by a strongly electron-withdrawing group in fact enhanced the reactivity of these systems without sacrificing their high stability.[38] Thus, $Ru(CF_3CO_2)_2(IMesH_2)(=CH-2-(2-PrO)-C_6H_4)$ was a highly active catalysts in RCM both at 45°C and 20°C, respectively, exceeding known ruthenium-based catalysts in catalytic activity.

TONs up to 1,800 and 1,400, respectively, were achieved in the RCM of DEDAM. High activity was also observed in enyne metathesis and ring-opening-cross metathesis using norborn-5-ene and 7-oxanorborn-5-ene-derivatives. A monolith-supported version of this catalyst was prepared and used in continuous flow experiments (Scheme 4).[39] TOFs of 0.11 s^{-1} were observed, TONs were >500. It is worth mentioning that the TONs obtained with these two supported versions so far exceed all published data on supported well-defined metathesis catalysts.

Acknowledgement

References

[1] Penczek, S., Kubisa, P., Szymanski, R., 1991, *Makromol. Chem. Rapid Commun.*, **12**: 77–80.

[2] Matyjaszewski, K., 1993, *Macromolecules*, **26**: 1787–1788.

[3] Peters, E. C., Švec, F., Fréchet, J. M. J., Viklund, C., Irgum, K., 1999, *Macromolecules*, **32**: 6377–6379.

[4] Schrock, R. R., 1990, *Acc. Chem. Res.*, **23**: 158–165.

[5] Schrock, R. R., 1993, *Ring-Opening Polymerization*, 1st ed., Hanser, Munich, pp. 129–156.

[6] Švec, F., Tennikova, T. B., Deyl, Z., 2003, *Monolithic Materials: Preparation, Properties and Application* (In: J. Chromatogr. Libr., Ed.), Elsevier, Amsterdam, Vol. 67, pp. 1–773.

[7] Švec, F., 2004, *LC-GC: LC Column Technol. Suppl.*, **June**: 18.

[8] Švec, F., 2005, *LC-GC Europe*, **18**: 17–20.

[9] Švec, F., Huber, C. G., 2006, *Anal. Chem.*, **78**: 2100–2107.

[10] Švec, F., Geiser, L., 2006, *LCGC North America*, **24(S4)**: 22–27.

[11] Buchmeiser, M. R., 2007, *Polymer*, **48**: 2187–2198.

[12] Sinner, F., Buchmeiser, M. R., 2000, *Angew. Chem.*, **112**: 1491–1494.

[13] Mayr, B., Tessadri, R., Post, E., Buchmeiser, M. R., 2001, *Anal. Chem.*, **73**: 4071–4078.

[14] Buchmeiser, M. R., 2004, *New. J. Chem.*, **28**: 549–557.

[15] Buchmeiser, M. R., 2003, Metathesis-Based Polymers for Organic Synthesis and Catalysis, In: *Polymeric Materials in Organic Synthesis and Catalysis*, 1st ed., Wiley-VCH, Weinheim, pp. 1–559.

[16] Buchmeiser, M. R., 2005, *Metathesis Polymerization from and to Surfaces*, In: Adv. Polym. Sci. (Surface-Initiated Polymerization I), Springer, Berlin/Heidelberg/New York, Vol. 197, pp. 137–172.

[17] Love, J. A., Morgan, J. P., Trnka, T. M., Grubbs, R. H., 2002, *Angew. Chem.*, **114**: 4207–4209.

[18] Halász, I., Martin, K., 1978, *Angew. Chem.*, **90**: 954–961.

[19] Bandari, R., Prager-Duschke, A., Kühnel, C., Decker, U., Schlemmer, B., Buchmeiser, M. R., 2006, *Macromolecules*, **39**: 5222–5229.

[20] Lubbad, S., Mayr, B., Huber, C. G., Buchmeiser, M. R., 2002, *J. Chromatogr. A*, **959**: 121–129.

[21] Mayr, B., Hölzl, G., Eder, K., Buchmeiser, M. R., Huber, C. G., 2002, *Anal. Chem.*, **74**: 6080–6087.

[22] Gatschelhofer, C., Magnes, C., Pieber, T. R., Buchmeiser, M. R., Sinner, F. M., 2005, *J. Chromatogr. A*, **1090**: 81–89.

[23] Sinner, F. M., Gatschelhofer, C., Mautner, A., Magnes, C., Buchmeiser, M. R., Pieber, T. R., 2008, *J. Chromatogr. A.*, **1191**: 274–281.

[24] Sedláková, P., Miksik, I., Gatschelhofer, C., Sinner, F. M., Buchmeiser, M. R., 2007, *Electrophoresis*, **28**: 2219–2222.

[25] Buchmeiser, M. R., Lubbad, S., Mayr, M., Wurst, K., 2003, *Inorg. Chim. Acta*, **345**: 145–153.

[26] Lubbad, S., Buchmeiser, M. R., 2003, *Macromol. Rapid Commun.*, **24**: 580–584.

[27] Eder, K., 2007, *Macromol. Rapid Commun.*, **28**: 2029–2032.

[28] Eder, K., Reichel, E., Schottenberger, H., Huber, C. G., Buchmeiser, M. R., 2001, *Macromolecules*, **34**: 4334–4341.

[29] Bandari, R., Knolle, W., Prager-Duschke, A., Buchmeiser, M. R., 2007, *Macromol. Chem. Phys.*, **208**: 1428–1436.

[30] Bandari, R., Knolle, W., Buchmeiser, M. R., 2007, *Macromol. Symp.*, **254**: 87–92.

[31] Bandari, R., Elsner, C., Knolle, W., Kühnel, C., Decker, U., Buchmeiser, M. R., 2007, *J. Sep. Sci.*, **30**: 2821–2827.

[32] Bandari, R., Knolle, W., Buchmeiser, M. R., 2008, *J. Chromatogr. A.*, **1191**: 268–273.

[33] Bandari, R., Knolle, W., Buchmeiser, M. R., 2007, *Macromol. Rapid Commun.*, **28**: 2090–2094.

[34] Sinner, F., Buchmeiser, M. R., 2000, *Macromolecules*, **33**: 5777–5786.

[35] Mayr, M., Mayr, B., Buchmeiser, M. R., 2001, *Angew. Chem.*, **113**: 3957–3960.

[36] Krause, J. O., Lubbad, S., Mayr, M., Nuyken, O., Buchmeiser, M. R., 2003, *Polym. Prepr. (Am. Chem. Soc., Div. Polym. Chem.)*, **44**: 790–791.

[37] Krause, J. O., Lubbad, S., Nuyken, O., Buchmeiser, M. R., 2003, *Adv. Synth. Catal.*, **345**: 996–1004.

[38] Krause, J. O., Wurst, K., Nuyken, O., Buchmeiser, M. R., 2004, *Chem. Eur. J.*, **10**: 777–784.

[39] Krause, J. O., Lubbad, S. H., Nuyken, O., Buchmeiser, M. R., 2003, *Macromol. Rapid Commun.*, **24**: 875–878.

SYNTHESIS OF BIODEGRADABLE MATERIALS AND CHEMICAL SENSORS VIA ROMP

EZAT KHOSRAVI[*], IZABELA CZELUSNIAK, GEORGI GRANCHAROV, RITU KATAKY, ALAN M. KENWRIGHT, AND CHRIS W. G. ANSELL
Polymer IRC, Durham University, Durham DH1 3LE, UK

Abstract: This chapter will aim to (A) demonstrate that ring opening metathesis polymerisation (ROMP) is a power tool in macromolecular engineering and (B) show the usefulness of the ruthenium initiators in the synthesis of highly functionalised macromolecules. It will be shown that the combination of these two important characteristics allows the design and synthesis of polymers with novel topologies for target applications. The first example discussed is the design and synthesis of polymeric biodegrabable materials with controlled degradation. The second example discussed is the synthesis and characterisation of polymeric ionophoric channels based on 7-oxanorbosrnenes, as chemical sensor.

1. Synthesis of Biodegradable Materials

1.1. INTRODUCTION

Biodegradable polymers and copolymers prepared from cyclic esters, such as glycolide (GL), lactide (LA) or ε-caprolactone (CL) have been widely used as sutures, drug delivery carriers and implants to ensure a temporary mechanical or therapeutic function, as well as cell scaffolds in tissue engineering.[1–4] These polymers decompose via hydrolysis of the ester bonds in an aqueous environment and give readily-absorbable degradation products (CO_2 and H_2O).[4] All the practical uses of these materials involve their biodegradable character and thus their decomposition profile has to be matched to the requirements of the application. The degradation rate of the polymeric material depends on many factors, including the polymer composition, molecular weight distribution, the presence of catalysts, and the geometry of the device.[2, 5–7] As a consequence, there is increasing

interest in methods that allow the preparation of polymers which degrade in a controlled fashion. In this respect the preparation of tailored macromolecular architectures remains an important challenge in biodegradable materials. Various materials based on polyhydroxyacids with a broad range of properties have been obtained by copolymerisation of different comonomers,[8, 9] ring opening polymerisation (ROP) with multifunctional initiators[10] and also by combination of different polymerisation techniques.[11–15]

The work reported here involves the synthesis of well-defined biodegradable graft copolymers with polylactide (PLA) side chains and oxanorbornene backbones via ring opening metathesis polymerisation (ROMP).[16] The presence of the oxygen in 7 position makes the backbone more hydrophilic[17] and hence increases the biocompatibility of the backbone.

1.2. RESULTS AND DISCUSSION

1.2.1. *Synthesis of PLA Macromonomers*

PLA macromonomers terminated with an oxanorbornyl group were synthesized by ROP of D,L-lactide in the presence of mono or di-alcohol derivatives of oxanorbornene as an initiator (Scheme 1). Stannous octoate, also known as tin(II) 2-ethylhexanoate, $Sn(Oct)_2$, was chosen as catalyst for three reasons. First, $Sn(Oct)_2$ is one of the most widely used compounds for initiating the ROP of various lactones and lactides.[18, 19] It is easy to handle and soluble in common organic solvents. Second, this catalyst is highly efficient and allows almost complete conversions even at low concentration.[20] Finally, $Sn(Oct)_2$ has been accepted as a food additive by the U.S. FDA because its toxicity is extremely low compared to other heavy metal salts.
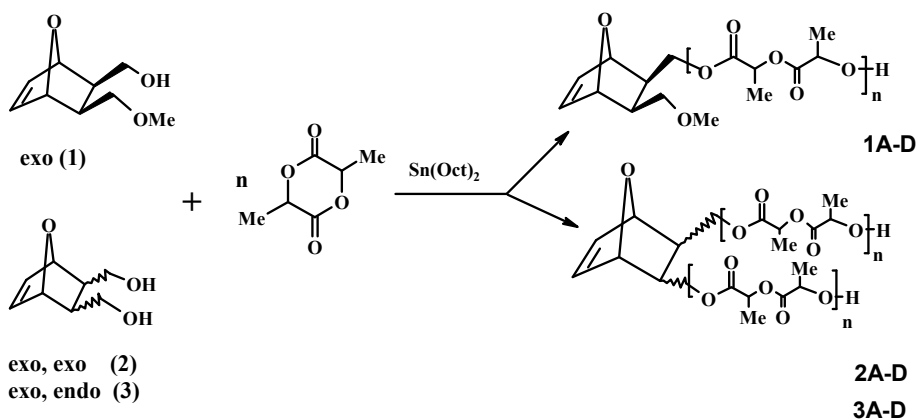
Scheme 1. Synthesis of PLA macromonomers with one (1) and two PLA chains (2 and 3).

A series of macromonomers with different PLA chain length were prepared and characterised (**1A–D**, **2A–D**, **3A–D**), Scheme 1. Their characteristics are presented in Table 1. All PLA macromonomers were characterised by ^{1}H NMR spectroscopy and Size Exclusion Chromatography (SEC). The oxanorbornyl end-group of the PLA chain is readily observed by ^{1}H NMR spectroscopy. The main evidence for attachment of the oxanorbornyl group is the chemical shift of the methylene groups. For example, after ROP of LA initiated by alcohol **2** signals corresponding to methylene protons shifted to lower frequency (down to 4.33 and 4.06 ppm). It is possible to calculate the PLA/oxanorbornene molar ratio by integration of the methylene protons of PLA and the olefinic protons of the oxanorbornyl group and, therefore, calculate the average number of LA units in PLA chain end-capped with oxanorbornene group (degree of LA polymerisation, DP). For low molecular weight PLA macromonomers (up to 25 LA units per chain) these values agree within experimental error with the theoretical value. However, with higher molecular weight PLA macromonomers, similar calculations do not provide any useful information. This is explained by the large differences in intensity between signals due to PLA and oxanorbornene.

TABLE 1. Characterisation of PLA macromonomers (M) synthesised by ROP of LA catalysed by Sn(Oct)$_2$.[a]

ROH	[LA]/ [OH]	M	Time (h)	Theor M_n	SEC Analysis			^{1}H-NMR Analysis	
					M_n	PDI	DP	M_n	DP
1	5	**1A**	24	890	–	–	–	1,030	6
	10	**1B**	24	1,610	1,430	1.28	9	1,610	10
	25	**1C**	24	3,770	3,540	1.24	23	3,480	23
	50	**1D**	72	7,370	7,270	1.20	49	8,810	60
2	5	**2A**	24	1,600	–	–	–	1,600	5
	10	**2B**	24	3,040	3,470	1.22	11	3,040	10
	25	**2C**	72	7,360	5,690	1.27	19	5,340	18
	50	**2D**	7 days	14,560	6,900	1.90	23	14,840	51
3	5	**3A**	24	1,600	–	–	–	1,600	5
	10	**3B**	24	3,040	2,960	1.27	10	3,320	11
	25	**3C**	72	7,360	6,930	1.32	23	6,200	21
	50	**3D**	7 days	14,560	8,260	1.51	28	10,240	35

[a] Reaction conditions: [LA]$_0$= 1M; [LA]$_0$/[Sn(Oct)$_2$]$_0$ = 200; solv. PhMe, T = 70°C.

The lack of agreement between molecular weights of macromonomers measured by SEC against polystyrene standards and those calculated from ^{1}H NMR results arises from differences in the hydrodynamic volume of polystyrene relative to PLA macromonomer. The degree of LA polymerisation was in good agreement with the lactide-to-alcohol ratio only in the case of macromonomers with one PLA chain (**1A–D**). For macromonomers containing two PLA chains

(2A–D and 3A–D), the average number of LA units in the PLA chains decreased as the lactide-to alcohol molar ratio increased. These results can be explained by consideration of the mechanism of initiation involved in the reaction of alcohol with $Sn(Oct)_2$.[21–23] Impurities such as water or 2-ethylhexanoic acid, which are always present in commercial $Sn(Oct)_2$, may act also as co-initiators and hence increase the molecular weight distribution of PLA macromonomer.[23] Moreover, inspection of the MALDI-TOF mass spectra of the macromonomers proves the presence of an intermolecular transesterification side reaction.[24] The spectra show the presence of two distinct series of signals with higher and lower intensity. The higher intensity series comes from PLA macromonomers with an even number of lactoyl $(C(O)CH(CH_3)O)$ repeating units. However, the side-reaction leads to macromonomers with an odd number of lactoyl units, which is observable as the lower intensity series.

1.2.2. Synthesis of Graft Copolymers

Well-characterised macromonomers with one (**1A–D**) and two (**2A–D** and **3A–D**) PLA chains of varying lengths were subjected to ROMP using ruthenium Grubbs catalysts, **I–III**, Figure 1. These initiators are the most widely used initiators for ROMP due to their excellent functional group tolerance.[25–27] The living polymers were terminated using ethyl vinyl ether to give the final product. The molecular weight of the graft copolymer was controlled by varying the macro-monomer-to-initiator molar ratio [M]/[I]. All graft copolymers were characterised by SEC to estimate the amount of unreacted macromonomer. As discussed above, only relative, molecular weights can be calculated against polystyrene standards due to the different hydrodynamic volumes the copolymers.
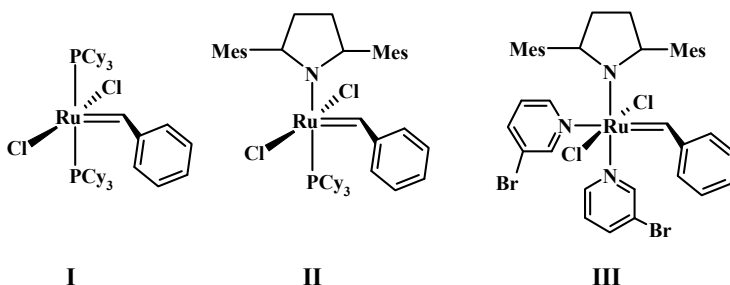
Figure 1. Well-defined Grubbs ruthenium initiators.

The graft copolymers (GC) prepared are shown in Scheme 2. The macro-monomer **1A** was polymerised well with ruthenium initiator **I** to produce GCP1. Examination of the ^1H NMR spectra of the copolymer showed no signals due to the oxanorbornyl end-group in the macromonomer. However, the SEC chrom-atogram of this product showed the presence of a major high molecular weight

peak and a minor low molecular weight peak. The low-molecular-weight peak had the same retention time as that of macromonomer **1A** and extended reaction times did not significantly diminish the intensity of this signal. Thus, we concluded that graft copolymers were contaminated with PLA homopolymer without an oxanorbornene end group (uncapped PLA) produced in a side reaction during ROP of LA.

The behaviour of these PLA macromonomers in ROMP is due to steric crowding, which develops between macromonomers as they are added to the growing graft copolymer.[14] In contrast to macromonomers having two PLA side chains on the same oxanorbornene unit (**GCP2** and **GCP3**), copolymers can be prepared from macromonomers with one PLA chain per unit (**GCP1**) with longer backbone and side-chains as a consequence of reduced steric hindrance.[28] We expected that difficulties with the synthesis of higher molecular weight copolymers by ruthenium initiator **I** could be overcome by using a more active initiator, namely the second generation ruthenium initiator **II**. The replacement of one of the phosphine ligands with an N-heterocyclic carbene ligand gives a complex which displayed dramatically improved metathesis activity, thermal stability and inertness towards oxygen and moisture compared with ruthenium initiator **I**. It is generally accepted that this ruthenium initiator is not an appropriate choice for the of ROMP of most monomer systems.[29] However, sterically hindered substrates with bulky substituents have been successfully polymerised to yield polymers with a low PDI.[14, 15] In our studies macromonomers containing two PLA chains (**2A–D** and **3A–D**) were subjected to ROMP by ruthenium initiator **II**. Although the ruthenium initiator **II** polymerised the sterically hindered endo,exo-macromonomer with 10 LA units in each chain (**3B**) to completion after 2 h, a broad molecular weight distribution of copolymer product was observed.

Since the ROMP of PLA macromonomers by ruthenium initiator **II** results in largely uncontrolled polymerisation processes, we decided to use ruthenium initiator **III**. Previous investigations have shown high activity of initiator **III** in the ROMP of endo,exo 2,3-disubstituted norbornene moieties.[30–32] In addition, in contrast to ruthenium initiator **II**, in the presence of this complex polymerisations exhibit much higher values of k_i relative to k_p and hence yield polymers with narrow molecular weight distributions.[26, 30, 31] When a green solution of ruthenium initiator **III** was added to a colourless solution of monomer, the colour immediately changed to yellow, which implies the immediate initiation of ruthenium initiator **III**. The polymerisations of PLA macromonomers with one short chain per oxanorbornene (**1B**) went to completion for [M]/[**III**] of 10 and 25. Experiments to polymerise macromonomers containing two exo-PLA chains (**2A–D**) with ruthenium initiator **III** resulted in high conversions at short reaction times. All the graft copolymers produced were contaminated with PLA homopolymer, as discussed above. The amounts of uncapped PLA estimated

from SEC chromatograms of the copolymers depended on the molar ratio of LA
to alcohol-substituted oxanorbornene and slightly increased with increasing
length of PLA chain in the macromonomer. Therefore, we used the difference
in solubility in CH_2Cl_2 between the macromonomers and copolymers to develop
a procedure for the purification of the graft copolymers. SEC chromatograms of
the purified white material showed only one high molecular weight peak due to
graft copolymers. The signal due to uncapped PLA observed in SEC chromato-
grams of the crude material disappeared after passing the crude material through a
silica column. Moreover, the purification method allowed the removal not only
of uncapped PLA but also of unreacted macromonomer. The PDI's for the
column-purified graft copolymers produced by ROMP using ruthenium initiator
III were in the range of 1.05 and 1.14, indicating a well-behaved polymerisation
reaction.
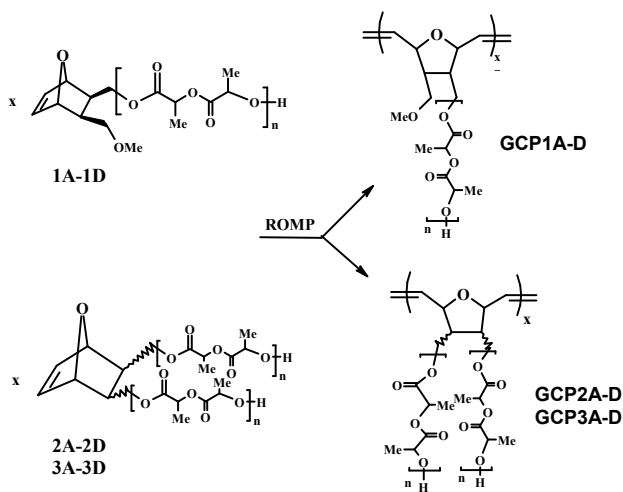
Scheme 2. ROMP of PLA macromonomers using Grubbs ruthenium initiators.

1.3. HYDROLYTIC DEGRADATION OF MACROMONOMERS AND GRAFT
COPOLYMERS

Various graft copolymers with 10 oxanorbornene units in the backbone chain
and varying lengths of PLA side-chains were selected for hydrolysis studies,
GCP1–GCP3, Figure 2. All experiments were carried out in phosphate buffered
saline (PBS) at 50°C. The influence of various parameters on the kinetics of
degradation has been examined including the polyoxanorbornene/PLA ratio,
different configurations of PLA side chain on polyoxanorbornene backbone
chain and the purification of copolymer. Before immersion, the specimens are
generally transparent and colourless (macromonomers) or slightly yellow

(copolymers). They became progressively whitish or yellowish with ageing time, and their brittleness also increased. Moreover, the degrading polymer samples became thinner and hollow as the hydrolysis time increased.
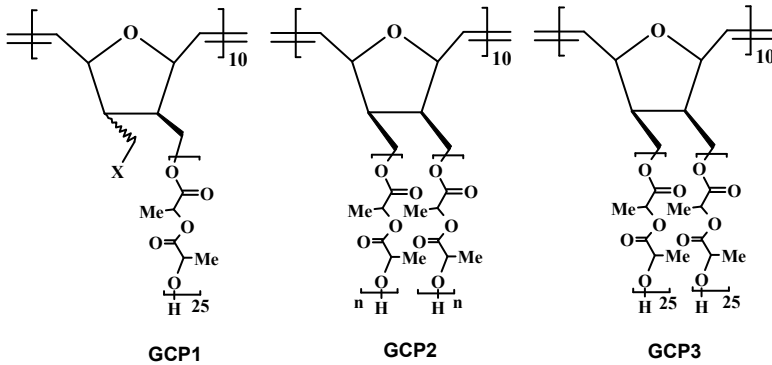
Figure 2. Graft copolymers **GCP1–GCPP3** used for the hydrolysis studies.

Figure 3 shows the changes of average molar weights as determined from SEC chromatograms of degraded graft copolymers bearing two *exo*-PLA side chains with different length (**GCP2**). The initial decrease of molecular weights was substantially smaller in the case of copolymers containing side-chains with 10 LA units. Additionally, the rate of molecular weight loss after the induction period was clearly higher for graft copolymer bearing long PLA chains. These results indicate that the proportion of oxanorbornene/LA units ratio in the copolymer plays an important role in the degradation of material and that shorter PLA chains lead to a lower rate of copolymer degradation.
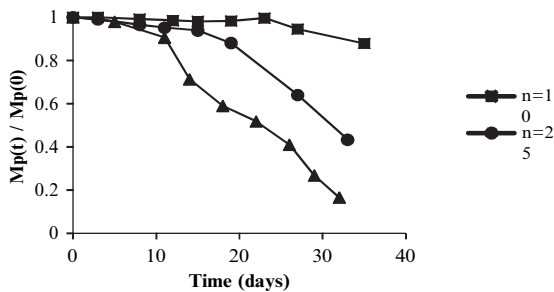
Figure 3. Degradation of *exo,exo*-copolymers with different length of PLA side-chains (GCP2) in PBS at 50°C.

The influence of the different configurations of PLA side chain (*endo/exo*) on the rate of degradation of these three types of graft copolymers (**GCP1–GCP3**)

was investigated by comparison of the degradation behaviour of copolymers with the same length of backbone and PLA side chains, Figure 4. Among the three copolymers, that with one PLA side-chain (**GCP1**) exhibits the fastest rate of degradation. This result implies that the presence of two PLA side chains on each oxacyclopentane ring in the backbone chain results in steric hindrance and therefore reduces the rate of degradation.
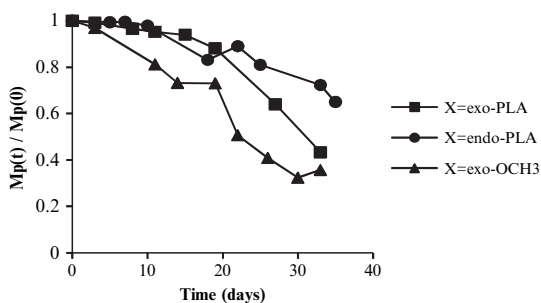
Figure 4. Degradation of various graft copolymers with endo/exo 25 LA units per chain in PBS at 50°C.

It has been established previously that one of the parameters that influence hydrolysis is the presence of impurities in the degradable material.[2] Thus, we decided to perform comparative studies of purified and unpurified *exo,exo*-copolymer (**GCP2**) degradations at 50°C. Unpurified *exo,exo*-copolymer with 25 LA units in each chain contained approximately 20% of uncapped PLA. As shown in Figure 5, degradation of the unpurified material was substantially faster than its purified counterpart. Moreover, the overall rate of degradation of this copolymer is essentially the same as the rate of degradation of macromonomer at the same hydrolysis time. These results clearly show that impurities, such as low molecular-weight PLA increase the rate of hydrolytic degradation of the final copolymer. This behaviour could be explained by the hydrolytic degradation mechanism previously proposed in the case of these graft copolymers. According to that theory heterogeneous degradation causes an increase in the number of carboxylic chain ends, which are known to autocatalyse the ester hydrolysis of PLA side-chains.[33] Studies of the factors governing the bioabsorption rate of L-PLA contaminated with unreacted monomer showed that impure PLA resorbed much more quickly than purified polymer.[34] The hydrolytic degradation was also dependent on the molecular weight of the polymer itself,[6] as well as on the presence of catalysts.[7] Thus, uncapped PLA present in our unpurified material degraded faster than the copolymer and therefore led to an increase in the overall degradation rate.
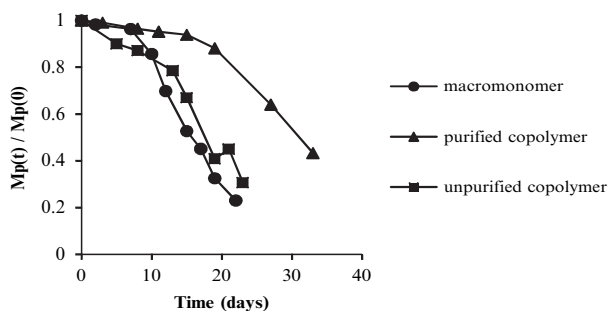
Figure 5. Effect of purification on degradation behaviour of *exo,exo*-copolymers (**GCP2**) with 25 LA units in each side-chains, in PBS at 50°C.

In summary, the synthesis of well-characterised polyoxanorbornene graft copolymers containing PLA grafts using a combination of two polymerisation mechanisms (ROP of lactide and ROMP of oxanorbornene derivatives) has been achieved. A series of well-characterised macromonomers with one *exo*- (**1A–D**) and two: *exo,ex*- (**2A–D**) and *endo,exo*-PLA chains (**3A–D**) were subjected to ROMP by three well-defined Grubbs' ruthenium initiators. The results using Grubbs first generation ruthenium initiator **I** showed that this initiator was ineffective for the polymerisation of macromonomers with two PLA side-chains (**2A–D** and **3A–D**). Although, Grubbs second generation ruthenium initiator **II** was much more active in the ROMP of macromonomers bearing two PLA chains (**2A–D** and **3A–D**), the polymerisation reactions were not well controlled in terms of the molecular weight distributions. Given these results, ruthenium initiator **III** was successfully applied to the synthesis of graft copolymers with long polyoxanorbornene backbone chain and long PLA grafts length.

The hydrolytic degradation of graft copolymers depended to a significant degree on the polyoxanorbornene-to-polylactide molar ratio in copolymers and the rate of degradation of the PLA is greatly reduced by attaching it to poly-oxanorbornene backbone chain. The degradation tests on materials based on pure PLA show 80% weight loss in about 80 days whereas the weight loss for our target graft copolymers is 40% over the same period of time. This clearly demonstrates that the rate of degradation of the PLA is greatly reduced by attaching it to polyoxanorbornene backbone chain.

In addition, the presence of PLA homopolymer as an impurity in the co-polymers significantly increases the rate of degradation of the final material. Therefore, we developed procedure for the purification of copolymers which allowed us to eliminate that factor from the degradation behaviour of the materials.

Our results indicate that, by changing the length of the polyoxanorbornene backbone chain and the PLA grafts, we can tailor the properties of the polymers under degradation to enhance their potential utility in biomedical applications.

2.   Synthesis of Polymeric Chemical Sensors

2.1. INTRODUCTION

The ionophoric properties and complexing ability of crown ethers were discovered by Pedersen in 1960.[35, 36] Crown ethers are well known for their ability to bind a cations of specific size, determined by extraction studies, isolation of complexes, and potentiometric titrations.[37, 38] The ionophoric properties of crown ethers towards specific ions have been systematically analysed, determined and progressively applied that is of great importance in drug-delivery studies, biological, medical and clinical analyses.

   The main objective of this work was the synthesis and characterisation of polymeric ionophores based on substituted 7-oxanorbornenes.[39]

2.2. SYNTHESIS OF MONOMERS

In our studies polymeric acyclic ionophores[40–42] based on a 7-oxanorbornenes were synthesised and characterised. A series of 5,6-substituted-7-oxanorbornene monomers (Figure 6) were prepared and were characterised and determined using ^{1}H and ^{13}C NMR.
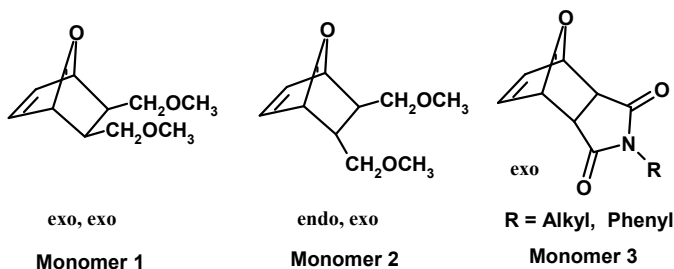
Figure 6. Structures of **Monomers 1–3**.

   Monomer 1, exo, exo-5,6-bis(methoxymethyl) oxanorbornene,[43, 44] was synthesised according to the Scheme 3. Pure exo norbornene dicarboxlic anhydride was prepared via Diels–Alder reaction of furan and maleic anhydride which was reduced to exo, exo-5,6-bis(hydroxylmethyl) oxanorbornene followed by the reaction with NaH and MI to form Monomer 1.
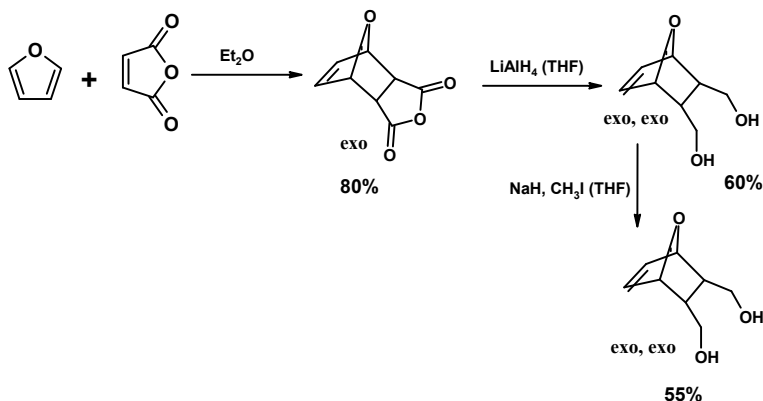
Scheme 3. Synthetic route for the **Monomer 1**.

Monomer 2, 5-endo-6-exo-bis(methoxymethyl)oxanorbornene, [43] was synthesised following Scheme 4. 5-endo-6-exo-bis(chlorocarbonyl) oxanorbornene[45] was prepared via prepared via Diels–Alder reaction of furan and fumaroyl chloride which was reduced to 5-endo-6-exo-bis(hydroxymethyl)oxanorbornene followed by the reaction with NaH and MI to form **Monomer 2**.
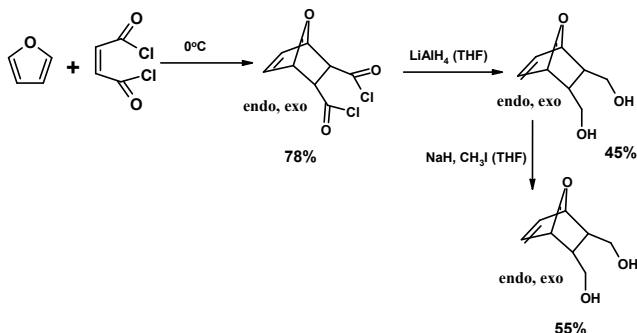
Scheme 4. Synthetic route for **Monomer 2**.

Monomer **3**, N-methyl-7-oxanorbornene-5,6-dicarboximide, was synthesised via Diels–Alder reaction of furan with maleimide in carius tube, Scheme 5.[46]
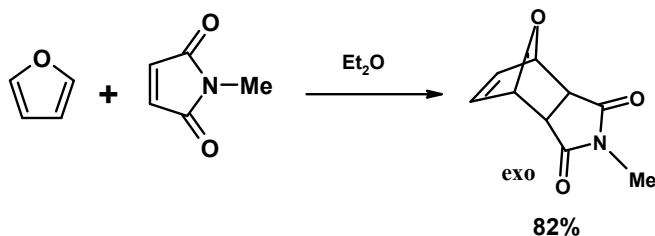
Scheme 5. Synthetic route for **Monomer 3**.

2.2.1. Synthesis of Polymers

Monomers 1–3 were subjected to ROMP using well-defined Grubbs first generation ruthenium initiator to prepare Polymers P1–P3 and the results are shown in Table 2.

TABLE 2. Results of ROMP of Monomers 1–3 to prepare Polymers P1–P3.

Polymer	Mon:Init.	Dp	Mn		PDI
			GPC	Calculated	
P1	25:1	25	6,000	4,600	1.13
	50:1	50	11,700	9,200	1.26
	100:1	100	22,600	18,400	1.35
P2	25:1	25	4,460	2,760	1.31
	50:1	50	5,320	4,600	1.39
	100:1	100	12,900	9,200	1.40
P3	25:1	25	25,200	8,950	1.26
	50:1	50	39,700	17,900	1.24
	100:1	100	76,600	35,800	1.29

The resulting polymers were characterised using proton and carbon NMR, and size exclusion chromatography (SEC). The structures of the resulting polymers are shown in Figure 7.
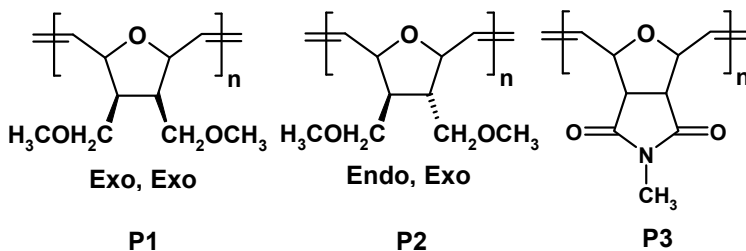
Figure 7. ROMP polymers **P1**–**P3** used for the studies.

The preliminary molecular model studies of these polymers indicate ability to form helical structures with all the THF oxygen facing into the interior of the helix, Figure 8.

This unique conformation allows these polymers in solution to act as useful acyclic ionophores. They bind cations like crown ethers through oxygen lone pair but unlike crowns their cavities are not preformed and they can bind to various cations depending on size and charge.
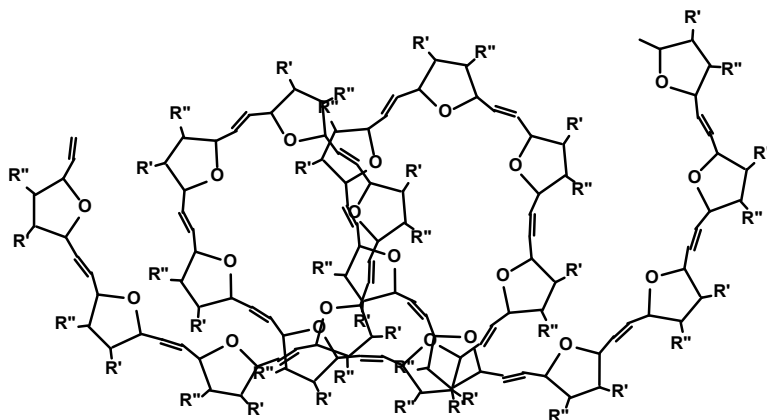
Helical structure of the polymers

Figure 8. Schematic representation of polymer chains forming helical structures with oxygen atoms facing interior of the helices.

A range of polymers (**P1**–**P3**) of different chain length (molecular weight) from various 7-oxanorbornene monomers were prepared to study the ion binding and ion selectivity properties. These monomers have different configuration of the substituents on furan ring which allows further systematic structural modifications of the basic polymer skeletons. Polymers **P1**–**P3** prepared by 5,6-substituted-7-oxanorbornene monomers were expected to exhibit potential ionophoric properties by having the ability to bind a different cations based on size and charge such as Li^+, K^+, Ca^{2+}, Ba^{2+} or even a big cation as methylene blue (MW = 373.9).[42]

Potentiometric investigations showed that all ROMP polymers (**P1**–**P3**) have ionophoric properties similar to those of standard ionophores in the case of small ions like Li^+ (d = 1.36 Å) and Na^+ d = 1.94 Å. For big cation like K^+ (d = 2.66 Å), good binding ability was observed for **P2** and **P3** polymers but not for **P1** polymer. The binding properties towards Ca^{2+} ions (d = 1.98 Å) are comparable to those of standard ionophores only in the case of **P1** and **P2** polymers with lowest molecular weight of Mn = 6,000 and 4,460, respectively.

The UV–VIS analyses for **P1** and **P2** polymers indicated that they exhibit ionophoric properties better than those of the crown ether towards MB^+ ions.

In summary, The acyclic polymeric ionophores (**P1**–**P3**) based on 5,6-sub-stituted-7-oxanorbornenes were synthesised by ROMP and fully characterised. Their ionophoric properties were analysed by potentiometry after incorporation in membranes and UV–VIS measurements. All ROMP polymers showed ionophoric properties similar to those of the standard ionophores for ions of different sizes.

However, the helical conformation and therefore the binding ability of these polymers are expected to be affected by the presence of the cis and trans double bonds along the backbone chain. It will be interesting to hydrogenate these polymers and compare the helical conformation and hence binding ability.

References

[1]   K.A. Athanasiou, G.G. Niederauer, C.M. Agrawal, *Biomaterials* **1996**, *17*, 93–102.
[2]   J.C. Middleton, A.J. Tripton, *Biomaterials* **2000**, *21*, 2335–2346.
[3]   T.J. Corden, I.A. Jones, C.D. Rudd, P. Christian, S. Downes, K.E. McDougall, *Biomaterials* **2000**, *21*, 713–724.
[4]   M. Vert, S.M. Li, G. Spenlehauer, P. Guerin, *J. Mater. Sci.: Mater. Med.* **1992**, *3*, 432–446.
[5]   Grizzi, H. Garreau, S. Li, M. Vert, *Biomaterials* **1995**, *16*, 305–311.
[6]   G. Schliecker, C. Schmidt, St. Fuchs, T. Kissel, *Biomaterials* **2003**, *24*, 3835–3844.
[7]   G. Swach, J. Coudane, R. Engel, M. Vert, *Biomaterials* **2002**, *23*, 993–1002.
[8]   H.S. Choi, T. Ooya, S. Sasaki, N. Yui, Y. Ohya, T. Nakai, T. Ouchi, *Macromolecules* **2003**, *36*, 9313–9318.
[9]   Q. Cai, J. Bei, S. Wang, *Polymer* **2002**, *43*, 3585–3591.
[10]   R. Kumar, W. Gao, R.A. Gross, *Macromolecules* **2002**, *35*, 6835–6844.
[11]   H. Shinoda, K. Matyjaszewski, *Macromolecules* **2001**, *34*, 6243–6248.
[12]   P. Lecomte, D. Mecerreyes, P.H. Dubois, A. Demonceau, A.F. Noels, R. Jerome, *Polym. Bull.* **1998**, *40*, 631–638.
[13]   D. Mecerreyes, D. Dahan, P.H. Lecomte, P.H. Dubois, A. Demonceau, A.F. Noels, R. Jerome, *J. Polym. Sci., Polym. Chem.* **1999**, *37*, 2447–2455.
[14]   S. Jha, S. Dutta, N.B. Bowden, *Macromolecules* **2004**, *37*, 4365–4374.
[15]   H.D. Maynard, S.Y. Okada, R.H. Grubbs, *Macromolecules* **2000**, *33*, 6239–6248.
[16]   I. Czelusniak, E. Khosravi, A.M. Kenwright, C.W.G. Ansell, *Macromolecules* **2007**, *40*, 1444–1452.
[17]   J.G. Hamilton, J. Kay, J.J. Rooney, *J. Mol. Catal. A: Chem.* **1998**, *133*, 83–91.
[18]   D.K. Gilding, A.M. Reed, *Polymer* **1979**, *20*, 1459–1464.
[19]   A.-C. Albertsson, M. Gruvegard, *Polymer* **1995**, *36*, 1009–1016.
[20]   A.J. Nijenhuis, D.W. Grijpma, A.J. Pennings, *Macromolecules* **1992**, *25*, 6419–6424.
[21]   M. Ryner, K. Stridsberg, A.C. Albertsson, *Macromolecules* **2001**, *34*, 3877–3881.
[22]   H.R. Kricheldorf, I. Kreiser-Saunders, C. Boettcher, *Polymer* **1995**, *36*, 1253–1259.
[23]   A.J. Nijenhuis, D.W. Grijpma, A.J. Pennings, *Macromolecules* **1992**, *25*, 6419–6424.
[24]   S. Penczek, R. Szymanski, A. Duda, J. Baran, *Macromol. Symp.* **2003**, *201*, 261–269.
[25]   P. Schwab, R.H. Grubbs, J.W. Ziller, *J. Am. Chem. Soc.* **1996**, *118*, 100–110.
[26]   J.A. Love, J.P. Morgan, T.M. Trnka, R.H. Grubbs, *Angew. Chem. Int. Ed. Engl.* **2002** *41*, 4035–4037.
[27]   J. Huang, H.-J. Schanz, E.D. Stevens, S.P. Nolan, *Organometallics* **1999**, *18*, 5375–5380.
[28]   A.C.M. Rizmi, E. Khosravi, W.J. Feast, M.A. Mohsin, A.F. Johnson, *Polymer* **1998**, *39*, 6605–6610.

[29] C.W. Bielawski, R.H. Grubbs, *Angew. Chem., Int. Ed. Engl.* **2000**, *39*, 2903–2906.
[30] C. Slugovc, S. Demel, S. Riegler, J. Hobisch, F. Stelzer, *Macromol. Rapid Commun.* **2004**, *25*, 475–480.
[31] T.-L. Choi, R.H. Grubbs, *Angew. Chem. Int. Ed.* **2003**, *42*, 1743–1746.
[32] C. Slugovc, S. Riegler, G. Hayn, R. Saf, F. Stelzer, *Macromol. Rapid Commun.* **2003**, *24*, 435–439.
[33] G.G. Pitt, M.M. Gratzl, G.L. Kimmel, J. Surles, A. Sohindler, *Biomaterials* **1981**, *2*, 215.
[34] T. Nakamura, S. Hitomi, S. Watanabe, Y. Shimizu, K. Jamshidi, S.-H. Hyon, Y. Ikada, *J. Biomed. Material Res.* **1989**, *23*, 1115–1130.
[35] C.J. Pedersen, *J. Am. Chem. Soc.*, **1967**, *89*, 7017.
[36] C.J. Pedersen, H.K. Frendsdorf, *Angew. Chem., Int. Ed. Engl.*, **1972**, *11*, 16.
[37] H.K. Frensdorf, *J. Am. Chem. Soc.*, **1971**, *93*, 600.
[38] H.K. Frensdorf, *J. Am. Chem. Soc.*, **1971**, *93*, 4684.
[39] R. Kataky, G. Grancharov, E. Khosravi, *Analyst* **2005**, 130, 1351.
[40] D.J. Cram et al., *J. Am. Chem. Soc.*, **1977**, *99*, 2564.
[41] S. Smith, W.J. Shultz, M.C. Etter, A.V. Pocius, *J. Am. Chem. Soc.*, **1980**, *102*, 7981.
[42] R.H. Grubbs, B. Novak, *J. Am. Chem. Soc.*, **1988**, *110*, 960.
[43] Sh.-Y. Lu, J. Amass, N. Majid, D. Glennon, A. Byerley, P. Quayle, F. Heatley, C. Booth, St. Yeates, J. Padget, *Macromol. Chem. Phys*, **1994**, *195*, 1273
[44] Sh.-Y. Lu, P. Quayle, F. Heatley, C. Booth, St. Yeates, J. Padget, *Macromolecules*, **1992**, *25*, 2692.
[45] L. Paquette, T. Kravetz, P. Charumilind, *Tetrahedron*, **1986**, *42(6)*, 1789.
[46] T. Viswanathan, J. Jethmalani, *J. Appl. Polym. Sci.*, **1993**, *48*, 1289.

RUTHENIUM CATALYSTS BEARING O-CHELATING CARBOXYLATE LIGAND: POTENTIAL CHEMO-SWITCHABLE ROMP CATALYSTS

RAFAL GAWIN AND KAROL GRELA[*]
Institute of Organic Chemistry, Polish Academy of Sciences, Kasprzaka 44/52, 01-224 Warsaw, Poland

Abstract: In this chapter novel ruthenium complexes such as carboxylates are described. Chemical and thermal activation of new complexes providing highly active metathesis catalysts is discussed. Unique structural motif allow to introduce new carboxylate and sulfonate derived ligands without use of silver or thallium salts. Structure–activity relationship is investigated.

1. Introduction

The tremendous success of olefin metathesis is largely due to the evolutionary development of active, well-defined ruthenium-based catalysts. [1] In the case of Grubbs' first-generation precatalyst, **1a**, major progress has been attained by optimizing the ligand sphere around the ruthenium center. Key advances include the development of *N*-heterocyclic carbene (NHC) complexes (e.g. Grubbs' second-generation catalyst **1b)** and derivatives containing a chelating 2-alkoxy-benzylidene (e.g. Hoveyda's catalyst **2**) or indenylidene **3** (Figure 1).[1]

In some specific cases it is necessary to control activity of catalyst during process. The most obvious example is ring opening metathesis polymerization (ROMP).[2] It is demanded to precisely mix substrates with temporary inactive catalyst to avoid uncontrollable reaction. Afterward catalyst could be activated thermally or chemically to provide controllable polymerization reaction.

N-chelating catalysts are most common members of latent family catalysts. van der Schaaf et al. reported catalyst **4**, bearing chelating pyridine derivative (Figure 2).[3] Schrodi reported second generation of catalyst **4**.[4] Slugovc reported synthesis of catalyst **5**, bearing chelating imine derivative.[5] Barbasiewicz

et al. reported synthesis of quinoline and quinoxaline catalysts **6**.[6] These complexes have low activity at room temperature and became active at elevated temperatures.

a: L = PCy₃   b: L =

(SIMes)

| a: | ⇨ | *I-generation* |
| b, b': | ⇨ | *II-generation* |

b': L =

(IMes)
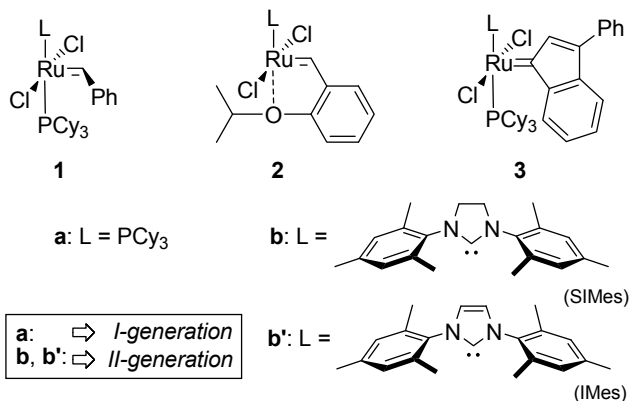
Figure 1. Modern olefin metathesis ruthenium catalysts. PCy₃ – tricyclohexylphosphine.

Much less common are *O-* and *S*-chelating complexes. Grela et al. reported synthesis of catalyst **7** bearing benzylidene ligand substitued with diethylamine function.[7] Complex **7** posses low activity and can be activated by addition of acids to form quaternary ammonium derivative with high catalytic activity.

Independently groups of Grela and Lemmcoff reported synthesis of sulphur containing analogs of Hoveyda catalyst **8**.[8] Szadkowska et al. obtained sulfinyl catalyst **9**.[9] These catalysts have low activity at room temperature and can be activated thermally.

4, L = PCy₃, SIMes   **5**, L = SIMes   **6**, X = CH, N
                                                          L = SIMes

7, L = SIMes   **8**, R = Me, Et, *i*-Pr, Ph, *t*-Bu   **9**, R = 4-C₆H₄
                          L = SIMes, IMes   L = IMes
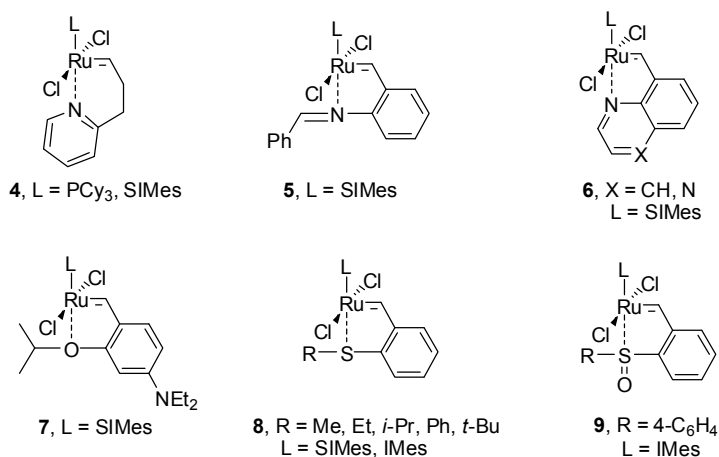
Figure 2. Latent ruthenium catalysts.

2. Synthesis of Ruthenium Carboxylate Catalysts

Grela et al. reported synthesis of novel class of ruthenium catalysts bearing carboxylate ligand **13a** with interesting features (Scheme 1).[10]
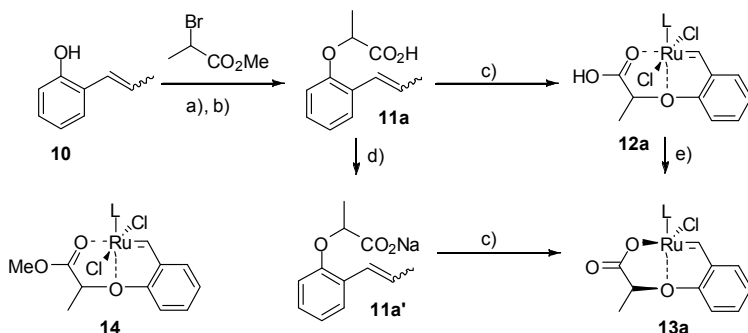
Scheme 1. Synthesis of ruthenium carboxylate complex **13a**. Conditions: (a) K_2CO_3, Cs_2CO_3, DMF, rt, 24 h (b) LiOH, THF, rt, 24 h (c) **1b**, DCM, 40°C, 30 min. or **3b**, toluene, 80°C, 30 min. (d) NaOH e) SiO_2 (silica gel chromatography).

Starting from commercial 2-propenylphenol **10** and methyl 2-bromopropionate ligands **11a** was readily obtained (Scheme 1). Reaction with Grubb's second generation catalyst **1b** or second generation indenylidene catalyst **3b** and standard purification procedure (chromatography and crystallization) provided unexpectedly cyclized complex **13a** instead of **12a** (84% yield). NMR of crude reaction mixture and after column chromatography shows that cyclization takes place during column chromatography (benzylidene proton shift 16.73 ppm before and 16.52 ppm after). Same reaction with sodium salt of acid **11a** gave directly cyclized complex **13a**. Based on mass spectrometry, NMR spectroscopy, elemental analysis and X-ray analysis (Figure 3) we assigned structure of new complex to **13a**.
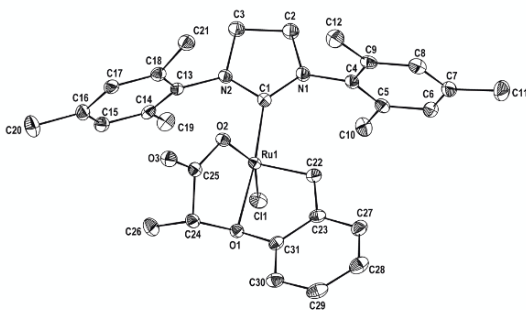
Figure 3. Solid state structure of **13a**.

Addition of 1 eq of hydrochloric acid in diethyl ether to a solution of **13a** in dichloromethane (DCM) and stirring for 5 min followed by precipitation with *n*-hexane, evaporation and drying provided complex **12a** (Scheme 2). Complex **13a** was also treated with triflic acid and perfluorononanoic acid to form new complexes **15** and **16**. After silica gel chromatography **13a** was obtained irrespective of which acid was used.

13a

12a: X=Cl
15: X=CF$_3$SO$_3$
16: X=C$_8$F$_{17}$CO$_2$

13a
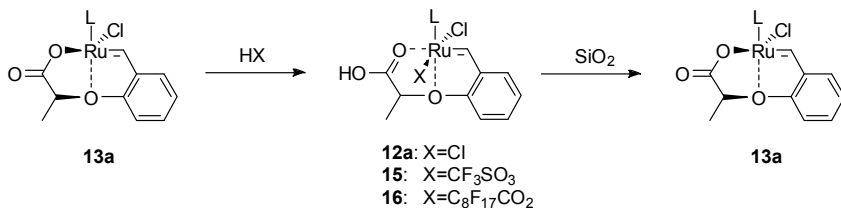
Scheme 2. Synthesis of complexes **12a**, **15** and **16**.

The activity of new catalysts was compared in standard metathesis reaction – ring closing metathesis (RCM) of diethyl diallylmalonate **17** (Scheme 3).
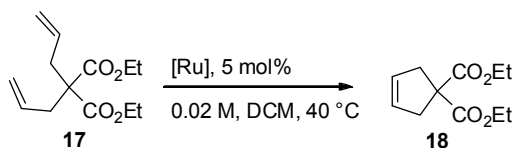
Scheme 3. Model metathesis reaction.
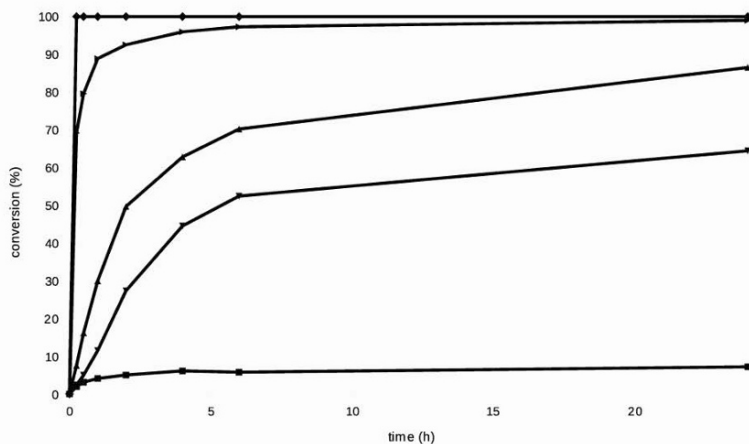
Figure 4. Comparison of activity of complexes **13a** (■), **12a** (▶), **15**(▼), **16** (▲) and **14** (◀) in RCM of **17**. Conditions: 5 mol% catalyst, 40°C, DCM, 24 h.

It is worth mentioning that new complexes **12a**, **15** and **16** were formed *in situ* by addition of 1 eq of proper acid to solution of **17** and **13a** (Figure 4). Complex **12a** with chlorine was most active from new complexes. Complexes with perfluorononanoic **16** and triflic acid **15** were less active. It was not surprising that complex **14** bearing tridentate ligand was almost inactive. Surprisingly complex **12a** is much less active than corresponding **14** (Scheme 1).[11] The explanation for this fact may be the presence of an equilibrium which takes place during reaction (Scheme 4).
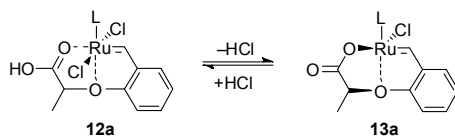
Scheme 4. Possible equilibrium during metathesis reaction.

Although, crystal structure of **12a** was not obtained we believe that other reason may be due to a stronger bond (compared to **14**) between ruthenium and carboxylate moiety. The behaviour of complex **12a** in reaction with bases is interesting. Reactions were followed by NMR. The reaction of **12a** in CD$_2$Cl$_2$ and 1 eq of sodium methoxide gives no **13a** due to insolubility of base. Reaction with 1 eq of pyridine gives a mixture of **12a** and cyclized **13a** in ratio 1:1, whereas the reaction with 1 eq of potassium *t*-amylate gives only cyclized **13a**.

This interesting possibility of "turning on" in acidic conditions and "turning off" in basic conditions might be useful in ROMP or in tandem multistep reactions where one of the steps is incompatible with active ruthenium species.

Complex **13a** posses another interesting feature – it can be also activated thermally. While **13a** is inactive at room temperature it became active at elevated temperatures. The mechanism of thermal activation of **13a** is not understood. We believe that it may be due to break of ruthenium–carbon double bond in the presence of substrate (Scheme 5).
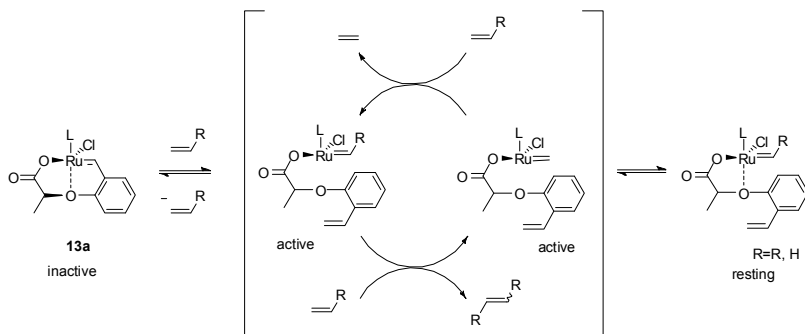
Scheme 5. Possible mechanism of thermal activation of **13a**. trough ruthenium–carbon double bond break.

Anionic ligands of ruthenium coordination sphere are very labile.[12] It is possible that in thermal conditions the activation is due to anionic ligand exchange between two molecules of **13a** resulting in bi-nuclear, active complex **19** (Scheme 6).
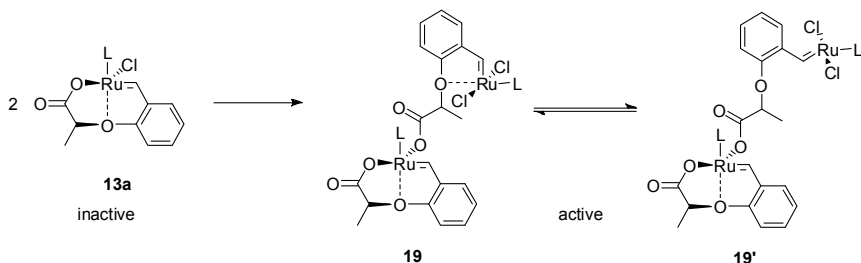
Scheme 6. Possible mechanism of thermal activation of **13a**. trough anionic ligand exchange.

We became interested in analogs of **13a** and investigated structure–activity relationship study. Series of new carboxylates **13b**–**g** were obtained.
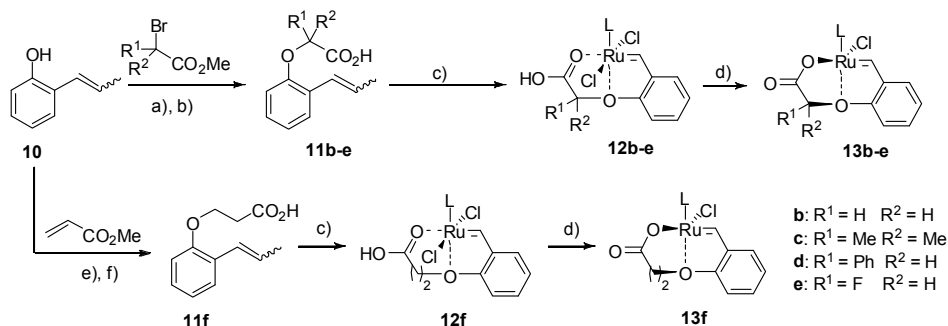
Scheme 7. Synthesis of ruthenium catalysts bearing carboxylate function. Conditions: (a) K_2CO_3, Cs_2CO_3, DMF, rt, 24 h (b) LiOH, THF, rt, 24 h (c) **1b**, DCM, 40°C, 30 min. or **3b**, toluene, 80°C, 30 min (d) SiO_2 (silica gel chromatography) (e) Triton-B, reflux (f) LiOH, THF, rt, 24 h.

Starting from **10** and 2-bromoester ligands, **11b**–**e** were readily obtained (Scheme 7). Reaction with second generation indenylidene catalyst **3b** and standard purification procedure (chromatography and crystallization) provided cyclized complexes **13b**–**e**. Ligand **12** was obtained in Michael addition of **10** to methyl acrylate followed by hydrolysis. Reaction with second generation indenylidene catalyst **3b** provided homologue complexes **13f**. Unfortunately, complexes **13e** and **13f** were not stable.

Starting from 4-nitrophenol **20** ligand **24** was obtained in five steps (Scheme 8). Reaction with **3b** provided complex **13g**.
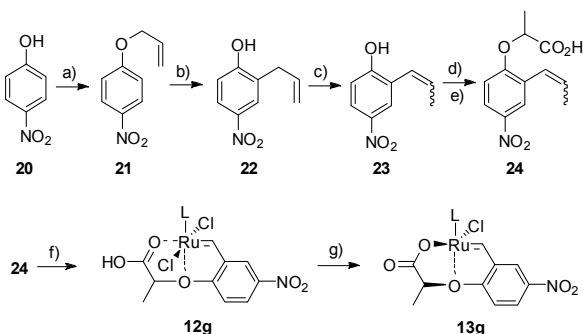
Scheme 8. Synthesis of complex **13g**. Conditions: (a) K_2CO_3, allyl bromide, DMF, rt, 24 h (b) 195°C, PhOPh, 8 h (c) $(PPh_3)_3RuHClCO$, toluene, reflux, 24 h (d) Methyl 2-bromopropionate, K_2CO_3, Cs_2CO_3, DMF, rt, 24 h (e) LiOH, THF, rt, 24 h (f) **1b**, DCM, 40°C, 30 min. or **3b**, toluene, 80°C, 30 min (g) SiO_2 (silica gel chromatography).

Complexes **13a–g** were transformed back to corresponding **12a–g** in reaction with hydrochloric acid. Activity of complexes **12a–g** were compared in RCM of **17** (Scheme 9).
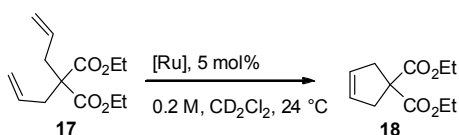
Scheme 9. Model metathesis reaction.
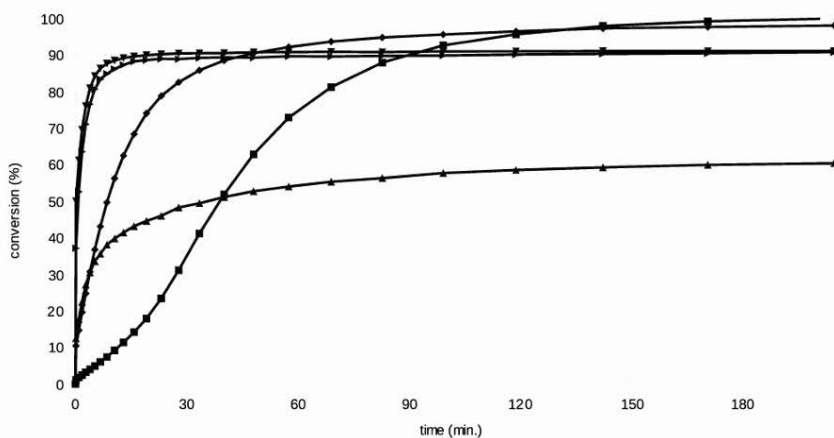
Figure 5. Comparison of activity of complexes **12 c** (■), **12a** (♦), **12d** (►), **12g** (▼), **12b** (▲) in RCM of **17**. Conditions: 5 mol% catalyst, 24°C, CD_2Cl_2.

Complex **12b** ($R^1 = R^2 = H$) was quite unstable and in RCM of **17** only 60% conversion was achieved. Complex **12c** ($R^1 = R^2 = Me$) was little less active than **12a**, but in a prolonged reaction time gives the highest conversion. Complex **12g** due to nitro substituent was the most active reaching 90% conversion in 15 min. Unfortunately, the total conversion was not achieved. Interestingly, complex **12d** ($R^1 = Ph$, $R^2 = H$) has almost identical reaction profile to that of the nitro substituted **12g**.

Solid state structures were determined for complexes **12c** and **13g** (Figures 6 and 7).
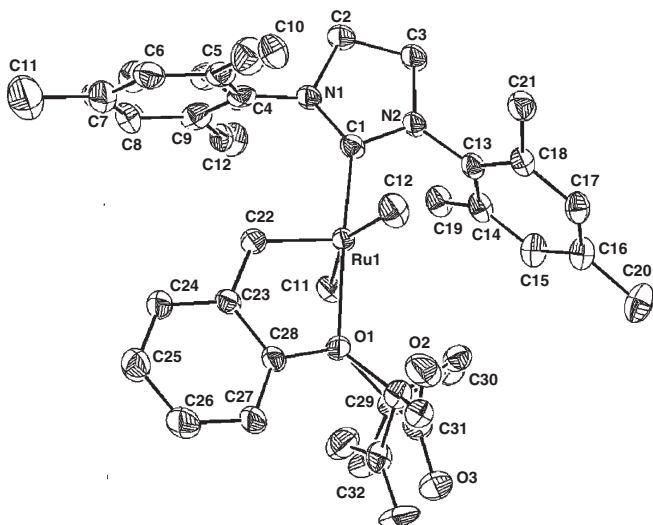
Figure 6. Solid state structure of complex **12c**.
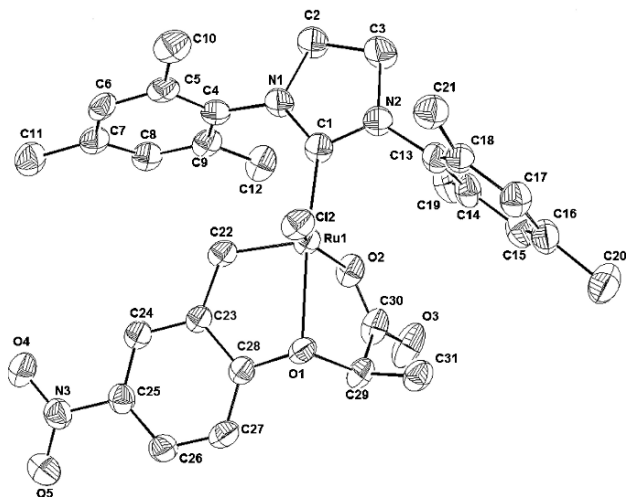
Figure 7. Solid state structure of complex **13g**.

3. Summary and Outlook

In summary, we reported ruthenium catalysts **13** bearing carboxylate ligand which posses interesting properties. It is almost inactive at room temperature and can be activated by various acids or thermally. Unique structural motif of carboxylate allow to introduce new carboxylate derived ligand (free, tagged or supported) without the use of any silver of thallium salt. New catalytic system has a wide range of controllable activity through tuning structure of complex **13** and different acids used for activation.

4. Typical procedure for synthesis of complexes 13.

Ligand **11a** (49.5 mg; 0.24 mmol) or **11a'** (0.24 mmol), CuCl (23.8 mg; 0.24 mmol) and DCM (10 mL) were placed in a Schlenk flask. Afterward carbene complex **1b** (169.8 mg; 0.20 mmol) was added and the resulting solution was stirred under argon at 40°C for 40 min. From this point forth, all manipulations were carried out in air with reagent-grade solvents. The reaction mixture was concentrated under vacuum and resulting material was dissolved in ethyl acetate (ca. 10 mL), white solid was filtered off and the filtrate was concentrated under vacuum. The product was purified by column chromatography on silica gel (Merck, grade 9385, 230–400 mesh, no pre-treatment). Elution with c-hexane-ethyl acetate (2:1) (ca. 200 mL) then c-hexane-ethyl acetate (1:1) removes **14** as a green band. The solvent was evaporated and product dissolved in small amount of DCM, then t-butyl methyl ether was added until green crystals precipitated. The precipitate was filtered off, washed with n-pentane and dried in vacuum to afford complex **13a** (104.8 mg, 84%) as a green solid. ^{1}H NMR (500 MHz, CDCl$_3$): δ = 16.52 (s, 1H), 7.49–7.52 (m, 1H), 7.11 (s, 2H), 7.06 (s, 2H), 7.02–7.05 (m, 1H), 6.97 (d, J = 8.23 Hz, 1H), 6.95 (d, J = 7.57 Hz, 1H), 4.65 (q, J = 7.02 Hz, 1H), 4.21 (s, 4H), 2.47 (bs, 6H, 2.39 (s, 6H), 2.37 (s, 6H), 1.19 (d, J = 7.02 Hz, 3H); ^{13}C NMR (125 MHz, CDCl$_3$): δ = 293.3, 210.3, 181.5, 154.6, 146.7, 139.3, 138.8, 130.0, 129.6, 129.4, 126.6, 122.2, 119.1, 84.1, 51.4, 21.0, 19.00, 18.8, 18.5. IR (film from CH$_2$Cl$_2$): v = 3,483, 3,044, 2,977, 2,919, 2,861, 2,736, 1,662, 1,607, 1,594, 1,571, 1,483, 1,451, 1,401, 1,376, 1,318, 1,297, 1,269, 1,185, 1,151, 1,100, 1,069, 1,017, 944, 918, 879, 846, 795, 752, 734, 700, 645, 617, 577, 501, 471, 438, 421 cm^{-1}; HRMS (FD/FI): m/z calcd for C$_{31}$H$_{35}$N$_2$O$_3$^{35}Cl^{102}Ru: [M$^+$] 620.1380 found, 620.1357; elemental analysis (%) calcd for C$_{31}$H$_{35}$N$_2$O$_3$ClRu (620.16): C 60.04, H 5.69, N 4.52, Cl 5.72; found: C 59.92, H 5.69, N 4.55, Cl 5.48.

Acknowledgements

References

[1]   (a) Trnka T M, Grubbs R H (2001) Acc Chem Res 34:18–29 (b) Grubbs R H
        (2003) Handbook of Metathesis, Wiley-VCH, Weinheim, p. 1204 (c) Schrock R
        R, Hoveyda A H (2003) Angew Chem 115:4740–4782; Angew Chem Int Ed
        42:4592–4633 (d) Connon S J, Blechert S (2003) Angew Chem 115:1944–1968;
        Angew Chem Int Ed 42:1900–1923 (e) Astruc D (2005) New J Chem 29:42–56
        (f) Dragutan V, Dragutan I, Verpoort F (2005) Platinum Metals Rev 49:33–40

[2]   Szadkowska A, Grela K (2008) Curr Org Chem 12:1631–1647

[3]   van der Schaaf P, Kolly R, Kirner H-J, Rime F, Muhlebach A, Hafner A (2000) J
        Organomet Chem 606:65–74

[4]   Ung T, Hejl A, Grubbs R, Schrodi Y (2004) Organometallics 23:5399–5401

[5]   Slugovc C, Burtscher D, Stelzer F, Mereiter K (2005) Organometallics 24:2255–
        2258

[6]   Barbasiewicz M, Szadkowska A, Bujok R, Grela K (2006) Organometallics
        25:3599–3604

[7]   (a) Kirschning A, Gułajski Ł, Mennecke K, Meyer A, Busch T, Grela K (2008)
        Synlett 2692–2696 (b) Gułajski Ł, Michrowska A, Narożnik J, Kaczmarska Z,
        Rupnicki L, Grela K (2008) ChemSusChem 1:103–109 (c) Michrowska A,
        Gułajski Ł, Kaczmarska Z, Mennecke K, Kirschning A, Grela K (2006) Green
        Chem 8:685–688

[8]   (a) Kadyrow R, Rosiak A, Tarabocchia J, Szadkowska A, Bieniek M, Grela K
        (2008) Catalysis of Organic Reactions, Chemical Industries Series, White M G,
        Ed Taylor & Francis, London, CRC Press, Vol. 123, p. 568 (b) Ben-Asuly A,
        Tzur E, Diesendruck C E, Sigalov M, Goldberg I, Lemcoff N G (2008)
        Organometallics 27:811–813 (c) Kost T, Sigalov M, Goldberg I, Ben-Asuly A,
        Lemcoff N G (2008) J Organomet Chem 693:2200–2203

[9]   Grela K, Szadkowska A, Kadyrow R (2007) Neuartige schwefelhaltige Metathese
        Katalysatoren DE Patent Application 102007020694.3 (Degussa AG)

[10]   Gawin R, Makal A, Woźniak K, Mauduit M, Grela K (2007) Angew Chem Int
        Ed 46:7206–7209

[11]   Bieniek M, Bujok R, Cabaj M, Lugan N, Lavigne G, Arlt D, Grela K (2006) J
        Am Chem Soc 128:13652–13653

[12]   (a) Tanaka K, Bohm V P W, Chadwick D et al. (2006) Organometallics 25:5696
        (b) Braddock D C, Tanaka K, Chadwick D et al. (2007) Tetrahedron Lett
        48:5301–5303

DESIGN AND APPLICATION OF LATENT OLEFIN METATHESIS CATALYSTS FEATURING *S*-CHELATING ALKYLIDENE LIGANDS

ANNA SZADKOWSKA* AND KAROL GRELA*
Institute of Organic Chemistry, Polish Academy of Science, Kasprzaka 44/52, 01-224 Warsaw, Poland

Abstract: This review article is devoted to recent advances in the design and application of so-called "dormant" or "latent" ruthenium olefin metathesis catalysts bearing S-chelating alkylidene ligands. Selected ruthenium complexes containing *S*-donor ligands, which possess controllable initiation behaviour are presented. Applications of these complexes in olefin metathesis are described.

Keywords: Catalysis; Metathesis; Ligand design; Dormant catalyst; Latent catalyst

1. Introduction

The tremendous development in the area of olefin metathesis has cumulated in the Nobel Prize in Chemistry being awarded in 2005 to Chauvin, Schrock and Grubbs for their seminal work in this field.[1] Olefin metathesis demonstrates an outstanding importance in catalytic chemistry which stands among a handful of important ways to create carbon–carbon bonds and to build advanced natural and non-natural compounds. Until now, several types of this reaction have been studied and widely described to facilitate many organic transformations and strategies (Figure 1).[2]

Currently, the efficient olefin metathesis catalysts have focused on increasing stability and perfectibility. Synthetic chemists were provided with well-defined catalysts, with enhanced activities and stability, as well as with fast initiation in a range of metathesis reactions.[2] Selected commercially available two families of catalysts: molybdenum and ruthenium are presented in Figure 2. Importantly, the ruthenium catalysts [3] could be handled in air and are compatible with various functionalized substrates, such as esters, amides, ketones, aldehydes and even alkenes bearing protic functionalities like hydroxy and carboxylic groups.[2] Contemporary, Ru-catalysts promote metathesis not only in the neutral organic solvents traditionally used for metathesis (dichloromethane and toluene) but also in protic organic solvents and water.[4]
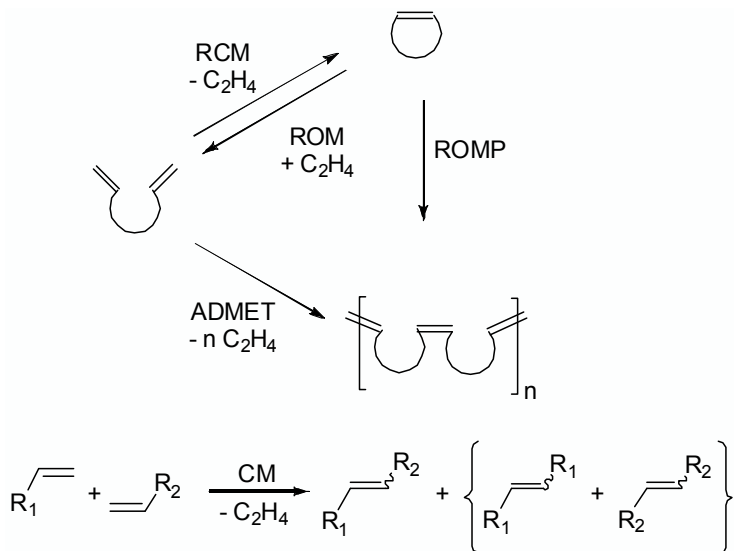
Figure 1. Well-known variants of olefin metathesis reaction: RCM = ring-closing metathesis; ROM = ring-opening metathesis; ROMP = ring-opening metathesis polymerization; ADMET = acyclic diene metathesis polymerization; CM = cross metathesis.
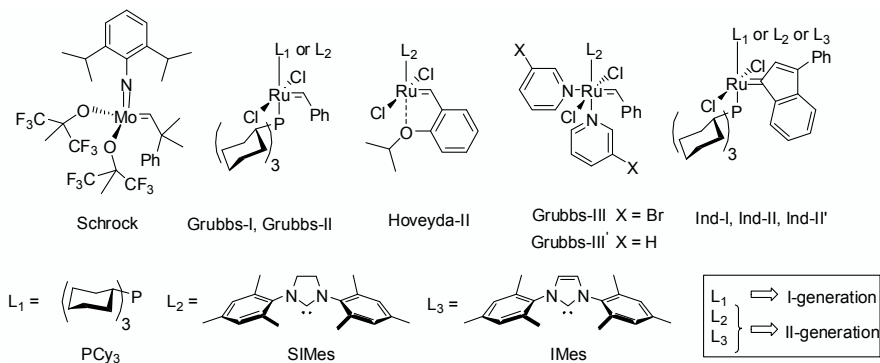
Figure 2. Selected commercially available catalysts.

According to the postulated mechanism, phosphine-free precatalysts of type $L'LX_2Ru=CRR'$ (**Grubbs, Ind**), initiate by dissociating a PR_3 (ligand L) to form 14 electron complex **A**, while in case of the Hoveyda-type precatalysts (**Hoveyda**), whereas L is a tethered ether ligand, the initiation requires breaking of the Ru–O chelation as a first step (Figure 3).[5–7] According to the so-called "boomerang mechanism" the propagating 14-electron species **B** and **C**, formed during the initiation step, can re-coordinate to 2-isopropoxystyrene, regenerating the initial precatalyst at the end of reaction.[6, 7]
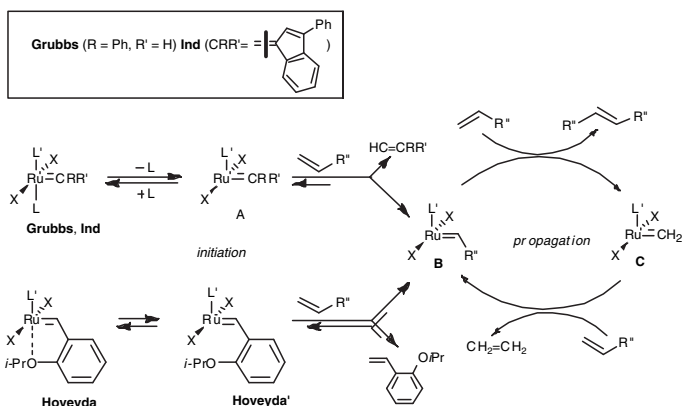
Figure 3. Plausible mechanism of a CM reaction catalysed by Grubbs, indenylidene, and Hoveyda-type initiators.

In some strategies of olefin metathesis it could be beneficial if the complex initiation is controllable. During some industrial set-ups of the ROMP reaction it is required that a mixture of a monomer and an initiator can be processed (or stored) before the metathesis process occurs.[8–10] Ruthenium catalysts shown in Figure 2 are comparatively fast initiators. Therefore, few precatalysts of reduced initiation speed have been prepared. This important class of so-called "latent" or "dormant" catalysts[10] involves complexes bearing Schiff-base ligands, dangling 2-pyridinylcarbinol ligands.[11] Another opportunity that allows to control the initiation speed is based on tethering a donor ligand (L) to the ruthenium center *via* the alkylidene group. The presence of a N→Ru or O→Ru chelate favours the "sleeping" precatalyst over it's metathesis active coordinatively unsaturated form (Figure 4).[12–17] When the initiation step (controlled by temperature, light or a chemical agent) will start and the first catalytic turnover will finish, the donor will no longer be tethered and catalysis should proceed quickly. This switch in catalyst structure from chelated to non-chelated one brings about this strategy interesting for fine-tuning of the initiation speed. This chapter concentrates on new ruthenium catalysts bearing chelating *S*-alkylidene ligands that are representative for the second strategy.
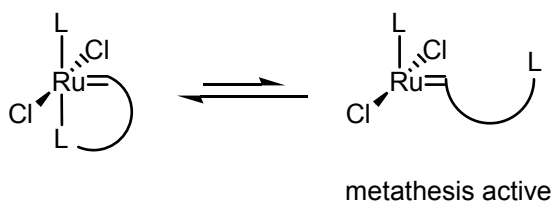
metathesis active

Figure 4. Ruthenium catalyst bearing a chelating alkylidene ligand.

The great impact of a N→Ru or O→Ru chelating in metathesis precatalysts, and their influence on catalytic activity was examined widely in detail (Figure 5).[12–17]
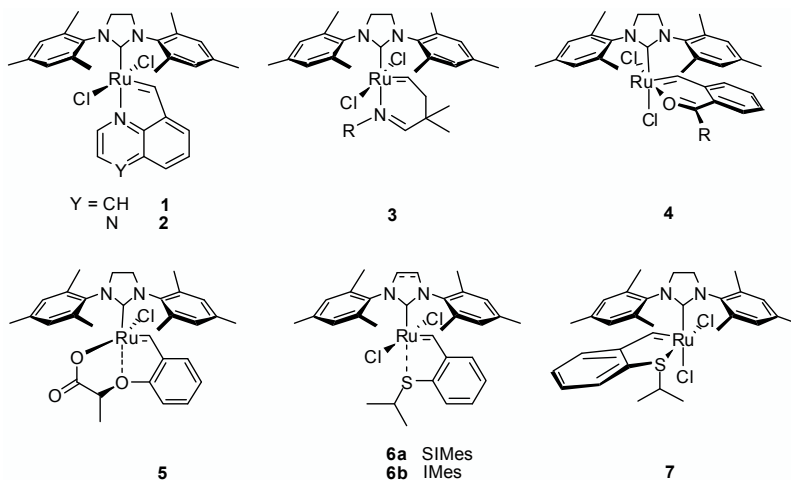
Figure 5. Ruthenium catalysts bearing a chelating alkylidene ligand.

Recently, the new class of sulfur-containing Ru-catalysts **6a**, **6b** and **7** has been revealed independently by Lemcoff and Grela (Figure 5).[12, 18, 19] Although **6–7** show very low activity at room temperature, these initiators posses remarkably good stability and can potentially be suitable in high-temperature applications.

Recently, we devoted our attention to a new family of sulfur and sulfoxide-bearing ruthenium complexes and examined their applicability as initiators in olefin metathesis. The results described in this chapter were a subject of a patent application.[18b]

2.   Preparation and Performance of S-Donor Catalysts

2.1.   SYNTHESIS OF CATALYSTS AND THEIR LIGAND PRECURSORS

New complexes **6a** and **6b** were conveniently obtained from the **Ind-II** and **Ind-II** catalysts, respectively. The preparation of the (2-vinyl)phenyl substituted sulphides is straightforward using recently established routes (Scheme 1).[19]
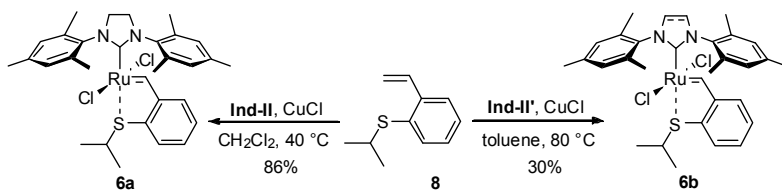
Scheme 1. Ruthenium catalysts bearing *S*-chelating alkylidene ligand.

2.2. GENERAL PROCEDURE FOR INITIATORS 6A AND 6B

A Schlenk equipped with a stirring bar charged with **Ind-II** or **Ind-II** catalysts (0.21 mmol) and CuCl (23.1 mg, 0.23 mmol). The Schlenk was flushed with argon and charged with anhydrous toluene (10 mL). A corresponding styrene (0.64 mmol; 113.5 mg) in anhydrous dichloromethane or toluene (10 mL) was then added. The resulted solution was stirred at 80°C for 35 min (for **6a**) or 1 h (for **6b**). After this step, all manipulations can be done without a protective atmosphere of argon. The resulting mixture was concentrated *in vacuo*, and the residue was re-dissolved in AcOEt and the solution was passed through a Paster pipette containing a small amount of silica gel and evaporated to dryness. The solid was collected and washed a few times with AcOEt and with cold *n*-pentane to yield the chelated catalysts as green microcrystals.

2.3. X-RAY SOLID STATE STRUCTURES AND CATALYTIC ACTIVITY OF 6A AND 6B

The solid state structure of complex **6a** is shown on Figure 6. Similar to parent oxygen-chelating ether complex **Hov-II**, the solid state structure of **6a** shows a distorted square-pyramidal structure with the benzylidene moiety at the apical position. The *N*-aryl ring is located above the benzylidene moiety resulting in the relatively close contact of the benzylidene proton with the π-aromatic system of the mesityl group.
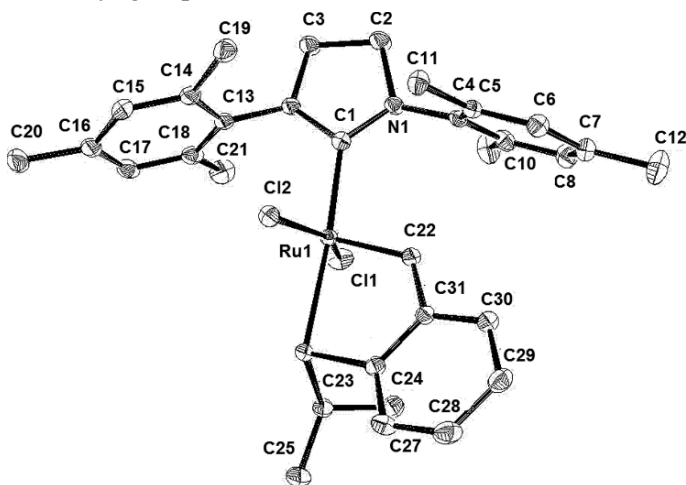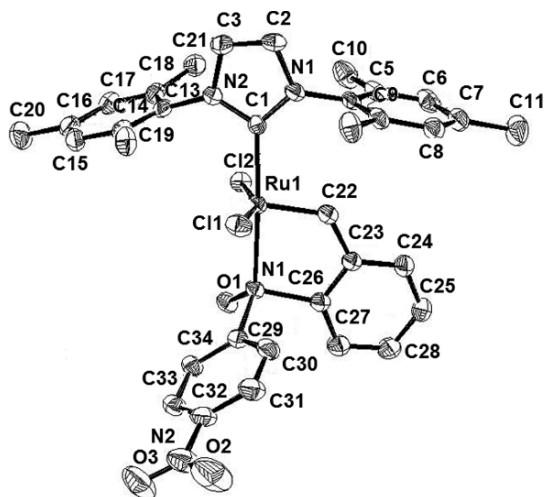

Figure 6. Solid state structure of **6a** with thermal ellipsoids at 50% probability. Hydrogen atoms were omitted for clarity.

We put our effort to examine the efficiency of the new catalysts **6a** and **6b**. Interestingly, both initiators showed no reaction at room temperature in typical

RCM transformations (Scheme 2). After heating to 80°C for 24 h, chelating sulfur catalysts **6a** and **6b** were achieved, respectively, with 51% and 22% conversion of diallyamide **9a**. Using the same conditions, complex **6a** proceed the ring-closing of **10a** with 28% conversion and **6b** with 13% conversion. Unexpectedly, we noticed that enyne cycloisomerisation of **11a** for latent catalysts was running quite fast. Just after 1 h, GC chromatography indicated 99% conversion for **6a** and 68% conversion for **6b**.

9a, A = NTs R=H   **9b**, A = NTs R=H
10a, A = C(CO$_2$Et)$_2$ R=Me   **10b**, A = C(CO$_2$Et)$_2$ R=Me

11a   **11b**
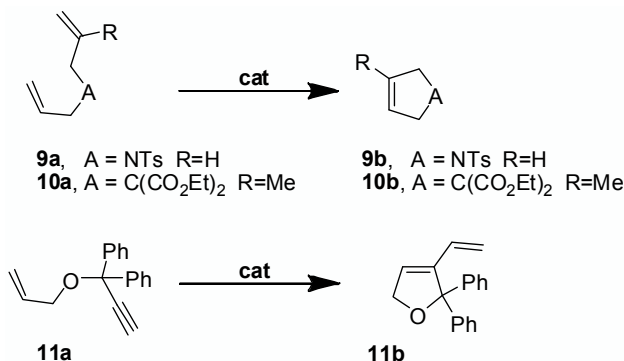
Scheme 2. Model metathesis reactions for catalytic activity of **6a** and **6b**. Conditions: 5 mol% of catalyst, 80°C, toluene, 24 h.

In order to "awake" **6a** and **6b** initiators, we decided to oxidize the sulfur chelating atom to obtain sulfoxide complex **16a**.

3. Preparation and Performance of S(O)-Donor Catalysts

3.1. SYNTHESIS OF CATALYSTS AND THEIR LIGAND PRECURSORS

The commercially available 2-bromothiophenol **12** was transformed into a sulfoxide-bearing ligand precursor **15a**, using oxidation of sulfide **14a** with Oxone[TM][20] and Suzuki-Miyaura cross-coupling with potassium vinyl trifluoroborate as key steps (Scheme 3).[21]
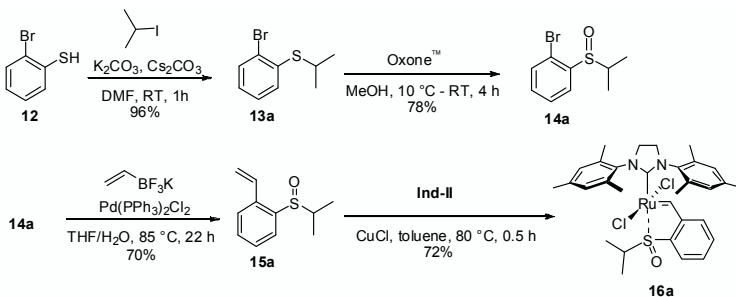
Scheme 3. Synthesis of Ru-initiator **16a** and its precursor.

The final step was performed in presence of CuCl, in toluene at 80°C leading to formation of **16a** as green crystals in 72% yield. Perfectly stable and air-tolerant complex **16a** was characterized by ^{1}H and ^{13}C NMR spectroscopy. Catalyst **16a** showed moderate activity in ring-closing metathesis (RCM) and enyne cycloisomerisation (Scheme 4).
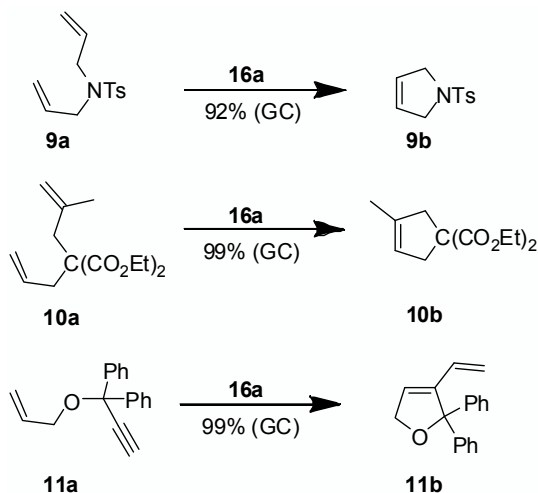
Scheme 4. Catalytic activity of 1**6a** in RCM and enyne cycloisomerisation. Conditions: for reactions with **9a** and **11a**: 1 mol% of **16a**, CH$_2$Cl$_2$, 24°C, 6 h. For reaction with **10a**: 1 mol% of **13a**, toluene, 80°C, 1 h.

We have also investigated the influence of the nature of the NHC ligand and of the substituent at the sulfoxide moiety on the catalytic activity of the resulting ruthenium complexes. Interestingly, initiator **17a** with IMes ligand, turned out to be inactive at room temperature after 48 h, in RCM reaction of **9a**. The complex **17a** started to be more active at elevated temperatures. Kinetic data for **17a** encouraged us study the influence of the substituents R attached to the sulfur center on the catalyst activity (Figure 7). The design of complexes **17b**, **17c** and **17d** was based on idea that applying steric bulk close to chelating sulfur fragment could result in higher increase of catalytic activity. To further expand the scope of sulfoxide Ru-catalyst, we attempted to examine catalysts **17e** and **17f**, to incorporate smaller substituents and electronic effects to chelating sulfur fragment. All catalysts **17a–f** were prepared according to the general method shown on Figure 7 and yields obtained during syntheses of these complexes are shown in Table 1.
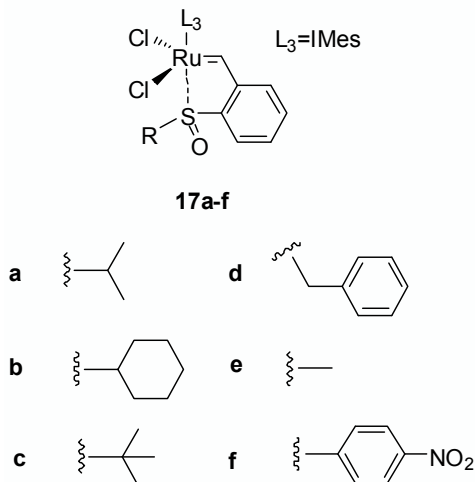
17a-f

Figure 7. IMes Ru-initiators **17a-f** with different substituents.

TABLE 1. Preparation of Ru-initiators **17a–f**.

	R	13%	14%	15%	17%
a	*i*-Pr	96	78	70	60
b	Cy[(a)]	53	75	70	57
c	*t*-Bu[(b)]	58	69	70	57
d	Bn[(c)]	94	72	69	57
e	Me[(d)]	92	62	67	33
f	*p*-NO$_2$C$_6$H$_4$[(e)]	84	68	74	60

If not stated otherwise, conditions shown on Scheme 3 were used. Special alkylation conditions: (a) CyBr, KF/CsF, DMF, reflux, (b) *t*-BuOH, H$_2$SO$_4$/H$_2$O, −10°C → RT, (c) BnCl, K$_2$CO$_3$/Cs$_2$CO$_3$, DMF, RT, (d) MeI, K$_2$CO$_3$/Cs$_2$CO$_3$, DMF, RT, (e) *p*-NO$_2$C$_6$H$_4$F, K$_2$CO$_3$, EtOH, 70°C.

3.2. GENERAL PROCEDURE FOR INITIATORS 16 AND 17A−F

A Schlenk equipped with a stirring bar charged with ruthenium catalysts (**Ind-II** or **Ind-II**) (0.17 g, 0.2 mmol) and CuCl (0.03 g, 0.24 mmol). The tube was flushed with argon and charged with anhydrous toluene (10 mL). A corresponding styrene (0.4 mmol) in anhydrous toluene (5 mL) was added. The resulted solution was stirred at 80°C for 20–30 min. After this step, all manipulations can be done

without a protective atmosphere of argon. The resulting mixture was concentrated in vacuum, and the residue was re-dissolved in AcOEt and the solution was passed through a Paster pipette containing a small amount of cotton and evaporated to dryness. Concentrated crude mixture was purifed by column chromatography (using eluents:cyclohexane/ethyl acetate 10:1 to 1:1 v/v). The solid was collected and washed a few times with mixture of solvents: AcOEt or methylene chloride with cold *n*-pentane (yield 33–60%). All obtained catalysts were green solids or crystals.

3.3. X-RAY SOLID STATE STRUCTURE OF 17F AND CATALYTIC ACTIVITY OF 17A–F

The ruthenium carbenes **17a–f** posses very good air, moisture and thermal stability and can be handled in air and stored for extended periods of time (more than 6 months at +5°C) without decomposition or diminishing of their activity. Only complex **17b** seems to be less stable. All complexes were characterized by ^{1}H and ^{13}C NMR spectroscopy, in addition the solid state structure of **17f** was determined by X-Ray crystallography (Figure 8). Solid state structures show, that the sulphur atom is coordinated to the ruthenium atom, similar to parent chelating thioether-type Hoveyda catalyst **Hoveyda-II**. Unlikely to the structure **7** introduced by Lemcoff et al. our initiators posse *trans*-geometry.[12, 18, 19, 22]

Figure 8. Solid state structure of **17f** with thermal ellipsoids at 50% probability. Hydrogen atoms were omitted for clarity.

The structure of **17f** show general similarity and follow the shape of Hoveyda catalyst. The C2–C3 bond in the central coordinating heterocyclic carbene is a proper double bond, and the heterocyclic ring is planar in the case of all the three structures. In **17f** the benzylidene moiety is nearly coplanar with

imidazole ring (C22–Ru1–S1–C28 torsion angle being about –2°). Additionally C4–C9 ring in **17f** is located exactly above the benzylidene, and both Mes substituents are bent with respect to the imidazole plain, as the N1–C4 and N2–C13 bonds are not coplanar with the imidazole. The selected torsion angles illustrate this behaviour.

It was interesting to compare the structures of sulfoxide-based catalyst **17f** with the structure of Hoveyda analogue with oxygen replaced by sulphur, **6a**. While the overall structure similarity is significant, two differences seem important. The first difference is the Ru–S bond length, which in the case of all sulfoxide catalyst **17f** is 2.33Å while in the case of thioether **6a** gets as long as 2.44 Å. The second difference is in the relative orientation of the benzylidene moiety with respect to the ruthenium and the plane of the imidazole ring, measured by C22–Ru1–S1–C28 torsion angle. For sulfoxide derivative **17f**, the torsion is always negative, but for the thioether **6a** the same torsion is significantly positive (adopting the value of 16°).

As illustrated in Figures 9–11, the catalysts **17b** and **17c** containing more bulky substituents R were more active in model metathesis reaction than less bulky **17e** and **17d**. To provide more comprehensive picture of structure–reactivity relationship of this class of initiators, we prepared complex **17f**, which showed even higher activity then **17c**. Surprisingly, catalyst **17f**, was still inactive in room temperature, in ring closing metathesis of **14**, but at elevated temperatures (40°C and 80°C) initialized faster than **17a**. Having a panel of differently substituted sulfoxide catalysts **17a–f**, we summarized that, steric effects seem to play decisive role in increasing catalytic activity.
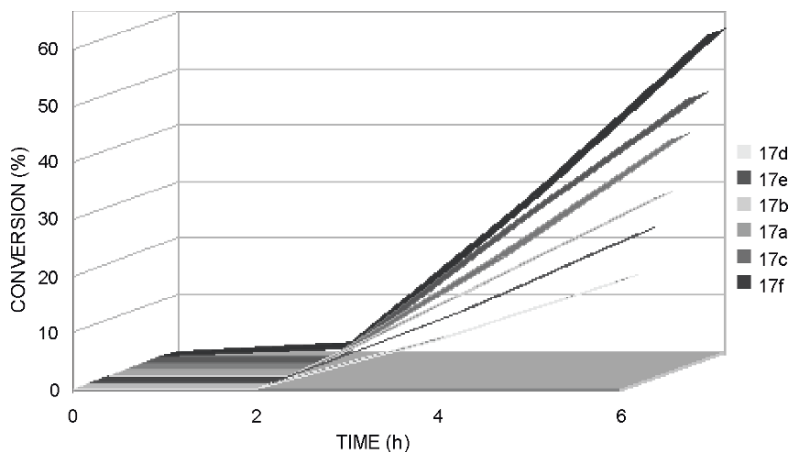
Figure 9. Catalytic activity of IMes Ru-initiators in RCM of **9a**. (Conditions: 1 mol% catalyst, 40°C, dichloromethane, 6 h).
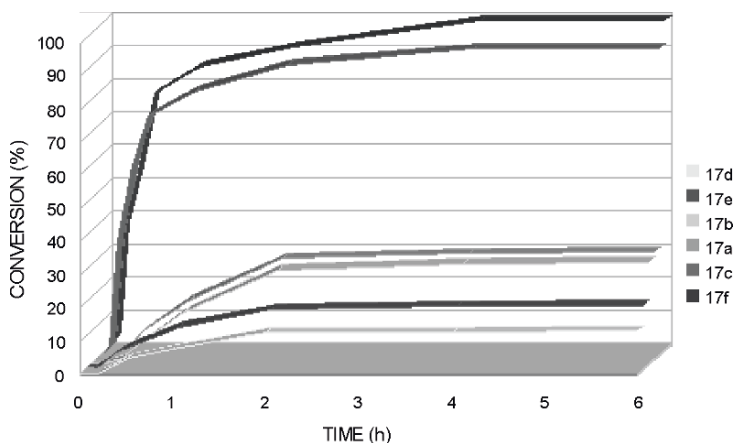
Figure 10. Catalytic activity of IMes Ru-initiators in RCM metathesis of **10a**. (Conditions: 5 mol% catalyst, 80°C, toluene, 6 h.)
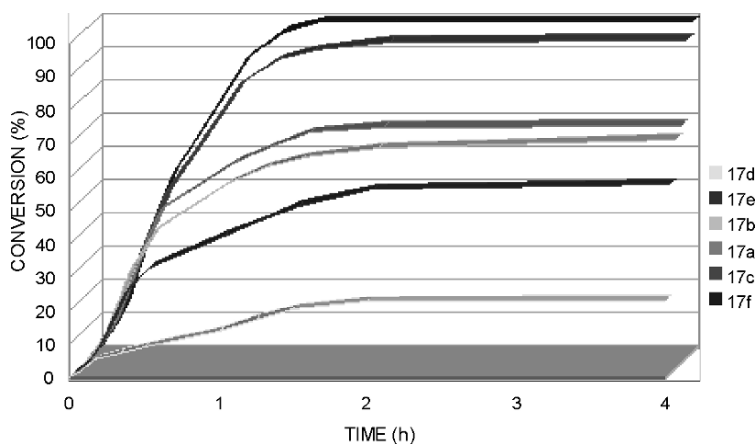
Figure 11. Catalytic activity of IMes Ru-initiators in enyne metathesis of **11a**. (Conditions: 5 mol% catalyst, 40°C, dichloromethane, 6 h.)

Having established the application profile of the sulfoxide catalysts in the formation of di- and trisubstituted C-C double bonds, we focused our efforts on the most demanding case, the formation of the tetrasubstituted carbon–carbon bonds (Scheme 5). It is believed that di(methylallyl)-malonate (**18a**) is a very challenging model substrate of ruthenium catalysts, giving with **Grubbs-II** and **Hoveyda-II** only 17% and 6% of yield, respectively (5 mol%, CH_2Cl_2, 30°C,

96 h). Catalyst **Grubbs-II′**, applied at higher temperature, was reported to give only 47% of the product (5 mol%, toluene, 80°C, 22 h, GC yield). [6b, 23] Therefore, we selected this reaction as a trial in our study.
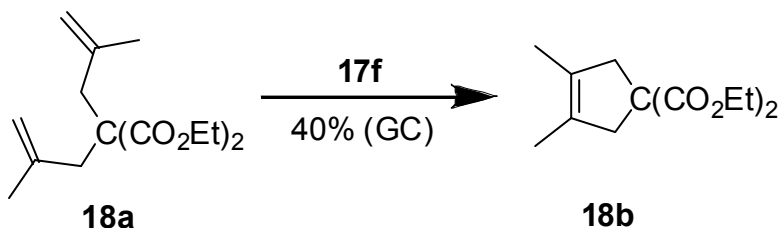
Scheme 5. RCM of **18a**. Conditions $c_{18a} = 0.02$ M, 1 mol% of **17f**, toluene, 110°C, 20 h.

It was found that sulfoxide chelate, **17f**, effected the RCM of substrate **18a** in slightly higher yield (40% conversion measured by GC) than **Grubbs- II** (32% according to GC), although use of rather forcing conditions (1 mol% catalyst, 110°C, toluene, 20 h) was necessary.

4.   Conclusions

In conclusion, development of perfectly stable and thermally or chemically switchable metathesis initiators is of increasing importance. Latent metathesis initiators can allow production of highly sophisticated polymer architectures that are hardly realizable with other polymerization methods. Potential applications of such catalysts are not limited to polymer chemistry, but can be also used in multi-transformation or multi-component synthetic sequences involving a metathesis step. In such design, an initiator, present in a reaction mixture in a latent form, can be switched-on when required. It was recently demonstrated that sulphide- and sulfoxide chelating ligands can be used for the formation of stable Ru-initiators. The activity of the resulted chelated Ru-benzylidene complexes can be fine-tuned by altering the steric and electronic prosperities of the chelating ligand. The most promising complex **17f** combines excellent thermodynamic and air stability with good catalytic activity at elevated temperatures. Prosperities of the family of S-chelated Ru-benzylidene complexes as initiators in ROMP will be studied and reported due course.

Acknowledgements

References

[1]   The Nobel Prize in Chemistry for 2005, jointly awarded to Yves Chauvin, Robert H. Grubbs and Richard R Schrock "for the development of the metathesis method in organic synthesis". For more reading see:http://nobelprize.org/nobel_prizes/chemistry/laureates/2005/chemadv05.pdf

[2]   For selected reviews on olefin metathesis, see: (a) Trnka T M, Grubbs R H (2001) Acc Chem Res 34:18–29 (b) Grubbs R H (2003) Handbook of Metathesis. Wiley-VCH, Weinheim, Germany (c) Connon S J, Blechert S, (2003) Angew Chem Int Ed 42:1900–1923 (d) Astruc D (2005) New J Chem 29:42–56 (e) Since 2003, Sigma-Aldrich has exclusively offered some Grubbs and Hoveyda–Grubbs catalysts (incl. **Grubbs-I**, **Grubbs-II** and **Hoveyda-I**, **Hoveyda-II**) produced by Materia Inc. Strem Chemicals now offers a selection of ruthenium (incl. **Ind-I**, **Ind-II**, **Ind-II'**) and molybdenum catalysts, many of which in collaboration with Degussa, Ciba Speciality Chemicals, Umicore, and Zannan Pharma

[3]   Precisely, the common Ru-based olefin metathesis catalysts should be called pre-catalysts: "Compounds that are well-characterised, and that under some conditions will catalyse the metathesis of olefin, but that have not been proven to be essentially identical to the active species for the metathesis reaction, are not well-defined catalysts. They are precursors, or (pre)catalysts." Schrock R R (2004) J Mol Catal A Chem 213:21–30

[4]   (a) Burtscher D, Grela K, (2008) Angew Chem. doi:10.1002/anie.200801451 (b) Gułajski Ł, Michrowska A, Narożnik J, Kaczmarska Z, Rupnicki L, Grela K (2008) ChemSusChem 1:103–109

[5]   Śledź P, Mauduit M, Grela K (2008) Chem Soc Rev 37:2433–2442

[6]   (a) Love J A, Morgan J P, Trnka T M, Grubbs R H (2002) Angew Chem 114:4207–4209 (2002) Angew Chem Int Ed 41:4035–4037 and references therein (b) Kingsbury J S, Hoveyda A H (2005) J Am Chem Soc 127:4510–4517 (c) for an interesting interpretation, see: Maechling S, Zaja M, Blechert S (2005) Adv Synth Catal 347:1413–1422; (d) Bieniek M, Michrowska A, Usanov D, Grela K (2008) Chem Eur J 14:806–818

[7]   Hoveyda A H, Gillingham D G, Van Veldhuizen J J, Kataoka O, Garber S B, Kingsbury J S, Harrity J P A (2004) Org Biomol Chem 2:8–23

[8]   Buchmeiser M R (2000) Chem Rev 100:1565–1604

[9]   Asrar J (1993) J Appl Polym Sci 47:289–293

[10]   Usually, catalysts that are inert to a given olefinic substrate at room or slightly above room temperature are called "latent" or "dormant" initiators. Since the initiation rate depends not only on the catalyst structure but also on alkene, solvent and temperature, these terms should be used with a great care

[11]   (a) Denk K, Fridgen J, Herrmann W A (2002) Adv Synth Catal 344:666–670 (b) Jordaan M, Vosloo H C M (2007) Adv Synth Catal 349:184–192 (c) De Clercq B, Verpoort F (2002) Adv Synth Catal 344:639–648 (d) Chang S, Jones II L, Wang C, Henling L, Grubbs R H (1998) Organometallics 17:3460–3465 (e) van der Schaaf P, Kolly R, Kirner H J, Rime F, Muhlebach A, Hafner A (2000) J Organomet Chem 606:65–74

[12]   Szadkowska A, Grela K (2008) Curr Org Chem 12:1631–1647

[13] Ung T, Hejl A, Grubbs R H, Schrodi Y (2004) Organometallics 23:5399–5401

[14] (a) Barbasiewicz M, Szadkowska A, Bujok R, Grela K (2006) Organometallics 25:3599–3604 (b) Gstrein X, Burtscher D, Szadkowska A, Barbasiewicz M, Stelzer F, Grela K, Slugovc C (2007) J Polym Sci Part A Polym Chem 45:3494–3500 (c) Slugovc C, Burtscher D, Stelzer F, Mereiter K (2005) Organometallics 24:2255–2258

[15] (a) Grela K, Harutyunyan S, Michrowska A (2002) Angew Chem Int Ed 41:4038–4040 (b) Michrowska A, Bujok R, Harutyunyan S, Sashuk V, Dolgonos G, Grela K (2004) J Am Chem Soc 126:9318–9325 (c) Gułajski Ł, Michrowska A, Bujok R, Grela K (2006) J Mol Catal A 254:118–123 (d) Fürstner A, Thiel O R, Lehmann Ch W (2002) Organometallics 21:331–335 (e) Slugovc C, Perner B, Stelzer F, Mereiter K (2004) Organometallics 23:3622–3626 (f) Gawin R, Makal A, Wozniak K, Mauduit M, Grela K (2007) Angew Chem Int Ed 46:7206–7209 (g) Barbasiewicz M, Szadkowska A, Grela K (2008) Chem Eur J 14:9330–9337

[16] (a) Wakamatsu H, Blechert S (2002) Angew Chem Int Ed 41:794–796 (b) Wakamatsu H, Blechert S (2002) Angew Chem Int Ed 41:2403–2405 (c) Gessler S, Randl S, Blechert S (2000) Tetraherdron Lett 41:9973–9976 (d) Bieniek M, Bujok R, Cabaj M, N. Lugan N, Lavigne G, D. Arlt D, Grela K (2006) J Am Chem Soc 128:13652–13653 (e) Bieniek M, Bujok R, Stępkowska H, Jacobi A, Hagenkötter R, Arlt D, Jarzembska K, Woźniak K, Grela K (2006) J Organomet Chem 691:5289–5297 (f) Michrowska A, Gułajski Ł, Kaczmarska Z, Mennecke K, Kirschning A, Grela K (2006) Green Chem 8:685–688 (g) for an overview on Hoveyda-Grubbs catalysts, see: A. Michrowska A, Grela K (2008) Pure Appl Chem 80:31–43

[17] Hejl A, Day M W, Grubbs R H (2006) Organometallics 25:6149–6154

[18] (a) Kadyrow R, Rosiak A, Tarabocchia J, Szadkowska A, Bieniek M, Grela K (2008) Catalysis of Organic Reactions, Chemical Industries Series. White M G (Ed.) Taylor & Francis, London, (b) Grela K, Szadkowska A, Kadyrow R (Degussa AG, 2007) "Neuartige schwefelhaltige Metathese Katalysatoren", DE Patent Application 102007020694.3

[19] (a) Ben-Asuly A, Tzur E, Diesendruck C E, Sigalov M, Goldberg I, Lemcoff N G (2008) Organometallics 27(5):811– 813 (b) Kost T, Sigalov M, Goldberg I, Ben-Asuly A, Lemcoff N G (2008) J Organomet Chem 693:2200–2203

[20] McCarthy J R, Matthews D P, Paolini J P (1998) Organic Syntheses Coll 9:446–452

[21] Molander G A, Brown A R (2006) J Org Chem 71:9681–9686

[22] For other cis-configurated Hoveyda complexes, see: Barbasiewicz M, Bieniek M, Michrowska, Szadkowska A, Makal A, Woźniak K, Grela K (2007) Adv Synth Catal 349:193–203

[23] Clavier H, Nolan S P (2007) Chem Eur J 13:8029–8036

NOVEL CYCLOPOLYMERIZATION DERIVED CONJUGATED POLYENES: SMART MATERIALS FOR ELECTRONICS AND SENSORS

MICHAEL R. BUCHMEISER
Leibniz-Institut für Oberflächenmodifizierung e.V. (IOM), Permoserstraße 15, D-04318 Leipzig, Germany; Institut für Technische Chemie, Universität Leipzig, Linnéstraße 3, D-04103 Leipzig, Germany

Abstract: The metathesis-based cyclopolymerization of 1,6-heptadiynes using late transition metal catalysts is summarized. In this context, results obtained with binary, ternary, and quaternary catalytic systems as well as well-defined molybdenum- and ruthenium-based catalysts will be presented. Special consideration is given to the advancements in catalyst design and mechanistic understanding that have been made in this area during the last few years, which allow the tailor-made synthesis of poly(ene)s. In addition, supported versions of ruthenium-based cyclopolymerization-active systems will be summarized. Finally, selected structure-dependant properties will be outlined where applicable.

1. Introduction

Fully conjugated polymers based on poly(ene)s and related structures represent interesting materials for many applications in the fields of organic (semi-)conductors, optoelectronics, and photonics.[1–6] Unfortunately, poly(acetylene) as the simplest representative of this class of compounds suffers from insolubility, lack of processability, and insufficient stability versus oxygen. Substituted poly(acetylene)s somehow overcome these problems. They are accessible *via* three different routes. The first, ADMET (acyclic diene metathesis) polymerization, is a metathesis-based condensation reaction of α,ω-dienes[7, 8] and is nowadays widely used in the synthesis of poly(*p*-phenylenevinylene)s (*PPVs*) and its

derivatives, respectively.[9–15] This polymerization technique is characterized by a comparable easy setup and many catalysts in principle suitable for metathesis polymerization may be used for these purposes.[14] Nevertheless, preference is nowadays given to well-defined catalytic systems in order to obtain well-defined polymers and to avoid comparably low molecular weights.[16]
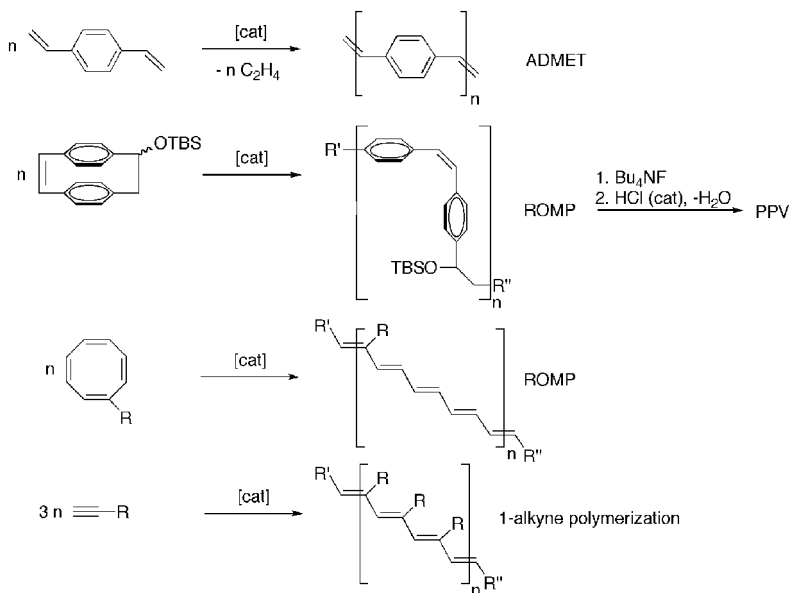
Scheme 1. Metathesis-based polymerization techniques for the synthesis of conjugated materials.

A detailed description of this polymerization method is given in Ref. [17]. The second approach to poly(ene)s, ROMP (ring-opening metathesis polymerization), is restricted to particularly designed poly(ene) precursors such as substituted and unsubstituted cyclooctatetraenes or paracyclophenes.[13–23] The third, alkyne polymerization, allows in principle a wide range of structural variations once a suitable initiator monomer system has been identified (Scheme 1).[18–25] However, despite their outstanding and promising role in the development of conjugated materials, poly(ene)s based on poly(acetylene)s were never able to fulfill these high expectations. Consequently, conjugated materials are nowadays generally based on poly(thiophene)s, poly(pyrrole)s, poly(thiazole)s, poly(p-phenylene)s, PPV and related materials.[26–28] With these systems, a large variety of conjugated polymer-based devices such as organic field transistors,[29, 30] diodes, light-emitting diodes,[27, 31–33] photodiodes, polymer grid triodes, light emitting electrochemical cells, optocouplers, etc. is available.[28, 34, 35]

A major reason for the failure of poly(ene)s in form of poly(acetylene)s in the above-mentioned applications is related to their inherent instability versus moisture and oxygen and their high proneness towards decomposition/

rearrangement in the partially oxidized/doped state. Nevertheless, similar to poly(thiophene), poly(pyrrole), poly(*p*-phenylene)s, PPV, etc., poly(ene)s stablized by appropriate ligand systems and/or incorporated into cyclic structures are believed to exhibit similar stability. In the following, the basic concepts as well as realized structures shall be outlined.

2. Cyclopolymerization of 1,6-Diynes

The cyclopolymerization of 1,6-heptadiynes represents a powerful alternative to 1-alkyne polymerization.[36, 37] Introduction of a ligand in the 4-position of the 1,6-heptadiyne generally improves the solubility of the resulting polymers. Thus, substituted heptadiynes possess good solubility in common organic solvents (e.g. C_6H_6, toluene, CH_2Cl_2, $CHCl_3$), good long-term stability towards oxidation and high effective conjugation lengths.[25, 36, 38, 39] So far, the cyclopolymerization of a large number of uncharged[25, 36, 37, 39–51] and ionic monomers with substituents at the 4-, respectively 2- and 5-position has been investigated.[52–57] In most cases binary and ternary catalysts have been employed.

2.1. POLYMER STRUCTURE

In terms of polymer structure, the cyclopolymerization of 1,6-heptadiynes usually yields poly(ene)s that contain a mixture of five- and six-membered rings (Figure 1).
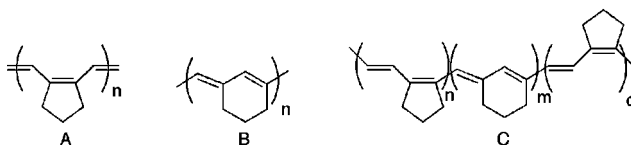
Figure 1. Possible ring structures of poly(1,6-heptadiynes) prepared via cyclopolymerization. Poly(cyclopent-1-enevinylene)s (A); poly(cyclohex-1-ene-3-methylidene)s (B); and mixed structures (C).

It is important to note that these two ring structures generally occur *within one single polymer chain* as shown in C and not in form of a mixture of polymer chains either consisting of five- or six-membered rings. The structures of these polymers may be determined by ^{13}C-NMR, since the carbonyl carbon and the quaternary carbon are especially sensitive to the ring size. Nevertheless, the *cis/trans* configuration of the exocyclic double bond or the *s-cis/s-trans* configuration of the backbone single bond in poly(cyclohex-1-ene-3-vinylene)s as well as the configuration of the double bonds in poly(cyclopent-1-ene-1-vinylene)s cannot be

determined, thus impeding to distinguish between the two possible idealized planar conformational isomers.

2.2. STEREOSELECTIVE CYCLOPOLYMERIZATION

2.2.1. *Diethyl Dipropargylmalonate (DEDPM)*

In order to understand the polymer structures that are obtained in the polymerization of 1,6-heptadiynes, one needs to consider all possible polymerization mechanisms. Thus, in case 1,6-heptadiynes are subject to cyclopolymerization using well-defined Schrock catalysts, polymerization can proceed *via* two mechanisms. One is based on a monomer insertion, where the first alkyne group adds to the molybdenum alkylidene in a way that a disubstituted alkylidene is formed, which then reacts with the second terminal alkyne group to form poly(ene)s consisting of five-membered repeat units. In analogy to 1-alkyne polymerization, one refers to this type of insertion as α-insertion again (Scheme 2).
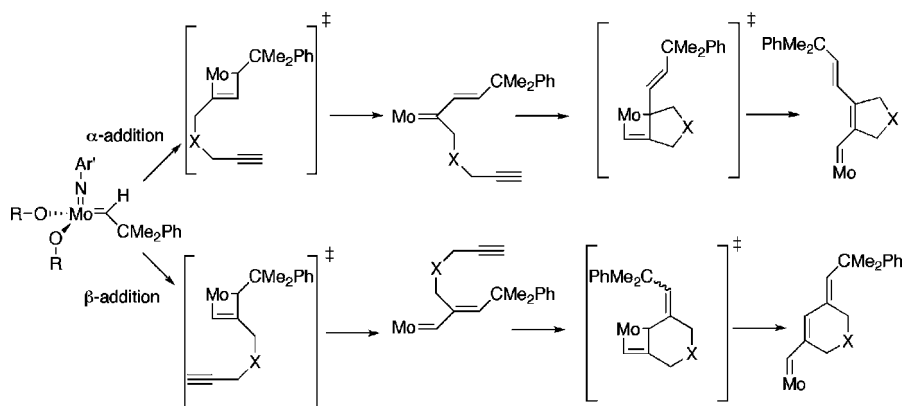
Scheme 2. Two possible reaction pathways and resulting ring structures in the cyclopolymerization of 1,6-heptadiynes.

Vice versa, the monomer can add to the initiator in a way that a monosubstituted alkylidene is formed. This sequence, again referred to as *ß-addition*, yields poly(ene)s based on six-membered rings. Poly(DEDPM) *exclusively consisting of six-membered rings* was first prepared using the molybdenum imido alkylidene complex Mo(*N*-2-*tert*-Bu-C$_6$H$_4$)(CH-*tert*-Bu)(O$_2$CCPh$_3$)$_2$.[25, 39] Here the bulky ligands (i.e. the carboxylates) forced the monomer to undergo selective *ß-addition* by sterically preventing any other approach to the CNO-face.[23] These findings were in accordance with the concept of "small alkoxides" developed by Schrock et al. for this type of initiators.[22, 24] Nevertheless, it should be emphasized that both Schrock et al.[58] and others[59] already underlined the important role of substituents at the arylimido ligand, which can

totally invert the mode of insertion with the same set of alkoxides.[59] The structure of poly(DEDPM) consisting solely of cyclohex-1-ene-3-vinylene units was identified by ^{13}C-NMR as described above.

The polymerization of DEDPM for the synthesis of poly(1,2-cyclopent-1-enylene-vinylene)s required some significant tuning of the Schrock-type initiator. In order to obtain a polymer consisting virtually solely of cyclopent-1-ene-1-vinylene units, small alkoxides were required in order to allow α-addition. Unfortunately, the use of small alkoxides turned out to be a necessary, yet not sufficient prerequisite. In fact, some additional modifications in catalyst design had to be carried out. These modifications were related to some basic properties of molybdenum complexes of the type Mo(NAr´)(CHCMe$_2$Ph)(OR´)$_2$. Generally speaking, these compounds exist in form of two rotamers.[23, 58] The one isomer with the 2-phenylpropyl group pointing towards the imido ligand is called the *syn*, the one with this group pointing away from the imido group is called the *anti* rotamer. These two rotamers interconvert with a rate that depends on both the electronic and steric effects around the Mo-center, thus allowing to tune their reactivity and selectivity.[23, 58, 60, 61] Even more important, the *syn* and *anti* rotamer possess significantly different reactivities, the *anti* rotamer being the more reactive one.

These properties have already been used for the synthesis of a large variety of stereoregular norborn-2-ene- and norbornadiene-based polymers.[23, 58, 59, 62, 63] In these polymerizations, addition of a base such as quinuclidine has a strong impact on polymerization. Though a base is believed to be not coordinated to molybdenum during insertion,[24] it strongly influences the reactivity of the entire system.[19, 60] On one hand, the presence of a base particularly at low temperature favors the formation of (coordinated) *anti* rotamer since it stabilizes this isomer.[58] On the other hand, it enhances the relative reactivity of the *syn* isomer. Fluoroalkoxide-based initiators such as Mo(N-2,6-Me$_2$-C$_6$H$_3$)(CHCMe$_2$Ph)(OCMe(CF$_3$)$_2$)$_2$ were not capable of forming poly(DEDPM) solely consisting of five-membered repeat units.[36] Neither addition of quinuclidine nor lower polymerization temperature significantly changed this situation. Since syn-anti interconversion is slow in these complexes, the final geometry of a cyclopolymerization-derived polymer must at least be influenced if not governed by both the relative reaction rates of the *syn* and *anti* isomer and the rate of interconversion. If this was true, initiators based on non-fluorinated *alkoxides* had to be expected to allow the preparation of the target polymer since they generally show fast syn-anti interconversion. As a matter of fact, Schrock initiators containing non-fluorinated alkoxides could be used for the living polymerization of DEDPM to produce poly(ene)s solely based on five-membered rings.[64, 65] Thus, low-temperature-initiated polymerization of DEDPM using Mo(N-2,6-*iso*-Pr$_2$-C$_6$H$_3$)(CHCMe$_2$Ph)(OCH(CH$_3$)$_2$)$_2$ as catalyst yielded virtually solely poly(cyclopent-1-ene-1-vinylene)s. The same polymer was obtained using either

Mo(N-2,6-Me$_2$-C$_6$H$_3$)(CHCMe$_2$Ph)(OC(CH$_3$)$_3$)$_2$·quinuclidine or Mo(N-2,6-*iso*-Pr$_2$-C$_6$H$_3$)(CHCMe$_2$Ph)(OC(CH$_3$)$_3$)$_2$·quinuclidine. In this case polymerizations were conducted at room temperature. Again, the polymer structure was assigned by ^{13}C-NMR as described above.

2.2.2. Polymerization of Chiral Monomers

Chiral monomers, i.e. monomers containing at least one asymmetric carbon allow to retrieve further information about the actual configuration of a poly(ene) and the relative orientation of the repetitive units (i.e. tacticity). The cyclopolymerization of the chiral monomers di-(1S, 2R, 5S)-(+)-menthyl dipropargylmalonate and 4-(ethoxycarbonyl)-4-(1*S*, 2*R*, 5*S*)-(+)-menthoxycarbonyl-1,6-heptadiyne to yield poly(ene)s consisting virtually solely of five-membered rings was accomplished using Mo(N-2,6-*iso*-Pr$_2$-C$_6$H$_3$)(CHCMe$_2$Ph)(OC(CH$_3$)$_3$)$_2$ and Mo(N-2,6-*iso*-Pr$_2$-C$_6$H$_3$)(CHCMe$_2$Ph)(OC(CH$_3$)$_3$)$_2$·quinuclidine, respectively. The ^{13}C-NMR spectrum of poly(4-(ethoxycarbonyl)-4-(1*S*, 2*R*, 5*S*)-(+)-menthoxycarbonyl-1,6-heptadiyne) indicated a polymer containing virtually solely five-membered repeat units. In addition, only one single set for each type of carbon was observed, indicative for a highly tactic base. Keeping the restrictions in terms of symmetry described above in mind, either a *cis* or *trans-st* structure can be assigned. A 500 MHz ^{1}H-^{1}H-correlated spectrum did not show any coupling between the olefinic protons, nevertheless, a *trans*-structure could be derived from analysis of the double bonds located next to the end groups. Therefore, an *alternating cis–trans* conformation was assigned to the polymer. If this was true, then the polymer possessed a *syndiotactic* base. Nevertheless, since there could be some small, undetectable coupling, this assignment remains, though highly probable, still speculative.

2.3. LIVINGNESS

While classical catalysts usually result in ill-controlled polymerization systems, well-defined *Schrock* initiators cyclopolymerize 1,6-heptadiynes in a living manner, in most cases a class VI living manner according to Matyjaszewski.[66] Polymers prepared on the base of one single repetitive unit (i.e. poly(cyclopent-1-ene-1-vinylene)s and poly(cyclohex-1-ene-3-vinylene)s, respectively) by the action of the Schrock catalysts described above were prepared in a truly living way and were therefore well defined in terms of molecular weight and molecular weight distribution. It is worth mentioning, that the accurate determination of molecular weights with such rigid structures requires the use of absolute methods such as light scattering rather than relative methods such as calibration versus poly(styrene).[64, 65]

2.4. INITIATORS BASED ON M-N-BU$_4$SN-ETOH-QUINUCLIDINE (M= MOCL$_5$, MOOCL$_4$)

An important aspect in the large-scale synthesis of any material is costs. Despite their superiority, *Schrock* initiators are characterized by limited commercial availability and high sensitivity versus oxygen and moisture. Classical ternary systems have been investigated for this reason, yet were not able to compete with Schrock systems in terms of materials properties (i.e. definition, purity, etc.) so far. Nevertheless, there is still significant interested in the use of alternative systems in the cyclopolymerization of 1,6-heptadiynes. While standard ternary systems behaved as expected, yielding ill-defined polymers without any control over molecular weight, the addition of quinuclidine turned out to be a milestone in this area of research.[64, 65] Thus, DEDPM was cyclo-polymerized by MoCl$_5$-*n*-Bu$_4$Sn-EtOH-quinuclidine (1:1:5:1) and MoOCl$_4$-*n*-Bu$_4$Sn-EtOH-quinuclidine (1:1:2:1) to produce poly(DEDPM) *exclusively based on 1,2-(cyclopent-1-enylene)-vinylene units*. The initiator efficiency of MoOCl$_4$-*n*-Bu$_4$Sn-EtOH-quinuclidine (1:1:2:1) was as high as 91%, the highest value ever reported for such systems, whereas the efficiency for the corresponding MoCl$_5$-based initiator was ≤67%. The absorption maximum λ_{max} for poly(DEDPM) was 587 nm, close to that one found for poly(DEDPM) prepared by a *Schrock* initiator (592 nm, *vide infra*). A maximum effective conjugation length N_{eff} of 49 (*THF*) was calculated therefrom. A plot of number of monomers (*N*) added versus molecular weights (M_n) as determined by light scattering showed a linear dependence for both initiators. Multistage polymerizations of DEDPM indicated for both initiator systems that the catalytic species were active for at least 6 h in the presence of monomer *yet did not fulfill the criteria of a living polymeri-zation*, i.e. stability of the active chain end in the *absence of monomer*. Despite identical polymers were produced, this had to be regarded as a significant disadvantage compared to well-defined Schrock initiators, which generally provide truly living polymerizations.

2.5. RUTHENIUM-BASED CYCLOPOLYMERIZATION SYSTEMS

Grubbs-Herrmann (e.g. RuCl$_2$(1,3-bis(2,4,6-trimethylphenyl)-4,5-dihydroimi-dazolin-2-ylidene)(CHPh)(PCy$_3$)) respectively Grubbs-Hoveyda catalysts (e.g. RuCl$_2$(1,3-bis(2,4,6-trimethylphenyl)-4,5-dihydroimidazol-2-ylidene)(CH(2-(2-PrO-C$_6$H$_4$))[67] are air and moisture-stable metathesis catalysts with remarkable activity, sometimes rivaling that of highly active Schrock catalysts.[68] Nonetheless, despite their activity in ring-opening metathesis polymerization (ROMP), ring-closing, enyne and ring-opening cross metathesis reactions, none of the existing systems was capable of polymerizing alkynes or cyclopolymerizing 1,6-heptadiynes so far. Recently, Buchmeiser and Nuyken et al. reported on the

successful synthesis of a modified Grubbs-Hoveyda catalyst that was capable of cyclopolymerizing of 1,6-heptadiynes in both a living and stereoregular way.[69, 70] With the development of these catalytic systems, one of the last gaps between molybdenum- and ruthenium-based metathesis catalysts was closed.

Ru(CF$_3$COO)$_2$(1,3-dimesityl-4,5-dihydroimidazl-2-ylidene)(CH-(2-(2-PrO-C$_6$H$_4$))), initially developed as a highly efficient and active catalyst for ring-closing, enyne and cross metathesis[71] possesses an enhanced polarization across the ruthenium–carbon double bond, which directly translates into an increased reactivity, thus allowing the cyclopolymerization of DEDPM. Nevertheless, though highly active, this catalyst did not allow a living polymerization setup[72] in the polymerization of DEDPM. Consequently, catalyst variations were carried out to overcome this problem. Exchange of the 2-(2-propoxy)benzylidene ligand by the 2,4,5-trimethoxybenzylidene ligand[73] resulted in Ru(CF$_3$COO)$_2$(1,3-dimesityl-4,5-dihydroimidazol-2-ylidene)(CH-(2,4,5-(MeO)$_3$-C$_6$H$_4$)). This compound turned out to be an excellent catalyst for the cyclopolymerization of DEDPM, allowing full control over molecular weight.[69] Similar to polymerizations carried out with well-defined Schrock initiators, polymerizations of DEDPM with this catalyst in methylene chloride proceeded in a class VI living manner.[66] In terms of microstructure, poly(DEDPM) prepared by this catalyst consisted again virtually solely (>96%) of 1,2-cyclopent-1-enylenevinylene units as shown by ^{13}C-NMR measurements.[64, 65] The polymerization mechanism was proposed to follow that of molybdenum-based cyclopolymerizations[36] as evidenced by ^{1}H-NMR. Here, the disappearance of the starting alkylidene at δ = 17.58 ppm and the appearance of new alkylidene signals at δ = 15.63, 18.67, 19.90, 20.84 and 21.63 ppm was observed.

Using MALDI-TOF spectroscopy, 2-propoxybenzylidene was found as end group in *all* polymers prepared by the action of Ru(CF$_3$COO)$_2$(1,3-dimesityl-4,5-dihydroimidazl-2-ylidene)(CH-(2-(2-PrO)-C$_6$H$_4$))), indicating the absence of any chain transfer reactions. The polymerization of chiral 4-(ethoxycarbonyl)-4-(1*S*, 2*R*, 5*S*)-(+)-menthoxycarbonyl-1,6-heptadiyne by this catalyst again proceeded in a stereo- and regioselective way. The ^{13}C-NMR spectrum of poly (4-(ethoxycarbonyl)-4-(1*S*, 2*R*, 5*S*)-(+)-menthoxycarbonyl-1,6-heptadiyne) was identical to the one recorded with a sample of this polymer prepared by the action of a Schrock catalyst. Consequently, the same structure, i.e. a *st* poly(*trans*-1,2-(cyclopent-1-enylene)vinylene) with >98% stereoregularity was assigned.[64, 65] This finding was of particular interest, since polymers prepared via ring-opening metathesis polymerization (ROMP) using other Ru-based catalysts revealed a *trans*-content ≤90% and low stereoregularity.[68, 74]

In an extension to this work, Buchmeiser et al. performed a systematic variations in the catalytic system in order to further improve the entire polymerization system.[70] For this purpose, 14 metathesis initiators, i.e. the Hoveyda catalyst RuCl$_2$(IMesH$_2$)(CH-2-(2-PrO)-C$_6$H$_4$), as well as Ru(CF$_3$COO)$_2$(IMesH$_2$)

(CH-2-(2-PrO)-C$_6$H$_4$), Ru(CF$_3$CF$_2$COO)$_2$(IMesH$_2$)(CH-2-(2-PrO)-C$_6$H$_4$), Ru-(CF$_3$CF$_2$CF$_2$COO)$_2$(IMesH$_2$)(CH-2-(2-PrO)-C$_6$H$_4$), RuCl$_2$(IMesH$_2$)(CH-2,4,5-(MeO)$_3$-C$_6$H$_2$), Ru(CF$_3$COO)$_2$(IMesH$_2$)(CH-2,4,5-(MeO)$_3$-C$_6$H$_2$), Ru(CF$_3$CF$_2$COO)$_2$(IMesH$_2$)(CH-2,4,5-(MeO)$_3$-C$_6$H$_2$), Ru(CF$_3$CF$_2$CF$_2$COO)$_2$ (IMesH$_2$)(CH-2,4,5-(MeO)$_3$-C$_6$H$_2$), RuCl$_2$(IMes)(CH-2-(2-PrO)-C$_6$H$_4$), Ru(CF$_3$COO)$_2$(IMes)(CH-2-(2-PrO)-C$_6$H$_4$), RuCl$_2$(IMesH$_2$)(CH-2-(2-PrO)-5-NO$_2$-C$_6$H$_3$), Ru(CF$_3$COO)$_2$(IMesH$_2$)(CH-2-(2-PrO)-5-NO$_2$-C$_6$H$_3$), Ru(CF$_3$CF$_2$COO)$_2$(IMesH$_2$)(CH-2-(2-PrO)-5-NO$_2$-C$_6$H$_3$), and Ru(CF$_3$CF$_2$CF$_2$COO)$_2$(IMesH$_2$)(CH-2-(2-PrO)-5-NO$_2$-C$_6$H$_3$) (IMes=1,3-dimesitylimidazol-2-ylidene; IMesH$_2$=1,3-dimesityl-4,5-dihydroimidazol-2-ylidene, Figure 2) were investigated for their polymerization activity for DEDPM. Class VI living polymerization systems could be generated
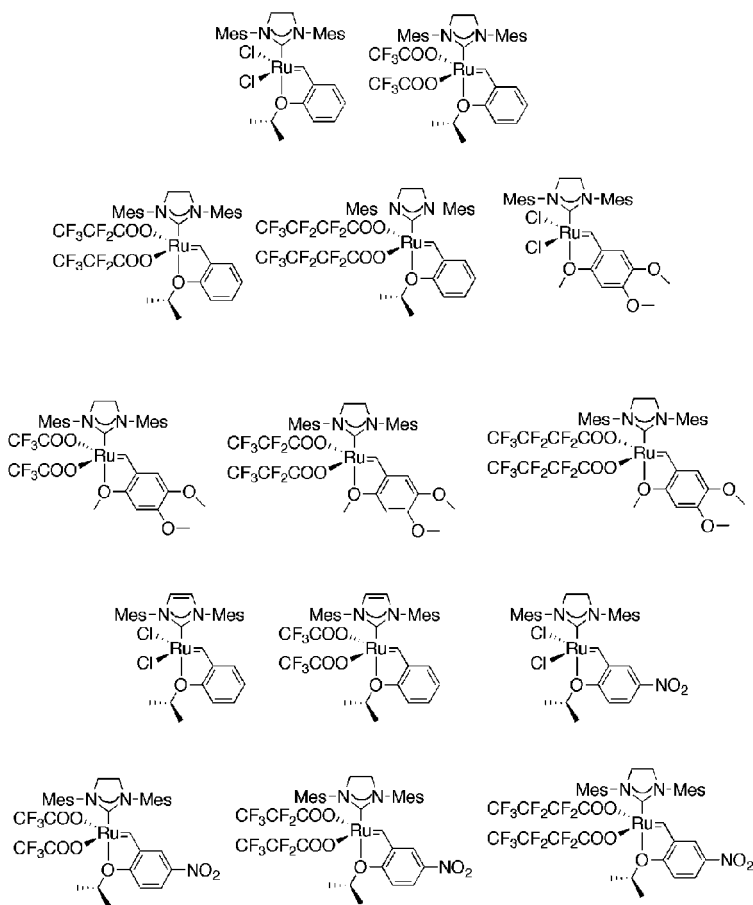
Figure 2. Ru-based initiators used in a systematic study on the cyclopolymerization of DEDPM.

with initiators $Ru(CF_3COO)_2(IMesH_2)(CH-2,4,5-(MeO)_3-C_6H_2)$, $Ru(CF_3CF_2COO)_2$ $(IMesH_2)(CH-2,4,5-(MeO)_3-C_6H_2)$, $Ru(CF_3CF_2CF_2COO)_2(IMesH_2)(CH-2,4,5-$ $(MeO)_3-C_6H_2)$, containing the $(CH-2,4,5-(OMe)_3-C_6H_2)$ group and initiators $Ru(CF_3COO)_2$ $(IMesH_2)(CH-2-(2-PrO)-5-NO_2-C_6H_3)$, $Ru(CF_3CF_2COO)_2(IMesH_2)$ $(CH-2-(2-PrO)-5-NO_2-C_6H_3)$, and $Ru(CF_3CF_2CF_2COO)_2(IMesH_2)(CH-2-(2-$ $PrO)-5-NO_2-C_6H_3)$ containing the $(CH-2-(2-PrO)-5-NO_2-C_6H_3)$ group. From these systematic variations in catalyst structure, the following conclusions were drawn: In order to be suitable for the living cyclopolymerization of DEDPM, (i) the replacement of both chlorine ligands with strongly electron withdrawing carboxylic salts such as $CF_3(CF_2)_{x=0-2}COOAg$ is required; (ii) the NHC has to be electron rich.

In addition, the living character of the polymerization of DEDPM strongly correlates with the steric and electronic situation at the benzylidene ligand. Therefore, the weaker the coordination of the oxygen fragment to the Ru-core is, the lower the values for k_p/k_i are, resulting in increased insertion efficiencies. Both types of initiators mentioned above fulfilled these criteria. These initiators gave raise to 100% α-insertion of the monomer, resulting in the formation of poly(acetylene)s containing virtually solely (>96%) five-membered ring structures. The use of larger fluorinated carboxylates turned out to further reduce chain-transfer reactions resulting in poly(ene)s with low PDIs.

2.6. BLOCK-COPOLYMER SUPPORTED RUTHENIUM-BASED CYCLOPOLYMERIZATION SYSTEMS

One of the many advantages of ruthenium based catalysts is their tolerance to polar functional groups and water as a reaction medium. Consequently, reactions that could be carried out under aqueous conditions appeared favorable. One of the possibilities to run polymerizations under aqueous conditions is the location of a suitable catalyst within a micelle. While the use of sodium dodecylsulfonate (SDS) as micelle-forming reagent clearly failed, immobilization of the catalyst on a micelle-forming support was successful. The synthetic route necessary for the realization of a polymer-bound catalyst had to fulfill two requirements. On the one hand, perfect mimics of $Ru(CF_3COO)_2(IMesH_2)(CH-(2,4,5-(MeO)_3-C_6H_4)$ had to be generated in order to maintain its reactivity and stereoselectivity. On the other hand and in contrast to conventional suspension/emulsion poly-merization, the catalyst had to be permanently linked to the block copolymer amphiphile. Only under these conditions, the catalyst was located in the hydro-phobic micellar core upon micelle formation of the functionalized block copolymer in water, where also the monomer was dissolved. Preparation of the functionalized block copolymers was accomplished by first reacting an amphiphilic, poly(2-oxazoline)-derived copolymer, $Me_{30}Non_6(PenOH)_2Pip$, bearing two randomly distributed hydroxyl groups in the side chain of the hydrophobic

block with hexafluoroglutaric anhydride followed by deprotonation with aqueous NaOH and reaction with $AgNO_3$ to yield a polymer-bound silver carboxylate. The last steps entailed its reaction with the catalyst precursors $RuCl_2$(1,3-bis(2,4,6-trimethylphenyl)-4,5-dihydroimidazol-2-ylidene)(CH-2-(2-PrO)-C_6H_4 and $RuCl_2$(1,3-bis(2,4,6-trimethylphenyl)-4,5-dihydroimidazol-2-ylidene)(CH-2,4,5-(OMe)$_3$-C_6H_2),[73] respectively, followed by reaction with silver trifluoroacetate to endcap unreacted chloro groups of the catalysts. In course of this two-step chlorine exchange, the corresponding ruthenium compounds were fixed to the support to yield the poly(2-oxazoline)-immobilized catalyst $Me_{30}Non_6$((PenOCO(CF$_2$)$_3$COO)(CF$_3$COO)Ru(CH-2,4,5-(OMe)$_3C_6H_2$)(IMesH$_2$))$_{0.8}$(PenOCO(CF$_2$)$_3$COOAg)$_{1.2}$Pip (Scheme 3). The successful and selective immobilization was evidenced by ^{1}H-NMR. Thus, the immobilized system was characterized by one single alkylidene signal at $\delta =$ 17.51 ppm, which perfectly fist the chemical shift for the alkylidene signal in the homologous compound Ru(CF$_3$COO)$_2$(IMesH$_2$)(CH-(2,4,5-(MeO)$_3$-C_6H_4) at $\delta =$ 17.58 ppm. Poly(DEDPM) prepared with the block copolymer-immobilized initiator in water was characterized by comparably low polydispersity indices (PDIs) <1.40 compared to poly(DEDPM) prepared by Ru(CF$_3$COO)$_2$(IMesH$_2$)(CH-2-(2,4,5-(MeO)$_3$-C_6H_3).
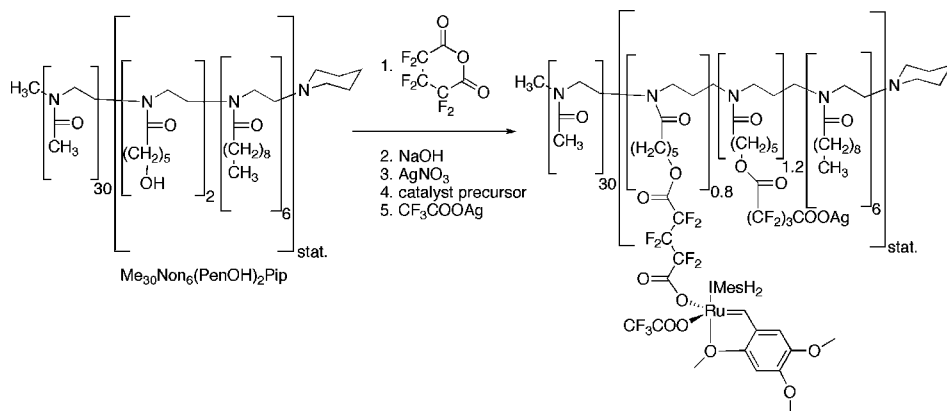
Scheme 3. Cyclopolymerization-active Ru-based initiator immobilized to a micelle-forming block-copolymer.

Due to the increased concentration of DEDPM within the micelles, reaction times required to reach complete conversion were reduced to 30 min compared to 2 h with the parent catalyst indicating the catalytic effect of the micellar nanoreactors formed in aqueous medium. Stabilized by the amphiphilic structure of the block-copolymer, the poly(acetylene) lattices could be stored over 2 weeks without any change in terms of latex particle size, molecular weight and UV–Vis absorption maximum.

2.7. CYCOPOLYMERIZATION OF HEPTADIYNES BASED ON QUATERNARY AMMONIUM SALTS

In an extension to DEDPM and related monomers, the cyclopolymerization of polar, ionic N,N-dibutyl-N,N-dipropargylammonium bis(trifluoromethylsulfonyl) imide (**M1**), N,N-dimethyl-N,N-dipropargylammonium bis(trifluoromethyl-sulfonyl)imide (**M2**), N,N-dipropargylmorpholinium bis(trifluoromethylsulfonyl)-imide (**M3**) and N-propyl-N,N-dipropargylamine (**M4**) using different well-defined Schrock- and trifluoroacetate-modified Grubbs-type initiators was investigated. The Ru-based initiators allowed for the polymerization of **M1**–**M3** with average isolated polymer yields around 25–40%, however, poly-**M2** and poly-**M3** thus prepared consisted >95% of five-membered ring structures, i.e. (3,4-(1H-2,5-dihydropyrrolylene)vinylene)s units. In contrast, the use of the Schrock type initiator Mo(N-2,6-iPr$_2$-C$_6$H$_3$)(CHMe$_2$Ph)(OC(CH$_3$)(CF$_3$)$_2$)$_2$ allowed for quantitative polymer yields, whereas, poly-**M2** was based on both five- and six-membered, i.e. (3,5-(1,2,5,6-tetrahydropyridinylene)methylidene) cyclic units. Polymers were synthesized with molecular weights M_n < 21,800 g/mol and polydispersity indices in the range of 1.04 < PDI < 1.37 and 1.01 < PDI < 1.08 with Ru- and Mo-based initiators, respectively. They were additionally investigated for their thermal stability and ionic conductivity. Finally, the solvato-chromic behavior of the polymers prepared was studied. Particularly, solutions of poly-**M1** prepared by the action of Ru-based initiators displayed a high sensitivity towards traces of water in N,N-dimethylformamide.

3. Conclusions

Cyclopolymerization has experienced dramatic improvements in terms of mechanistic understanding and definition of the resulting polymers and materials, respectively. The knowledge about complex catalytic systems has reached a level that allows the straightforward tailor-made synthesis of materials with designed properties. The materials described here are currently under investigation for their peculiar physical properties such as conductivity, photoconductivity and applications in sensors. Despite these interesting and useful applications, which are certainly more located in the areas of physics or chemical engineering, one should not forget that any successful realization of "advanced materials" is dependant on synthetic chemistry to a major extent. Furthermore, interdisciplinary research as the one described here, crossing the borders between organic, organometallic, physical, and polymer chemistry, is required.

Acknowledgement

References

[1] Skotheim, T. A., Elsenbaumer, R. L., Reynolds, J. R., 1997, Handbook of Conducting Polymers, 2nd ed., Marcel Dekker, New York.

[2] Brédas, J. L., Silbey, R. J., 1991, Conjugated Polymers, Kluwer, Dordrecht.

[3] Heeger, A. J., 2001, *Angew. Chem.*, **113**: 2660–2682.

[4] MacDiarmid, A. G., 2001, *Angew. Chem.*, **113**: 2649–2659.

[5] Shirakawa, H., 2001, *Angew. Chem.*, **113**: 2642–2648.

[6] Schottenberger, H., Buchmeiser, M. R., 1998, *Recent Res. Dev. Macromol. Res.*, **3**: 535–550.

[7] Wagener, K. B., Boncella, J. M., Nel, J. G., Duttweiler, R. P., Hillmyer, M. A., 1990, *Makromol. Chem.*, **191**: 365–374.

[8] Wagener, K. B., Boncella, J. M., Nel, J. G., 1991, *Macromolecules*, **24**: 2649–2657.

[9] Wolf, A., Wagener, K. B., 1991, *Polym. Prepr. (Am. Chem. Soc., Div. Polym. Chem.)*, **32**: 535–536.

[10] Thorn-Csányi, E., Kraxner, P., 1997, *Macromol. Chem. Phys.*, **198**: 3827–3843.

[11] Thorn-Csányi, E., Kraxner, P., 1997, *J. Mol. Catal.: A Chem.*, **115**: 21–28.

[12] Thorn-Csányi, E., Kraxner, P., 1997, *Macromol. Symp.*, **122**: 77–81.

[13] Müllner, R., Winkler, B., Stelzer, F., Tasch, S., Hochfilzer, C., Leising, G., 1999, *Synt. Met.*, **105**: 129–133.

[14] Schlick, H., Stelzer, F., Tasch, S., Leising, G., 2000, *J. Mol. Catal. A: Chem.*, **160**: 71–84.

[15] Thorn-Csányi, E., Herzog, O., 2004, *J. Mol. Catal. A: Chem.*, **213**: 123–128.

[16] Brzezinska, K., Wolfe, P. S., Watson, M. D., Wagener, K. B., 1996, *Macromol. Chem. Phys.*, **197**: 2065–2074.

[17] Baughman, T. W., Wagener, K. B., 2005, *Progr. Polym. Sci.*, **176**: 1–42.

[18] Krouse, S. A., Schrock, R. R., 1988, *Macromolecules*, **21**: 1885–1888.

[19] Schlund, R., Schrock, R. R., Crowe, W. E., 1989, *J. Am. Chem. Soc.*, **111**: 8004–8006.

[20] Schaffer, H. E., Chance, R. R., Knoll, K., Schrock, R. R., Silbey, R. J., 1990, Conjugated Polymeric Materials: Opportunities in Electronics, Optoelectronics, and Molecular Electronics, Kluwer, Dordrecht, p. 365.

[21] Saunders, R. S., Cohen, R. E., Schrock, R. R., 1991, *Macromolecules*, **24**: 5599–5605.

[22] Schrock, R. R., Luo, S., Zanetti, N. C., Fox, H. H., 1994, *Organometallics*, **13**: 3396–3398.

[23] Schrock, R. R., 1995, *Polyhedron*, **14**: 3177–3195.

[24] Schrock, R. R., Luo, S., Lee Jr., J. C., Zanetti, N. C., Davis, W. M., 1996, *J. Am. Chem. Soc.*, **118**: 3883–3895.

[25] Schattenmann, F. J., Schrock, R. R., 1996, *Macromolecules*, **29**: 8990–8991.

[26] Hide, F., Díaz-García, M. A., Schwartz, B. J., Heeger, A. J., 1997, *Acc. Chem. Res.*, **30**: 430–436.

[27] Sheats, J. R., Chang, Y.-L., Roitman, D. B., Stocking, A., 1999, *Acc. Chem. Res.*, **32**: 193–200.

[28] Fox, M. A., 1999, *Acc. Chem. Res.*, **32**: 201–207.

[29] Horowitz, G., 1998, *Adv. Mater.*, **10**: 365–377.

[30] Sirringhaus, H., Tessler, N., Friend, R. H., 1998, *Science*, **280**: 1741–1744.

[31] Brédas, J.-L., Cornil, J., Beljonne, D., Santos, D. A. D., Shuai, Z., 1999, *Acc. Chem. Res.*, **32**: 267–276.

[32] van Hutten, P. F., Krasnikov, V. V., Hadziioannou, G., 1999, *Acc. Chem. Res.*, **32**: 257–265.

[33] Wang, Y. Z., Epstein, A. J., 1999, *Acc. Chem. Rev.*, **32**: 217–224.

[34] Alivisatos, A. P., Barbara, P. F., Castlemann, A. W., Chang, J., Dixon, D. A., Klein, M. L., McLendon, G. L., Miller, J. S., Ratner, M. A., Rossky, P. J., Stupp, S. I., Thompson, M. E., 1998, *Adv. Mater.*, **10**: 1297–1336.

[35] Chen, C. H., Shi, J., Tang, C. W., 1997, *Macromol. Symp.*, **125**: 1–48.

[36] Fox, H. H., Schrock, R. R., 1992, *Organometallics*, **11**: 2763–2765.

[37] Fox, H. H., Wolf, M. O., O'Dell, R., Lin, B. L., Schrock, R. R., Wrighton, M. S., 1994, *J. Am. Chem. Soc.*, **116**: 2827–2843.

[38] Choi, S.-K., Gal, Y.-S., Jin, S.-H., Kim, H.-K., 2000, *Chem. Rev.*, **100**: 1645–1681.

[39] Schattenmann, F. J., Schrock, R. R., Davis, W. M., 1996, *J. Am. Chem. Soc.*, **118**: 3295–3296.

[40] Jang, M. S., Kwon, S. K., Choi, S. K., 1990, *Macromolecules*, **23**: 4135.

[41] Ryoo, M. S., Lee, W. C., Choi, S. K., 1990, *Macromolecules*, **23**: 3029.

[42] Kim, Y. H., Choi, K. Y., Choi, S. K., 1989, *J. Polym. Sci., Part C*, **27**: 443.

[43] Kim, Y.-H., Kwon, S.-K., Choi, S. K., 1994, *J. Macromol. Sci., Pure Appl. Chem.*, **A31**: 2041.

[44] Han, S. H., Kim, U. Y., Kang, Y. S., Choi, S.-K., 1991, *Macromolecules*, **24**: 973–976.

[45] Jin, S. H., Cho, H. N., Choi, S. K., 1993, *J Polym. Sci. A – Polym. Chem.*, **31**: 69–74.

[46] Lee, H.-J., Oh, J. M., Choi, S. J., Kim, H.-K., Choi, S. K., 1994, *Polym. Bull.*, **32**: 433.

[47] Lee, J.-H., Park, J.-W., Oh, J.-M., Choi, S.-K., 1995, *Macromolecules*, **28**: 377–379.

[48] Kim, Y.-H., Kwon, S.-K., Lee, J.-K., Jeong, K. G., Choi, S. K., 1995, *J. Macromol. Sci., Pure Appl. Chem.*, **A32**: 1761.

[49] Kwon, S.-K., Kim, Y.-H., Choi, S.-K., 1995, *J. Polym. Sci., Polym. Chem. Ed.*, **33**: 2135–2140.

[50] Cho, H.-N., Lee, J.-Y., Kim, S.-H., Choi, S. K., Kim, J. Y., 1996, *Polym. Bull.*, **36**: 391.

[51] Kim, Y. H., Kwon, S. K., Choi, S. K., 1997, *Macromolecules*, **30**: 6677–6679.

[52] Gal, Y.-S., Choi, S.-K., 1995, *Eur. Polym. J.*, **31**: 941–945.

[53] Tlenkopatchev, M. A., Navarro, J., Sanchev, C., Canseco, M. A., Ogawa, T., 1995, *Vysokomol. Soedin.*, **37**: 1212.

[54] Kang, K. L., Cho, H. N., Choi, K. Y., Choi, S. K., Kim, S. H., 1993, *Macromolecules*, **26**: 4539–4543.

[55] Kim, S.-H., Choi, S.-J., Park, J.-W., Cho, H.-N., Choi, S.-K., 1994, *Macromolecules*, **27**: 2339–2341.

[56] Zhang, N., Wu, R., Li, Q., Pakbaz, K., Yoon, C. O., Wudl, F., 1993, *Chem. Mater.*, **5**: 1598–1599.

[57] Choi, D.-C., Kim, S.-H., Lee, J.-H., Cho, H.-N., Choi, S.-K., 1997, *Macromolecules*, **30**: 176–181.

[58] Schrock, R. R., Lee, J.-K., O'Dell, R., Oskam, J. H., 1995, *Macromolecules*, **28**: 5933–5940.

[59] Buchmeiser, M. R., Schuler, N., Kaltenhauser, G., Ongania, K.-H., Lagoja, I., Wurst, K., Schottenberger, H., 1998, *Macromolecules*, **31**: 3175–3183.

[60] Schrock, R. R., Crowe, W. E., Bazan, G. C., DiMare, M., O'Regan, M. B., Schofield, M. H., 1991, *Organometallics*, **10**: 1832–1043.

[61] Oskam, J. H., Schrock, R. R., 1992, *J. Am. Chem. Soc.*, **114**: 7588–7590.

[62] Totland, K. M., Boyd, T. J., Lavoie, G. G., Davis, W. M., Schrock, R. R., 1996, *Macromolecules*, **29**: 6114–6125.

[63] Buchmeiser, M. R., Schuler, N., Schottenberger, H., Kohl, I., Hallbrucker, A., 2000, *Des. Monomers Polym.*, **3**: 421–446.

[64] Anders, U., Nuyken, O., Wurst, K., Buchmeiser, M. R., 2002, *Angew. Chem.*, **114**: 4226–4230.

[65] Anders, U., Nuyken, O., Wurst, K., Buchmeiser, M. R., 2002, *Macromolecules*, **35**: 9029–9038.

[66] Matyjaszewski, K., 1993, *Macromolecules*, **26**: 1787–1788.

[67] Garber, S. B., Kingsbury, J. S., Gray, B. L., Hoveyda, A. H., 2000, *J. Am. Chem. Soc.*, **122**: 8168–8179.

[68] Bielawski, C. W., Grubbs, R. H., 2000, *Angew. Chem.*, **112**: 3025–3028.

[69] Krause, J. O., Zarka, M. T., Anders, U., Weberskirch, R., Nuyken, O., Buchmeiser, M. R., 2003, *Angew. Chem.*, **115**: 6147–6151.

[70] Krause, J. O., Nuyken, O., Buchmeiser, M. R., 2004, *Chem. Eur. J.*, **10**: 2029–2035.

[71] Krause, J. O., Wurst, K., Nuyken, O., Buchmeiser, M. R., 2004, *Chem. Eur. J.*, **10**: 777–784.

[72] Darling, T. R., Davis, T. P., Fryd, M., Gridnev, A. A., Haddleton, D. M., Ittel, S. D., Matheson Jr., R. R., Moad, G., Rizzardo, E., 2000, *J. Polym. Sci., Part A*, **38**: 1706–1708.

[73] Grela, K., Kim, M., 2003, *Eur. J. Org. Chem.*, **6**: 963–966.

[74] Hamilton, J. G., Frenzel, U., Kohl, F. J., Weskamp, T., Rooney, J. J., Herrmann, W. A., Nuyken, O., 2000, *J. Organomet. Chem.*, **606**: 8–12.

NEW MEMBRANE MATERIALS VIA CATALYTIC POLYMERIZATION OF BIS(TRIMETHYLSILYL)-SUBSTITUTED NORBORNENE TYPE MONOMERS

MAXIM V. BERMESHEV, MARIA L. GRINGOLTS, LUDMILA E. STARANNIKOVA, ALEXEI V. VOLKOV, AND EUGENE SH. FINKELSTEIN[*]
A.V.Topchiev Institute of Petrochemical Synthesis, Russian Academy of Sciences, 29, Leninskii prospect, 119991 Moscow, Russia

Abstract: In this work we summarize our results of investigation on ring-opening metathesis (ROMP) and addition polymerization (AP) of a range of norbornene, norbornadiene and tricyclononene monomers containing two Me_3Si-substituents. The tested monomers exhibited different reactivity in ROMP and AP. The new polymers obtained demonstrated high gas permeability and allowed defining some correlations between features of their chemical structure and gas separation characteristics.

Keywords: Silyl norbornenes; ROMP; Addition polymerization; Gas permeability

1. Introduction

Gas separation membranes offer a number of benefits over other gas separation technologies. Gas separation membrane units are smaller than other types of plants, and therefore have relatively small footprints. They are cheaper, easy in operating, and environmentally friendly.[1]

Norbornenes are attractive monomers for synthesis of membrane polymers. On the one hand, norbornene derivatives can be polymerized according to three different schemes leading to polymers having different structures of main chains (Scheme 1).[2–6] On the other hand, they are accessible compounds which can be synthesized by Diels–Alder reactions of cyclopentadiene and olefins containing various substituents.[7, 8]
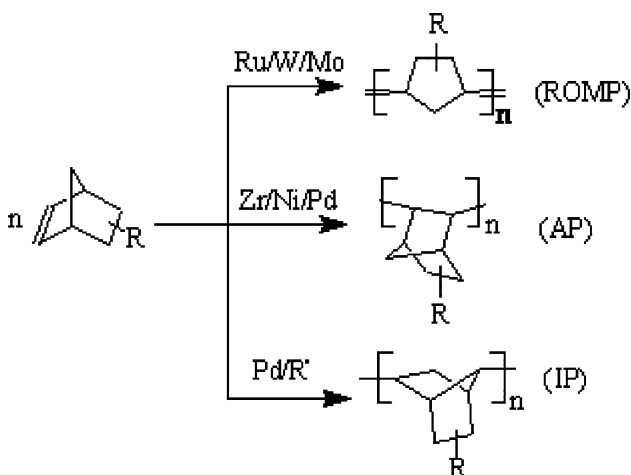
Scheme 1. Three different routes for the polymerization of norbornene monomers.

Earlier, we have shown that the presence of side Me₃Si-substituent in polynorbornenes is responsible for a rise of one of the most interesting and distinctive properties of non-porous polymer films, such as high gas transport parameters.[9–11] It was found that metathesis polymer of 5,6-bis(trimethylsilyl)norbornene containing two Me₃Si-groups per a monomer unit had much better gas transport properties than the corresponding metathesis polymer of 5-trimethylsilylnorbornene containing one Me₃Si-group per a monomer unit.

The aim of this work was synthesis and polymerization of norbornenes bearing two silyl-groups according to ROMP and AP mechanisms and investigation of membrane properties of the corresponding polymers.

2. Results and Discussion

Norbornene and norbornadienes derivatives namely 5,6-bis(trimethylsilyl)norbornene (**1**),[11] 5,5-bis(trimethylsilyl)norbornene (**2**),[12] 2,3-bis(trimethylsilyl)norbornadiene (**3**)[13] and 3,4-bis(trimethylsilyl)tricyclononene-7 (**4**),[14] were synthesized by Diels–Alder reaction of cyclopentadiene and corresponding silyl-ethylenes and silyl-acetylene or thermal condensation of quadricyclane and the corresponding silyl-ethylene.

2.1. RING-OPENING METATHESIS POLYMERIZATION (ROMP)

ROMP of all the obtained monomers has been performed using Ru- and W-catalyst systems with various mol ratio monomer/catalyst (Scheme 2, Table 1).
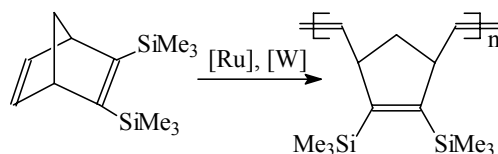
Scheme 2. ROMP of silyl norbornenes with Ruthenium and Tungsten based initiators.

Table 1 shows that Grubbs first generation ruthenium initiator was the most active in ROMP of majority of the tested silyl-norbornenes. Unfortunately, it was inactive in ROMP of monomer **2.** $RuCl_3$/ethanol turned out to be inactive in ROMP of monomer **3**. W-containing catalyst was suitable for all studied monomers and it was more active than $RuCl_3$/ethanol. It allowed achieving polymers with higher molecular weight. Cis/trans double bond ratio was determined from carbon NMR of the polymers. Chemical shifts of the corresponding allylic carbon atoms were fairly resolved and a signal located in a high field was assumed to cis-forms. Different catalysts led to polynorbornenes with different microstructure. For example, the simplest catalyst system, $RuCl_3$/ethanol, gave polymers with preferable amount of trans double bonds, while tungsten hexachloride – 1,1,3,3-(tetramethyl)disilacyclobutane-1,3 led to polynorbornenes containing approximately equal amounts of cis and trans double bonds. Grubbs first generation initiator was more selective in cis/trans double bond formation than W-catalytic system and less selective than $RuCl_3$/EtOH. Thus, we synthesized a range of metathesis polynorbornenes, **I–IV**, with different location of Me_3Si-substituents, Figure 1.

TABLE 1. ROMP of bis(trimethylsilyl)-substituted norbornene type monomers over Ru- and W-containing catalytic systems.

Catalyst (Cat)	Mon.(M)	M:Cat	Yield (%)	Mw^b ($\times10^{-3}$)	Mw/Mn^b	Tg (°C)	Cis^c (%)
$RuCl_3$/EtOH[d]	2	50:1	50	100	1.5	196	2
	3	50:1	0	–	–	–	–
	4	50:1	80	800	2.1	131	5
WCl_6^a/TMDSCB[e]	2	100:1	98	1,500	3.2	203	60
	3	100:1	98	1,600	2.8	183	71
	4	100:1	98	1,000	1.6	129	47
Grubbs first G^a	2	500:1	0	–	–	–	–
	3	1,000:1	98	220	1.2	189	11
	4	1,500:1	98	800	1.8	123	22

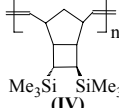[a] 25°C, toluene, 24 h.

[b] Determined by GPC relative to polystyrene standards.

[c] ^{13}C NMR data.

[d] 65°C, chlorobenzene, ethanol, 15 h.

[e] TMDSCB – 1,1,3,3-tetramethyldisilacyclobutane-1,3.
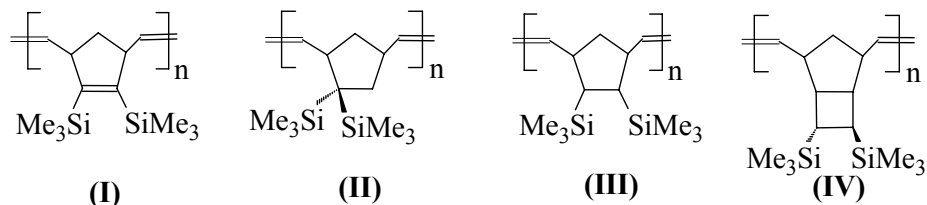
Figure 1. Structures of polymers obtained from ROMP of silyl norbornene monomers.

2.2. ADDITION POLYMERIZATION (AP)

We tested the synthesized monomers in AP. Earlier it was found good activity of (Nph)$_2$Ni-MAO for addition polymerization of 5-(trimethylsilyl)norbornene,[14] and we used the same system ((Nph)$_2$Ni-MAO) as a catalyst.

We examined behavior of monomer **2** at different mol ratios monomer/ (Nph)$_2$Ni/MAO but the formation of the corresponding addition homopolymer was not found. At the same time this monomer could copolymerize with norbornene. It resulted in obtaining the corresponding copolymer (Scheme 3, Table 2). The existence of unimodal MWD and not very wide PDI as well as good solubility of the copolymer in aromatic and chlorinated aliphatic hydrocarbon solvents confirmed that the reaction product was a random copolymer. It should be noted that the addition homopolymer of norbornene is insoluble in these solvents.
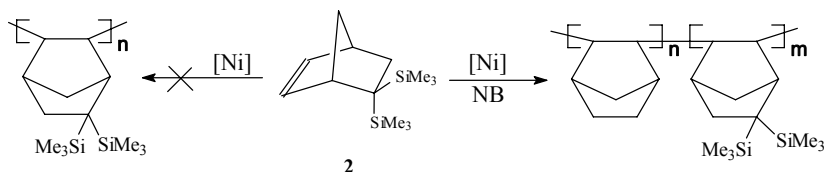
Scheme 3. Addition homo- and copolymerization of silyl norbornene using Ni based catalyst.

^{1}H and ^{13}C NMR spectra indicated that the copolymer did not contain double bonds, confirming addition polymer structure.

Unlike bis-(trimethylsilyl)norbornenes, norbornadiene **3** in the addition polymerization conditions cyclodimerized according to [2 + 2] scheme, and no polymer was observed in final reaction mixtures (Scheme 4). The structure of the cyclodimer was established with X-ray analysis and NMR spectroscopy.[13]
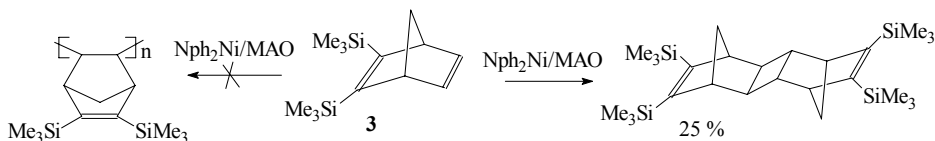
Scheme 4. Formation of cyclodimerized adduct.

At the same time norbornadiene **3** was able to copolymerize with norbornene, but not with norbornadiene. In the case of copolymerization with norbornene three parallel processes took place: cyclodimerization of **3**; co-cyclodimerization of both monomers and addition copolymerization resulting in the formation of low molecular weight toluene soluble copolymer (Table 2, Scheme 4). Homo-cyclodimerization led to formation of only one isomer (as it was mentioned above) while co-cyclodimerization led to two codimer isomers.

Monomer **4** was active both in addition homo- and copolymerization (Scheme 5). The structure of the homopolymer was confirmed by NMR spectro-scopy. At room temperature the homopolymer was obtained with moderate yield. It had low molecular weight (Table 2) and $T_g = 168°C$. The yield of the homopolymer was 80% At 90°C. Copolymerization of **4** with norbornene (initial ratio 1/1) proceeded with a high yield of copolymer.
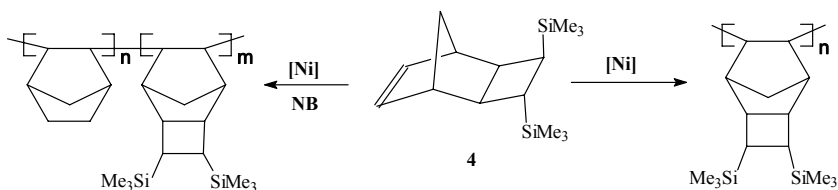
Scheme 5. Addition homo- and copolymerization of silyl norbornene monomers using Ni based catalyst.

The formation of the random copolymer was confirmed by narrow PDI and by complete solubility in aromatic solvents (unlike norbornene homopolymer). According to ^1H and ^{13}C NMR spectra all the obtained copolymers did not contain double bonds and had the structure of addition polymers.

TABLE 2. Addition homo- and copolymerization of silicon-substituted norbornene-type mono-mers (M) with norbornene (NB).

Monomer (M)	[M]/[NB]/[Cat[a]] (m/m/m)	Time (h)	Yield of copolymer (wt%)	Copolymer's composition[b] (mol%)		Mw[c]	Mw/Mn
				M	NB		
1[14]	100/100/1	96	51	17	83	17,800	2.1
2	200/200/1	168	30	18	82	65,000	1.9
3	200/200/1	168	8	25	75	20,000	2.2
4	600/0/1	90	80[d]	100	–	30,000	2.2
	200/200/1	168	95	42	58	205,000	2.3

[a] (Nph)₂Ni:MAO = 1:100 m/m, RT, toluene.

[b] ^1H NMR data.

[c] Determined by GPC relative to polystyrene standards.
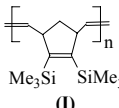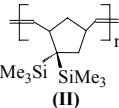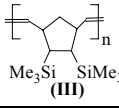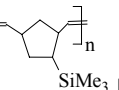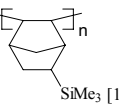
[d] 90°C.

It should be noted that Tg data turned out to be not informative, because all the synthesized copolymers did not show any glass transition up to thermal decomposition temperature (330°C, DSC).

2.3. GAS-TRANSPORT PROPERTIES OF THE OBTAINED ROMP POLYMERS

Earlier we published some results about gas-transport properties of ROMP poly(5-(trimethylsilyl)norbornene) and poly(5,6-bis(trimethylsilyl)norbornene).[9–11] In this work we show some new results concerning ROMP polymers obtained from monomers **2**, **3**, **4**.[15] Several permeation coefficients and the corresponding selectivities are shown in Table 3. It is obvious that for all obtained poly(bis(tri-methylsilyl)norbornene)s introduction of the second Me_3Si-substituent in a monomer unit of ROMP polynorbornenes substantially increases permeability

TABLE 3. Gas transport parameters of silyl-substituted polynorbornenes.

Polymer	Tg (°C)	, Barrer					$\alpha = P_i/P_j$			
		H_2	O_2	N_2	! O_2	! H_4	H_2/N_2	H_2/CO_2	O_2/N_2	CO_2/CH_4
(I)	183	254	71	20	358	48	12.7	5.3	3.6	7.5
(II)	203	218	54	14	277	27	15.6	8.1	3.9	10.3
(III)	167	375	95	25	445	45	15	8.3	3.8	9.9
(IV)	129	227	89	24	396	55	9.5	4.1	3.7	7.2
$SiMe_3$ [9]	113	227	89	24	396	55	9.5	4.1	3.7	7.2
$SiMe_3$ [16]	>340	790	1,680	780	297	4,350	5.7	2.1	2.6	5.5

coefficients for light gases in comparison with ROMP poly(5-(trimethylsilyl)
norbornene). However, any extra significant improvement of these parameters
by changing positions of two SiMe$_3$-groups was not achieved.

It should be noted that addition poly(5-(trimethylsilyl)norbornene) had much
better permeation coefficients than ROMP poly(bis(trimethylsilyl)norbornene)s.
ROMP-poly(bis(trimethylsilyl)norbornene)s had also better gas transport char-
acteristics than ROMP poly(5-(trimethylsilyl)norbornene). These facts allow us
to hope that addition poly(3,4-bis(trimethylsilyl)tricyclononene-7) will possess
better membrane properties than addition poly(5-(trimethylsilyl)norbornene).

Acknowledgement

References

[1]   Mulder M. Basic Principles of Membrane Technology. Dordrecht, Kluwer, 1998.
[2]   Makovetskii KL. Polym. Sci. Ser. C. 2008; 50: 22–38.
[3]   Ivin KJ, Mol JC. Olefin Metathesis and Metathesis Polymerization. San Diego,
        CA: Academic Press, 1997.
[4]   Grubbs RH (Ed.). Handbook of Metathesis. Weinheim. Wiley-VCH, 2003.
[5]   Gaylord NG, Deshpande AB, Mandal BM, Martan M. J. Macromol. Sci. Chem.
        A. 1977; 11/5: 1053–1070.
[6]   Peetz RM, Moustafa AF, Kennedy JP. J Polym Sci Part A Polym Chem. 2003;
        41: 732–739.
[7]   Diels O, Alder K. Ann. 1928; 460: 98.
[8]   Stockmann H. J. Org. Chem. 1971; 26: 2025–2029.
[9]   Finkelshtein ESh, Bespalova NB, Portnykh EB, Makovetskii KL, Ostrovskaya
        IYa, Shishatskii SM, Yampolskii YuP, Plate NA, Kaliuzhnyi NE. Polym. Sci. A.
        1993; 35: 589.
[10]   Bondar V, Kukharskii Yu, Yampolskii Yu, Finkelshtein E, Makovetskii K. J.
        Polym. Sci. Part B: Polym. Phys. 1993; 31: 1273−1283.
[11]   Finkelshtein ESh, Gringolts ML, Ushakov NV, Lakhtin VG, Soloviev SA,
        Yampol'skii YuP. Polymer 2003; 44: 2843−2851.
[12]   Bermeshev MV, Gringolts ML, Lakhtin VG, Finkel'shtein Esh. Petroleum Chem.
        2008; 48: 302–308.
[13]   Gringolts ML, Bermeshev MV, Makovetsky KL, Finkelshtein ESh, Eur. Pol. J.
        2009; 45: 2142–2149.

[14] Finkelshtein ESh, Makovetskii KL, Gringolts ML, Rogan YV, Golenko TG, Lakhtin VG, Filatova MP. J. Mol. Cat. A Chem. 2006; 257: 9–13.
[15] Gringolts ML, Bermeshev MV, Starannikova LE, Rogan YV, Yampolskii YuP, Finkelshtein ESh. Polym. Sci. Ser. C. 2009, 51, in press.
[16] Finkelshtein ESh, Makovetskii KL, Gringolts ML, Rogan YV, Golenko TG, Starannikova LE et al. Macromolecules. 2006; 39(20): 7022–7029.

PART 5. OTHER POLYMERIZATION METHODS

LIGHT INDUCED PROCESSES FOR THE SYNTHESIS OF POLYMERS WITH COMPLEX STRUCTURES

YASEMIN Y. DURMAZ, M. ATILLA TASDELEN,
BINNUR AYDOGAN, MUHAMMET U. KAHVECI,
AND YUSUF YAGCI[*]
*Department of Chemistry, Istanbul Technical University,
34469 Maslak, Istanbul, Turkey*

Abstract: Light induced reactions are based on the absorption of light that excites the electrons of a molecule and can, under favorable circumstances, lead to dissociation, isomerization, abstraction, electron or energy transfer, and bond formation. These reactions have been the subject of many studies in various fields including organic chemistry, molecular biology, electronics etc. Light induced reactions can advantageously be utilized in the field of polymer chemistry. Among them, light induced polymerization is of enormous commercial importance. Techniques such as curing of coatings on wood, metal and paper, adhesives, printing inks and photoresists are based on photopolymerization. There are some other interesting applications, including production of laser video discs and curing of acrylate dental fillings. In this chapter, general methods for the light induced polymerization processes involving radical and ionic reactions are described. Special emphasize is devoted to their application to more complex macromolecular structures such as block, graft and star copolymers, and polymer nanocomposites based on clay and metal.

1. Introduction

Polymerization initiated by light induced processes, referred as photopolymerization, has found many applications including printing inks, adhesives, surface coating, microelectronics, printing plates and 3D microfabrication. In these applications, a photosensitive molecule, as a polymerization initiator, is

excited by irradiation leading to the formation of reactive species capable of converting liquid monomer mixtures into solid structures. Besides energy, cost and environmental considerations, light induced processes have the advantage of providing homogeneous conditions and high reactivity that cannot be achieved by conventional systems.

Light induced polymerizations are used not only in the formulations containing bi- and multi-functional monomers leading to the formation of cross-linked networks, but also synthesis of linear and complex macromolecular structures such as block and graft copolymers, and star polymers. Additionally, the photo-polymerization strategy can be of general use in the syntheses of metal and clay/polymer nanocomposites. Both radical and cationically acting systems have successfully been employed, and the mechanisms of initiation have been studied in detail. Compare to the cationic mode, free radical photoinitiation is in more advanced state because of the availability of wide range of monomer formulations and photoinitiators with broad spectral sensitivity in UV and visible range. Many efforts have been paid to develop photoinitiators for both polymerizations acting at different wavelength ranges.

In this paper, we describe photochemical routes for the synthesis of novel complex macromolecular structures and hybrid nanocomposites possessing linear and crosslinked polymeric structures as well as inorganic components. Such hybrid nanocomposites will be potentially attractive in size related bio, electronic and catalytic applications. Before discussing the preparation of such complex macromolecular structures, it is essential to present photoinitiating systems for the examples recently reported in the authors' laboratory.

2. Photoinitiating Systems

2.1. PHOTOINITIATING SYSTEMS FOR FREE RADICAL POLYMERIZATION

Photoinitiated radical polymerization may be initiated by both cleavage (type I) and H-abstraction type (type II) initiators. The radical generation processes of type I and type II photoinitiators are entirely different. While type I photoinitiators generate initiating radicals by a unimolecular cleavage reaction, type II initiators undergo bimolecular hydrogen abstraction reactions. The main cleavable photo-initiators include benzil dimethyl ketal, benzoin ethers, alkyl hydroxyphenyl ketones, dialkoxyacetophenones, benzylcyclohexanol, amino alkylketones, acylphosphine oxides and acyl germanes. Except for acylphosphine oxide and acylgermane photoinitiators, the cleavage takes place at carbon–carbon bond. Long wavelength and visible light active acylphosphine oxide and acylgermane photoinititors undergo cleavage at carbon–phosphorous and carbon–germane bonds upon irradiation, respectively (Scheme 1).[1, 2]
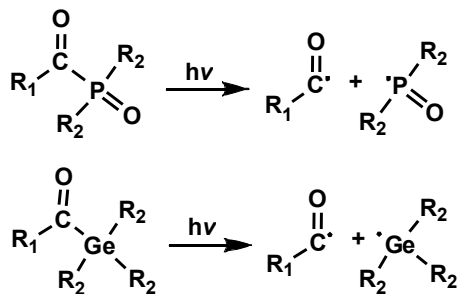
Scheme 1. Photoinduced cleavage of acylphosphine oxides and acylgermane initiators.

Photolysis of aromatic ketones, such as benzophenone, thioxanthones, benzil, and quionones, in the presence of hydrogen donors, such as alcohols, amines, or thiols, leads to the formation of a radical produced from the carbonyl compound (ketyl type radical) and another radical derived from the hydrogen donor. The photopolymerization of vinyl monomers is usually initiated by the radical produced from the hydrogen donor. The ketyl radicals are usually not reactive toward vinyl monomers due to the steric hindrance and the delocalization of unpaired electron. The overall mechanism of the photoinitiation is represented in Scheme 2 on the example of thioxanthone.
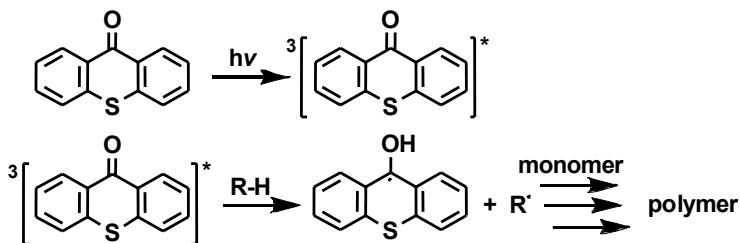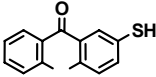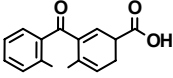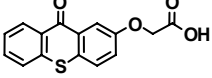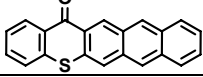
Scheme 2. Photoinitiated free radical polymerization by using thioxanthone.

One of the disadvantages of type II systems concerns high usage of high volatile and odorous amines as hydrogen donors.[3] Poly(ethylene oxide) and poly(ethylene imine) based dendrimers of the following structures have been successfully used as polymeric hydrogen donors to replace low molecular weight amines in the formulations. As it will be shown later, these molecules act as precusors for graft and star copolymers (*vide infra*).

As part of our efforts to avoid problems associated with the amine hydrogen donors, we have recently reported several new thioxanthone derivatives as photoinitiators for free radical polymerization. Interestingly, these photo-initiators do not require an additional coinitiator, that is, a seperate molecular hydrogen donor. The stuctures and the mode of action of such one-component photoinitiators are shown in Table 1.

Besides hydrogen donors, photoinitiators themselves can be incorporated into polymeric structures. This way, the macromolecules having covalently bonded chromophoric groups overcome the problems associated with high volatility and high migration often observed with low molar mass analogous. The two recent examples concern attachment of thioxanthone photoinitiators into polymers as pendant groups by photoinitiator synthesis from the polymeric precursors[9] and by taking advantage of two click reactions, namely Diels–Alder and 1,3-dipolar cycloaddition reactions.[10]

TABLE 1. Thioxanthone based one-component photoinitiators.

Photoinitiator	Structure	Mode of action	Ref.
2-Mercaptothioxanthone		Hydrogen abstraction	[4, 5]
2-(9-Thioxanthone-2-thio) acetic acid		Hydrogen abstraction	[6, 7]
2-(9-Thioxanthone) acetic acid		Hydrogen abstraction	[6, 7]
Thioxanthone-anthracene		Endoperoxide formation	[8]

2.2.   PHOTOINITIATING SYSTEMS FOR CATIONIC POLYMERIZATION

Although several non-salt structured cationic photoinitiors were reported, most of the photoinitiated cationic polymerization applications are based on oniums-salt type initiators, namely diaryliodonium, triarylsulphonium and *N*-alkoxy pyridinium salts. Upon photolysis, these initiators undergo irreversible photo-fragmentation to produce cation radicals and Bronsted acids capable of initiating cationic polymerization (Scheme 3).[11]
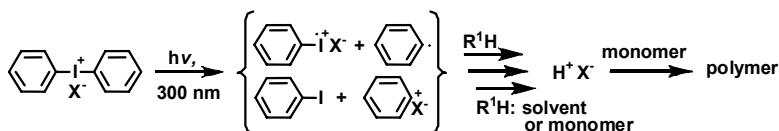
Scheme 3. Photoinitiated cationic polymerization by using iodonium salt.

Unfortunately, onium salts have absorptions at 300 nm regions which limit their use in various applications including curing of pigmented systems. In order to have longer wavelength activity partciularly at visible range several indirect methods were proposed. Adaption of the initiating system to longer

wavelengths can be achieved in three ways: (i) oxidation of free radicals by onium salts (also called free radical promoted cationic polymerization), (ii) electron transfer between photoexcited sensitizer and onium salt, and (iii) electron transfer in photoexcited charge transfer complexes of certain onium salts.[12] For example, we have recently shown that acylgermane based photoinitiators can successfully be used in free radical promoted cationic polymerization of appropriate monomers. Because of the fact that these free radical photoinitiators exhibit long wavelength characteristics (due to the well-known interaction of the lone pair of the carbonyl oxygen with the free d-orbitals of the germanium), the spectral sensitivity of cationic polymerization was easily extended to the visible range. As can be seen from Figure 1, typical onium salt, diphenyl iodonium salt is transparent at the visible range where acyl germane photoinitiator strongly absorbs the light.
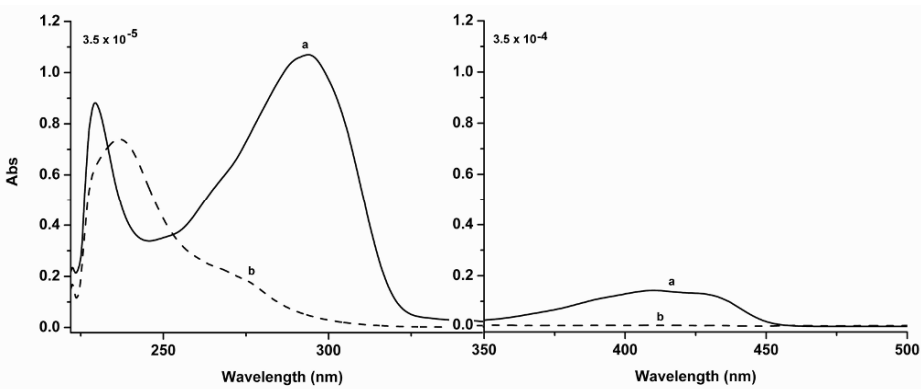
Figure 1. Optical absorption spectra of benzoyltrimethylgermane (BTG) (**a**) and $Ph_2I^+PF_6^-$ (**b**) in CH_2Cl_2.

Typical acylgermane photoinitiator, benzoyltrimethylgermane (BTG) in conjunction with an iodonium salt was shown to be active in initiating cationic polymerization of various monomers at wavelengths up to 450 nm.[13] Detailed polymerization and radical scavenging experiments revealed that trimethyl germyl radicals formed from the homolysis of carbon german bonds in the primary step undergo electron transfer reaction yielding germanium cations capable of initiating cationic polymerization (Scheme 4).
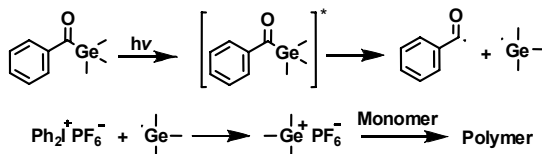
Scheme 4. Photoinitiated cationic polymerization by using benzoyltrimethylgermane in the presence of $Ph_2I^+PF_6^-$.

Polynuclear aromatic hydrocarbons can also induce photoinitiated cationic polymerization at long wavelengths. Quite unusual example of this type of photosensitization by using a dithienothiophene derivative, namely 3,5-diphenyldithieno [3,2-b:2,3-d] thiophene (DDT), was recently reported.[14] This compound, known as a precursor for conducting polymers, absorbs light at above 350 nm (Figure 2) and initiates the polymerization in the presence of iodonium salt.
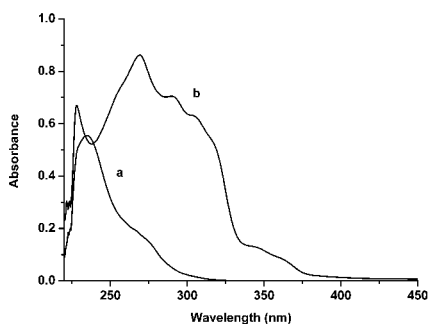
Figure 2. UV spectra of 3.5×10^{-5} M $Ph_2I^+PF_6^-$ (a) and 3.5×10^{-5} M 3,5-diphenyldithieno[3,2-b:2,3-d]thiophene (DDT) (b) in CH_2Cl_2.

A mechanism (Scheme 5) involving formation of exciplex and subsequent electron transfer from excited DDT to iodonium ions was proposed.
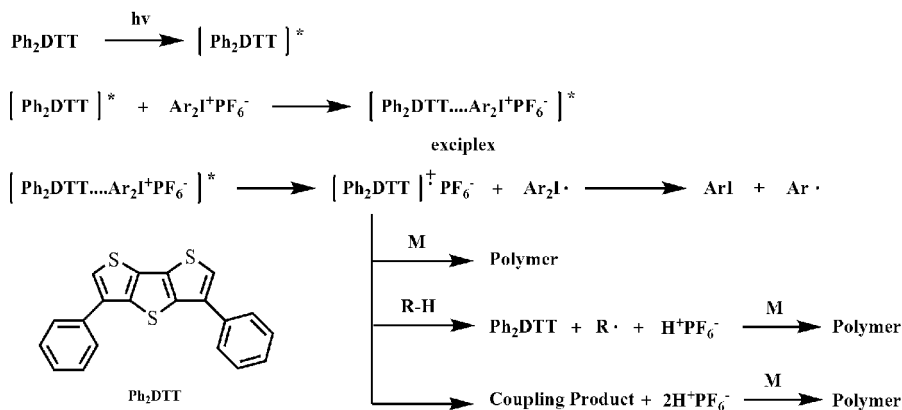
Scheme 5. Photoinitiated cationic polymerization by using 3,5-diphenyldithieno[3,2-b:2,3-d] thiophene (DDT) in the presence of $Ph_2I^+PF_6^-$.

How wide photoinitiated cationic polymerization can be used in different applications on an industrial scale depends on the economical and environmental advantages offered by the particular process involved. For example, vinyl ethers can be rapidly photopolymerized by cationic means which overcomes limitations of molecular oxygen inhibition and avoids problems related to monomer toxicity associated with the more conventional free radical polymerization of acrylates which are widely used in industrial applications. Recently introduced initiating system for the polymerization of this class of monomers, consisting of diphenyliodonium halides and a zinc halide Lewis acid further eliminates the use of toxic arsenic and antimonate based anions. [15, 16] Such polymerization can successfully be performed in aqueous medium in the presence of the water-tolerant Lewis acid, ytterbium triflate.[17] Obviously, this process would open new pathways for many applications employing waterborne systems. The polymerization consists of two-steps; (i) photoinduced adduct formation and (ii) subsequent propagation with the aid of $Yb(OTf)_3$ (Scheme 6). The fast polymerization exhibited an explosive character so that the monomer conversion and molecular weights of the resulting polymers are very dependent on the experimental conditions, such as temperature and stirring manner.

The following sections will focus on the light induced reactions in the synthesis of polymers with complex structures. Subjects to be discussed include: (i) block and graft copolymers by photopolymerization, (ii) star polymers by photopolymerization, and (iii) *in situ* synthesis of metal or clay/polymer nano composites by light induced processes.
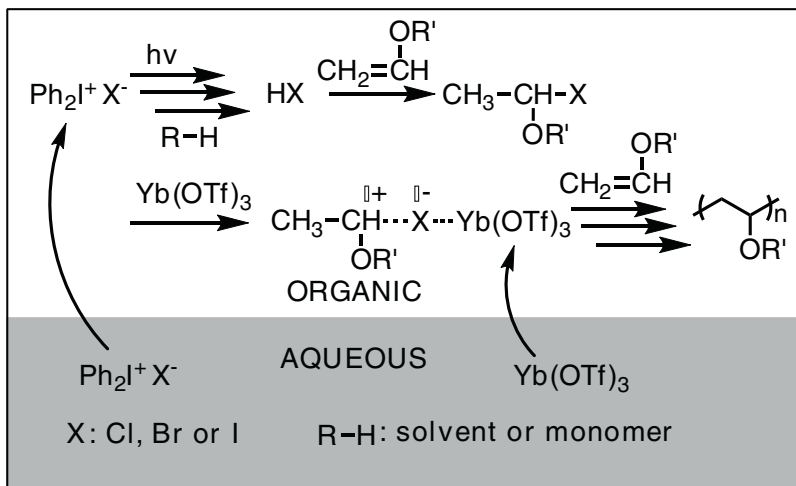
Scheme 6. Photoinitiated cationic polymerization of vinyl ethers in aqueous medium.

2.3. SYNTHESIS OF BLOCK, GRAFT AND STAR COPOLYMERS BY LIGHT INDUCED PROCESSES

In general photoinitiating systems in classical polymerization of monofunctional monomers do not provide control over the molecular weight and structure. However, they still contribute to the synthesis of various macromolecular structures. In particular, block and graft copolymers can be prepared by using main chain and side chain polymeric photoinitiators, respectively (Scheme 7). By photolysis, active sites are produced at the chain ends or side chains, which serve as initiating moieties in the polymerization of a second monomer. In this manner, copolymers with almost quantitative block or graft yields can be obtained, for the fact that side reactions and, thus, homopolymer formation are minimized as a result of the low polymerization temperature. A wide range of monomer combinations have been studied, and the detailed strategies and mechanisms were discussed.[18–20] Herein, we present recent examples to demonstrate the versatility of the light induced processes for block, graft and star copolymer formation.
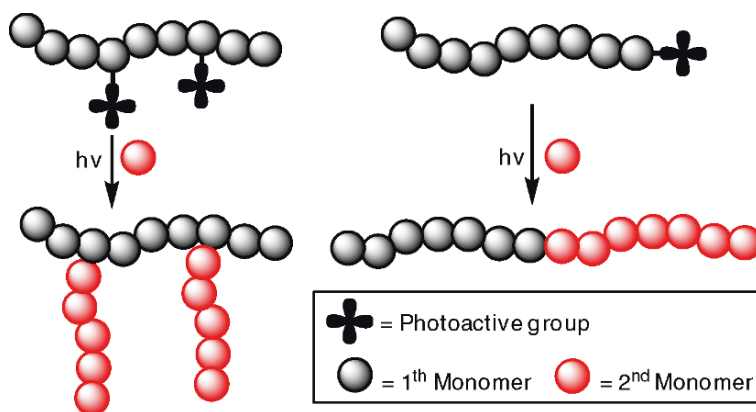
Scheme 7. Photoinitiated block and graft copolymerization.

In block copolymerization the most important step is the incorporation photoactive groups at polymer chain ends. For this purpose, usually controlled polymerization methods were employed as they yield polymers with well-defined structure and desired functionality. In a recent study,[21] photoactive morpholine-4-dithiocarbamate terminated polystyrene was prepared by the reaction of dibrominated polystyrene, obtained by Atom Transfer Radical Polymerization (ATRP), with morpholine-4-dithiocarbamate sodium salt in dimethyl formamide. The capability of this photoactive precursor polymer to act as a photoinitiator for the block copolymerization of methyl acrylate (MA) was examined (Scheme 8).[21] Polymerization shows a "living" character at up to 25% conversions and produces well-defined polymers with molecular weights

close to those predicted from theory and relatively narrow polydispersities ($M_w/M_n \sim 1.40$). Both functionalization and light induced steps involve controlled polymerization processes.
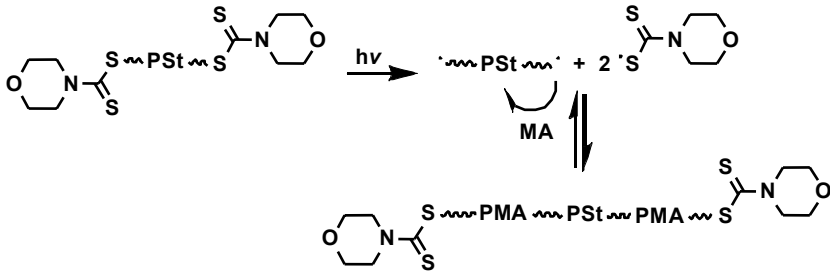
Scheme 8. Block copolymerization of polystyrene with methyl acrylate by photoiniferter process.

When poly(ethylene oxide) (PEO) is used as hydrogen donors in photoinitiated free radical polymerization of methyl methacrylate by using benzophenone or thioxanthone as photosensitizers, graft copolymers consisting of hydrophilic backbone and hydrophobic side chains are readily formed (Scheme 9A).[22] A similar hydrogen abstraction strategy was applied to exterior methylenes of poly(propylene imine) based dendrimers yielding star copolymers (Scheme 9B).[23]
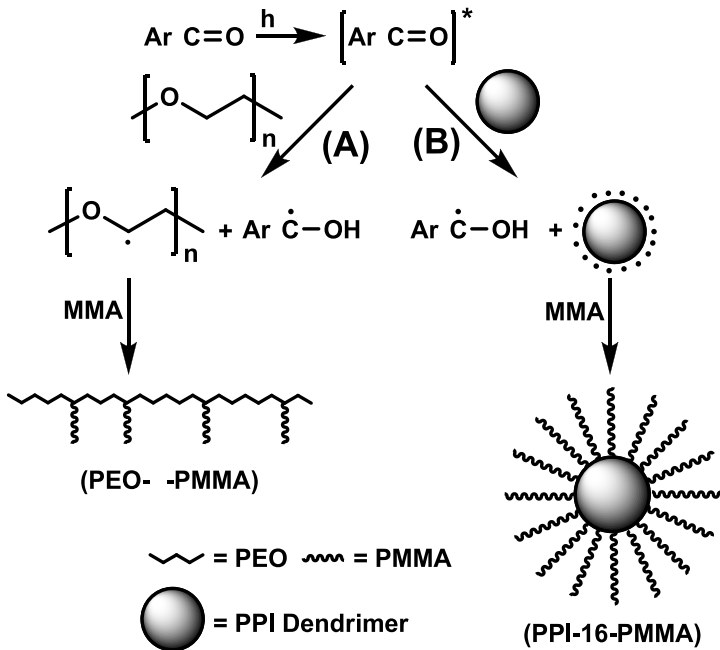
Scheme 9. Synthesis of graft and star copolymers by light induced hydrogen abstraction process.

The effect of generation number of the dendrimer on photoinitiation efficiency and molecular weight of the resulting polymers was investigated. Glass transition temperatures and particle size measurements of the resulting polymers indicated the presence of nearly stretched polymer chains around the dendrimers.

2.4. LIGHT INDUCED SYNTHESIS OF METAL/POLYMER NANOCOMPOSITES

Nanocomposite materials containing metal nanoparticles and polymer matrix may exhibit novel physical and chemical properties that are of high scientific and technological importance. These materials combine the physical properties of small size metal nanoparticles with those of polymeric materials in a beneficial manner. Many advanced optoelectronic and sensor devices are based on the fabrication of these materials.[24–27] Because of their high surface free energy, nanoparticles tend to agglomerate. A key challenge for a potential technological use is the achievement of homogeneous dispersion of the thermodynamically unstable nanoparticles. Various methods have been applied. Generally, applied methodology is detaining nanoparticles during the preparation by adding protecting agents or setting them in an inert environment. Among them, photochemical methods involving light induced reduction of metal ions such as Ag and Au complexes are of particular interest as they find a wide range of application including synthesis of metallic colloids, and metallization and patterning of films.

Recently, we have introduced a novel approach for the preparation of metal–polymer nanocomposites, in which nanoparticle formation and UV crosslinking process were accomplished in one pot by simply irradiating appropriate formulations, obtaining the homogeneous distribution of the nanoparticles within the polymer network without any macroscopic agglomeration. Silver or gold nanoparticles and initiaing species were formed in a single redox process. Acrylate and epoxy resins polymerizing by free radical and cationic mechansims, respectively, were successfully used in the preparation of such composites (Table 2).

TABLE 2. Light induced synthesis of metal/polymer nanocomposites.

Polymer matrix	Metal nanoparticle	Photoinitiator	Polymerization mechanism	Ref.
Epoxy	Silver	DMPA-AgSbF6	Cationic	[28]
Silicon epoxy	Silver	CQ/Amine-AgSbF6	Cationic	[29]
Acrylate	Gold	Irgacure 2959	Radical	[30]
Silicon epoxy	Gold	CQ/Amine-Rhodorsil 2074	Cationic	[31]

Scheme 10 shows typical reactions for the *in situ* synthesis of silver and gold-cross-linked epoxy nanocomposites by photoinduced electron transfer and cationic polymerization processes. Simply irradiating the mixture containing epoxy resin and metalic salt the presence of a visible light photoinitiator, camphorequinone (CQ) without necessity of an external reducing agent, leads to the formation of desired composites. Compared to chemical cross-linking of metal nanoparticle decorated polymer matrices, the method described here is quite attractive since it allows for simultaneous metal nanoparticle and network formation which secures the resulting structure, and permits long-term stability.
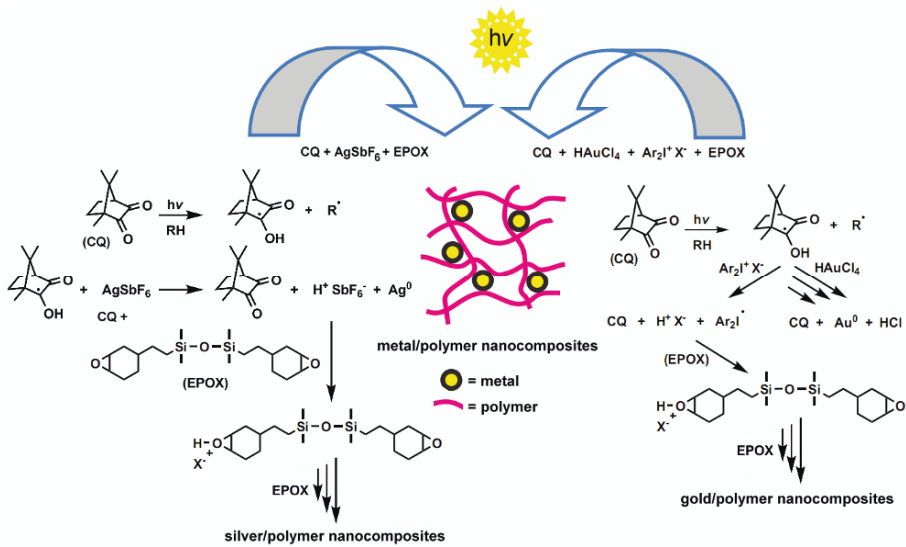
Scheme 10. Light induced synthesis of metal/epoxy nanocomposites.

2.5. LIGHT INDUCED SYNTHESIS OF CLAY/POLYMER NANOCOMPOSITES

Polymer-layered clay nanocomposites receive interest beacuse of their improved physical and chemical properties due to small size or large surface area of the clay with nanoscale dimension.[32–34] Although many methods have been tested, the dispersing *in situ* polymerization may be the most desirable method for preparing nanocomposites because the types of nanoparticles and the nature of polymer precursors can be selected. Photopolymerization methodology allows in situ synthesis of polymer nanocomposites using organophilic montmorillonite (MMT) as the layered clay. MMT clay was ion-exchanged with photosensitive molecule which acts as both suitable intercalant- and photo-initiator. These modified clays were then dispersed in a selected monomer in different loading

degrees to facilitate in situ photopolymerization.[35] The overall process is presented in Scheme 11.
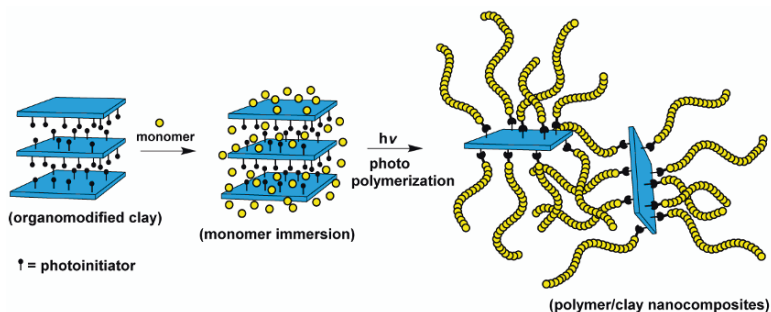
Scheme 11. Light induced synthesis of clay/polymer nanocomposites.

Versatality and convenience of the method was recently demonstrated by using organo modified clay with N-phenacyl,N,N-dimethylanilinium hexafluoro phosphate (PDA) in the polymerization of methyl methacrylate. Polymerization through the interlayer galleries of clay resulted in the formation of exfoliation/ intercalation structures.

References

[1]   Hageman, H. J. *Prog. Org. Coat.* 1985, **13**, 123–150.
[2]   Gruber, H. F. *Prog. Polym. Sci.* 1992, **17**, 953–1044.
[3]   Vazquez, B., Levenfeld, B., Roman, J. S. *Polym. Int.* 1998, **46**, 241–250.
[4]   Karasu, F., Arsu, N., Yagci, Y. *J. Appl. Polym. Sci.* 2007, **103**, 3766–3770.
[5]   Cokbaglan, L., Arsu, N., Yagci, Y., Jockusch, S., Turro, N. J. *Macromolecules* 2003, **36**, 2649–2653.
[6]   Aydin, M., Arsu, N., Yagci, Y., Jockusch, S., Turro, N. J. *Macromolecules* 2005, **38**, 4133–4138.
[7]   Aydin, M., Arsu, N., Yagci, Y. *Macromol. Rapid Commun.* 2003, **24**, 718–723.
[8]   Balta, D. K., Arsu, N., Yagci, Y., Jockusch, S., Turro, N. J. *Macromolecules* 2007, **40**, 4138–4141.
[9]   Temel, G., Arsu, N., Yagci, Y. *Polym. Bull.* 2006, **57**, 51–56.
[10]   Gacal, B., Akat, H., Balta, D. K., Arsu, N., Yagci, Y. *Macromolecules* 2008, **41**, 2401–2405.
[11]   Yagci, Y. *Macromol. Symp.* 2000, **161**, 19–35.
[12]   Yagci, Y. *Macromol. Symp.* 2004, **215**, 267–280.
[13]   Durmaz, Y. Y., Moszner, N., Yagci, Y. *Macromolecules* 2008, **41**, 6714–6718.
[14]   Aydogan, B., Gundogan, A. S., Ozturk, T., Yagci, Y. *Macromolecules* 2008, **41**, 3468–3471.
[15]   Kahveci, M. U., Tasdelen, M. A., Yagci, Y. *Macromol. Rapid Commun.* 2008, **29**, 202–206.

[16] Kahveci, M. U., Tasdelen, M. A., Yagci, Y. *Polymer* 2007, **48**, 2199–2202.
[17] Kahveci, M. U., Tasdelen, M. A., Cook, W. D., Yagci, Y. *Macromol. Chem. Phys.* 2008, **209**, 1881–1886.
[18] Muftuoglu, A. E., Yagci, Y., Se, K. *Turk. J. Chem.* 2004, **28**, 469–476.
[19] Yagci, Y., Schnabel, W. *Prog. Polym. Sci.* 1990, **15**, 551–601.
[20] Muftuoglu, A. E., Tasdelen, M. A., Yagci, Y. Photoinduced Synthesis of Block Copolymers, in: *Photochemistry and UV Curing : New Trends*, J. P. Fouassier (Ed.), Research Signpost, Trivandrum, Ch. 29, pp. 343–353, 2006.
[21] Durmaz, Y. Y., Karagoz, B., Bicak, N., Yagci, Y. *Polym. Int.* 2008, **57**, 1182–1187.
[22] Tasdelen, M. A., Moszner, N., Yagci, Y. *Prog. Org. Coat.* 2009, in submitted.
[23] Tasdelen, M. A., Demirel, A. L., Yagci, Y. *Eur. Polym. J.* 2007, **43**, 4423–4430.
[24] Watson, K. J., Zhu, J., Nguyen, S. T., Mirkin, C. A. *Pure Appl. Chem.* 2000, **72**, 67–72.
[25] Park, J. H., Lim, Y. T., Park, O. O., Kim, J. K., Yu, J. W., Kim, Y. C. *Chem. Mat.* 2004, **16**, 688–692.
[26] Shenhar, R., Norsten, T. B., Rotello, V. M. *Adv. Mater.* 2005, **17**, 657–669.
[27] de Loos, F., Reynhout, I. C., Cornelissen, J., Rowan, A. E., Nolte, R. J. M. *Chem. Commun.* 2005, 60–62.
[28] Sangermano, M., Yagci, Y., Rizza, G. *Macromolecules* 2007, **40**, 8827–8829.
[29] Yagci, Y., Sangermano, M., Rizza, G. *Polymer* 2008, **49**, 5195–5198.
[30] Yagci, Y., Sangermano, M., Rizza, G. *Chem. Commun.* 2008, 2771–2773.
[31] Yagci, Y., Sangermano, M., Rizza, G. *Macromolecules* 2008, **41**, 7268–7270.
[32] Alexandre, M., Dubois, P. *Mater. Sci. Eng. R.* 2000, **28**, 1–63.
[33] Okamoto, M. *Mater. Sci. Tech-Lond.* 2006, **22**, 756–779.
[34] Ray, S. S., Okamoto, M. *Prog. Polym. Sci.* 2003, **28**, 1539–1641.
[35] Nese, A., Sen, S., Tasdelen, M. A., Nugay, N., Yagci, Y. *Macromol. Chem. Phys.* 2006, **207**, 820–826.

RECENT ADVANCES IN THE FUNCTIONALIZATION OF ALIPHATIC POLYESTERS BY RING-OPENING POLYMERIZATION

PHILIPPE LECOMTE[*] AND CHRISTINE JEROME
*Center for Education and Research on Macromolecules,
University of Liege, B6 Sart-Tilman, B-4000 Liege, Belgium*

Abstract: Two main strategies aiming at synthesizing aliphatic polyesters bearing pendant functional groups will be reported. The first one is based on the synthesis and the polymerization of lactones substituted by various functional groups. The direct grafting of functional groups onto aliphatic polyesters is the second strategy. Last but not least, the association of these two strategies is very promising in order to overcome their respective limitations.

Keywords: Ring-opening polymerization; Aliphatic polyester

1. Introduction

Biodegradable and biocompatible aliphatic polyesters are well-known biomaterials. Attachment of functional groups along the chain is highly desirable to tailor macroscopic properties such as crystallinity, hydrophilicity, biodegradation rate, bioadhesion and mechanical properties. Besides, pendant functional groups can be used to covalently attach molecules or probes of biological interest.

Aliphatic polyesters can be synthesized either by polycondensation or by ring-opening polymerization. At the one hand, the control imparted to polycondensation is limited. At the other hand, ring-opening polymerization (ROP) of lactones and lactides is a well-established process for the synthesis of aliphatic polyesters with predictable molecular weight, narrow molecular weight distributions, and well-defined end-groups. This review aims at reporting recent advances in the synthesis of functionalized aliphatic polyesters synthesized by ROP.

Two main strategies allowing synthesizing aliphatic polyesters bearing pendent functional groups might be distinguished.[1] The first one is based on the synthesis and polymerization of lactones substituted by a functional group.[2] It is worth pointing out that the copolymerization of lactones with other functionalized monomers such as epoxides and carbonates is beyond the scope of this review.

The direct grafting of functional groups onto aliphatic polyesters is the second strategy.

2. Ring-Opening Polymerization of Lactones Substituted by a Functional Group

In 1997, Tian et al. reported the synthesis of 1,4,8-trioxaspiro[4.6]-9-undecanone by the Baeyer-Villiger oxidation of 1,4-dioxaspiro[4.5]dedcan-8-one. This cyclic monomer was homopolymerized[3] and copolymerized[4] with oxepan-2-one (εCL for ε-caprolactone) as shown in Scheme 1.

The functionalization of aliphatic polyesters by hydroxyl groups leads to increase in their hydrophilicity. Pendant hydroxyl groups are also very useful for further macromolecular engineering. For instance, ROP initiated by pendant hydroxyl groups is a route towards comb-shaped polyesters. Toward this end, the ketal groups of poly(εCL-co-oxepane-1,5-dione) were deprotected into ketones, which were finally reduced by sodium borohydride into pendant hydroxyl groups (Scheme 1).
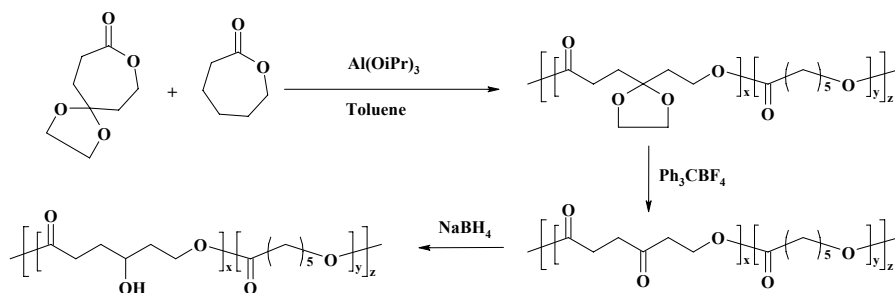
Scheme 1. Synthesis of PCL with pendent OH groups.

Later on, ketone-containing polyesters were synthesized by the more direct ROP of εCL and oxepane-1,5-dione, which was again synthesized by the Baeyer-Villiger oxidation of cyclohexane-1,4-dione (Scheme 2).[5] Nevertheless, aluminum isopropoxide was not an efficient initiator because the complexation with the ketone competes with the complexation with the ester, which is the first step of ROP. This problem was overcome by using tin(IV) alkoxides as initiators, which tolerates the presence of ketones, for reasons which yet remains unclear.
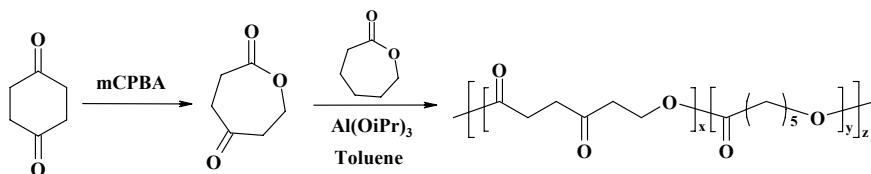
Scheme 2. Synthesis and polymerization of oxepane-1,5-dione.

In order to prepare aliphatic polyesters with pendant hydroxyl groups, 5-triethylsilyloxyoxepan-2-one (γEt$_3$SiOϵCL for 5-triethylsilyloxy-ϵ-caprolactone) was synthesized from cyclohexane-1,4-diol in three steps as shown in Scheme 3.[6, 7] The protection of the hydroxyl group prior to the Baeyer-Villiger is mandatory because hydroxyoxepan-2-one obtained by reaction of 4-hydroxy-cyclohexanone is not stable and rearrange into 5-(2-hydroxyethyl)dihydrofuran-2(3H)-one (Scheme 4).[8] γEt$_3$SiOϵCL was copolymerized with ϵCL in order to obtain the corresponding statistical copolyesters.[6, 7] The deprotection of the hydroxyl group turned out to be difficult even under optimized conditions, especially for copolyesters with a γEt$_3$SiOϵCL content higher than 50% due to the noxious transesterification reaction of an internal ester by the released hydroxyl group, which results in the formation of a five-membered lactone.[7] As a rule, the protecting group has to be stable enough to avoid deprotection prior to polymerization and has to be deprotected under mild conditions under which no degradation of the polyester takes place. These two conditions are contradictory and it is sometimes difficult to find a good compromise. To this respect, Hedrick et al. reported the synthesis and the polymerization 5-(benzyloxy)-oxepan-2-one. The benzyloxy group was deprotected by catalytic hydrogenolysis, which avoids the use of acidic conditions.[9] Last but not least, the intramolecular rearrangement can be avoided just by changing the structure of the lactone, which avoids the use of protection/deprotection reactions. Recently, several teams reported the synthesis of several stable lactones substituted by hydroxyl groups such as 5-(2-hydroxyethyl)oxepan-2-one,[10] 4-hydroxy-4-methyltetrahydro-2H-pyran-2-one,[11] 6-(hydroxymethyl)-1,4-dioxan-2-one,[12] and 5-(hydroxymethyl)-1,4-dioxan-2-one[13] (Scheme 5). It is worth recalling that these monomers are nothing but AB inimers, whose polymerization is a route to hyperbranched aliphatic polyesters.
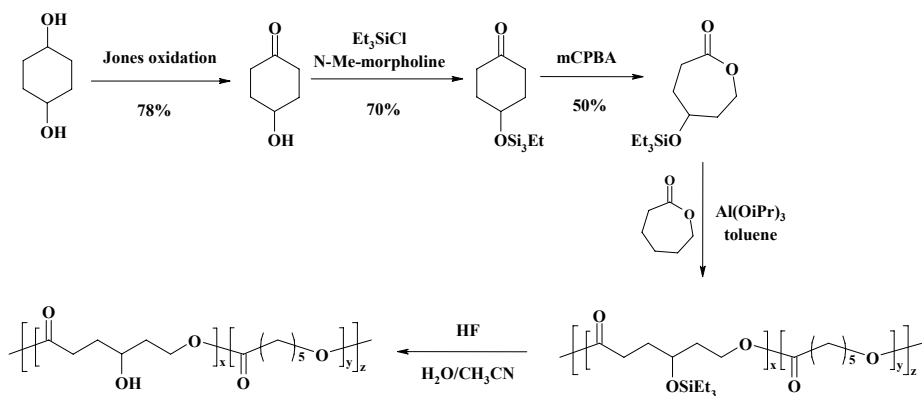
Scheme 3. Synthesis and polymerization of γEt$_3$SiOϵCL.
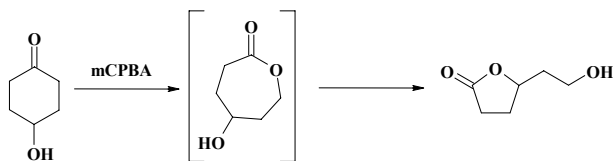
Scheme 4. Baeyer-Villiger oxidation of 4-hydroxycyclohexanone.
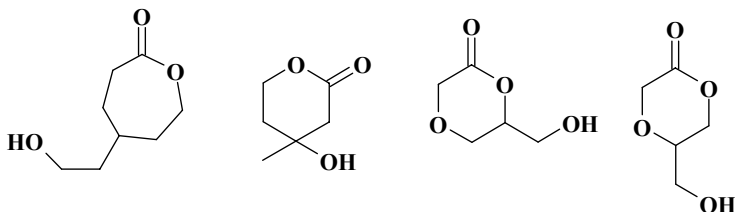
Scheme 5. Stable lactones bearing hydroxyl groups.

Very recently, Feijen et al. reported the synthesis of 3-(2-phenylethyl)-1,4-dioxane-2,5-dione and 3-methyl-6-(2-phenylethyl)-1,4-dioxane-2,5-dione, from serine (Scheme 6).[14] These monomers were homopolymerized and copolymerized with L-lactide[14] and εCL[15] A very similar procedure was implemented by Gerhardt et al. to synthesize 3-methyl-6-(2-phenylethyl)-1,4-dioxane-2,5-dione.[16]
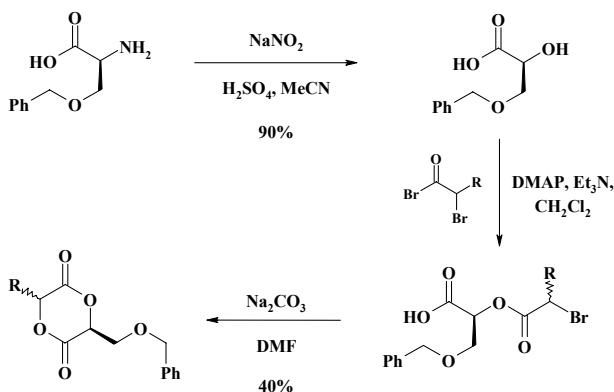
Scheme 6. Synthesis and polymerization of 3-(2-phenylethyl)-1,4-dioxane-2,5-dione and 3-methyl-6-(2-phenylethyl)-1,4-dioxane-2,5-dione.

The synthesis of lactones substituted by protected diols such as 7-oxooxepan-4-yl 5-methyl-2-phenyl-1,3-dioxane-5-carboxylate[9] was also reported (Scheme 7).

Interestingly, Vert et al. investigated the synthesis and polymerization of 3-(2,2,2′,2′-tetramethyl-4,4′-bi-1,3-dioxol-5-yl)-1,4-dioxane-2,5-dione (DIPAGYL),

which is nothing but a dilactone substituted by two acetonide groups, which can be partially deprotected into diols (Scheme 8).[17]
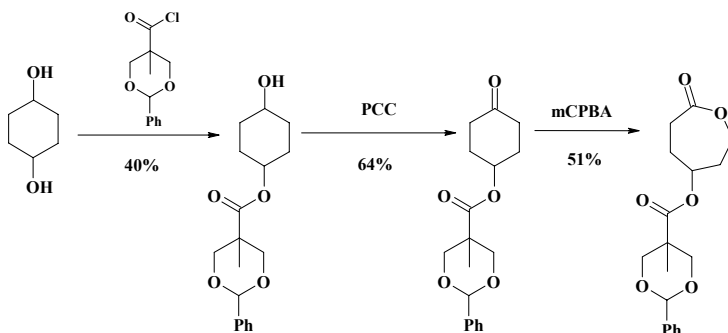
Scheme 7. Synthesis of 7-oxooxepan-4-yl 5-methyl-2-phenyl-1,3-dioxane-5-carboxylate.
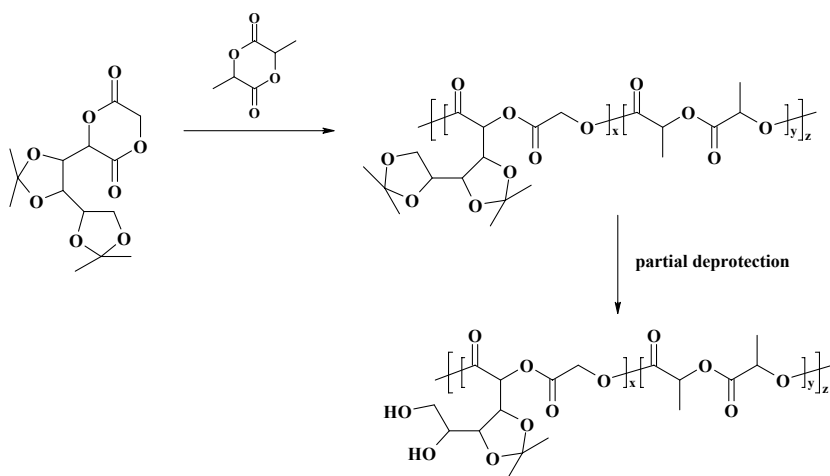
Scheme 8. Copolymerization of DIPAGYL with lactide.

The synthesis and the polymerization of lactones substituted by amines are less common even tough they have a great potential for many applications. The synthesis of 4-(trifluoroacetyl)-1,4-oxazepan-7-one by a three-step process was reported by Hedrick et al. (Scheme 9). The deprotection of the amino group turned out to be complicated by the sensitivity of the aliphatic polyester. NaBH$_4$ was the most efficient reagent surveyed and mild conditions as well as short reaction times were required to minimize degradation.[9] More recently, Gerhardt et al. reported the synthesis of benzyl [(3,6-dioxo-1,4-dioxan-2-yl)methyl]carbamate from lysine (Scheme 10).[16]
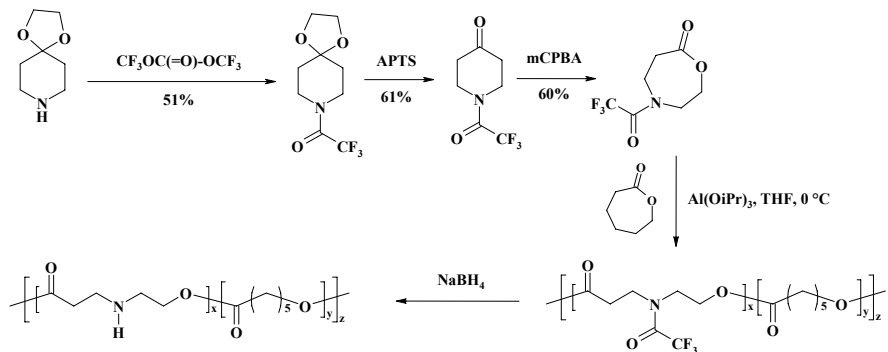
Scheme 9. Synthesis and polymerization of 4-(trifluoroacetyl)-1,4-oxazepan-7-one.[9]
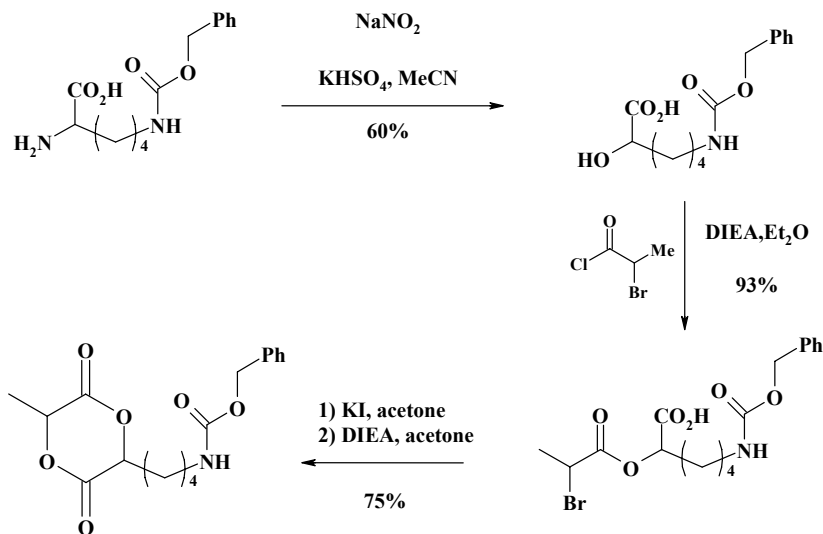
Scheme 10. Synthesis and polymerization of benzyl [(3,6-dioxo-1,4-dioxan-2-yl)methyl]carbamate.[16]

The functionalization of aliphatic polyesters by carboxylic acids is another approach allowing increasing their hydrophilicity. Carboxylic acids being not tolerated by aluminum and tin alkoxides, which are the initiators for ROP, it was again necessary to use protection/deprotection reactions. At the one hand, Lecomte et al. reported on the silyl-protected 7-oxooxepane-4-carboxylic acid (Scheme 11).[18] At the other hand, Hedrick et al. proposed to protect the carboxylic as benzyl or t-butyl esters as an alternative.[9] The deprotection after polymerization was easily carried out under non degrading conditions. Nevertheless, the purification of the monomer turned out to be a key issue due to undesired deprotection of the carboxylic acid. Due to the presence of acidic impurities, the homopolymerization was not easy to carry out. This problem was tackled by using t-butyldiphenylsilyloxy protecting groups more stable than the more

usual t-butyldimethylsilyloxy protecting groups. The polymerization was controlled when initiated by aluminum isopropoxide. It is worth noting that the polymerization of phenyl 4-oxooxetane-2-carboxylate (or benzyl β-malolactonate) yields poly(benzyl β-malolactonate), which can finally be deprotected into poly(β-malic acid) by catalytic hydrogenation, as recently reviewed elsewhere.[19]
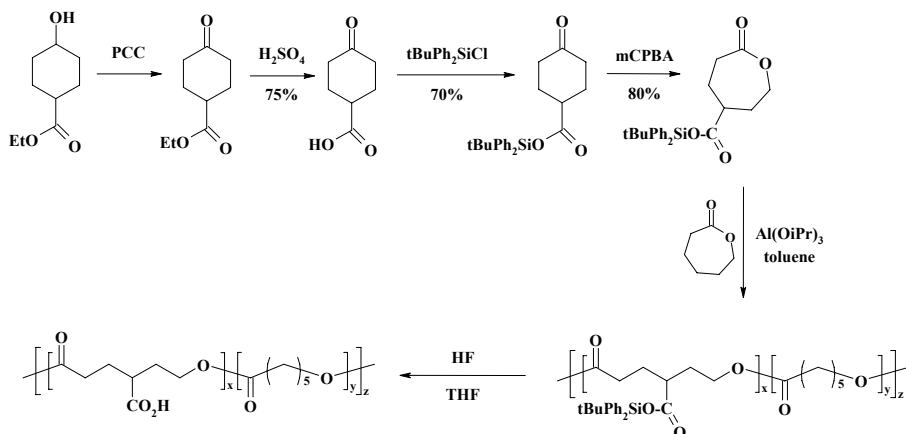
Scheme 11. Synthesis and polymerization of the silyl-protected 7-oxooxepane-4-carboxylic acid.

Very recently, Gerhardt et al. reported on the synthesis of benzyl 3-(5-methyl-3,6-dioxo-1,4-dioxan-2-yl)propanoate from glutamic acid (Scheme 12).[16]
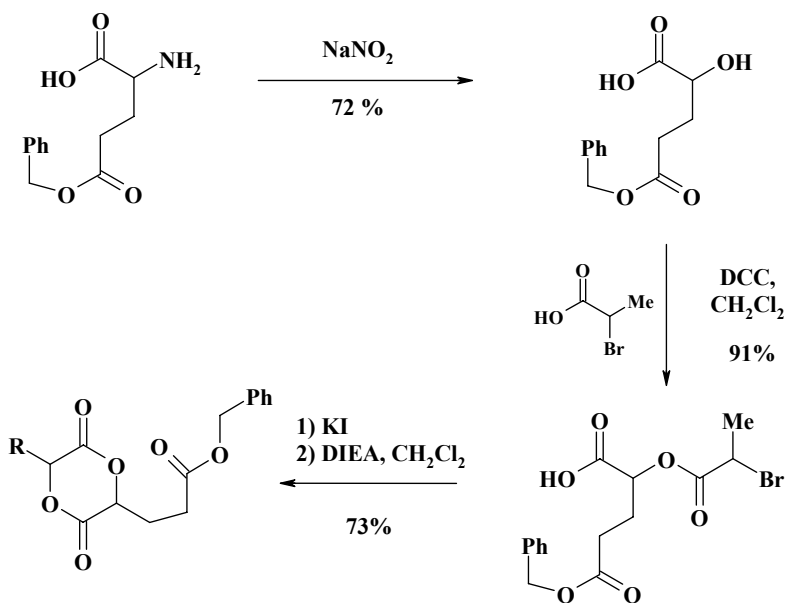
Scheme 12. Synthesis and polymerization of benzyl 3-(5-methyl-3,6-dioxo-1,4-dioxan-2-yl)propanoate.

Much attention has been paid on the synthesis of halogen-containing aliphatic polyesters because the halogen function can be used for further chemical transformations such as elimination and quaternization reactions.[20] Detrembleur et al. reported the synthesis of 5-bromooxepan-2-one (γBrεCL for γ-bromo-ε-caprolactone) synthesized by a three-step strategy shown in Scheme 13.[21] The homopolymerization of γBrεCL and its copolymerization with εCL was under control when aluminum isopropoxide is used as an initiator.
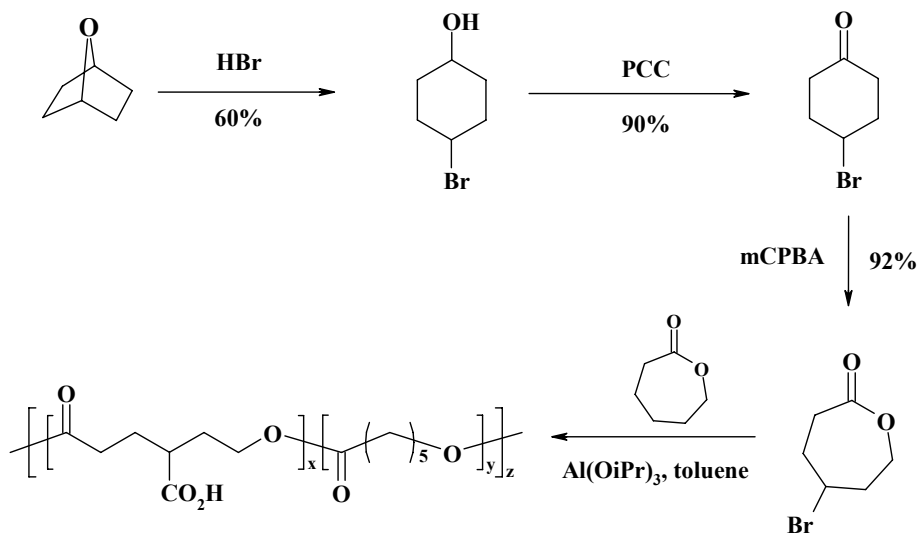
Scheme 13. Synthesis and polymerization of benzyl 3-(5-methyl-3,6-dioxo-1,4-dioxan-2-yl) propanoate.

Later on, a more direct strategy was implemented by Lenoir et al. who reported the synthesis of 3-chlorooxepan-2-one (αClεCL for α-chloro-ε-caprolactone) in only one step by the Baeyer-Villiger oxidation of 2-chlorocyclohexanone (Scheme 14).[22] It is worth noting that the Baeyer-Villiger reaction is not 100% selective as witnessed by the formation of 7-chlorooxepan-2-one as a minor isomer. It is mandatory to carefully remove 7-chlorooxepan-2-one prior to polymerization because this isomer inhibits the polymerization by a mechanism shown in Scheme 15. A slight drawback of αClεCL compared to γBrεCL is its lower thermal stability at room temperature and αClεCL needs to be stored at −20°C. The polymerization of this monomer was not under control when initiated by aluminum alkoxides for reasons which remain unclear. Nevertheless, this polymerization of αClεCL can be successfully initiated by tin(IV) alkoxides[22] and by alcohols in the presence of tin octoate.[23] More recently, the same approach was used by Wang et al. to synthesize 3-bromoooxepan-2-one but the thermal stability of this monomer was not mentioned.[24]
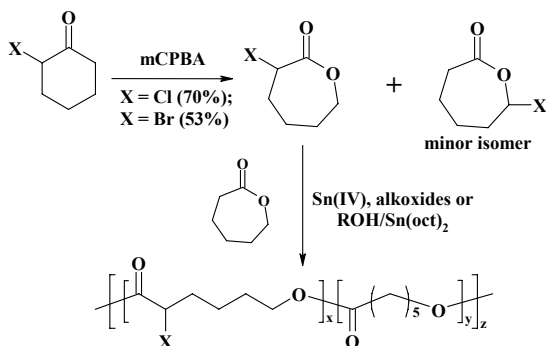
Scheme 14. Synthesis and polymerization of αClεCL and αBrεCL.
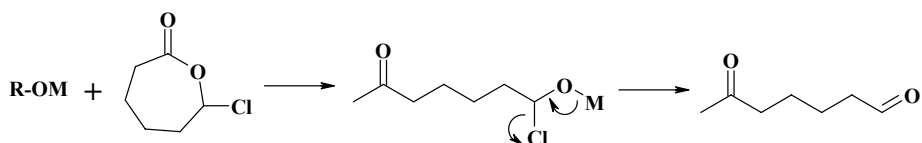
Scheme 15. Inhibition mechanism of ROP in the presence of 7-chlorooxepan-2-one.

The synthesis of unsaturated aliphatic polyesters is highly desirable because they can be crosslinked and also the double bond can be converted into other functionalities, for instance by dihydroxilation and epoxidation reactions.[20, 25]

Mecerreyes et al. proposed the synthesize of 7-(prop-2-en-1-yl)oxepan-2-one by the Baeyer-Villiger oxidation of 2-(prop-2-en-1-yl)cyclohexanone but this reaction was not very efficient because epoxidation of the double bond could not be avoided, which limits the yield (Scheme 16).[26]
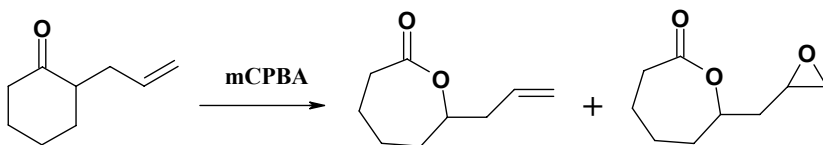
Scheme 16. Synthesis of 7-(prop-2-en-1-yl)oxepan-2-one.

Lactones functionalized with an endocyclic double bond were obtained by the elimination reaction of αClεCL.[27] Nevertheless, this reaction was again not selective because a mixture of 6,7-dihydrooxepin-2(5H)-one and of 6,7-dihydrooxepin-2(3H)-one was obtained (Scheme 17). The two isomers were separated by chromatography. Interestingly, 6,7-dihydrooxepin-2(3H)-is an unusual monomer, which can be polymerized by two distinct mechanism. At the one hand, the ROP can be initiated by aluminum alkoxides.[27] At the other hand, the polymerization can also be carried out by a ring-opening metathesis mechanism. Indeed, 6,7-dihydrooxepin-2(3H) was successfully mediated by the Schrock's catalyst, even though the control of the polymerization was poor.[28]
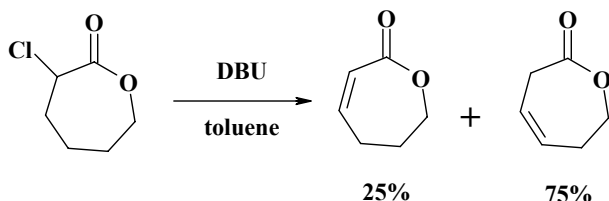
Scheme 17. Synthesis of 7-(prop-2-en-1-yl)oxepan-2-one.

After these first reports, more selective syntheses were reported. Lou et al. reported the selective synthesis of 6,7-dihydrooxepin-2(5*H*)-one by a strategy based on the elimination of a selenoxide shown in Scheme 18.[29]
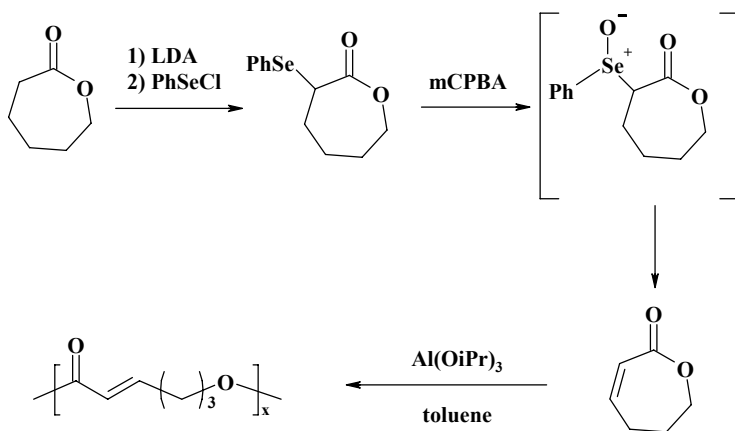
Scheme 18. Synthesis of 6,7-dihydrooxepin-2(5H)-one.

Emrick et al. reported on the synthesis of 3-(prop-2-en-1-yl)tetrahydro-2*H*-pyran-2-one by reaction of tetrahydro-2*H*-pyran-2-one (δVL for δ-valerolactone) and LDA into the corresponding enolate followed by reaction with 3-bromoprop-1-ene (Scheme 19). It is worth nothing that the yield of this reaction depends the size of the lactone, as shown by the lowest yield obtained for the allylation of εCL even under optimized conditions. 3-(prop-2-en-1-yl)tetrahydro-2*H*-pyran-2-one was homopolymerized and copolymerized with εCL by ethanol the presence of Sn(OTf)$_2$.[30] In another work, Emrick et al. reported on the synthesis of 7-oxaspiro[4.5]dec-2-en-6-one by a strategy based on ring closing metathesis as shown in Scheme 20.[31]
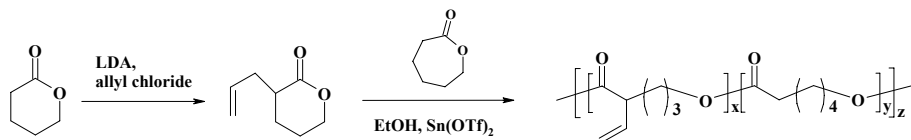
Scheme 19. Synthesis and polymerization of 3-(prop-2-en-1-yl)tetrahydro-2*H*-pyran-2-one.
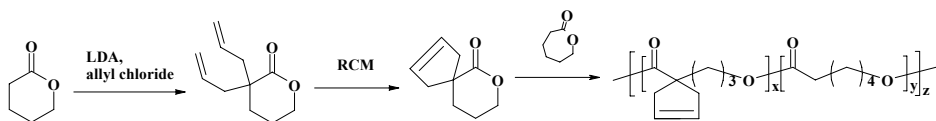
Scheme 20. Synthesis of 7-oxaspiro[4.5]dec-2-en-6-one.

Interestingly, the synthesis and the polymerization of 3-(prop-2-en-1-yl)-1,4-dioxane-2,5-dione, which is nothing but an allyl-substituted glycolide, was reported by Hennink et al. (Scheme 21).[25]
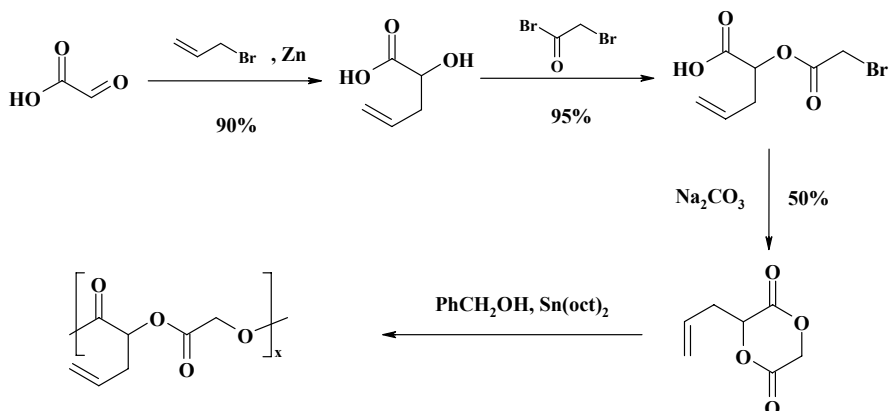
*Scheme 21.* Synthesis and polymerization of 3-(prop-2-en-1-yl)-1,4-dioxane-2,5-dione.

7-oxooxepan-4-yl prop-2-enoate is the first reported example of a difunctional monomer polymerizable by two different controlled processes: ROP and atom transfer radical polymerization (ATRP).[32] This monomer was synthesized by a three-step strategy shown in Scheme 22 and was homo- and copolymerized with εCL by ring-opening by using aluminum isopropoxide as an initiator. Later on, a two-step backbiting reaction was observed during this polymerization, which results in the formation of 2-(5-oxotetrahydrofuran-2-yl)ethyl prop-2-enoate by the mechanism shown in Scheme 23.[33] Nevertheless, the extent of this side reaction is less important as long as the temperature is low and the reaction is stopped rapidly after complete monomer conversion. The driving force of this side reaction is the very favorable formation of a five-membered ring. In order to overcome this issue, the acrylic functionality was introduced in another position. Toward this end, Li et al. synthesized 1-(2-oxooxepan-3-yl)ethyl prop-2-enoate by a three-step process shown in Scheme 24.[34] It is worth noting that all these lactones substituted by acrylic groups are not stable owing to noxious radical reactions. These lactones have to be stored in the presence of a radical scavenger at −20°C.
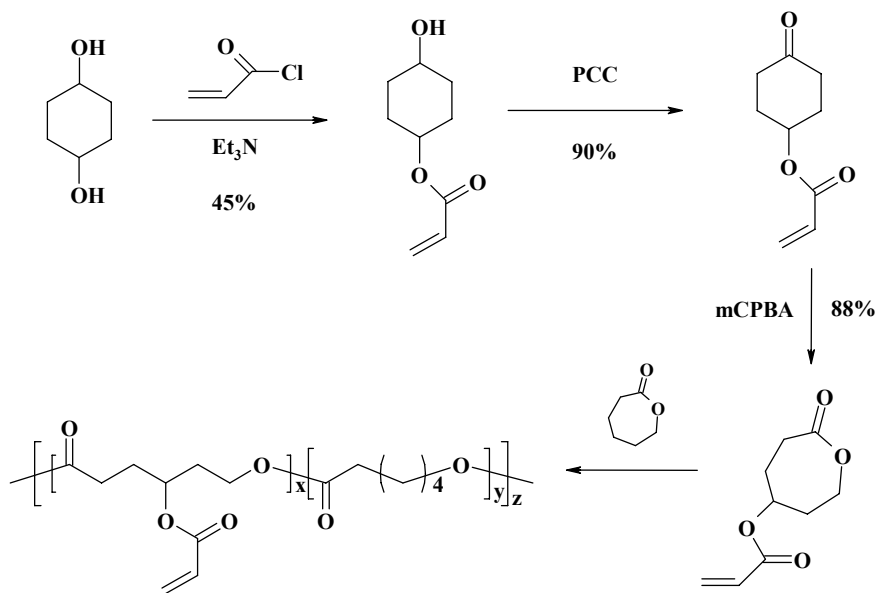
Scheme 22. Synthesis and polymerization of 7-oxooxepan-4-yl prop-2-enoate.[32]
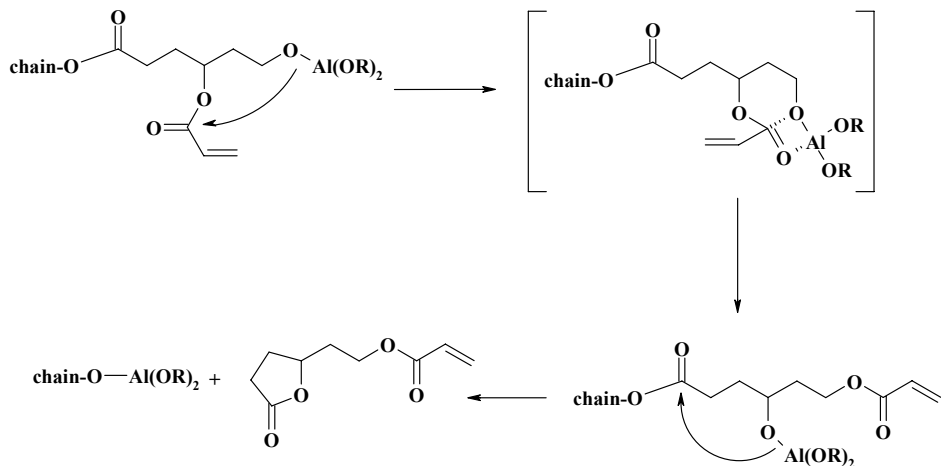

Scheme 23. Two-step backbiting reaction in the polymerization of 7-oxooxepan-4-yl prop-2-enoate initiated by aluminum isopropoxide.[33]
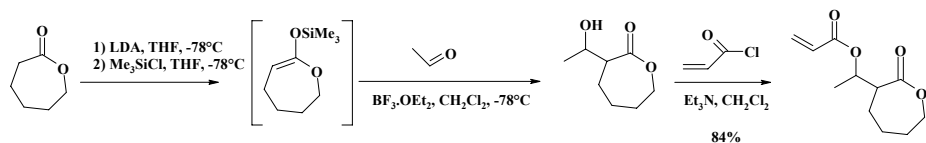
Scheme 24. Synthesis of 1-(2-oxooxepan-3-yl)ethyl prop-2-enoate.[34]

3. Direct grafting of Functional Groups onto Aliphatic Polyesters

The synthesis of lactones substituted by functional groups requires too often a multi-step synthesis at the expense of the final yield, which can be quite low. In order to tackle these drawbacks, the grafting of functional groups onto preformed polyester chains is a very appealing approach because a wide range of functional groups can be attached from a single precursor and the synthesis of substituted monomers is no more required, which is a huge advantage. Besides, the functionalization of aliphatic polyesters by alcohols and carboxylic acids is very efficient without using protection and deprotection reactions because functionalization takes place after polymerization. A representative example was reported by Vert et al.,[35,36–38] who metallated PCL by LDA with formation of a poly(enolate), which was then reacted with several electrophiles for further functionalization. (Scheme 25). The implementation of this strategy is however limited by unavoidable chain degradation in competition with chain metallation. It is difficult to reach functionalization efficiencies higher than 30%, which can be a limitation for several applications.
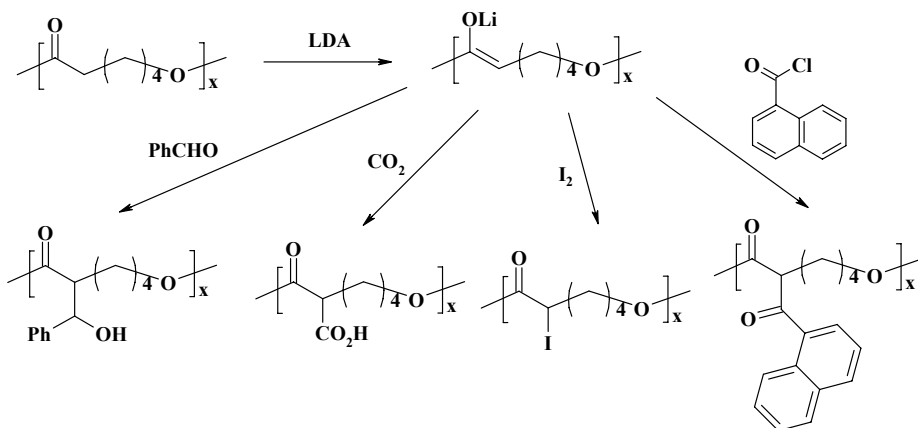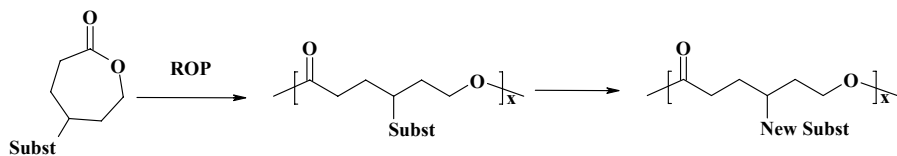

Scheme 25. Chemical derivatization of PCL by an anionic route.

4. Ring-Opening Polymerization of Suitably Substituted eCLs Followed by Derivatization of the Substituent

In order to tackle the problems inherent to the routes discussed earlier, it appears that a combination of these two strategies into a two-step process might be a valuable alternative (Scheme 26).[1] Thus, εCL substituted by a suitable functional group is first polymerized, followed by the derivatization of the substituent into various functional groups. A wide range of aliphatic polyesters could accordingly be made available from a single precursor.

Scheme 26. ROP of substituted ωCL followed by its chemical derivatization into various functional aliphatic polyesters.

For this strategy to be successful, the following criteria should be satisfied: (1) The synthesis of the substituted monomer should be as direct as possible and the yield should be high (2) this monomer should comply with controlled (co)-polymerization, (3) the envisioned derivatization reactions should be carried out under mild conditions in order to (i) avoid chain degradation, (ii) avoid protection/deprotection of the functions to be incorporated, (iii) favour quantitative reaction even at high content of functional groups.
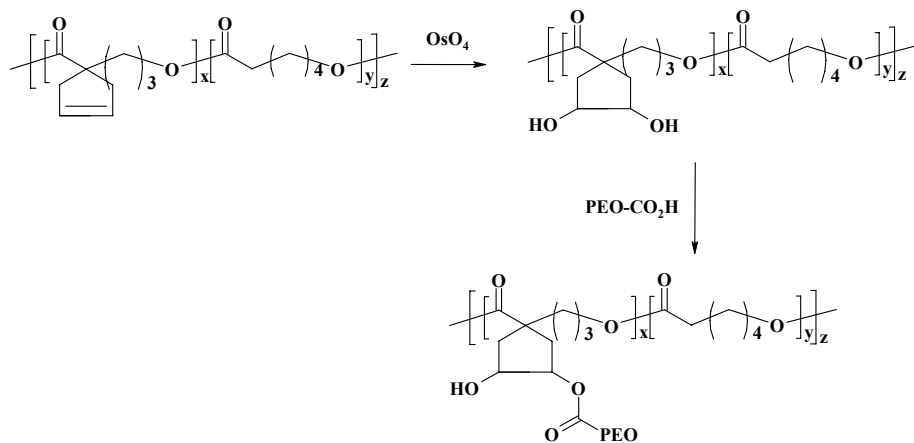
Scheme 27. Grafting of PEO onto PCL according to Emrick et al.[27]

An example of this strategy was reported by Emrick et al. who implemented an esterification reaction of carboxylic acid-terminated PEO and a copolyester attached by pendant hydroxyl groups (Scheme 27).[31] This process could be easily extended to other functionalizations just by changing the structure of the carboxylic acid. The main limitation of this approach relies on tedious synthesis of aliphatic polyesters bearing pendant alcohols, as pointed out in "Polyelectrolyte Stars and Cylindrical Brushes Made by ATRP: New Building Blocks in Nano-technology".

Mayes et al. reported the grafting of aminooxy-terminated PEO onto the ketone groups of poly(εCL-*co*-oxepane-1,2-dione) (Scheme 28).[39] The synthesis of the starting polyester is direct as shown in Scheme 2. Nowadays, these

functionalizations have been extended to hydrazines[40] and to other aminooxy small molecules.[41, 42] It is also worth noting that the coupling of amines by reductive amination was investigated by Wooley et al. but the efficiency turned out to be not sufficient.[43] One important issue is the low solubility of co-polyesters with a high content of oxepane-1,2-dione in many organic solvents, which might limit the extent of functionalization.
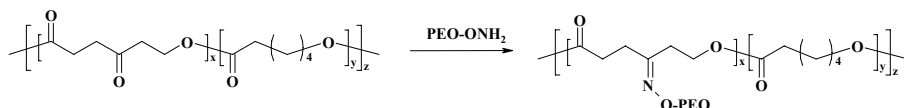
Scheme 28. Grafting of PEO onto PCL according to Mayes et al.

Recently, thiols were added onto pendant acrylate groups of PCL.[44] For example, thiol end-capped PEO was added onto the pendant acrylic groups of PCL (content of acrylic units = 18 mol%) in the presence of pyridine (THF, room temperature, 300 h [pyridine]/[thiol]/[acrylate] = 15/10/1). The poly(CL-*g*-EO) graft copolymer was formed as result of 65% conversion of the acrylic units. These experimental conditions were extended to the addition of mercapto-acetic acid, the acrylic conversion being 71% after 75 h. Interestingly, no degradation was observed and no cumbersome protection/deprotection reaction was needed. Nevertheless, the Michael reaction is not quantitative and there is a risk of cross-linking through the residual acrylic groups.
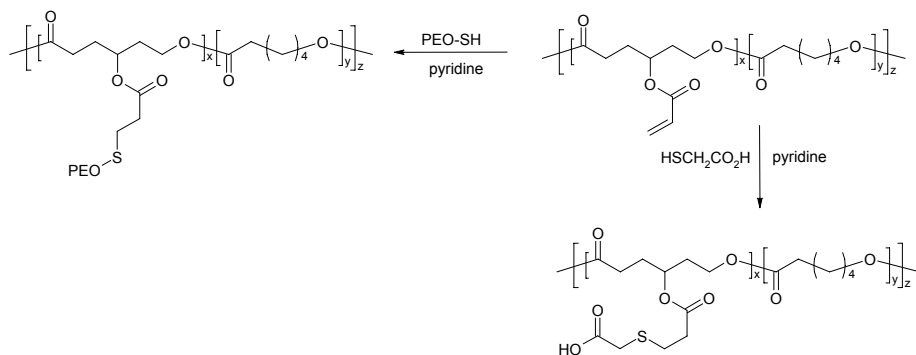

Scheme 29. Derivatization of pendent acrylic unsaturations of PCL by Michael addition.

In a similar approach, thiols were grafted onto PCL attached with pendant epoxides.[20, 27] Nevertheless, the synthesis of aliphatic polyesters bearing pendant epoxides is quite complicated because a two-step approach is needed; the synthesis of unsaturated aliphatic polyesters being the first step and the epoxidation of double bonds being the second step.

The synthesis of α-chlorinated PCL is straightforward (Scheme 14) and chlorides activated by a carbonyl group are well suited to react by atom transfer

radical addition (ATRA). Several alkenes substituted by various functional groups were grafted onto PCL by ATRA mediated by CuBr/Me$_6$TREN (Scheme 30).[45] No protection was needed and no chain degradation was observed by SEC. Moreover, ATRA of α-methoxy, ω-acrylate-PEO (M_n (PEO = 750) onto poly (αClεCL-co-εCL) (M_n = 17,500 ; 48 αClεCL units) yielded a graft copolymer, with nine PEO grafts.[46] However, 18 chlorinated units per chain were lost by reduction during ATRA. The situation got worse when but-3-enoic acid was used because only reduction was observed. Interestingly, no parasitic reduction of the chlorides occurred by using HMTETA instead of Me$_6$TREN as a ligand but the activity of the catalyst was decreased. ATRA took place with a moderate yield of 32% after 24 h. Increase of the temperature (85°C instead of 65°C) allows reaching completeness but chains were then degraded simultaneously. The stoichiometric amount of the copper catalyst with respect to activated chlorides, which is needed in ATRA, contaminates the final polyester, which may be unacceptable depending on the end-use of the polymer.
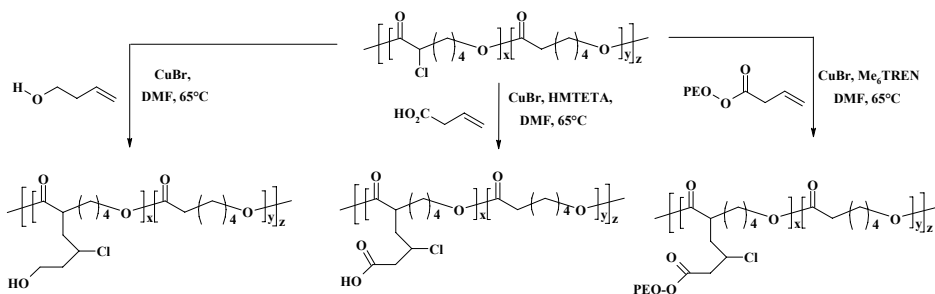
Scheme 30. Derivatization of the α-chloride pendant groups of PCL by ATRA.

5. Conclusions

Nowadays, the synthesis of aliphatic polyesters bearing pendant functional groups remains challenging. The synthesis and the ROP of a wide range of functional lactones have been reported. Nevertheless, a multi-step synthesis of the monomer is often required and the global yield might be low. The direct functionalization of aliphatic polyesters is a very direct approach. Nevertheless, many reactions used until now are not quantitative or are performed under conditions which are not mild enough to prevent degradation from occurring. It is thus highly desirable to implement more efficient reactions and copper mediated azide–alkyne cycloaddition, which is nothing but the most widely used "click" reaction, is very promising.

Acknowledgement

References

[1] Ph. Lecomte, R. Riva, S. Schmeits, J. Rieger, K. Van Butsele, C. Jérôme, R. Jérôme, *Macromol. Symp.* 240, 157–165 (2006).

[2] X. Lou, C. Detrembleur, R. Jérôme, *Macromol. Rapid Commun.* 24, 161–172 (2003).

[3] D. Tian, Ph. Dubois, Ch. Grandfils, R. Jérôme, *Macromolecules* 30, 406–409 (1997).

[4] D. Tian, Ph. Dubois, R. Jérôme, *Macromolecules* 30, 2575–2581 (1997).

[5] J.-P. Latere, Ph. Lecomte, Ph. Dubois, R. Jérôme, *Macromolecules* 35, 7857–7859 (2002).

[6] F. Stassin, O. Halleux, Ph. Dubois, C. Detrembleur, Ph. Lecomte, R. Jérôme, *Macromol. Symp.* 153, 27–39 (2000).

[7] S. Gautier, V. d'Aloia, O. Halleux, M. Mazza, Ph. Lecomte, R. Jérôme, *J. Biomater. Sci. Polym. Edn.* 14, 63–85 (2003).

[8] C. G. Pitt, P. Ingram, R. W. Hendren, *J. Polym. Sci.: Part A: Polym. Chem.* 25, 955–966 (1987).

[9] M. Trollsas, V. Y. Lee, D. Mercerreyes, P. Löwenhielm, M. Möller, R. D. Miller, J. L. Hedrick, *Macromolecules* 33, 4619–4627 (2000).

[10] M. Liu, N. Vladimirov, J. M. J. Fréchet, *Macromolecules* 32, 6881–6884 (1999).

[11] F. Tasaka, Y. Ohya, T. Ouchi, *Macromol. Rapid Commun.* 22, 820–824 (2001).

[12] X.-h. Yu, J. Feng, R.-x. Zhuo, *Macromolecules* 38, 3244–6247 (2005).

[13] P. G. Parzuchowski, M. Grabowska, M. Tryznowski, G. Rokicki, *Macromolecules* 39, 7181–7186 (2006).

[14] M. Leemhuis, C. F. van Nostrum, J. A. W. Kruijtzer, Z. Y. Zhong, M. R. ten Breteler, P. J. Dijkstra, J. Feijen, W. E. Hennink, *Macromolecules* 39, 3500–3508 (2006).

[15] C. A. M. Loontjens, T. Vermonden, M. Leemhuis, M. J. van Steenbergen, C. F. van Nostrum, W. E. Hennink, *Macromolecules* 40, 7208–7216 (2007).

[16] W. W. Gerhardt, D. E. Noga, K. I. Hardcastle, A. J. Garcıa, D. M. Collard, M. Weck, *Macromolecules* 7, 1735–1742 (2006).

[17] K. Marcincinova Benabdillah, J. Coudane, M. Boustta, R. Engel, M. Vert, *Macromolecules* 32, 8774 (1999).

[18] Ph. Lecomte, V. D'aloia, M. Mazza, O. Halleux, S. Gautier, C. Detrembleur, R. Jérôme, *Polym. Preprints, Am. Chem. Soc.*, 41(2), 1534–1535 (2000).

[19] O. Coulembier, P. Degée, J. L. Hedrick, P. Dubois, *Prog. Polym. Sci.* 31, 723–747 (2006).

[20] C. Detrembleur, M. Mazza, O. Halleux, Ph. Lecomte, D. Mecerreyes, J. L. Hedrick, R. Jérôme, *Macromolecules* 33, 7751–7760 (2000).

[21] C. Detrembleur, M. Mazza, O. Halleux, Ph. Lecomte, D. Mecerreyes, J. L. Hedrick, R. Jérôme, *Macromolecules* 33, 14–18 (2000).

[22] S. Lenoir, R. Riva, X. Lou, C. Detrembleur, R. Jérôme, Ph. Lecomte, *Macromolecules* 37, 4055–4061 (2004).

[23] R.-S. Lee, Y.-T. Huang, *J. Polym. Sci.: Part A: Polym. Chem.* 46, 4320–4331 (2008).

[24] G. Wang, Y. Shi, Z. Fu, W. Yang, Q. Huang, Y. Zhang, *Polymer* 46, 10601–10606 (2005).

[25] M. L. Leemhuis, N. Akeroyd, J. A. W. Kruijtzer, C. F. van Nostrum, W. E. Hennink, *Eur. Polym. J.* 44, 308–317 (2008).

[26] D. Mecerreyes, R. D. Miller, J. L. Hedrick, Ch. Detrembleur, R. Jérôme, *J. Polym. Sci., Polym. Chem.* 38, 870–875 (2000).

[27] X. Lou, C. Detrembleur, Ph. Lecomte, R. Jérôme, *J. Polym. Sci.: Part A: Polym. Chem.* 40, 2286–2297 (2002).

[28] X. Lou, C. Detrembleur, Ph. Lecomte, R. Jérôme, *e-polymers.* 34, 1–12 (2002).

[29] X. Lou, C. Detrembleur, Ph. Lecomte, R. Jérôme, *Macromolecules* 34, 5806–5811 (2001).

[30] B. Parrish, Quansah J. K. T. Emrick, *J. Polym. Sci.: Part A: Polym. Chem.* 40, 1983–1990 (2002).

[31] B. Parrish, T. Emrick, *Macromolecules* 37, 5863–5865 (2004).

[32] D. Mecerreyes, J. Humes, R. D. Miller, J. L. Hedrick, Ph. Lecomte, Ch. Detrembleur, R. Jérôme, *Macromol. Rapid. Commun.* 21, 779–784 (2000).

[33] X. Lou, C. Detrembleur, Ph. Lecomte, R. Jérôme, *Macromol. Rapid Commun.* 23, 126–129 (2002).

[34] H. Li, R. Jérôme, Ph. Lecomte, *Polymer* 47, 8406–8413 (2006).

[35] S. Ponsart, J. Coudane, M. Vert, *Biomacromolecules* 1, 275–281 (2000).

[36] B. Saulnier, S. Ponsart, J. Coudane, H. Garreau, M. Vert, *Macromol. Biosci.* 4, 232–237 (2004).

[37] M.-H. Huang, J. Coudane , S. Li, M. Vert, *J. Polym. Sci., Polym. Chem.* 43, 4196–4205 (2005).

[38] B. Nottelet, J. Coudane, M. Vert, *Biomaterials* 27, 4948–4954 (2006).

[39] I. Taniguchi, A. M. Mayes, E. W. L. Chan, L. G. Griffith, *Macromolecules* 38, 216–219 (2005).

[40] E. L. Prime, J. J. Cooper-White, G. G. Qiao, *Aust. J. Chem.* 59, 534–538 (2006).

[41] B. A. Van Horn, R. K. Iha, K. L. Wooley, *Macromolecules* 41, 1618–1626 (2008).

[42] B. A. Van Horn, K. L. Wooley, *Soft Matter* 3, 1032–1040 (2007)

[43] B. A. Van Horn, K. L. Wooley, *Macromolecules* 40, 1480–1488 (2007).

[44] J. Rieger, K. Van Butsele, P. Lecomte, C. Detrembleur, R. Jérôme, C. Jérôme, *Chem. Commun.* 274–276 (2005).

[45] R. Riva, S. Lenoir, R. Jérôme, Ph. Lecomte, *Polymer* 46, 8511–8518 (2005).

[46] R. Riva, J. Rieger, R. Jérôme, Ph. Lecomte, *J. Polym. Sci.: Part A: Polym. Chem.* 44, 6015–6024 (2006).

THERMALLY DEGRADABLE MALEIMIDES FOR REWORKABLE ADHESIVES

OSAMA M. MUSA[1*], XINNAN ZHANG[1], GANG-CHI CHEN[1], ANDREW COLLINS[2], SOLOMON JACOBSON[1], PAUL MORGANELLI[2], AND YADUNANDAN L. DAR[1]
[1]*Bridgewater Applied Research Group, National Starch and Chemical Company/ICI, 10 Finderne Ave. Bridgewater, NJ 08807*
[2]*Emerson & Cuming, 46 Manning Road, Billerica, MA 01821*

Abstract: New thermosetting materials were developed for reworkable adhesive applications by introducing acetal ester groups as thermally degradable linkages into maleimide compounds. The synthesis of compounds containing maleimide functionality and acetal ester linkages was conducted by a one-step neat reaction from commercially available materials. The polymerization process and thermal degradation of the synthesized materials were studied. It was found that the acetal ester linkage degraded rapidly above 225°C and introduction of this linkage into the adhesive formulation led to improved reworkability of adhesively bonded substrates. A mechanism for reworkability was proposed based on insight provided by experimental and modeling work.

1. Introduction

Thermosetting materials have been widely used in a variety of applications such as coatings, encapsulants, and adhesives.[1–3] However, many traditional thermosetting materials display poor tractability after curing, which limits their use in those applications for which degradable or reworkable polymers are advantageous. For example, the reworkability of an adhesive used to adhere semiconductor chips to substrates is desired because it is expensive to discard an assembled printed circuit board (PCB) with only one failed chip. The use of an adhesive that will melt or decompose to allow removal of individual chips for repair or replacement would be an advantage for semiconductor manufacturers. In addition, reversible or degradable adhesives are applicable to a variety of fabrication processes to increase process efficiency.

In order to develop adhesives that are reworkable, thermally degradable linkages are introduced into the crosslinkable structures. The decomposition of the degradable crosslinkers upon heating leads to a decrease in crosslinking density and modulus of the adhesive, allowing chip removal and replacement. A variety of degradable linkages have been studied both in academia as well as in industry. For example, Tesero and Sastri developed epoxy resins containing disulfide linkages, which decomposed upon treatment with triphenylphosphine.[4, 5] A series of crosslinkers containing secondary or tertiary ester linkages were developed.[6–10] Upon heating, the thermally labile ester linkages decomposed and led to degradation of the crosslinked network. In addition, Wudl and coworkers reported the use of retro Diels–Alder reactions for thermally reversible materials.[11, 12] More recently, Wong and coworkers introduced thermally degradable carbamate and carbonate linkages into epoxy-based adhesive form-ulations to facilitate the rework process.[13–15] However, most of degradable thermosetting materials that have been reported in the literature are based on traditional epoxy resin systems.

Recently, a variety of radical based systems have been developed for adhesives and electronic packaging applications. These systems are advantageous due to their fast cure speed as well as other material specific advantages. For example, maleimide-based materials[16–19] are found to have better adhesion and low shrinkage after curing. In addition, maleimide functionality cannot only be homopolymerized efficiently but can also be copolymerized with a variety of functional groups, such as styrenic, vinyl ether, acrylate, and methacrylate. However, these systems can be intractable after curing and not suitable for applications where adhesive removal is desired, such as debonding adhesives and reworkable adhesives. Therefore, in our study, reworkable maleimide com-pounds have been developed and their polymerization process and degradation behavior have been analyzed. These novel materials provide the advantages offered by maleimide adhesives in a reworkable adhesive system.

The reworkable maleimide-based crosslinkers were prepared by introducing degradable acetal ester linkages into multi-functional maleimides (Figure 1). Acetal ester linkages were chosen because the degradation of acetal linkages has been demonstrated in variety of other applications.[20, 21] For example, Fréchet and coworkers have incorporated acetal or ketal linkages into a polymer backbone for pH-sensitive polymers for polymer therapeutics and drug delivery applications.[22] Buchwalter and Kosber have introduced acetal linkages into epoxy resins for reworkable adhesives, which could be slowly dissolved into acid-containing organic solvents.[23] In this paper, we describe a unique approach where the acetal ester linkages were introduced into maleimide-based compounds by a one-pot neat reaction from commercially available materials. These multifunctional maleimide compounds can polymerize into highly crosslinked networks, which can degrade upon further heating as shown in

Figure 1. The thermal degradation behavior was analyzed by differential scanning calorimetry (DSC), thermogravimetic Analysis (TGA), thermal desorption gas chromatography with mass spectrometric detection (GC-MS), and hot-stage Fourier transform infrared spectroscopy (FTIR). Molecular modeling was also used to study the thermal degradation process in order to understand the mechanism of degradation as well as to guide experimental effort. Additionally, we report the results of adhesion tests for reworkable adhesive applications.
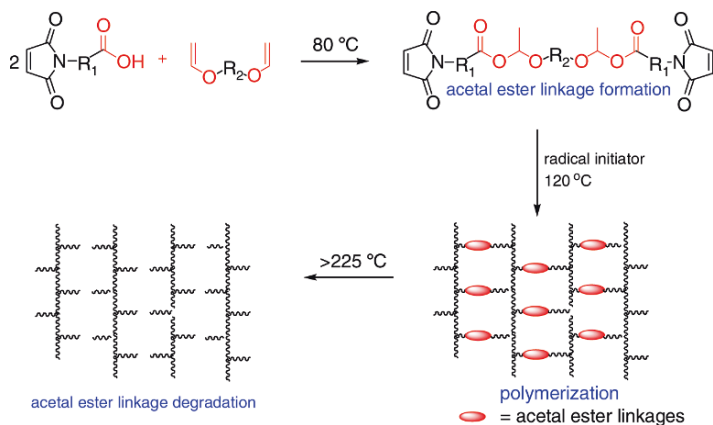
Figure 1. Schematic diagram of synthesis, polymerization, and decomposition of bismaleimides containing acetal ester linkages.

2. Results and Discussion

2.1. SYNTHESIS

The synthesis of maleimide compounds containing acetal ester linkages was conducted by a one-step neat reaction using a maleimide compound with carboxylic acid functionality and a vinyl ether. The preparation of the bismaleimide **1** was performed by slow addition of carboxylic acid into vinyl ether at 90°C as shown in Scheme 1. It was found that reversing the addition process caused gelation, most likely due to a large amount of acid leading to cationic polymerization of the vinyl ether. When running the reaction under a N_2 atmosphere, gelation was also observed, indicating that a small amount of oxygen is necessary to inhibit the possible polymerization of vinyl ether and maleimide functionalities. In addition, a small excess of carboxylic acid leads to lead to complete reaction of the divinyl ether. The residual acid can be effectively removed by Amberlyst A21 or basic alumina treatment.
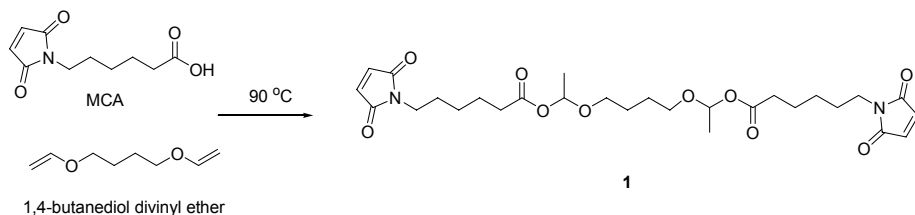
Scheme 1. Synthesis of compound **1** containing acetal ester linkages.

TABLE 1. Viscosities of compounds **1–5**.

Compound	Structures	Viscosity at 25°C (mPa·S)
1		5,000
2		>100,000
3		3,800
4		13,000
5		313

Five materials containing acetal ester linkages and maleimide functionality were synthesized via a similar synthetic method and their viscosities are listed in Table 1. It was found that the viscosities of the resulting maleimide compounds varied significantly when changes to the backbone. Compound **2** displayed a large increase in viscosity upon introduction of a cycloaliphatic backbone. However, introduction of a diethylene glycol backbone leads to a slight decrease of the viscosity as compared to compound **1**. Viscosity also increased considerably when a shorter maleimide carboxylic acid was used as a starting material for compound **4** as compared to compound **3**. When only one maleimide functionality was present, such as monofunctional maleimide **5**, the viscosity of the resulting compound is much lower than the bismaleimides.

2.2. DSC AND TGA

The polymerization process of these materials was studied by DSC. Figure 2 shows the curing profile of compound **1** initiated by USP-90MD (2 wt%). The polymerization was initiated at 105°C and reached a maximum at 121°C with the heat of polymerization of 389 J/g. The peak after ~220°C suggests possible degradation of acetal ester linkages. This peak was also observed for compounds **3–5**.[25] A control experiment was conducted with a bismaleimide without
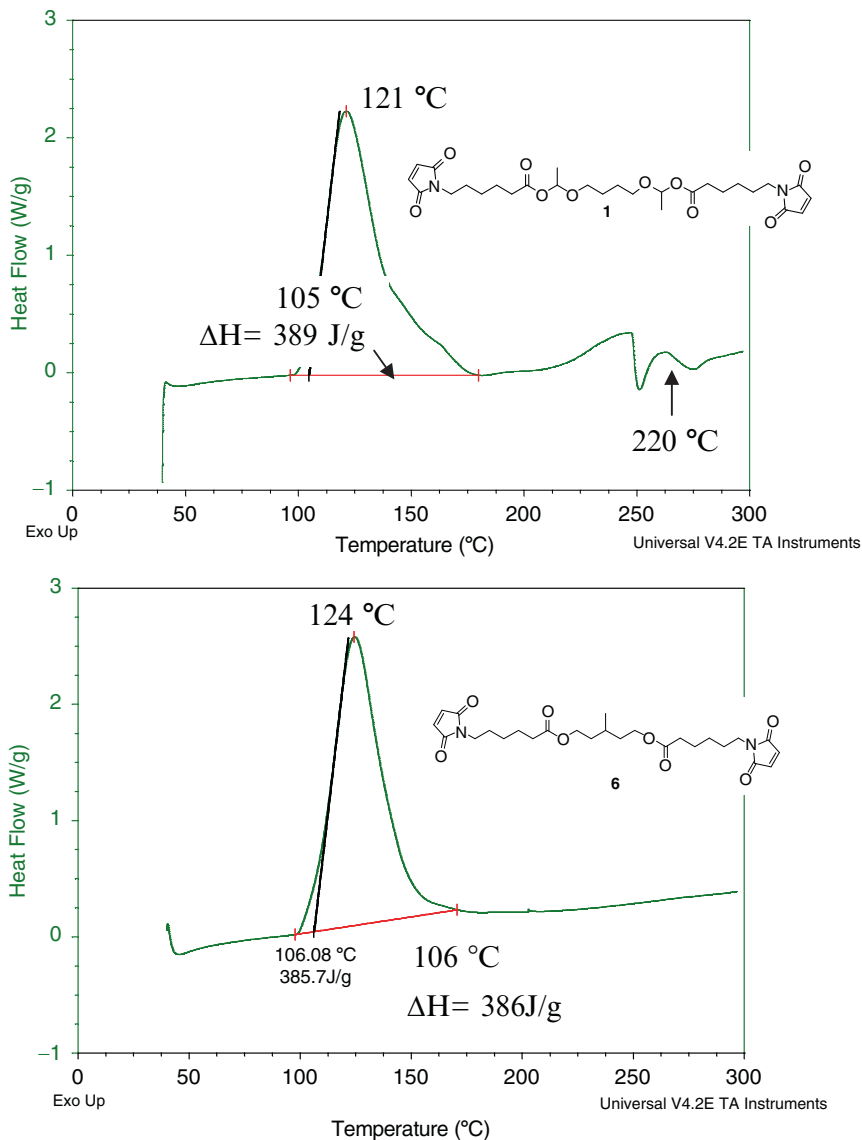

Figure 2. DSC of compounds **1** and **6** with 2 wt% USP-90MD.

the acetal ester linkage (compound **6**).[26] No peak was observed above 175°C. The polymerization processes of compounds **3**–**5** can be found in the Supporting Information.

The thermal degradation behavior of compounds **1**, **3**, **4**, and **5** was studied by TGA of the polymerized samples. The results for compound **1** are shown in Figure 3.
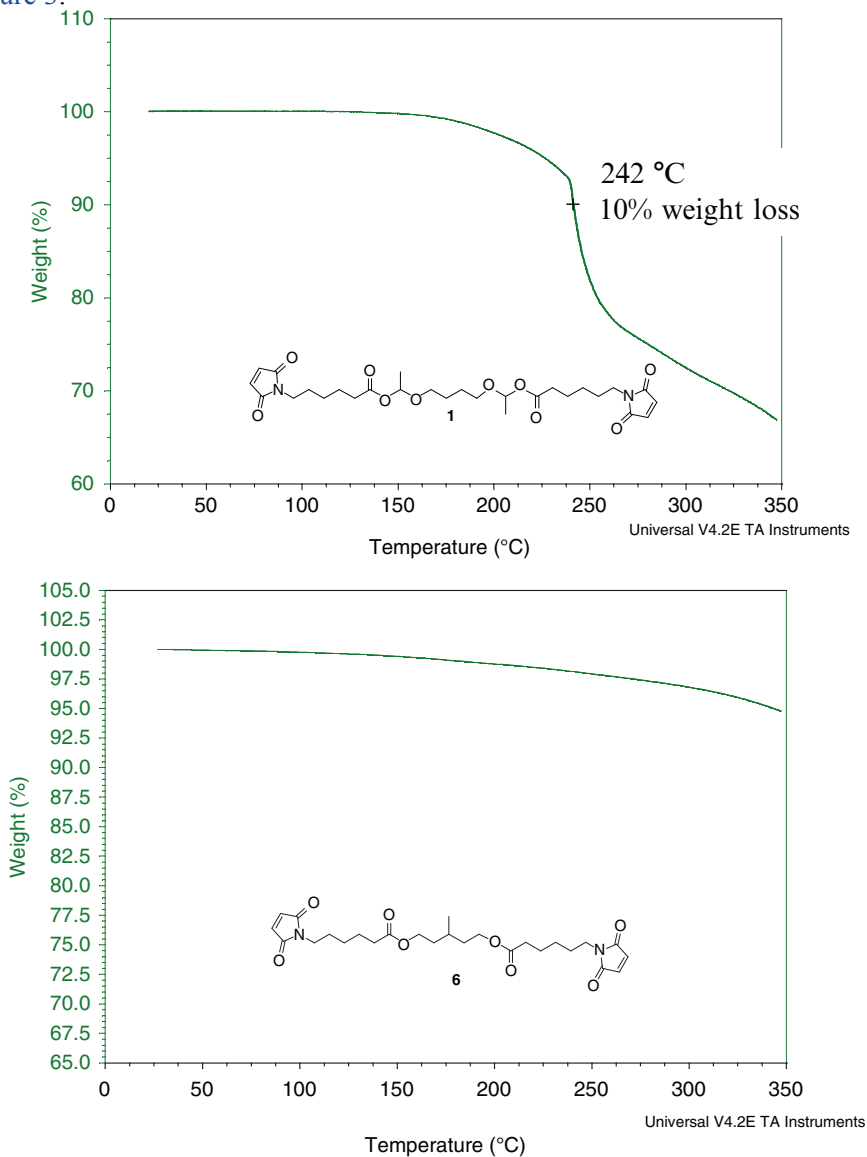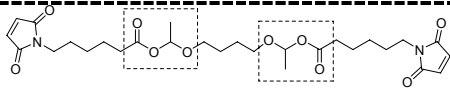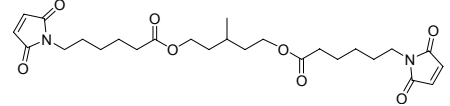
Figure 3. Degradation behavior of compounds **1** and **6** by TGA.

The curing experiment was conducted by heating a mixture of **1** (98 wt%) and USP-90MD (2 wt%) to 120°C for 10 min. The polymerization temperature was chosen based on the curing peak measured using DSC. The polymerized **1** displayed a 10% weight loss at 242°C by TGA. The detailed decomposition pathway is discussed in the proposed degradation mechanism section. Compounds **3–5** displayed similar degradation behavior by TGA as shown in the Supporting Information.[25]

2.3. REWORK TESTING

The rework test was performed by testing the adhesion of the polymerized materials in an electronic package at high temperature. The mixture of compound **1** and USP-90MD was used as underfill[24] in a standard electronic package, followed by curing at 120°C for 10 min. The adhesion of the cured underfill was tested by die shear test at both ambient temperature and 150°C after exposing to 250°C for 2 min to simulate the rework condition.[27] Compound **6** (see Table 3), a bis-maleimide without acetal ester linkage, was also tested as a reference molecule. The adhesion results are summarized in Table 2.

TABLE 2. Die shear adhesion of cured **1** and **6**.

	25°C adhesion	150°C adhesion (after exposing to 250°C for 2 min)
1	35.2 kg	2.3 kg
6	44.9 kg	18.6 kg

The adhesion strength of cured compound **1** dropped significantly from 35.2 kg (room temperature) to 2.3 kg (150°C) after it was held at 250°C for 2 min. However, the adhesion of cured compound **6** without the acetal ester linkage is much higher after 250°C exposure. In addition, board damage was observed for cured compound **6** during the die shear test due to cohesive failure of the substrate, demonstrating poor reworkability. The die shear data suggests that the acetal ester linkage indeed caused a large decrease in adhesion strength after exposing to elevated temperature, which facilitates the rework process.
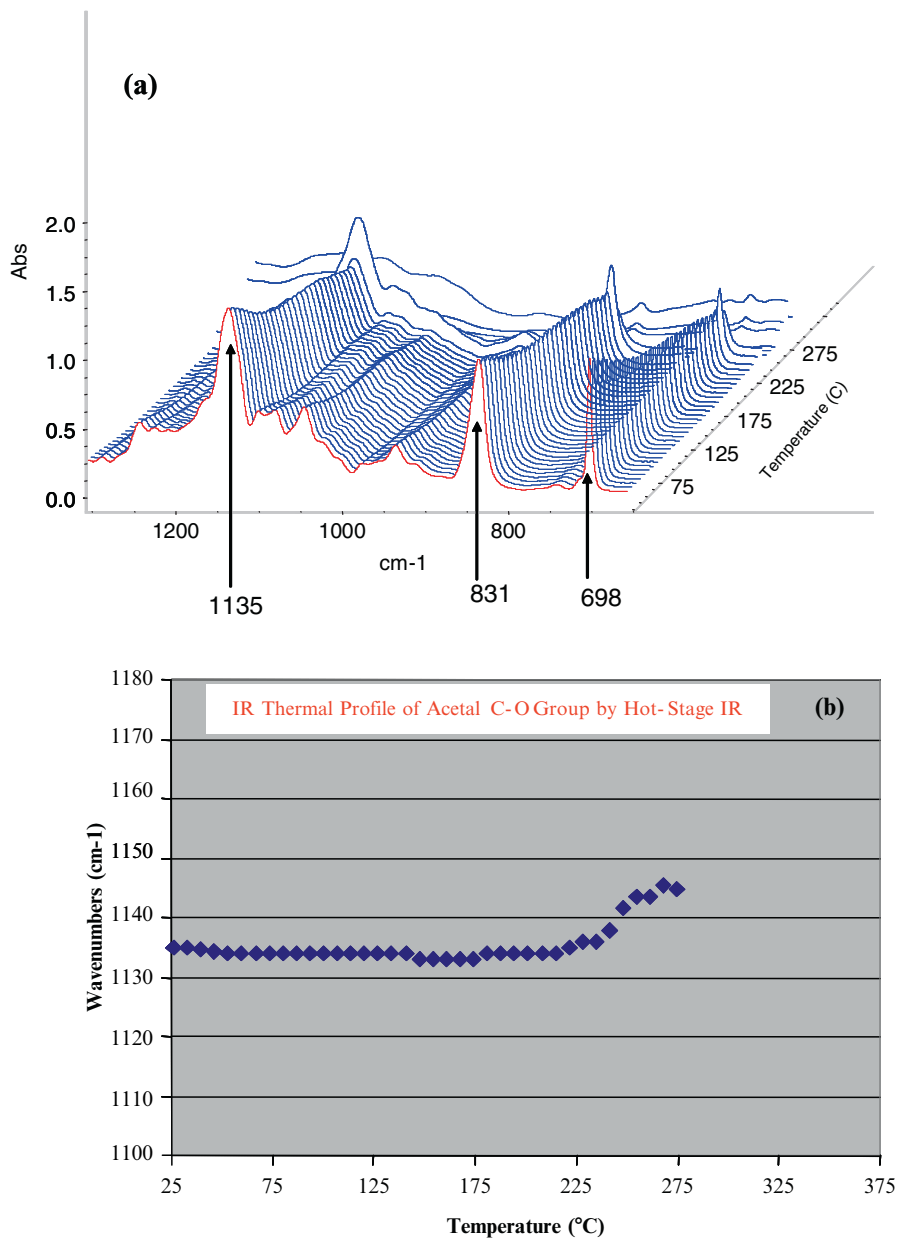
Figure 4. Degradation behavior of compound **1** by hot-stage IR: (**a**) three-dimensional IR (**b**) graph of acetal C–O stretch versus temperature.

2.4. THERMAL DEGRADATION STUDY BY HOT-STAGE IR

In order to confirm the degradation temperature and understand the decomposition mechanism at the molecular level, hot-stage FTIR of compound **1** was conducted as shown in Figure 4. Figure 4a shows the FTIR spectra plotted as a function of temperature ranging from 25°C to 275°C. At ~250°C, the intensity of several peaks in the figure decreased significantly, suggesting decomposition. Particularly, the acetal C–O peak (~1,135 cm^{-1}) dropped in intensity indicating that the decomposition occurred at this linkage. The peaks at 831 and 698 cm^{-1} correspond to C–H stretching of the maleimide functionality. The decrease of these peaks suggests that self-polymerization occurred upon heating. The decomposition not only led to intensity decline but also to a frequency shift of the breaking bond in the IR spectra.

In order to identify the initial degradation temperature, the frequency of the acetal C–O stretching was plotted with temperature as seen in Figure 4b. The C–O stretching frequency started to shift at 225°C, suggesting the decomposition of this linkage initiated from ~225°C. The changes in peak intensity and wavenumber suggest that the experimentally observed breakdown in network structure is caused by the degradation of one of the acetal C–O linkages. The thermal degradation temperature indicated by hot-stage FTIR spectrum is consistent with the DSC and TGA data discussed above.

2.5. MOLECULAR MODELING AND SIMULATION OF THE THERMAL DEGRADATION MECHANISM

The experimental observations suggest that the C–O bond in the acetal linkage decomposes to break the polymer network and enable reworkability. The most likely pathway for acetal thermal degradation mechanism involves cleavage of the C–O with abstraction of an adjacent hydrogen atom, forming a vinyl ether and an alcohol.[28] The degradation products are shown in Scheme 2:
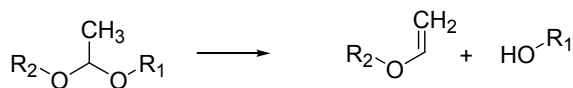
Scheme 2. Pyrolysis of an acetal bond.

Thermal degradation of the acetal linkage was studied. In order to do this we define a reaction coordinate based on the observations of the molecular dynamics simulation. Here, the thermal degradation pathway can be defined by elongation of the weak C–O bond. The molecular energy was calculated for several points along this reaction pathway. For each point, all aspects of the

molecular geometry were optimized, except the C–O bond of interest which was forced to elongate in small increments. Figure 5 plots the computed energy as a function of the C–O bond length. The reaction energy barrier (E_b) was determined by subtracting the starting energy from the maximum energy along the reaction path, while the heat of the reaction (ΔE) was determined by subtracting the starting energy from the energy of the final point (products) of the pathway.
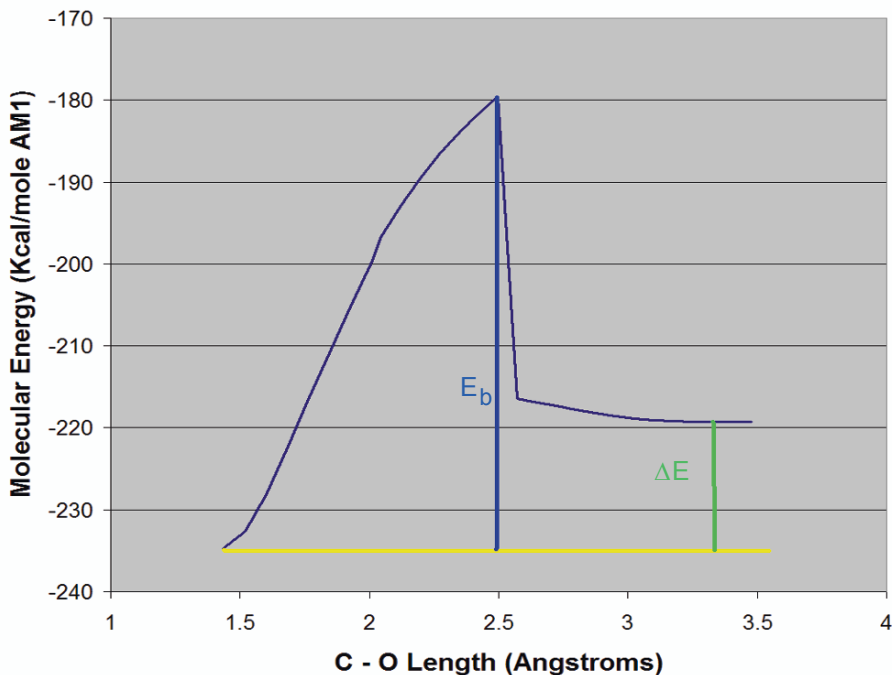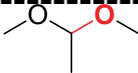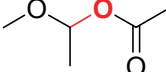

Figure 5. Computed energy along the reaction path for the thermal decomposition of an acetal ester linkage.

The calculation results (Table 2) indicated that introduction a C=O group next to the acetal linkage led to a significant decrease of both activation energy (~45 kcal/mol) and ΔE (~46 kcal/mol). Therefore, an acetal linkage next to a C=O group is predicted to be weaker than an acetal next to aliphatic groups. The results in Table 3 show that substitution near the acetal can have a significant effect on thermal degradation, and suggest that the acetal ester is a promising candidate; therefore we have focused our studies on materials that utilize this linkage.

TABLE 3. Computed reaction energy barriers[a] and heats of reaction for acetal linkage decomposition.

	E_b (kcal/mol)	ΔE (kcal/mol)
	99.29	61.37
	53.94	15.09

[a] Results were obtained for a "gas phase" reaction, which may be higher than energy barriers obtained from solution reaction rate data.[29]

2.6. THERMAL DEGRADATION STUDY BY GC-MS

Thermal desorption GC-MS was conducted on cured bismaleimide **1** to analyze the degradation products.[30] After heating at 250°C for 10 min, volatilized components were collected and analyzed by GC-MS. The main decomposition product is a cyclic acetal (Figure 6). Small amounts of acetaldehyde and butanediol were also present. These results are consistent with the molecular modeling studies and the hot-stage IR data.
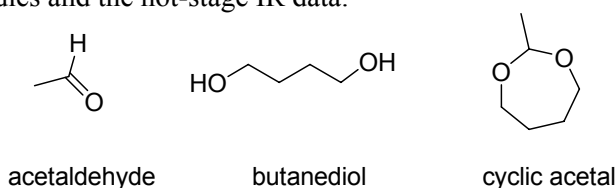

acetaldehyde   butanediol   cyclic acetal

Figure 6. Structures of major (cyclic acetal) and minor (acetaldehyde and butanediol) decomposition products at 250°C.

2.7. PROPOSED MECHANISM

We propose that the degradation of the bismaleimide resins proceed according to reaction Scheme 3. Molecular modeling showed that the first step in this mechanism is the decomposition of the C–O bond next to the C=O group of compound **1** to give a carboxylic acid and vinyl ether. Under acidic condition, the vinyl ether hydrolyses to form an alchohol and acetaldehyde. Then, the hydroxyl functionality can back-bite the other acetal ester linkage to form the cyclic acetal material observed in GC-MS analysis and another molecule of the carboxylic acid (blue arrow). The other acetal ester linkage can also decompose in a similar way to the first acetal group to form acetaldehyde and butanediol (green arrow); however, this is believed to be a minor side reaction since these components were only observed in small amounts by GC-MS. All the degradation products are consistent with the results of the GC-MS thermal degradation study.
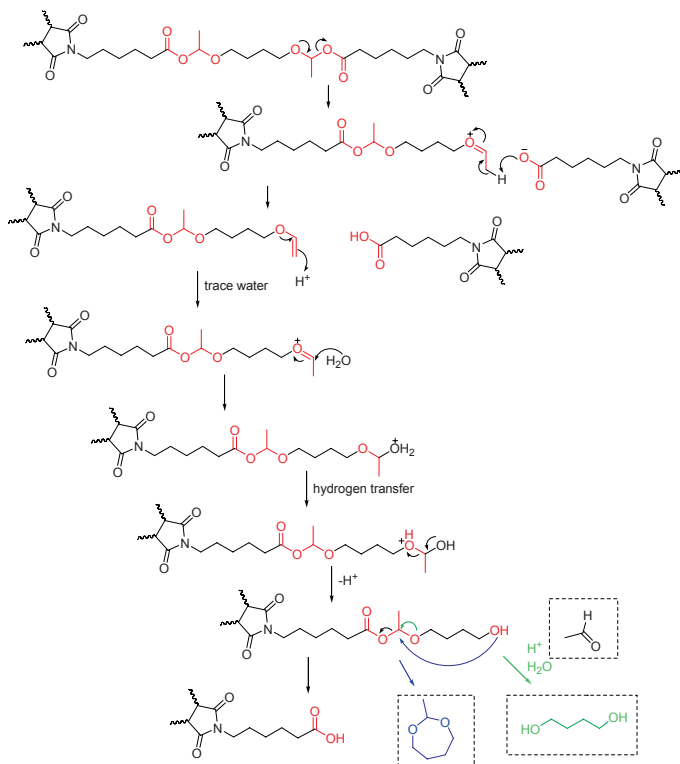
Scheme 3. Proposed degradation mechanism of cured **1**.

3.   Conclusions

A series of maleimides containing acetal ester linkages have been synthesized
by a neat one-step reaction from commercially available materials. The curing
behavior and degradation were studied by DSC, TGA, hot-stage FTIR, and
thermal desorption GC-MS. DSC data indicated that maleimide functionality
can be efficiently polymerized under radical condition. DSC, TGA, and hot-
stage IR suggested that the degradation of the acetal ester linkage initiated
from ~225°C and reached a maximum at ~250°C. The rework test of cured
compound **1** indicated that introduction of the acetal ester linkage leads to a
significant decrease of adhesion strength after exposing to high temperature,
which could facilitate the chip removal process. A degradation mechanism
was proposed based on mechanistic guidance from hot-stage FTIR, thermal
desorption GC-MS, and molecular modeling.

References and Notes

[1] Shirai, M. Prog. Org. Coat. 2007, 58, 158.
[2] Woods, J. G.; Morrill, S. D. (Henkel Corporation) U.S. Patent 6,916,890, July 12, 2005.
[3] Woods, J. G.; Torres-Filho, A.; Yaeger, E. K.; Wang, J. (Henkel Corporation) U.S. Patent 6,887,737, May 3, 2005.
[4] Tesero, G. C.; Sastri, V. J. Appl. Polym. 1990, 39, 1425.
[5] Sastri, V. J.; Tesero, G. C. J. Appl. Polym. 1990, 39, 1439.
[6] Yang, S.; Chen, J. S.; Korner, H.; Breiner, T.; Ober, C. K. Chem. Mater. 1998, 10, 1475.
[7] Ogino, K.; Chen, J. S.; Ober, C. K. Chem. Mater. 1998, 10, 3833.
[8] Ramis, X.; Salla, J. M.; Mas, C.; Mantecón, A.; Serra, A. J. Appl. Polym. Sci. 2004, 92, 381.
[9] Giménez, R.; Fernandez-Francos, X.; Salla, J. M.; Serra, A.; Mantecón, A.; Ramis, X. Polymer 2005, 46, 10637.
[10] Mas, C.; Ramis, X.; Salla, J. M.; Mantecón, A.; Serra, A. J. Polym. Sci. Part A Polym. Chem. 2006, 44, 1711.
[11] Loy, D. A.; Wheeler, D. R.; Russick, E. M.; McElhannon, J. R.; Saunders, R. S. (Sandia Corporation) U.S. Patent 6,337,384, January 8, 2002.
[12] Chen, X.; Wudl, F.; Mal, A. K.; Shen, H.; Nutt, S. R. Macromolecules 2003, 36, 1802.
[13] Wang, L.; Wong, C. P. J. Polym. Sci. Part A Polym. Chem. 1999, 37, 2991.
[14] Wang, L.; Li, H.; Wong, C. P. J. Polym. Sci. Part A Polym. Chem. 2000, 38, 3771.
[15] Li, H.; Wang, L.; Jacob, K.; Wong, C. P. J. Polym. Sci. Part A Polym. Chem. 2002, 40, 1796.
[16] Mison, P.; Sillion, B. Adv. Polym. Sci. 1999, 140, 137.
[17] Gacal, B.; Cianga, L.; Agag, T.; Takeichi, T.; Yagci, Y.; J. Polym. Sci. Part A Polym. Chem. 2007, 45, 2774.
[18] Liu, Y. L.; Hsieh, C. Y.; J. Polym. Sci. Part A Polym. Chem. 2006, 44, 905.
[19] Agag, T.; Takeichi, T.; J. Polym. Sci. Part A Polym. Chem. 2006, 44, 1424.
[20] Li, R. C.; Broyer, R. M.; Maynard, H. D.; Polym. Sci. Part A Polym. Chem. 2006, 44, 5004.
[21] Themistou, E.; Kanari, A.; Patrickios, C. S.; Polym. Sci. Part A Polym. Chem. 2007, 45, 5811.
[22] Jain, R.; Stanley, S. M.; Fréchet, J. M. J. Macromolecules, 2007, 40, 452.
[23] Buchwalter, S. L.; Kosbar, L. L. J. Polym. Sci. Part A Polym. Chem. 1996, 34, 249.
[24] Luo, S.; Wong, C. P.; J. Adh. Sci. Technol. 2004, 18, 275.
[25] The polymerization of compound **2** was not conducted because its high viscosity made the mixing process difficult.
[26] Compound **6** was synthesized according to the procedure: Musa, O. (National Starch and Chemical Company) U.S. Patent 6,803,406, October 12, 2004.

[27] The die shear tests were conducted at 150°C because the upper temperature limit
      for the die shear testing equipment is 150°C. Exposure to 250°C for 2 min prior
      to the die shear measurements is to simulate the rework condition.

[28] Smith, M. B.; March, J. In March's Advanced Organic Chemistry; Fifth Edition,
      Wiley, New York, 2001; Chapter 17, pp. 1328–1329.

[29] The significance of the reaction medium on reaction rate has been reported by
      Thames, S. J. Coatings Technol. 1990, 62(784), 51.

[30] The cured sample was prepared by heating a mixture of 98 wt% compound **1** and
      2 wt% USP-90MD at 120°C for 10 min.

POLYURETHANES WITH METAL CHELATE FRAGMENTS IN THE BACKBONE AND WITH COORDINATION METAL COMPOUNDS NANOSTRUCTURED SYSTEMS

YURI SAVELYEV
Institute of Macromolecular Chemistry of NAS of Ukraine,
48, Kharkovskoe schosse, 02160 Kiev, Ukraine

Abstract: Novel polyurethanes with metal chelates and nanostructured based systems have been synthesized. Polyurethane formation processes was carried out via the formation of intermediates under the influence of metal β-diketonates with metal containing cores. Peculiarities of the polyurethane supramolecular organization and the nature of the metal chelate atom exists in the obtained systems properties.

Keywords: Polyurethanes; Metal chelates; Nanostructured systems; Structure properties

1. Introduction

Elaboration of the polymers with high functionality – is a main stream of chemical material science. Polyurethanes have found commercial applications as multi-purpose coatings, having high mechanical properties (elasticity and mechanical firmness, stability to the wear); solvent-based adhesives and sealings; biomaterials owing to their hypothetic biocompatibility, etc. The wide range of different approaches of constructing of macromolecules of thermoplastic polyurethane elastomers is rather evident, and there is a variety of possibilities to set different specific structures of the macromolecular chain; that's why one has to consider the PUs not as a class of polymers only, but as a good and effective method for directed construction of macrochains with purposed structure.[1] Modification of polyurethanes (PU) with coordination metal compounds via formation of metal mediated systems during PU reaction and metal cores formation within PU rigid blocks or on their boundary allows to regulate PU properties. That is why hydrazine and its derivatives are very perspective as PU chain extenders owing to (a) being reactive bifunctional reagents, they easily form polymers with different classes of organic multifunctional compounds;

(b) high cohesion energy of the hydrazide fragments of the PU macromolecular determines the character of intermolecular interactions, that becomes apparent in special properties of the polymers and (c) high activity of hydrazide's groups in complex formation with metal cations.
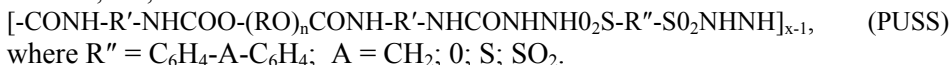
2. Polyurethanes with Metal Chelate Fragments in the Backbone

2.1. URETHANE-TRANSITION METAL ACETYLACETONATE SYSTEMS: CATALYSTS AND MODIFIERS

Traditional scheme of PU formation includes two steps. At the first step one obtains the prepolymer (PP) through interaction of oligoether (I) and diisocyanate (II). At the second step, the PP is extended by a stoichiometric quantity of the bifunctional compounds with active H-atom – dihydrazides (III) of carbonic (PUS) or arylsulfonic (PUSS) acids. Polyurethane-semicarbazides' (PUS) and polyurethane-sulfosemicarbazides (PUSS) elementary chain fragment may be represented as:

HO-R-OH (I) + 2OCN-R′-NCO(II) → OCN-R′-NHCOO-R-OCONH-R′-NCO   (PP)

n(PP) + nH$_2$NHNOC-R″-CONHNH$_2$ (III) →

[-CONH -R′-NHCO-R-OCHN-R′- NHCONHNHOC-R″-CONHNH-]$_{n-1}$,   (PUS)

where R, R′, R″ = Aг or A1k-.

[-CONH-R′-NHCOO-(RO)$_n$CONH-R′-NHCONHNH0$_2$S-R″-S0$_2$NHNH]$_{x-1}$,   (PUSS)

where R″ = C$_6$H$_4$-A-C$_6$H$_4$; A = CH$_2$; 0; S; SO$_2$.
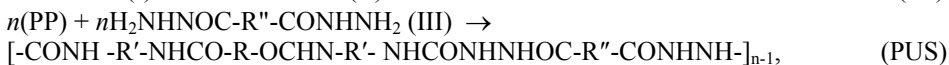
The tertiary amines, organotin compounds and transition metal β-diketonates are active catalysts of those reactions. The transition metal acetylacetonates, M(AA)n, as transition metal β-diketonates representatives (Figure 1), are interesting both as catalysts and modifiers of the PU systems.
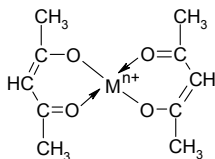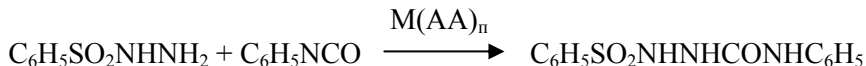

Figure 1. M(AA)$_n$,M = Cu(II), Zn(II), Pb(II).

2.1.1. Model Systems: Intermediates

Study of the model reactions of urethane formation: isocyanate – phenylisocyanate (PhIC) and compound with active H-atom – benzene sylphonylhydrazide (BSH) in the presence of transition metal β-diketonates – M(AA)п , as catalyst:

$$C_6H_5SO_2NHNH_2 + C_6H_5NCO \xrightarrow{\quad M(AA)_\text{п} \quad} C_6H_5SO_2NHNHCONHC_6H_5$$

has shown that the process passes through intermediate products formation.[2] Conditioned schemes of the latter may be presented as:

"M(AA)$_n$•Isocyanate" ("M/I") and "M(AA)$_n$•Hydrazide" ("M/H").

Intermediate "M/I" formation is carried out due to intraspheric coordination of NCO-group with metal atom. The statistic number of "M/I" intermediates has been exist: (i) π-complexes, formed by the atoms of transition metals on bonds –N=C– >C=O; (ii) intermediates, formed by donor–acceptor interaction owing to unshared electron pair of N- and O-atoms. Intraspheric coordination are being approved by noticeable inhibiting effect of small additives of pyridine on catalytic properties of M(AA)п, formed intraspheric complexes with the last one. Addition of pyridine into reaction medium leads to decreasing of reaction rate.[2] Obviously, an equilibrium stage between intermediates and initial reagents exists:

$$RNCO + M(AA)_n \leftrightarrow RNCO\bullet M(AA)_n \leftrightarrow [RNCO\bullet M(AA)_{n-1}]^+ + (AA)^-$$

The decrease of reaction rate constant at the addition of a mass of (MAA)n in a quantity comparable with concentration of M(AA)п into reaction testifies to this fact. Essential increase of acetylacetone (HAA) concentration, in ten times in comparison with M(AA)n concentration, should lower an observed rate constant, just as it was expected (Table 1).

TABLE 1. Influence of M(A$_n$A) and addition of acetyl acetone (HAA) on the observed reaction rate constant in reaction of BSH with PhIC, benzene, 25°C.

M^{n+}	$[M(AA)_n] \cdot 10^4$ (mol/L)	K_{obs} (L/mol/s)		
		[HAA] = 0	[HAA] = $[M(AA)_n]$	$[HAA]_n = 2 \cdot 10^{-3}$
Fe^{3+}	1	0.0679 ± 0.004	0.0530 ± 0.003	0.0453 ± 0.003
Zn^{2+}	2	0.1230 ± 0.001	0.0898 ± 0.005	0.0411 ± 0.004
Ni^{2+}	0,5	0.1080 ± 0.007	0.0822 ± 0.005	0.0474 ± 0.004

[a] For non-catalytic reaction k$_o$ = 0.0408 ± 0.003 L/mol/s.

IR spectroscopy analysis of preoperatively obtained intermediates "M/H" has shown : (i) a reduction of stretching vibration band frequency of SO$_2$-group (range 1,310–1,160 cm^{-1}); (ii) a reduction of stretching vibration band frequency of M-O of AA-cycle (range 400–450 cm^{-1}); (iii) frequency reduction in

the range of 600–690 cm^{-1} (superposition of the stretching vibration bands of M-O of M(AA)$_n$ cycle and vibrations of pseudo-aromatic cycle of M(AA)$_n$; (iv) the shift of bands in area of 3,200–3,400 cm^{-1}, specified the stretching vibrations of N-H. Thus, it could be concluded that the formation of intermediate "M/H" occurred by intraspheric coordination of O-atom of hydrazide SO$_2$-group to metal atom and exterior coordination: H-bond of hydrazide NH-group with O-atom of the first coordinating sphere of M(AA)$_n$.

2.2. POLYURETHANE-SULFOSEMICARBAZIDES WITH ACTIVE ADDITIVES OF M(AA)N

Analysis of the processes, taking place in polymer systems, has proved their similarity to model systems: intraspheric coordination of O-atom of hydrazide SO$_2$-group in macrochain PUSS or CO-group of PUC fragment to metal atom; external coordination of NH-group of hydrazide fragment of macrochain with O-atom of the first coordinating sphere of M(AA)$_n$ due to H-bond formation.

2.2.1. Polyurethanes Performance

The problem of creation of PUs with prescribed set of physical-chemical properties can be solved by variation of their chemical structure, and through directed choice of catalysts for urethane formation and modifying additives as well. The optimum for the last case is in combining of those two functions in one initial element. The nature of M(AA)$_n$ central atom is the main factor of determination of the character of complex formation with hydrazide fragments of PU macrochain, and its principal influence on polymer system properties.

The catalyst additives Zn(AA)$_2$, Co(AA)$_2$ and Fe(AA)$_3$ introduced into the samples of the PUSSs based on *iso*-phtalic acid increase the temperature of the 5% mass loss (T_5, °C) on 40–50°C. To increase substantially the thermal stability of the PUSSs based on arylsulfonic acid, the modifying additives in amount ≥2% is needed. This provides that the complex formation condition is followed: NHNHSO$_2$:M(AA)$_n$ = 1:1. Inhibition mechanism for thermo-destruction processes can be explained as follows. The addition of the M(AA)$_n$ leads to the compaction of the polymer packing resulting from the coordination cross-linking; this impedes diffusion of oxygen to the bulk of the polymer. At temperatures up to 300°C the rate of the destruction process is proportional to concentration of diffusing oxygen. Effect of the M(AA)n on destruction processes consists in inhibition of the hydroperoxide – the branching agent of the process.

UV-Stability was investigated for the PUS (PU 1–2) and PUSS (PU 3–7). Composition and some properties of PUS and PUSS with M(AA)$_n$ additives are represented in the Table 2. Stability of polyurethanes to UV-irradiation is evaluated by means of coefficients characterizing preservation of polymer sample tensile strength (K$_\sigma$) and elongation at the break point (K$_\varepsilon$): K$_\sigma$ =

$(\delta_{exp}/\delta_{init})\bullet100\%$, $K_{\varepsilon} = (\varepsilon_{exp}/\varepsilon_{init}) \bullet100\%$, where δ_{exp} and ε_{exp} – values of experimental parameters, and δ_{init} and ε_{init} – values of initial parameters. Character of inhibition of the photo-destruction processes is determined mostly by the nature of the $M(AA)_n$ central atom. The largest effect of increase of photo-stability at UV-radiation exposition during 200 h is noted for PUSS, containing $Ni(AA)_2$. In this case Ks characterizing preservation of polymer sample's tensile strength (K_{σ}) and elongation at the break point (K_{ε}) are equaled 100%. The role of the $Ni(AA)_2$ in inhibition of the processes of photo-destruction is reduced, probably, first of all due to the termination of hydroperoxide homolytic decomposition (Figure 2, A). Studies of the UV-radiation influence on PU, effected in the absence of oxygen (in inert atmosphere), show also the inhibiting effect of the $Ni(AA)_2$ on photo-destruction. So, $Ni(AA)_2$ acts through the mechanism of suppression of excited states as an UV-absorber. Role of the $Fe(AA)_3$ in inhibition of PU destruction process is, obviously, in the compaction of the polymer packing resulting from the coordination cross-linking; this impedes diffusion of oxygen into the bulk of the PU.

Stability of PUSS to the radiolysis is evaluated by means of coefficients characterizing preservation of PU tensile strength (K_{σ}) and elongation at the break point (K_{ε}). The value of K_{σ} after irradiation with 100 Mrad doze increases up to 200% for PUSS with $Co(AA)_3$ additives, the parameter K_{ε} takes the minimal value – 78 %. At irradiation of the $Zn(AA)_2$ modified PUSS with 50 Mrad doze, the values of K_{σ} and K_{ε} are 49.2% and 48.5%, respectively. Irradiation of the PU with accelerated electrons leads to beginnings of excited states, and as a result, to bridged bonds owing to molecular chain breaks and combinations. Stabilization effect of the $M(AA)_n$ at radiolysis of PUSS is, possibly, related to the oxidation–reduction processes which decrease the oxidation number of metal during the hydroperoxide destruction.. Inhibiting activity of the $M(AA)_n$ in the process of radiolysis with accelerated electrons of the PU varies in the order: Co(III) > Cr(III) > Fe(III) >> Zn(II).

TABLE 2. Composition and some properties of PUS and PUSS.

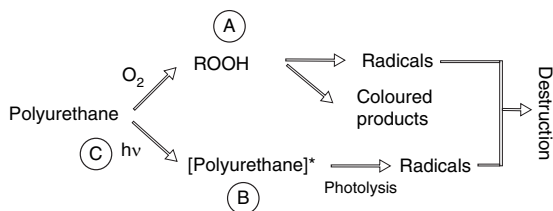| PUs	Chain extender	Exposition (h)	M+/[c] (wt%)	Kε (%)	Kδ (%)
1	$1,3\text{-}C_6H_4(CONHNH_2)_2$	200	–	42.2	13.8
2	$1,3\text{-}C_6H_4(CONHNH_2)_2$	200	$Fe^{3+}/2.0$	73.7	96.6
3	$O(C_6H_4SO_2NHNH_2)_2$	200	–	48.4	8.0
4	$O(C_6H_4SO_2NHNH_2)_2$	200	$Fe^{3+}/2.0$	65.0	95.6
5	$CH_2(C_6H_4SO_2NHNH_2)_2$	200	–	39.2	35.2
6	$CH_2(C_6H_4SO_2NHNH_2)_2$	200	$Ni^{2+}/0.6$	100.0	100.0
7	$CH_2(C_6H_4SO_2NHNH_2)_2$	150	$Zn^{2+}/1.2$	61.0	87.1

Figure 2. Scheme of the PU photo-destruction.

3.   Non-linear Polyurethane/Transition Metal Acetylacetonates Systems

3.1.   POLYURETHANE BASED ON UNSYMMETRICAL DIMETHYLHYDRAZINE

The use of the unsymmetrical dimethylhydrazine, $(CH_3)_2NNH_2$, (UDMH), in chemistry of macromolecular compounds, has been directed mostly towards its application for the polymer modifications. Abnormalities in reaction ability of tertiary atom of nitrogen in UDMH lead to formation of hydrazinium-compounds. Violation of the reagents stoichiometric ratio during PU formation at two-step synthesis leads to obtaining of cross-linked polymer. A different result is obtained at processing the polyurethane PP, dissolved in DMF by UDMH. At increase of molar part of the PP by 2, 5, 10 and even 20 times macromolecular compounds, dissolvable in DMF, are formed. From the solutions polymer films were obtained, with physic-mechanical properties specific for traditional polyurethane elastomers. A complex approach includes: (i) evaluation of the average number molecular weights (Mn) of PU by analysis of terminal group; (ii) determination of the number of amide and associate hydrazide groups by potentiometric non-aqueous titration; (iii) evaluation of the number of atoms of nitrogen in PU samples by Kieldale method; and (iv) determination of the Mn of some elastomers by the method of ebullioscopy.[1] Possible macrochain structures of the PU on the basis of UDMH (Figure 3).

In the case of the ratio PP:UDMH = 1:1 and 2:1 (with using of tin butyldilaurate as catalyst) only oligomers or low-molecular elastomers with linear structure are formed, in all the other cases the PUs with hypothetic branched [comb-like] structure through formation of biuret structures are formed. The biuret formation is confirmed by the fact that introduction of phosphoric acid to the reaction system prevents the formation of biuret bonds. Study of the catalysts' activity in the reaction of urethane formation allows to order the catalysts as follows: $Sn(AA)_2Cl_2 > TDBDL > TEA$.

[-OCHN-R-NHCOO-R$_1$-OCONH-R]$_3$-NHN(CH$_3$)$_2$ (A)

{-OCHN-[-R-NHCOO-R$_1$-OCONH-R-NCO-]$_n$-NHN(CH$_3$)$_2$

|

CONH-R-NHCOO-R$_1$-OCONH-R-NHCO-}- (B)

{-OCHN-[-R-NHCOO-R$_1$-OCONH-R-NCO-]$_n$-NHN(CH$_3$)$_2$

|

CONH-R-NHCOO-R$_1$-OCON-R-NCO-}

|

CONH-R-

-NHCOO-R$_1$-OCONH-R-NHCO-]- (C)

Figure 3. Possible macrochain structures of the PU based on UDMH: linear (A) and branched (B, C) structures.

Use of hydrazine derivative as a CE and M(AA)$_n$ as a catalyst in the reaction of PU formation results in the formation of intermediate "M/H", which participates in the acceleration of reaction. Taking into account that, metal β-diketonates play a catalytic role in the reactions of PU formation between TDBDL and TEA, the highest activity of Sn(AA)$_2$Cl$_2$ cannot be explained only by formation of the Sn(AA)$_2$Cl$_2$•UDMH. Ability of the UDMH to form the hydrazinium-cations:

This makes it possible to assume that the reaction of PU formation with participation of the UDMH goes with formation of reaction centers of ionic nature. The ability of UDMH as PU macrochain end group to form hydrazinium-structure was used for functionalizing of polymers:

3.1.1. Small-Angle X-Ray Scattering Measurements

According to SAXS data, PU's are the micro-heterogeneous amorphous systems, in which the depth of microphase segregation is determined by compatibility of flexible (oligoether) and hard fragments of macrochain (Table 3).

These data shows that as the PP/UDMH ratio decreases (from 2 to 20), the structural homogeneity of hard blocks increases and promotes the increase of the α$_{seg.}$

TABLE 3. SAXS data of selected PUs: angle of interferential maximum $2\Theta_{max}'$, Bregg' period D, and segregation level α_{seg}.

PUs	$2\Theta max'$	D	α_{seg}
G1/1	25	21	0.23
PU 2/1	30	17.5	0.17
PU 5/1	32	16	0.29
PU 10/1	42	12.5	0.54

4.   Polyurethanes with Metal Chelate Fragments in the Backbone

4.1.   POLYURETHANES BASED ON TRANSITION METAL B-DIKETONATES

Poly(amide-urethane)s, PAU, were synthesized by traditional two-steps method. The PP is extended by a stoichiometric quantity of the transition metal acetyl-acetonates $Cu(AA)_2$, $Zn(AA)_2$, $Pb(AA)_2$ and $Sn(AA)_2Cl_2$. IR study of interaction between NCO-group of PP and γ-H atom of CH-group of the chelate ring of $M(AA)_n$ proves the formation of PAU: disappearing of deformation vibrations of γ-H atom of acetylacetonates $\delta CH \sim 1{,}190$ cm^{-1}, appearance of absorption bands at 1,640 and 3,360 cm^{-1} (stretching vibrations νCO and νNH-groups of amide fragments, accordingly) in the IR-spectra, that testifies to amide grouping -CO-NH- formation in reaction product. According to kinetic study of model systems: "PhIC– $M(AA)_n$" investigated $M(AA)_n$ form the following row of activity in reactions of urethane formation: $Sn(AA)_2Cl_2 > Cu(AA)_2 > Zn(AA)_2 > Pb(AA)_2$.[3]

4.1.1. IR spectroscopy

IR spectra of polyurethanes, registered by the method of multiple attenuated total reflectance IR spectra (ATR IR-spectra) for the: PAU, containing $Cu(AA)_2$ in the main chain as extender of PP (sample PAU-3); PU, containing dihydrazide of isophthalic acid (DHIA) as extender of PP (sample 1); PU, containing DHIA as extender of PP (mole ratio 1:1), and $Cu(AA)_2$ as modifying additive (the ratio of DHIA:$Cu(AA)_2$ = 2:1) (sample 75) are presented in Figure 4. As it is seen, at addition of $Cu(AA)_2$ as modifying additive into PUS (sample 75), the position of the bands of semicarbazide fragments' carbonyl groups (1,658 cm^{-1}) and associated C=O-groups (1,705 cm^{-1}) and non-associated (1,730 cm^{-1}) of urethane fragments is preserved. However, an increase of a fraction of non-associated C=O-groups is observed, testifying to redistribution of intermolecular bonds in polymer at addition of $Cu(AA)_2$. In the IR-spectrum of the surface in comparison with IR spectrum of transmittance, the increase of relative intensity of absorption band of amide fragments (in comparison with urethanes) was observed. It testifies to the presence in the surface layer of PAU of the most part

of PU chain units with acetylacetonates fragments. This may be a determinant factor of biological activity of the PU.
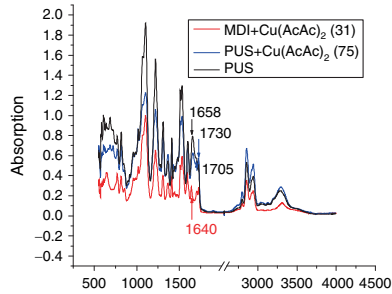

Figure 4. IR spectra of the P(A)U.

4.1.2. Wide-Angle X-Ray Investigations

The analysis of the WAXS diffractograms of PAUs (Figure 5) shows the dual (amorphous-crystalline) structure of the metal acetyl acetonate urethane containing PU. This is indicated by appearance against a background of so-called "amorphous halo" with maximum at $2\theta \approx 20°$ of two diffraction maxima (pointed with arrows) with angular positions ($2\theta_m$) at 21.1° and 26.4° (samples PAU 1,2,3). The appearance of addition diffraction maxima on X-ray diffraction patterns of PAU, containing acetyl acetonates of two-valence metals (Zn, Cu, Pb) should be noted. These maxima characterize the crystalline structure of low molecular weight compounds, probably $M(AA)_n$. This effect is more typical for the Cu- and, particularly, the Pb-acetylacetonate chain extenders.

In the latter case, the intensity of the diffraction maxima practically exceeds the intensity of the maxima related to the urethane-containing polymer phase. Display of crystalline structure from the acetyl acetonates of two-valence metals in the PU bulk indicates that only a (not calculated) fraction of the metal-chelate component takes part in the poly-addition reaction. Based on the WAXS data, this quantity decreases in the following order: $Cu(AA)_2 > Zn(AA)_2 > Pb(AA)_2$. It means, that reactivity of $M(AA)_n$ with PP decreases in the row: $Sn[(AA)Cl]_2 > Cu(AA)_2 > Zn(AA)_2 > Pb(AA)_2$. Consequently the non-reacted part of acetyl acetonates of two-valent metals segregates into separate regions, coordination of these metal-chelates with polar groups in hard segments (HS) of the PUs, through hydrogen-bonding interactions with O-atoms of the outer sphere of the metal acetyl acetonate, which exists in the PAU bulk as active cores. An estimate of the crystallite effective size L was obtained using Sherrer's method. Non-reacted (with PP) Zn- and Pb-acetyl acetonates have crystallites with size around 9.1 nm, while the size of the HS crystallites of the PUs under study is approximately 5.3 nm. Such elements may play a role of nanostructuring elements.
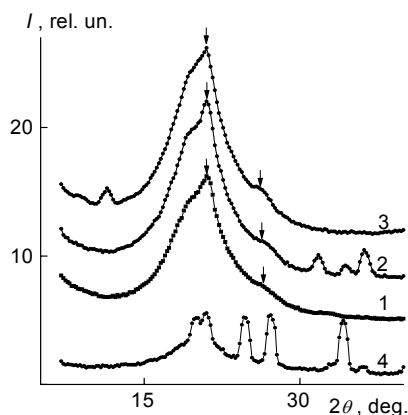
Figure 5. WAXS data of PAU with acetylacetonates of Sn (1), Zn (2), Cu (3) and Pb (4) in hard blocks.

4.1.3. Thermally Stimulated Depolarization Currents (TSDC) Studies

Thermograms for the PAU-1 (Sn(AA)$_2$Cl$_2$), PAU-2 (Zn(AA)$_2$), PAU-3 (Cu(AA)$_2$) and PAU-4 (Pb(AA)$_2$) are presented on the Figure 6. Scaled spectra in the region of the glass-transition α peak are given in the inset. From this figure some conclusion may be made. (i) The TSDC spectra of all samples present similar structure with traditional four main peaks in the extended temperature window –230°C to +50°C. The first two peaks, in the order of increasing temperature, correspond to secondary relaxations denoted as δ (with $T_\delta \sim -$ 195°C) and γ ($T_\gamma \sim -165$°C) modes. (ii) The second signal (γ mode) is considered to arise from crankshaft motions of (CH$_2$)$_n$ sequences with attached dipolar groups. (iii) The α peak, at about –60°C, is polar and located close to the calorimetric glass transition temperature. For the PAUs the α-relaxation peak arises from the reorientation of the polar soft segments of the chain during the glass transition of the PAU amorphous micro-phase rich in soft segments. (iv) The peak above the α relaxation mode is associated with interfacial Maxwell-Wagner-Sillars (MWS) polarization, i.e. mesoscopic transport of charge carriers and trapping at interfaces arising from the microphase-separated structure of PAU. Intense conductivity signals appear above ~0°C. Conductivity is especially strong in the case of the PU-Sn(1) sample.[3] This phenomenon is attributed to the presence of the chloride electric-charge balancing anions in the structure of the chain-extender, which provides new space-charge carriers and probably new and/or modified conduction paths. Based on the trends followed by the glass-transition temperature values (T_α), the difference of the peak temperatures of the MWS and the α relaxation signals ($T_{MWS} - T_\alpha$), and the α relaxation strength

($\Delta\varepsilon_\alpha$) in each PAU sample, degree of microphase separation (DMS) increases in the row: AU-3 ≤ PAU-4 < PAU-1 < PAU-2.

Figure 6. Thermograms for the PAU.

4.2. POLYURETHANES BASED ON AZA-MACROCYCLIC COMPLEXES

PU's were synthesized according to PP technique,[4] Figure 7. As chain extender the aza-macrocyclic complex of perchlorates of Ni(II) or Cu(II) with 3,10-(α-hydroxyethyl) – 1,3,5,8,10,12-hexaza-cyclotetradecane (AMC) was used.

These systems may be considered as macromolecular metal chelates. They are characterized by coordinative bonds between the ion and the chain and by the presence of one ion in each monomer unit.

[-OCHN-R$_1$-CONH-R$_2$-NHCOO-R$_3$-OCONH-R$_2$-NHCO-]$_n$

$R_1 =$

$R_2 =$ ⟨benzene⟩-CH$_2$-⟨benzene⟩- ; $R_3 =$ -[(CH$_2$)$_4$-O]$_n$- ,

Figure 7. Azamacrocyclic complex. M – Cu^{2+} (PU402), Ni^{2+} (PU 398); n in R$_3$ is 14.

4.2.1. Differential Scanning Calorimetry (DSC) Studies

Figure 8 shows DSC thermograms of the PU 398(Ni) and PU 402(Cu). The occurrence of specific heat capacity jumps (ΔC_{p1}) at the glass transition temperature (T_{g1}) of the soft-segment-rich micro-phase (SS microphase) and of

endothermic enthalpy relaxations at the softening points (T_{s2}) of the hard-segment-rich micro-domains (HS micro-domains) on the thermo-grams of both samples is typical for PU in general.

Parameters of thermal transitions are only slightly affected by the nature of the metal cation, however, in a trend suggesting higher degree of microphase separation (DMS), in the sample 398. This is indicated by the lower T_{g1} value, −52°C, (more homogeneous soft segment, SS, microphase), the lower ΔC_{p1}, 0.27 and the higher T_{s2} 127°C (better packing of hard segment (HS) in more homogeneous HS micro-domains).
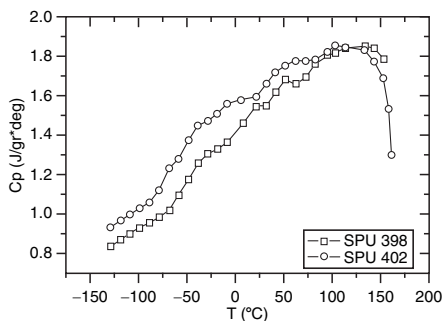
Figure 8. Specific heat capacities of PU 398 (squares) and PU 402 (circles), second heating run (samples quenched in liquid nitrogen after the first heating run), heating rate of 2°C/min.

4.2.2. Small-Angle X-Ray Scattering (SAXS) Studies

In contrast to the weak indications for a higher DMS in PU 398 provided by DSC experiments, the SAXS data are more decisive in that respect. The SAXS patterns in Figure 9 indicate quite different DMS. A distinct peak around 2Θ nearly 30′ for PU 398 is the evidence for the existence of a regular macro-lattice of HS macro-domains (i.e. reasonably high DMS) with the mean inter-domain spacing (*L*) nearly 17.5 nm, while a smooth decay of the SAXS curve for PU 402 suggests the absence of large-scale structural heterogeneities (i.e. negligible DMS).

These differences will be rationalized taking into consideration two alternative mechanisms by which the M^{2+} cations can influence the structure of PUs. On the one hand, electrostatic interactions promote of positively charged M^{2+} cation can coordinate two HS moieties; hence in absence of unfavourable steric hindrances from the aza-crown there is a possibility for two pairs of coordinated HS moieties to join together and to form the co-ordinated interchain aggregates, structurally different from ordinary HS micro-domains. The ClO_4-anions, in their turn, can form the ion-molecular hydrogen bonds by electrostatic interactions,
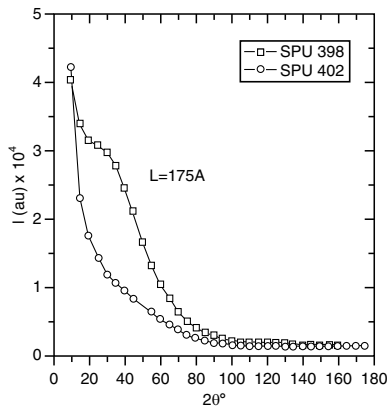
Figure 9. SAXC curves for PU 398 (squares) and PU 402 (circles).

with the protons of urethane groups; as a result, the density of interchain urethane–urethane hydrogen bonds is decreased, and the tendency of HS for self-aggregation becomes weaker. It follows, therefore, that the DMS will be lower, the larger the contribution of the second mechanism. In view of these considerations, higher DMS of the PU398 may be attributed to the predominant contribution of the first mechanism, whereas the opposite should be true for the PU 402. Probably such differences may be explained by the ability of the additional coordination of the O-atom perchlorite anion ClO_4^- on fifth and sixth coordination sites of the Cu-atom.

5. Biological Activity of the Polymers or Microorganism Attack – Polymer Counteraction

Most materials, including polymers, are sensitive to microorganisms' attack that causes essential economic losses as a result of biodeterioration of the performance. Processes of biocorrosion of materials, induced by microorganisms (firstly mold fungi) are considered also in respect to their influence on human body, since a colonization of polymer materials by microorganisms produces centers of increased dangerous infection. The problem of biological corrosion is seen during long-term human stay in a closed space such as in spaceship, submarine, airplane, medical institutions, military camps, and penal system institutions. In these cases, the polymer materials should be stable to the destructive action of microorganisms, but also biologically active and nontoxic for human.

5.1. BIOLOGICAL ACTIVITY OF THE PU OF LINEAR AND BRANCHED
      STRUCTURES, CONTAINING METAL-CONTAINING MODIFIRES

The following micromycets' test-cultures have been used for biological activity
study: *Aspergillus niger spp., Penicillium spp., Paecilomyces varioti, Fusarium
moniliforme, Trichoderma viride, Alternaria alternate.* Polymers of linear and
branched structures with active inorganic fungicidal additives [tin (II) and zinc
(II) chlorides ($ZnCl_2$, $SnCl_2$) and zinc (II) acetylacetonate ($Zn(AA)_2$) in a
quantity from 0,1 till 5 wt%] which can participate in complex formation with
semicarbazide and urethane fragments and macrochain end-group according to
mechanism of (A) add/or (B) or (C) (Figure 10) are stable to fungi attack. Their
degree of biodeterioration is insufficient, that is proved by retention of physical
properties: K_δ and $K_\epsilon > 95\%$.

(A)   (B)   (C)
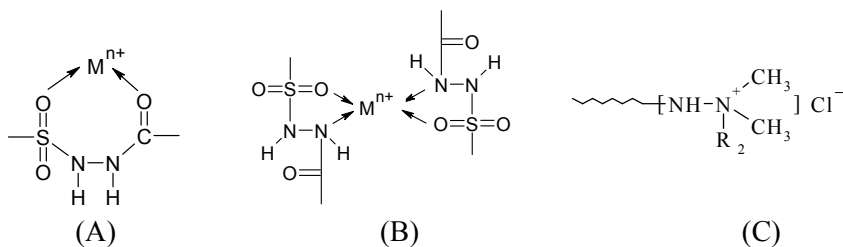
Figure 10. Complex formation. (A) intramolecular and/or (B) intermolecular interaction
or (C) transforming UDMH end-group to the hydrazinium structure.

5.1.1. *Study of Possible Adaptation of Microorganisms to the PUs*

As we can see from the Table 4 all of studied polymers are fungicidal ones.
How can we connect the bioactivity of the PU with its structure? One of the
explanations may be the next. Polyurethanes as phase-separated systems are

TABLE 4. Fungi steady of modified polyurethanes.[a]

PUs	Estimation of the fungi growth(in units per day)							
	5	10	15	20	25	30	32	46
1c[b]	3	3	3	4	4	4	4	4
2	0	0	0	0–1	0–1	0–1	0	0
3	0	0	1	1	1	1	1	1
4	0	0	0	1	1	0	0	0
13c[b]	3	3	4	5	5	5	5	5
14	0	1	1	1	1	1	1	0
15	0	0	0	1	1	1	0	0
16	0	0	0	0..1	0…1	0..1	0	0

[a] Evaluation criteria of fungi growth.[5]

[b] c Polyurethanes without additives.

subjected to influence of external factors, including metabolites of mould fungi: water, carbonic acids, etc. Introduction into the PU system of metal-organic compounds, able to complex-formation with hydrazide fragments, essentially influence on degree of ordering of domain structure. The ratio of bands' intensities in the region of 1,540 cm^{-1} (δ NH-groups non-associated) in comparison with ν_{benz} =1,600 cm^{-1} does not change after the action of used micromycets test-cultures for all systems. It testifies to stability to their action.

5.2. POLYMERS, CONTAINING IN THE MAIN CHAIN METAL-ORGANIC FRAGMENTS – POLYAMIDOURETHANES (PAU)

Synthesized PU's are stable to microorganism attack and they possess fungicidal activity.[6] Study of spores' viability on the PAU surface allows to determine from 38 standard test-cultures of microorganisms', used for inoculation, only two cultures on PU-Cu, and one by one on PU-Zn and PU-Sn. They were the very aggressive extremophiles: mold fungi *Penicillium* and *Aspergillus*. Viability of micromycets' spores (Figure 11) arranged: on PU-Sn – 3 days, on PU-Zn – 6 days, on PU-Cu – 10 days. The fungicidal activity of the PAU may be connected with their surface peculiarities. In accordance to above-mentioned data of the IR-spectrum (Figure 4) of the surface of the PAU (in comparison with IR-spectrum of transmittance), the increase of relative intensity of absorption band of amide fragments (in comparison with urethanes) was observed. It testifies to the presence in the surface layer of PAU of the most part of polymer chain units with AA-fragments.
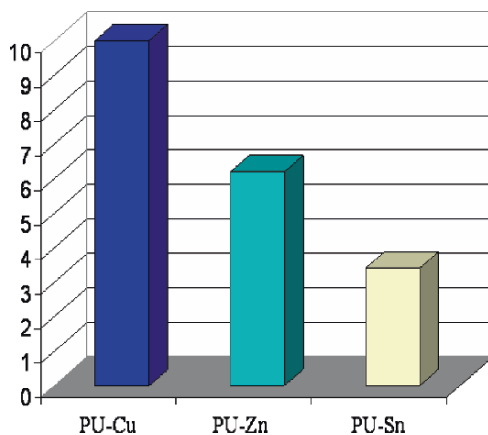
Figure 11. Viability of spores on the film surface of PU.

Comparison of relative intensities of absorption bands in the area of 1,640 cm^{-1} (stretching vibrations of CO of amide fragments) of PAU surfaces shows, that the relative intensity of this band (Sn-containing PAU, sample 28) increases such of Cu-contained PAU (sample 31). It is the result of higher concentration of amide bonds, and consequently, Sn^{4+} atoms in the surface layers of PAU in comparison with it bulk. Thus, the introduction into the PU matrix of metal-containing compounds, able to complex-formation with hydrazide fragments of macromolecule and/or inclusion of metal-containing fragments into the macro-molecule structure allows to impart the PU with fungicidal properties. Since for the given systems the direct contact "microorganism-polymer" is absent, the reason of biological activity should be explained by influence of metal containing centers on structural organization – the degree of ordering of domain structure. The use of such approach allows avoiding the diffusion of metal-containing component on the surface of polymer material that prevents their toxic action on living organism. It was confirmed by *in vitro* and in *vivo* studies (with the use of experimental animals).

6. Conclusions

Novel polyurethanes with metal chelates systems have been synthesized. Polyurethane formation processes carries out *via* the formation of intermediates under influence of metal β-diketonates with metal containing cores formation. Obtained systems were described as metal containing nanosystems that include nanoscale structures both of organic nature (self-similar micro heterogeneities typical for segmented PU) and metal containing coordination junction cores within the microphase or at the boundary. Peculiarities of the polyurethane supramolecular organization and of metal chelate atom nature determine obtained PU systems' properties.

References

[1]   Yu.V. Savelyev, In "*Handbook of Condensation Thermoplastic Elastomers*", Wiley-VCH GmbH&Co. KgaA, 2005, p. 355.
[2]   A. Grekov, Yu. Savelyev, V. Veselov. *J. Organic Chem.* 21 (1985) N12, 1232.

[3]I.M. Kalogeras, M. Roussos, Yu.V. Savelyev et al. *Eur. Phys. J. E.* V 18 (2005) 467.
[4]G. Georgoussis, A. Kanapitsas, P. Pissis, Yu.V. Savelyev et al. *Eur. Polym. J.* 36 (2000) 1113.
[5]*International Standard ISO 846:1997 (E).*
[6]Yu. Savelyev, L. Robota, O. Savelyeva et al. *Acta Astronautica* 64 (2009) 36.

NANOSTRUCTURED SELF-ASSEMBLING SYSTEMS BASED ON FUNCTIONAL POLY(URETHANE/SILOXANE)S

YURI SAVELYEV

Institute of Macromolecular Chemistry of NAS of Ukraine,
48, Kharkovskoe schosse, 02160 Kiev, Ukraine

Abstract: Novel hybride organo-inorganic systems based on urethane-, urea-crown ether- and siloxane-containing monomers and oligomers have been developed by sol-gel method. Structure–properties relationships were discussed.

Keywords: Hybrid; Organic–inorganic; Crown ethers; Polyurethanes; Polysiloxanes

1. Introduction

Combination of organic and inorganic components allows creating a unique hybrid based materials. Polyurethanes have found commercial applications as multi-purpose coatings, solvent-based adhesives and sealing, biomaterials etc.[1] Siloxane-based elastomers are characterized, mainly, by heat resistance and water repellence. Combination of the properties of above-mentioned polymers allows obtaining hybrid materials with target characteristics.

   At first sight, hybrid materials look like bi-phase, in which organic and inorganic phases are mixed in a scale from nanometric till sub-nanometric. Therefore, it is evident that properties of such materials will be determined not just as a sum of single phases, but as internal interaction of their interfaces. The nature of surfaces interaction at the interface is put on the basis of classification of those materials. The first group contain the substances with weak bonds (hydrogen, Van-der-Vaals or electrostatic ones) between organic and inorganic components. The second group contains the materials with strong chemical bonds between two phases; they perform hybrid network composites. Of course the weak bonds may also be present in the second group materials.[2] Application of these innovative materials promises new achievements in many branches: mechanics, environment, biology and medicine, optics, electronics, etc. The most employed route of obtaining of hybrid nanocomposites is sol-gel method.[3]

It consists of hydrolysis of alkoxy silanes or corresponding compounds with multi(hydroxides) formation accordingly to the Scheme 1:

$$\equiv SiOEt + H_2O \longrightarrow \equiv SiOH + EtOH$$

$$\equiv SiOH + HOSi\equiv \longrightarrow \equiv Si-O-Si\equiv + H_2O$$

$$\equiv SiOH + EtOSi\equiv \longrightarrow \equiv Si-O-Si\equiv + EtOH$$
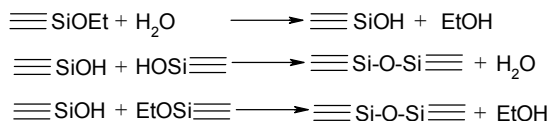
Scheme 1. Preparation of hybrid nanocomposites by hydrolytic polycondensation reaction.

Varying of organic substructure in a molecule-precursor leads to the self-organization of the solids during a primary hydrolysis. In order to develop a hybrid material of such type, the series of three-functional silanes, which may be used as precursors in sol-gel synthesis, is required, Figure 1.

$$
X-R'-\underset{\underset{OR}{|}}{\overset{\overset{OR}{|}}{Si}}-OR
$$

R = -CH$_3$, -C$_2$H$_5$

R' = Alk, Ar

X = -NH$_2$, -Cl, -OCH$_2$-CH$-$CH$_2$, -O-$\overset{\overset{O}{||}}{C}$-$\overset{\overset{CH_3}{|}}{C}$=CH$_2$; -Si(OAlk)$_3$
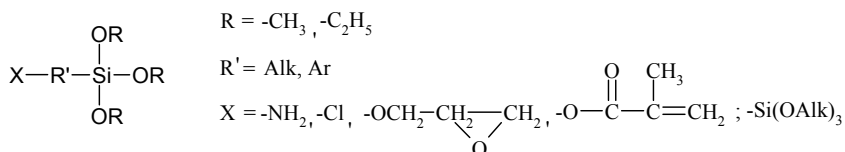
Figure 1. Three-functional silanes as precursors in sol-gel synthesis of hybrid nanocomposites.

The most promising for realization of this idea is bis-silanes of type (RO)$_3$Si–R′–Si(OR)$_3$. It is determined by the fact, that bis-silanes provide wide structural capacities in design of such hybrid materials due to the possibility of choosing the spacer both from the nature and geometry points of view, associated with two three-alkoksisilane groups. The presence of various other groups in spacer chain and their interaction may result in self-association of precursors, and in formation of a final material with predictable morphology. So, an introduction of the macro-heterocyclic compounds into a macrochain is the route of the additional self-assembling processes as a result of coordinative cross-linking owing to ion–dipole interaction of the crown ether cavity and metal cation with the formation of the sandwich-type intermolecular complexes.

$$
X-R'-\underset{\underset{OR}{|}}{\overset{\overset{OR}{|}}{Si}}-OR
$$
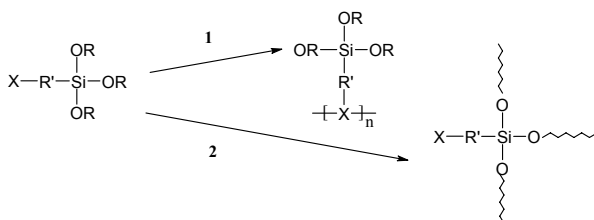
Scheme 2. Different ways for the formation of hybrid polymer; (1) formation of polymer chain in organic component, (2) formation of polymer chain in inorganic component.

Two principal ways of hybrid polymer formation may be performed, Scheme 2. First, polymer chain formation starts in organic component and second, polymer chain formation starts in inorganic component. Depending on which structures we need, we choose the synthetic scheme. For example: the widely used polymer modification with polyhedral oligomer silsesquioxanes (POSS) accordingly to this scheme is the case of preliminary polycondensation of inorganic component. Thus, various preliminary prepared structures can be introduced into the final polymer.[4]

1.1. HYBRID ORGANIC–INORGANIC MATERIALS: METHODS OF FORMATION

The wide choice of the organosilanes allows using the different schemes of hybrid organic–inorganic material formation. So, when isocyanate-propyl-triethoxy-silane (ICPTES), which contains the isocyanate group, is used, precursor for the formation of the hybrid may be obtained by the reaction with polyether. This polyether from can play a role of the complex formation for metal cations, and also it allows to obtain material with purposed properties.[5]

Another way of the Hybrid organic–inorganic materials formation is using amine-containing triethoxysilanes, which can react with isocyanate groups. That allows creating hybrid organic–inorganic materials using the methods of poly-urethane chemistry.[6]

2. Inorganic Materials with Urethane and Urea Fragments

The nature of organic component and conditions of hydrolytic polycon-densation (the character of non-aqueous solvent and catalyst, regulations of gelation, etc.) and gel treatment (the conditions of ageing, washing and drying) essentially influence on properties and morphology of the final products. Those materials in which organic and inorganic components are associated by urethane and urea fragments are perspective for use as polymer electrolytes, biomedical, photoluminescence, photochromic etc. optical materials.

2.1. POLY(URETHANE-UREAS-SILSESQUIOXANE) P-UU-SI

A multistage process was used for the synthesis of organic–inorganic hybrid materials. Generally, it was the two-stage process.[7] In the first stage, the bis(triethoxy)silane oligomer was obtained by reaction of diisocyanate (DIC) or macro-diisocyanate (PP) with 3-aminopropyltrietoxy-silane (APTES) with organic spacer formation, Scheme 3. In the second stage, an organic–inorganic hybrid material was obtained by sol-gel method, Scheme 4.
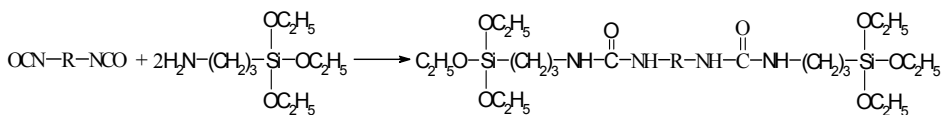
Scheme 3. Synthesis of bis(triethoxy)silane oligomer as organic spacer.
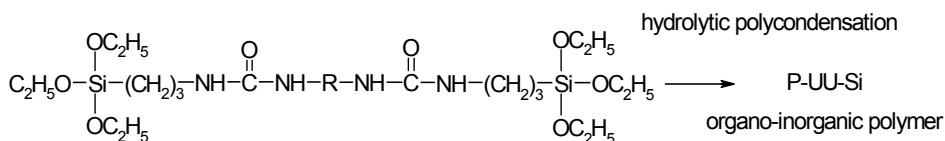
Scheme 4. Preparation of organic-inorganic polymer by hydrolytic polycondensation reaction.

Having received macro-diisocyanates on the basis of various diols, one can control the properties of final organic–inorganic systems, as well as introduce a different organic structures or functional groups. This stage displays an enormous potential for development of such materials. The ethylene glycol, diethylene glycol and butanediol as diol component and hexamethylene diisocyanate, isophorone diisocyanate and diphenylmethane diisocyanate – 4,4′-methylene-bis (p-phenyl isocyanate) as second component were used.

Obtained macro-diisocyanate (PP) was used for the synthesis of two series of silica-containing hybrid materials. In the first series the ratio of PP:APTES was 1:1, in the second – 1:2 (mol). The completeness of reaction was controlled by IR spectroscopy– till complete exhausting of NCO-groups (2,200-2,300 cm^{-1}). Hydrolytic polycondensation was carried out at the composition ratio APTES: water:fluoride-ion = 1:1.5:0.01 (mol). The transparent gel was formed during 20–30 min. The opalescence was observed. Obtained gels were dried in a vacuum until half-transparent, glass-like xerogels were formed.

2.1.1. IR-Spectra of Poly(Urethane-Ureas-Silsesquioxane) P-UU-Si

The IR-spectra of xerogels, obtained with the use of 1,4-butanediol, ethyleneglycol and diethyleneglycol at the ratio of DIC/APTES = 1:1 (samples 1–3) and 1:2 (samples 4–6). There are three intensive absorption bands at ~2,860, ~2,930 i 3,309–3,322 cm^{-1} for all studied samples, which assigned to $\nu_{simmetric}$(CH), $\nu_{asimmetric}$(CH) and ν(NH), correspondingly. They refer to presence in xerogels of methylene and amide sites, the latter participate in hydrogen bonding. The quantity and profiles of intensive absorption bands in the region of 1,250–1,750 cm^{-1} are dependent on the PP:APTES ratio. In case of 1:2 ratio, there is an intensive absorption band at 1,695 cm^{-1} (spectrum 4) in the IR-spectrum of 1,4, butanediol based xerogel. In the case of xerogels synthesized on the basis of ethylene and diethyleneglycol based precursors, the intensive absorption band

at ~1,706 cm^{-1} (sample 5,6) are observed. The two first bands can be assigned to the stretching vibration of CO (amide I), the third one – to the deformation vibration of CNH (amide II) of urethane and urea groups, correspondingly. IR spectra of xerogels, obtained at the ratio of UP:APTES = 1:1 (sample 1–3), are similar to those described above. However, there are some differences. The absorption band at 1,687–1,706 cm^{-1} (amide I) has no shoulder, and the other intensive band (amide II) is shifted to the low-frequency area at ~16–26 cm^{-1}. It may indirectly point to the presence of allophanate and biuret fragments in these samples, because their appearance leads to the less ordering structures. It is ought to note that IR spectra of all samples include the absorption band in the range of 1,033–1,057 cm^{-1}. This band may be assigned to the stretching vibrations of siloxane bonds, which were formed during the reaction of hydrolytic poly-condensation of trietoxysililyc groups.

2.1.2. Thermogravimetric(TG) and Differential Thermogravimetric(DTG) Studies of the P-UU-Si

We can see from Figure 2 that TG/DTG/DTA curves of samples obtained on the basis of hexamethylene diisocyanate and 1,4-butane diol at the molar ratio DIC/APTES, 1:1 (1) and 1:2 (2). According to TG/DTG data, the destruction of materials begins at a temperature higher than 220°C. Till 420°C the process runs in two stages   with maximal rates at 310°C and 350°C (sample, obtained at the ratio of UP:APTES = 1:1) and at 310°C and 370°C (sample, obtained at the ratio of UP:APTES = 1:2), correspondingly. Two endothermic peaks are observed in the DTG curve. It can be supposed that the first stage of destruction is connected with destruction of urea and urethane groups, and the second one – with destruction of methylene chains. The intensity of endothermic peaks is in proportion to the UP content. The complete weight loss, as it was expected at the ratio of 1:1, is somewhat higher (80%, wt.), than at the ratio of 1:2 (72%, wt.). According to TG and DTG curves, the beginning of destruction of studied polymers is higher than 220°C. Till 420°C a process passes through two stages with the maximum rates at 310°C and 350°C (for sample 1, the ratio 1:1) and 310°C and 370°C (for sample 2, the ratio 1:2). Based on the literature data, it can be supposed that the first stage is caused by the decomposition of carbamide and urethane groups, the second one – is caused by the decomposition of ether chains. The total weight loss at the ratio of 1:1, as it was awaited, was somewhat higher (80%, wt), than at the ratio of 1:2 (72%, wt). Thus, as a result of interaction of 1,4-butanediol based PP with APTES the precursors are easily formed. The hydrolytical polycondensation of obtained precursors in the presence of fluoride-ion as catalyst leads to the formation of transparent gels. Subsequent treatment of the gels allows obtaining the hybrid organic–inorganic materials, which contain urea, urethane, allophanate and biuret fragments. Obtained materials are thermally stable till 220°C.
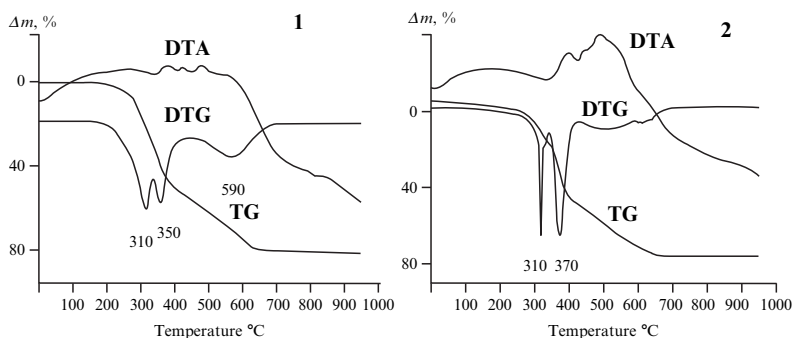
Figure 2. DTA, TG, DTG curves of samples obtained on the basis of hexamethylene diisocyanate and 1,4-butane diol at the molar ratio DIC/APTES=1:1 (1) and DIC/APTES= 1:2 (2).

2.2. POLY(URETHANE-UREAS-SILSESQUIOXANE) ON THE BASIS OF CROWN ETHER-CONTAINING PRECURSOSR P-UU-CE-SI

Crown ethers, as macro-heterocyclic compounds, are widely used ones due to the complex formation. That is why scientists are interested in their use for HOIM development. Hybrids on the basis of these functionalised crown ethers with inorganic components have been reported.[8] Conclusion concerning a violation of complex formation, when crown ether cycles are positioned close to units of inorganic component, has been made. However, this should be expected since the inorganic component forms three-dimensional network. The use of the systems with simultaneous content of urea and crown-ether fragments has been described.[9] These systems are considered as potential membranes. It worth saying, that such a way is one of the classic ways of crown ethers use.

2.2.1. Synthesis

For the synthesis of hybrid organic–inorganic material (HOIM), the precursors comprising trialkoxyl groups $(RO)_3SI-$ are used with further hydrolytical poly-condensation with formation of an advanced network of polysiloxane bonds. Synthesis of nanohybrid materials is based on self-organization of precursors of sol-gel synthesis – derivatives of trifunctional bis-silanes with using of diols, hydrazides and crown ethers, having specific properties (molecular weight, complex formation ability in regards to metal cations and neutral molecules, kinetic flexibility, etc.). The latter essentially determines the morphology of solid state and properties of materials. Such approach is a powerful way of direct creation of hybrid nanomaterials for optical, electronic, sorption and some other technologies. The synthesis of poly-urethane-urea-silsesquioxanes with crown ether fragments, P-UU-CE-Si, may be presented,[10] Scheme 5.

→ polycondensation → **HOIM**
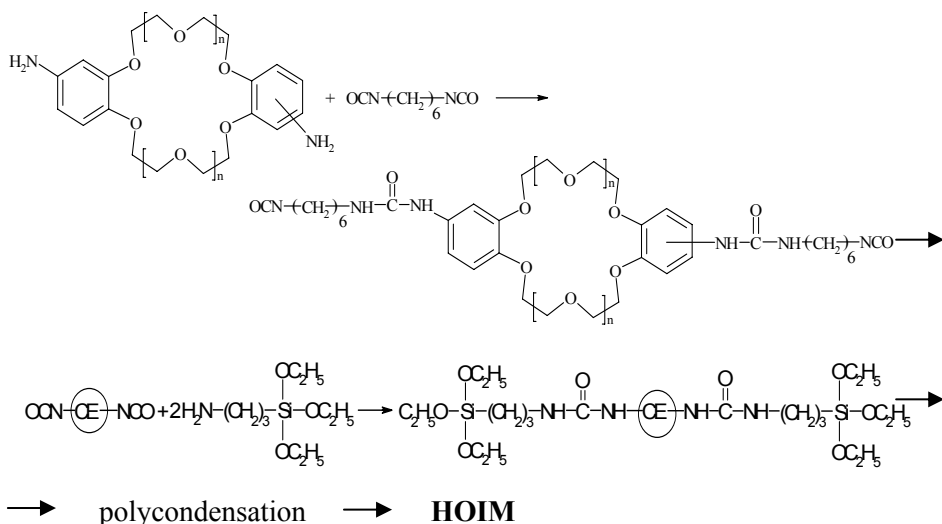
Scheme 5. Scheme of the HOIM synthesis. CE – fragment of the diamine dibenzo-18(24,30)-crown-6(8,10).

The use of urethane and urethane-urea fragments as the spacers provides the regulation of the degree of interchain interaction. The embedding into the spacer's structure of macro-heterocyclic fragments provides the systems with ability of specific complex formation. Besides, it is a potential possibility of systems' self-association under the introduction of metal cation, as the result of coordination cross-linking of macromolecules through ion–dipole interaction of macro-heterocycle cavity and metal cation with intermolecular sandwich-type complex formation. The composition of the poly(urethane-urea-silsesquioxane)s on the basis of crown ether-containing precursors P-UU-CE-Si are presented in the Table 1.

TABLE 1. Composition of the P-UU-CE-Si.

No.	DA/1 (mol)	DA/2 (mol)	DA/3 (mol)	HMDI (mol)	PF (mol)	PEG300 (mol)	PEG600 (mol)	PEG1000 (mol)	APTES (mol)	ω(DBCE) (wt%)
1	1	–	–	2	–	–	–	–	2	30.7
2	–	1	–	2	–	–	–	–	2	35.5
3	–	–	1	2	–	–	–	–	2	39.7
–4	1	–	–	4	–	2	–	–	2	17.0
5	1	–	–	4	–	–	2	–	2	13.2
6	1	–	–	4	2	–	–	–	2	10.2
7	1	–	–	4	–	–	–	2	2	10.2

DA/1-DADB18C6, DA/2-DADB24C8, DA/3-DADB30C10.

The dibenzo-18-crown-6, dibenzo-24-crown-8 and dibenzo-30-crown-10 (DBCE) were used. We modify the organic spacer by introduction of polyethylene glycols: PEG-300 and PEG-600, as well as polyoxytetramethylene glycol, POTMG-1000 (PF), in order to delete the centers of cross-linking of macro-heterocycles. The hybrid bridge polysilsesquioxanes with covalent-bonded crown-ethers: urea-containing (samples 1–3) and urethane(urea)-containing (samples 4–6) have been obtained.[10]

2.2.2. Catalytic Polycondensation of Crown Ether-Containing Precursors

It should be noted that during catalytic polycondensation of crown ether-containing precursors, the higher rates of gel formation in comparison with urethane bis-silanes without crown ether fragments (studied earlier) have been observed. This can be explained by rising of nucleophilicity of fluoride–ion upon binding of counter-ion NH_4^+ by crown ether cavity and as a result the generation of "naked" anion, Figure 3.
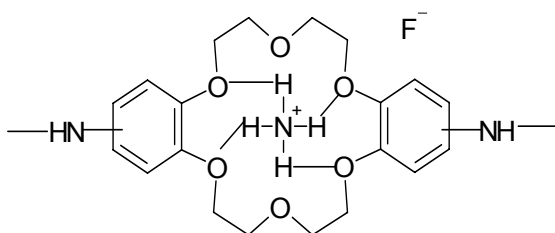
Figure 3. The "naked" anion generation.

2.2.3. IR Spectroscopy

IR spectra of HOIM on the basis of DADBCE urethane(urea) derivatives both non-containing oligoethers (P-UU-CE-Si/1,2,3) and containing oligoethers (P-UU-CE-Si/4,5,6) are practically similar (Figures 4 and 5), however they differ
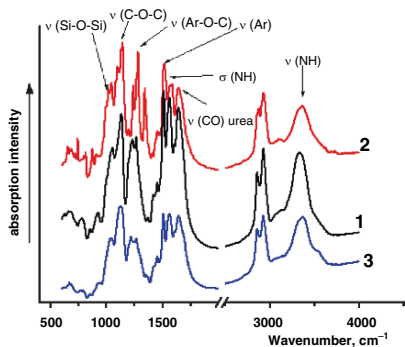
Figure 4. IR-spectra P-UU-CE-Si/1, 2, 3.
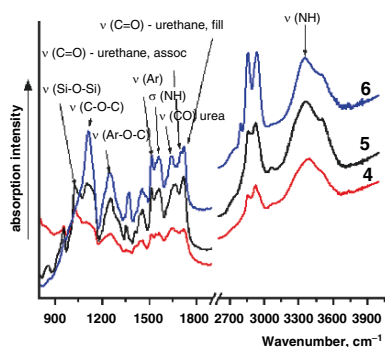
Figure 5. IR-spectra P-UU-CE-Si/4, 5, 6.

by additional absorption bands, indicating the presence of urethane fragments in the HOIM structure (such as Amide 1 band of urethane fragments).

Comparative analysis of IR spectra of initial DADB -18(24,30)-C-6(8,10) and based HOIM (Figure 6) has shown the presence of absorption bands, typical both for initial DADBCE and for HOIM including corresponding DADBCE, proved the inclusion of DADBCE fragments into HOIM structure.
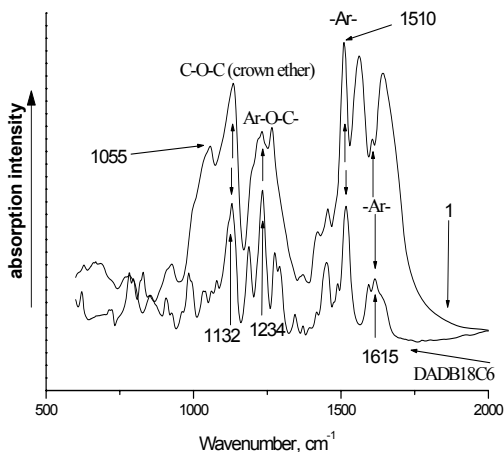
Figure 6. IR-spectra of initial DADB18C6 and based polyurethane-urea-crown ether-silsesqioxane (P-UU-CE-Si/1).

2.2.4. Thermo-stability of P-UU-CE-Si

Analysis of thermo-oxidative destruction of the systems (Figure 7) has shown that the temperatures of the active destruction increase with oligoethers' intro-duction. The highest temperature was observed for the sample with polyether of MW 1,000. The weight loss till 200°C by the samples 4,5 based on oligoethers olyethylene glycol, which is more polar in comparison with polytetramethylene glycol is possibly the result of difficulty of the solvent (DMF) residue removal. Then, approximately starting from 300°C, the weight losses for these systems become less in comparison with urea-based systems.

There are two main explanation of the thermo-stability of polymers of different structure. Organosiloxanes: in this case, even at 950°C the full combustion was not registered. It was interpreted as a little accessibility of organic radicals in polyorgano-siloxanes for oxidation. Organic polymers: the main factor of thermo-oxidative stability is the level of intermolecular interactions.

Analysis of thermo-oxidative destruction of synthesized systems has shown that the temperatures of active destruction increase with oligoethers' introduction. The highest temperature was observed for the sample with polyether of MW of 1,000.
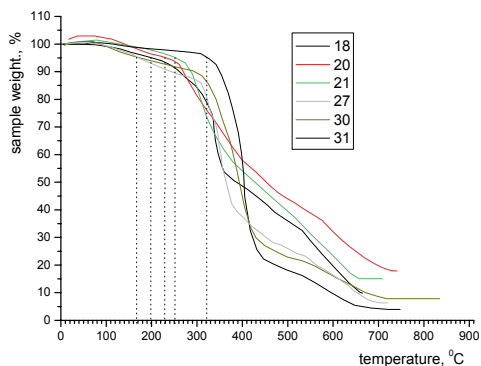
Figure 7. TG curves of studied samples.

For the confirmation of the hypothesis, that the main factor of thermo-oxidative stability is the level of intermolecular interactions for studied systems IR spectroscopy investigations were carried out (Figures 8 and 9). IR-spectra analysis may provide the information not only about the presence in polymer of chemical structure of some fragments, but it can indicate the different supra-molecular structural peculiarities of samples. The analysis of position and character of absorption bands of Amide I and ν(NH) testifies to the participation of urethane and urea fragments of HOIM in formation of associates owing to hydrogen bonding between H-atoms of NH-groups and O-atoms of urethane and urea fragments. The shift of the maxima of the bands ν(NH) and ν(C=O)Amid I of urea fragments to the low-frequency region along with distinct display of associated carbonyl groups' band (ν(C=O)Amid 1 of urethane fragments – 1,700 cm^{-1}) relatively to the internal standard (CH2-goup band) allows to place studied systems accordingly to degree of association of their hard blocks as following:

P-UU-CE-Si-4< P-UU-CE-Si-5< P-UU-CE-Si-6.
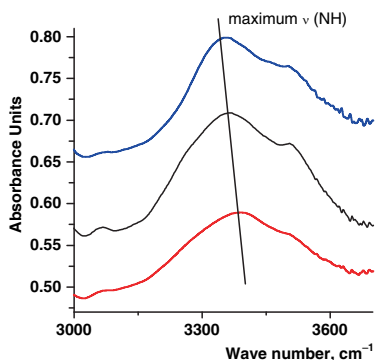
Figure 8. IR-spectrum of absorption area of ν(CO) urethane and urea (specimen 4–6).
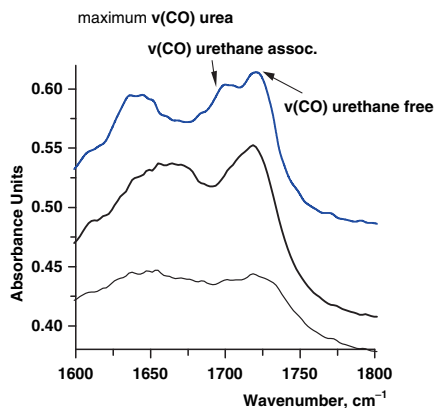
Figure 9. IR-spectrum of absorption ν(N-H) (specimen 4–6).

It should be noted that the content of Si-O-Si fragments in this case is essentially less and this factor may be considered less significant. Although, it is worth paying attention to it, since the content of Si-O-Si fragments may be easily increased (by tetra-ethoxysilane introduction on the stage of heterolytic polycondensation). The intensive absorption peaks have been observed which testify to presence of silica substance. The peaks with lower intensity at 2,924 and 1,653 cm^{-1} indicate the incomplete combustion of organic fragments. The specimen was heated up to 960°C that practically fully disrupt the organic specimens.
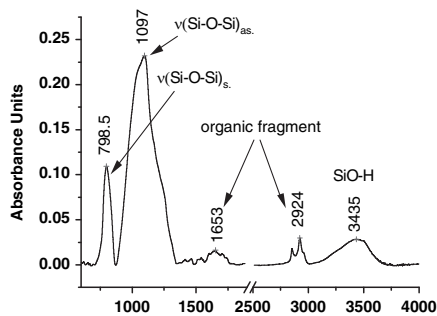
Figure 10. IR-spectrum of specimen 7.

The investigations of the thermo-stability of the similar systems Polyurethane/ Polyoctahedralsilsesquixanes based on the hybrid systems of isocyanate-function-alized POSS (8NCO:1POSS)/PEG 600 is known.[11] Thermo-stability of this hybrid is lower than the initial POSS; the start of decomposition is 190°C.

2.2.5. WAXS Study of P-UU-CE-SI

The fragments of crystal structure in P-UU-CE-Si-2 confirmed by the IR data, were also observed in X-ray data (Figure 11), which is specific only for this sample. Two broad maxima in the range of medium and small scattering angles (M1, M2) as well as the presence of A maximum were observed at WAXS profiles for amorphous samples P-U-Si-(1,3). Beside the described maxima, a number of narrow crystal peaks is observed for WAXS profile of P-UU-CE-Si-2 (Kn,), Table 2. Figure 12 presents WAXS profiles of linear polyurethanes samples PU-1, PU-2, PU-3 based on 4,4′-methylene-bis (p-phenyl isocyanate) and oligooxytetrametylene glycol and the same diamino-dibenzo-18(24,30)-crown-6(8,10). Investigations were carried out with the aim of understanding of the character of noted maxima. The crystal peaks observed for PU-2 и P-UU-CE-Si indicate that K peaks belong to the structural peculiarities of DADB24C8, since both samples include in their chemical structures the fragments of DADB24C8.

The maximum A, typical for all samples, is an evidence of amorphous character of materials' short ordering.[1]
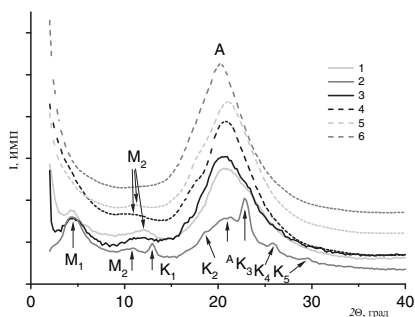
Figure 11. WAXS profiles of P-UU-CE-Si 1, 2, 3, 4, 5, 6.
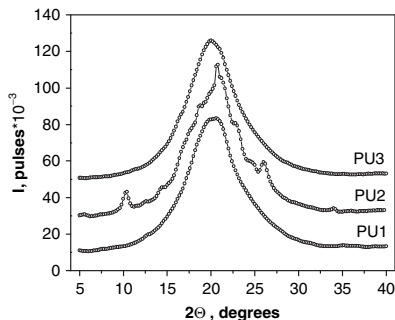
Figure 12. WAXS profiles of linear poly-urethanes PU-1, PU-2, PU-3.

The maximum M1, by analogy with similar bridge hybrid organic–inorganic systems, may be attributed to the formation by inorganic sites of phase-homogeneous domains, which have a short order of mutual location in organic matrix. Thus, the only case of amorphous-crystal structure is conditioned by specific peculiarities of used diamino-dibenzo-crown ether. It was confirmed by analysis of linear polyurethane, containing the same diamine.

TABLE 2. WAXS profiles for P-UU-Cr-Si; peaks Mn, Kn and A.

No.	Peak sign	Interpack distance, d (nm)	Angle of scattering, 2Θ, (grad)
1	M_1	2.229	4.4
	M_2	0.806	12.2
	A	0.474	20.8
2	M_1	2.229	4.4
	M_2	0.890	11.0
	K_1	0.755	13.0
	K_2	0.524	18.8
	A	0.470	21.0
	K_3	0.436	22.6
	K_4	0.383	25.8
	K_5	0.334	29.6
3	M_1	2.127	4.6
	M_2	0.832	11.8
	A	0.473	20.8

Analysis of the data of Wide-angle X-ray Scattering for the samples of Polyurethane-Polyoctahedralsilsesqvioxaness based on ester, isophorone diiso-cyanate and dimethyl propionic acid, which can serve to some extent as analogue for the studied systems is described.[12] Unfortunately, even in the case of POSS use, the WAXS data does not provide the answer regarding the ordering of inorganic component of the system. But at the same time, they provide information about the distance between inorganic sites.

2.2.6. Computer Modelling: Molecular Design

Figure 13 presents the result of Computer modelling for sample 1. It was obtained by the method of molecular mechanics MM3, realized in Tinker program. The distance d between inorganic components, which serves as partial characteristic of the structure has been evaluated by X-ray method. It was used for simulation of the structure of studied samples. It allows to visualize the structure. It can be seen that the sample's structure is not linear, but it has a tendency to spiral-like organization.
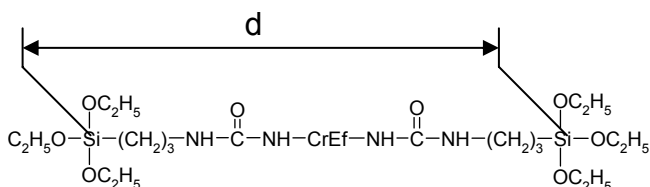
D in our model from WAXS for P-UU-CE-Si-1: 2,229 Hm
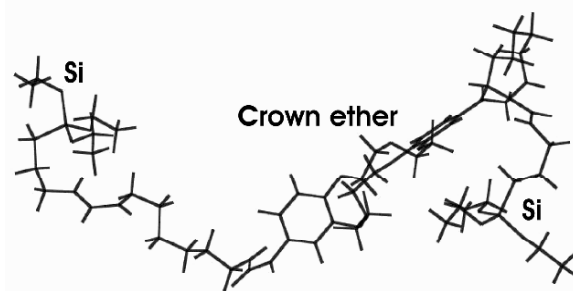
Figure13. Scheme of the structure of studied samples.

Formation of supramolecular structures for such systems is possible owing to the presence of the macro-heterocyclic fragments in the polymeric chain by the way of creation of sandwich – type structure: "crown ether fragment of organic spacer●metal cation● crown ether fragment of organic spacer" (Figure 14).

Structuring the effect of Metal salt, Barium dichloride, was carried out by inclusion of the salt into the precursor of hydrolytic polycondensation. As a result

the poly(urethane-urea-crown ether-silsesquioxane) network, a self-associated system, was formed. The first act of self-association was the cross-linking and the second act was the network formation due to polycondensation process.
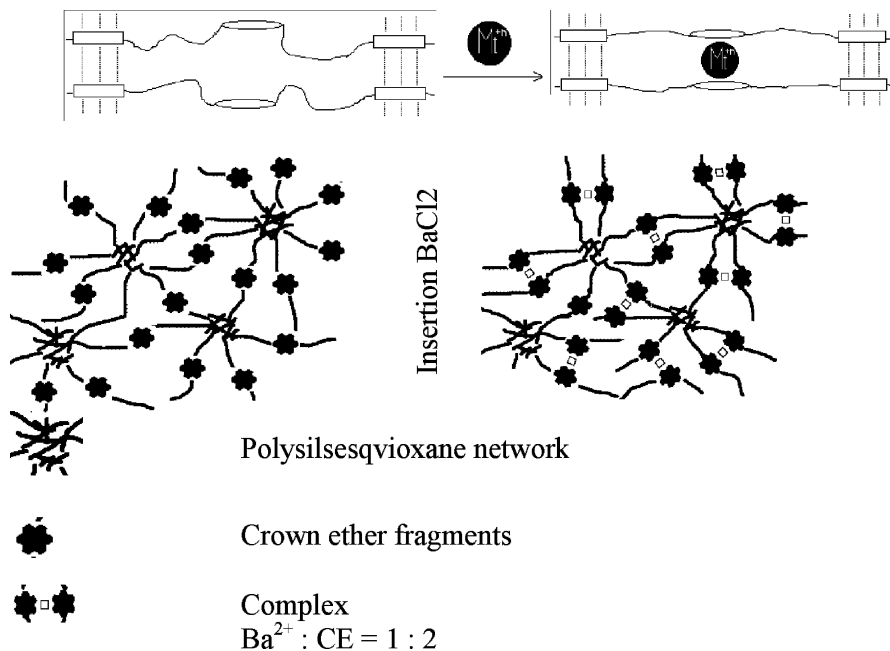
Figure 14. Scheme of the structure formation: "crown ether fragment of organic spacer●metal cation● crown ether fragment of organic spacer".

3.   Conclusions

Novel hybrid organo-inorganic systems based on urethane-, urea- crown ether- and siloxane-containing monomers and oligomers have been developed by sol-gel method. According to WAXS data, used in the method of molecular mechanic simulation and their comparison with DSC data, the different types of structural organization of organic fragments in two series of samples can be supposed. In the series of the HOIM based on urea-containing spacer, the chain twists as spiral-like structure, while in the series based on urethane(urea)-containing spacer the partial producing of lamellar formations is taking place.

Introduction of oligoethers and increase of their molecular weight results in increasing the start temperature of their decomposition. We suppose that this is connected with strengthening of interactions between organic chains of the hybrids. This is confirmed by IR-spectra in the area of urethane and urea groups' vibrations. Obtained novel bridge organic-inorganic urethane(urea)-silsesquioxane hybrids

with macro-heterocyclic fragments in organic chain are perspective as poly-functional materials, firstly, as sorbets.

They are interesting for studying of multi-level processes of self-organization under the influence of complex-formation processes of organic spacer.

Acknowledgement

References

[1] Y.V. Savelyev, In "Handbook of Condensation Thermoplastic Elastomers, Wiley-VCH GmbH&Co. KgaA, 2005, p. 355.
[2] G. Kickelblick, *Prog. Polym. Sci.* 28 (2003) 83.
[3] J.C. Brinker, G.W. Scherer, *Sol-Gel Science: The Physics and Chemistry of Sol-Gel Processing*. San Diego, CA: Academic Press, 1990.
[4] T. Zhang, K. Xi, H. Chen et al., *J. Appl. Polym. Sci.* 91 (2004) N1, 190.
[5] S.M. Gomes Correia et al., *Electrochimica Acta* 47 (2002) 2421.
[6] J. Luo et al., *Polymer* 48 (2007) 4368.
[7] Y. Savelyev, L. Robota, Yu. Zub et al., *Ukr. khim. zhourn.* 72 (2006) N11, 64.
[8] G. Dubois et al., *J. Mater. Chem.* 10 (2000) 1091.
[9] S. Cerneaux, N. Hovnanian, *J. Membrane Sci.* 247 (2005) 87.
[10] V. Sierov, V. Litvyakov, Y. Savelyev et al., *Proc. Nat. Acad. Sci. Ukr.*, 7 (2008) 135.
[11] D. Neumann et al., *J. A.C.S.* 124 (2002) N47, 13999.
[12] A.K. Nanda et al., *Macromolecules* 39 (2006) 7037.

Cu-CONTAINING POLYMER NANOCOMPOSITES ON THE BASIS OF SOME (CO)POLYMERS OBTAINED USING NOVEL NON-METALLOCENE TYPE Ti-CONTAINING CATALYSTS

ELNARA KALBALIYEVA[*], REYHAN ALIYEVA, AND AKIF AZIZOV

Institute of Petrochemical Processes of National Academy of Sciences of Azerbaijan, Khodjaly Ave, 30, AZ 1025, Baku, Azerbaijan

Abstract: Polyethylenes and ethylene/1-hexene copolymers with various thermodynamic and structural parameters in the presence of novel non-metallocene type Ti-containing efficient catalytic systems, and Cu-containing polymer nanocomposites were prepared. Polyolefins and composites have been investigated using such methods as Differential Scanning Calorimetry, IR spectroscopy and X-ray phase analysis. It is shown that introduction of Cu-containing particles (Cu/Cu$_2$O) having sizes lower than 10 nm, determined by EMR method, in polymer matrix allows to obtain metal-polymer composites with improved thermal properties.

Keywords: Ethylene (co)polymerization; Polyethylene; Ethylene/1-hexene copolymer; Nanocomposites; Ti-phenolate catalytic systems

1. Introduction

The preparation of metal-polymer composites (MPC) on the basis of various polymer matrices and investigation of their properties is of importance from practical point of view. Such metal-polymer nanocomposites (MPNC) possess unique optical, magnetic, catalytic and other properties.[1–5]

The present article is devoted to some results of investigation of the properties of Cu-containing nanocomposites on the basis of polyethylene and ethylene/1-hexene (EH) copolymers, obtained in the presence of novel non-metallocene type Ti-containing catalyst.[6–9]

2.   Synthesis

Synthesis of novel non-metallocene Ti-phenolate precursors (TPP) were fulfilled in an aromatic solvent (benzene or toluene) refluxed and distilled over metallic sodium by interaction of $TiCl_4$ and various sterically hindered substituted phenols (2,6-bis(morpholylmethyl)-4-methylphenol, 2,6-ditertbutylphenol, 2-morpholylmethyl-4-methylphenol, 2-pyperidinylmethyl-4-methylphenol, $2,2^1$-methylenebis[-6-(1-methylcyclohexyl)-4-methylphenol)] at molar ratio of initial components of 1:1-2, correspondingly. HCl liberated as a result of reaction remained in product composition thus forming Ti-containing complexes with grafted ammonium ligands,[6] which are orange powders after removing the solvent.

(Co)polymerization processes were carried out in a 200 ml stainless steel (X18H10T) autoclave equipped with a magnetic stirrer. Temperature in reaction zone was maintained by ultrathermostat and measured by thermocouple. The pressure in the reactor was controlled by manometer. After the completion of the reaction, the active catalyst was decomposed by 10% alcohol solution of HCl. Polymer was filtered and washed with acidified ethanol, then with distilled water and dried under reduced pressure at 60–70°C to the constant weight.

Density of (co)polymer samples in the form of pressed tablets with 1 mm thickness was determined by picnometric method using aqueous-alcohol solution at 20°C. MPC was prepared by addition of aqueous solution of aqueous Cu acetate (II) – $[Cu(CH_3COO)_2 \times H_2O]$ to the solution of polymer in high-boiling organic solvent at 180–195°C in the medium of inert gas.

3.   Results and Discussion

Recently, we have stated that high efficient catalysts of ethylene (co)polymerization could be prepared by interaction of abovementioned phenolate ligands.[6–12] The transition metal-based compound such as $TiCl_4$ and aluminum organic activator, were used directly in the polymerization reactor (one pot synthesis). Upon interaction of the phenol substituents with $TiCl_4$ in hydrocarbon solution, HCl is liberated which reacts with nitrogen-containing substituent in ortho-position of phenyl ring leading to the zwitterionic type salts, Scheme 1.

It is supposed that the presence of grafted ammonium salt in the composition of phenolate ligand of the precursor complex facilitates the formation of metal-cation active polymerization sites.

Ionic liquid type ammonium salts with [MAOCl]⁻ type counter-ion arising upon interaction of the precursor salts with aluminum organic compounds are the best activators compared to the corresponding chloride salts due to its weak-coordinating character. It is noteworthy that these catalytic systems allow obtaining the various polymer matrices which differ by structure, crystallinity,

density, molecular, thermal-physical and other characteristics that are important for preparation and studying of MPC.
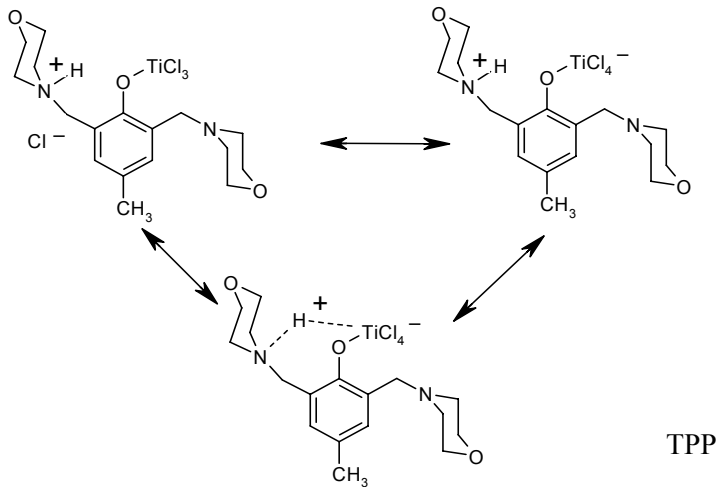
Scheme 1. Ti phenolate precursor (TPP) used as initiator for the polymerization of ethylene and copolymerization of ethylene with 1-hexene.

Some results of ethylene (co)polymerization in the presence of novel TPP and the comparison with conventional catalyst $CpTiCl_2$ are given in Table 1. The table shows the activities of catalytic systems ranges 684–11,878.3 kg product/mole cat. $\times$ h, crystallinity degrees (χ) of samples prepared determined by DSC analysis are 70.2–73.6% for PE, and 31.6–53.9% for copolymers, correspondingly. The degree of branching and unsaturation of obtained PE were determined by IR spectroscopy. It was revealed that the prepared PE samples have linear structure and contain insignificant amount of double bonds and methyl branching. By X-ray phase analysis method it was established that the degree of crystallinity of PE obtained are different depending on catalytic system used. The results of the analysis show that it is possible to obtain various polymers depending on chosen TPP and (co)polymerization conditions. These (co)polymers were used as polymer matrices to prepare Cu-containing MPNC. The sizes of metal-containing particles in polymer matrices have been calculated from EMR spectra data according to.[14, 15] It was revealed that MPC prepared contain in their composition metal/metal oxide particles having sizes lower than 10 nm. Some regularities of ultradispersion of Cu-containing particles in MPNC have been studied depending on structure and branching degree of primary polymer matrix. Comparative X-ray phase analysis of polymer matrix and Cu-containing MPC on its basis shows considerable changes up to 10–15% in the crystallinity degree of polymer matrix after introduction of metal-containing particles compared to the primary polymer. The results of above investigations

show that during thermal decomposition of Cu (II) acetate in the presence of (co)polymer in the medium of inert gas the formation of ultradispersed Cu/Cu_2O particles takes place.

TABLE 1. Ethylene/1-hexene (co)polymerization in the presence of TPP and some parameters of (co)polymers obtained.

Sample	Polyethylene (PE)			Ethylene/1-hexene (EH) copolymer		
	PE-1	**PE-2**	**PE-3**	**EH-1**	**EH-2**	**EH-3**
Catalytic system	$CpTiCl_2$ + $EtAlCl_2$ + MAO	TPP + $EtAlCl_2$ + MAO	TPP + $EtAlCl_2$	$CpTiCl_2$ + $EtAlCl_2$ + MAO	TPP + $EtAlCl_2$ + MAO	TPP + $EtAlCl_2$
Ti: Al, mole	1:600	1:600	1:300	1:600	1:600	1:300
Density (g/cm^3)	0.96	0.95	0.97	0.93	0.93	0.93
Activity (kg product/mole cat. × h)	11,878	10,076	4,264	3,000	1,400	684
χ^a by DSC (%)	74	70	72	54	35	32

Conditions: catalyst concentration – 10^{-4} mole/L, $P_{ethylene}$ – 6 atm, temperature – 22°C, time – 40−50 min, solvent – toluene.

[a] χ were determined from ratio $\Delta H_{melt}/\Delta H_{melt.100\%} \times 100$, where $\Delta H_{melt.100\%} - \chi$ 100% of crystalline PE, which is 269.9 J/g according to literature data.[13]

DSC analysis of EH copolymers and MPNC performed in the atmosphere of air also shows the changes of thermo-physical parameters of polyolefin matrix after insertion of metal-containing particles (Figures 1 and 2). DSC curves of copolymer EH-1 obtained in the presence of conventional catalyst $CpTiCl_2$ (Table 1), and MPNC are given in Figure 1. As is seen from the curve (Figure 1, cr. 1), EH-1 has melting temperature $T_m = 135°C$, melting enthalpy $\Delta H_m = 158$ J/g and crystallinity $\chi = 54\%$. Oxidation with the formation of peroxide-hydroperoxide groups in the defect sites of the main chain of copolymer occurs at 234–280°C, while thermo-oxidative decomposition, followed by intensive exothermal effect $\Delta H_m = 5,367$ J/g takes place at 452°C. According to DSC data of MPNC (Figure 1, cr. 2) its thermodynamic parameters has changed: $T_m = 124°C$, $\Delta H_m = 68$ J/g, $\chi = 23\%$, i.e., crystallinity of composite decreases ~ 2.3 times, T_m decreases ~11°C. With regards to the oxidation processes, as it is seen

from DSC curve of the composite, exo-effect following the formation of peroxide-hydroperoxide compounds is observed at $t_1 = 358°C$ ($\Delta H_1 = 788.5$ J/g) and $t_2 = 427°C$ ($\Delta H_2 = 879$ J/g), while full oxidative destruction takes place at 488.13°C. So MPNC at least in the area of 20–340°C shows best thermal stability, than initial EH-1.
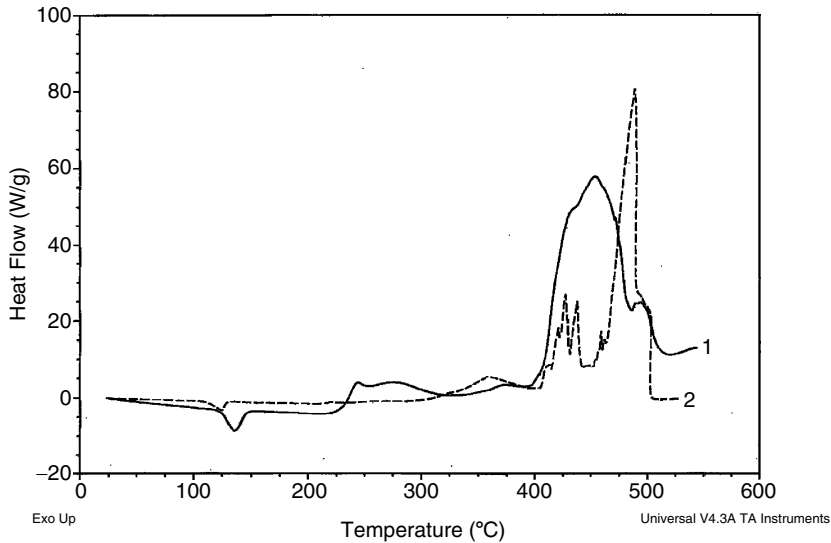
Figure 1. DSC curves of EH-1 (1), MPNC on its basis (2).

DSC curves of copolymer EH-2 obtained in the presence of novel catalyst TPP (Table 1) and MPNC are given in Figure 2. As it is seen (Figure 2, cr. 1), for EH-2 sample: $T_m = 125°C$, $\Delta H_m = 102$ J/g, $\chi = 35\%$. Preliminary oxidation starts from t ~ 226°C, the first exo-effect maximum appears at ~255°C. Then the series of exothermal effects is observed at 313°C; 334°C; 368°C; 397°C; 419°C; 510°C, following full thermo-oxidative destruction of the copolymer. DSC investigations of MPNC on the basis of EH-2 showed that it has the following thermodynamic characteristics: $T_m = 127°C$, $\Delta H_m = 47$ J/g, $\chi = 16\%$, i.e., T_m of the composite shifts to the area of high temperatures only by 2°C, while ΔH_m and χ decrease more than two times. Thermo-oxidative stability of composite also changes compared to the initial copolymer. Exo-effect following preliminary oxidation with the formation of peroxide-hydroperoxide compounds is practically absent. Up to 430°C, on the DSC curve, there are insignificant exo-effects upon heating in the atmosphere of air. Such exothermal effects are observed at 480°C and 508°C with $\Delta H = 934$ and 2,240, correspondingly. Conducted DSC investigations allow to conclude that exothermal effects following oxidation on the defect sites of copolymer chains are considerably

hindered in both composites that provides for a possibility of using these composites as thermo-stable ones in a wide range ($\sim$ up to 350°C for MPNC (EH-1) and $\sim$ to 450°C for MPNC (EH-2)).

From DSC data apart from T_m, ΔH_m and χ, the melting entropy ΔS_{melt}, conformation entropy ΔS_{conf} have also been calculated (Table 2). All the data obtained testify to the decrease of thermodynamic parameters of the studied polymers upon dispersing in them Cu-containing nanoparticles. However, the thermo-oxidative stability of the polymer matrix increases considerably.
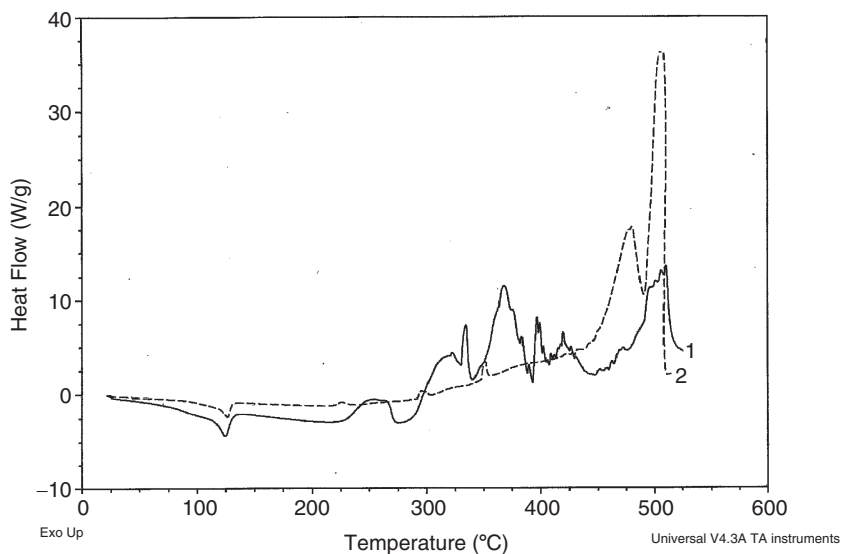
Figure 2. DSC curves of EH-2 (1), MPNC on its basis (2).

TABLE 2. Thermodynamic parameters of PE, EH and MPNCs on their basis.

No.	Sample	T_m (°C)	ΔH_m (J/g)	ΔS_{melt} (J·g/°C)	ΔS_{conf} (J·g/°C)	χ^* (%)
1	PE-1	135	199	0.487	0.389	74
2	MPNC (PE-1)	131	99	0.244	0.195	37
3	PE-2	134	190	0.466	0.373	70
4	MPNC (PE-2)	133	90	0.222	0.178	33
5	EH-1	135	158	0.387	0.310	54
6	MPNC (EH-1)	124	68	0.172	0.137	23
7	EH-2	125	102	0.255	0.204	35
8	MPNC (EH-2)	127	47	0.116	0.093	16

4. Conclusions

It has been established that by introducing nano-sized Cu particles into polymer matrix it is possible to obtain MPNC with controllable thermo-physical properties on the basis of polyolefin matrices (PE, EH) obtained using novel Ti-containing organometallic catalytic systems. Addition of a little amount of metal even in the branched copolyethylene matrix increases its thermal stability considerably. It is suggested that changes of thermodynamic parameters and increase of thermo-oxidative stability as a result of doping polyolefin matrices by metals are conditioned by formation of ultradispersed metal-containing nanoparticles having sizes of lower than 10 nm. These particles apparently have increased activity in quenching singlet oxygen and/or decomposition of the intermediate peroxides and hydroperoxides arising at the defect sites of polymer matrix. Besides nanoparticles form distinguishing structures of polymer matrix that also causes increase of thermo-oxidative stability of a composite.

Composites obtained can be used as functional nanomaterials with predictable thermal, magnetic, optical and catalytic properties.

References

[1] Mio, M.J., Moor, J.S. Supramolecular aufbau: folded polymers as building blocks for adaptive organic materials, MRS Bull. 2000, 25:36–41.

[2] Sergeev, G.B. Nanochemistry, Moscow, CDU, 2006.

[3] Aliyeva, R.V. Metal-containing nanoparticles and polymer composites on their basis, processes of petrochemistry and oil refining, 2007, 5(32):54–65.

[4] Pomogailo, A.D., Rozenberg, A.S., Ufland, I.E. Metal nanoparticles in polymers, Chemistry, Moscow, 2000.

[5] Azizov, A.H., Ismailov, E.S., Martynova, G.S., Aliyeva, R.V., Kalbaliyeva, E.S., Vakhshouri, A.R., Maharramov, M.J. Influence of magnetic field on polyethylene with nanosized metal oxide component, Europolymer Conference-2008 (EUPOC 2008), Gardnano, Lake Gardo, Italy, 1–5 June 2008.

[6] Azizov, A.H., Aliyeva, R.V., Bagirova, Sh.R., Mamedova, R.Z., Kalbaliyeva, E.S., Azizbeili, H.R., Khanmetov, A.A., Guliyev, B.V. Method for preparing single site catalysts for ethylene (co)polymerization, Azerbaijanian Patent I 20080048, 2008.

[7] Azizov, A.H., Aliyeva, R.V., Martynova, G.S., Kalbaliyeva, E.S., Vakhshouri, A.R., Bagirova, Sh.R., Azizbeili, H.R. XVIII Mendeleev Congress on General and Applied Chemistry. Moscow, Russia. 2007. September 23–28. 1434.

[8] Kalbaliyeva, E.S., Aliyeva, R.V., Azizov, A.H., Martynova, G.S., Vakhshouri A.R. 2nd International IUPAC Conference on Green Chemistry, Moscow, Saint Petersburg, September 14–19, 2008.

[9] Azizov, A.H., Aliyeva, R.V., Kalbaliyeva, E.S., Bagirova, Sh.R., Mamedova, R.Z., Azizbeyli, H.R., Vakhshouri, E.R. Europacat–VIII, Turku/Abo. Finland. 2007. August 26–31.

[10] Kalbaliyeva, E.S., Azizov, A.H., Ismailov, E.G., Aliyeva, R.V., Abbasov, Y.A. Whole-Russia Conference of candidates of international Charitable Society named after K.I.Zamaraev. Novosibirsk. Russia. 2007. May 17–19. 2004.

[11] Aliyeva, R.V., Azizov, A.H., Bagirova, Sh.R., Mamedova, R.Z., Kalbaliyeva, E.S., Azizbeyli, H.R. VII Russian Conference (with International participation) "Mechanism of catalytic reactions". Saint-Petersburg. Russia. 2006. July 3–8. 184.

[12] Azizov, A.H., Aliyeva, R.V., Kalbaliyeva, E.S., Bagirova, Sh.R., Mamedova, R.Z., Azizbeili, H.R., Guliyev, B.V. III International Conference Catalysis: Fundamentals and Application, Novosibirsk. Russia. 2007. July 4–8. 169.

[13] II Kim, Chang-Sik Ha J. Mol. Cat. A: Chemical 210, 2004. 47.

[14] Masimov, E.A., Ismailov, E.G., Guseinov, V.I. Interpretation of EPR spectra of $Cu(NO_3)_2*3H_2O/H_2O$/polyethylene glycol and $Mn(NO_3)_2*6H_2O/H_2O$/polyethylene glycol systems/Baku, BSU No. 40, 1999, 48.

[15] Kopp, K.E., Weiss, B.P., Maloof, A.C., Hojotolah, V. and et al. Chains, clums and strings: Magneto-Fossil taphonomy with ferromagnetic resonance spectroscopy Earth and Planetary Science Letters, 2006, 247:10–25.

SUBJECT INDEX